FIELD INVESTIGATIONS AND HYDROLOGICAL STUDIES OF TWO UNSTABLE, UNSATURATED SOIL SLOPES IN SAINT LUCIA, WEST INDIES

A Thesis Submitted to Newcastle University

In Partial Fulfillment for the Degree of Doctor of Philosophy

by

Roosevelt Adolph Isaac
M.Sc., P.Eng., C.Eng., MIMMM, MCIM

Department of Civil Engineering and Geosciences

Newcastle University

Newcastle Upon Tyne, NE1 7RU

The United Kingdom

March 2014

ABSTRACT

Classical soil mechanics as presented by Karl Terzaghi assumed that the soil is in a fully saturated state. However, in tropical areas of the world residual and colluvial soil slopes exist in an unsaturated condition and the traditional theories and methods of slope stability analysis cannot be readily applied. However, situations may arise when unsaturated soils rapidly become saturated during rainstorms and the traditional theories do apply.

The quick response of pore water pressure to rainfall intensity in a multi-layered residual soil and colluvium has been studied and reported in this research project. The effect of infiltration into a slope of variable saturated hydraulic conductivity values on stability was also examined. It was found that for a multi-layered residual soil the rapid infiltration of water into the more permeable soil layer causing saturation had a relatively quick impact on pore water pressure increase and hence the stability of the slope even though the overlying residual soils of lower saturated hydraulic conductivity remained unsaturated. In tropical areas which experience heavy rainfall periods during the wet season followed by very dry spells for several months of the year the infiltration process particularly in multi-layered unsaturated residual soil slopes is not fully understood.

This thesis attempts to address this problem with the objective of contributing to the understanding of the hydrological processes taking place in a multi-layered unsaturated residual soil slope and a colluvial slope and to demonstrate how quickly the unsaturated soils become saturated and unstable during a 24-hour rainstorm event. The study includes the use of field instrumentation, laboratory testing and finite element numerical analysis to determine the changes in pore water pressure and instability in the two slopes due to infiltration during rainstorms. The sites selected for the study are located on the Caribbean island of Saint Lucia in the West Indies. Both sites experienced land slippage during heavy rainfall events.

A study of the cause of the slope failures of a colluvial soil slope derived from weathered basalt and a residual soil slope from weathered parent andesite rock. The effect of the hydrological process induced by variable rainfall patterns and their effect on the stability of the two slopes unstable are examined. Pore water pressure and matric suction were measured in the field at both sites with tensiometers manufactured by Soil Moisture Equipment Corporation, Santa Barbara, California, and were installed at variable depths at specified locations on the slopes. Slope inclinometers, standpipe piezometers and rainfall gauges were also used for field instrumentation. The combined seepage and limit equilibrium slope stability analyses were conducted using the soil properties from the field and laboratory testing programs. The software Slope/W and Seep/W from Geo-Slope International Ltd, Calgary, Alberta, Canada were used for modeling the slope failures.

The results of the study indicate the sensitivity of the relationship between variable pore water pressures, suction and the degree of saturation as expressed by the Soil Water Characteristic Curve (SWCC).The effect of these stress variables on the stability of the two slopes are also presented. Several areas are highlighted where additional research work is required such as the need to accurately identifying soil parameters for unsaturated residual soils and colluvium both in the field and laboratory. Of particular concern is the accurate measurement of the saturated hydraulic conductivity and suction of these materials which contribute to the frequent occurrence of catastrophic landslides during the rainy season on the Caribbean island of Saint Lucia.

ACKNOWLEDGEMENTS

Firstly, I would like to thank Mr. Dick Forth of the Department of Geotechnical Engineering at Newcastle University for taking me on as a research student and who visited the island of Saint Lucia where I gave him a tour of the study sites at the initial stage of the study. Mr. Forth pointed out to me that the topic of the research would be challenging but it would be a great contribution to the development of the island. Upon Mr. Forth's retirement from the University, Dr. Mohamed Rouinia accepted my plea for his guidance as my supervisor and I wish to thank him very much for accepting me and guiding me through to the completion of the research study.

I also wish to extend special thanks to the technicians in the Soil Mechanics laboratory at Newcastle University for their assistance with the more complex test procedures. My sincere appreciation go out to Mr. Grant Staines and Ms Kath Liddell of the Department of Chemical Engineering and Advanced Materials of Newcastle University for their excellent work on the Scanning Electron Microscopy and the X-Ray Diffraction analyses of soil samples from the study sites. I would also like to acknowledge the work of Mr. Philip Green of the Department of Geochemistry who performed the chemical tests on soil samples from the study sites.

Mr. Fred Beadle of the Rock Mechanics laboratory at Newcastle University performed specialized tests on rock samples transported from Saint Lucia and his efforts are greatly appreciated. I would like to extend very special thanks to Mr. Trevor Whitfield formerly of the Rock Mechanics laboratory who used his specialized skills to produce the petrographic thin sections from rock samples of basalt and andesite from Saint Lucia.

The numerical analyses were performed using the commercial geotechnical software SEEP/W and SLOPE/W from Geo-slope International of Calgary, Canada. I wish to extend special thanks to the support team at the company for their patience and tolerance in helping me along with understanding the complicated aspects of the software program which was vital for the completion of the research study.

Not to be forgotten are the dedicated technicians of Strata Engineering Consultants Ltd who were very helpful in accumulating field and laboratory data for the project and who assisted with the graphical presentation of the data. So I must extend special thanks to Dave, Arnnel, Antonius and Garvey for their much appreciated contribution to this project. Philo provided some stress relief during the course of the study. Mike provided continuous moral support.

Finally, I wish to thank my wife Griselda for her moral support and patience when the workload became tiresome and frustrating and the encouragement to keep on going was always there.

DECLARATION

The work presented in this dissertation was carried out in conjunction with the Department of Civil Engineering and Geosciences at Newcastle University in the United Kingdom. This thesis is the result of my efforts and any quotation from, or description of the work of others is acknowledged herein by reference to the sources, whether published or unpublished.

This dissertation is unlike any other that I have submitted for any degree, diploma or other qualification at any other university or institution of higher learning. No part of this thesis has been or or is being concurrently submitted for any such degree, diploma or other qualification.

This document is within the required length of 80,000 words and consist of
240 figures and 34 tables.

****

Roosevelt Adolph Isaac

I dedicate this dissertation to my late parents Adolphus and Rose Agatha Isaac who gave me the temperament and sustenance to live a productive life.

TABLE OF CONTENTS

LIST OF FIGURES

LIST OF TABLES

CHAPTER 1

INTRODUCTION

1.1 Background

Land degradation in mountainous tropical regions of the world is primarily caused by landslide activity induced by periods of intense rainfall during the wet season. In the Caribbean region, this phenomenon is quite prevalent on the volcanic islands which form an archipelago extending from the southern tip of the Florida peninsula in the United States of America to the northern shores of Venezuela in Latin America.

The geomorphology of these volcanic islands is dominated by rugged mountainous terrain resulting from tectonic uplift and deep valley incisions carved into the volcanic rocks which make up most of the geological formation of these islands and by slopes comprised of extensive deposits of unsaturated residual soils derived from the weathering of the parent rock and colluvial material transported downslope.

During the wet season, which normally extends from July to December, these soil deposits become saturated or partially saturated due to infiltration and as a result become unstable and collapse causing loss of life and substantial damage to civil works and property.

1.2 Scope of the Thesis

Research work on the engineering behavior of the residual soils on the Caribbean island of Saint Lucia is limited to studies conducted by Anderson and Kemp in 1985 to predict the pore water pressure conditions in road cut slopes in residual soils.

This current research work aims to reveal the hydrogeological processes which contribute in the triggering mechanism of a shallow and deep-seated landslides in two unstable, unsaturated soil slopes with contrasting geomorphology and hydrologic settings. The study also aims to establish the rate of infiltration in a multi-layered unsaturated residual soil slope from parent andesite rock and a colluvial soil slope from parent basalt rock and demonstrate how quickly these slopes become saturated and unstable during a 24-hour rainstorm.

The final aim of the research is to establish the relationship between surface water infiltration and saturation of the unsaturated soils and pore water pressure changes at various depths which result in a reduction of the shear strength and hence slope instability.

In the unsaturated state the slopes under study are stable and are of minor concern. During 24-hour rainstorms of 654 mm and 488mm as experienced in Saint Lucia during the wet season, these slopes rapidly become saturated and unstable and are of major concern to the authorities and the public at large since major devastation results. Therefore, an unsaturated analysis of the slopes was not addressed in this thesis and the emphasis was placed on the saturated condition when slope failure actually occurs. The research also demonstrates that the presence of a hydrogeological feature such as a confined aquifer of higher saturated hydraulic conductivity in the residual soil slope affects the pore water pressure response and stability of the slope.

These aims were achieved through field instrumentation and monitoring, laboratory testing procedures and numerical analyses which were used to achieve the following objectives:

i) Determine the mineral composition of the parent andesite and basalt rock formations and the mineralogical composition of the residual soil and colluvium. In order to achieve this, the following tasks were undertaken:

- petrographic analysis by preparation of thin sections (slides) of the parent rocks to present a true realization of the mineralogical constitution of the rocks and interpreting the rock forming minerals used in the description of the rock types using a microscope
- determine the mineral composition and fabric of the residual soil and colluvium using X-ray diffraction and Scanning Electronic Microscope analyses. An assessment of soil fabric is essential for a proper evaluation of soil structure

ii) Undertake a series of field instrumentation and monitoring programmes to determine surface runoff, infiltration, pore water pressure responses at variable depths and subsurface deformation during a natural rainstorm of 24-hour duration. This was achieved by:

- installing rain gauges, standpipe piezometers and slope inclinometers and tensiometers to monitor pore water pressure response to rainfall at variable depths and the associated subsurface deformation
- measurement of surface runoff and infiltration in the field during an actual 24-hour rainstorm event
- determination of the hydraulic conductivity of the subsoils using falling head permeability tests in the field

iii) To undertake a series of tests on laboratory prepared specimens to determine the engineering properties of the subsoils. This was accomplished by the following tasks:

- borehole drilling and the recovery of disturbed and undisturbed soil samples for laboratory testing
- determine the index properties of the subsoils
- determine the shear strength parameters for the subsoils in direct shear and tri-axial tests
- determine the chemical composition of the subsoils

iv) To perform numerical analyses of the seepage conditions in the slopes (SEEP/W) during the rainstorm based on predicted and field data to better understand how quickly surface water infiltrates and saturates an unsaturated residual and colluvium and affect the stability of the slope (SLOPE/W). Particular attention will be given to the effect this has on the shear strength of the subsoils and the factor of safety of the slopes during a 24-hour rainstorm by using a finite element software package to accomplish the following tasks:

- develop a numerical model for seepage conditions in the slopes and generate a finite element mesh with defined boundary conditions and the material properties
- conduct a 'steady state' seepage analysis to establish the initial pore water pressure conditions in the slopes
- conduct a 'transient' seepage analysis to show the changes taking place within the slopes with time
- incorporate the results obtained during the transient process analysis into SLOPE/W to establish the changes taking place with time in the factor of safety and stability of the slope as a result of surface infiltration

1.3 Thesis Layout

The thesis is organized in a series of Chapters following the introduction:

Chapter 2 presents a historical literature review of rainfall induced slope instability in Saint Lucia and the interaction farming and community development practices on slope instability.

Chapter 3 Considers the current theoretical understanding of unsaturated soil as related to rainfall, infiltration, seepage and slope instability. A literature review of current research documentation of rainfall induced instability in unsaturated soils is presented.

Chapter 4 provides a detailed description of the geology and geomorphology of the Barre de L'isle and the Windjammer Landing Beach Resort research study sites and the field investigation and instrumentation implemented. Monitoring procedures and data assimilation are also included.

Chapter 5 presents the results of the laboratory tests and field instrumentation results for the two sites under study and a comparison is made of the results. A discussion and analysis is made for each site.

Chapter 6 provides an analysis of the field instrumentation data.

Chapter 7 **N**umerical modeling of the Barre de L'isle and Windjammer Landing Beach Resort research sites are presented and discussed. The chapter outlines the Geo-slope model structures of Slope/W and Seep/ W and the fact that they uniquely incorporate rainfall, seepage, infiltration and slope instability in saturated and unsaturated soils. Seep/W can utilize an evaporative flux by applying a negative flux along the ground surface but this study emphasizes pore water pressure changes during periods of intensive rainfall during which time evapo-transpiration is assumed to be negligible. This assumption should not be a significant limitation on the numerical analysis study for this project.

Chapter 8 concludes this thesis with a summary of the project and its key findings and provides recommendations for future research work on rainfall induced slope instability. The need for the development of a landslide hazard warning system for Saint Lucia is strongly emphasized.

CHAPTER 2

LITERATURE REVIEW OF LANDSLIDE ACTIVITY IN SAINT LUCIA

2.1 Introduction

Saint Lucia is one of the Caribbean islands which form the Antillian arc which begins at the Florida peninsular in the United States of America and terminates at Trinidad & Tobago off the north coast of Venezuela in South America. The island lies at Latitude 13^{o} 43 N and 14^{o} 07 N and Longitude 60^{o} 55 W and 61^{o} 05 W between the island of Martinique in the north and Saint Vincent in the south. It has a land mass of approximately 616 square kilometers and a population of 163,267 inhabitants with the majority (64,344) living in the capital city of Castries (2001 census). The location map of Saint Lucia is shown in Figure 2.1. A map of the Physical Features of Saint Lucia is shown in Figure 2.2.

Information on the problem of land degradation due to landslides on the island of Saint Lucia is well documented in published and unpublished reports, including DeGraff, 1985, DeGraff et al, 1989 and Prior and Ho, 1972. The historical record of tropical storms and hurricanes which have affected the island of Saint Lucia from 1938 to the present, suggests that during this period there were at least thirteen major landslide-producing storm events on the island. In addition to these, landslides invariably develop on an annual basis during the rainy season (July to December) or during high rainfall periods of non-storm years of the type experienced at high frequency and widespread distribution of these slope failures are evidence that landsliding is a dominant erosional process on the island.

Several types of landslides have been documented in Saint Lucia, including debris flows, debris slides, rockfalls, rock slides and landslide complexes. Of the several landslide types, debris flows are the most common and are the main contributor to land degradation. These flows occur in soil or weathered rock, are typically small in size and are initiated as shallow failures in the upper regions of the slope. The failed material, saturated with water becomes mobilized, flows downslope and carves deep erosion channels. Debris flows also erode the upper slopes of road beds, leading to the collapse of several road foundations. The significant volume of soil and other landslide debris carried by these flows to streams result in increased sedimentation of rivers, the coastline and contributes to flooding downstream.

O'Keefe and Conway (1977) of the University of Bradford, conducted a survey of a disaster history of St Lucia with a focus on storm events from 1938 to 1996. The survey highlighted the importance of the banana industry on the macro-economics of the island. However, the natural rugged topography of the island does not ideally favour the cultivation and transport and thus the delivery of the banana crop.

The clearing of the permanent vegetation on hillslopes for banana cultivation presents a high potential for rainfall induced landslides. The roots of the banana plant are shallow and provide little resistance to slope instability during periods of heavy rainfall.

2.2 Disaster History of Saint Lucia with a Focus on Storm Events

O'Keefe and Conway (1977) and Rogers (1997) report on the disaster history of Saint Lucia with respect to rainfall induced landslide events from data collected from extensive library search and from the archives of Saint Lucian newspapers. A summary of their findings follow:

2.2.1 Ravine Poisson/Ravine Crebiche Landslides: (1938)

Ravine Poisson is a small agricultural community located in the Cul de sac valley in close proximity to the toe of the north slope of the Barre de L'isle mountain range. The area is accessible by the main Castries / Vieux Fort highway which disects the valley to access the Barre de L'isle mountain range and the southern region of the island. Reports from the descendants of families that survived the disaster indicate that the landslide occurred on a hillside located to the east of the current Castries / Vieux Fort highway. The slope of the slide area is approximately 40 degrees with a crest elevation recorded at 335 meters from topographic maps.

DeGraff et al, 1989 report this event as one of the worst landslide disasters in the Eastern Caribbean. The landslide occurred on November 21, 1938 after the region experienced 244 mm of rainfall in one day from a tropical storm (O'Keefe and Conway, 1977). Rainfall distribution for the year was irregular and abnormal and was reported at 965 mm above the 50 year average. The main road across the central highland of Saint Lucia known as the Barre de L'isle was blocked by a landslide. For eighteen days, landslides had prevented passage along this road connecting the capital, Castries with the southeastern part of the island. A workforce of several hundred inhabitants was present near Ravine Crebiche and neighboring Ravine Poisson laboring to clear the road. This was the result of eight days of continuous rainfall.

DeGraff, et al, 1989 reports as follows : 'At 9.00 am on Monday, November 21, 1938, a landslide from Ravine Crebiche swept into the area where workmen were clearing the previous landslide debris. An hour later, a second landslide issued from neighboring Ravine Poisson. The areas engulfed by these landslides were described as "a sea of mud".

DeGraff et al (1985) calculated that in Saint Lucia, Saint Vincent and Dominica, the average annual cost for landslide damage to roads ranges from US$ 115,000 to US$ 121,000 in normal years. They also calculated that in an average year the cost of repairing landslide damage to roads throughout the Caribbean amount to U$$ 15 million.

2.2.2 Ravine Poisson, Barre de L'isle, L'Abbaye Landslides: (1939 &1940)

Data on these landslide events is limited and details of the exact location of the landslides are not available. Three villages on the island were destroyed by a tropical storm on January 7, 1939 with 100 persons reported dead (O'Keefe and Conway, 1977). On August 7, 1940 Ravine Poisson, Barre de L'isle and L'Abbaye communities were badly damaged by a tropical storm. There was extensive damage to livestock and plantations. Roads and walls which were built after 1939 were destroyed.

2.2.3 Ravine Poisson Landslide: (1954)

Farmers severely affected by this storm event on December 12, 1954 which totally destroyed a whole year's output of staple crops and bananas. Recorded rainfall for the year was 3,277 mm. Ravine Poisson was badly hit by landslides (O'Keefe and Conway).

2.2.4 The Barre de L'isle Landslide (1980)

On August 3, 1980 a landslide was triggered on the Barre de L'isle mountain range by the passing of Hurricane Allen. The landslide blocked the main East Coast road on Saint Lucia connecting the capital city of Castries to the east coast villages of Dennery and Micoud and the southern town of Vieux Fort. This disrupted the main route used to transport tourists arriving at the international airport at Vieux Fort in the south to hotels and tourist facilities in the northern part of the island (Degraff et al, 1989). The landslide affected the main road to the extent that clearing the road would not restore access to the southern part of the island. The road was later restored by the construction of a masonry retaining wall at the toe of the slide and three gabion structures within the failed area to stabilize the slope. The gabion were placed at an average cost of US$3.00 per cubic meter (Ministry of Communication & Works, Government of Saint Lucia). The cost included excavation of the site as well as the construction of the gabion structures. The entire repair cost approximately $ US172,000 (Degraff et al, 1989).

2.2.5 Tropical Storm 'Debbie' (1994)

In recent times, landslide events and their impact on the socio-economic structure of the island of Saint Lucia has increased. This is attributed to i) the increase in frequency and severity of low pressure systems which affect the Lesser Antilles and ii) the encroachment of forested areas by agricultural farming, in particular bananas(Rogers, 1997).

On September 9, 1994, the island of Saint Lucia was struck by Tropical Storm 'Debbie'.
Six rainfall gauging stations were operational throughout the storm, with recorded 24 hour totals ranging from 230 mm to 360 mm. Maximum recorded one hour rainfall intensities reached 90 mm/hr at Union Research Station of the Government of Saint Lucia with an estimated peak one hour intensity in the upper Roseau Valley of 141 mm/hour (Saint Lucia Meteorological Services).

The short duration, high intensity rainfall experienced during Tropical Storm 'Debbie' forms the most critical storm profile type for Saint Lucia's small, steep catchments. This, in combination with the already saturated soil conditions due to antecedent rainfall, resulted in high discharges in the rivers, in particular in those whose catchments drain the steep slopes on the central mountain range of Mount Gimie.
More than 400 landslides were reported to have occurred as a result of Tropical Storm 'Debbie', resulting in loss of soil, trees and crops which contributed to the debris and sediments which dammed rivers and damaged adjoining farmland. More than 90 per cent of the landslides occurred in the upper reaches of the watersheds with landslides occurring in every main drainage area in some catchments (Rogers, 1997). A large portion of the landslides were shallow debris flows, ten to twenty metres in width, originating close to ridge crests. Debris and rock slides occurred principally along roads.

The floods caused four deaths, twenty four persons were injured, six persons were reported missing, thirty seven were made homeless and five hundred displaced persons had to be accommodated in temporary shelters

2.2.6 The Millet Primary School Landslide (1995)

The landslide at the Millet Primary School occurred as a result of heavy incessant rainfall during hurricane 'Iris' during the month of September, 1995. The landslide raised some concern about the safety of the students and the facility and an urgent appeal was made by members of the Government of Saint Lucia for the implementation of immediate remedial slope stabilization measures to eliminate the risk of further instabilities developing within the slope that may result in serious consequences regarding the safety of the students and the school building.

The subsoil stratigraphy at the site consisted of a reddish brown, stiff to very stiff residual soil of medium plasticity overlying highly weathered andesite bedrock. The residual soil is approximately 2.5 m in thickness. In the landslide area a 2.0 m thick layer of soft, dark brown, clayey colluvium overlayed the weathered bedrock. Groundwater seepage was observered at a depth of 0.75 m below ground surface in a test pit located in the landslide area.

The results of the two (2) direct shear strength tests conducted on the soils at the site were as follows:

Material	Unit Weight	Effective Cohesion C'		Effective Angle of Internal Friction ϕ'	
	(kN/m^3)	(kPa)		(degrees)	
Residual Soil	17.0	peak	residual	peak	residual
		26.0	10.0	20.0	14.0
Colluvium	15.0	21.0	3.0	12.0	6.0

A commercially available computer programme 'STABL' was used to perform a back-analysis of the failed slope on the southwest side of the building and to assess the stability of the existing northwest slope. The analysis utilized the Janbu limit equilibrium method for a translational mode of slope failure.

The results of the analysis showed that in its present state of partial saturation, with a natural moisture content of 33.0 % to 39.0 % and a slope gradient of approximately 30^{o} the computed factor of safety of the the stable northwest slope was 1.3.

2.2.7 The Boguis Landslide (1998)

The agricultural community of Boguis located approximately 14 kilometres east of the capital city of Castries experienced disturbing ground movements in early September 1998 which resulted in the appearance of cracks in masonry walls and the development of tension cracks on the ground surface.

The site is bordered to the north by a forested gully and to the south by the Boguis elementary school and playground. The Marquis river flows northward along the east boundary of the site and banana farmland flourishes of the river floodplain. The toe of the failed mass of slope debris was about 8.0 m above the level of the floodplain at an inclination of 28^{o}.

The monitoring of ground surface movement was performed with extensometers placed across tension cracks and vertical differential displacement was measured with a tape at selected points within the slide area. The result of the field monitoring programme was as follows:

1) Extensometer

Monitoring Period	Total Horizontal Displacement (mm)
October 1 – 6, 1998	25.0
October 1 – Nov. 4, 1998	230.0

2) Tape Measurement

Monitoring Period	Monitoring Points	Horizontal Displacement (mm)	Vertical Displacement (mm)
Sept. 28 – Oct. 1, 1998	1	0.0	100.0
	2	270.0	30.0
	3	150.0	120.0
	4	20.0	150.0
	5	0.0	30.0

The local geology at the site is of Early Tertiary volcanic basalt and andesite rocks which form the oldest and most highly folded rocks on the island. Some colluvial and terrace sands are present. The subsoil stratigraphy is composed of a colluvium material overlying weathered bedrock. The colluvial deposit is composed mainly of an agglomerate rhyolitic tuff containing large weathered rock fragments up to 1.0 m in diameter and gravel within a silty clay matrix. The rock fragments are angular and moderately to highly weathered. The silty clay matrix material is reddish brown in colour and exhibits high plasticity characteristics.

A triaxial shear strength test was performed on the undisturbed sample of colluvium recovered from the site. The results of the test are as follows:

Unit weight, γ	= 19.0 kN/m^3
Effective cohesion, C'	= 12.0 kPa
Effective Angle of Internal Friction, ϕ'	= 15^o

Figure 2.3 contains a photograph of failed slope at Boguis.

2.2.8 The Black Mallet/Maynard Hill Landslide (1999)

2.2.8.1 Introduction

The problem of slope instability at the residential community at Black Mallet/Maynard Hill located in the southeast region of the capital city of Castries in Saint Lucia was brought to public attention with dramatic force on October 7, 1999 when approximately 80,000 cubic metres of colluvial material 'flowed' downslope toward the Marchand River causing the destruction of several residences and ruptured public utilities servicing the community.

Numerous tension cracks developed on the main roads in the community and at various locations on the hill slope. Several concrete residences showed evidence of distress with numerous cracks developing on walls and several water and sewer mains were ruptured. A total of 300 persons were displaced as a result of the landslide and 60 residences were destroyed.

2.2.8.2 Site Description

The residential community of Black Mallet/Maynard Hill is located at the toe of the north slope of Morne Fortune in the southeastern region of the capital city of Castries, Saint Lucia. The area of slope instability is bordered to the north by the Marchand River, a tributary which meanders northward into the main Castries River.

The natural course of the Marchand River is controlled by the geologic structure of the sediments along its banks. In the slide area, the river actively undermined the embankment deposits and test borings and excavations indicated the presence of andesite bedrock formation at a depth of approximately 1.5 meters below the riverbed.

Figures 2.4 and 2.5 show instrumentation monitoring at Black Mallet/Maynard Hill

2.2.8.3 Field Investigations

The field investigation is the central and decisive part of a study of landslides and landslide prone areas. The investigation serves two essential purposes, namely:

i) to identify areas subject to sliding when future construction is being planned and

ii) to define features and environmental factors involved in an existing landslide

Unstable areas prone to sliding usually exhibit symptoms of past movement and incipient failure; most of these can be identified in a field investigation before design. Such investigations can show how to prevent or at least minimize future movements and they can suggest alternative areas that are less likely to slide.

A number of features require study in a field investigation including:

i) topography
ii) geology
iii) groundwater regime
iv) weather conditions
v) history of slope alterations

2.2.8.3.1 Standpipe Piezometers (SP)

A total of five (5) boreholes were drilled for piezometer installation to depths varying from 6.0 metres to 8.3 metres below existing ground surface at selected locations within the slide area. Standard Penetration Tests (SPT) were conducted at regular intervals of depth in all the boreholes and recovered disturbed and undisturbed soil samples were used for laboratory testing.

2.2.8.3.2 Slope Inclinometers (SI)

Five (5) boreholes were drilled to depths ranging from 6.5 metres to 11.0 metres for slope inclinometer installation. The boreholes were drilled at a distance of approximately 1.5 metres from the standpipe piezometers to observe any correlation between groundwater level fluctuations and subsurface movement.

2.2.8.4 Laboratory Procedures

The recovered disturbed and undisturbed soil samples from the field investigation were placed in plastic bags and sealed to retain their natural moisture content. The disturbed soil samples were used to determine the engineering characteristics for remedial slope stabilization design.

The results of direct shear strength tests on the recovered soil samples were as follows:

Table 2.1 Summary of the Direct Shear Strength Tests Results for Black Mallet Site

Borehole No.	Material	Depth (m)	Unit weight (kN/m^3)	Effective cohesion C' (kPa)		Angle of Internal Friction ϕ' (degrees)		Source
				peak	residual	peak	residual	
SP99-BM-1	colluvium	5.8	18.0	37.5	20.0	9.0	6.0	Trintoplan
SP99-BM-2	colluvium	5.5	17.9	11.0	4.4	5.5	4.5	Trintoplan
SP99-BM-4	colluvium	2.2	18.1	17.3	14.0	15.0	6.0	Trintoplan

2.2.8.5 Subsoils Condition

2.2.8.5.1 Colluvium

The general subsoil stratigraphy at the site consist of colluvial material overlying highly weathered andesite bedrock. The colluvium deposit consisted of boulders, cobbles, gravel deposited within a sandy, clayey silt matrix and ranges in thickness from 4.0 metres to 6.0 metres.

Most values of the natural moisture content for this material ranged from 12.0 % to 36.0 %. The colluvium may be described generally as a sandy, clayey inorganic silt of low to medium plasticity.

The grain size distribution curves indicate this material to consist of 22.4 % sand, 42.6 % silt and 34.9 % clay.

The 'N'- values from the Standard Penetration Test (SPT) ranged from 2 blows to 46 blows per 300 mm which is indicative of a soft to very stiff material. The 'N'-value generally increased with depth.

2.2.8.5.2 Silty Sand

The silty sand layer varied in thickness from 2.0 metres to 4.3 metres. This material consists of 27.6 % gravel, 57.6 % sand and 14.8 % silt with moisture contents ranging from 14 % to 26.7 %. The sand contained rock fragments, quartz and feldspar minerals.

The 'N'- value from the Standard Penetration Test ranged from 10 blows to 44 blows per 300 mm.

2.2.8.5.3 Highly Weathered Andesite Bedrock

The andesite bedrock at the site is fractured, very dense and was classified as highly weathered in accordance with the weathering classification proposed by Anon (1977) as outlined in Table 3.1 of Section 3.5.4 of this Thesis.

2.2.8.6 Liquefaction Potential

The term 'liquefaction' as used in this thesis is defined as follows:

> Liquefaction – is a phenomenon wherein a mass of soil loses a large percentage of its shear resistance when subjected to undrained monotonic, cyclic or shock loading, and flows in a manner resembling a liquid until the shear stresses acting on the mass are as low as the reduced shear resistance.

The loss in shear resistance is due to the conversion of the mass from a practically drained condition, at which it can sustain the in situ stresses to a practically undrained condition of shear. Liquefaction can occur in saturated sands and silts and some gravels (Castro, 1975).

Soils sheared to large strains eventually reach a 'steady state' of deformation.
Poulos (1981) presented the following definition of the 'steady state' of deformation:

> " The 'steady state' of deformation for any mass of particles is that state in which the mass is continuously deforming at constant volume, constant normal effective stress, constant shear stress and constant velocity. The 'steady state' of deformation is achieved only after all particle orientation has reached a statistically steady-state condition and after all particle breakage, if any, is complete so that the shear stress needed to continue deformation and the velocity of deformation remain constant".

Poulos (1981) stated that liquefaction, as defined above, involves large unidirectional shear deformations, and thus one would expect that during liquefaction failures the soil will tend towards the 'steady state' of deformation. If the shear strength at the 'steady state' is lower than the applied shear stress in the ground, then, in principle, it is possible for liquefaction occur. Conversely, if the 'steady state' shear strength is greater than the shear stress in the ground, then liquefaction cannot occur because the associated unidirectional deformations are not possible.

A careful examination of the definition of liquefaction stated above indicates the following two explicit conditions:

i) liquefaction involves large, unidirectional shear deformations, which usually occur at a relatively rapid rate when failure occur in situ so that the soil appears to be flowing

ii) liquefaction requires the presence of 'driving' shear stresses significantly greater than the shear strength of the soil after the loss of shear resistance. These driving shear stresses supply the driving force which produces the large and rapid deformation.

2.2.8.7 The Application of Liquefaction to the Black Mallet/Maynard Hill Landslide

One of the most common index properties for estimating the liquefaction potential of saturated sands is the 'N' value from the Standard Penetration Test (ASTM D 1586-84). Case histories published by the Japanese Geotechnical Society (1998) support the use of the Standard Penetration Test 'N' values in most liquefaction evaluations for the following reasons:

i) the Standard Penetration Test 'N' value is an index property reflecting soil density and fabric and thus could have a good correlation with liquefaction strength.

ii) the Standard Penetration Test is primarily a shear strength test under essentially undrained conditions, while many of the other field tests are conducted under drained conditions.

iii) numerous case histories of soil liquefaction during past earthquakes in Japan are on record, based on which empirical correlation between the Standard Penetration Test 'N' value and liquefaction strength are developed.

iv) the Standard Penetration Test yields representative samples of soil from which index properties such as grain size distribution and fines content can readily be determined.

2.2.8.8 Hydrology and Hydrogeology

In situ falling head hydraulic conductivity tests were performed in the standpipe piezometers installed at the site as specified by the United States of America Department of the Navy, Naval Facilities Engineering Command- 1974 (NAVFAC), for a cased borehole with a perforated extension of length 'L'.

The results of the hydraulic conductivity tests were as follows:

Table 2.2 Results of Falling Head Hydraulic Conductivity Tests

Borehole No.	Depth (m)	Soil description	Hydraulic Conductivity {cm/sec^{-1}}
SP99-BM-1	6.5	sand	2.8×10^{-4}
SP99-BM-2	7.0	sand	4.3×10^{-3}
SP99-BM-3	3.0	colluvium	1.4×10^{-6}
SP99-BM-4	3.5	colluvium	3.7×10^{-5}
SP99-BM-5	4.0	colluvium	1.1×10^{-6}

2.2.8.9 Instrumentation Monitoring

Standpipe Piezometers

The groundwater levels recorded in the piezometers were as follows:

Table 2.3 Initial and Current Groundwater Levels

Borehole No.	Depth (m)	Initial Piezometric level (m) (30/10/99)	Current Piezometric level (m) (5/12//99)
SP99-BM-1	6.5	3.0	4.1 (pinched at 5.6m)
SP99-BM-2	7.0	3.0	dry (pinched at 3.9m)
SP99-BM-3	3.0	5.5	3.5
SP99-BM-4	3.5	2.0	3.5 (pinched at 2.5m)
SP99-BM-5	4.0	5.2	5.2

Slope Inclinometer

The slope inclinometer provides useful quantitative information by defining the level of maximum lateral movement. It provides the most definitive early warning system of an impending slope failure in comparison with other forms of instrumentation. Ground movement causes the slope indicator casing to move from its initial position to a new position. The rate, depth and magnitude of this displacement are calculated by comparing data from the initial survey data from subsequent surveys. The inclination is measured by two forced-balanced servo-accelerometers. One accelerometer measures the tilt in the plane of the inclinometer wheels ('A') axis. The other accelerometer measures tilt in the vertical plane perpendicular to the wheels ('B') axis.' The cumulative displacement at a depth of 7.9m in inclinometer SI99-BM-1 was recorded at 39.6mm.

2.2.8.10 Slope Stability Analysis

The Limit Equilibrium method for slope stability analysis was used in this design to determine the magnitude of the factor of safety. When a slope has failed the factor of safety is unity and the analysis can then be used to estimate the average shearing resistance along the failure surface. The factor of safety is that factor by which the shear strength parameters may be reduced in order to bring the slope into a state of limiting equilibrium along a given slip surface.

A commercially available slope stability analysis software 'G'SLOPE' developed by Mitre Software Corporation of Edmonton, Alberta, Canada was used to perform back-analyses of the failed slope (cross-section A-A')and in the design of slope remedial stabilization works.

A cross section A-A' was selected for slope stability analysis and is shown in Figure 2.6**.** The analyses utilized the simplified Janbu limit equilibrium method of slices for an irregular slip surface.

Back-analysis performed on the sand layer indicated the shear strength at failure was $\phi' = 21$ degrees.

Section A-A': the computed factor of safety (FS) prior to the excavation of 1.5m at the toe of the slope was 1.29. The computed FS after the excavation was 1.24. When a seismic coefficient of 0.03g was applied the computed FS was 1.07.
The following soil parameters from laboratory tests at the University of the West Indies in Trinidad were utilized in the effective stress stability analyses:

Table 2.4 Summary of Direct Shear Strength Test Results for Slope Stability Analysis

Material	Unit Weight γ (kN/m^3)	Effective cohesion c' (kPa)	Effective Angle of Internal Friction ϕ' (degrees)	Source
Surcharge (15 kPa)				
Colluvium	18.0	0.0	9.0	UWI
Sand	20.0	0.0	27.0	UWI
Bedrock	-1 (infinitely strong)			

2.2.8.11 Discussions and Recommendations

2.2.8.11.1 Causes of the Slope Failure

The Black Mallet/Maynard Hill slope has been in a steady state of deformation or creep for a period of years prior to failure. This is evident in the presence of old cracks observed on several concrete structures and reports from residence of frequent disturbing noises during periods of heavy rainfall and seismic activity. Soil creep or slow gravitational movement of the surface soils from frequent periods of wetting and drying appears to occur virtually throughout the study area. Although individual movements have been small, cumulative movement over a period of time may have had a negative effect on the performance of the slope. The main contributing factors which triggered the landslide at Black Mallet/Maynard Hill include the following:

- poor drainage conditions available at the site to divert surface runoff downslope and away from the site
- the existence of leaking septic tanks for waste disposal from the residences
- the build up of hydrostatic or artesian pressure in the confined sand aquifer

- the presence of loose, saturated sand in the aquifer which may have liquefied and caused instability in the slope

- the low shear strength of the colluvium material

- seismic events prior to and at the time of the landslide are the main contributing factors which triggered the slope failure.

2.2.8.11.2 Ground Bio-Engineering

The removal of the natural vegetation on slopes has been identified by this author as the single most important misuse of land in Saint Lucia. Deforestation of lands, particularly on steep slopes for farming has led to an increase in landslide activity during the rainy season. Erosion and land slippage problems can therefore be closely related with the expansion of farming and community development.

Forest cover provides the following advantages to slope stabilization:

i) foliage intercepts rainfall, causing absorptive and evaporative losses that reduce rainfall available for infiltration into the soil
ii) roots extract moisture from the soil which is lost to the atmosphere via transpiration, leading to lower pore water pressures developing and a lower groundwater table
iii) roots reinforce the soil, increasing soil shear strength
iv) tree roots may anchor into firm strata, providing support to the upslope soil mantle through buttressing and arching
v) roots bind soil particles at the ground surface, by reducing susceptibility to erosion

Selected species of natural tropical vegetation have been used on a limited basis by land owners for several decades in Saint Lucia to assist in controlling soil erosion and slope instability in road cuts, steep slopes and on river banks. Clark (1996) identifies the most common plant species used locally as follows: Glyricidia sepium (glory cedar); Bambusa vulgaris (Bamboo);Hibiscus pernambucinsis (Mahomang); Hibiscus elatus (Blue Mahoe); Mangifera indica (Mango); Cecropia pelata (Bois canon); and Vertivieria zizaniodes (Vertiver grass).

The existing landslide scars and tension cracks on the failed slope at Black Mallet / Maynard Hill will be subjected to further degradation from rainfall eroding material from the exposed soil surface. Appropriate slope stabilization techniques should be applied to control the detachment of soil particles and their subsequent transportation to the landslide scar. The protection of the landslide area from the direct impact of rainfall and the flow of running water is necessary.

2.2.9 Barre de L'isle Ridge Landslide (2005)

2.2.9.1 Introduction

During the month of July 2005, a landslide occurred on the Barre de L'isle ridge in the interior of the island following an intensive rainstorm. The slide debris blocked the main road and caused an interruption of vehicular traffic flow along the main highway to the eastern and southern parts of the island. A field investigation was carried out to determine the causes of slope failure and to mitigate remedial slope stabilisation measures.

2.2.9.2 Site Description

The Barre de L'isle ridge is the main east to west divide of the island. The highest point on the ridge is at approximately 440 metres and the existing road is steep and tortuous. The landslide occurred on the eastern slope of the mountain ridge at elevation 245metres where the principal road link between the capital city of Castries and the eastern and southern sections of the island converge in a sharp curve with gradual slopes on both sides of the main road. Evidence of numerous tension cracks and slumping were observed on the road surface and on the adjacent northern and southern slopes of the road cut. Photographs of the site are included in Figure 2.7 and Figure 2.8.

2.2.9.3 Field Investigations

Two (2) boreholes were drilled to depths ranging from 16.8metres to 18.3 metres below existing ground surface on the north and south slopes to assess the subsurface soil conditions. Recovered soil samples were classified in the field and one (1) undisturbed Shelby tube sample was recovered for shear strength testing.

A standpipe piezometer was installed in each borehole to monitor groundwater level fluctuations. Two (2) boreholes were drilled to depths of 17.0 metres and 19.0 metres below existing ground surface for inclinometer installation. The boreholes were located at a distance of approximately 1.0 metre from the piezometer locations in order to observe any correlation between groundwater fluctuations and subsurface movements.

One (1) undisturbed Shelby tube samples was packaged and transported by air freight to the University of the West Indies in Trinidad for direct shear strength testing in their soil mechanics laboratory.

Table 2. 5 Summary of Direct Shear Strength Test Results for Barre de L'isle Site

Borehole No.	Material	Depth	Unit weight	Effective cohesion		Effective Angle of Internal Friction		Source
			γ	c'		ϕ'		
		(m)	(kN/m^3)	(kPa)		(degrees)		
				peak	residual	peak	residual	
BH05-BS-2	residual soil	6.0	18.0	24	6.0	27	22	UWI

Figure 2.18 Shows the Direct Shear Strength Graph

2.2.9.4. Subsoils Condition

The general subsoil stratigraphy at this site consists of a layer of compact, rusty brown, clayey, silty sand overlying a sandy, clayey silt residual soil deposit which in turn overlies the highly weathered andesite bedrock. The clayey, silty sand is compact, low to non-plastic with excessive oxidation. The sandy, clayey silt layer is a firm to stiff residual soil of medium plasticity and contains thin layers of volcanic ash. The highly weathered andesite is dense to very dense and contains derelict discontinuities.

A silty sand seam was encountered in the residual soil deposit at a depth of nine (9) metres below ground surface in borehole BH05-BS-2 (North).

2.2.9.5 Hydrology and Hydrogeology

Groundwater levels in boreholes BH05-BSL-1 and BH05-BSL-2 were recorded at depths of 8.8 metres and 5.5 metres respectively, below existing ground surface..

Rainfall data for the Barre de L'isle site during the period of January to December, 2005 was obtained from the Department of Water Resources, Ministry of Agriculture, Fisheries and Forestry of the Government of Saint Lucia. A maximum rainfall of 377 mm occurred during the month of January 2005 and a minimum of 50.6 mm was recorded during the month of March 2005.

2.2.9.6 Conclusions and Recommendations

An interpretation of the results of the field instrumentation is required in order to determine the mechanics and causes of the slide and remedial stabilization measures required at this site. This should include slope stability analyses, seepage analyses and the collection of additional field data.

Remedial stabilization of the slope at this site would include one or a combination of the following:

i) surface and subsurface drainage
ii) the installation of passive piles on the slope
iii) the installation of soil nails
iv) relocation of the existing roadway to an alternate route to bypass the unstable area

2.2.10 Windjammer Landing Beach Resort Landslide (2005)

2.2.10.1 Introduction

A landslide occurred at the Windjammer Landing Beach Resort during the month of July, 2005 causing extensive damage to a few high priced Villas, roads, buried utility services, retaining walls and posed an immediate threat to the Administration building and Villas upslope. Previous studies of slope instability at this site had been conducted and reported by engineering consultants from 1989 to 2004. A site investigation was carried out during the period of August 8th – October 8th, 2005 to investigate the cause of slope instability and to implement remedial slope stabilization measures.

2.2.10.2 Site Description

The Windjammer Landing Beach Resort is a tourist destination located between two volcanic peaks on the northwest coast of the island of Saint Lucia at Labrelotte Bay in the district of Gros Islet. The geomorphological features at the site represent a colluvial deposit which has accumulated between the two peaks and could not be eroded by run-off as on the beach side where the colluvium and weathered basalt bedrock is exposed. The colluvium deposit at the beach front was not washed away by the sea because of the presence of the resistant exposed basalt rock face.

The area of slope failure is not typical of the rest of the Windjammer Landing Beach Resort property because of its location between the two volcanic peaks where the colluvium has accumulated. The areas of the site outside this setting are more stable and not prone to ground movement.

The site contains several highly priced Villas constructed on a steep hillside which slopes to the west and rises to approximately 160 metre elevation. The Villas are constructed in cut and fill areas in the hillside which is composed of highly weathered basalt.

Fresh basalt is exposed in an outcrop on the hillside upslope of Bougainvillea Lane. The lower portion of the slope is composed of colluvial material which was transported downslope by erosion.

Figure 2.9 shows the extent of the toe of the slide. Tension cracks were visible on the ground surface as a result of creep. Some of the Villas showed signs of distress and deformation as shown in Figure 2.10 to Figure 2.13. Photographs of the remedial works at the site are presented in Figure 2.14 to Figure 2.17

2.2.10.3 Field Investigations

Seven (7) boreholes were drilled to depths ranging from 5.2 metres to 21.3 metres below existing ground surface for standpipe piezometer installation. Seven (7) slope inclinometers were installed at approximately 1.0 m distance from the piezometer locations to monitor any correlation between groundwater fluctuations and subsurface movement.

Dewatering wells of 150 mm diameter PVC casing were installed in close proximity to each standpipe piezometer and were pumped regularly to reduce the pore water pressures in the subsoils.

A falling head test was conducted in one of the dewatering wells to determine the hydraulic conductivity, (k) of the colluvium. The results of the test showed the hydraulic conductivity value as 2.3×10^{-4} cm/sec.

Appendix A contains the borehole logs for the 2005 landslide site investigation at the Windjammer Landing Beach Resort.

2.2.10.4 Laboratory Procedures

Geocon Incorporated conducted laboratory tests on the colluvial material at the Windjammer Landing Beach Resort during their investigation in 1989. The results of the tests are as follows:

Unit Weight	γ	=	15.7 kN/m^3
Cohesion	c’	=	1.2 kPa
Angle of Internal Friction	ϕ’	=	27^o

In 1997, Geotech Associates Ltd of Trinidad used the following soil parameters in their stability analysis of the west slope at the Windjammer Landings Beach Resort:

Sand/silt/clay :	Unit Weight	γ	=	18.0 kN/m^3
(collovium)	Cohesion	c’	=	0.0 kPa
	Angle of Internal Friction	ϕ’	=	32^o
Weathered :	Unit weight	γ	=	18.0 kN/m^3
bedrock	Cohesion	c’	=	0.0 kPa
	Angle of Internal Friction	ϕ’	=	45^o

Two (2) additional undisturbed bulk samples were recovered from excavations on the upper and lower slopes during the remedial stabilization program. Two rock core samples were packaged and transported by air freight by this author to the University of Newcastle upon Tyne in the United Kingdom for uniaxial compressive strength tests, point load tests and Cerchar abrasivity tests.

The results of the shear strength tests are as follows:

Table 2.6 A Summary of the Soil Properties

Borehole No.	Material	Depth (m)	Unit Weight γ (kN/m^3)	Effective Cohesion C' (kPa) peak	Effective Cohesion C' (kPa) residual	Angle of Internal Friction ϕ'(degrees) peak	Angle of Internal Friction ϕ'(degrees) residual	Uniaxial Compressive Strength (MPa)	Source
BH05-STD-1	Colluvium	4.9	19.0	40.0	--	23.0	--	--	UWI
BH05-STD-1	Colluvium	9.4	16.9	7.0	13.0	30.0	13.0	--	UWI
Upper Slope (Excavation)	Colluvium	2.4	18.6	3.0	7.5	38.0	16.5	--	UWI
Lower Slope (Excavation)	Colluvium	3.0	17.5	4.5	1.0	27.5	23.0	--	UWI
TP06 - 1 (Villas 37/38)	Weathered Bedrock	6.0	19.4	5.0	2.0	39.0	30.0	--	UWI
BH05-STA-1	Rock core	11.3	26.0	--	--	--	--	59.0	UN'cle
BH05-STD-1	Rock core	11.6	25.8	--	--	--	--	53.0	UN'cle

2.2.10.5 Subsoils Condition

2.2.10.5.1 Colluvium

The general subsoil stratigraphy at the site consists of 3.0m to 10.5m of colluvium overlying highly weathered basalt bedrock.

Most values for the natural moisture content of this material ranged from 7.9 % to 66.1 %. The higher values were found in samples containing a high clay content.

Thinly interbedded layers and isolated pockets of slickensided, light gray volcanic ash deposits exist within the colluvium. These layers of volcanic ash may have further reduced the shear strength of the colluvium to a value lower than that observed in laboratory isolated layers of volcanic ash could not have been assumed based on surface conditions.

A sample of volcanic ash recovered from the site was sent to the University of Western Ontario (Canada) for X-Ray Diffraction Analysis tests. The test results indicated that there were no clay minerals present and no montmorillonite was detected

The presence of slickensides in the volcanic ash layers is an indication that the material has historically experienced some degree of shear displacement or could be assumed to be prone to future displacement under certain conditions.

2.2.10.5.2 Highly Weathered Basalt (Bedrock)

Weathered rock outcrops are fully exposed at the site along Bougainvillea Lane and in road cuts further upslope. The rock mass contains numerous relic discontinuities with silty, clayey, sand infilling. Groundwater seepage was observed on the exposed rock face at Bougainvillea Lane during the site investigation and appears to have been contributed by infiltration of surface water from the 'boulder field' upslope.

2.2.10.6 Hydrogeology

The probable pattern of groundwater flow at the site is downslope (east to west) through the colluvium and weathered bedrock, with the potential to generate "artesian" pressures in the lower parts of the slope. This assumption is supported by the observation of groundwater seepage on the beach front at the toe of the west slope.

Hydrological studies included obtaining precipitation data for the years 2000 – 2005 from the Water Resources Unit of the Government of St. Lucia. The weather station is located at Trouya in the vicinity of the Windjammer Landing Beach Resort.

The mean monthly rainfall recorded at Trouya for July, August and September, 2005 was 199 mm; 163 mm, and 173 mm, respectively.

Artesian pressure was observed in piezometer SP05-STB-1 and dewatering well DW05-STB-1 at Station 'B' 30 days after installation. Pumping tests were conducted in the dewatering well at station 'B' by Windjammer Landing Beach Resort personnel to measure the rate of well recharge.

The hydraulic conductivity (k) of the colluvium was determined in a falling head test from the dewatering well (DW05-STB-1) in accordance with the standards specified by the United States Department of the Navy, Naval Facilities Engineering Command – 1974 (NAVFAC), for a cased borehole with a perforated extension of length 'L'.

The hydraulic conductivity value for the colluvium as measured during the pumping test at Station 'B' is 2.3×10^{-4} cm/sec.

2.2.10.7 Slope Stability Analysis

The Limit Equilibrium method was used to analyse the stability of the slope by assuming a potential failure surface with the soils along this failure surface providing shear resistance. A knowledge of the groundwater conditions prevailing at the time is important input in carrying out such analyses. The factor of safety is that factor by which the shear strength parameters may be reduced in order to bring the slope into a state of limiting equilibrium along a given slip surface.

Three (3) slope sections: Profile 2 (Station C), Profile 3 (Station B) & Profile 4 (Station A) were selected to perform effective stress stability analyses for remedial slope stabilization. Profile 3 (Station B) was selected for back-analysis of the failed slope since it represented the worst case scenario with a full-head (artesian pressure) condition.

A total of ten (10) cross-sections along the three slope profiles were selected for stability analysis to determine the factor of safety for the remedial slopes as shown in plan in Figure 2.18.

The stability analyses utilized the simplified Janbu limit equilibrium method of slices for an irregular slip surface. A potential slip surface is selected and the potential sliding mass is divided into a number of vertical slices and the stability of each slice is considered in turn, on the assumption that the factor of safety for each slice is equal to the factor of safety of each of the others.

Each slice is acted upon by its own weight which produces shearing and normal forces on its vertical boundaries and shearing and normal forces along its base. The shearing and normal forces acting on the vertical boundaries depend on the stress-deformation characteristics of the material comprising the sliding mass.

The factor of safety 'FS' of a slope is usually defined as the ratio of available shear strength to shear stress on the critical surface.

The back-analysis performed at station "B" on the failed slope was to determine the shear strength of the soil mass at failure. In order to conduct this exercise, the technique applied involved analyzing the original slope geometry and piezometric levels before failure and working backwards by altering the shear strength parameters of the subsoils until a factor of safety of unity is achieved.

A full head condition was assumed to represent the artesian pressure conditions observed at station "B" and a value of zero cohesion was assumed for the colluvium layer. The results of the back-analysis show the effective shear strength of the colluvium layer at failure was $\phi' = 19^o$.

A distributed surcharge load of 20.0 kPa was used to represent the equivalent surcharge applied by the Villa on the slope for the back-analysis.

The following soil parameters were utilized in the effective stress stability analyses:

Table 2.7 A Summary of the Direct Shear Strength Results

Material	Unit Weight γ (kN/m^3)	Effective Cohesion C' (kPa)	Effective Friction angle ϕ' (degrees)	Seismic Coefficient (g)
Surcharge 20.0 kPa)	-	-	-	
Colluvium	17.0	0.0	19.0	0.2
Rock Fill	20.0	0.0	45.0	0.2
Bedrock	20.0	0.0	35.0	0.0

2.2.10.8 Summary of Slope Stability Analyses

The results of the slope stability analysis for the remedial slope stabilisation at Station 'B' with a rockfill buttress produced factors of safety ranging from 1.93 to 5.07. When a seismic coefficient of 0.2 g was applied the factor of safety was reduced, ranging from 1.15 to 2.39 respectively.

2.2.10.9 Remedial Slope Stabilisation Measures

The urgency to stabilise the slope required the immediate use of the available equipment and technology on the island. The importation of heavy equipment from abroad would require some delay in implementing remedial slope stabilisation measures with consequences.

The slope was stabilized using a soil replacement approach since it provided for immediate implementation of remedial stabilization with the equipment and technology available on the island. This involved the removal of the weak colluvium soil on the failed slope and replacing this material under careful engineering control with competent quarried boulders arranged in layers and finer quarry waste material placed over each layer of boulders to fill the voids.

Three (3) subsurface drains were installed at low points in the topography to channel the flow of groundwater in the rockfill on the upper slope to the lower slope. The drains were 450 mm in diameter and composed of corrugated HDPE plastic pipe. The drainage pipes were installed by excavating a 2.0m wide trench to the base of the rockfill in the upper slope.

2.2.10.10 Conclusions

The instability of the slope at the Windjammer landing Resort was brought about by an unusual combination of factors, including the presence of artesian pressures and evidence of inclusions of thinly interbedded volcanic ash layers, which could not have been reasonably anticipated from previous geotechnical investigations and only detected in this case by: i) the fact that the site investigation was carried out during conditions of high rainfall and ii) evidence exposed in the sides of the excavations for construction of the remedial rockfill "hard points".

The causes of the landslide are both "Natural" and "Developed" and may be summarized as follows:

The colluvial material within the slope is naturally of marginal stability as a result of its geological formation. The material is firm to very stiff and is composed mainly of silt, sand and clay with rock fragments. The newly discovered thinly interbeded layers of slickensided volcanic ash which may be bentonitic in nature exist within the matrix of the colluvial material and may reduce the shear strength to values lower than that assumed in previous studies.

2.2.10.11 Recommendations & Implementation

1. It is recommended that a program of long term field instrumentation and monitoring be implemented at the site at the Windjammer Resort. The instrumentation program should include the installation of slope inclinometers, piezometers, tensiometers, a rainfall gauge and survey prisms located at appropriate positions at the site. The measurement of run-off and infiltration rates are necessary to develop a numerical model for the site. The instrumentation program should be implemented as soon as possible to commence a long term record of slope activity.

2. A cover protection for the rockfill at the 'hard points' is required to minimize the infiltration of surface runoff. A number of expedients are available to achieve this objective which should consider concurrently geotechnical and landscape engineering factors. One recommended geotechnical scheme would be a 100 mm thick layer of 75 mm minus quarry waste be placed over the surface of the rockfill and compacted to a minimum of 95 per cent of the corresponding standard Proctor, maximum dry density.

3. A geotextile fabric should be placed over the compacted fill prior to placing a 100 mm thick layer of topsoil as a growth medium. The topsoil should be seeded with Bermuda grass or any other suitable vegetal cover. This is subject to review, however, based on the agricultural and landscaping factors involved etc.

2.2.11 The Tapion Landslide (2004)

2.2.11.1 Introduction

The initial landslide at the suburban residential community of Tapion occurred on September 26, 2004 when approximately 1,800 cubic metres of colluvial material 'flowed' downslope at a site west of the capital city of Castries in Saint Lucia. Two (2) concrete residential structures were severely damaged and adjacent residences had to be abandoned. An investigation of the cause of the landslide was carried out by this author at the request of the Chief Engineer in the Ministry of Works of the Government of Saint Lucia. A report was submitted to the Ministry at that time highlighting the immediate need for remedial slope stabilization measures to be implemented to arrest the moving soil mass. No remedial slope stabilization works were implemented at the site over the past six (6) years.

On July 9, 2010 additional ground movements occurred at the site during a period of intensive rainfall which caused additional slope movement at the crest and toe of the old landslide causing severe damages to a residential building at the crest which had survived the 2004 landslide.

2.2.11.2 Site Description

The area affected by the landslide was about 1,250 m^2 with an overall slope gradient of 15^o. The slope extends eastwards towards a very steep cut in weathered rock. The site is bordered to the north, south and west by residential buildings. Surface runoff is collected by an earth drain located on the east side of the access road which channels waste water to a collector ditch downslope.

2.2.11.3 Field Investigations

The field investigation consisted of drilling three (3) boreholes in the slide area to depths ranging from 8.0 m to 10.0 m below existing ground surface utilizing a track-mounted DHM-163R drill rig with a motorized cathead. One (1) test pit was excavated to a depth of 6.0 m in the slide area with a track-mounted excavator. Disturbed soil samples were recovered from the standard penetration test performed at regular intervals of depth in nthe boreholes. Two (2) undisturbed 'shelby tube' samples were recovered from the boreholes for shear strength testing. The disturbed soil samples were used to determine the natural moisture content, grain size distribution and plasticity index of the subsoil.

The field instrumentation consisted of installing a standpipe piezometer in the three (3) of the boreholes on completion of drilling to monitor groundwater level fluctuations. A total of nine (9) survey stations were established at selected locations within and around the slide area to monitor horizontal and vertical ground displacement. The location of the slide area, boreholes and monitoring points are shown in plan in Figure 2.19.

2.2.11.4 Subsoils Condition

The general subsoil stratigraphy at the site consisted of a sandy clayey colluvial deposit overlying a silty sand layer which in turn overlies highly weathered basalt agglomerate bedrock. At some locations in the slide area, the colluvial material had been removed for building construction.

The colluvium ranged in thickness from 2.0 m to 3.0 m and consisted of a brown, clayey sandy silt of low plasticity. The natural moisture content of the material ranged from 36.0 % to 62.8 %. The grain size distribution consisted of 40.6% sand, 50.0% silt, 9.4% clay. The 'N'- value from the Standard Penetration Test ranged from 8 blows per 300 mm to 27 blows per 300 mm, indicative of a loose to compact material. The groundwater level as measured in the installed standpipe piezometers varied from 2.75 m to 7.5 m below existing ground surface. The groundwater table follows the natural topography of the slope in an east to west direction.

2.2.11.5 Laboratory Testing

The results of two (2) direct shear strength tests performed on soil samples recovered from the field investigation are as follows in Table 2.8 :

Table 2.8 Direct Shear Strength Test Results for Tapion Landslide Site

Borehole No.	Material Description	Depth	Bulk Unit weight γ'	Effective Cohesion C'		Effective Angle of Internal Friction	
		(m)	(kN/m^3)	(kPa)		(ϕ'^o)	
				peak	residual	peak	residual
BH04-1	colluvium	2.5	17.7	23.2	10.5	35.5	26.8
BH04-2	silty sand	1.2	17.6	7.6	1.5	38.0	28.0

2.2.11.6 Slope Stability Analysis

Detailed examination of the soil profile within the slide area confirmed the critical slip surface to be located at a depth of 2.5 m below the ground surface at the contact between the colluvium and the silty sand layer.

Slope stability analyses were performed utilized the simplified Janbu limit equilibrium method of slices for an irregular slope geometry. A back-analysis of the slope indicated the shear strength of the colluvium at failure was $\phi' = 29.4^{o}$

A distributed load of 50 kPa was used in the analysis to represent the equivalent surcharge applied by the residential structures on the slope.

The computed factor of safety of the slope at failure was 0.681. The computed factor of safety of the slope with remedial 'French' drains installed at a depth of 2.5 m below ground surface to reduce the pore water pressure conditions was 1.652. The computed factor of safety of the slope with 'French' drains and a toe buttress was 1.773.

2.2.11.7 Cause of Slope Failure

The main factors that affected landslide initiation at Tapion are as follows:

- the presence of poorly maintained surface drains at the crest of the slope which were incapable of diverting surface run-off away from the slope resulting in rainfall infiltration and saturation of the colluvium
- the building up of excess pore water pressure in the colluvial material due to infiltration or the possible existence of subsurface flow channels
- the presence of a loose, porous saturated colluvial material with a high liquefaction potential
- ground borne vibrations from recent seismic activity in the area may have assisted in triggering slope failure by reducing the shear strength of the saturated colluvium causing liquefaction.

The slope failure at Tapion was initiated at the toe of the slope and regressed uphill by a progressive mechanism. Residents at the toe of the slope reported persistant groundwater seepage beneath their houses throught the year and flooding of the lower portion of the slope during heavy rains. Visual inspection of the area by this author confirmed the presence of groundwater seepage and ponding of surface water at some locations on the lower part of the slope.

Figure 2.20 to Figure 2.23 show photographs of the Tapion landslide area and damaged structures.

2.2.11.8 Remedial Slope Stabilisation Measures

Remedial slope stabilization at the site consisted of controlling surface runoff, altering the slope geometry by flattening the slope to 15^{o} and installing a 'French' drain to control groundwater. The construction of a toe buttress will provide sufficient dead weight or artificially reinforced restraint near the toe of the unstable soil mass to assist in slope stabilization by ensuring an adequate factor of safety against slope failure.

2.2.12 Hurricane 'TOMAS' (2010)

On Saturday October 30, 2010 Hurricane 'TOMAS' ravaged the island of Saint Lucia with maximum sustained winds of 160 km/hr and rainfall up to 668 mm as a Category 2 system . The hurricane was initially classified as a Category 1 system with sustained winds of 120 km/hr but was later upgraded to a Category 2 system. Strong winds began at about 10:00 am on Saturday morning and subsided around 8:00 am on Sunday October 31, lasting for a period of 22 hours.

Two (2) persons were confirmed dead and three (3) persons missing at the community of Colombette and four (4) persons dead and one (1) person missing at the village of Fond St. Jacques as a result of landslide activity during hurricane 'TOMAS'.

The Government Meterological Centre reported rainfall measurements at various locations on the island over a 24 hour period as follows:

Location	Rainfall .
Hewanorra International Airport (Vieux Fort – South)	347.3 mm
George F.L.Charles Airport (Castries – West)	682.0 mm
Soufriere (West)	668.0 mm
Forestierre (Castries – Central)	633.0 mm
Windjammer Landing Resort (Gros Islet – North)	130.0 mm

Rooftops, power lines and trees were blown away by the strong winds and several bridges collapsed due to overflowing rivers. The heavy rains caused saturation of the ground and triggered several landslides some more severe than others.

The main triggering mechanism causing the landslides was the intensive and prolonged rainfall which saturated the subsurface soils resulting in an increase of the groundwater regime which in turn caused an increase in the soil pore water pressure. This resulted in a loss in shear strength of the subsoils resulting in the mobilization of the subsoils on slopes.

The most pronounced landslides occurred at Colombette and Fond St. Jacques (Soufriere); the Barre de L'isle Ridge (Dennery) and in communities east and south of the capital city of Castries, such as the Morne, Derriere Fort, Bagatelle, Forestierre, Babonneau, Millet, Marc and Trois Piton.

Recent climatic conditions in Saint Lucia indicate that a drought condition in 2008 preceded hurricane ‘TOMAS’ with very high rainfall intensity. Whereas the return period of the rainfall was of the order of 180 years, the likelihood of a drought to be followed by a storm event of this magnitude is even more unusual, probably with a return period of 1000 years.

The drought coindition in Saint Lucia in 2008, therefore, set the stage for extremely high potential for surface erosion and mass movents on slopes in the event of normal wet season. Even if the wet season were to be of normal levels, the effect of the drought on the soil/rock regime would have resulted in a severe hazard condition in respect to mass movements on slopes. The Government Meterological office in Saint Lucia was informed by the Caribbean Institute for Meteorology and Hydrology that in terms of total daily rainfall, this event was classified as a 1- in-180 year event, making hurricane ‘TOMAS’ a very extreme event with regards to rainfall and well in excess of a 100 year event.

A summary of the major landslides that were triggered by the heavy rainfall are presented in Table 2.9. Figure 2.24 – Figure 2.27 contain photographs of the devastation left by hurricane ‘TOMAS’ on Saint Lucia.

Table 2.9 A Summary of Major Landslides in Saint Lucia during Hurricane 'TOMAS', October 30, 2010 (Roosevelt Isaac)

Landslide	Description of Failure Mechanism	Potential Hazards	Proposed Mitigation	Notes/ Comments
Colombette An extensive slide which resulted in loss of life, damage to the main arterial roadway and significant mass wasting.	Very rapid debris avalanche as a result of an increase in the Pore water pressures within the subsoils.	The soil mass is likely to expand through increased sliding and creep. This could affect the integrity of the roadway and the utilities within the easement. Soil erosion is causing a major environmental impact on the surrounding area including the marine reserve.	**Short Term**: Clear roadway, provide surface drainage, flatten the slope for increase stability and build retaining walls along roadway cuts. **Long Term**: Realign the roadway, use subsurface drainage, use soil reinforcement and plant trees along the exposed slopes.	The area is unsuitable for development unless a major mitigation project to improve slope stability is undertaken. The risk after development may be higher than usually accepted.
Fond St. Jacques An extensive slide which resulted in loss of life, damage to roadway infrastructure including two bridges, significant mass wasting and the destruction of residences.	Very rapid debris avalanche as a result of an increase in the pore water pressures within the subsoils.	There is evidence of soil creep which could lead to additional slippage at the landslide site. Significant instability may occur during or after extreme rainfall or earthquake.	**Short Term**: Evacuate area within the slide zone. Provide adequate surface drainage and implement a river training program. **Long Term:** Redesign the landscape to improve slope stability. Evaluate the area for stability of residential settlement. Plant trees on slopes and install relief wells for springs.	Development restrictions are required to limit and control activities which could affect the stability of the area. The potential of other landslides exists for other larger slopes surrounding the area based on a similar mechanism of failure.
Barre D'Isle A series of landslides along the mountains and within the roadway cut and fill sections ….continuing **Barre D'Isle** Damaging roadway and utility infrastructure.	Slow to rapid debris flow as a result of an increase in the pore water pressure within the subsurface soil layer	There is evidence of soil creep which could lead to additional slippage along the roadway. Significant instability may occur during or after extreme rainfall or earthquake.	**Short Term**: Evacuate area within the slide zone. Provide adequate surface drainage and implement a river training program. **Long Term:** Develop an alternate route to bypass areas which may require highway bridges and tunnels.	Development and cultivation restrictions may be required.

Millet A series of landslides along the access roadway to the main water supply of St. Lucia.	Slow to rapid debris flow as a result of an increase in the pore water pressure within the subsurface soil layer.	There is evidence of soil creep which could lead to additional slippage along the roadway. Significant instability may occur during or after extreme rainfall or earthquake.	**Short Term:** Clear roadway and provide adequate surface drainage to control storm water. Flatten and or bench slopes to increase slope stability. **Long Term:** Improve slopes along roadway.	The roadway needs to be improved with a focus of uninterrupted access to the Dam site.
East and South Hills of Castries A series of landslides within residential communities impacting, roadways, utilities and residences.	Slow to rapid debris flow as a result of an increase in the pore water pressure within the subsurface soil layer.	There is historical evidence of creep which became extensive landslides, impacting lives and infrastructure. Significant instability may occur during or after extreme rainfall or earthquake.	**Short Term:** Clear Roadway and provide adequate surface drainage to control storm water. Flatten and/ or bench slopes to increase slope stability. **Long Term:** Implement comprehensive storm water management plan. Improve slopes along roadways along with retaining structures to improve overall stability of area.	Residents need to control runoff to reduce slope instability. Overall strategy on storm water management needs to be implemented.

2.3 Regional Geology

The Antillean arc of Caribbean islands is geologically young, probably not exceeding 50 million years, and is predominantly of volcanic origin. In general, the islands were formed by the accumulation of lava flows and volcanic ash deposits, initially on the seabed, followed by seabed uplift. During the gradual uplifting process, the emerging islands were colonised by coral reef caps and after emergence coastal reefs developed (Newman, 1965).

There is abundance of volcanic activity at eight sights within the arc, including hot springs, sulphurous streams, gas vents, near surface hydrothermal hot spots and recent lava and ash eruptions at St. Vincent Soufriere and Montserrat Soufriere.

The island of Saint Lucia and the associated undersea ridge on which it is perched are located approximately 150 kilometres from the east edge of the Caribbean plate where it meets the North American plate. The Caribbean plate in underthrust by the North American plate which passes down into the mantle where melting occurs (Lindsay et al, 2002).

The most pronounced topographic feature is the Barre de L'isle, a mountain range extending centrally down the length of the island. The highest mountain is Mount Gimie (950 m), is located in the southwestern part of the mountain range. Heavily forested ridges dominate the eastern and western sides of the Barre de L'isle mountain range and descend to the coast. On the western side of the ridge at Soufriere, two spectacular Pitons (cone shaped pinnacles of solid lava from residual volcanic plugs) dominate the topography. The northern part of the island has smaller rounded hills and shallow valleys. The southwestern part of the island is characterized by fan-shaped slopes dipping gently towards the coast and are cut by narrow and deep valleys (Lindsay et al, 2002)

Saint Lucia is almost entirely volcanic with the oldest rocks, largely rhyolite, andesite and various basalt lavas, dating from the early Tertiary period of about 50 million years. These older rocks are found at the surface in the extreme north and southern parts of the island and probably underly the most recent rocks found elsewhere.

Newman, (1965) divided the volcanic rock formations in Saint Lucia into three broad categories, from oldest to youngest, namely : the Northern Series, the Central Series and the Southern Series with respect to their location in the northern, central and southern parts of the island.

i) The Northern Series

These deposits consists of highly deformed and eroded basalts and andesite lavas and pyroclastic deposits. The oldest of these represent the earliest volcanic activity on the island of Saint Lucia. There are no known hot fumaroles in this geologic formation although there is a relative large area of warm spring activity and weak diffuse fumarole activity in Ravine Raisinard on the south flank of Mount Monier. This weak geothermal activity does not suggest the possibility of future volcanic activity in the northern part of Saint Lucia.

ii) The Central Series

Many andesite lavas and clastic deposits are found in the central part of the island. They extend along the southeast coast and appear to be younger than the deformed basaltic rocks in the northern series but are not of recent origin. The rocks of this series were deposited following an increase in sea level across the Lesser Antilles approximately 25 million years ago. The region is heavily forested and consist of inaccessible highlands in the central part of the island. There are no hot fumaroles in this series although a few hot springs are said to exist in forested areas. There is some evidence of hydrothermal activity in the central part of the island and some trace elements have been found in the upper reaches of a few rivers in this part of the island. It is not anticipated that any volcanic activity is likely to occur in the central series although more research work is required in this area to confirm this.

iii) The Southern Series

Many small basaltic andesite lava deposits are found in the southern part of Saint Lucia. They age between 5 – 10 million years which shows in the subdued topography of the landforms in this series. There are no hot fumaroles associated with this series. There are several instances of 'cold' fumarolic activity and gas vents located in areas of highly altered rock within the southern series.

Most of the volcanic rocks in Saint Lucia occur as pyroclastic, varying from coarse agglomerates and breccias, agglomeratic ashes to fine ashes and tuffs although coarser fragmental rocks predominate. The basalts, however are often seen as dykes or flows especially in the north of the island where they also occur as agglomerates (Lindsay et al, 2002).

The most recent centre of volcanic activity in Saint.Lucia lies to the southwest of the town of Soufriere, within what appears to be remnants of a caldera. It consists of a series of volcanic vents and a vigorous high temperature geothermal field associated with the Qualibou depression, a large arcuate structure that formed in southwest Saint Lucia about 300 thousand years ago as a result of a huge landslide or structural collapse
(Lindsay et al, 2002).

A shower or series of showers of dacitic type ash containing abundant bi-pyramidal quartz crystals have fallen at a relatively recent date over most of St. Lucia, especially in the south and central parts. The effects of this layer of ash over different underlying materials can be seen in many soil profiles.

Approximately 25 million years ago there was a period of general submergence of the entire Lesser Antilles and during this period, there was a development of coral reefs which were later uplifted above sea level (Newman, 1965).

Along the coast there are beds of mixed sedimentary and volcanic materials with well developed bedding and stratification. Most beach sands are a mixture of calcareous coral and shell fragments and particles derived from the volcanic rocks.

2.3.1 Petrographic Analysis from Thin Sections of the Basalt and Andesite Rocks found in Saint Lucia

Two thin section slides from basalt and andesite rock samples from Saint Lucia were prepared by technicians in the rock mechanics laboratory of the University of Newcastle upon Tyne. The petrographic analysis of the mineralogical composition of the rocks were done by this author. The following petrographic descriptions are based on two thin sections, one of the Blue Rock Quarry basalt and the other of the RG Quarry andesite formation.

2.3.1.1 Blue Rock Quarry - Basalt

Classification**:** Pyroxene Phyric Basalt

General Description:

This sample is moderately fresh holocrystalline porphyritic basalt containing phenocrysts of plagioclase, clinopyroxene, rare orthopyroxene, and magnetite in a very fine grained matrix. Clinopyroxene phenocrysts are moderately altered around their edges and along fractures to a chlorophaeite-like assemblage, presumably consisting of chlorite, serpentine and iron hydroxide (Figure 2.28 and Figure 2.29). Orthopyroxene is rare and, when observed, typically less altered than clinopyroxene (Figure 2.29).

The matrix is a very fine grained aggregate of predominantly plagioclase and clinopyroxene with carbonate and chlorophaeite alteration products of either original glass or mafic minerals.

Modal abundances:
Phenocrysts: Vol. % Comments
Plagioclase; minor carbonate alteration
Clinopyroxene; alteration to chlorophaeite
Orthopyroxene
Opaques (magnetite)
Total 55 %

Matrix: Vol. % Comments
Plagioclase
Clinopyroxene
Alteration (Chlorophaeite) alteration of glass or mafic minerals
Apatite trace
Rutile trace
Zircon trace
Total 45 %

2.3.1.2 RG Quarry - Andesite

The extreme alteration and lack of a chemical analysis precludes classification.

General description:

This sample is extremely altered with scant evidence of the original mineralogy remaining. The alteration of the mafic minerals to serpentine is shown in Figure 2.30. Other mafic minerals if they existed, and one would anticipate hornblende to have been present if the rock is an andesite, are completely replaced by serpentine (Figure 2.31). These different textures may be explained by different precursor minerals such as coexisting clinopyroxene ($CaMgSi_2O_6$) and orthopyroxene ($MgSiO_3$). Plagioclase phenocrysts are moderately altered to carbonate and have fractures containing serpentine and carbonate (Figure 2.30)

The matrix consists of a complex intergrowth of original plagioclase and carbonate and serpentine alteration products. Both the matrix carbonate and serpentine occur as patches and veins or fracture fillings that can cross-cut the phenocryst minerals.
Modal abundances:

Phenocrysts: Vol. % Comments
Plagioclase ; moderate alteration to carbonate
Pyroxenes; undifferentiated pseudomorphic replacements
Opaques (magnetite)
Total 45 %

Matrix: Vol. % Comments
Plagioclase
Carbonate ; alteration product
Serpentine ; alteration product
Apatite trace
Epidote; alteration product
Total 55 %

Figure 2.32 shows a photograph of the Basalt Formation mining operation at the Blue Rock Quarry. A photograph of the mining of the Andesite Formation at RG Quarry is shown in Figure 2.33. The Geological Map of Saint Lucia is presented in Figure 2.34.

2.4 Climate

St. Lucia has a tropical climate with average daily temperatures of about 27^o Celcius with a maximum of 31^o Celcius. Average annual rainfall varies from 1500mm in the drier coastal zones to 4500mm in the central mountains (OAS, 1984). A dry season extends from January to June and a wet season from July to December. The seasons are not always distinct, however, and rainfall can be variable. Typically, 30% to 40% of the rainfall occurs during the dry season. Very wet months can occur in the dry season and dry months can occur during the wet season.

The high interior of the island receives the most rainfall with a high proportion of this being orographic. With the central water-divide being closer to the west than the east coast and this distance being only 8-9 km, rainfall on the west coast tends to be higher than that on the east coast. The vegetation of the interior consist of tropical rain forest. Savannah grass and shrubs dominate the drier coastal regions. An appreciable part of the rain forest in the interior has been replaced by banana and vegetable farming. The island lies in the hurricane belt and in the past has suffered from extreme high winds and torrential rains during August and October.

Figure 2.35 contains the Rainfall Map of Saint Lucia with rain gauge stations locations throughout the island.

2.5 Seismicity

2.5.1 General

Volcanic and seismic activity in Saint Lucia is monitored by the Seismic Research Unit at the University of the West Indies in Trinidad and Tobago. A continuous seismic monitoring system was established in Saint Lucia in 1982. In 2001, the seismic network was upgraded and now comprises 7 stations that transmit data to a complete seismograph network located at Moule-a-chique at the southern extremity of the island. The computer at Moule-a-chique automatically transmits data to the Seismic Research Unit in Trinidad twice daily through an internet link and data can be retrieved on demand through the telephone system.

In January, 2001 a 12-station GPS2 network system was installed and a 23-pin leveling profile established close to the Sulphur Springs geothermal field in Soufriere. Results from the GPS are complemented with distance measurements (EDM) wherever possible. The ground deformation network is measured annually.

2.5.2 A Review of Historical Earthquake Events in Saint Lucia

Saint Lucia lies in a transition zone where the rate of seismic activity is increasing. The Seismic Research Centre reports that there have been at least five swarms of shallow earthquakes in Saint Lucia in the last 100 years. They occurred in 1906, 1986, 1990, 1999 and 2000. At least three of these swarms seem to have been triggered by a larger tectonic earthquake. The last tectonic earthquake of note was of magnitude 7.75 in 1953 and caused partial collapse of buildings previously damaged by fire and caused some damaged to buildings in the capital city of Castries.

In 1906, Saint Lucia was shaken by a large tectonic earthquake which was felt in the neighbouring islands of Grenada and Dominica. Numerous aftershocks and tremors were felt in the neighbouring islands for several months following the event. There have been periods of low seismic activity interrupted by shallow earthquakes beginning in 1986 when there were 12 earthquakes occurred in a single day of which four were felt.

In May and June of 1990, there were shallow earthquakes felt, the largest was of magnitude 4.5 on the Richter scale. Little damage resulted in the vicinity of the epicenter which was located at Mount Gomier in the southern part of Saint Lucia.

Between April and June of 1999, 105 volcanic earthquakes were recorded in southern Saint Lucia. They were recorded at only one station and none were reported felt.

Between July and November 2000, 27 earthquakes occurred in a single day. None of these earthquake events were directly related to the Soufriere Sulphur Springs, the area of most recent volcanic activity on the island. Most of these earthquakes were from older basaltic centres which were previously regarded as being extinct.

A review of seismological data from Gutenberg and Richter indicates several historical earthquakes with magnitude 7.0 to 7.7 on the Richter scale within 100 kilometers of Saint Lucia. It is assessed that the area would fall into Zone 3 with a maximum ground acceleration of 0.33g.

2.5.3 Earthquake Design Criteria

On November 29th, 2007 Saint Lucia experienced an earthquake of magnitude 7.3 on the Richter Scale at a depth of 121 kilometers. The epicenter of the earthquake was located close to the east side of the island of Martinique.

The largest engineering structure built on the island of Saint Lucia is the Roseau Dam which was designed by Klohn Crippen Ltd of Calgary, Alberta, Canada. The determination of seismic risk at the site of the dam was characterized by a design basic earthquake and a maximum design earthquake which is synonomous with the `maximum credible` earthquake for high hazard dams and was assumed to have a Richter magnitude of 8.0 to 8.5.

The stability of a slope can be seriously affected by the shaking caused by earthquakes. The effect of the earthquake may be twofold; firstly, the accelerations caused by the ground movement will induce an inertial force into the slope material which will provide an extra overturning moment, and secondly, the vibration may cause pore pressure build up in the slope thus causing loss of frictional strength. Both effects will reduce the factor of safety of the slope and may lead to failure if the slope is subject to ground movement of sufficient magnitude and duration.

The design basic earthquake (DBE) would be an event with an annual probability of exceedance of 0.0021which is equivalent to a 10% chance of exceedance over a 50-year period. The predicted mean plus one standard deviation peak horizontal ground acceleration value for this event, would lie between 10% and 15% of gravity (Shepherd, et al 1987a)…. In order to estimate the ground motion at a site, a suitable distance-attenuation relationship is required. To date, there has not been sufficient strong motion data recorded to allow a regional attenuation relationship to be developed for Saint Lucia (Shepherd, 1987a). Therefore, relationships developed for other parts of the world have been used to estimate a range of possible values for peak ground acceleration…. . The predicted peak horizontal ground acceleration for the two postulated MCE events ranges from .10 g to .37 g, depending on the magnitude and the attenuation law assumed. The mean value is .23 g.

The seismic coefficient ‘g’ is an empirical value which depends upon accelerations caused by an earthquake. Seed et al., (1978) states : “…virtually any well built embankment dam on a firm foundation can withstand moderate earthquake shaking, with peak accelerations of about 0.2g with no detrimental effects .”

The great majority of the historical and recorded earthquakes used in the probabilistic analysis of the DBE were tectonic earthquakes. There have been some earthquakes in the region associated with volcanic activity and eruptions, for example on Dominica and Montserrat. Earthquakes of this type can do a great deal of damage, but their effects are generally confined to a local area, thought usually to be less than 2 kilometres in radius. Robson (1964) does attribute a long series of small earthquakes felt in Saint Lucia in 1906 to possible volcanic activity, but Saint Lucia is not considered to be significantly at risk from this type of earthquake (Shepherd). It is recommended that the design earthquake should be assumed to be within Zone 3 with a design earthquake of 7.5 at a distance of 25 to 100 kilometres.

A map of earthquake activity in the Eastern Caribbean is shown in Figure 2.36 for the period of March 15 – 31, 2011 (After Seismic Research Unit, University of the West Indies). Figure 2.37 contains a map of earthquake activity in the Eastern Caribbean Region for the period of April 1 – 15, 2011 (After Seismic Research Unit, University of the West Indies, Trinidad & Tobago).

THIS PAGE DELIBERATELY LEFT BLANK

Figure 2.1 Location Map of Saint Lucia

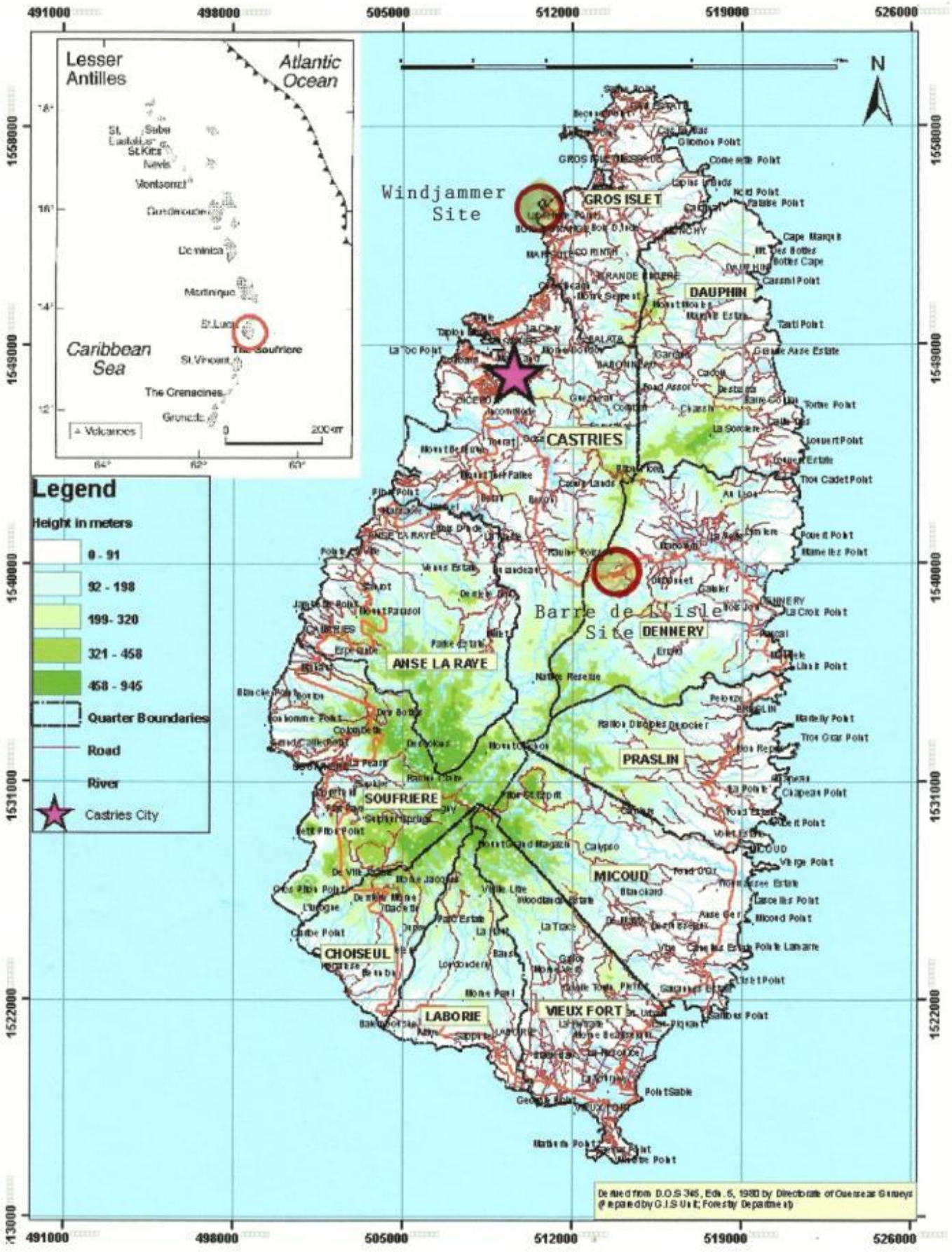

Figure 2.2 Map of Physical Features of St. Lucia (OAS)

Figure 2.3 Failed Slope at Boguise

Figure 2.4 Wheeled inclinometer probe for measuring deflection in the inclinometer casing

Figure 2.5 Recording data from the probe as it passes through the inclinometer casing

	Gamma kN/m3	C kPa	Phi deg	Piezo Surf.	Ru
SURCHARGE	18	0	9	1	0
COLLUVIUM	18	0	9	2	0
SAND	20	0	27	3	0
BEDROCK	(Infinitely Strong)				

Strata Engineering - St. Lucia
PB99-015
BLACK MALLET LANDSLIDE
6 December 1999
SECTION A - A' ANALYSIS
BEFORE EXCAVATION

F = 1.288 (Janbu)

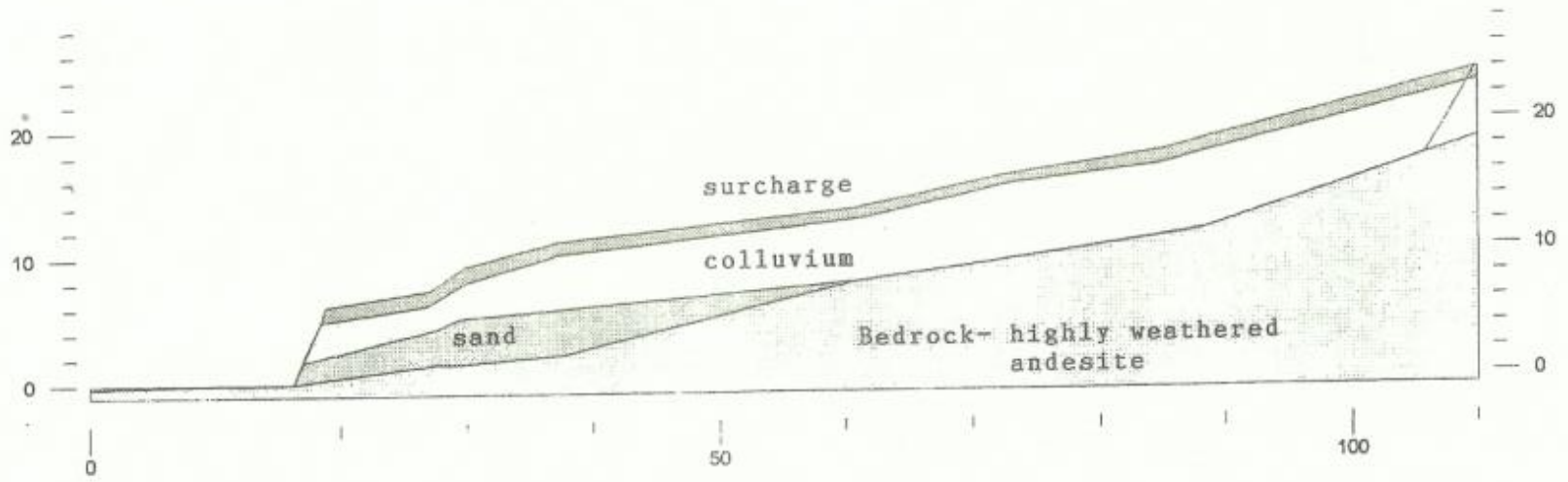

Figure 2.6 Cross-Section A-A' Slope Stability Analysis
Black Mallet/Maynard Hill

Figure 2.7 West Limit of Barre de L'isle 2005 Landslide

Figure 2.8 East Limit of Barre de L'isle 2005 Landslide

Figure 2.9 Extent of slope failure at Windjammer Landing

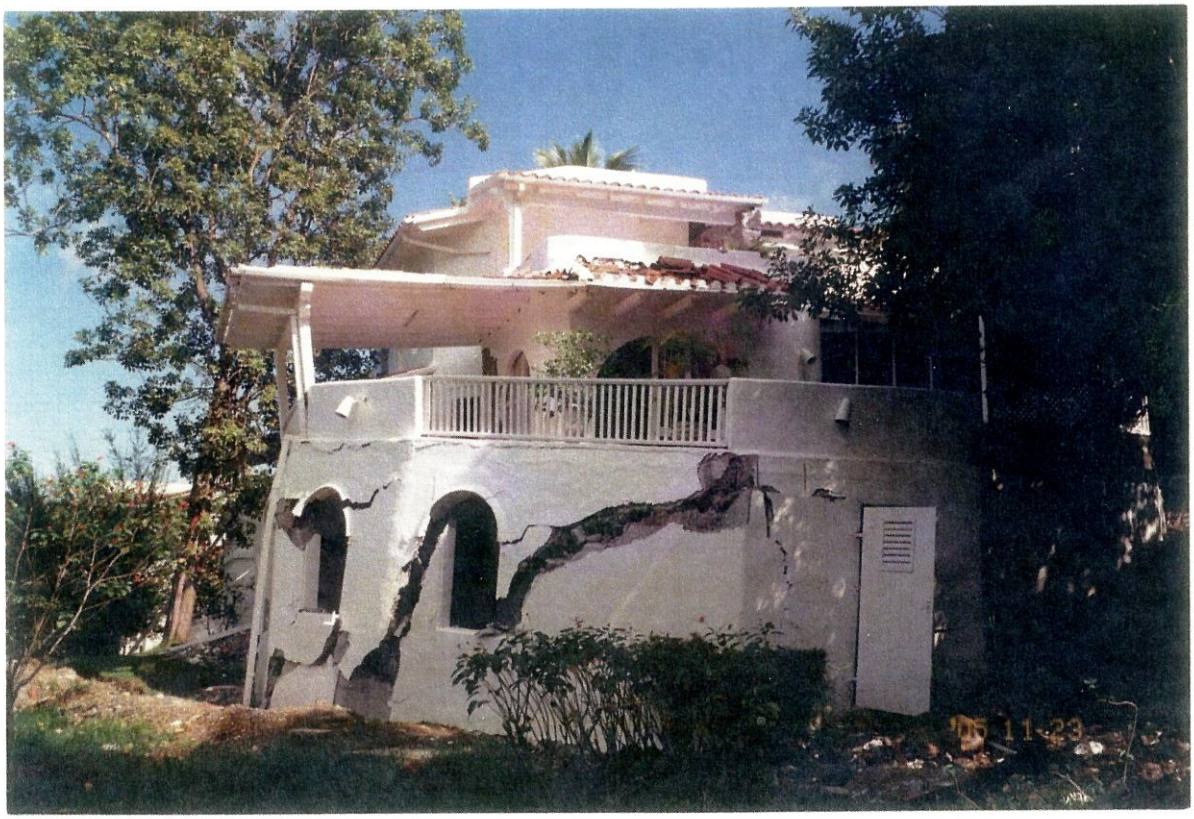

Figure 2.10 Damaged Villas 17/18 at Windjammer Landing

Figure 2.11 Retaining wall collapse at crest of slope

Figure 2.12 Retaining wall collapse at toe of slope

Figure 2.13 Instrumentation in Failure Zone
Winjammer Landing Beach Resort

Figure 2.14 Remedial works - Excavation of failed colluvium at Windjammer Landing Resort

Figure 2.15 Remedial works - Placement of rock fill buttress at Windjammer Landing Resort

Figure 2.16 Rock buttress construction
Windjammer Landing Beach Resort

Figure 2.17 Completed rock buttress
Windjammer Landing Beach Resort

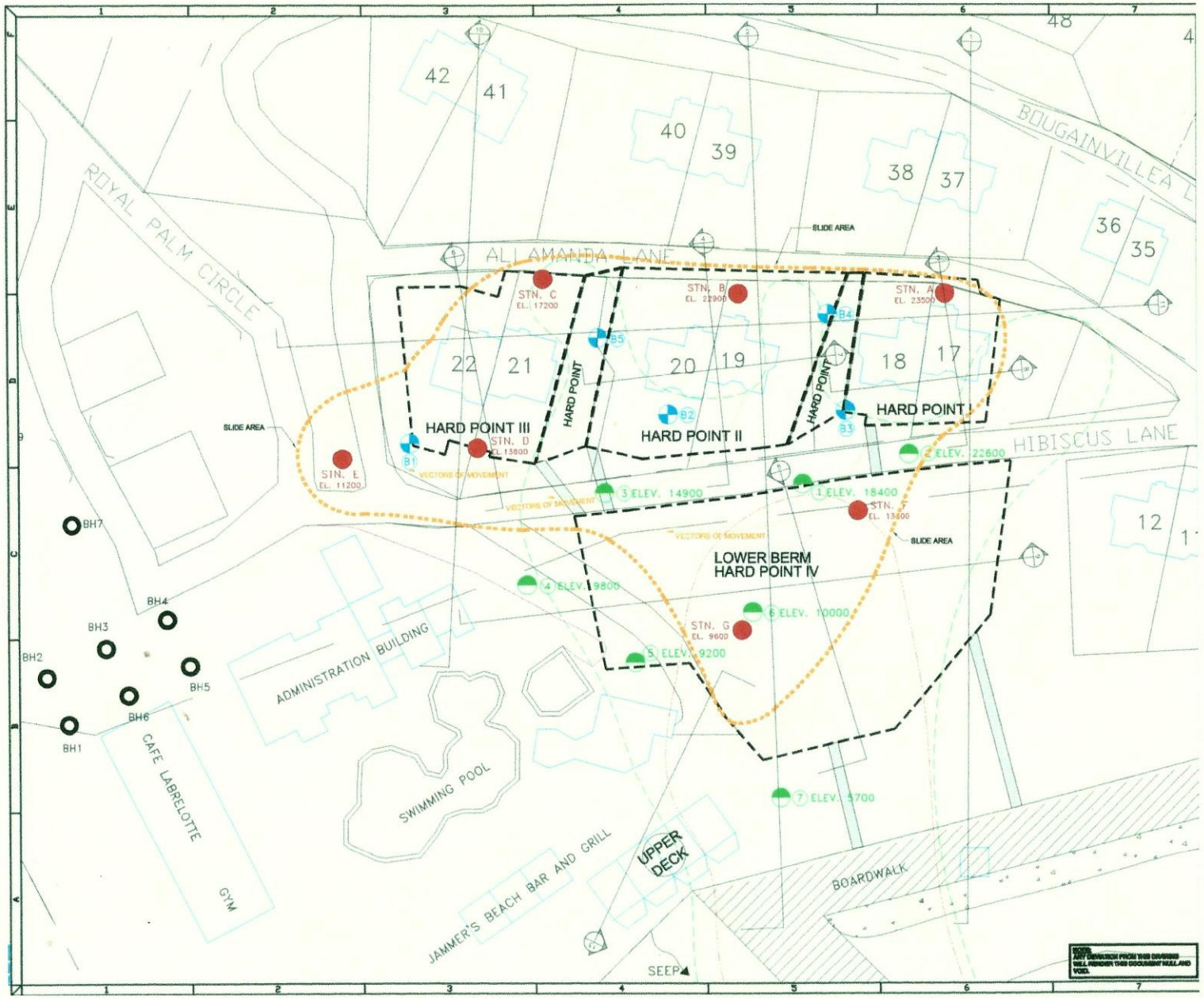

Figure 2.18 Plan of Cross-Sections for Slope Stability Analysis Windjammer Landing Beach Resort (After EllisDon,2007)

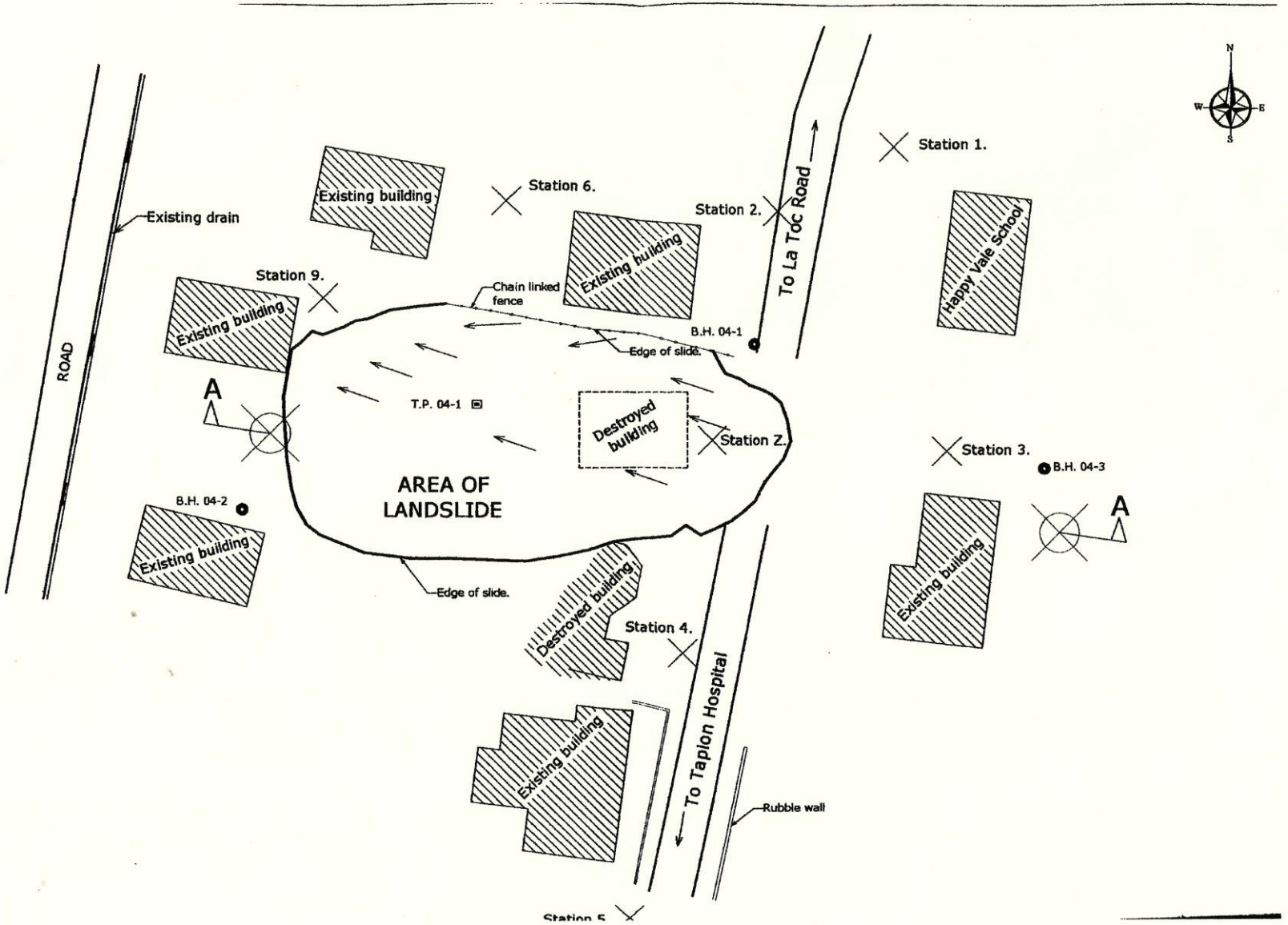

Figure 2.19 Site Plan of the Tapion Landslide (2004)

Figure 2.20 Ground displacement in access road at Tapion slide

Figure 2.21 Damaged roadway and structures downslope Tapion slide

Figure 2.22 Foundation failure at crest of Tapion slide

Figure 2.23 Structural collapse downslope of Tapion slide

Figure 2.24 Colombette Landslide, Saint Lucia (2010)

Figure 2.25 Fond Saint Jacques Landslide, Saint Lucia (2010)

Figure 2.26 Guesneau Landslide, Saint Lucia (2010)

Figure 2.27 Trois Piton Landslide, Saint Lucia (2010)

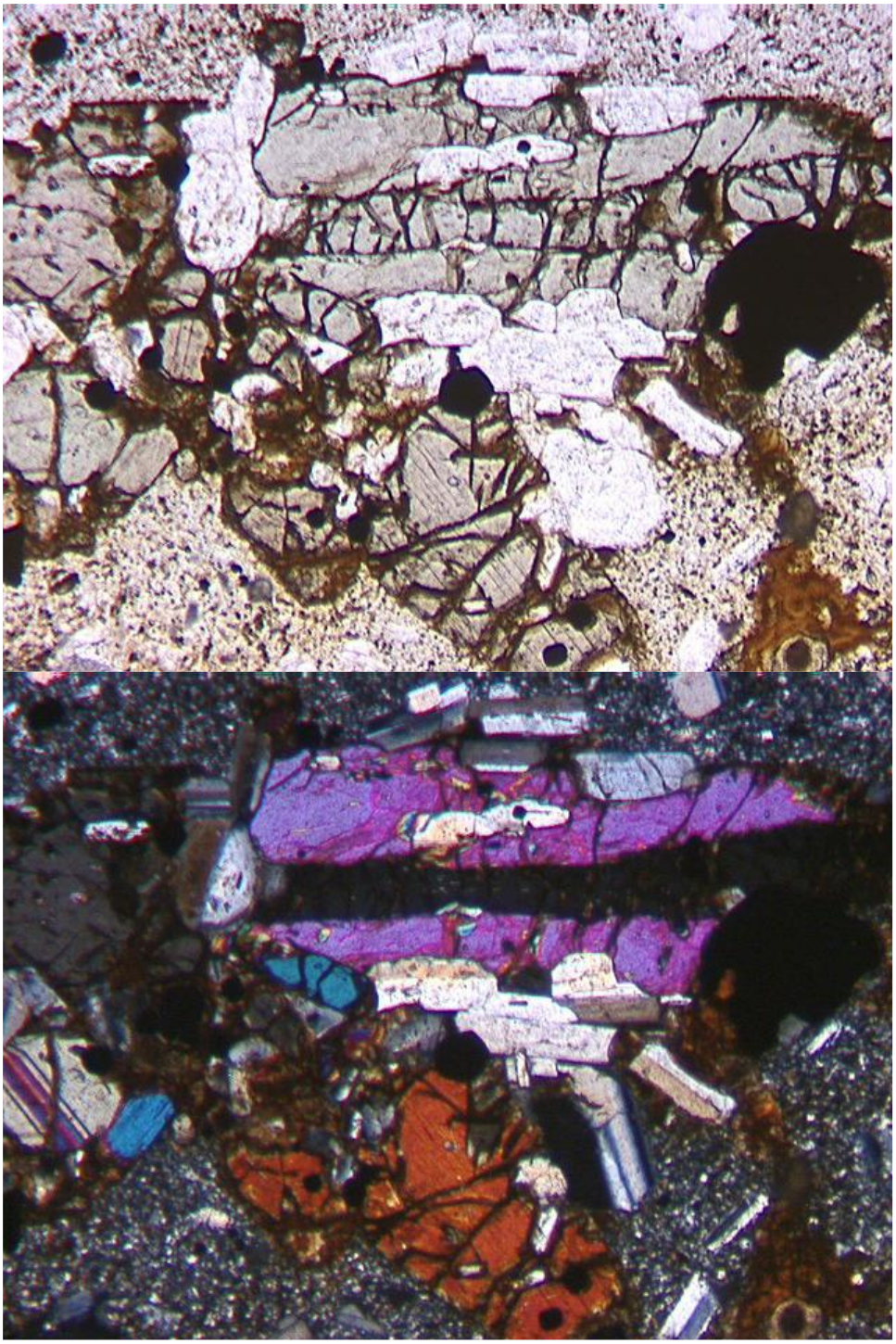

Figure 2.28: Bule Rock Quarry – Basalt : Glomeroporphyritic texture involving plagioclase (pl), clinopyroxene (cpx), orthopyroxene (opx), and magnetite (mt). Alteration of cpx to chlorophaeite (likely including chlorite, serpentine, and iron hydroxide) is evident around grain edges and along fractures. A single elongate orthopyroxene grain is oriented E-W in the upper third of the top image and is at extinction (dark) in the lower image.

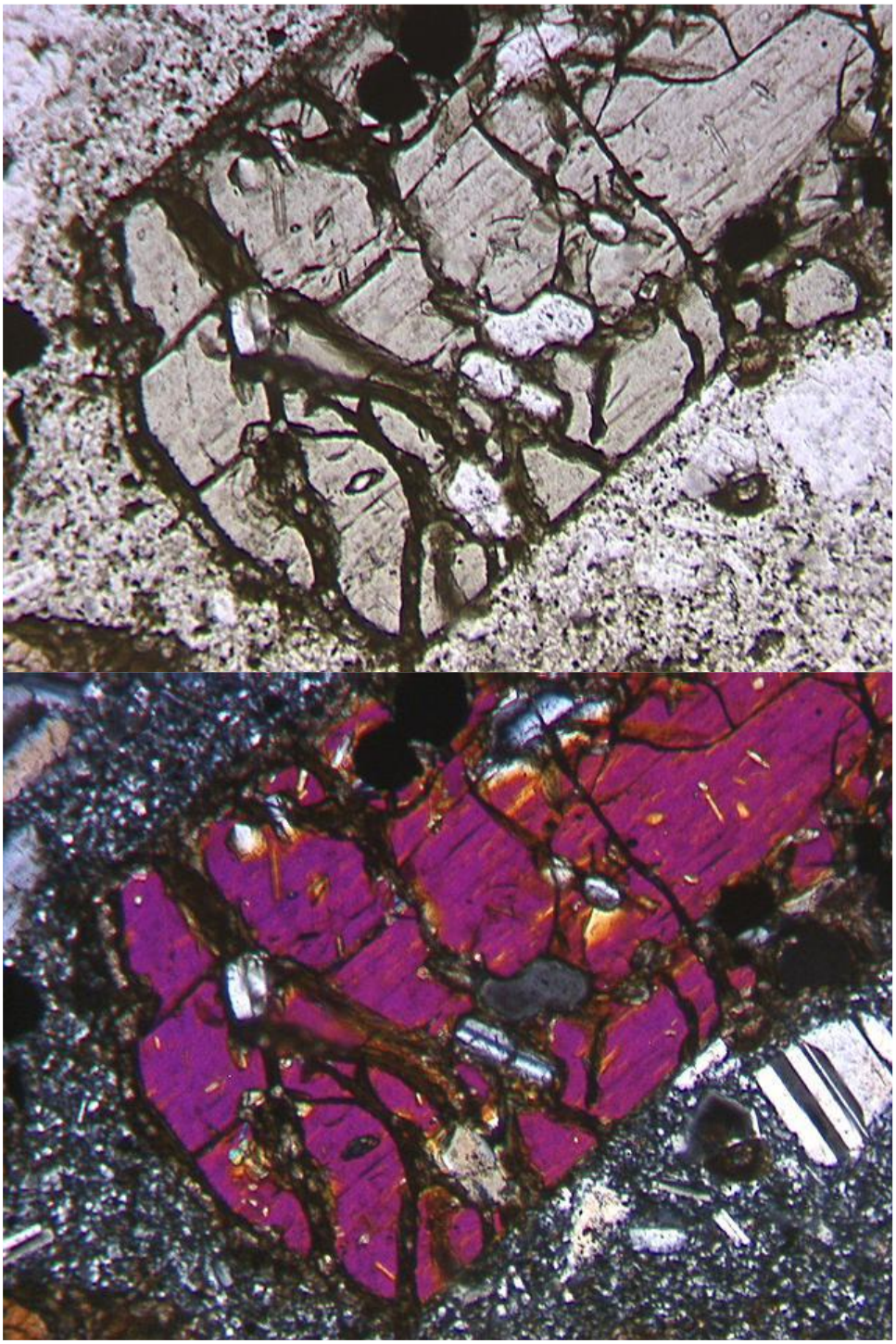

Figure 2.29: Blue Rock Quarry – Basalt : Clinopyroxene grain showing chlorophaeite alteration along fractures and grain margins. Plagioclase and apatite inclusions are evident in the cpx, indicating earlier crystallization of these phases.

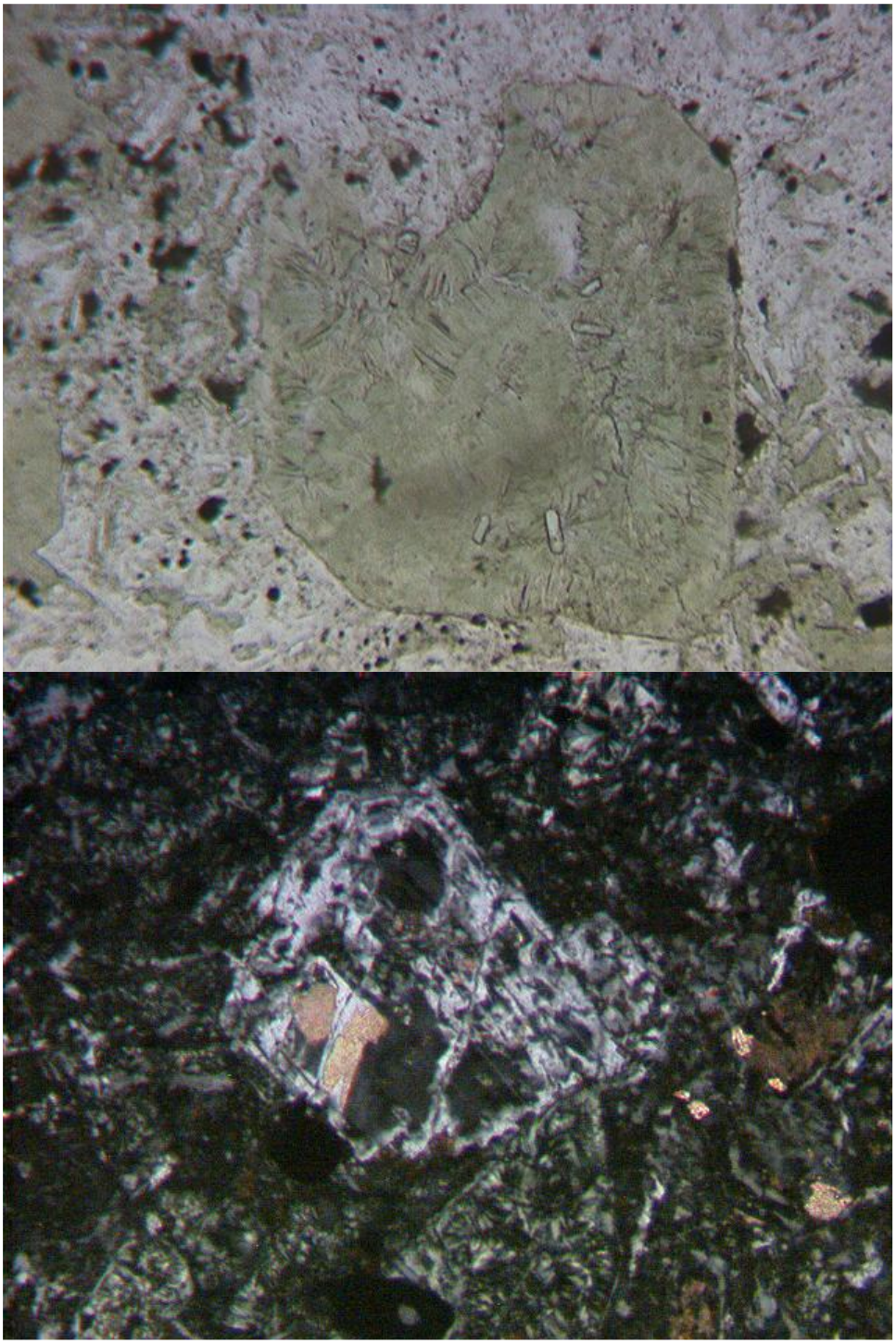

Figure 2.30: RG Quarry – Andesite : Plagioclase phenocryst that is altered to carbonate (light orange colored material in lower image) with cross-cutting fractures of serpentine. Large uniformly green areas (top image) are serpentine replacement of mafic phenocrysts. The surrounding matrix is a serpentine, carbonate, and plagioclase intergrowth.

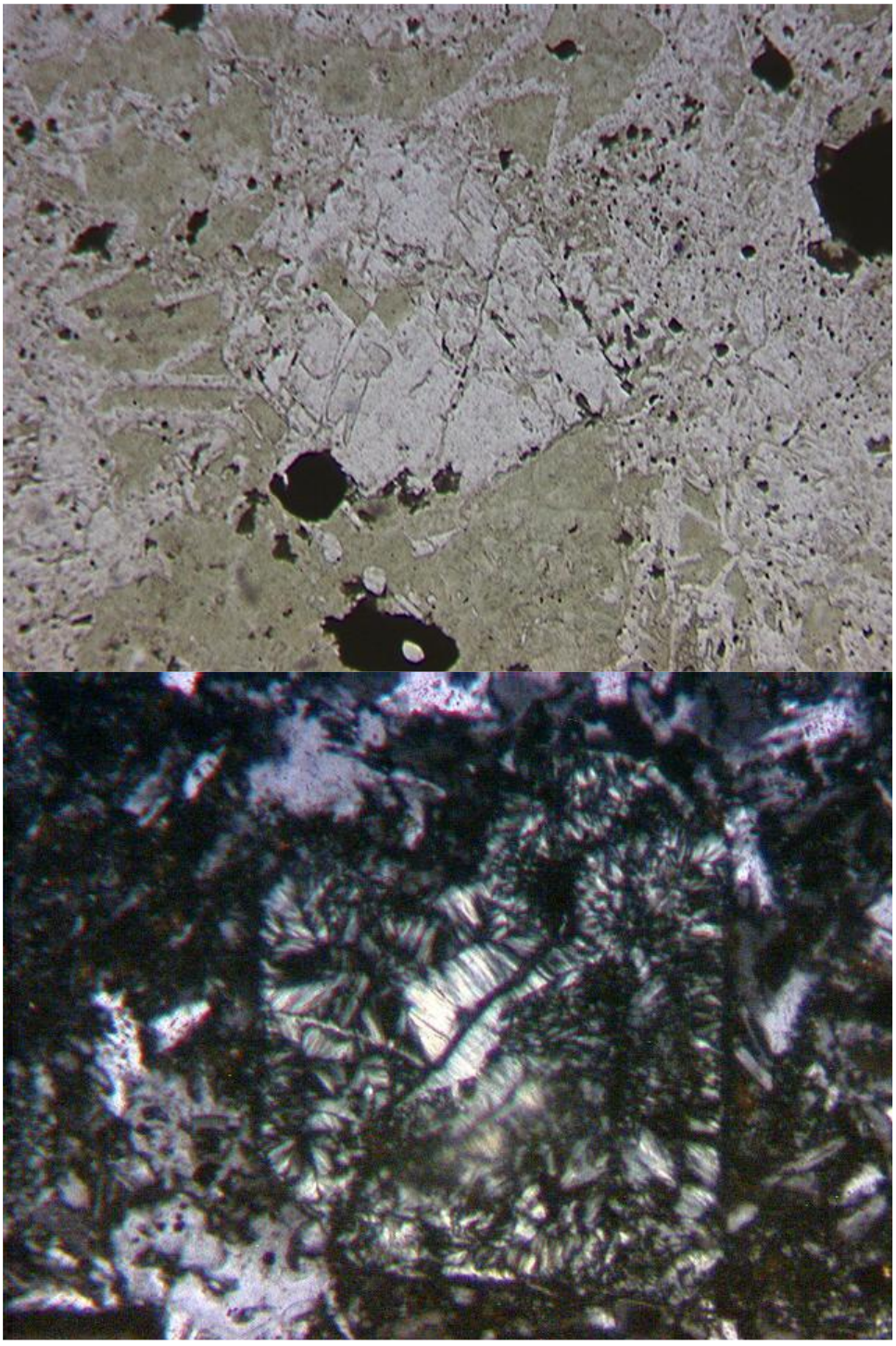

Figure 2.31: RG Quarry – Andesite : Euhedral grain, believed to have been pyroxene based on external morphology, which has been completely pseudomorphed by serpentine. Small elongate inclusions of apatite are visible in the upper image.

Figure 2.32 Basalt Formation at Blue Rock Quarry, Saint Lucia

Figure 2.33 Andesite Formation at RG Quarry, Saint Lucia

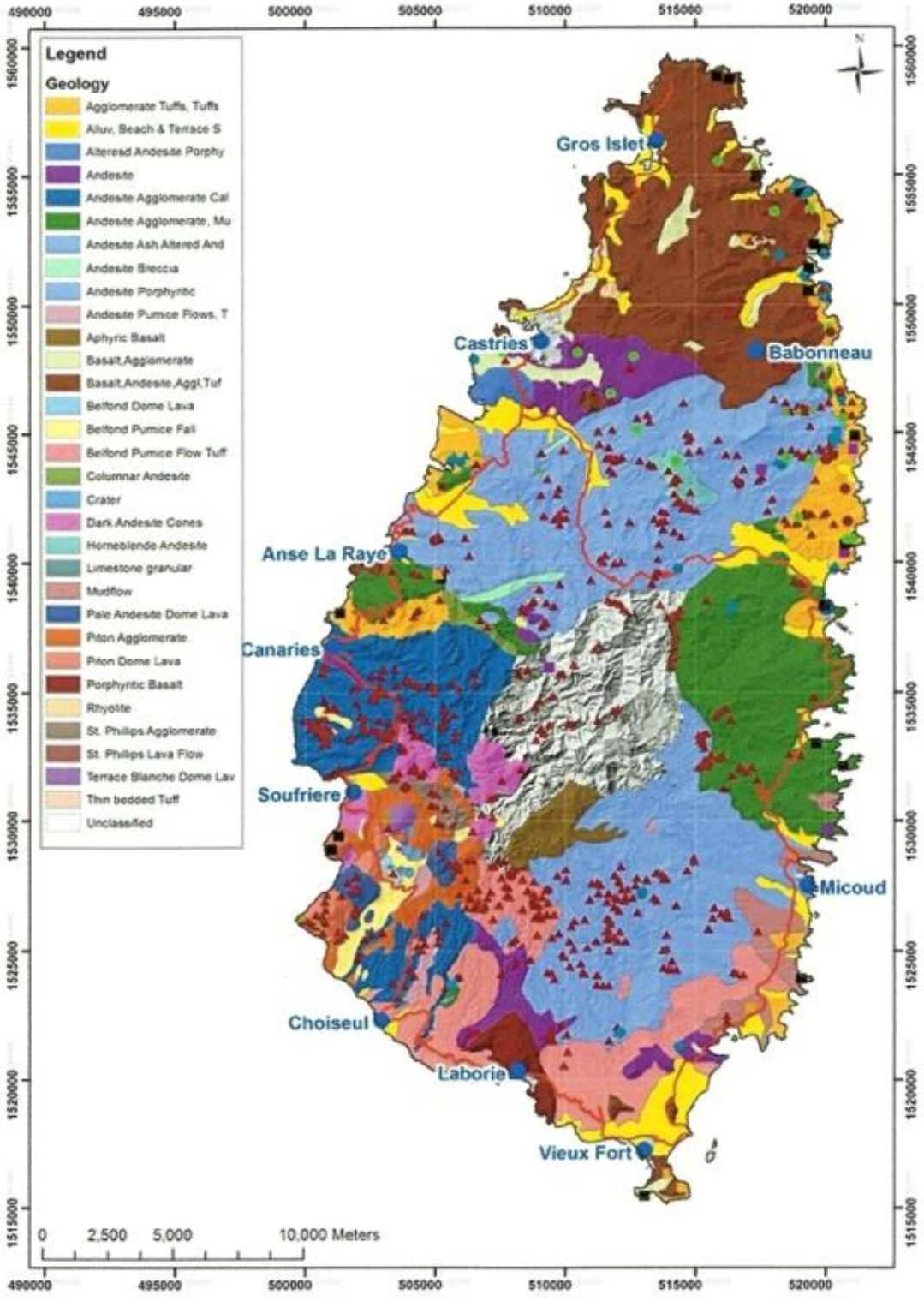

Figure 2.34 Geological Map of Saint Lucia

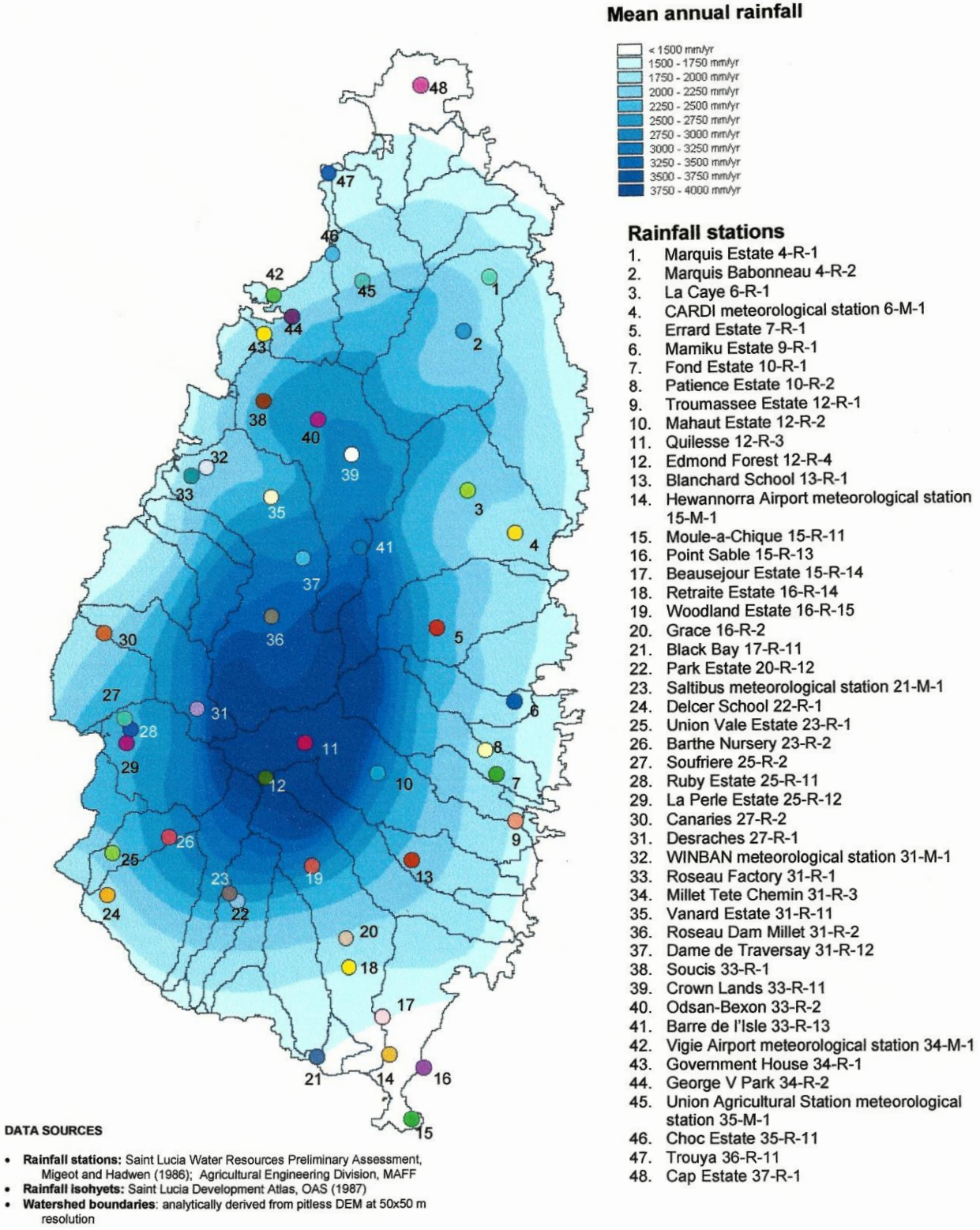

Figure 2.35 Annual rainfall distribution and rainfall stations with watershed boundaries superimposed. (After the Organization of American States (OAS)

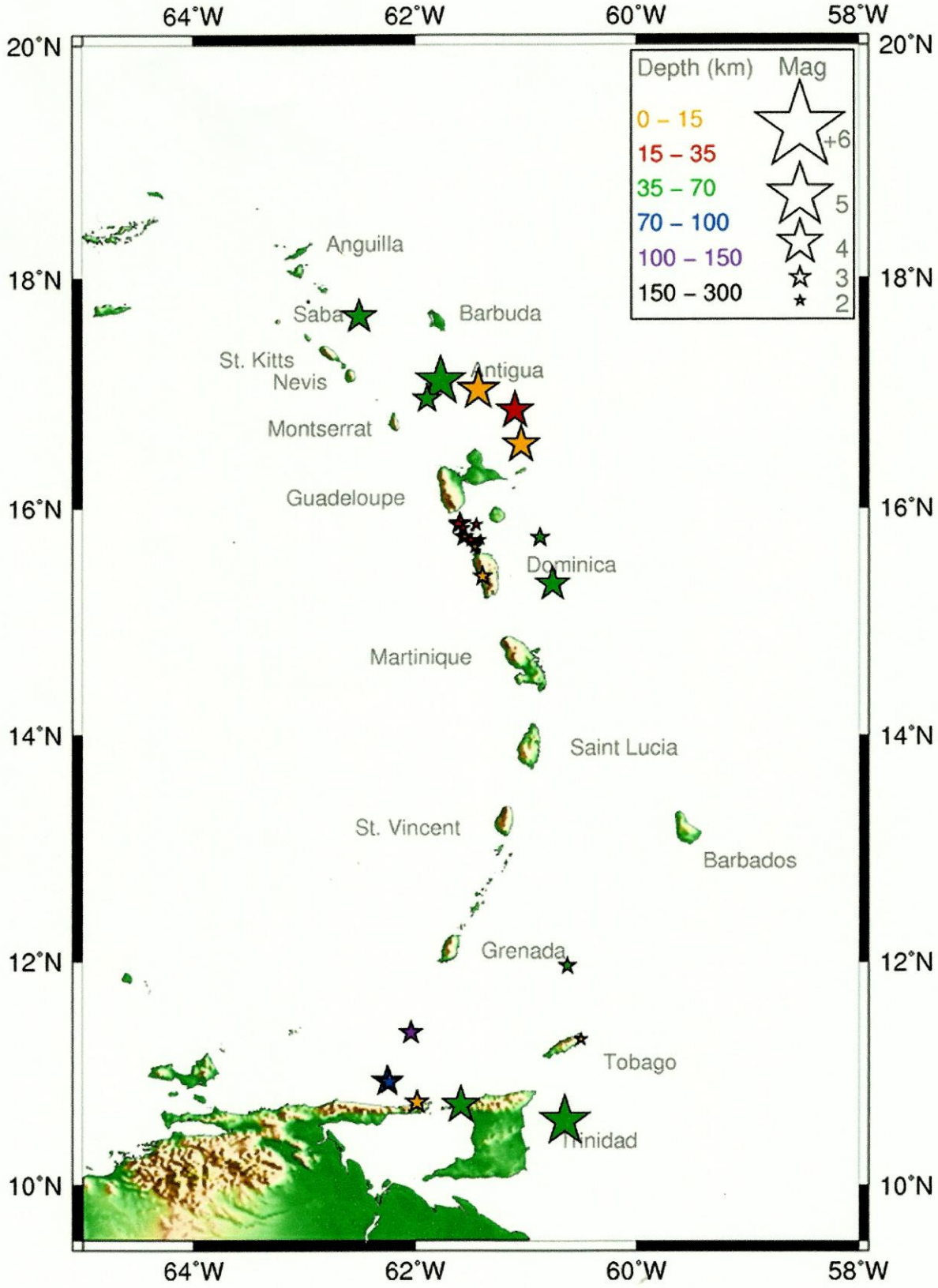

Figure 2.36 Map of Earthquake Activity in the Eastern Caribbean for 15-31 March, 2011 (After Seismin Research Centre - UWI, Trinidad & Tobago)

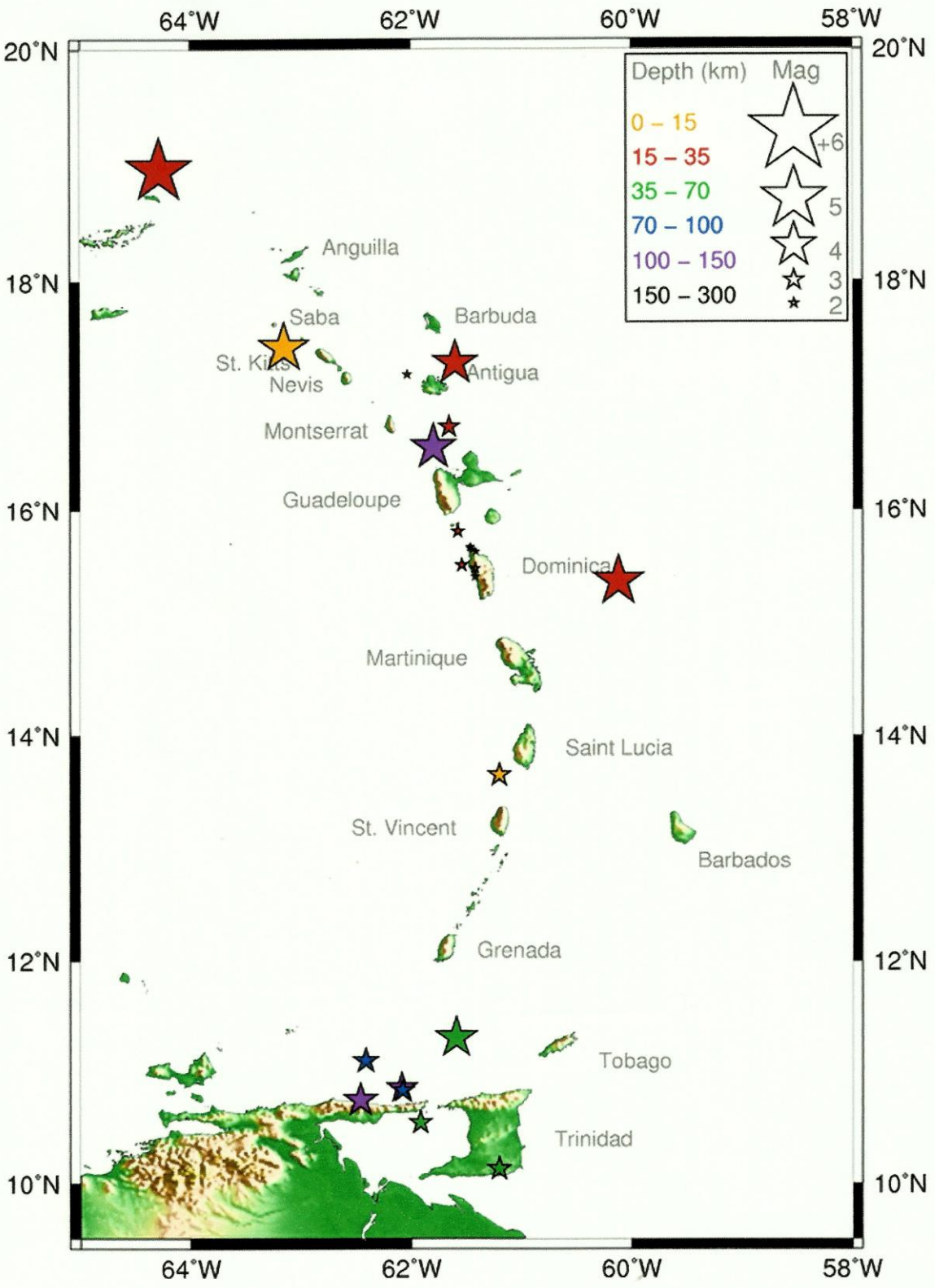

Figure 2.37 Map of Earthquake Activity in the Eastern Caribbean for 1 - 15 April, 2011 (After Seismic Research Centre - UWI, Trinidad & Tobago)

CHAPTER 3

ACADEMIC LITERATURE REVIEW

3.1 Introduction

Landslides triggered by intensive rainfall events are a common phenomenon in the tropical islands of the Caribbean, but detailed studies of these occurrences are limited. Several studies have been conducted by researchers in other tropical countries such as Hong Kong, Singapore and Malaysia in order to understand the response to unsaturated residual soil slopes to different rainfall conditions and the effect of infiltration on the pore water pressure conditions within the slope. Several steep slopes in residual soils remain stable for long periods during dry weather conditions but tend to lose shear strength by developing positive pore water pressures during saturation by rainfall resulting in the development of instabilities within the slope.

In addition to be comprised of a solid, water and air phase, Fredlund and Morgenstern (1977) concluded that a fourth phase exist in unsaturated soils at the air-water interface. They refer to this fourth phase of unsaturated soils as the contractile skin. The contractile skin is flexible and exists throughout the soil structure. An unsaturated or partially saturated soil condition indicates that the pore water saturation is any value less than unity (Lu and Likos, 2004)

3.2 The State of Stress in an Unsaturated Soil

Stress state variables reflect the state of stress in a soil. The number of stress state variables required for the description of the stress state of a soil is dependant on the number of phases involved. For an unsaturated soil, the stress state variables consist of the total stress, the pore water pressure and the pore air pressure. Consideration of the contractile skin as a fourth phase warrants the support to the theoretical justification of two independent stress states, $(\sigma - u_a)$ and $(u_a - u_w)$ for an unsaturated soils (Fredlund and Morgenstern, 1977)

Bishop (1959) suggested an equation for effective stress as follows:

$$\sigma' = (\sigma - u_a) + \chi\,(u_a - u_w) \qquad (3.1)$$

Where,

σ' = effective normal stress
σ = total normal stress
u_a = pore air pressure
u_w = pore water pressure
$u_a - u_w$ = negative pore water pressure or matric suction
χ = a parameter related to the degree of saturation of the soil

The term $(\sigma - u_a)$ represents the component of net normal stress applicable to bulk soil. The product $\chi(u_a - u_w)$ represents the interparticle stress due to suction (suction stress).

Fredlund et al (1978) used two independent stress state variables $(\sigma - u_a)$ and $(u_a - u_w)$ to formulate the shear strength of an unsaturated soil. The resulting equation follows:

$$\tau = c' + (\sigma - u_a)\tan \phi' + (u_a - u_w) \tan \phi^b \quad (3.2)$$

Where,

c' = effective cohesion
$(\sigma - u_a)$ = net normal stress state on the failure plane at failure
u_a = pore-air pressure on the failure plane at failure
ϕ' = angle of internal friction associated with the net normal stress state variable
$(u_a - u_w)$ = matric suction on the failure plane at failure
ϕ^b = angle indicating the rate of increase in shear strength relative to matric suction

The shear strength equation for an unsaturated soil is transformed to the shear strength of a saturated soil. As the soil approaches saturation, the pore water pressure u_w, approaches the pore air pressure, u_a, and the matric suction, $(u_a - u_w)$ goes to zero, that is , the pore air pressure is in equilibrium with the pore water pressure $(u_a = u_w)$.

The equation for the shear strength of a saturated soil is written as:

$$\tau = c' + (\sigma - u_w)\tan \phi' \quad (3.3)$$

Fredlund and Rahardjo (1993) state that the parameter ϕ^b (the angle of increase in shear strength due to matric suction, $u_a - u_w$) is always less than or equal to the saturated angle of internal friction, ϕ'. They show how matric suction $(u_a - u_w)$, net normal stress $(\sigma - u_a)$, and shear stress (τ), interrelate to produce a three-dimensional failure surface for the extended Mohr-Coulomb failure envelope as shown in Figure 3.1. They explained that the figure shows a planar failure envelope intersecting the shear axis, giving a cohesion c'. The failure envelope has slope angles ϕ' and ϕ^b with respect to the $(\sigma - u_a)$ and $(u_a - u_w)$ axes. The angles are assumed to be constants and the cohesion c' and the slope angles are strength parameters relative to the stress state variables.

3.2.1 Shear Strength from Matric Suction Stress State Variable, ϕ^b

Fredland and Morgenstern (1977) proposed the use of $(\sigma - u_a)$ and $(u_a - u_w)$ as independent stress stete variables for unsaturated soils. From this emerged the theory that the shear strength of an unsaturated soil consisted of an effective cohesion c', and a derivation from both $(\sigma - u_a)$ and $(u_a - u_w)$. This led to the introduction of the angle, ϕ^b, which relates to the shear strength contribution from the matric suction stress state variable.

Ho and Fredlund (1982) analysed test results on various soil samples reported in the literature and and using Equation 3.2 above found that ϕ^b was typically one-third to two-thirds of the effective angle of internal friction. In their study they found that the average angle of friction for decomposed granite was 15.3^o and the average angle of friction with respect to suction was about 13.8^o.

Fredlund (1979) suggested that as the degree of saturation approached 100 percent, the pore air pressure and the pore water pressure would become equal, matric suction ($u_a - u_w$) would go to zero and pore water pressure could be substituted for pore air pressure in the applied stress variable ($\sigma - u_a$). As a result, the c' and ϕ' strength parameters could be evaluated in the conventional manner for saturated soils.

This theory is supported by Rahardjo (2002) who states that under special conditions when a soil is saturated the pore water pressure equals the pore air pressure and the matric suction ($u_a - u_w$) diminishes. The stress state variables then become a single effective stress ($\sigma - u_w$). The stress state variables control the shear strength and volume change behavior of the soil.

Rahardjo (1991) showed that an increase in the ϕ^b angle results in an increase in the cohesive component of shear strength and the factor of safety of an unsaturated slope. As infiltration occurs as a result of rainfall the value of ϕ^b decreases as saturation increases and the factor of safety of the slope decreases.

Hossain (2010) indicated that maximum changes in matric suction near the ground surface occur initially and as the rainfall intensifies matric suction values at greater depths are affected. In his analysis of the stability of a residual soil slope in Bangladesh it was found that the factor of safety decreased as matric suction was reduced as the soil became saturated. He found that matric suction increased in the dry season and decreased substancially during the wet season.

Yeh et al (2006) investigated the effect of the degree of saturation on slope stability in sand, loam and clay soil samples. It was found that the effective degree of saturation of the sandy soil was relatively sensitive to rainfall events as a result of the large pores in the sand that allows relatively short capillary rise and the air entry value of sand is lower than that for clay. They also showed that the clayey soil had the lowest variation in rainfall events since the air entry value is greater than for sand. They concluded that infiltration of rainwater into an unsaturated slope impairs slope stability by decreasing matric suction and as a result the effect of ϕ^b, thereby increasing the moisture content of the soil which may trigger shallow slides.

Since this research project is focused on the changes taking place in the pore water pressure and matric suction in an unsaturated residual soil and colluvium slopes when they become saturated and unstable during rainstorms, ϕ^b was not used in the finite element numerical analysis.

3.3 The Soil-Water Characteristic Curve (SWCC)

The relationship between the water content and the suction of a soil is commonly referred to as the Soil-Water Characteristic Curve or SWCC. The physical and physicochemical mechanisms responsible for soil suction depends on the water content of the unsaturated soil-water-air system. At relatively low values of water content and correspondingly high values of suction, the pore water is adsorbed to the soil particles in thin layers and the dominant mechanism contributing to suction are the adsorption effects controlled by the surface properties of the soil particles. Alternatively, at high values of water content and the resulting low suction, the dominant pore water retention mechanism is capillarity, which is controlled by the soil particle, the pore structure and the pore size distribution.

Lu and Likos (2004) show typical soil-water characteristic curves for sand, silt and clays in Figure 3.2 and Figure 3.3**.** The surface adsorption at the high suction range for sands is relatively low due to the small surface area and low charges on the sand particles and capillarity is the dominant suction mechanism. Silty soil particles have a larger surface area than sand and therefore can adsorb greater amounts of water than the sand particles. The surface area of clays are much larger than sands or silts and is electrically charged and therefore has a higher capacity for adsorpion.

3.4 Steady State Water Flow

Water flow through unsaturated soils is governed by Darcy's law with the addition that the coefficient of permeability is assumed to be a function of suction, water content or some other variable and negative pore - water pressure.

The coefficient of permeability usually varies for unsaturated soils whereas for saturated soils it is constant. Fredlund and Rahardjo (1993) state that the variation of the coefficient of permeability of a saturated soil can be contributed to a heterogeneous distribution of the soil solids, whereas for an unsaturated soil it is more appropriate to consider the heterogeneous volume distribution of the pore-water due to matric suction in the soil.

3.4.1 One-Dimensional Flow

Steady state flow conditions require that for continuity the volume of water flowing in and out of an element must be equal:

$$\left(\upsilon_{wy} + \frac{\delta \upsilon_{wy}}{\delta y} \delta y \right) \delta x \, \delta z - \upsilon_{wy} \, \delta x \, \delta z = 0$$

where,

υ_{wy} = water flow rate across a unit area of the soil in the y-direction

$\delta x, \delta y, \delta z$ = dimensions in the x,y,and z-directions, respectively

3.4.2 Two-Dimensional Flow

For two-dimensional steady-state flow in an unsaturated soil, continuity can be expressed as follows:

$$\left(\upsilon_{wx} + \frac{\delta \upsilon_{wx}}{\delta x} \delta x - \upsilon_{wx} \right) \delta y \, \delta z + \left(\upsilon_{wy} + \frac{\delta \upsilon_{wy}}{\delta y} \delta y - \upsilon_{wy} \right) \delta x \, \delta z = 0$$

3.5 The Physical and Chemical Weathering of Rocks

3.5.1 General

Weathering is the result of the alteration of rocks by means of textural, chemical and mineralogical changes induced by a change in the physical, physico-chemical and chemical environment. Physical weathering causes a physical breakdown of the parent rocks but the rock fragments retain their original chemical and mineralogical composition. In chemical weathering, the rock forming minerals are vulnerable to attack by water, oxygen, and carbon dioxide of the new near surface environment to form new minerals which are in more stable equilibrium with the prevailing atmospheric conditions.

3.5.2 Physical Weathering of Rocks

Physical weathering involves the disintegration of parent rocks into angular blocks, cobbles, gravel, sand, silt and rock flour. Gidigasu (1976) states that the main factors which enhance physical weathering are:

i) the periodical temperature changes, erosional forces and the disintegrating action of plants and animals.

ii) The roots of plants grow through openings in rocks in search of moisture and nutrients. Animals burrowing through the ground disturbing the soil and rock. Human activities such as mining, tunneling, excavating etc. contribute to the disintegration of rock.

3.5.3 Chemical Weathering of Rocks

New minerals are produced from the process of chemical weathering. The near-surface agents of weathering which attack the primary minerals in the fresh rock include oxygen, water, carbon dioxide and organic acids from decayed vegetation.

The various chemical processes involved in the weathering of rocks include solution, ion-exchange, hydration, carbonation, oxidation and reduction. These processes may act simultaneously, some more rapidly than others and some more effectively in the alteration of one mineral than another (Gidigasu, 1976).

3.5.4 Residual Soils

Residual soils are formed from the physical and chemical weathering of rock-forming minerals into materials rich in 1:1 clay lattice minerals and constituent elements (Fe, Al, Ti, and Mn). They have a vertical soil section or a soil profile which consists of a distinct layering termed the soil horizon. These soil horizons are a reflection of the weathering process. The soil profile also has a weathering aspect that gives rise to a vertical weathering profile that is a critical aspect from the engineering perspective (Gidigasu, 1976).

Three main stages have been identified in the weathering process (Gidigasu, 1976):

i) Decomposition - is characterized by physico-chemical breakdown of primary minerals and the release of constituent elements (SiO_2, Al_2O_3, Fe_2O_3, CaO, MgO, K_2O, Na_2O, etc.) which appear in simple ionic forms.

ii) Laterisation/Oxidation – involves the leaching, under appropriate drainage conditions, of combined silica and bases and the relative accumulation or enrichment from outside sources of oxides and hydroxides (mainly Al_2O_3, Fe_2O_3, TiO_2).

iii) Dessication/Dehydration - involves partial or complete dehydration of the oxide rich materials and secondary minerals. The dehydration of colloidal hydrated iron oxides involves loss of water, and the concentration and crystallization of the amorphous iron colloids into dense crystalline iron minerals such as; limonite, goethite, and hematite.

The weathering profile consist of material that shows progressive stages of transformation or 'grading' from fresh rock to completely weathered material toward the ground surface. Continuous attempts have been made over the years to develop methods for the description or classification of rock weathering and residual soils.

Weathering profiles have been investigated by many researchers such as Little (1969), Anon (1977) and Wesley (1988) for a descriptive scheme for grading the degree of weathering. Figure 3.4 contains the classification system proposed by Little. Examples of a few classification schemes are shown below:

Anon, (1977) and Wesley is illustrated in Table 3.1. A scheme for the description of the weathering grades of rock masses from Wesley is shown in Figure 3.5

Table 3.1 Scale of Weathering Grades of Rock Mass (Table 8 of Anon, 1977)

Term	Description	Grade
Fresh	No visible sign of material weathering; perhaps a slight discolouration on major discontinuity surfaces.	I
Slightly Weathered	Discolouration indicates weathering of rock material and discontinuity surfaces. All the rock material may be discoloured by weathering	II
Moderately Weathered	Less than half of the rock material is decomposed or disintegrated to a soil. Fresh or discoloured rock is present either as a continuous framework or as corestones.	III
Highly Weathered	More than half of the rock material is decomposed or disintegrated to a soil. Fresh or discoloured rock is present either as a discontinuous framework or as corestones.	IV
Completely Weathered	All rock material is decomposed and or disintegrated to soil. The original mass structure is still largely intact.	V
Residual Soil	All rock material is converted to soil. The mass structure and material fabric are destroyed. There is a large change in volume, but the soil has not been significantly transported	VI

Wesley (1988) proposed classification schemes for residual soils and soils groups which are shown in Table 3.2 and Table 3.3, respectively.

A comparison of the weathering grades of andesite from RG Quarry in Saint Lucia is presented in Figure 3.6**.**

Figure 3.7 shows a cut in a residual soil slope at the RG Quarry with corestones present.

Wesley (1988) proposed a practical system for classifying residual soils based on distinguished characteristics that identify them from transported soils (colluvium). These include the presence of specific clay minerals found only in residual soils, or to the presence of unweathered or partially weathered rock, relic discontinuities and other planes of weakness and inter-particle bonds. He grouped them under the headings of composition and structure.

Structure refers to the soil condition in situ and undisturbed. Macro-structure includes all features visible to the naked eye, such as layering, discontinuities, fissures, pores, presence of unweathered or partially weathered rock and other relic structures from the parent rock. Micro-structure includes fabric, inter-particle bonding, aggregation of particles, pore sizes and shapes etc.

The proposed classification by Wesley (1988) is shown in Table 3.2 and Table 3.3.

Residual soils are divided into three groups:

i)	Group A:	Soils without a strong mineralogical influence
ii)	Group B:	Soils with a strong mineralogical influence derived from clay minerals also found in transported soils
iii)	Group C :	Soils with a strong mineralogical influence derived from clay minerals only found in residual soils

Table 3.2 Classification of Residual Soils (after Wesley & Irfan, 1988)

Grouping System		Common Pedological Names Used for Group	Descriptive Information on in situ state	
Major Division	Sub-Group		Parent Rock	Information on Structure
Group A (Soils without a strong mineralogical influence)	(a) Strong macro structure influence	Give names if appropriate	Give details of type of rock from which the soil has been derived	Describe nature of structure - stratification, reflecting parent rock - fractures, fissures faults etc -Presence of partially weathered rock (state % and physical form, e.g. 50% corestones
	(b)Strong micro Structure influence	Give names if appropriate		Describe nature of micro-structure or evidence of it -effect of remoulding, sensitivity -liquidity index or similar index
	(c)Little or no Structure	Give names if appropriate		Describe evidence for little or no structural influence
Group B (soils strongly influenced By commonly occurring minerals)	(a) Montmorillonite (Smectite group)	Black cotton soils Black clays, Tropical Black earths, Grumusols vertisols		Describe any structural effects which may be present, or other aspects relevant to engineering properties. Evidence of swelling behavior, extent of surface cracking in dry weather, slickensides below surface etc.
	(b) Other Minerals			
Group C (soils strongly influenced by clay minerals essentially found only in residual soils)	(a) Allophane sub Andosols, Andepts	Volcanic ash soils		Give basis for inclusion in this group. Describe any structural influences, either macro-structure or micro-structure
	(b)Halloysite sub group	Tropical red clays, Latosols, Oxisols, Ferralsols		
	(c) Sesquioxide sub Group (gibbsite, geothite, haematite	Lateritic soils, Laterits, ferrlitic soils, Duricrusts		Give basis for inclusion in this group. Describe structural influences-especially cementation effects of the sesquioxides

Table 3.3 Characteristics of Residual Soils (after Wesley & Irfan, 1988)

Group		Examples	Means of identification	Comments on likely engineering properties and behaviour
Major Group	Sub-Group			
Group A (Soils without a strong mineralogical influence)	(a) Strong macro-structure influence	High weathered rocks from acidic or inter-mediate igneous rocks, and sedimentary Rocks	Visual Inspection	This is a very large group of soils (including the 'saprolites') where behavior (especially in slopes) is dominated by the influence of the discontinuities, fissures, etc.
	(b)Strong micro-Structure influence	completely weathered rocks formed from Igneous and sedi-mentary Rocks	Visual inspection, and evaluation of sensitivity liquidity index, etc	These soils are essentially homogeneous and form a tidy group much more amenable to systematic evaluation and analysis than group (a) above. Identification of nature and role of bonding (from relict primary bonds to weak secondary bonds) important to understanding behaviour
	(c)Little structural influence	Soils formed from very homogeneous rocks	Little or no sensitivity uniform appearance	This is a relatively minor sub-group. Likely to influence behave similarly to moderately overconsolida-ted soils
Group B Soils influenced by commonly occurring minerals	(a) Smectite (Montmorillonite group)	Black cotton soils, many soils formed in tropical areas in poorly drained conditions	Dark colour (grey to black) and high plasticity suggest soils of this group	These are normally problem soils found in flat (soils strongly or low strength, high compressibility, and high swelling and shrinkage characteristics.
	(b) Other Minerals			This is likely to be a minor sub-group.
Group C (soils strongly influenced by clay minerals essentially) found only in residual soils	(a) Allophane group	Soil weathered from volcanic ash in the wet tropics and in	Very high natural water contents, and irreversible changes on drying	These are characterized by very high natural water contents, and high liquid and plastic limits. Engineering properties are generally good, though in some cases high sensitivity could make handling and compaction difficult.
	(b)Halloysite group	Soils largely derived from older volcanic Rocks; especially tropical red clays	Reddish colour, well drained topography and volcanic parent rock are useful indicators	These are generally very fine grained soils, of low to medium plasticity, but low activity. Engineering properties are generally good, (Note that there is often overlap between allophone and halloysitic soils).
	(c) Sesquioxide group	This soils group loosely referred to as 'lateritic',	Granular, or nodular appearance	This is a very wide group, ranging from silty clay to coarse sand and gravel.

As a result of more extreme weathering conditions the chemical process may proceed more extensively and rapidly to produce destructive forms of residual soils. Laterites, which are extensively leached soils are an example of such soils (Gidigasu, 1976). In humid, tropical climates when intense weathering involving leaching occurs, soils rich in iron and aluminium oxides are left behind giving the soil a deep red colour and are referred to as laterites. Most of the depth of a residual soil will usually not be subject to laterisation. Because of their mode of formation, laterites usually occur as fairly shallow strata of limited depth. Laterites are often used as backfill for road and embankment construction. Saprolites are highly or completely weathered rocks that contain soil like materials but retain the original relic rock structure. Saprolites may occur in profiles of any depth. These altered residual soils are low in silica content.

3.5.5 Colluvium

Colluvium is generally referred to as sediments transported from their place of origin and deposited downslope by landslides, surface erosion, outwash, mud flow, debris flow or fluvial activity, amongst others. Fookes (1997) indicated that landslide debris is known to extend 1 to 2 kilometres across footslopes and accumulate over weathered to depths exceeding 10 metres. Residual soils are usually covered by 1 to 5 metres of colluvial sediment at the base of which is usually a resistant gravel deposit of up to 2 metres in thickness.

Fookes (1997) highlighted the diagnostic features of the transported soil horizons of colluvium to include : the absence of rock structure; selective sorting by particle size; weak stratification; fining downslope; absence or weak development of soil structure and presence of foreign rock material derived from upslope site.

The contact between colluvium and the residual soil is often marked with a difference in particle size distribution, colour and chemical composition. Colluvial processes are very active in Saint Lucia and have been encountered on many engineering projects on the island by this author. The colluvial deposits usually occur on the lower portion of slopes and they tend to have different engineering characteristics and behaviour than residual soils.

3.6 Rainfall-induced Landslides in Unsaturated Residual Soils

Extensive research studies have been carried out to investigate the correlation between rainfall and landslide activity in tropical regions. Toll (1990) proposed a framework for unsaturated soil behavior which incorporates total stresses and suctions in the soil based on the critical state model used for saturated soils. He pointed out that for unsaturated soils the soil fabric is not significantly damaged during shear and that total stress and suction contribute to shear strength by two stress ratios that are dependant on the degree of saturation of the soil. He also stated that the soil fabric is protected by matric suction and is maintained even under shear or compressive stresses. However, when the soil becomes completely saturated in a rainstorm and becomes unstable as highlighted in this study, matric suction is reduced to zero and the shear strength of the soil becomes greatly reduced and the soil fabric does become altered as failure occurs.

The effect of a high permeability zone in a residual soil profile consisting of pervious and impervious layers has been acknowledged and reported in the recent past by Terzaghi and Peck (1967) and I quote: " Within the zone of weathering of the insoluable types of rocks, it is by no means uncommon for the coefficient of permeability of the weathered rock to increase from very small values near the ground surface to maximum values close to the boundary between weathered and sound rock. Thus, the zone of rock weathering forms a relatively impervious skin resting on a pervious layer. If water enters the pervious layer through a gap in the skin or through open fissures in the sound rock, artesian conditions may develop in the pervious zone and the impervious top layer may slide down the slope even if the inclination is very gentle." This theory by Terzaghi and Peck is in support of the results of this study which deals with similar geological conditions with similar results.

Rulon and Freeze (1985) investigated the effect of seepage on heterogeneous slopes in a laboratory experiment which showed how complex saturated and unsaturated flow systems develop in materials of variable saturated hydraulic conductivity values that lead to the development of multiple seepage faces, perched water tables and unsaturated zones in the slope. They also showed how the hydrogeological setting in a slope contributes significaltly to the overall stability. The study clearly illustrated the pore pressure and hydraulic head distribution in the layered slope and how the various saturated hydraulic conductivity values of the materials generate multiple seepage faces that affect the stability of the slope. In their studies, Rulon and Freeze did not consider the rate at which saturation of the subsoils occurred and how slope failure may still occur due to the presence of hydrogeological features such as confined aquifers, even with the presence of the unsaturated wedge shaped zones in the upper soil layers.

Lam et al (1987) developed a transient seepage two-dimensional model for saturated – unsaturated soils which considers flow in both the saturated and unsaturated zones. Examples were drawn which showed that the phreatic line is not a flow line since it was shown that water flows across the phreatic line into the unsaturated zone. They showed that during the early stages of the infiltration process, water flows through the unsaturated zone based on the location of an impermeable layer of different saturated hydraulic conductivy than the surrounding soil. There was no attempt in their study to analyse the strength or stress behavior of the soil. Yeh and Harvey (1990) conducted a study to determine the hydraulic conductivity of unsaturated heterogeneous coarse, medium and layered sands by laboratory experimentation.

They used two homogeneous sands and one-layered sand composed of the two homogeneous sands and applied the steady state flux control method in their experiment. The averaged hydraulic conductivity of the two homogeneous sands was compared with the measured hydraulic conductivity of the layered sand. The results indicated that the mean of the hydraulic conductivity suction curves of the coarse and medium sands fitted the measured hydraulic conductivity suction curves of the layered sand.

According to Toll (1990) the effective stresses are difficult to define and examined from unsaturated tests within the critical state framework and that some approximation to an equivalent effective stress can be formulated which in some cases cannot be applied.
To solve this problem he proposed a critical state framework which treats the stress variables (q, $p - u_a$, $u_a - u_w$) separately and also incorporates the soil fabric. Toll states that the results of this model for unsaturated soil behavior incorporates stress state variables and the degree of saturation as a controlling variable.

Leong and Rahardjo (1997) examined the variable permeability functions available for unsaturated soils, namely; empirical equations, macroscopic models and statistical models. They expressed the advantages and limitations of each model and showed how the more sophisticated statistical model can be degenerated to the simpler empirical model by making simple assumptions which can result in the derivation of the coefficient of permeability indirectly from the soil-water characteristic curve. They showed that by using the lowest value of volumetric water content of the soil-water characteristic curve and the volumetric water content corresponding to the matric suction of 10^6 kPa, a better coefficient of permeability can be obtained by making simple assumptions.

Shen (1998) investigated the relationship between suction and slope stability in Hong Kong using field measurements of suction, development of a model for predicting change in pore water pressure and quantifying the effect of suction on shear strength. He concluded that for unsaturated residual soils a considerable amount of suction is contributed to shear strength due to dilatency of unsaturated soils as a result of aggregation of soil particles compared to saturated soil at the same confining total stress. In his study he found that in order to maintain specified suction values, the effective permeability had to be 2, 3 and 4 orders of magnitude less permeable than the soil. He postulated that the critical state line of the soil at constant suction changes a s suction changes and a critical state surface is formed in the three dimensional plot with suction included as one of the axes as a stress variable.

Ng and Shi (1998) performed numerical studies on the effects of rainfall on pore-water pressure in unsaturated slopes resulting in slope instability in Hong Kong. They included parameters such as intensity and duration of rainfall, saturated permeability, the presence of an impeding layer and conditions of surface cover. Based on the results of their study, they concluded that the response of negative pore-water pressure and the groundwater table is mainly controlled by the infiltration flux, saturated permeability, the slope of the soil-water characteristic curve and the boundatry conditions. They also found that for a given slope there exist a critical saturated permeability and a critical rainfall duration with regards to the effect of rainfall infiltration on slope stability.

Jiao et al (2000) showed the effect of a confined aquifer of high permeability material in a weathered rock profile generates high pore water pressures resulting in slope instability in Hong Kong. The hydrogeological characteristics of the weathered rock profile was found to contributed to deep seated slope failures in a conceptual model. They emphasize that in a high hydraulic conductivity zone at depth the groundwater level can rise even though the wetting front has not reached the groundwater level by infiltration through a more impermeable zone. This occurs when there is recharge from an uphill source which results in a build up of excess pore water pressures that may initiate slope instability. The effect of hydrogeological features at depth in residual soils is open for research sinc there is very little data on this phenomenon.

Gasmo et al (2000) conducted a parametric study to identify parameters that influenced rainfall-induced instabilities in residual soil slopes using the finite element seepage model SEEP/W and the limit equilibrium slope stability model SLOPE/W. He concluded that slope height and angle had little effect on the infiltration characteristics of the slope and that infiltration rates may be greater than the coefficient of permeability of the soil if the rainfall is of greater intensity than the coefficient of permeability. He also suggested that the transient pore water pressure distribution was the main triggering mechanism for rainfall-induced slope failures.

Tsaparas et al (2000) studied the influence of rainfall sequences on the seepage conditions in a residual soil slope using finite element seepage analysis. For this study it was assumed that infiltration was continuous and a unit flux boundary condition was applied along the surface of the slope. The results of the study showed that if 25 mm of antecedent rainfall is distributed continuously on the slope surface for a duration of 5 days, this would be the most significant contribution to pore water pressure increase during rainstorms. The critical slip surface was at a shallow depth of about 1.0m where the initial conditions were ineffective since at the end of the rainfall event the pore water pressures tend to become positive as air entry into the soil commenced.

Aung et al (2000) studied the microstructure characteristics of residual soils in Singapore and its influence on the soil water characteristic curve (SWCC). They concluded that the mineralogy and microfabric of residual soils control the slope of the SWCC due to more restricted range of micropore sizes. They found that the SWCC was flatter at greater depths at high matric suctions. Low et al (2000) measured infiltration and suction in a heterogeneous residual soil in Malayasia and suggest that prolong rainfall is more effective in triggering slope failures than heavy rainfall. They highlighted that geological features in the soil such as mineral veins assist in increasing rainfall infiltration and bare slopes caused a greater decrease in matric suction than grassed slopes.

Ng and Pang (2000) in their studies showed that for prolonged rainfall periods the analysis using a wetting Soil-Water Characteristic Curve would predict adverse pore-water pressure distribution with depth than those from a dry Soil-Water Characteristic Curve. They suggest in using a wet SWCC for infiltration problems. Yagi et al (2000) attempted to show some correlation between matric suction and slope failure by using critical rainfall to predict slope failure of an unsaturated soil slope in Japan. Field measurements of matric suction and rainfall were used to establish the initial conditions for predicting the critical rainfall required to initiate slope failure. A relationship was developed between matric suction and no-rainfall days from which they suggested that it is possible to determine the critical rainfall required to predict rainfall-induced slope failure.

Zhang et al (2000) used in situ experiments to show that the presence of geological discontinuities in rock joints can affect the infiltration pattern in slopes. They pointed out that in their research it was found that seepage through the more permeable joint zone which behaved as a ‘perched aquifer’ caused saturation of the surrounding soil even though the soil below the joint remained unsaturated. They also concluded in their study that where the lateral flow through the joint is greater than the discharge rate in a spring at the toe of the slope, excess pore water pressures tend to build up and the slope may fail quickly in response to rainfall even though the slope as a whole remains unsaturated.

They also pointed out that there may be a significant time lag between slope failure and infiltration from rainstorms if the groundwater table is located at a significant depth.

Toll (2001) investigated the occurrence of major and minor landslides in Singapore and found that the majority of landslides triggered by rainfall were shallow, less than 10m in height. He sighted that the conditions for slope failure are dictated by total rainfall, i.e antecedent and daily. He observed that the few major landslides (>10m) that were rainfall-induced occurred on slopes with angles greater than 27^{o}. He also cited that based on limited data, the conditions that would trigger major landslides in Singapore would be 320 mm of rainfall over a period of 16 days. In this research study it was found that in Saint Lucia the threshold for slope failure in colluvium from parent basalt rock was 120mm of rainfall over a 24-hour period. It was also found that the conditions that would generate major deep seated landslides in residual soils varied as experienced during Hurricane 'TOMAS' when major slope failures occurred during a 650mm rainfall event of 24-hour duration and there were residual slopes of variable steepness that withstood the 'stress test' of 'TOMAS" and did not collapse. Further research work is required into this phenomenon.

Bommer and Rodriguez (2002) conducted a study on earthquake-induced landslides in the residual and volcanic soils Central America and showed that rainfall played a role in the susceptibility of slopes to earthquake shaking and slope instability. However, they emphasized that the simultaneous effect of rainfall and earthquake shaking on slope stability requires further examination.

Chowdhury and Flentje (2002) examined the main uncertainties associated with the occurrence of rainfall induced landslides and found that spartial variability of site conditions, local geology and rainfall contribute significantly to the uncertainty of landslide hazard. They concluded that the assessment of hazard, vulnerability and risk required the use of observational approaches, the analysis of rainfall data and the relationship between rainfall magnituide and slope movement. Their study emphasizes the need for subsurface monitoring and the determination of threshold rainfalls that initiate landslide movement.

Ng et al (2003) in their study of the performance of an unsaturated expansive soil slope in Hong Kong found that high initial soil suctions occurred within the top 1.0m of soil which induced an upward flux of water both in the vertical direction and along an inclined slope. A downward flux of water and moisture occurred at depths greater than 1.5m. The pore water pressure responses, horizontal stress and soil deformation to rainfall showed a 1 – 2 day delay.

A perched water table developed at a depth of 1.5m which was attributed to the presence of tension cracks at depth. The presence of the perched water table led to a decrease in shear strength of the soil due to expansion of the dry soil upon wetting. However, the study did not include the effect of the findings on slope stability in numerical analysis.

Blatz et al (2004) used a transient time-dependant seepage modeling approach to assess the infiltration mechanism during a long period of rainfall that led to failure of two shallow slopes in Winnipeg, Manitoba, Canada. The study included field and laboratory investigations and advanced numerical modeling to determine the cause of failure. The modeling was done using SEEP/W and SLOPE/W to conduct combined seepage and slope stability analyses. The results of the study showed that the rainfall resulted in dissipation of matric suction which in turn caused a reduction in shear strength of the soil. They also concluded that the most significant parameter to determine the mode of instability was the environmental boundary conditions and the changes in soil suction.

Collins and Znidarcic (2004) developed a method for integrating rainfall into conventional slope stability analyses showing the various possible mechanisms of slope failure in saturated and unsaturated soils using the commercially available software SEEP/W and SLOPE/W.
In their study they used one-dimentional flow modeling and an infinite slope analysis to predict the triggering mechanism that initiate rainfall induced slope failure. They found that for coarse-grained soils with high infiltration rates will develop increased pore water pressure and failure will be initiated by seepage forces within the slope. On the other hand, for fine-grained soils with lower infiltration rates, slope failure would be as a result of a decrease in shear strength due to a reduction of matric suction. They also pointed out that the failure depth is controlled by the shear strength of the soil and also by the hydraulic conductivity of the soil.

Zan et al (2004) studied the effects of rainfall intensity, duration, rainfall pattern and evapotranspiration rate on infiltration and pore water pressure responses in China. The study concluded that infiltration into an unsaturated soil is dependant of the saturated permeability and the desaturation coefficient of the soil. At intermediate values of saturated permeability, rain water will infiltrate into the soil to some degree and will be retained resulting in a decrease in the pore water pressure. The desaturation coefficient controls the rate of decreasing pore water pressure or increasing matric suction. A clayey soil will have a lower desaturation rate than a sandy soil and the saturated coefficient of permeability decreases gradually with an increase in matric suction.

Zhang et al (2004) conducted an analytical analysis of rainfall in unsaturated soils and used three hydraulic parameters namely, the water storage capacity, the saturated permeability and the desaturation coefficient in expressing the soil-water characteristic curve. They concluded that the effect of the desaturation coefficient and the saturation permeability were much more significant than that of the water storage capacity. They discussed that the soil profile is significant in influencing the pore water pressure characteristics. For a soil profile composed of a permeable layer overlying a less permeable layer, the negative pore water pressure at the interface of the two layers may drop significantly and may become positive if the rainfall duration is large enough.

Cai et al (2004) used numerical analyses to determine the effect of rainfall on slope stability in Japan. Pore water pressures induced by rainfall were computed using transient seepage through unsaturated and saturated soils and a shear strength reduction technique was applied in the slope stability analysis. The results of the study indicated that the hydraulic charactersitics of the soil greatly influenced the increase in pore water pressure from rainwater infiltration causing a decrease in slope stability. The effect of matric
suction on the stability of the slope decreased and eventually disappeared as the soils became saturated by rainfall infiltration. They noted that slopes with low permeability soils failed only if the rainfall lasted for a long enough period regardless of the intensity. Slopes with highly permeable soils failure took place during short periods of rainfall with a greater intensity.

Li et al (2005) conducted field measurements of soil moisture and matric suction in a residual soil in Hong Kong in a study of rainfall-induced slope failures. They observed that the advance of the 'wetting front' was dependant on rainfall intensity, the unsaturated hydraulic conductivity function and initial water content of the soil. Infiltration caused by the antecedent rainfall contributed to the decrease in matric suction and an increase in the pore water pressures in the soil causing a rise in the groundwater table resulting in a reduction in shear strength and slope instability. The results of their experiments in analyzing rainfall infiltration indicated that the infiltration rate was about 70 % of the total rainfall and that rainfall infiltration mainly increased the soil moisture content.

Studies by Rahardjo et al (2005) on the response of a residual soil slope to rainfall in Singapore showed that a rainfall may contribute 40 % to 100 % of its total volume as infiltration depending on the amount of precipitation. The percentage of rainfall contributing to infiltration decreases with an increase in the rainfall amount. In the study infiltration, runoff and pore water pressure increase due to rainfall were shown to be influenced by antecedent rainfall. They emphasize that in their study the characteristics of the rainfall process, runoff, and pore water pressure changes had relevance to rainfall-induced instability in residual soil slopes.

Tohari and Sarah (2006) conducted a study on the effect of hydrologic factors on the stability of steep volcanic residual soil slopes in Indonesia. Their objectives were to determine the soil-water characteristic curve and unsaturated permeability function for the volcanic residual soil; determine the unsaturated shear strength function for the volcanic residual soil and evaluate the stability of the slope during rainfall. The results of their study showed that the volcanic residual soils at the study site showed low air-entry values of about 10 kPa and a high effective friction angle of 35o and a matric suction, ϕ^b, of 10^o which decreased at matric suction values higher than the air-entry value of the soils.

They also found that infiltration of water did not cause an increase in the groundwater level, but formed a perched watertable near the ground surface and that prolonged suction in the slope contributed to the stability of the slope during rainstorms.

Gofar et al (2006) examined the mechanism causing a slope failure in Indonesia using transient seepage analyses in a combination of VADOSE/W and SLOPE/W 2002 software.The study utilized field observation and available documented data and the seepage pattern and seepage forces were were computed in VADOSE/W then imported into SLOPE/W for stability analysis. The results of the study showed that the formation of tension cracks on the slope during the dry season allowed faster infiltration of surface water into the slope causing seepage forces to develop and flow along the soil layers. This resulted in an increase in the soil moisture content and hence a reduction in the shear strength of the subsoils which initiated slope failure. Therefore, it was assumed that the presence of the tension cracks accelerated infiltration and failure of the slope which would not have occurred if there were no tension cracks on the surface of the slope.

Yang et al (2006) conducted laboratory studies to determine the behavior of unsaturated layered finer over coarser soils during infiltration. They concluded that rainfall of higher intensity and longer duration increased the pore water pressure build-up in the finer soil more than rainfall with lesser intensity and shorter duration before steady-state infiltration was reached. This applied for conditions when the rainfall intensity was either greater or lesser than the saturated hydraulic conductivity of the finer soil. In addition, they found that at the initial stage of infiltration the infiltration rate could be higher than the saturated hydraulic conductivity of the finer soil layer due to the large hydraulic gradient.

Sassa et al (2010) developed an integrated model that simulates the initiation and motion of earthquake and rain –induced rapid landslides in their study of a landslide mass of 36 million m3 that killed over 1,000 people in the Phillipines in 2006. They found that heavy rainfall occurred the day before the landslide but was not the triggering mechanism that caused the landslide. A small earthquake occurred five days after the rainfall and they concluded that the seismic event triggered the slide. The seismic event did not occur simultaneously with the rainfall. From this author's perspective, it is unlikely that an earthquake event will occur simultaneously with a rainstorm and the case to ignore earthquake loading of saturated natural slopes during rainstorms need to be developed by further research.

The numerical analyses conducted by the various researchers listed above indicate the complex nature of infiltration and seepage in residual soils and show that further research is required to fully understand these mechanisms and how they affect the stability of natural and man-made slopes in tropical terrain. Currently, there is no single and solitary explanation for these mechanisms and researchers are working steadily to achieve a solution. While one researcher's theory may be in conflict with others, constructive criticism is necessary and helpful in achieving common understanding of the infiltration and seepage processes despite current limitations. Various factors have been shown to contribuite to rainfall-induced slope instability in addition to rainfall intensity and duration. The antecedent soil moisture and saturated hydraulic conductivity of the soils also play a major role in the infiltration and seepage processes in residual soil slopes and additional research work is necessary, particularly in the study of infiltration and infiltration into multi-layered residual soil slopes.

3.7 Preliminary Research Study on The Barre de L'isle Ridge in Saint Lucia

During the period of October 1978 – October 1984, a research project was carried out on the Barre de L'isle mountain range in Saint Lucia by Professor M.G. Anderson and M.J. Kemp of Bristol University in the United Kingdom, to monitor Pore Water Pressure Conditions in Road Cut Slopes in Saint Lucia. The project was referred to as Research Scheme R3426 and was financed by the British Overseas Development Administration.

The objectives of the study were as follows:

a) the development of field instrumentation suitable for the monitoring of both positive and negative pore pressures in road cut slopes in developing countries.

b) the development of a prediction model for soil suction and positive pore pressures in residual soils based on readily available field data.

c) to evaluate whether, for the particular slope materials examined, soil suction was required for slope stability at any point along possible failure surfaces.

d) to examine the impact of material property variability upon from objective (c)

e) to determine whether in the context of stability analyses of residual soils, any field guidelines could be established for cut slope design that did not entail a full and detailed laboratory and site investigation approach that is standard practice in the developed world.

The research project was divided into four phases, namely :

a) that of establishing a field site area and securing Government approval and assistance in the field.

b) the development of field monitoring methods for soil suction/ pore pressure monitoring. This was undertaken at Bristol University and selected aspects were investigated at Bedford College, University of London.

c) establishment of a field investigation programme in Saint Lucia, for both soil suction/pore pressure and soil strength monitoring having secured the necessary agreements in (a) above.

d) laboratory strength testing at Bristol University.

The sites selected for the study were located on the Barre de L'isle mountain ridge along the main east coast road link between the capital city of Castries and the eastern and southern sections of the island. A total of ten (10) sites were selected for the study with field work being carried out between the period of September 1978 – September 1981. The location of the sites are shown in Figure 3.8 and Figure 3.9.

Figure 3.10 shows the plan layout of Site No. 10.

The field instrumentation used for this research project included the following:

i) Portable transducer/Digital voltmeter (DVM) system
ii) Transducer and single tensiometer system for continuous monitoring of soil water potential
iii) Jetfill Tensiometers
iv) Automatic Scanivalve
v) Standpipe piezometers
vi) Autographic raingauge

i) The portable transducer/DVM system was capable of responding as rapidly as possible to soil water potential changes triggered by relatively high frequency, short duration tropical storms and should be free from significant disturbances induced by relatively high temperatures and humidities.

ii) The transducer and single tensiometer system was used to record soil water potentials on a continuous basis in order to ensure that the 'worst' pore water pressure conditions could be detected. This equipment could only be used for 'spot' sample readings.

iii) Jetfill Tensiometers have the advantage of direct reading of pore pressures from the gauge at the top of the instrument. They are inexpensive and can be de-aired from the plunger at the top of the instrument

iv) The Automatic Scaniclave represents a more complex system which can record both positive and negative soil water potentials from 22 tensiometers at variable time intervals and requires minimal manual attention since data is recorded on paper from a solid state cartridge

v) Standpipe piezometers were installed to monitor groundwater level response to infiltration.

vi) The autographic raingauge was used for accurate precipitation monitoring. It was initially installed at the top of the Barre de L'isle but later relocated to one of the study sites.

Soil sampling consisted of obtaining undisturbed samples for direct shear and triaxial testing. Thin walled tins were designed to recover the samples of dimensions 100mm x 100mm x 30mm for direct shear testing. The tins were designed with sharp edges and were steadily pushed into the soil. Once filled with soil, the tins were dug out of the ground and sealed air tight with wax. Cylindrical samples for triaxial testing were of dimensions 100mm x 200mm x 200mm and were recovered in galvanized tubes designed with sharp edges and pushed into the soil until full of soil. The tubes were then dug out and waxed. The recovered soil samples were transported to the United Kingdom for laboratory testing at Bristol University.

Anderson and Kemp (1985) used the soil water potential data recovered from the field instrumentation installed at the ten (10) sites during the period of 1978 – 1982, to develop pore water pressure prediction models based on storm rainfall, material permeability and soil water potential responses.

The criteria used for the development of the prediction models were as follows;

a) predictions using Material Permeability and Storm Precipitation for Straight Slopes

b) predictions using Qualitative and Quantitative Site Factors and Storm Precipitation

c) the influence of Slope Plan Curvature on Soil-water Potentials

a) Predictions Using Material Permeability and Storm Precipitation for Straight Slopes

Anderson and Kemp (1985) plotted the pore pressures collected in the data base for the straight slopes in sites 1-9 from 1978 – 1982 against total storm rainfall and material permeability to produce the graph shown in Figure 3.11 which shows the relationship between soil water potential and rainfall. The grouping of pore water pressure (soil-water potential) values recorded when plotted in association with total storm precipitation and material permeability are illustrated in the figure.

The figure illustrates that there is an increase in negative pore water pressures when rainfall intensity decreases for soils of high permeability. They used this information to develop a statistical multiple regression model for soil water potential (ψ) at 60 cm depth at the slope base as a function of storm precipitation (p,mm) and soil permeability (k,cms^{-1}).

The model was developed from 82 observations:

$$\Psi_{60} = - 324.32 + 0.85\ p – 48.65 \log k \qquad (1)$$

Figure 3.12 shows the actual and predicted soil water potential results for the nine (9) sites.

b) Predictions using Qualitative and Quantitative Site Factors and Storm Precipitation

In the case of Site 1 which was located in a topographic depression, Anderson and Kemp (1985) used a procedure which included this anomaly into the predicted model. They assigned each site to a group which they defined as both qualitative and quantitative by assigning dummy variables to each group. The results of this procedure produced the following equation to represent the regression model which shows the relationship between storm precipitation and soil-water potential for the 82 observations :

$$\Psi_{60} = - 36.36 – 9.99D_1 – 180.21D_2 – 109.69D_3 + 57.53D_4 + 0.56p - 012D_1p + 0.60D_2p + 0.65D_3P – 0.30D_4p \quad \text{(for p = 0.001 level)} \qquad (2)$$

Where,

Ψ = soil water potential

Figure 3.13 shows the graph produced when actual versus predicted values are plotted.

Soil water potential indicates the tendency of soil water to move due to gravity, osmosis, pressure or surface tension. It is defined as the work water can do as it moves from its present state to the reference state. The reference state is the energy of a pool of water at an elevation defined to be zero i.e. when all pores are filled with water. As the soil dries out, soil water potential decreases and becomes increasingly more negative. When the soil water potential is high, it means that soil water is held loosely, is highly available and ready to move elsewhere.

Anderson and Kemp (1985) state that this model is capable of incorporating groups of different characteristics to predict the pore-water pressures from storm precipitation and site topography.

c) The Influence of Slope Plan Curvature on Soil-water Potential

In cases where the road-cut topography varied to that of a straight slope, Anderson and Kemp (1985) used three statistical analyses to describe the effect of variable site topography on pore-water pressure generation. They developed models for each permeability group using partial correlations and multiple regression:

i) Partial Correlations

By subdividing the sites into three permeability groups (10^{-3}, 10^{-4} and 10^{-6} cms^{-1}), they derived some correlation between slope plan curvature and soil-water potentials, ($r_{\psi c.p.}$).
They showed that when the effect of precipitation is controlled, slope topography and soil-water potentials are closely associated and the dominating topographic element is slope plan curvature. The partial correlation for the three permeabilities are shown in Table 3.4.

Table 3.4 Partial Correlations (After Anderson and Kemp, 1985)

Permeability Group ($cm\ s^{-1}$)	Partial Correlations[a]					Sample Size
	$r_{\psi a.p}$	$r_{\psi l.p}$	$r_{\psi c.p}$	$r_{\psi c.pa}$	$r_{\psi a.pc}$	
10^{-3} ($5 \times 10^{-4} - 5 \times 10^{-3}$)	0.17	0.78***	0.81***	0.81***	0.31	47
10^{-4} ($5 \times 10^{-5} - 5 \times 10^{-4}$)	0.66***	-0.22	0.66***	0.15	0.91***	36
10^{-6} ($9 \times 10^{-7} - 5 \times 10^{-5}$)	-0.64***	-0.01	0.56***	0.02	-0.93***	51

*** Significant at 9.99 per cent level

[a] For example, $r_{\psi a.p}$ correlation between soil-water potential (y) and slope angle (a) with precipitation (p) controlled (l is slope length, c is slope curvature.

Table 3.4 shows that when precipitation, (p) and slope angle, (a) are controlled, the relationship between soil-water potential, (ψ) and slope plan curvature, (c) is significant at high permeability, whereas when 'p' and 'c' are controlled, the ψ-a relationship is significant for low permeability soils.

ii) Multiple Regression

Using topographic slope characteristics and slope plan curvature as basic controls over soil-water potentials, Anderson and Kemp (1985) formulated a multiple regression analysis to developed a predictive model, using soil-water potential (ψ) as the dependant variable for each permeability group and the topographic indices slope angle (a), slope plan curvature (c) and slope length (l), as independent variables.
The prediction equations for each saturated permeability group are:-

k : 1×10^{-3} cm s^{-1} $y = -165.78 + 0.75p + 3.08c$

k : 1×10^{-4} cm s^{-1} $y = -136.15 + 0.72p + 1.69c$

k : 1×10^{-6} cm s^{-1} $y = -31.83 + 0.45p + 0.54c$

Table 3.5 provides the explained variance and significance for each of the nine (9) sites.

Table 3.5 Significance Levels and Coefficients of explanation (%) for Multiple Regression relationships between Permeability and Precipitation and Site Topographic indices for the three (3) Permeability Groups (After Anderson and Kemp, 1985)

Permeability groups (cm s-1) (saturated)	Independent variables (%)			Sample Size
	p.a	p.l	p.c	
1 x 10 $^{-3}$	22**	83***	87***	47
1 x 10 $^{-4}$	70***	70***	70***	36
1 x 10 $^{-6}$	66***	43***	62***	51

Significant at 99 %; * Significant at 99.9 % (based on F test).
Note: p = storm precipitation (mm); a = slope angle (degrees); l = slope length (m); c = slope plan curvature (degrees). Largest storm precipitation included 203 mm, having an estimated recurrence interval of 12 years (Anderson 1981a).

Figure 3.14 illustrates the three (3) equations and how soil-water potential (y) increases in the more permeable materials based on the effect of slope plan curvature (c). Alternatively, materials of lower permeability show very little change in soil-water potential for given changes in slope plan curvature. Direct shear strength tests were carried out on four (4) undisturbed soil samples from four (4) of the study sites. The strength parameters c and ϕ for saturated drained peak and saturated drained residual are summarized in Table 3.6.

Table 3.6 Direct Shear Strength Test Results (After Anderson and Kemp. 1985)

Location	Peak Strength c (kPa)	Peak Strength ϕ (degrees)	Residual Strength c (kPa)	Residual Strength ϕ (degrees)
Site 3	6.8	36.72^o	2.22	34.97^o
Site 5	6.35	35.0^o	2.99	29.0^o
Site 7	13.8	25.78^o	4.60	16.8^o
Site 10	----	----	6.00	30.9^o

Suction controlled triaxial tests were also conducted in the laboratory on the recovered soil samples from the above noted sites in Table 3.6

Table 3.7 contains a summary of the tests results.

Table 3.7 Suction Controlled Triaxial Test Results (After Anderson and Kemp, 1985)

Location	Cell Stresses (kPa) σ_1	Cell Stresses (kPa) σ_3	Pore Water Conditions at Failure Threshold suction/pressure
Site 3	68.5	11.4	1 kPa Suction
Site 5	52.0	5.5	1 kPa Suction
Site 7	58.5	6.9	0 + 1 kPa Pressure
Site 10	112.0	30.0	0 kPa Suction

Anderson and Kemp (1985) used the results of the laboratory tests to conduct stability analyses on the slopes at the study sites in Saint Lucia to determine the factor of safety on critical slip surfaces using the Bishop Modified Method (1955).

The method of slices was used to calculate the factor of safety using the following expression:

$$F = \frac{\{ c^1 b + \tan \phi^1 (W - ub + x_n - x_{n+1}) \}}{1 + \tan\phi^1 \tan\alpha}$$

$$W \tan\alpha \qquad \frac{F}{1 + \tan^2\alpha}$$

Where;

F	=	factor of safety
x_n and x_{n+1}	=	co-ordinates of the slice
W	=	weight of slice
b	=	length of slip surface at base of slice
u	=	pore water pressure
α	=	angle tangent to the base of the slice

Groundwater levels used in the stability analyses assumed a worst case condition for the three (3) study sites corresponding to a storm event of at least one (1) in 1 year occurrence. Hydrostatic pore water pressures exist on the slip surface below the assumed groundwater levels and hydrostatic suction was defined above the groundwater levels in the stability programme such that the suction on the slip surface increased hydrostatically to the specified maximum, above which it remained constant.

The maximum suction applied varied from 0 kPa to 70 kPa. The results of the slope stability analysis for sites 3, 5 and 7 are shown in Figure 3.15 – Figure 3.17.

The slope at Site 10 failed in 1979 and was stabilized with gabion basket retaining structures. Anderson and Kemp (1985) performed stability analyses on this slope using both circular and non-circular slip surfaces and variable groundwater level conditions.

The results of the stability analysis is summerised in Table 3.8

Table 3.8 Computed Factors of Safety for Site 10 (After Anderson and Kemp, 1985)

Slip surface Type		Groundwater Level – Depth Below Surface (m)			
(Method of Analysis)		0.0	0.5	1.0	1.5
Non – Circular (Janbu)	F.S. =	0.986	1.051	1.111	1.147
Circular (Bishop)	F.S. =	1.193	1.286	1.301	----

The slope profile at site 10 is shown in Figure 3.18

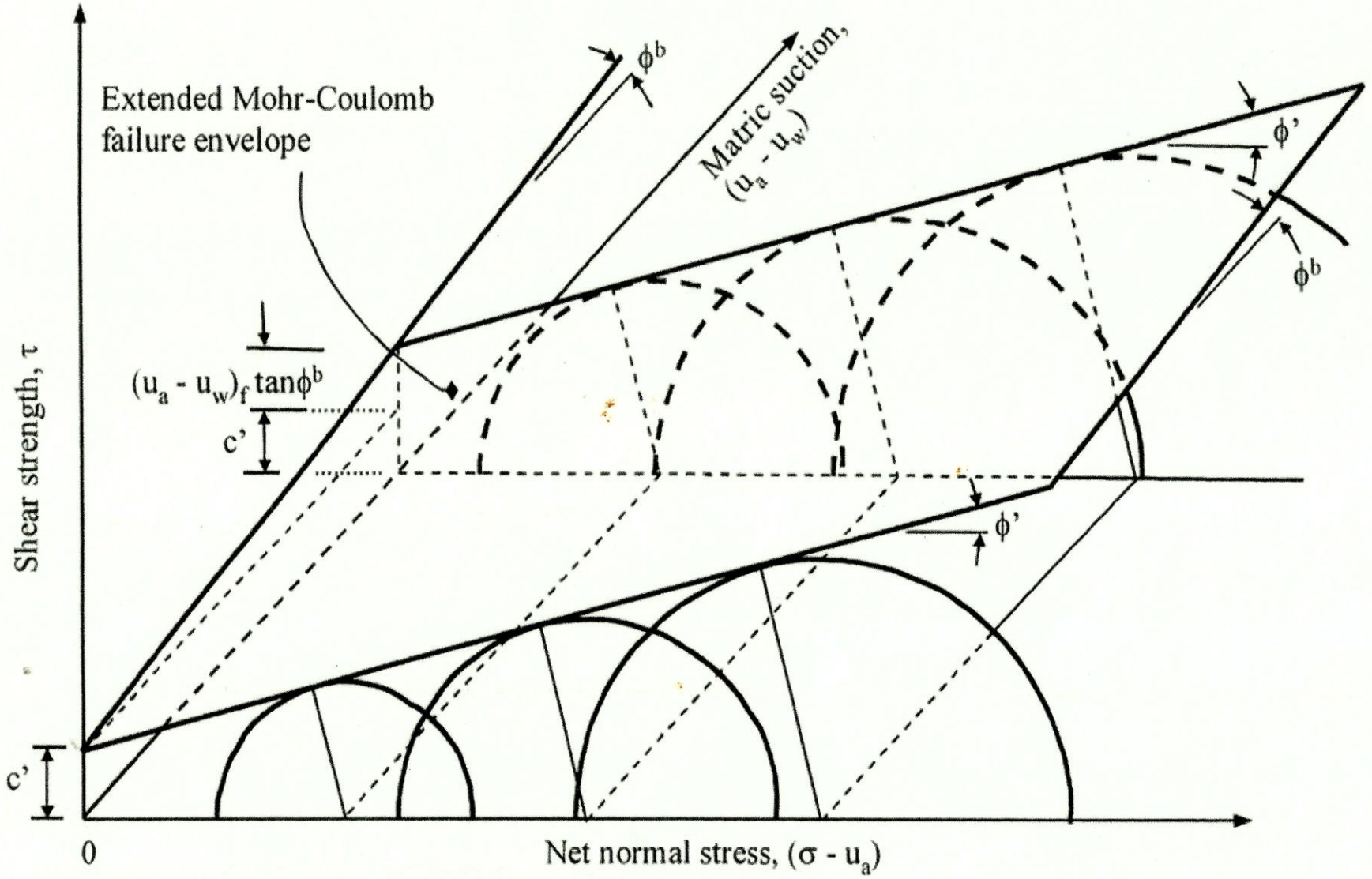

Figure 3.1 Extended Mohr Diagram for Unsaturated Soils (AFTER Fredlund and Rahardjo, 1993)

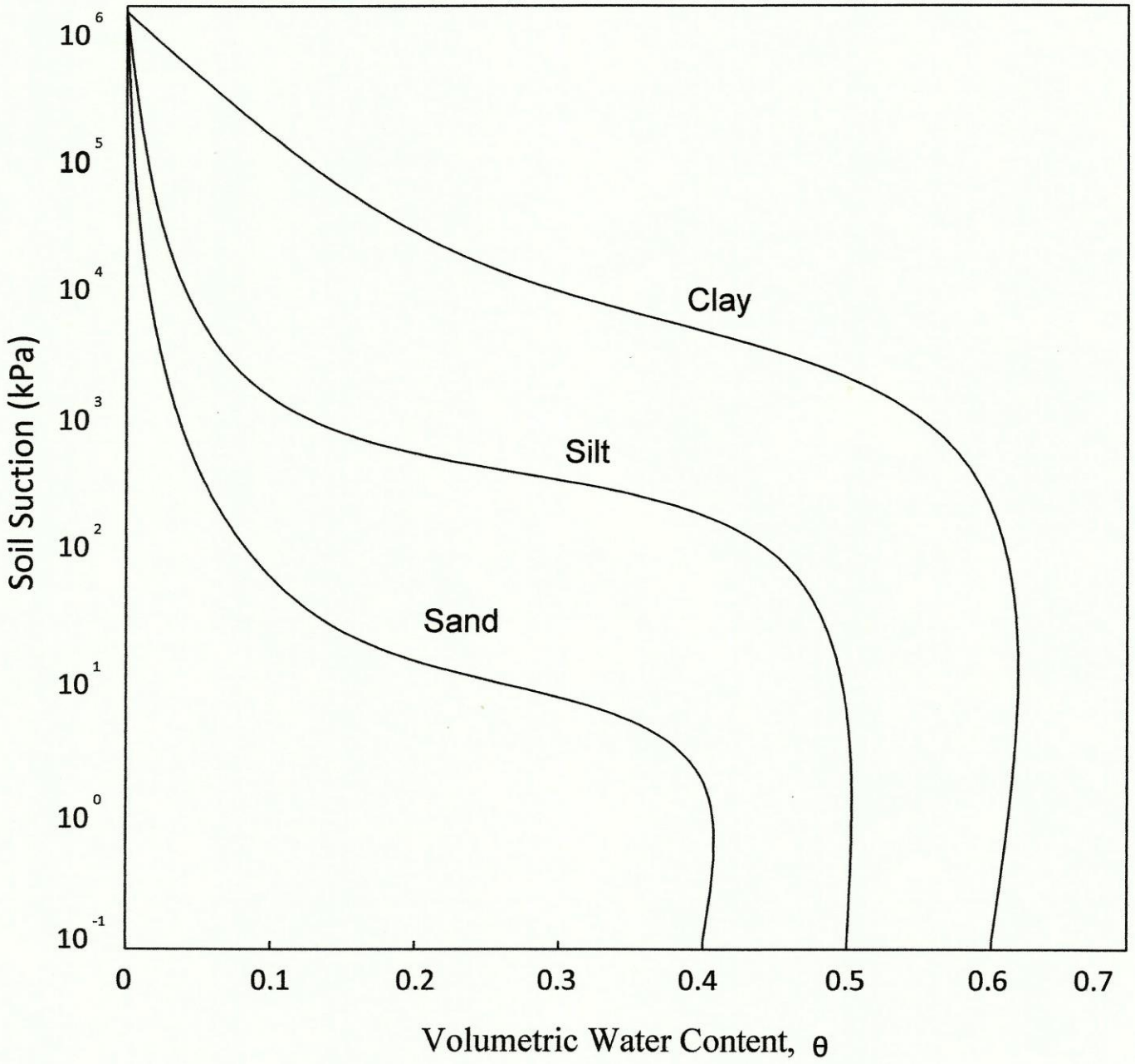

Figure 3.2 Soil water characteristic curve for sand, silt and clay (after Lu and Likos, 2004)

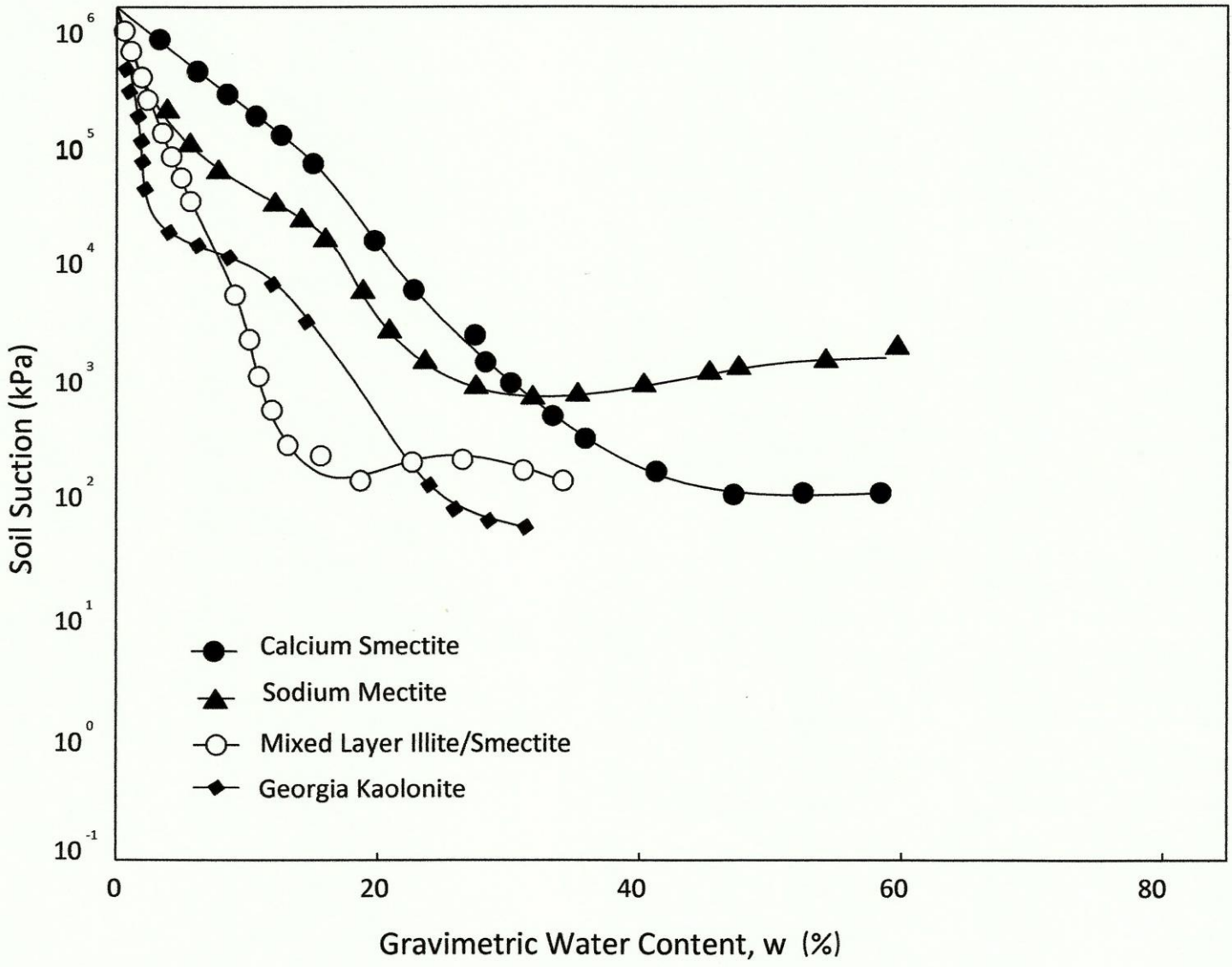

Figure 3.3 Soil water characteristic curve for four types of clays in a high suction range (after Likos, 2000)

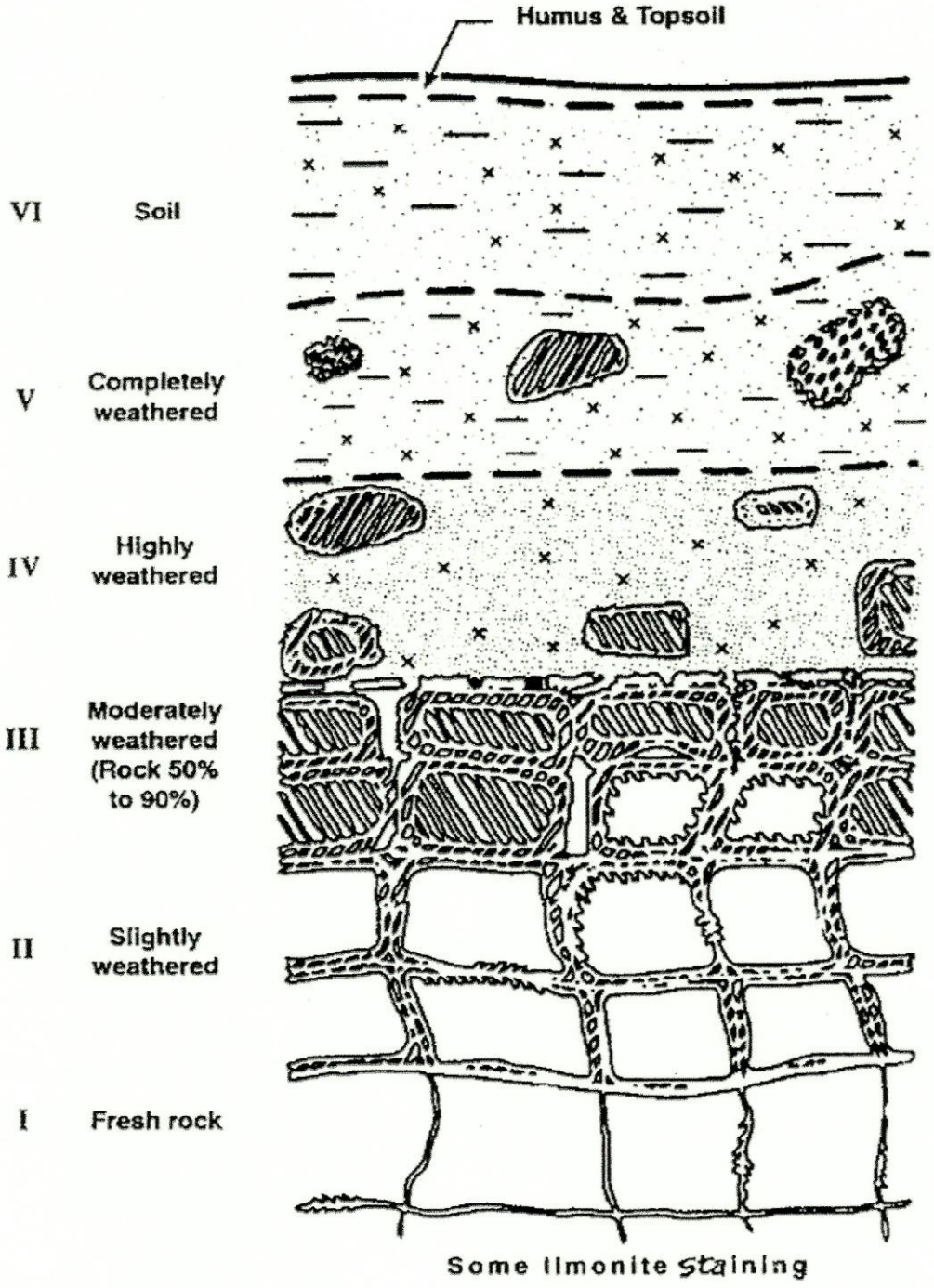

Figure 3.4 Classification of Residual Soils by the Degree of Weathering (After LITTLE, 1969)

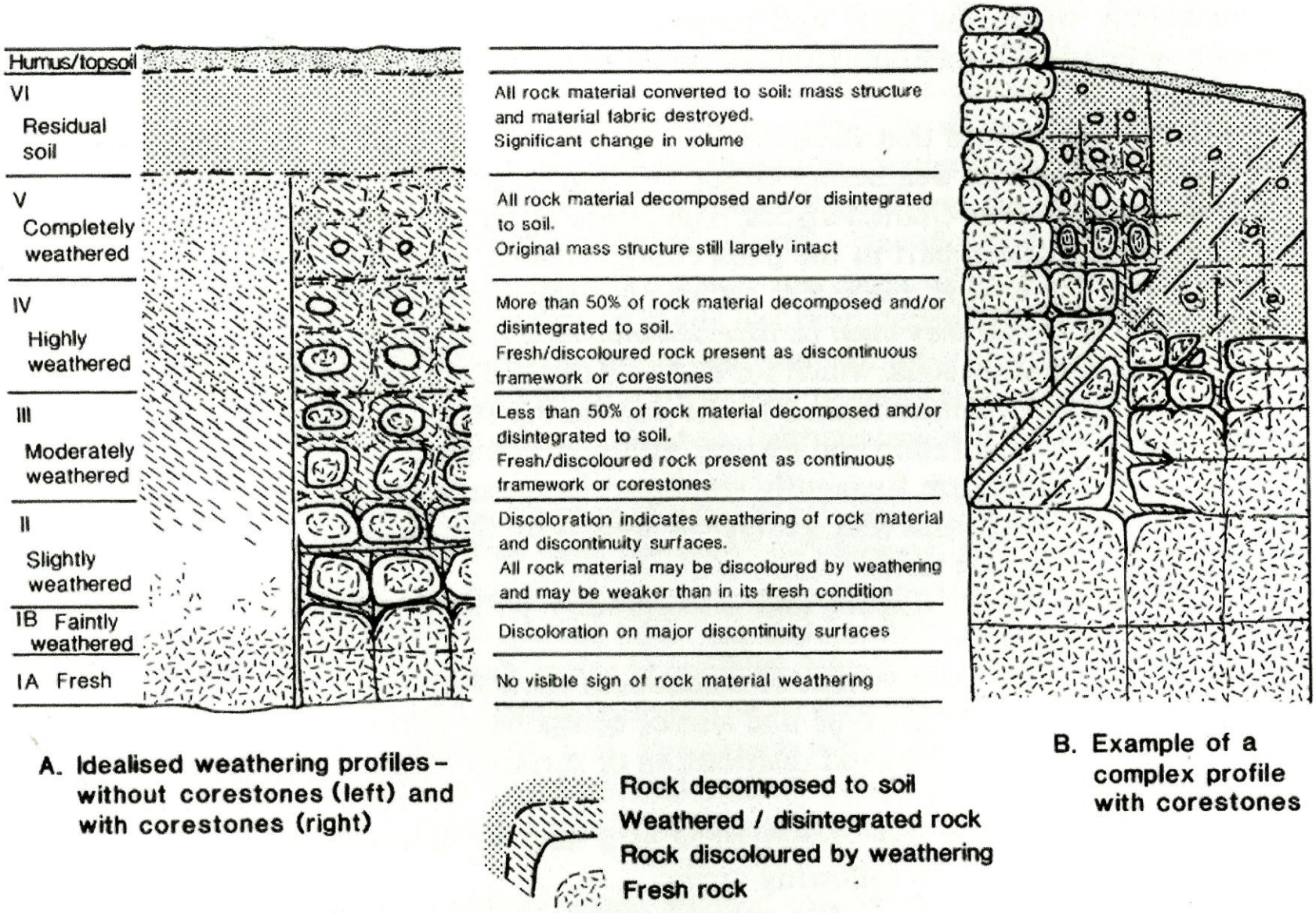

Figure 3.5 Scale of Weathering Grades of Rock Masses (After Wesley, 1988)

Figure 3.6 Weathering Grades of Andesite Formation At RG Quarry, Saint Lucia

1-residual soil
2-highly weathered
3-moderately weathered
4-slightly weathered
5-fresh rock

Figure 3.7 Cut in residual soil slope at RG Quarry, Saint Lucia

Figure 3.8 Location Map (After Anderson and Kemp, 1985)

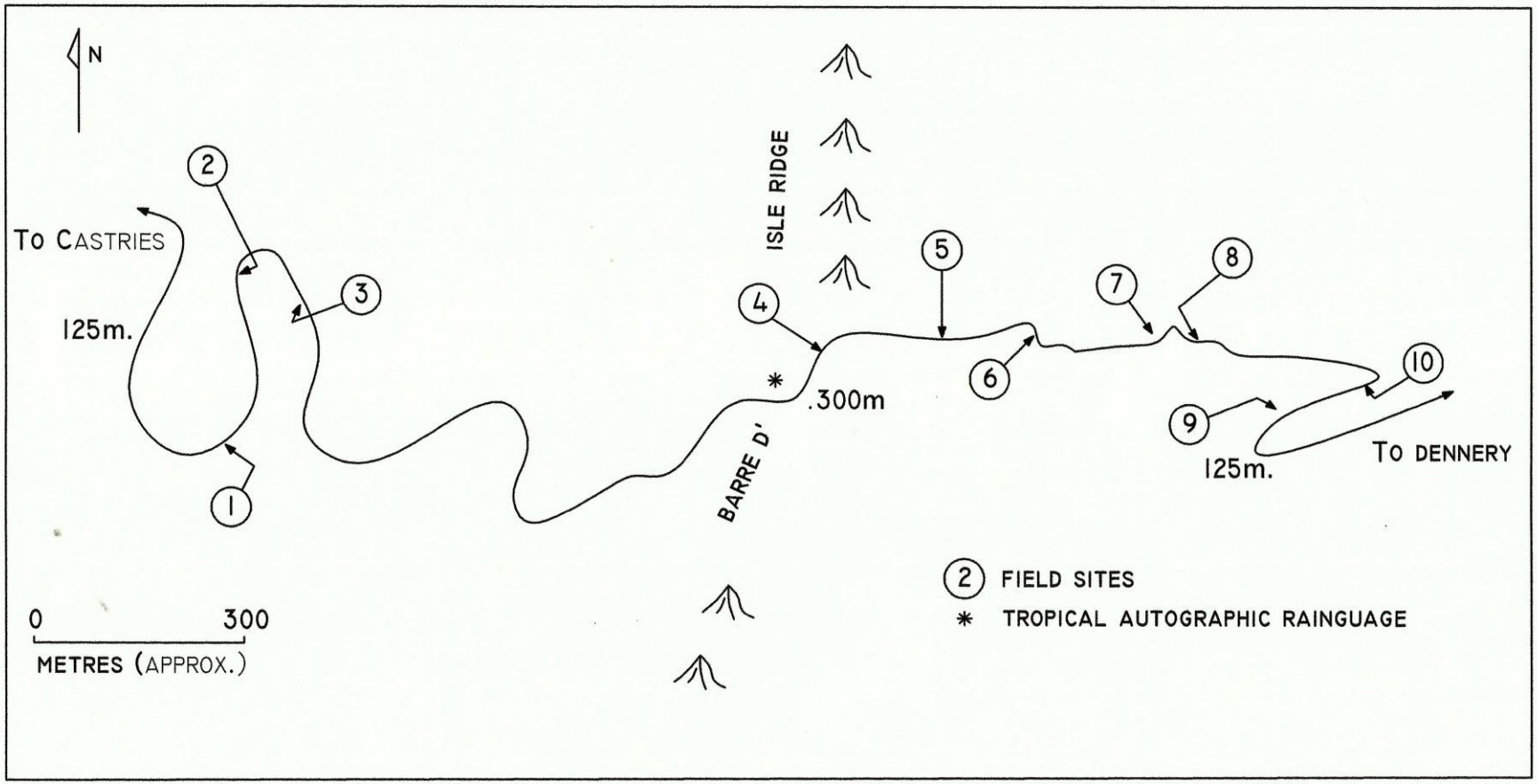

Figure 3.9 Field Sites (After Anderson & Kemp, 1985)

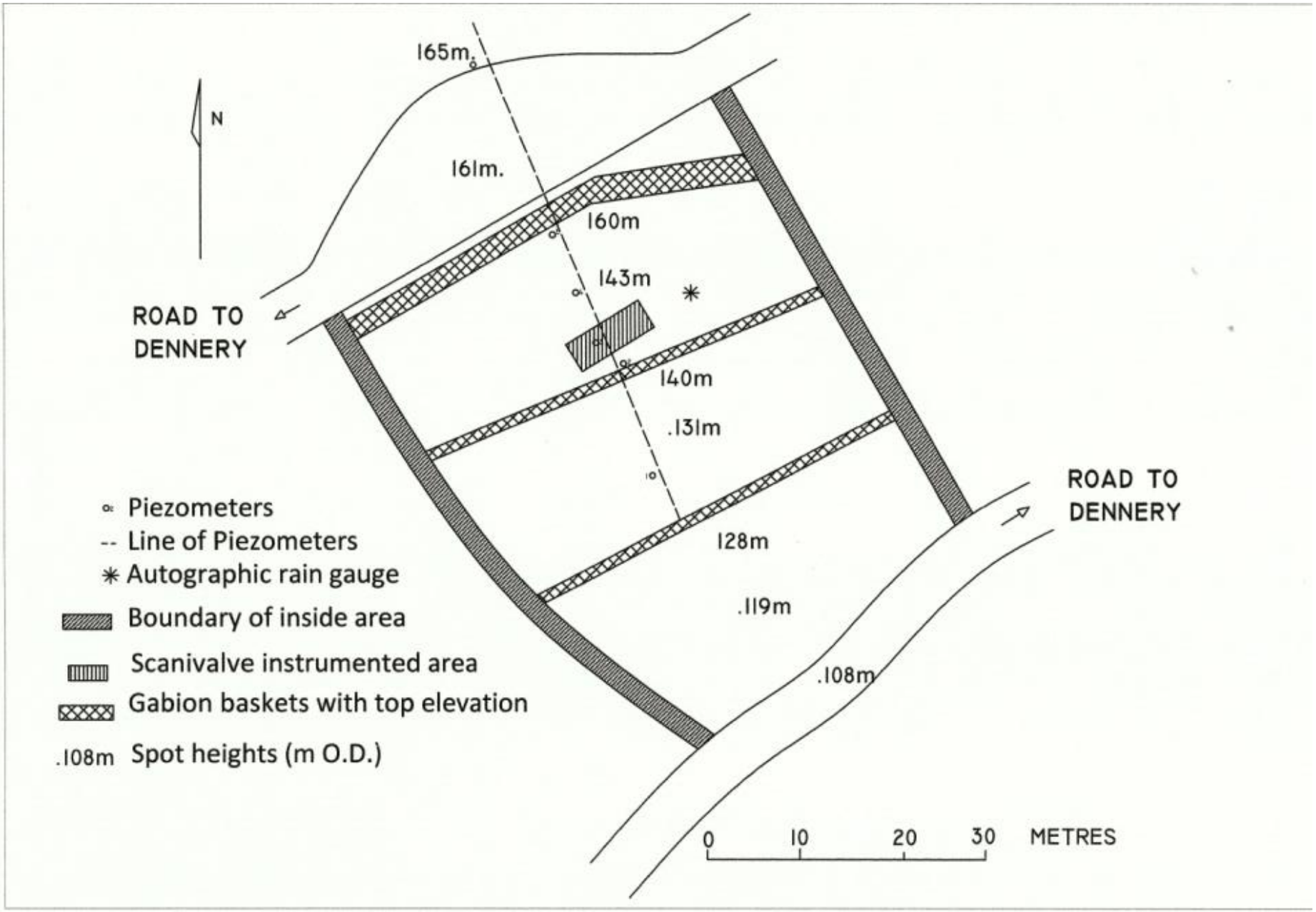

Figure 3.10 Site : 10 Plan of instrumentation (After Anderson & Kemp, 1985)

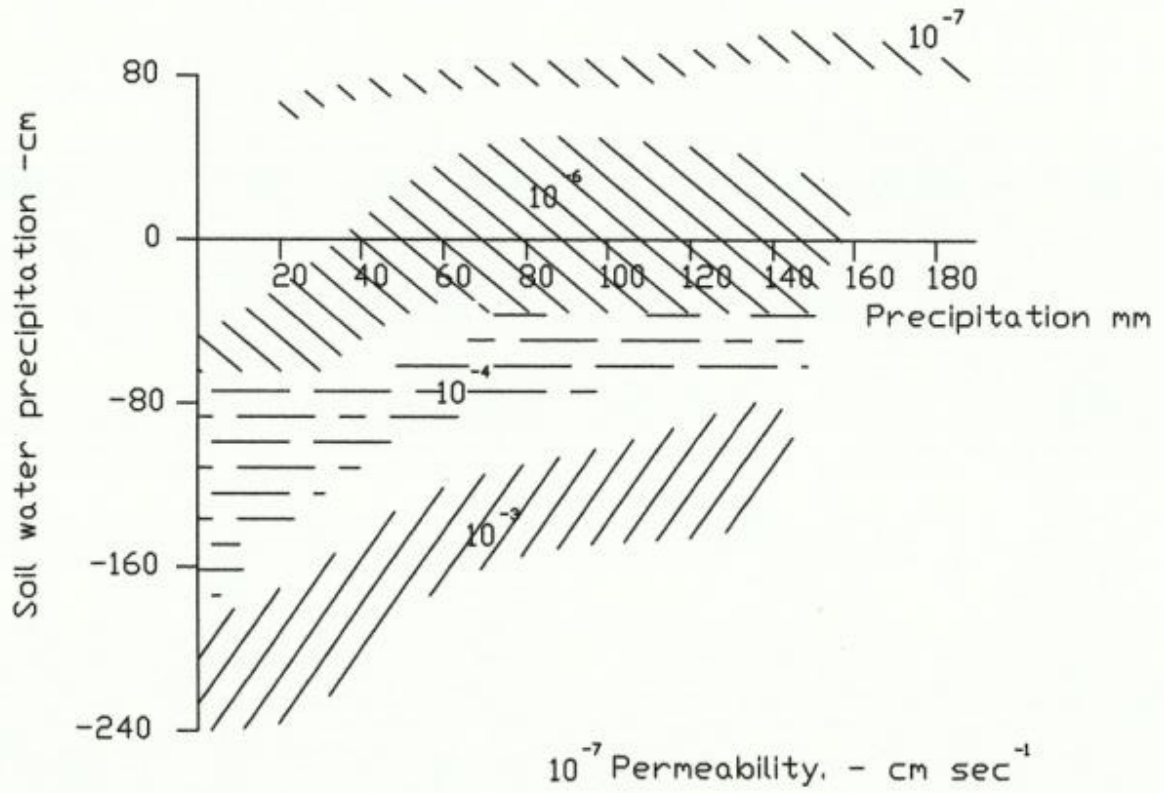

Figure 3.11 Relationship of permeability, precipitation and soil-water potential

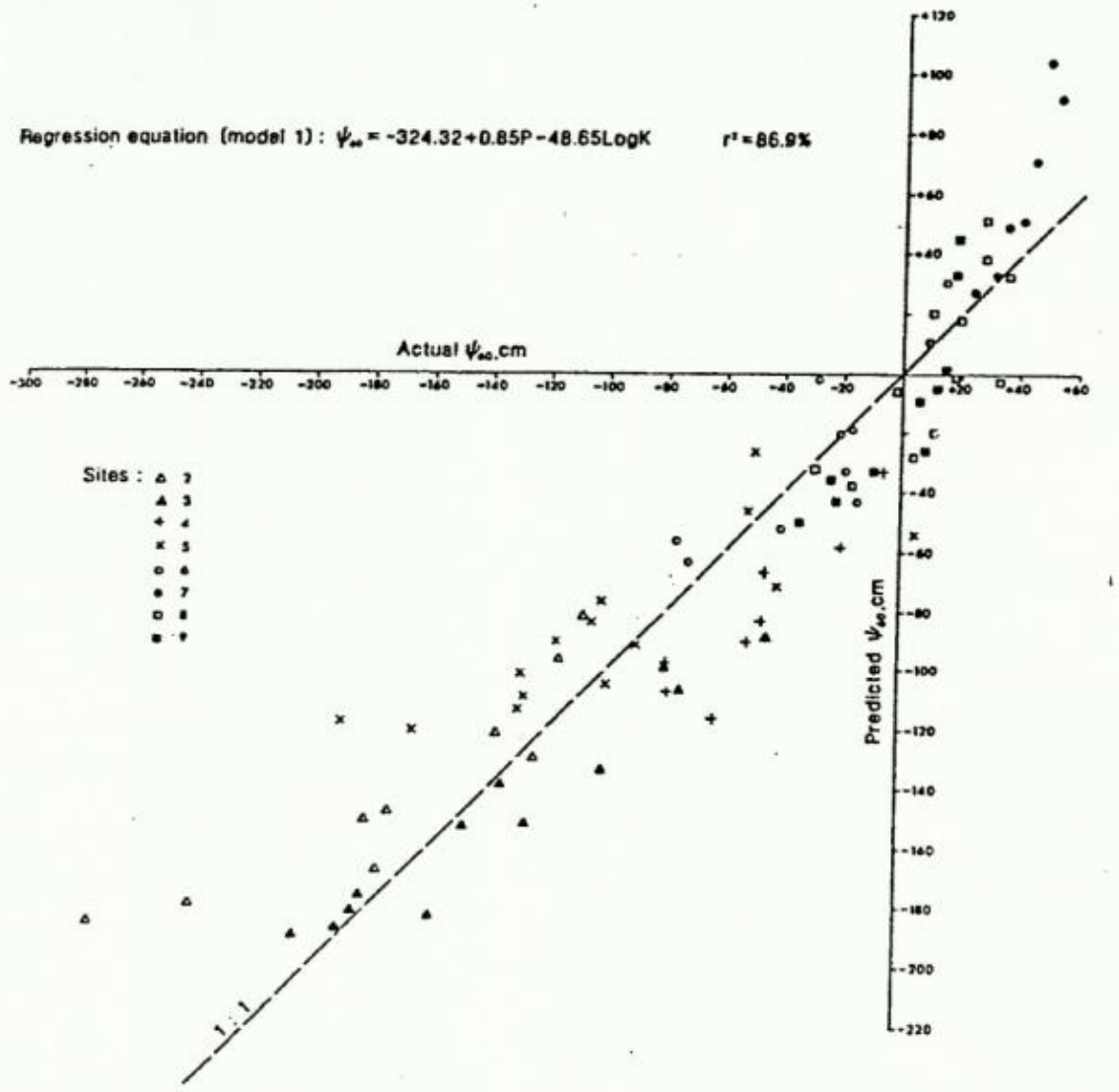

Figure 3.12 Actual and Predicted (equation 1) Soil-water Potentials (After Anderson and Kemp, 1985)

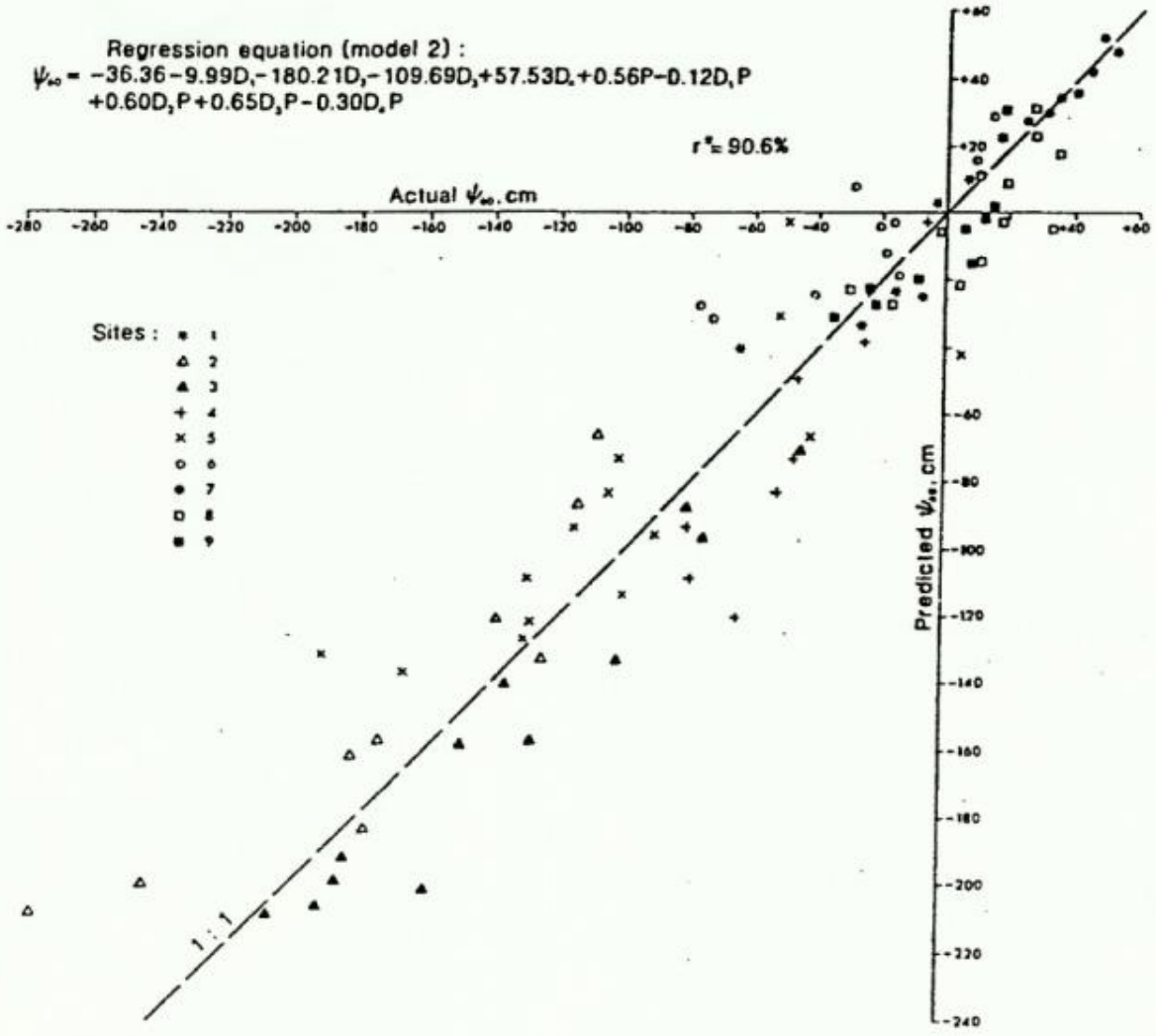

Figure 3.13 Actual and Predicted (equation 2) Soil-water Potentials (After Anderson and Kemp, 1985)

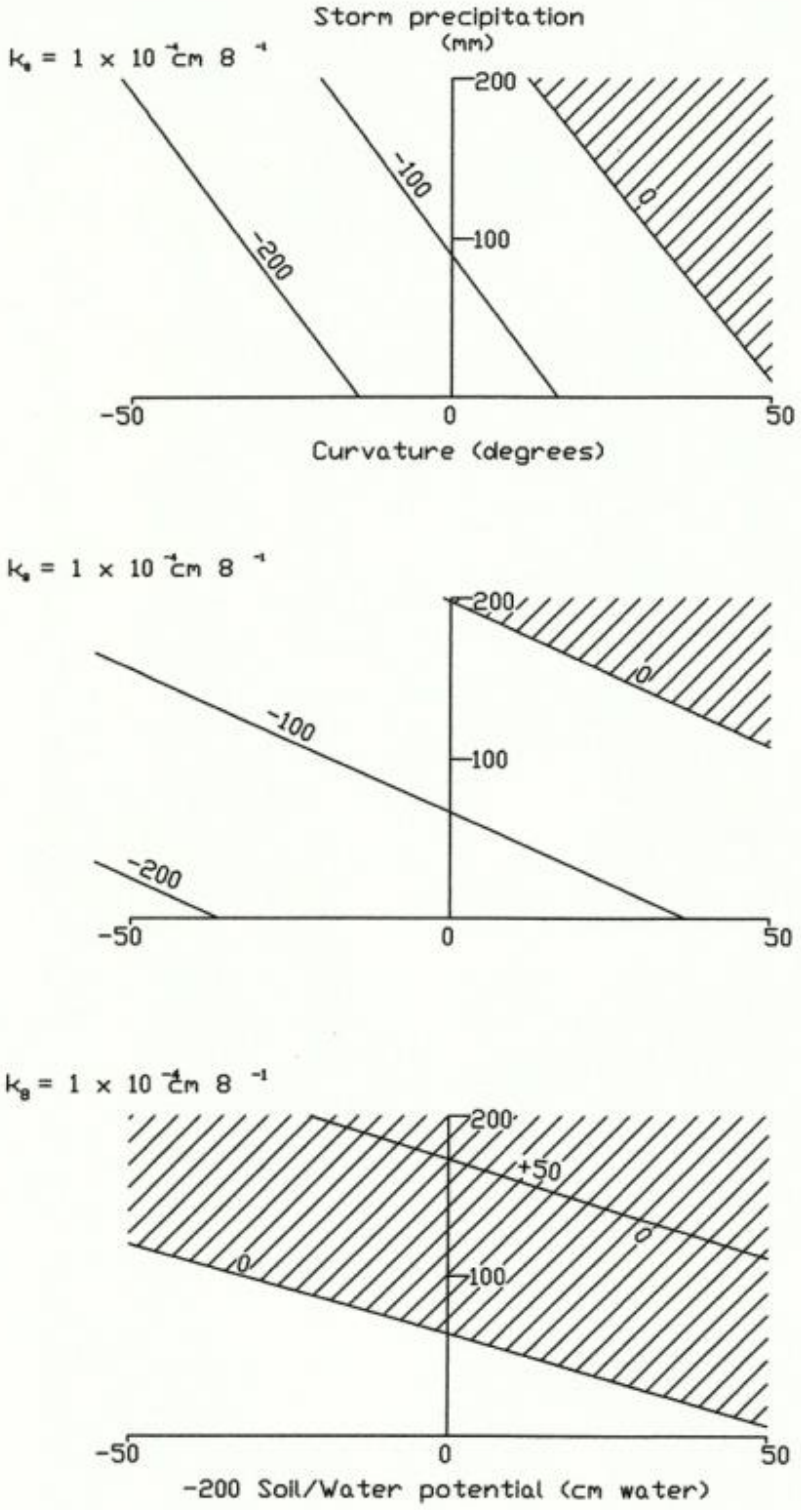

Figure 3.14 Plot of equations predicting soil-water potentials for each of three permeability group (after Anderson and Kemp, 1985)

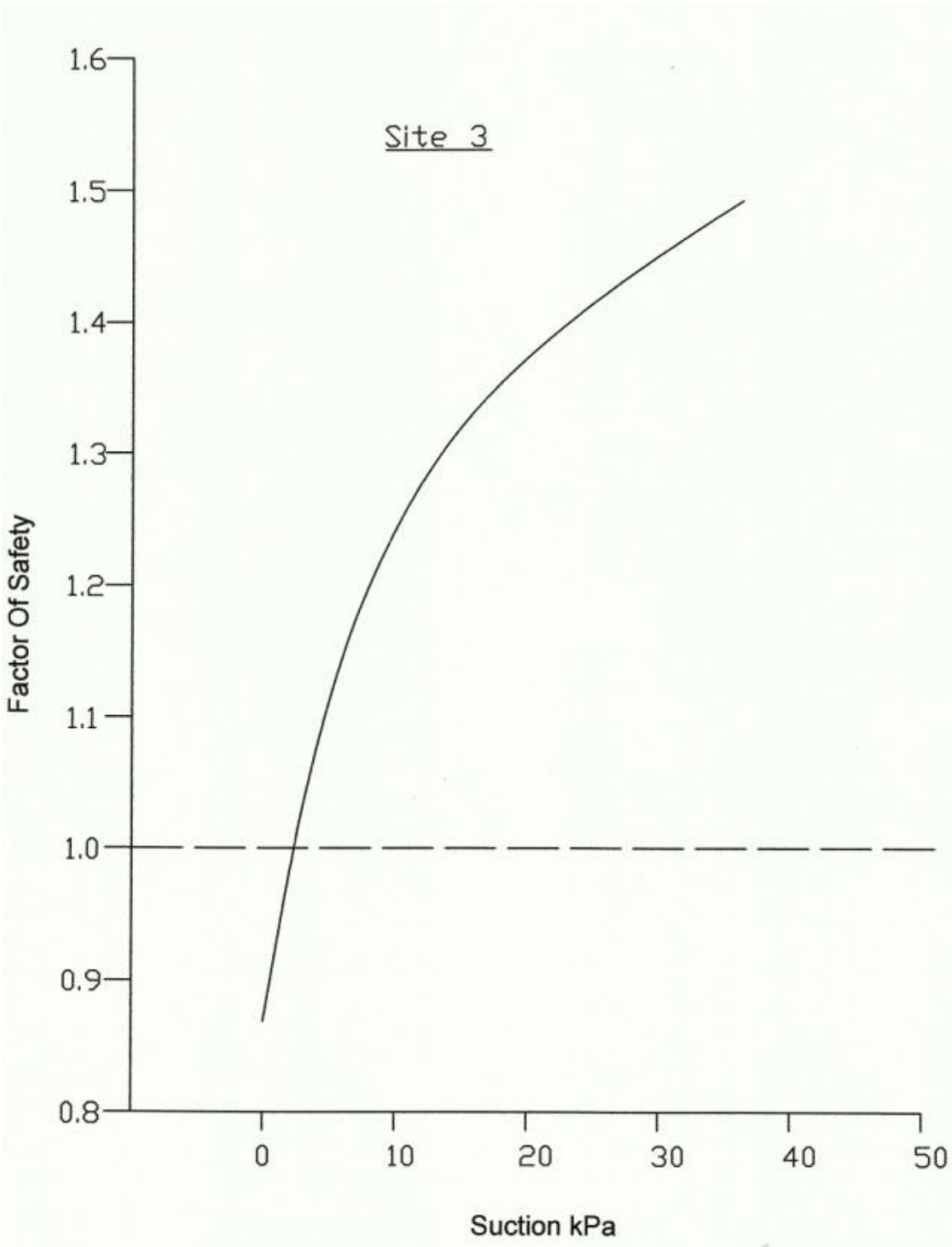

Figure 3.15 Factor of safety for various maximum suctions on the critical slip surface (after Anderson and Kemp)

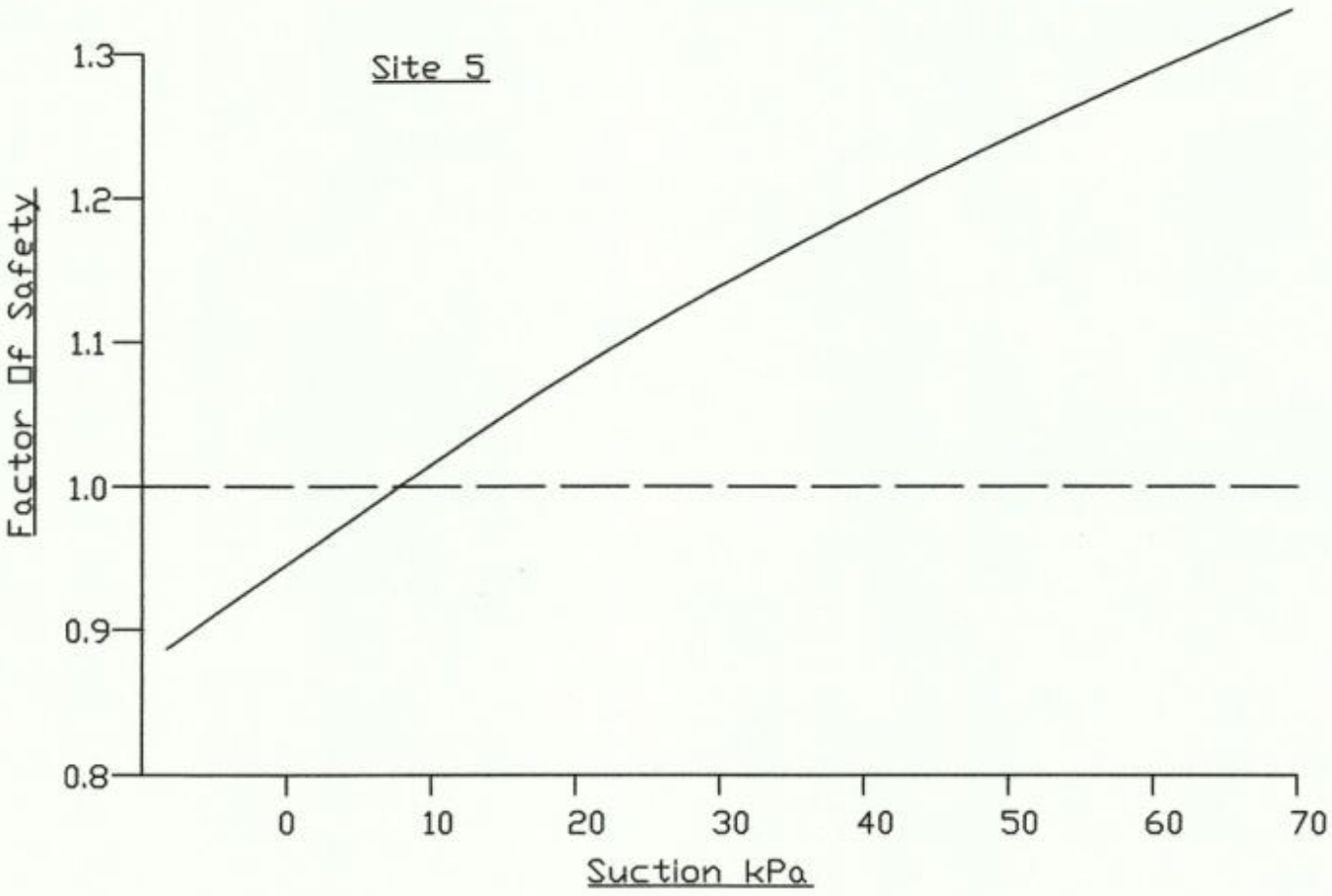

Figure 3.16 Factor of safety, for various maximum suctions on the critical slip surface (after Anderson and Kemp)

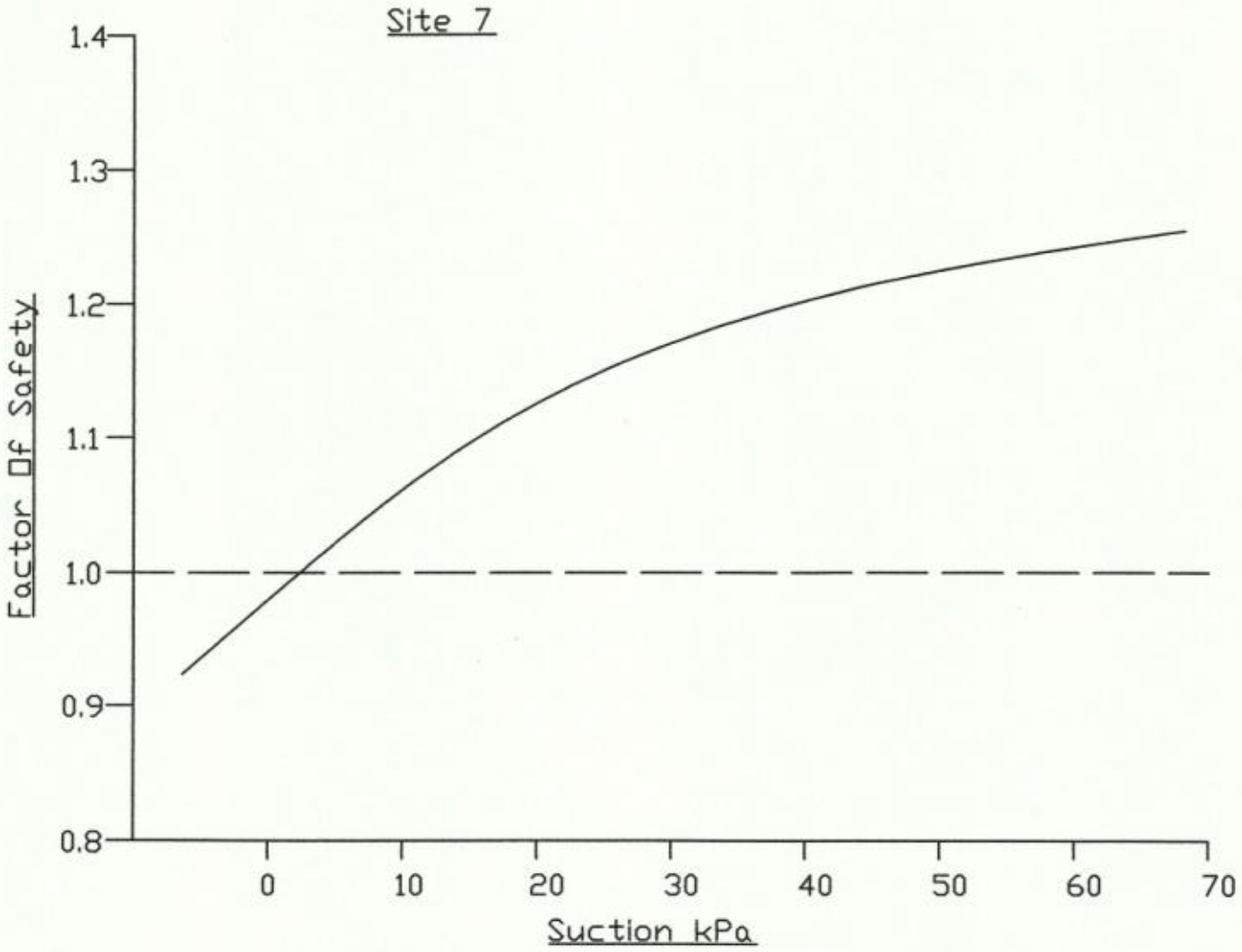

Figure 3.17 Factor of safety, for various maximum suctions on the critical slip surface (after Anderson and Kemp)

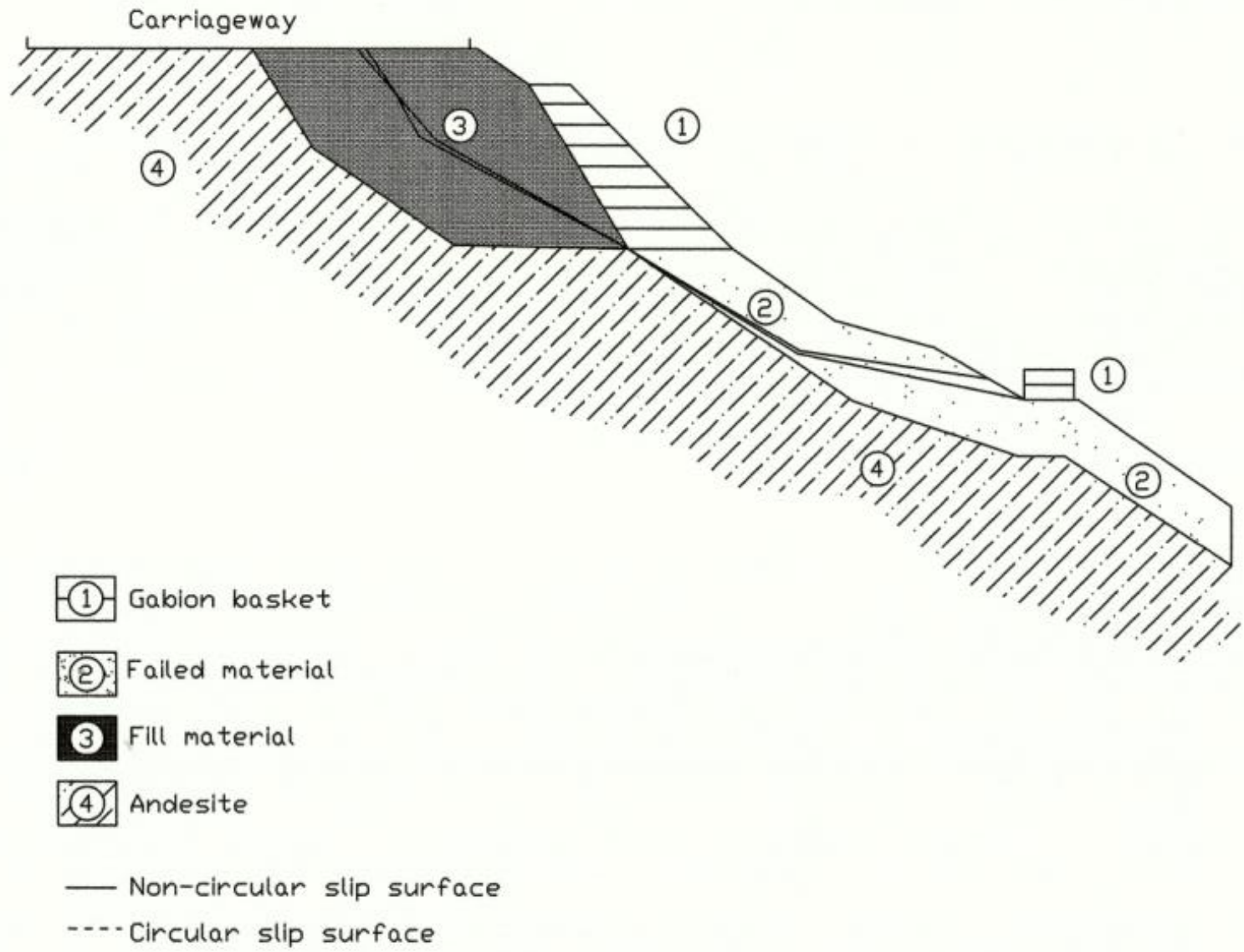

Figure 3.18 Slope Profile soil material types plus non and circular slip surface (after Anderson and Kemp)

CHAPTER 4

DESCRIPTION OF THE TWO STUDY SITES

4.1 Description of the Study Sites, Field Instrumentation and Monitoring Procedures

4.1.1 General

The two sites chosen for the research study were selected from the case histories outlined in Chapter 2, namely, the Barre de L'isle landslide (2005) and the Windjammer Landing Beach Resort landslide (2005). The location and description of the two sites are detailed in Sections 2.2.9 and 2.2.10 of Chapter 2 of this thesis. The sites were selected for this study based on the following conditions:

i) the author's familiarity and hands on experience with the site conditions
ii) the availability of field and laboratory data from previous site investigations carried out by this author
iii) easy access by motor vehicle
iv) both sites had experienced recent rainfall-induced slope failures
v) the selected sites are of different geological origin

4.1.2 The Barre de L'isle Study Site

4.1.2.1 Introduction

The site of the 2005 landslide on the Barre de L'isle as referred to in Section 2.2.9 of this thesis was selected for the study and is shown on the topographic map in Figure 4.1. The slope has a moderate gradient of about 21^{o} and is located within an area which was deforested and used for banana and vegetable farming. There are a few drainage ditches and gullies which start within the study and continue northward down the slope. The residual soil at the site is derived from weathered andesite and can be seen in numerous road cuts along the main road. Figure 4.1a presents a cross-section of the Barre de L'isle slope showing the subsoil stratigraphy and field instrumentation.

4.1.2.2 Hydrological Model for the Barre de L'isle Study Site

The science of hydrology is concerned with quantifying the various components into which rainfall is divided and understanding the physical processes by which water is eventually returned to the atmosphere. The hydrological cycle is the process through which rainfall passes before before being returned to the atmosphere. Figure 4.1b presents a hydrological model for the Barre de L'isle Study Site. Rainfall is intercepted and stored in the forest canopy and this represents the first component of the hydrological cycle to be lost directly back to the atmosphere. The interception of raindrops by the forest canopy is also a major factor in reducing soil erosion.

At the study site, the fruit and vegetable crops cultivated offer much less interception storage and soil erosion is increased. Stem flow and raindrop impact received by the soil surface contributes to infiltration and surface runoff. The infiltration capacity is dependant on the hydraulic conductivity of the soil. When the rate of rainfall exceeds the infiltration capacity of the soil, the result is surface runoff. Surface runoff was measured at 56 % over a period of 1 hour. The infiltration capacity of the soil at the site was measured at 44% of a total rainfall of 45 mm. There was no ponding of surface water at the site during the study period. Section 5.2.2.6 contains details of the test.

Infiltration of surface water caused a rise in the groundwater table as indicated in the standpipe piezometer installed at the site.. As the water flows downwards and encounters the silty sand layer it flows laterally in the aquifer and returns to the surface in the spring at the toe of the slope. Water is returned to the atmosphere by evaporation from the forest canopy, the ground surface and from the spring and surface flow in the gully at the toe of the slope.

4.1.2.3 Field Instrumentation at the Barre de L'isle Study Site

4.1.2.3.1 Introduction

The field investigation carried out at this site in 2005 is detailed in Chapter 2, Section 2.2.9 of this document. A supplementary subsurface investigation and instrumentation programme was conducted in December 2008 by this author to acquire additional subsurface information and to conduct additional shear strength tests and x-ray diffraction and scanning electron microscopy tests for this research study. Furthermore, the slope inclinometer and standpipe piezometer installed on the north side of the main road in the study area in the 2005 site investigation programme, were vandalized and had to be replaced for this study.

The standpipe piezometer and the slope inclinometer installed on the south side of the main road during the 2005 site investigation were not damaged. The supplementary field investigation and instrumentation consisted of drilling two boreholes to install one slope inclinometer and one standpipe piezometer for the research study.

Jet-fill tensiometers were installed to monitor negative pore-water pressures (matric suction) at variable depths in the slide area. A rain gauge was installed to measure rainfall and a flume was constructed at the site to monitor surface run-off.

Figure 4.2 shows the schematic layout of the instrumentation at the Barre de L'isle Study Site. A schematic of the slide area is shown in Figure 4.3.

4.1.2.3.2 Standpipe Piezometer

The following standard procedure method was used to install the standpipe piezometer:
A 100 mm diameter hollow steel casing is placed against the ground surface where the borehole is to be drilled and driven into the soil with a 135 kilogram weight hammer using a pulley system attached to a tri-pod stand. The soil enters the casing and when the required depth for testing is achieved the soil in the casing is drilled out using a wash boring tri-pod drill fitted with drill rods and a chopping bit.

Standard Penetration Tests (SPT) were conducted at 1.5m intervals of depth in the piezometer borehole in accordance with ASTM D 1586. To perform this test, a split spoon sampler was attached to the drill rods and lowered down the steel casing in the borehole until it rests on the layer of soil to be tested. It was then driven into the soil for a length of 450 mm by means of a 65 kg weight hammer free falling 760 mm for each blow.

The number of blows required to drive the last 300 mm was recorded and this figure was designated the 'N'- value of the soil. The first 150 mm of driving was ignored because of possible loose soil in the bottom of the borehole from the boring operations. After the sampler was removed from the borehole it was opened and its contents were examined.

The recovered disturbed soil samples were visually classified in the field, placed in plastic bags and sealed to retain their natural moisture content.

The soil classification system used for this project is in accordance with the Burmister Soil Classification System. A brief description follows:

COMPOSITION OF SOIL

A. Principle Soil Type

The principle soil type in each stratum represents at least 50% by weight of the material in the stratum.

B. Minor Soil Types

The descriptive terms "trace", "little", "some", "and" indicate the percentages by weight of the minor soil types in each stratum as follows:

Trace: < 10%	Some: 21 – 35%
Little: 11 – 20%	And: 35 – 50%

e.g. 30% silt is described as "some" silt
12% sand is described as "little" sand

The subsoil stratigraphy at the site consist of a reddish brown, firm to stiff, clayey, sandy silt residual soil of low to medium plasticity overlying highly weathered andesite bedrock. The residual soil layer is approximately 15.0 metres thick at this location.

The recovered disturbed soil samples were visually classified in the field and transported to the author's laboratory and tested to determine natural moisture content, grain size distribution and soil plasticity.

The drill was used to advance the borehole to bedrock at a depth of 15.0 m below existing ground surface. The borehole was advanced 1.0 m into the andesite bedrock and was terminated at a depth of 16.8 m.

The piezometer installations were conducted as follows:

The borehole was backfilled with crushed rock up to a depth of 12.0m below existing ground surface and a 1.5 m thick bentonite seal was placed on top of the crushed rock by dropping bentonite pellets through the steel casing used to advance the borehole. Thus the top of the bentonite seal at the base of the silty sand layer. A 1.5m thick layer of crushed rock was then placed to allow drainage fronm the silty sand into the piezometer slots to record groundwater fluctuations in the silty sand layer.

A 300 mm thick bentonite seal was then installed to prevent ingress of free water from the upper residual soil layers. The borehole was then topped to within 2.0m of ground surface with drill cuttings and then grouted to the ground surface. This procedure was applied to confirm that the groundwater levels recorded in the standpipe piezometer represented the pore pressure in the silty sand layer. An additional borehole was drilled near the toe of the slope and instrumented with a standpipe piezometer but was vandalized before any groundwater data was recorded.

A 38.0 mm diameter poly-vinyl chloride (PVC) plastic pipe was used as a piezometer to record groundwater levels. The lower 3.0 m length of the PVC plastic pipe was slotted at 150 mm intervals with a hacksaw and a sealed end lowered to the top of the bentonite seal at a depth of 14.5 m below ground surface by adding 6.0 metre lengths of plastic pipe connected on ends by couplings and sealed with PVC adhesive. The borehole was then backfilled to within 0.5 m of ground surface with drill cuttings.

A bentonite/cement slurry mix was then used to top the upper 0.5 metre of the borehole to form an impermeable seal to prevent the ingress of surface water into the piezometer prematurely. A cap was place over the top of the standpipe piezometer and is removed when recording groundwater levels.

A detailed borehole log for the piezometer borehole is shown in Appendix B.

Figure 4.4 **s**hows the areal extent of the Barre de L'isle landslide from the toe of the slope. Seepage of groundwater into a spring at the toe of the slope is shown in Figure 4.5.

Groundwater levels were measured in the standpipe piezometers by a dipmeter (model EL23-1757) manufactured by ELE International Ltd in the United Kingdom. The instrument is drum-mounted with an on/off indicator switch. A light and audible signal are activated when the probe touches the water when lowered down the piezometer with a cable attached. The cable is 50 metres long and is marked in metre intervals. Figure 4.6 contains a Photograph of ELE dipmeter used for monitoring groundwater levels in the standpipe piezometers

4.1.2.3.3 Slope Inclinometer

The slope inclinometer is a device used for monitoring deformation normal to the axis of a casing by means of a probe passing along the casing. It is used to determine the extent, rate and zone of landslide movement. The equipment used for this study was manufactured by the Slope Indicator Company, Mukilteo, Washington, USA.

The slope inclinometer has four components:

i) A permanently installed guide made of plastic and contains longitudinal grooves or slots for orientation of the sensor unit

ii) A portable probe containing a gravity-sensing transducer which is mounted in a carriage designed for operation in the guide casing

iii) A portable control readout unit at the surface supplies power, receives electrical signals and displays readings in digital format

iv) A graduated electrical cable linking the probe to the readout unit and is raised or lowered in the casing and transmits electrical signals to the surface

The following procedure was used to install the slope inclinometer:

The borehole for the installation of the slope inclinometer was drilled to a depth of 16.0 m below existing ground surface at a distance of about 1.0 m from the location of the standpipe piezometer in order to monitor any correlation between groundwater level fluctuations and slope movement. The base of the inclinometer casing was anchored 1.0 m into the weathered andesite bedrock. Soil sampling was not conducted in this borehole since it was in close proximity to the piezometer installation.

The slope inclinometer plastic casing sections were layed out in lengths and couplings marked to show the location of the alignment key. A bottom cap was placed at one end of the initial casing section, sealed with an ABS adhesive and taped to prevent loose soil or cement/bentonite grout from entering the casing.

The remainder of the casing was assembled by adding on sections connected with couplings and sealed with ABS adhesive. During the installation process, the axis of one pair of grooves was kept parallel to the anticipated direction of movement, i.e. downslope. This orientation was maintained throughout the installation process. A grout slurry composed of Portland cement, bentonite and water was used to backfill the borehole and to provide stability to the casing.

The slope inclinometer casing was installed in a vertical borehole which passed through a zone of suspected movement. The bottom of the casing was anchored in the weathered andesite bedrock which served as a reference. The slope inclinometer probe was then used to survey the casing and establish its initial position.

Figure 4.7 shows the tension cracks in the main access road at the crest of the slope.

4.1.2.3.4 Jet Fill Tensiometers

Pore water pressure response to infiltration in the slopes was measured by Jet-fill Tensiometers (model 2725) manufactured by Soilmoisture Equipment Corporation, Santa Barbara, California, U.S.A.

The tensiometer is an instrument used to measure soil suction or negative pore water pressure in soils. The instrument consists of a transparent plastic tube with a porous tip attached to the bottom, a vacuum gauge attached via an angled port on the side wall of the plastic tube and a flexible reservoir cover at the top which allows for convenient filling and sealing of stored water. When it is filled with water and inserted into the soil, water can move into and out of the tensiometer through the ceramic porous tip.

As the soil dries out and water moves out of the tensiometer, it creates a vacuum inside the tensiometer which registers on the gauge. When the vacuum created equals the soil suction, water stops flowing out of the tensiometer. The dial gauge reading is the direct measure of the force required to remove water from the soil. If the soil dries out further, additional water moves out until a higher vacuum level is achieved.

When water is added to the soil due to infiltration, the reverse process takes place and water from the soil enters the tensiometer through the porous ceramic tip, the vacuum level is reduced to equal the lower soil suction value. When enough water is added to the soil so that it is completely saturated, the gauge reading on the tensiometer will drop to zero. Since water can move back and forth from the tensiometer to the soil through the pores in the ceramic tip, the gauge reading is always in balance with the soil suction.

Model 2725 jet-fill tensiometer has a range of 0 – 100 centibars. At zero reading the soil is completely saturated for example after a heavy rainfall event. Positive pore water pressures are not recorded with this instrument. A reading of 0 - 10 centibars indicate a surplus of water or pore water pressure. At 10 – 20 centibars there is excess pore water pressure but also negative pore water pressure or suction begin to enter the soil. The practical limit is 80 - 85 centibars due to the effect of cavitation. Cavitation is the phenomenon where a small air bubble expands into a large air bubble due to the vacuum being created in the tensiometer. That was considered when taking readings. The accuracy of the instrument is (+,-) 1.5 % of the reading (Soil Moisture Company).

Figure 4.8 shows a photograph of the 2725 Jet Fill Tensiometer. A photograph of the jet- filled tensiometers installed at the site are shown in Figure 4.9.

4.1.2.3.5 Rain Gauge

An all weather rain gauge model 5477 supplied by Forestry Suppliers Inc. of Mississippi, U.S.A. was installed at the site to record rainfall data. The rain gauge apparatus weighs 1.0 kilogram and has a capacity of 27.9 cm x 2.0 mm. The instrument collects water at the top and funnels it into a removable inner tube graduated in metric units (cm). Overflow is collected in the outer chamber for later measurements. The rain gauge was mounted on a 2.0 metre high wooden post of dimensions 100 mm x 100mm with brackets supplied by the manufacturer.

The rain gauge was installed in a location downslope of the tensiometers, slope inclinometer and standpipe piezometer, where it was not obstructed by any trees or other structures that could have prevented it from receiving a fair sample of rain with wind blowing from any direction.

The all weather rainfall gauge is shown in Figure 4.10.

4.1.2.3.6 Surface Run- off Apparatus

Surface run-off at the study site was measured manually using a 19 litre bucket to collect the run-off water during an actual rainfall event and measuring the amount of water collected in a plastic container (beaker) graduated in metric units (cm).

A 4.0 m x 3.5 m ($14.0m^2$) area of the study site was marked off for run-off measurements. Strips of galvanized sheeting were pushed about 150 mm into the soil to establish the borders for the test. The galvanized strips protruded 600 mm out of the soil.

An opening was established in the galvanized boundary as a collection point for the surface run-off at a downslope corner of the test area. The boundaries guided the surface run-off toward the collection point. Data on surface run-off was collected during an actual rainfall event on a 5-minute interval to record the effect of rainfall intensity on surface run-off, groundwater level changes, and negative pore-water pressure changes (soil suction) during storm events.

Figure 4.11 contains a photograph showing the Run-off/Infiltration Measurement Area.

4.1.2.4 Instrumentation Layout at the Barre de L'isle Study Site

Pore-water pressure changes in the slope in response to infiltration were measured by standard jet-fill tensiometers. A total of fifteen (15) jet fill tensiometers were installed on the slope at the Barre de L'isle study site. They were arranged in three rows (A,B,C) in a small depression on the slope within the 2005 landslide area. The three rows of tensiometers were aligned on contour across the slope with 2.13 metre spacing downslope. Each row was designed to measure pore water pressures at depths of 3.0m, 2.1m, 1.5m, 0.9m, and 0.5 metre (designated columns 1 – 5) below existing ground surface. The tensiometers were spaced 0.6 metre apart (Rahardjo et al, 2003).

The layout of the study site was designed to include the slope inclinometer and the standpipe piezometer previously installed by this author. The tensiometer spacing and depths allowed for detailed pore-water pressure profiles across the slope.

The tensiometers were installed in pre-drilled boreholes using a hollow 25 mm diameter galvanized pipe driven into the soil with a hammer and the extruded manually with wrenches. The soil entered the hollow pipe and the required borehole was created for the tensiometer installation. The tensiometers were assembled in accordance with specifications supplied by Soilmoisture Equipment Corporation and installed manually by pushing the plastic tubing into the pre-drilled borehole until the porous ceramic tip was embedded into the soil at the bottom of the borehole.

The upper 5.0 cm of the borehole was sealed with a bentonite mix to prevent the ingress of surface water into the borehole.

The jet fill tensiometers were installed close to the standpipe piezometer, the slope inclinometer and the rain gauge to allow easy access and convenient monitoring of all the instrumentation.

The instrumentation was monitored as frequently as possible over a period of ten (10) months from January 28, 2009 to November 30, 2009 by a technician who recorded the data manually as observed in the field.

Figure 4.12 is a photograph of the instrument layout at the Barre de L'isle Study Site (looking north). Figure 4.13 shows a cross-section of the instrumentation installed and the subsoil stratigraphy at the Barre de L'isle Study Site.

4.1.2.5 In Situ Hydraulic Conductivity Test

The hydraulic conductivity of the residual soil at the study site was measured in a falling head test utilizing the standpipe piezometer installed. The test was conducted in accordance with the standards specified by the United States Department of the Navy, Naval Facilities Engineering Command – 1974 (NAVFAC), for a cased borehole with a perforated extension of length 'L'.

4.1.3 The Windjammer Landing Beach Resort Study Site

4.1.3.1 Introduction

On October 11, 2008 a shallow landslide occurred at the Windjammer Landing Beach Resort after a 120 mm rainfall event in an area north of the 2005 landslide detailed in Section 2.2.10 of Chapter 2 of this thesis. The landslide caused the rupture of buried utility lines and partially overturned a retaining wall located near the main entrance to the resort.
The slope instability occurred in the vicinity of two high scale Villas upslope and the safety of these structures was of great concern to management.

This author was authorized by personnel of the resort to conduct a site investigation to determine the cause of the slope instability and recommend remedial measures for slope stabilization. Figure 4.14 contains an aerial photograph of the 2005 landslide area and the current study site at the Windjammer Landing Beach Resort.

4.1.3.2 Field Instrumentation at the Windjammer Landing Beach Resort Study Site

4.1.3.2.1 Field Investigations

At the time of the field investigation, the retaining wall at the toe of the slope was bulging outward with several large cracks visible on the exposed face of the wall. Tension cracks were visible on the ground surface and power lines installed on the slope for ground lighting were in tension.

The overall slope is 90.0m long from the toe to Villa 43c at the crest. The slide area is approximately 30.0 m long and 15.0m wide and extends from the retaining wall to the Villa at a westward inclination of 18^{o}. Figure 4.15 shows the "bulging" retaining wall at the toe of the slope at the Windjammer Landing Beach Resort Study Site.

The field work consisted of drilling four (4) boreholes to a depth of 3.5 metres below existing ground surface to install two (2) standpipe piezometers and two (2) slope inclinometers at selected locations on the slope, utilizing a wash boring drill fitted with drill rods and a chopping drill bit. Two (2) test pits were manually excavated in close proximity to the boreholes to recover undisturbed bulk samples for shear strength and consolidation testing.

The standpipe piezometers and the slope inclinometers were installed during the period of October 29, 2008 to November 8, 2008.

In situ Standard Penetration Tests (SPT) were conducted at 0.75 metre intervals in two (2) of the boreholes in accordance with the American Society for Testing and Materials (ASTM) standard D 1586.

The recovered soil samples were visually examined and classified in the field, placed in plastic bags and sealed to preserve the natural moisture content. The disturbed soil samples were transported to the author's laboratory for index testing.

Two undisturbed bulk samples were packaged and transported by air freight to the University of the West Indies in Trinidad for shear strength, consolidation and swell testing in their soil mechanics laboratory.

4.1.3.2.2 Subsoils Condition

The general subsoil stratigraphy at the site consist of a thin layer of topsoil overlying colluvial material which in turn overlies the highly weathered basalt bedrock.

The colluvium layer is approximately 3.0 metres thick and is composed of a brown, medium plastic, firm to stiff, clayey, sandy silt deposit containing variable sizes of weathered rock fragments.

The 'N'-value from the Standard Penetration Test (SPT) for this material ranged from 5 blows to 44 blows per 300 mm, indicative of a soft to very stiff material.

The weathered basalt bedrock formation is very dense with 'N'-values in excess of 100 blows per 300 mm.

4.1.3.2.3 Standpipe Piezometer (SP)

The general procedure used for the standpipe piezometer installation at the Barre de L'isle study site was applied at the Windjammer Landing Beach Resort site. Two (2) standpipe piezometer boreholes were drilled to a depth of 3.0 metres below existing ground surface and were terminated at the colluvium/ bedrock contact zone.

Standard Penetration Tests (SPT) were conducted at 0.75 metre intervals of depth in each borehole. Disturbed soil samples were recovered from the drilling operation and preserved for laboratory index testing in the author's laboratory.

A 300 mm thick bentonite seal was installed at the base of the borehole to prevent any groundwater seepage from the underlying weathered basalt bedrock into the piezometer. The lower 1.5 metre section of a 38 mm diameter PVC plastic pipe was slotted with a hacksaw and lowered down the borehole with a plug inserted at the bottom end. The borehole was backfilled to within 300 mm of ground surface with drill cuttings placed around the piezometer. The borehole was then topped up to ground surface with a bentonite slurry to form a seal to prevent surface water from entering the piezometer prematurely. A cap was placed over the top of the piezometer and is removed when water levels are recorded.

Detailed logs for the standpipe piezometer boreholes are included in Appendix C.

Grain size distribution curves for the colluvium soil samples are contained in Appendix D.

4.1.3.2.4 Slope Inclinometer (SI)

Two (2) slope inclinometers were installed at the study site to monitor subsurface movements in the colluvium. The slope inclinometers were anchored to a depth of 0.5m into the weathered bedrock. A grout/cement slurry mix was placed around each slope inclinometer to stabilize the casing.

4.1.3.2.5 Jet Fill Tensiometers

Twelve (12) Jet Fill Tensiometers were installed on November 12, 2008 in an area of 6.0 m x 1.5 m dimensions in the landslide zone upslope from the 'bulging' retaining wall to monitor negative pore water pressures in the colluvium in response to rainfall events. The tensiometers were installed in close proximity to the standpipe piezometers and the slope inclinometers for convenient monitoring of all the instrumentation.

4.1.3.2.6 Rain Gauge

Rainfall data was recorded regularly and supplied by Windjammer Landing Beach Resort personnel from a rain gauge installed on their property. The rain gauge was mounted on the maintenance building about two (2) metres above ground, where it was not obstructed by any trees or other objects that would prevent the gauge from receiving a fair amount of rainfall from any direction.

4.1.3.3 Instrumentation Layout at the Windjammer Landing Beach Resort Study Site

The tensiometers were arranged on the slope in three (3) rows (A,B,C) each containing four (4) tensiometers at 0.5 metre spacing to form four (4) columns. The three rows were spaced 3.0 metres apart downslope.

The tensiometers were installed to measure negative pore water pressures across the slope at depths of 0.5 m, 1.0 m, 1.6 m, and 2.3 m.

The instrumentation at the Windjammer Landing Beach Resort study site was monitored for a period of six (6) months from October 29, 2008 to May 12, 2009 by a technician who manually recorded the data as observed in the field.

A schematic layout of the Instrumentation at the Windjammer Landing Beach Resort Study Site is shown in Figure 4.16**.** A Photograph of the layout of the instrumentation at the Windjammer Landing Beach Resort Study Site is presented in Figure 4.17.

4.1.3.4 In Situ Saturated Hydraulic Conductivity Tests

Falling head hydraulic conductivity tests were performed in the two (2) standpipe piezometers installed at the study site as detailed in Section 4.1.2.4

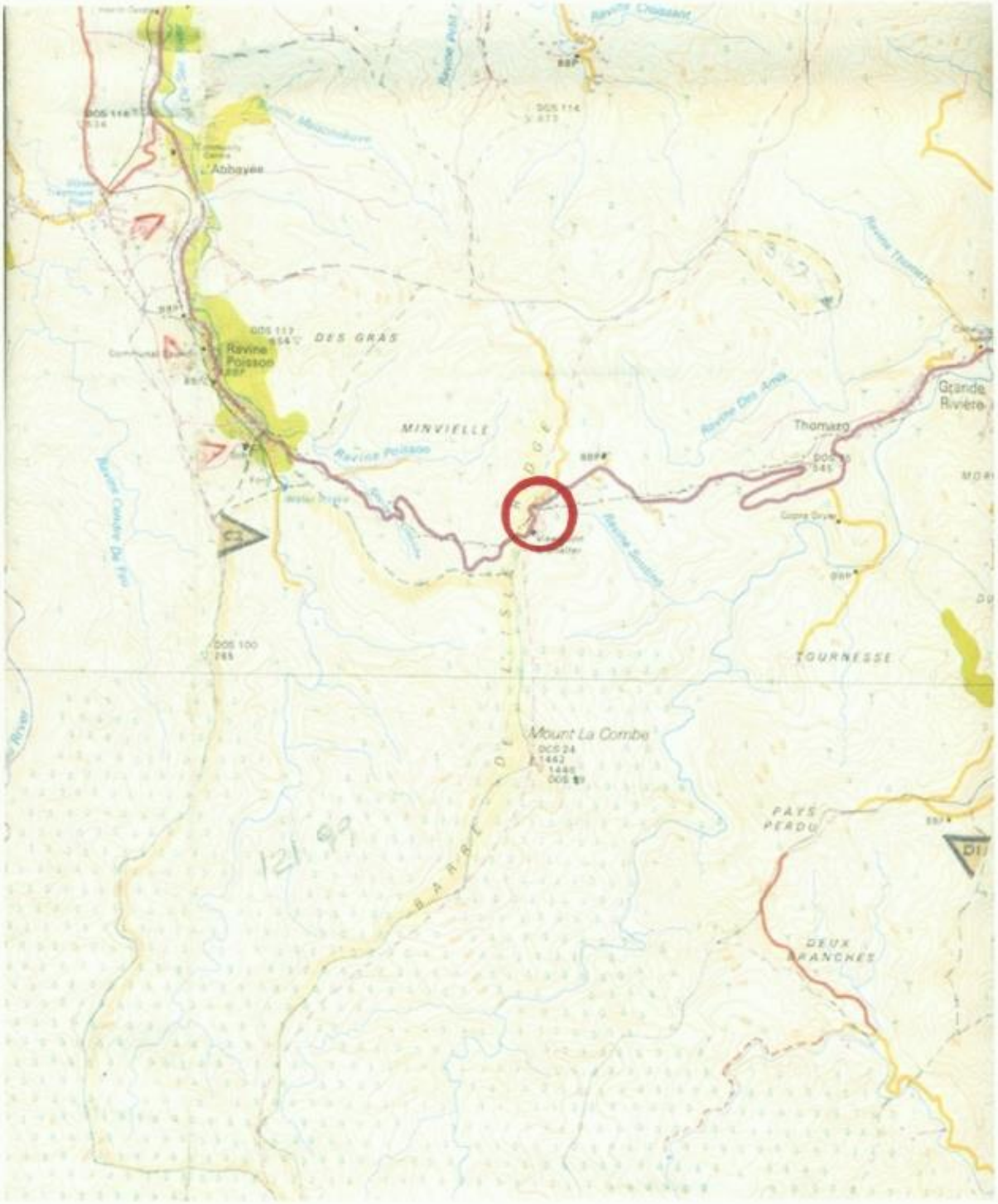

Figure 4.1 Location of the Barre de Lisle Study Site (After UK Government Overseas Survey,1981)

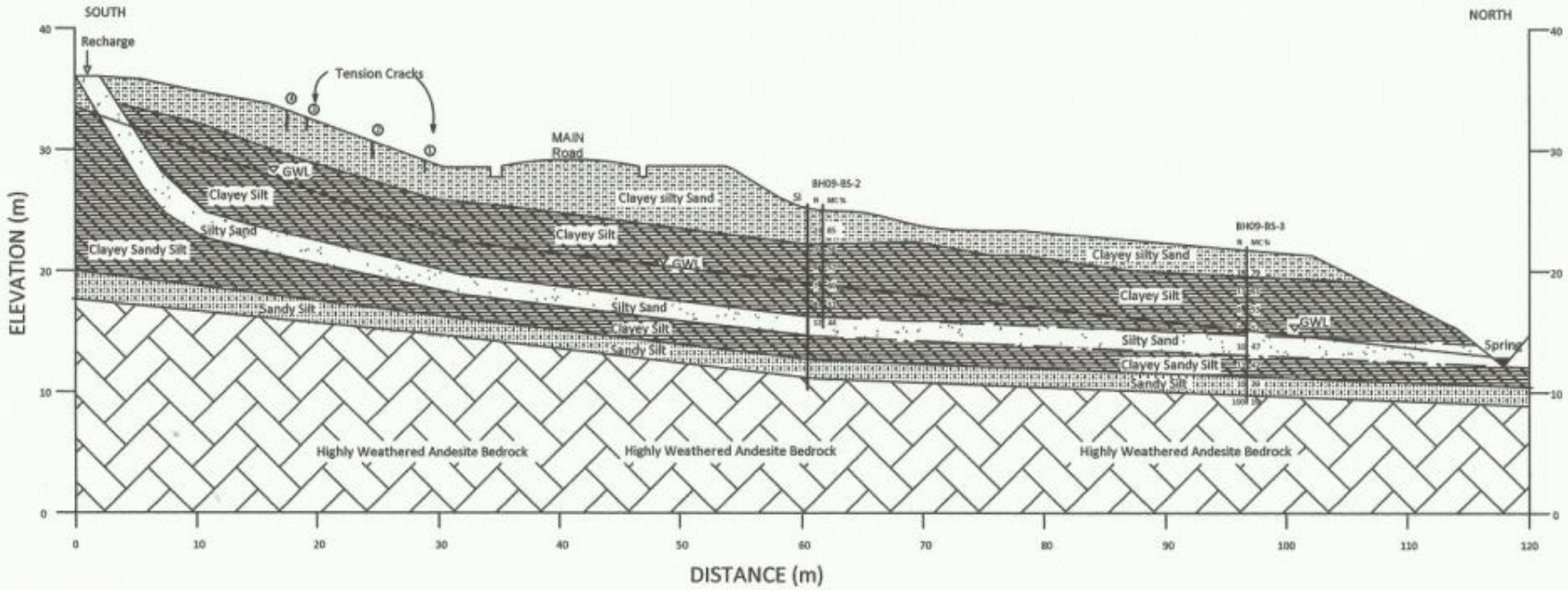

Figure 4.1a Cross Section of Barre de L'Isle Slope

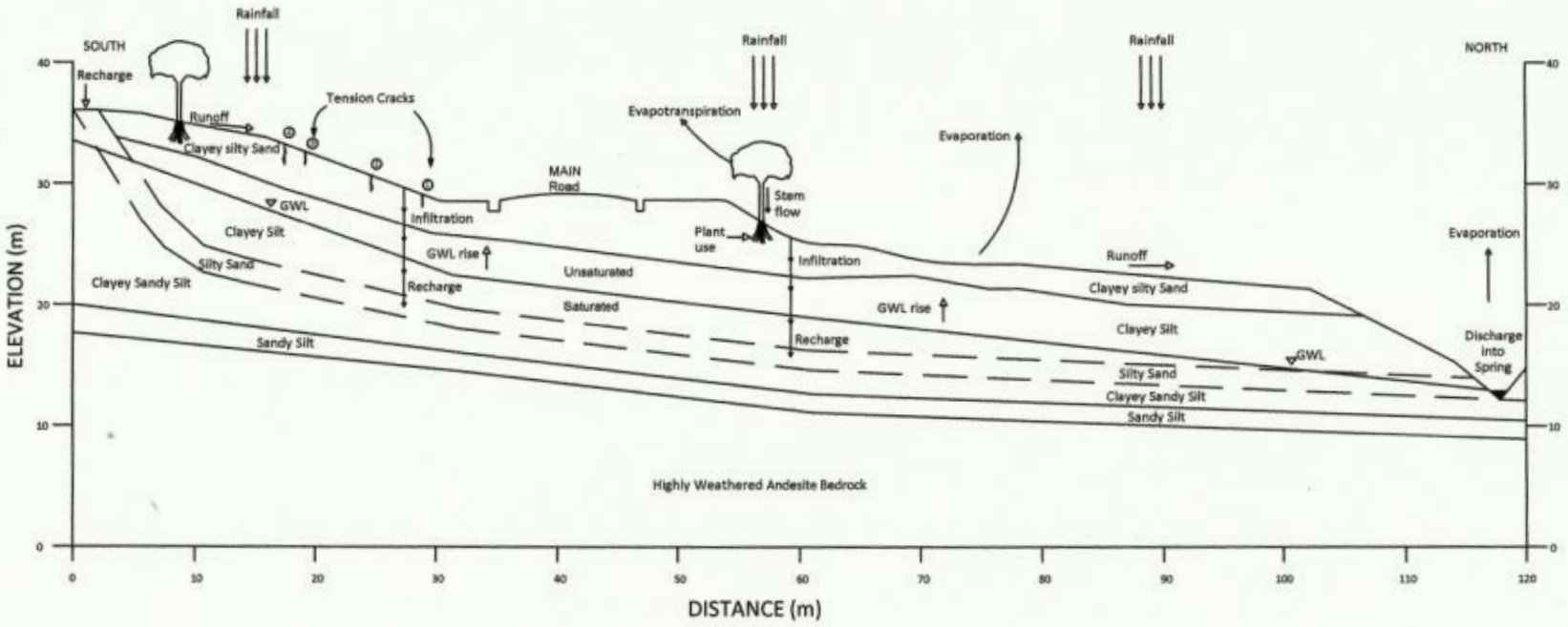

Figure 4.1b A Hydrological Model for Barre de L'Isle Study Site

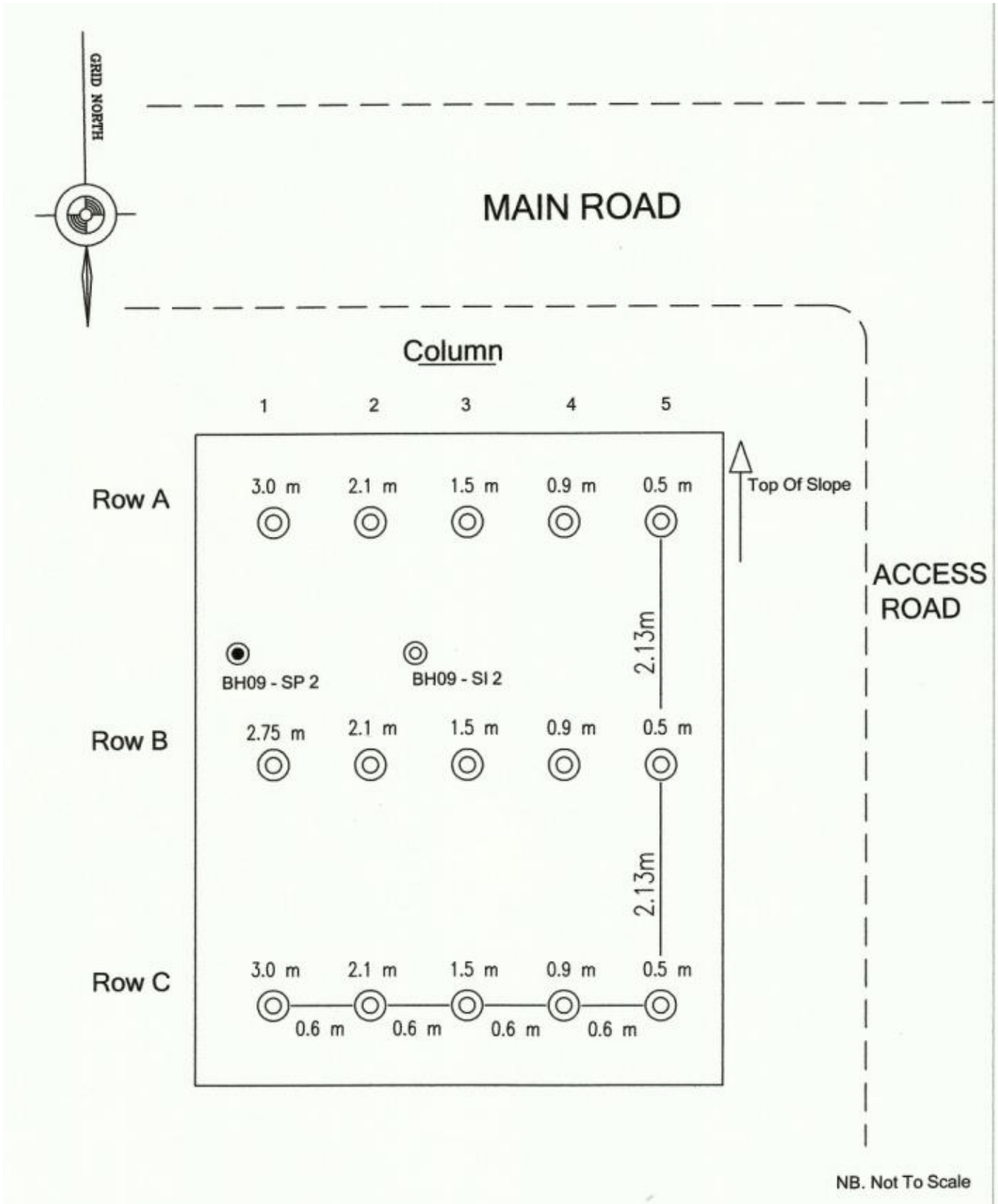

Figure 4.2 Schematic Layout of the Instrumentation at the Barre d'Isle Study Site

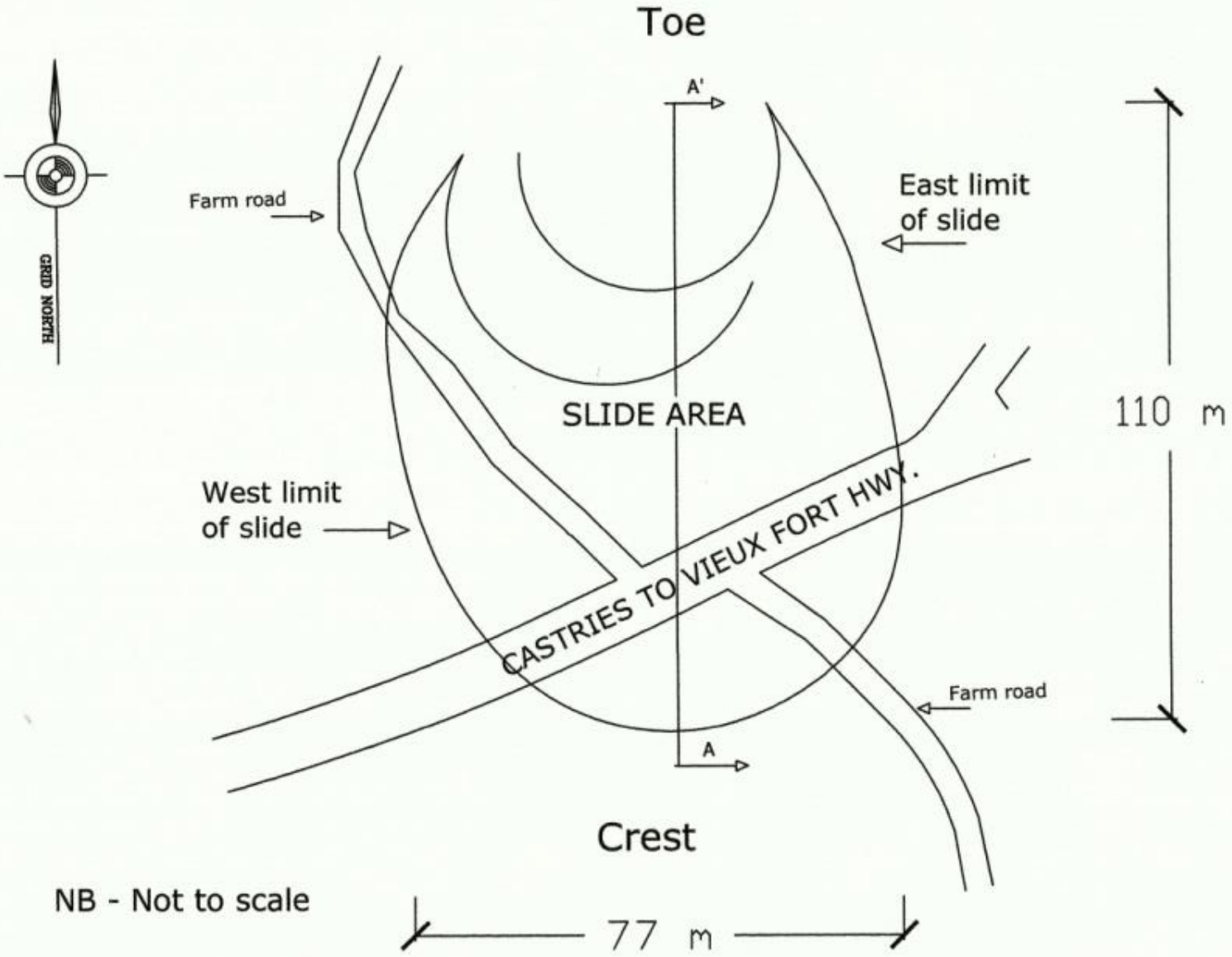

Figure 4.3 A Schematic layout of the slide area at the Barre d L'Isle

Figure 4.4 Areal extent of the Barre de L'isle landslide looking upslope

Figure 4.5 Seepage in a spring at the toe of the slope

Figure 4.6 ELE Dipmeter

Figure 4.7 Tension cracks in main access road pavement at the crest of the Barre de L'isle slope

Figure 4.8 Jet Fill Tensiometers

Figure 4.9 Jet Fill Tensiometers installed at the Study Site

Figure 4.10 All weather rain gauge

Figure 4.11 Run-off / Infiltration measurement setup

Figure 4.12 Instrumentation layout at the Barre de L'isle Study Site

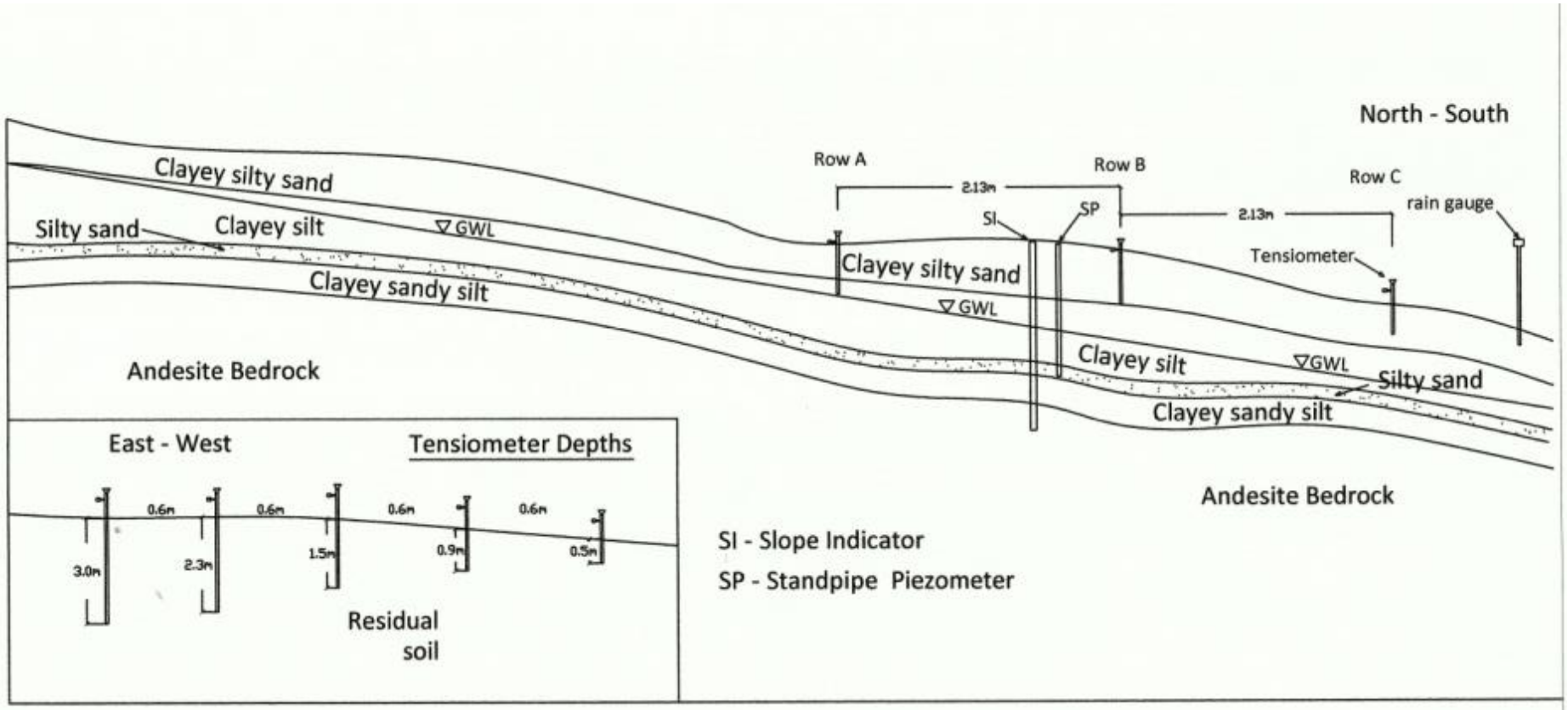

Figure 4.13 Cross - Section of the Barre d L'Isle subsoil stratigraphy and instrumentation

Figure 4.14 Aerial view of the 2005 landslide area and the current Study Site at the Windjammer Landing Beach Resort (After Windjammer, 2008)

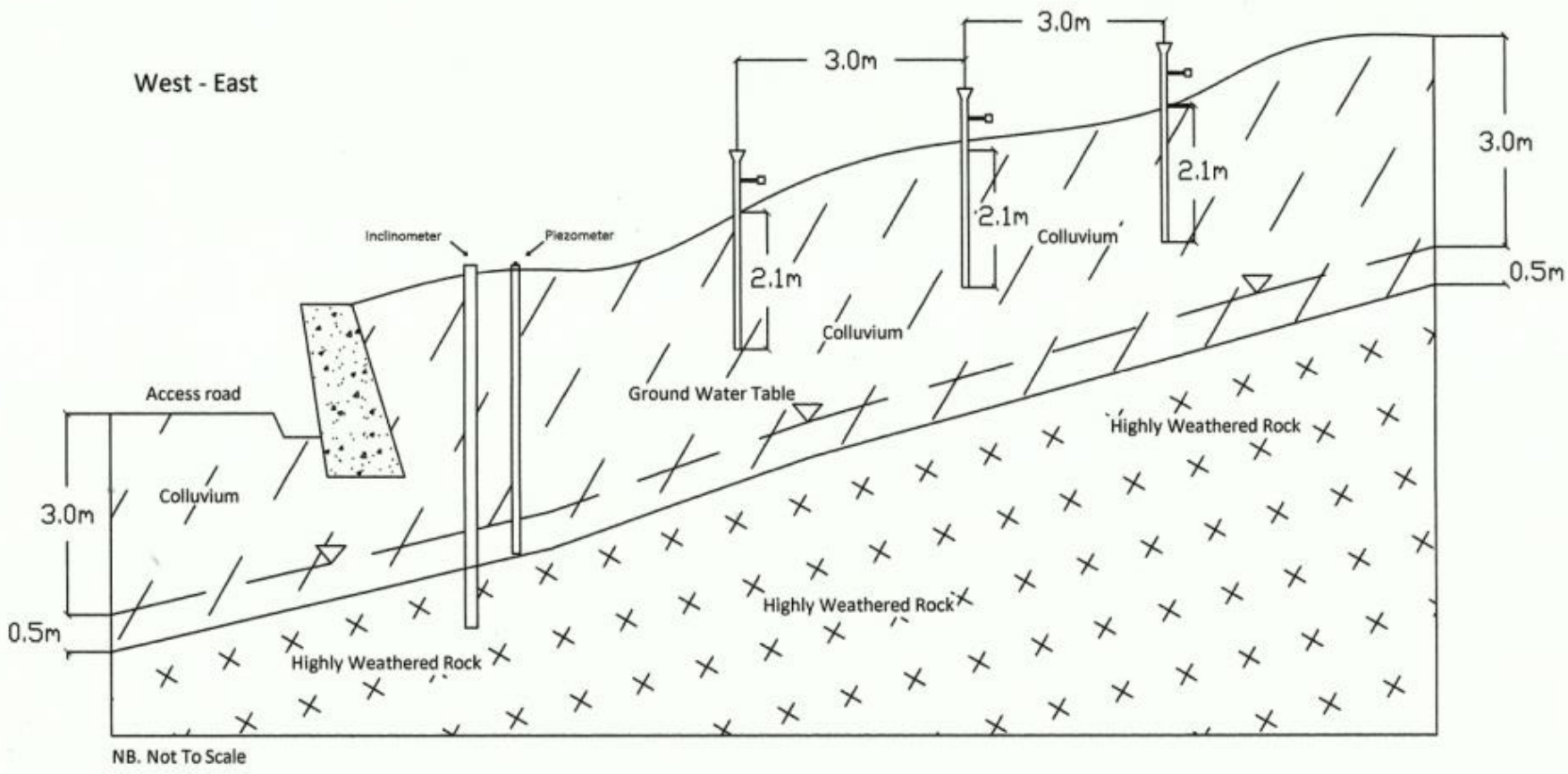

Figure 4.15 Cross Section of the slope with instrumentation at the Windjammer Landing Beach Resort Study Site

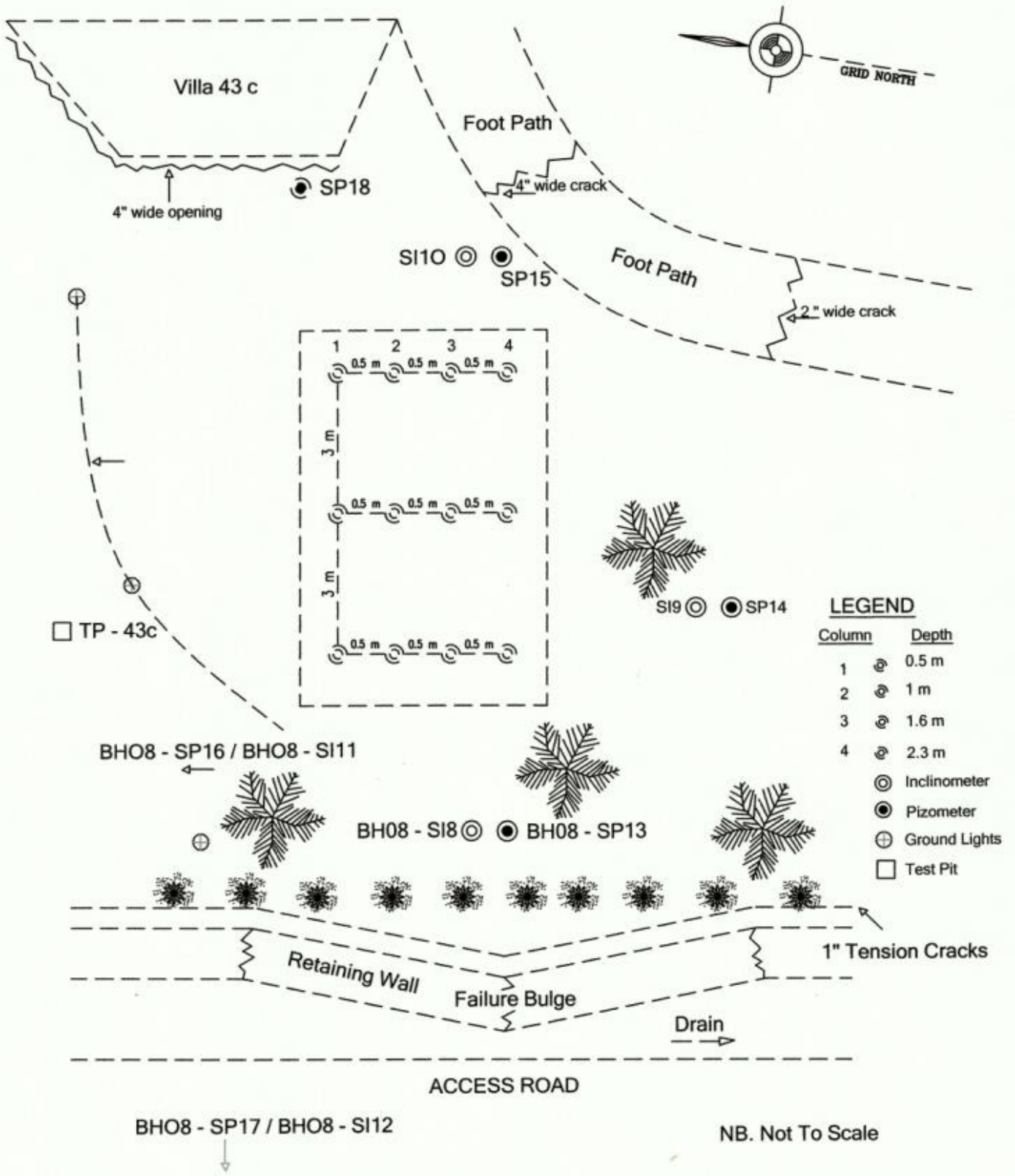

Figure 4.16 A Schematic layout of the Instrumentation at the Windjammer Landing Beach Resort Study Site

Figure 4.17 'Bulging' retaining wall at the Windjammer Landing Beach Resort Study Site

Figure 4.18 Layout of the Field Instrumentation at the Windjammer Landing Beach Resort Study Site

CHAPTER 5

The Results of Laboratory Tests and Field Measurements for the Barre de L'isle Ridge and Windjammer Landing Beach Resort Study Sites

5.1 Introduction

This chapter presents the results of the laboratory testing and the field instrumentation monitoring for both the residual soil deposit at the Barre de L'isle ridge and the colluvial material at the Windjammer Landing Beach Resort study sites.

The laboratory test results for the residual soil and colluvial soils from the study sites include index tests, direct shear strength tests, consolidation tests, specific gravity tests, loss on ignition tests, Cation Exchange Capacity (CEC), X-ray Diffraction Analysis (XRD) and Scanning Electron Microscopy (SEM). Laboratory tests on parent rock samples of andesite and basalt at variable stages of weathering include point load tests, cerchar abrasive tests, and uniaxial compressive strength tests.

Undisturbed soil samples were transported by air freight to the University of the West Indies in Trinidad for direct shear strength and consolidation testing in their soil mechanics laboratory. The index tests were performed by this author in his laboratory in Saint Lucia.

X-ray diffraction analysis, Scanning Electron Microscopy, point load tests, uniaxial compressive strength tests, Cerchar abrasive tests, Cation Exchange Capacity (CEC), specific gravity and loss on ignition tests were performed at the University of Newcastle upon Tyne on soil and rock samples transported by air freight from Saint Lucia to the United Kingdom by this author.

The field instrumentation monitoring provides details of rainfall data collected, piezometer readings, slope inclinometer data, surface run-off results and pore water pressure measurements at variable depths as recorded in the jet-fill tensiometers. The field monitoring of the two sites were conducted over different time periods due to delayed authorization to access the site by the property owners and also to climatic conditions which varied between the dry season (January –June) and the wet season (July – December).

The field monitoring of the instrumentation at the Barre de L'isle study site was for a period of ten (10) months dating from February 1, 2009 to December 31, 2009. There was no instrumentation monitoring for the month of May, 2009. The field instrumentation at the Windjammer Landing Beach Resort study site was monitored from November 14, 2008 to May 12, 2009, a period of six (6) months.

5.2 The Barre de L'isle Study Site

5.2.1 Laboratory Tests Results for Residual Soils from Parent Andesite Rock

5.2.1.1 Moisture Content

In December 2005, the groundwater level at the site was recorded at a depth of 5.5 metres below existing ground surface during the preliminary landslide site investigation.

The natural moisture content for soil samples recovered from the 2005 landslide investigation programme ranged from 33.2 % to 65.9 %. The average moisture content in the upper 6.0 metres of the residual soil profile above the groundwater table was 49.9 %. Below the groundwater table, the average moisture content was 40.6 %.

The natural moisture content for the residual soil samples recovered from this site during the supplementary site investigation in December 2008 ranged from 40.1 % to 84.4 %. The groundwater level was recorded at a depth of 6.0 metres below ground surface.

The average moisture content in the upper 6.0 metres of the residual soil profile above the groundwater table was 65.0 % . Below the groundwater table the average moisture content of the residual soil was 47.2 %.

Based on this premise, for the conceptual model it was assumed that the upper three (3) metres of the silty sand residual soil has an infiltration rate that allows rapid saturation of that layer during heavy rainfall events. The clayey silt layer which exist immediately below the more permeable upper silty sand layer has a lower saturated hydraulic conductivity than the upper layer and the infiltration rate in this soil layer is less.

The upper layer of residual soil has a high transmissivity which results in rapid infiltration during heavy rainfall. If this soil layer is continuous downslope, the pore water pressure will dissipate quickly at the end of the rainfall event since the storativity of the silty sand will be low due to natural drainage conditions.

A 2.0 m thick silty sand layer exists interbedded in the clayey silt residual soil at a depth of 9.0 m below ground surface at the location of the instrumentation. This highly permeable zone is believed to be recharged upslope by infiltration of surface water which is channeled underground through the subsoils and discharged in an active spring at the toe of the slope at a rate measured at 20 litres per minute.

Several underground springs are known to exist on the Barre de L'isle mountain ridge most of which provide local farmers with a year round supply of water for farm irrigation purposes. These springs sometimes develop "artesian" pressures during periods of intensive rainfall which may have been the cause of the slope instability at this study site.

The moisture content of samples of the weathered andesite bedrock varied between 18.0 % to 28.9 % .Moisture contents from another area of slope instability on the Barre de L'isle mountain ridge by previous investigations showed moisture contents ranging from 29 % to 45 % for the residual soils.

Residual soils from parent andesite rock have been encountered on engineering projects conducted by this author in other areas on the island of Saint Lucia and are outlined in the following paragraphs.

The Millennium Highway in Saint Lucia was constructed in 1994 along the northwest coast of the island between the capital city of Castries and the Cul de sac valley includes the construction of two short tunnels in andesite rock. The overburden material at both tunnel sites consists of residual soil overlying weathered andesite at one tunnel site and fresh andesite rock overlain by residual soil at the other site.

The natural moisture content of the residual soils from this project ranged from 8.0 % to 49.0 %. This range of moisture content for the residual soils at this site is much lower than that encountered at the Barre de L'isle study site since the coastal areas receive much less rainfall than the interior of the island.

Residual soils recovered from the Millet Landslide (Saint Lucia) by this author during the geotechnical site investigation in 1995 showed moisture content values ranging from 24.0 % to 64.0 %. These moisture content values are in close agreement to that from the Barre de L'isle study site since Millet is located in the interior of the island where the rainfall is highest.

Moisture content values of 28.8 % to 40.9 % was found for residual soil samples from parent andesite on a road project at Mabouya Valley bridge (Saint Lucia) located inland from the east coast of the island.

Wong, et al (2000) found the moisture content of a granitic residual soil from Singapore to be 48.4%

The moisture contents for the borehole at the Barre de L'isle study site are shown on the borehole log in Appendix B.

5.2.1.2 Atterberg Limits

The residual soil at the Barre de L'isle site was found to have a liquid limit of 57 % to 93 % and a plastic limit of 38 % to 49 %. The plasticity index ranged from 19 % to 49 %.

Residual soils tested from other unstable slopes on the Barre de L'isle mountain ridge from past investigations by this author and by Anderson and Kemp (1985) showed lower values with liquid limits of 33 % to 68 % and plastic limits of 25 % to 52 %. The plasticity index ranged from 8 % to 16 %.

This soil is classified by the Unified Soil Classification System (USCS – ASTM D 2487) as an elastic silt (MH). The sand seam encountered at a depth of 9.0 metres at the study site is classified as a silty sand (SM).

Residual soils from parent andesite rock at other locations on the island tend to fall below the 'A' – line of a Casagrande plasticity chart. This is characteristic of many tropical weathered soils (Gidigasu, 1976).

Soil samples from the Millennium Highway road project in Saint Lucia showed liquid limits of 27 % to 78 %; plastic limits of 17 % to 39 % and plasticity indices ranging from 6 % to 46 %.

At the Millet Primary School landslide in the interior, the liquid limit of residual soil samples ranged from 41 % to 87 % and the plastic limit from 25 % to 39 %. The plasticity index ranged from 17 % to 48 %.

Residual soil samples from the Mabouya Valley bridge project were found to have liquid limits ranging from 25 % to 61 % and plastic limits of 20 % to 30 %. Plasticity indices of 5 % to 35 % were recorded.

Toll et al, (2000) reported liquid limits of 42% to 47% and plastic limits of 28% to 29% for a granitic residual soil from Singapore. The index ranged from 13% to 19%.

Deutscher et al (2000) conducted tests on a granitic residual soil from a different site in Singapore and found liquid limits ranging from 13% to 39% and plastic limits of 7% to 31%. The soils from Singapore are classified as moderate to low plastic silts (MH).

Gidigasu, (1976) reported the results of tests on lateritic soils from Kenya of high clay content with liquid limits of 76% to 88% and plastic limits of 39% to 42%

Figure 5.1 Contains the Plasticity Chart for the soils tested at the Barre de L'isle study site.

5.2.1.3 Particle Size Distribution

The textural characteristics of the parent andesite rock is reflected in the residual soil developed from it. The degree of leaching in situ during weathering also influences the nature of the grading curves (Gidigasu, 1976).

Andesite is a fine grained igneous volcanic rock with a mineral composition of plagioclase feldspar, hornblende, biotite, olivine in a quartz matrix (Huang, 1962). The most stable rock forming silicate minerals are quartz, orthoclase feldspar and muscovite (acidic) and the least stable are olivine, augite and plagioclase feldspar (basic).

In a tropical climate with abundant moisture and high temperatures both acidic and basic rocks will decompose rapidly by the process of leaching, one more so than the other. Kaolinite, vermiculite and montmorillonite clay minerals are produced together with granular lateritic soils (Gidigasu, 1976).

The residual soil at the Barre de L'isle study site shows variation in particle size distribution. Samples recovered from the 2005 landslide investigation showed particle size distribution of 19 % sand; 63 % silt and 18 % clay. In comparison, the particle size distribution for samples recovered from the current site investigation showed a composition of 37 % sand (fine to medium/); 46 % silt and 17 % clay. Residual soils from parent andesite rock have been encountered on several major engineering projects on the island of Saint Lucia e.g., the Roseau Dam project in the interior of the island, the Millennium Highway in the northwest and the Watershed Management Project.

Particle size distribution for residual soil samples tested from these projects averaged about 30 % sand; 58 % silt and 12 % clay.

Residual soil samples from the Mabouya Valley bridge project (Saint Lucia) showed an average particle size distribution of 37 % sand; 35 % silt and 28 % clay.

The materials do not, however, appear to contain significant amounts of problematic clay minerals that would lead to unusual engineering properties.

The method of formation of these soils, by weathering of the parent bedrock and leaching out of soluble minerals, has led to a structure of aggregated clay particles (mostly kaolinite) that are clumped together to form silt sized nodules.

Toll et al (2000), found a granitic residual soil from Singapore to consist of 9% to 53% sand; 22% to 50% silt; and 25% to 31% clay. This soil was classified as clayey silt to silty sand (MH – SM).

Wong et al (2000) tested granitic residual soil samples from another site in Singapore and found them to contain 6% sand; 69% silt; and 25% clay. The samples were classified as a clayey silt (MH).

Figure 5.2 –Figure 5.11 show the particle size distribution curves for the soils at the Barre de L'isle Study **S**ite

5.2.1.4 Bulk Density

Bulk density values for tropical residual soils are abundant in the literature and are also available from various engineering projects in Saint Lucia, including the site under study.

Two bulk density tests were performed on undisturbed block samples from the Barre de L'isle study site which were transported to the University of the West Indies in Trinidad at the request of this author. The results of the tests suggest that the insitu bulk density of the residual soil from parent andesite rock within the study area was 17.90 kN/m^3

Residual soil samples from a previous landslide at another site investigated by this author on the Barre de L'isle mountain ridge investigated by this author suggests bulk density values ranging from 16.90 kN/m^3 to 17.30 kN/m^3.

Samples of residual soil from the Barre de L'isle mountain ridge were transported to the United Kingdom by this author and tested in the soil mechanics laboratory at the University of Newcastle upon Tyne by this author showed bulk density values ranging from 17.27 kN/m^3 to 17.95 kN/m^3.

Two undisturbed residual soil samples from another site at RG Quarry (andesite) in the Cul de sac valley near the capital city of Castries in the north were also tested by this author at the University of Newcastle upon Tyne and were found to have bulk density values ranging from 15.67 kN/m^3 to 17.90 kN/m^3.

Bulk density values of 17.66 kN/m^3 to 19.62 kN/m^3 were recorded for residual soil samples from the Millennium Highway project near the capital city of Castries in Saint Lucia.

A residual soil sample recovered from the Millet landslide showed a bulk density value of 17.00 kN/m^3. Soil samples from the Mabouya Valley bridge project showed bulk density values of 19.30 kN/m^3 to 19.40 kN/m^3.

These results indicate a wide range of bulk density values for residual soils from parent andesite rock from various locations on the island. This variation in bulk density value for this material is based primarily on the nature of the soils including the climatic conditions under which they were formed.

Wong et al (2000) reported a bulk density of 16.77 kN/m^3 for a granitic residual from Singapore.

5.2.1.5 Specific Gravity

Particle density or specific gravity is the ratio of the mass of a given volume of material to the mass of an equal volume of water at a temperature of 4^o C. The particle density or specific gravity values for soil particles are useful for all calculations involving void ratio, porosity or the degree of saturation. In soil mechanics, this would include compaction, consolidation, permeability, shrinkage limits tests and particle size distribution by sedimentation analysis (Gidigasu, 1976).

Gidigasu (1976) reports of quartz-rich decomposed rocks in tropical regions having specific gravity values between 2.55 and 3.00. He points out that the high specific gravity values found for laterite soils is associated with the gravel fractions in which the iron oxides are concentrated. In addition, he states that specific gravity values between 2.93 to 3.54 was found for lateritic soils by researchers in Uganda, Gambia and Ghana.

Residual soil samples from the Barre de L'isle study site were transported to the United Kingdom and tested by this author in the soil mechanics laboratory of the University of Newcastle upon Tyne and were found to have particle density values between 2.60 to 2.62.

Three residual soil samples from RG Quarry were tested by this author at the University of Newcastle upon Tyne and particle density values of 2.54 to 2.73 were recorded.

Particle density values between 2.61 and 2.67 were found for residual soil samples from the Millenium Highway project on the northwest coast of Saint Lucia.

Soil samples from the Mabouya Valley bridge project were tested for particle density by Trintoplan Consultants Ltd of Trinidad and values of 2.61 to 2.69 were recorded.

Taha et al (2000) have reported the specific gravity of a residual granite soil formation from Malayasia to range from 2.55 to 2.61.

5.2.1.6 Soil-Moisture Density

Residual soils are used extensively in Saint Lucia as a source of backfill material in the construction of road subbase, embankments and water retention facilities such as fish ponds and sediment settling ponds. The construction of these facilities require sound knowledge of the compaction of soil particles during the process of mechanical soil stabilisation.

One (1) residual soil sample from the Barre de L'isle study site was used to determine the moisture-density relationship using the standard Proctor test in accordance with ASTM D-698-91. The results of the test indicate an optimum moisture content of 24.0% and a maximum dry density value of 13.8 kN/m^3. Figure 5.12 shows the graph of the compaction test results.

5.2.1.7 Shear Strength Parameters

Fredlund and Rahardjo (1993) state that the extended Mohr-Coulomb shear strength envelope for unsaturated (residual) soils require that the shear strength parameters c',ϕ', and ϕ^b be determined in the laboratory. The laboratory equipment currently used to conduct triaxial and direct shear strength tests for saturated soils must be modified to achieve this requirement. The equation for the shear strength of an unsaturated (residual) soil can be expressed as:

$$\tau = c' + (u_a - u_w) \tan \phi^b + (\sigma_n - u_a) \tan \phi'$$

where,

τ = shear strength
c' = effective cohesion
ϕ^b = angle indicating the rate of increase in shear strength related to matric suction
σ_n = total normal stress
ϕ' = effective angle of shear resistance

Anderson and Kemp (1985) performed shear strength tests on residual soil samples from the Barre de L'isle mountain ridge in Saint Lucia using the conventional direct shear apparatus which they believe is adequate for testing the shear strength of residual soils. However, they recommend that the test must be run at a slow rate to ensure no build up of excess pore water pressure occurs. They recommend a rate of $0.012mm/min^{-1}$.

The results of the direct shear tests conducted by Anderson and Kemp (1985) on residual soil samples from the Barre de L'isle ridge are shown in Figure 5.13 to Figure 5.16.

Table 5.1.1 contains a summary of the direct shear strength tests.

.Table 5.1.1 Summary of Direct Shear Strength Tests – Barre de L'isle Ridge, Saint Lucia, (Anderson and Kemp, 1985)

	Peak Strength		Residual Strength	
Site	c (kPa)	ϕ	c (kPa)	ϕ
3	6.80	36.72^o	2.22	34.95^o
5	6.35	35.00^o	2.99	29.00^o
7	13.8	25.78^o	4.60	16.80^o
10	--	---	6.00	30.90^o

.Table 5.1.2 Summary of Direct Shear Strength Tests on Residual Soils from the Barre de Lisle, Saint Lucia,

	Peak Strength		Residual Strength		
Site	c (kPa)	ϕ	c (kPa)	ϕ	Source
Study site	24.0	27.0^o	6.0	22.0^o	Isaac (2005)
Study Site	4.0	38.0^o	---	----	Isaac (2008)
LUCELEC (Power Line)	20.0	27.0^o	---	----	Isaac (2008)

.Table 5.1.3 Summary of Direct Shear Strength Tests on Residual Soils from other Countries

	Peak Strength		Residual Strength		
Location	c (kPa)	ϕ	c (kPa)	ϕ	Source
Dominica, W.I.	-----	---	----	30.7^o- 38.4^o	Reading (1991)
Brazil	0 - 59	23.0^o – 33.0^o	----	------	Sridharan (1988)
Hong Kong	0 – 72	33.0^o – 40.0^o	----	------	Gidigasu (1976)
Singapore	12.0	33.0^o	----	------	Deutscher (2000)

A plot of the Mohr-Coulomb envelope for the direct shear test on the residual soil sample from the Barre de L'isle Study Site (2005) is presented in Figure 5.17. A plot of the Mohr-Coulomb envelope for the LUCELEC (2008) power line site is shown in Figure 5.18.

The test results of the peak shear strength shown in Table 5.1.1 and Table 5.1.2 are in close agreement with friction angle values ranging from 25.8^o to 38.0^o for the residual soils on the Bare de L'isle ridge. The shear strength of residual soils from other parts of the world are in good agreement with the Barre de L'isle residual soils as shown in Table 5.1.3. The cohesion intercept tends to vary widely based on clay component.

5.2.1.8 Cation Exchange Capacity (CEC)

The cation exchange capacity (CEC) of a soil refers to the sum of the negatively charged sites occurring mainly on alumino-silicate clay minerals and organic matter (Fookes, 1997). There is a direct relationship between cation exchange capacity and clay content. Sand and silt have little or no cation exchange capacity while organic matter show a variable capacity.

Cation exchange capacity is comprised of a permanent negative charge resulting from isomorphous substitution in clay minerals and a variable, pH-dependant negative charge attributed to organic matter (Fookes, 1997).

There is an abundance of information on the cation exchange capacity of clay minerals in the literature such as the findings of Grim (1968) which indicate CEC of the major clay minerals Kaolinite, Illite and Smectite (montmorillonite) to range from (meq/100g) 3–15, 10–40 and 60–150, respectively.

Gidigasu, (1976) attributes the low CEC values for laterized soils to be related to the coating of the specific surface of the clay particles by iron oxide during laterisation which reduces the surface activity of the clay particles.

Three (3) residual soil samples from the Barre de L'isle study site were analysed for CEC and exchangeable cations by technician Mr. Philip Green in the Department of Geochemistry at the University of Newcastle upon Tyne at the request of this author. The results indicated cation exchange capacities of 6.8, 9.8 and 10.1 meq/100g. Exchangeable cations results were:

Sodium (Na) 0.84, 1.07 and 1.22 meq/100g
Potassium (K) 1.68, 1.72 and 2.11 meq/100g
Calcium (Ca) 2.53, 2.85 and 3.03 meq/100g
Magnesium (Mg) 1.21, 1.29, and 1.32 meq/100g

Three (3) residual soil samples recovered from RG Quarry in Saint Lucia were also analysed and were found to have CEC values of 8.8, 9.4 and 9.7 meq/100g. Exchangeable cations were:

Sodium (Na) 0.47, 0.74, and 0.68 meq/100g
Potassium (K) 3.92, 4.41, and 4.50 meq/100g
Calcium (Ca) 4.01, 4.46, and 4.47 meq/100g
Magnesium (Mg) 2.86, 3.18, and 3.22 meq/100g

The analysis to determine the cation exchange capacity of the residual soil samples was in accordance with British Standard (BS 7755): Section 3.12, 1996; ISO 13536, 1995; Soil Quality, Part 3; Chemical Methods, Section 3.12, Determination of the potential cation exchange capacity and exchangeable cations using barium chloride solution buffered at pH = 8.1.

The results of the tests indicate that the exchangeable cations capacity for potassium, calcium and magnesium is higher for the residual soils at the RG Quarry site than for samples recovered from the Barre de L'isle study site. Only sodium cation was found to be at a lesser quantity.

5.2.1.9 Loss on Ignition

Loss on ignition is a rapid and accurate method used to determine the change in mass of a soil when heated to very high temperatures and allowing volatile substances to escape. The volatile materials usually consists of "combined water" (hydrates and hydroxyl compounds).

Loss on ignition was determined for two (2) residual soil samples from the Barre de L'isle study site. The tests were performed in the Department of Geochemistry at the Newcastle University at the request of this author.

The results indicated a loss of 5.1 % and 5.2 % of volatile substances from the soil samples.

Two (2) residual soil samples from RG Quarry were also tested and a loss of 7.7 % was reported for each sample.

5.2.1.10 Chemical Tests

Chemical analysis of residual soil samples from parent andesite from the Barre de l'isle study site were transported by this author to the Department of Geochemistry at the Newcastle University by technician Mr. Philip Green.

i) pH Value

Rainfall and vegetation appear to have very strong effects on the pH of residual soils. The higher the rainfall the greater the degree of leaching which results in lower pH values and the formation of an acidic medium in residual soils.

Two (2) residual soil samples from the Barre de L'isle study site were tested by this author and were found to have pH values of 4.89 and 4.90.

One water sample was collected from a spring source near the study site and another water sample was taken from the piezometer installed at the site. The water samples were tested at the Caribbean Environmental Health Institute in Saint Lucia and were found to have pH values of 7.3 and 7.5, respectively.

Two (2) residual soil samples from RG Quarry were analysed at the University of Newcastle upon Tyne and had pH values of 5.55 and 5.56.

ii) Sulphate Content

Soluble sulphate concentrations were analysed on three (3) residual soil samples from the Barre de L'isle study site and were found to contain amounts of 0.0034%, 0.0035% and 0.0034% . These very low sulphate concentrations may be due to the fact that sulphates and chlorides are very soluble and are removed from the soil during the early stages of the weathering process (Gidigasu, 1976).

Three (3) residual soil samples from RG Quarry showed soluble sulphate concentrations of 0.0073%, 0.0075% and 0.0110%

iii) Chloride Content

Chlorides tend to be removed from the soil during the early stages of weathering due to very low resistence to solution by infiltrating rainfall and leaching.

Chloride concentrations of 0.0027%, 0.0028% and 0.0030% were found from three (3) residual soil samples from the site which were tested at Newcastle University. Three (3) additional residual soil samples from RG Quarry showed chloride concentrations of 0.0025%, 0.0027% and 0.0035%.

iv) Calcium Carbonate Content

Calcium carbonate concentrations may vary in residual soils based on rainfall and vegetation. In areas of low rainfall and poor drainage conditions, calcium carbonate may occur in abundance (Felt, 1951).

High rainfall conditions and the resulting increase in leaching of the soils results in the reduced presence of calcium carbonate.

The results of tests on two (2) residual soil samples from the Barre de L'isle study site were tested at Newcastle University at the request of this author and showed calcium carbonate concentrations of 0.0090% and 0.0110%. Two (2) soil samples from RG Quarry were found to have calcium carbonate concentrations of 0.0191% and 0.0258%.

v) Organic Content

The amount of organic matter present in residual soils is strongly dependant on climate, vegetation and bacterial activity (Gidigasu, 1976). Mohr and Van Baren (1954) found that in well aerated tropical soils with average rainfall, the production and destruction of humus are in balance. Newill (1959) has shown that the organic matter content is more concentrated in the clay size fraction than in the coarser sized particles in lateritic soils.

Two (2) tests were performed at Newcastle University at the request of this author on residual soil samples from the Barre de L'isle study site and showed the presence of 1.711% and 1.759% of organics. Two (2) residual soil samples from RG Quarry were tested and were found to have organic contents of 2.854% and 3.041%.

5.2.1.11 X-Ray Diffraction Analysis (XRD)

X-ray diffraction analysis is used for identifying the minerals present in tropical soils, but is only appropriate for minerals with distinct crystallography (Queiroz de Carvalho et al, 1997). Modern X-ray diffractometers with crystal monochromators are capable of reliable mineralogical analysis of iron-rich tropical soils.

The grain size of the sample used in the analysis must be reduced to less than 5 to 10 microns. Powders can then be analysed as fillings in cavity mounts or as smear mounts on a glass slide. The powdered mineral is placed in a beam of X-rays which is diffracted through a number of angles by the crystal lattice of the sample. The atomic arrangement of the soil particles are thus determined and this provides a means to measure the spacings of the atomic planes in Angstroms. The atomic spacings are characteristic of the minerals producing them (Gidigasu, 1976).

All crystalline materials have unique X-ray diffraction patterns. The diffraction peaks are first identified and measured as an angle (2θ), which is twice the glancing angle (θ) of the diffracted X-ray beam.

The 2θ angles are then converted to lattice spacings (d) in Angstrom units (A) using the Bragg equation:

$$n\lambda = 2d\sin\theta$$

where,

- n = order of diffraction
- λ = wavelength of the incident X-ray beam
- d = distance between atomic layers in a crystal (lattice spacing)
- θ = angle of incidence (diffraction)

For clays, the highest spacing observed is the most important since it is the distance between the atoms and is the basal spacing.

Two (2) residual soil samples from the Barre de L'isle study site were transported by air freight by this author to the Newcastle University for X-ray diffraction studies in the School of Chemical Engineering and Advanced Materials.

The X-ray diffraction analyses were conducted by the laboratory technician Kath Liddell under the instructions of this author. The results of the analyses are presented in Figure 5.19 and Figure 5.20.

5.2.1.12 Scanning Electron Microscopy (SEM)

The scanning electron microscope is used in soil mechanics to identify the microfabric features or geometrical arrangement of particles and void spaces in a soil sample. The fabric of residual soils is the result of the initial fabric of the parent rock and the immediate environmental factors affecting the weathering process (Irfan, 1999). The inter-particle bonding of the grains result in the presence of true cohesion due to cementation.

Some weak bonding due to electrical attractive forces may exist in some clays or as a result of cementation generated by iron oxides (sexquioxides). The degree of bonding between the soil particles tend to affect the engineering properties of the soil.

The scanning electron microscope is useful in studying fine grained soils in both the transmissive and scanning modes and also the surface of weathered minerals in the sample. The electron beam is set to 100 Angstroms and the particle surface is scanned thereby stimulating emissions of electrons which are recorded and amplified. The output is passed through a cathode ray tube and the image formed has a magnification which depends upon the ratio of the lengths of the final and initial scanning movements
(Gillott, 1968).

The electron beam is focused on the surface of the specimen and the image that appears on the cathode ray tube highlights the secondary electrons in detail over the surface of the specimen. The resulting image on the cathode ray tube represents details of the variable geometric features of the specimen. The scanning electron microscope has the magnification capability of x30 to x100,000 based on the integrity of the specimen.

Collins (1985) classifies the microstructure of residual soils into three distinct levels:

i.) The Elementary level
ii.) The Assemblage level and,
iii.) The Composite level

i) The Elementary level is made up of silt, clay and sand size particles or clusters of clay size particles

ii) The Assemblage level comprises a larger number of clay or granular particles with defined boundaries consisting of :
- Matrices
- Aggregations
- Granular matrices

i) The Composite level consists of three categories:
- the composite microfabric
- relative abundance of reflecting the heterogeneity
- the degree of anisotropy

Two (2) air-dried lump residual soil samples from parent andesite rock from the Barre de L'isle study site and RG Quarry were subject to scanning electron microscopy (SEM) in the School of Chemical Engineering and Advanced Materials at the Newcastle University. The SEM analysis was performed by technician Grant Staines and his associates under the direction of this author. A JEOL Scanning Electron Microscope: Model JSM – 5300 LV was utilised for this exercise using magnifications x500 and x2000 for the Barre de L'isle sample (sample #1) and x750 and x2000 for the RG Quarry sample (sample #3).

Figure 5.20a shows the SEM peaks for Sample #1 from the Barre de L'isle study site.

The air-dried lump soil samples were prepared by the technicians and mounted on a hollow, cylindrical aluminium platen and examined under the Scanning Electron Microscope as shown in Figure 5.21 and Figure 5.22.

SEM images of magnification of x500 and x2000 of the Barre de L'isle study site residual soil sample are shown in Figure 5.23 and Figure 5.24. In accordance with the classification of Collins (1985) the soil shows an open, loosely bonded structure with clay size clusters in the elementary level at magnification x500 (Figure 5.23). At magnification x2000 (Figure 5.24) some weathering of the soil particles can be seen and the soil has large openings indicative of a high porosity.

Figure 5.25 shows the sample after saturation with water at x2000 magnification. The pores are filled with water and it appears that there is some alteration in the micro-textural orientation of the soil particles due to the increased pore water pressure ie, the soil particles have shifted around.

The SEM images of the soil sample from RG Quarry at magnification x750 and x2000 show similar micro-structural arrangement to that of the Barre de L'isle study site in both the dry and wet stages as shown in Figure 5.26 to Figure 5.28.

5.2.2 Field Tests Results for Residual Soil from Parent Andesite Rock

5.2.2.1 Standard Penetration Test (SPT)

The Standard Penetration Test (SPT) is an in situ dynamic penetration test designed to provide information on the engineering properties of soils. The test procedure is outlined in the British Standards (BS EN ISO 22476-3) and in the American Standards for Testing and Materials (ASTM) D1586. The purpose of the test is to provide an indication of the relative density of cohesionless soils such as sands and gravels, but it is also used to recover disturbed samples of silty and clayey soils.

A brief explanation of the test procedure is warranted here. To perform this test, a split spoon sampler is lowered down a pre-drilled borehole until it rests on the layer of soil to be tested. It is then driven into the soil for a length of 450 mm by means of a 65 kg weight hammer free falling 760 mm for each blow.

The number of blows required to drive the last 300 mm is recorded and this figure is designated the 'N' value of the soil. The first 150 mm of driving is ignored because of possible loose soil in the bottom of the borehole from the boring operations. The sampler is then removed from the borehole and its contents examined.

Standard Penetration Tests were performed on the subsoils at the Barre de L'isle Study site during the installation of the standpipe piezometer (BH09-BS-2). The results of the tests are shown in the graph in Figure 5.28a.

The residual soil deposit varies in particle size from a firm clayey silt to a compact silty sand layer and sandy silt. The highly weathered andesite parent rock is very dense.

5.2.2.2 Rainfall Data

Mean annual rainfall in Saint Lucia varies from 1450 mm at the Hewanorra Airport in the southern part of the island to approximately 3450 mm at Edmond Forest in the upper highlands. In general, rainfall is closely related to elevation, with the areas at sea level in the extreme north and south of the island receiving the least rainfall (mostly cyclonic, with some convectional rainfall). Adjacent areas in the Eastern Caribbean receive a mean annual rainfall of some 900mm, this being cyclonic. The high interior of the island receives the most rainfall, with a high proportion of this being orographic.

Historically, rainfall is consistently higher for the latter six (6) months of the year with maximum rainfalls being experienced in September to November. Conversely, February to May are the driest months with mean monthly minima varying between 45mm and 170mm.

The total rainfall experienced at the Barre de L'isle Study Site during the period of January 1st , 2009 – January 31st , 2010 was 7850.4 mm. Most of this amount of rainfall occurred during the wet season months of August to December (7366.2 mm). Rainfall for the dry season months of February to July was 484.2 mm. Rainfall data for the month of April, 2009 is not available. Figure 5.28b contains a graph of the rainfall during the period of February 1st, 2009 to January 31st, 2010.

Figure 5.29 to Figure 5.39 show the daily rainfall graphs for the Barre de L'isle Study Site for the period February 1st, 2009 to January 31st, 2010.

5.2.2.3 Standpipe Piezometer Data

A knowledge of excess pore water pressure conditions in the subsoils is required for calculation of the factor of safety of a slope. The measurement of excess pore water pressure within a saturated zone is most commonly carried out using piezometers installed in boreholes. The time taken for the piezometer to respond to a change in pore water pressure in the ground should be significantly short to give a meaningful accurate measure of the actual pore pressure. The response time will depend on the rate of change of groundwater pressures due to seasonal rainfall and individual storm events and the accuracy required.

Due to the various factors within the hydrological cycle that affect groundwater flows, and hence piezometer levels, a wide range of piezometric responses can be anticipated. The principle ways in which piezometers may respond to rainfall can be considered as either:

i) a storm response, being short term-hours to days
ii) a seasonal response, being longer term-months to years, or
iii) a combination of both effects.

Monitoring of the instrumentation at the study site provided the first stem in obtaining data necessary for slope stability analysis. Recorded groundwater level indicated a reliable estimate of the effect of pore water pressure fluctuations on the stability of the slope. Piezometer response to rainfall were recorded for the period of August 1st , 2009 to January 31st , 2010 at the Barre de L'isle Study Site. Because of the isolated location of the site some daily readings were not recorded. A graph of the standpipe piezometer readings is presented in Figure 5.40.

5.2.2.4 Jet Fill Tensiometer Data

The pore-water pressure response to rainfall and infiltration was measured by the jet-fill tensiometers installed at the site. The tensiometers were read frequently although it was not always possible to maintain daily readings due to the remote location of the site.
The tensiometers readings were carried out together with the rainfall and piezometer readings during the period of August 1st, 2009 to January 31st, 2010. The jet-fill tensiometer readings are illusrated from Figure 5.41a to Figure 5.41c.

5.2.2.5 Slope Inclinometer Data

The slope inclinometer installed at the Barre de L'isle Study Site was monitored during the period of June 24th 2009 to November 23rd, 2009. The inclinometer readings indicate that the shear zone is in a clayey silt residual soil layer at a depth of 12.2m (40.0 ft) below existing ground surface. The movement zone lies between a silty sand layer and a sandy silt layer which overlies the weathered andesite bedrock. As discussed in section 5.2.1.1 the silty sand layer is located at a depth of 9.0m below ground surface and it is this author's belief that the silty sand seam acts as a subterranean spring which is recharged from a source upslope from the study site and discharges in an active spring at the toe of the slope. This would explain the rapid pore pressure response in the standpipe piezometer during periods of intensive rainfall since the silty sand has a greater saturated hydraulic conductivity than the overlying residual soil. Figure 5.42 shows a graph of the incremental movement in the inclinometer during the monitoring period.

5.2.2.6 Surface Runoff/Infiltration

Surface soil infiltration rates represent the critical soil parameter determining how much rainwater will enter the soil and how much will run off for the event of each rain shower. A simple apparatus was used for the measurement of the runoff and infiltration rate at this site due to limited financial resources. The apparatus and the procedure used were described in Chapter 4 under the sub-heading 'Surface runoff Apparatus'.

The runoff and infiltration tests were carried during the actual rainfall event of October 7, 2009 when a total of 488 mm of rainfall was collected over a 24 hour period. The immediate surface run-off measured over a 60 minute period was 25 mm out of a total rainfall of 45 mm. The remaining 20 mm or 44 % of the total rainfall would have been temporarily held in the macro-pores in the soil and released over the following hours and days as lateral subsurface water flow through the soil profile. The resulting infiltration rate calculated was 5.6×10^{-6} m/sec.

5.2.2.7 Saturated Hydraulic Conductivity Test of Residual Soil

A falling head permeability test was conducted in the standpipe piezometer installed at the site in accordance with the standards specified by the United States Department of the Navy, Naval Facilities Engineering Command – 1974 (NAVFAC), for a cased borehole with a perforated extension of length 'L'.

The expression used to calculate the in situ saturated hydraulic conductivity test is explained in Section 4.4.2 of this thesis (In situ Hydraulic Conductivity Test).

The results of the test indicate that the saturated hydraulic conductivity of the residual soils at the Barre de L'isle study site was 9.0×10^{-5} m/sec.

The saturated hydraulic conductivity of the 2.0m thick sand layer encountered at 9.0 m in borehole BH09-BS-2 was estimated from the grain size distribution curve to be in the order of 1×10^{-3} m/sec (Cedergren, 1977).

5.3 Windjammer Landing Beach Resort Study Site

5.3.1 Laboratory Tests Results for Colluvium from Parent Basalt Rock

5.3.1.1 Moisture Content

The natural moisture content of the colluvium from parent basalt rock recovered in boreholes BH08-SP-13 to BH08-SP-15 and TP08-43C at the Windjammer Landing Beach Resort study site averaged at 36.8%, 28.4% and 32.6% respectively.

The moisture content of samples of colluvium recovered in boreholes BH08-SP-2 to BH08-SP-11 during the 2008 supplementary field instrumentation programme in the 2005 landslide area at the Windjammer Landing Beach Resort ranged from 5.4% to 60.8%.

The moisture content of colluvial soil samples from the 2005 landslide at the Windjammer Landing Beach Resort was recorded between 7.9% and 66.1%.

Colluvial soil samples from the Boguis landslide in 1998 showed moisture contents ranging from 18.1% to 51.8%.

5.3.1.2 Atterberg Limits

The colluvium recovered from boreholes BH08-SP-13 to BH08-SP-15 and test pit TP08-43C from the study site was found to have liquid limits ranging from 48% to 62% and plastic limits of 27% to 32%. Plasticity indices were from 21% to 30%.

Colluvial material collected during the 2008 supplementary field instrumentation program from boreholes BH08-SP-7 and BH08-SP-11 in the area of the 2005 landslide showed liquid limit values from 36% to 68% and plastic limits ranging from 26% to 36%. Plasticity indices were from 3% to 32%.

Colluvial soil samples recovered from the 2005 landslide investigation at the Windjammer Landing Beach Resort was found to have liquid limit values of 55% to 83% and plastic limits of 18% to 68%. Plasticity indices ranged from 15% to 41%.

Liquid limit and plastic limit values of 64% to 90% and 23% to 31% respectively, were found in colluvial soil samples from the Boguis landslide in 1998. Plasticity indices ranged from 36% to 62%. The high liquid limit values for the colluvium indicate the presence of montmorillonitic swelling clays.

The Plasticity Charts for the colluvium at the Windjammer Landing Beach Resort Study Site are contained in Appendix E.

5.3.1.3 Particle Size Distribution

The grain size distribution of the colluvium material at the study site consist of 26.4% sand; 59.9% silt and 13.7% clay.

Samples recovered from the 2008 supplementary field instrumentation programme at the Windjammer Landing Beach Resort were tested for grain size distribution and were found to contain 40% sand; 53% silt and 6% clay.

The grain size distribution for soil samples recovered during the 2005 landslide at the Windjammer Landing Beach Resort consist of 1.0% gravel; 26.5% sand; 61.7% silt and 10.8% clay.

5.3.1.4 Bulk Density

Bulk density values for two (2) samples of colluvium from the study site were 17.4 kN/m^3 and 17.5 kN/m^3. The bulk density of colluvium samples from the Boguis landslide was 19.8 kN/m^3.

Colluvium samples from the 2005 landslide at the Windjammer Landing Beach Resort were found to have the following bulk densities shown in Table 5.2.

Table 5.2 Summary of Bulk Density values for Colluvium at the 2005 Landslide at the Windjammer Landing Beach Resort

Borehole No.	Depth (m)	Bulk Density (kN/m^3)
TP06 - 2	3.0	17.5
BH05-STD-1	4.6	18.9
BH05-STD-1	6.0	20.0
BH05-STE-1	17.7	20.1
BH05-STC-1	4.9	20.4
TP06 – 1	6.0	20.4
BH05-STE-1	10.4	20.8

5.3.1.5 Specific Gravity

Undisturbed samples of colluvium recovered from the 2005 landslide at the Windjammer Landing Beach Resort were transported by aircraft to the University of Newcastle upon Tyne by this author for index testing in their soil mechanics laboratory. The tests conducted included particle density analyses which were performed by this author.
The results of the tests are shown in Table 5.3.

Table 5.3 Summary of Particle Density tests performed on colluvium soil samples from the 2005 landslide at the Windjammer Landing Beach Resort

Borehole No.	Depth (m)	Particle Density
BH05-STA-1	4.3	2.48
BH05-STB-1	3.6	2.56
BH05-STC-1	3.6	2.53
BH05-STD-1	2.4	2.65
BH05-STE-1	3.0	2.34
BH05-STF-1	3.6	2.30
BH05-STG-1	5.7	2.37

5.3.1.6 Soil - Moisture Density

One (1) soil-moisture density test was performed on a sample of colluvium recovered from the study site at the Windjammer Landing Beach Resort.

5.3.1.7 Direct Shear Strength Tests

Two (2) undisturbed samples of colluvium recovered in test pits TP08-43-1 and TP08-45-1 excavated in close proximity to the study site were transported by aircraft to the University of the West Indies (UWI) in Trinidad for shear strength testing in their soil mechanics laboratory. The soil samples were tested in direct shear as requested by this author. The results of the tests are presented in Table 5.4.

Table 5.4 Summary of Direct Shear Strength Tests results on samples of Colluvium from the Windjammer Landing Beach Resort Study Site

Test Pit No.	Material	Depth	Bulk Density	Effective Cohesion		Effective Angle of Internal Friction		Source
			γ	c'		ϕ'		
		(m)	(kN/m^3)	(kPa)		(degrees)		
				peak	residual	peak	residual	
TP08-43-1	colluvium	1.5	17.4	6.8	1.9	32.5	20.0	UWI
TP08-45-1	colluvium	1.5	17.5	12.1	3.5	24.0	22.5	UWI

Figures 5.43 and 5.44 illustrate the plots of the Mohr-Coulomb envelope for the soil samples tested.

5.3.1.8 X – Ray Diffraction Analysis (XRD)

Seven (7) air dried colluvium soil samples recovered from the 2005 landslide at the Windjammer Landing Beach Resort were prepared and analysed by X-ray diffraction by technicians in the School of Chemical Engineering and Advanced Materials under the supervision of this author. The samples of colluvium were recovered from the following boreholes;

Borehole No.	Depth (m)	File No.
SP05-STA-1	4.3	w-a-43.CAF
SP05-STB-1	3.6	w-b-36.CAF
SP05-STC-1	3.6	w-c-36.CAF
SP05-STD-1	2.4	w-d-24.CAF
SP05-STE-1	3.0	w-e-30.CAF
SP05-STF-1	3.6	w-f-36-CAF
SP05-STG-1	5.7	w-g-57-CAF

The X-Ray Diffraction analysis identified the following minerals in the samples of colluvium tested:

Albite	$Na(Si_3Al)\ O_8$
Antigorite	$Mg_3Si_2O_5(OH)_4$
Cristobalite	SiO_2
Montmorillonite	$(Na,Ca)_{0.33}\ (AlMg)_2(Si_4O_{10})(OH)_2.n(H_2O)$
Quartz	SiO_2

Figure 5.45 to Figure 5.51 illustrate the graphs of the the peaks of these minerals for each colluvium sample analysed.

Albite $\{Na(Si_3Al)\ O_8\}$ is a plagioclase feldspar mineral of the tektosilicate group with a specific gravity of 2.62. It is a sodium aluminium silicate which exhibits crystal twining as striations on the crystal face. It occurs in granites and pegmatite masses and in hydrothermal vein deposits and has a cleavage of right angle prisms (Hurlbut, 1971).

Tektosilicates have three-dimensional framework structures which result when each oxygen is shared between two silicons. One ion may sometimes replace another in the structure without altering the form of the crystal. This isomorphous substitution occurs in silicates and in other minerals.

Antigorite $\{Mg_3Si_2O_5(OH)_4\}$ is of the kaolinite-serpentine group of 1:1 layer silicate minerals and isomorphous substitution is limited. Antigorite occurs in the form of fibres and has a dark green to yellowish colour and greasy lustre. It has a hardness of 3.5 to 4 and does not have significant effect on the engineering properties of the soil (Hurlbut, 1971).

Montmorillonite $\{Na,Ca)_{0.33}\ (AlMg)_2(Si_4O_{10})(OH)_2.n(H_2O)\}$ is a 2:1 layer silicate with a layer charge of 0.25 – 0.6. The most distinctive characteristic of montmorillonite is that water and organic liquids can penetrate between the layers and cause an increase in volume and large swelling stresses are generated.

There are di-octahedral and tri-octahedral members of the group which exhibit ionic substitutions in the 2:1 layers which result in a negative charge which may be located in either the tetrahedral or octahedral sheet (Gillott, 1968). The charge is balanced by interchangeable layer cations.

Montmorillonite has a significant effect on the engineering properties of a clay because of its large increase in volume when in contact with water. This results in a marked decrease in the shear strength and stability of the clay.

Quartz $\{SiO_2\}$ is the second most abundant mineral in the earth's crust after feldspar. It is made up of a framework of SiO4 silicon-oxygen tetrahedral with each oxygen being shared between two tetrahedral.

Quartz has a trigonal crystal system made up of a six-sided prism terminating with six-sided pyramids at each end and is the most stable form of silicon dioxide. Pure quartz is colourless but other varieties are classified as milky, smokey, rose and others. It has a hardness of 7.0 on the Moh's scale (Hurlbut, 1971).

5.3.1.9 Environmental Scanning Electron Microscopy (ESEM)

Seven (7) air dried samples of colluvium were analysed in an Environmental Scanning Electron Microscope chamber (ESEM – Phillips XL Series) in the Department of Chemical Engineering and Advanced Materials at the Newcastle University by technician Grant Staines under the supervision of this author. The colluvium samples used for this analysis were selected at the same depth and borehole numbers used in the X-Ray Diffraction analysis, namely;

Borehole No.	Depth (m)
SP05-STA-1	4.3
SP05-STB-1	3.6
SP05-STC-1	3.6
SP05-STD-1	2.4
SP05-STE-1	3.0
SP05-STF-1	3.6
SP05-STG-1	5.7

Advantages of the ESEM include:

i) saturated specimens can be examined since any pressure above 609 Pa allows water to remain in its liquid state for temperatures above 0^{o} C., in contrast with the SEM which uses a vacuum

ii) electrically non-conductive specimens do not require the preparation techniques used in SEM to render the surface conductive

iii) the gas in the chamber is used as a detection medium producing imaging possibilities as opposed to SEM detectors

As a result of these advantages over the SEM, the ESEM processes specimens faster and more easily, avoiding complex and time consuming preparation methods. Gases, liquids and solids can be studied dynamically in situ and in real time. Biological specimens can be maintained fresh and alive. Therefore, the ESEM constitutes a radical breakthrough from conventional electron microscopy.

Observations by means of the ESEM performed on the colluvium samples show details of the microstructure of the minerals.

SP05-STA-1 (4.3m)
At x500 magnification **(**Figure 5.52), the soil particles are well bonded in a clayey matrix. At x2000 magnification (Figure 5.53), the soil particle surface is well bonded with no inter-particle pores.

SP05-STB-1 (3.6m)
At x500 magnification (Figure 5.54) the soil particles have a loosely bonded structure and is porous.

At x2000 magnification (Figure 5.55) fragments of weathered soil particles seem present on a moderately porous surface.

SP05-STC-1 (3.6m)
At x500 magnification (Figure 5.56) the soil particles show a loosely bonded structure with a moderately porous surface.

At x2000 magnification (Figure 5.57) the soil particles are loosely bonded and with a porous surface.

SP05-STD-1 (2.4m)
At x500 magnification (Figure 5.58) the soil particles show a well-bonded structure with low porosity.

At x2000 magnification (Figure 5.59) a well-bonded structure exist with low porosity.

SP05-STE-1 (3.0m)
At x500 magnification (Figure 5.60) the soil particles have a loosely bonded structure and a highly porous surface.

At x2000 magnification (Figure 5.61) a loosely bonded structure and a highly porous surface exist.

SP05-STF-1 (3.6m)
At x500 magnification (Figure 5.62) the soil particles have a loosely bonded structure and a highly porous surface

At x2000 magnification (Figure 5.63) the soil structure is loosely bonded with a highly porous surface.

SP05-STG-1 (5.7m)
At x500 magnification (Figure 5.64) the soil particles are moderately bonded with a slightly porous surface.

At x2000 magnification (Figure 5.65) there is moderate bonding of the soil particles and pore spaces are present on the surface of the specimen.

5.3.2 Field Tests Results for Colluvium from parent Basalt Rock

5.3.2.1 Standard Penetration Test (SPT)

The Standard Penetration Test (SPT) was performed in the colluvium in all the boreholes during the field investigation at the Windjammer Landing Beach Resort study site and during the 2005 landslide investigation. The tests were performed in accordance with the American Standards for Testing and Materials (ASTM) D 1586.

A graph of the 'N'-values from the Standard Penetration Test (SPT) for the colluvium in boreholes BH08-SP-13, BH08-SP-14 and BH08-SP-15 at the study site are shown in Figure 5.66**.**

SPT 'N'- Values for colluvium samples recovered from boreholes BH08-SP-2 to BH08-SP-11 during the 2008 Supplementary Field Instrumentation Programme at the Windjammer Landing Beach Resort are plotted in Figure 5.67 and Figure 5.68.

Figure 5.69 and Figure 5.70 contain graphs of the 'N'- Values for colluvium samples recovered from boreholes BH08-STA-1 to BH08-STG-1 at the 2005 landslide site.

5.3.2.2 Rainfall Data

Rainfall is quantified at a rain gauge station by measuring the amount of rain that falls during a specific period of time. Rainfall infiltration is considered a triggering factor in initiating slope instability by reducing the shear strength of the subsoils

At Trouya, where the Windjammer Landing Beach Resort is located, there is a Government owned rain gauge station in addition to the rain gauge station established at the Windjammer site for this study. Both stations were monitored manually and allowed one measurement per day. However, rainfall data for the period of January to May, 2009 is not available from the Government rain gauge station and is not included in this study. The rain gauge installed at Windjammer was vandalized during December 2008 and rainfall data is not available for the period of January to May 2009.

The rainfall data available for the period of January to August 2008 at the Trouya rain gauge station is presented from Figure 5.71 to Figure 5.78.

Figure 5.79 to Figure 5.85 present the available daily rainfall at the Windjammer Landing Beach Resort rain gauge station for the period of April to December 2008. The data is inconsistent but is helpful in assessing the rainfall conditions at the site during this period. Data for May and June 2008 is not available.

Based on the available rainfall data it is shown that the monthly rainfall average at the Windjammer Landing Beach Resort rain gauge station for the period April to September 2008 was about 140 mm and from October to December 2008 the amount of rainfall increased to almost 216 mm as shown in Figure 5.83 to Figure 5.85.

The daily rainfall from April to September 2008 is 19 mm as indicated in Figure 5.79 to Figure 5.82 which is less than the 24 mm average observed during the period from October to December 2008. Figure 5.82a contains a graph of monthly rainfall for the period of November 1, 2008 to April 30, 2009.

Note the intensive rainfall measurements of 120 mm and 95 mm experienced on October 11 and 12 respectively, which triggered the landslide at the study site and also at other locations on the island.

5.3.2.3 Standpipe Piezometer Data

The standpipe piezometers installed at the 2005 landslide site during the 2008 supplementary instrumentation programme showed some variations in groundwater level in response to rainfall during the monitoring period of June to December 2008, an indication of an increase in pore-water pressures as a result of infiltration during rainfall events. By examining the groundwater level records and their comparison with daily rainfall for the same period the following observations were made:

> The highest groundwater levels in the piezometers were recorded during the months of October and November 2008. During a period of heavy rainfall (120 mm) on October 11, 2008 most of the piezometers showed an increase in water level two to three days after the rainfall event. Therefore, there was a time lag before the highest water level was recorded in the piezometers. However, two of the piezometers showed a negative response to this rainfall event. This was probably due to malfunctioning of the piezometers as a result of faulty installation.

Figure 5.86 presents a graph of the 48-hour pore water pressure response in the standpipe piezometers at the 2005 landslide area to the rainfall event of October 11, 2008.

Figure 5.86a shows the piezometer readings for the period of November 1, 2008 to April 30, 2009 at the Windjammer Landing Beach Resort Study Site.

The pore water pressure increase in the piezometers during this rainfall event decreased slowly after reaching the highest level.

This rainfall event occurred prior to the installation of the instrumentation at the study site. Therefore, there was no piezometer response data for this rainfall event for the study site. Two (2) standpipe piezometers (BH08-SP-13 & BH08-SP-15) were installed at the study site during the period of October 29 to December 18, 2008. BH08-SP-13 was installed at the toe of the slide area and BH08-SP-15 was located at the top of the slope. The monitoring period for the instrumentation was from November 3, 2008 to May 12, 2009.

The piezometer data for November to May 2009 is plotted in Figure 5.87 to Figure 5.90.

5.3.2.4 Jet-Fill Tensiometers

The jet-fill tensiometers installed at the Windjammer Landing Beach Resort study site were monitored during the period of November 14, 2008 to May 12, 2009. The tensiometers were read simultaneously with the standpipe piezometers and the rainfall gauge. Figure 5.91 to Figure 5.93 contain graphs of the pore water pressure response to rainfall in tensometers in Row A, Row B and Row C at the Windjammer Landing Beach Resort Study Site.

5.3.2.5 Slope Inclinometer Data

Monitoring of slope inclinometers BH08-SI-8, BH08-SI-9 and BH08-SI-10 installed at the study site commenced on December 10, 2008.

The slope inclinometers installed in the 2005 landslide area during the 2008 supplementary instrumentation program were monitored from July 2008 to March 2009.
The data recorded indicated that subsurface displacement occurred at various depths at different rates and directions. The four (4) slope inclinometers i.e, BH08-SI-1; BH08-SI-2 ; BH08-SI-3 and BH08-SI-7 detected slow cumulative displacement (0.7mm to 4.8mm) within the colluvium layer over a period of four (4) months (August to November 2008).

Cumulative displacements of 1.4mm to 3.5mm in the colluvium layer were recorded in the slope inclinometers for the period of December 2008 to March 2009.

In all the inclinometers, displacement involved a casing length of 3.0m to 5.0m; with westward orientations at rates of approximately 1.0mm per month. The sliding surface within the 2005 landslide area is located at a depth of 3.0m to 5.0m below ground surface.

5.3.2.6 Saturated Hydraulic Conductivity Tests

The saturated hydraulic conductivity of the colluvium at the study site was determined from falling head permeability tests utilizing the standpipe piezometers installed in the boreholes. The tests were conducted in accordance with the standards specified by the United States Department of the Navay, Naval Facilities Engineering Command – 1974, for a cased borehole with a perforated extension of length 'L'.

Details of the test procedure are outlined in Section 4.4.2 'In Situ Hydraulic Conductivity Test' of this thesis. The results of the tests are as follows :

Table 5.5 Summary of Saturated Hydraulic Conductivity Tests Results for Colluvium at the Windjammer Landing Beach Resort Study Site

Borehole No.	Hydraulic Conductivity (m/sec)
BH08-SP-13	6.3×10^{-5} m/sec
BH08-SP-14	2.0×10^{-6} m/sec
BH08-SP-15	8.7×10^{-6} m/sec

The hydraulic conductivity of the colluvium encountered in the boreholes drilled during the 2008 Supplementary Instrumentation programme are presented in Table 5.6

Table 5.6 Summary of Hydraulic Conductivity Tests Results for Colluvium during the 2008 Supplementary Instrumentation Programme at the Windjammer Landing Beach Resort

Borehole No.	Hydraulic Conductivity (m/sec)
BH08-SP-2	1.6×10^{-5} m/sec
BH08-SP-3	6.4×10^{-7} m/sec
BH08-SP-4	2.0×10^{-7} m/sec
BH08-SP-5	4.7×10^{-7} m/sec
BH08-SP-6	4.0×10^{-7} m/sec
BH08-SP-7	1.0×10^{-7} m/sec
BH08-SP-8	2.4×10^{-7} m/sec
BH08-SP-10	3.2×10^{-6} m/sec
BH08-SP-11	4.5×10^{-7} m/sec

During the 2005 landslide investigation at the Windjammer Landing Beach Resort a pumping test was performed in borehole BH05-STB-1. The result of the test showed the colluvium to have a hydraulic conductivity of 2.3×10^{-4} cm/sec or 2.3×10^{-6} m/sec.

5.3.2.7 The Engineering Properties of Basalt and Andesite Rock Specimens from Saint Lucia

Laboratory index tests were performed on basalt and andesite rock samples collected from engineering projects at variable locations on the island of Saint Lucia to assess the engineering properties for design. The tests performed included uniaxial compressive strength tests, point load tests, cerchar abrasivity tests, and bulk density tests which were conducted in the rock mechanics laboratory of the University of Newcastle upon Tyne. Additional laboratory tests and rock classification were performed on rock samples by this author in Saint Lucia.

LIQUID AND PLASTIC LIMITS TEST REPORT

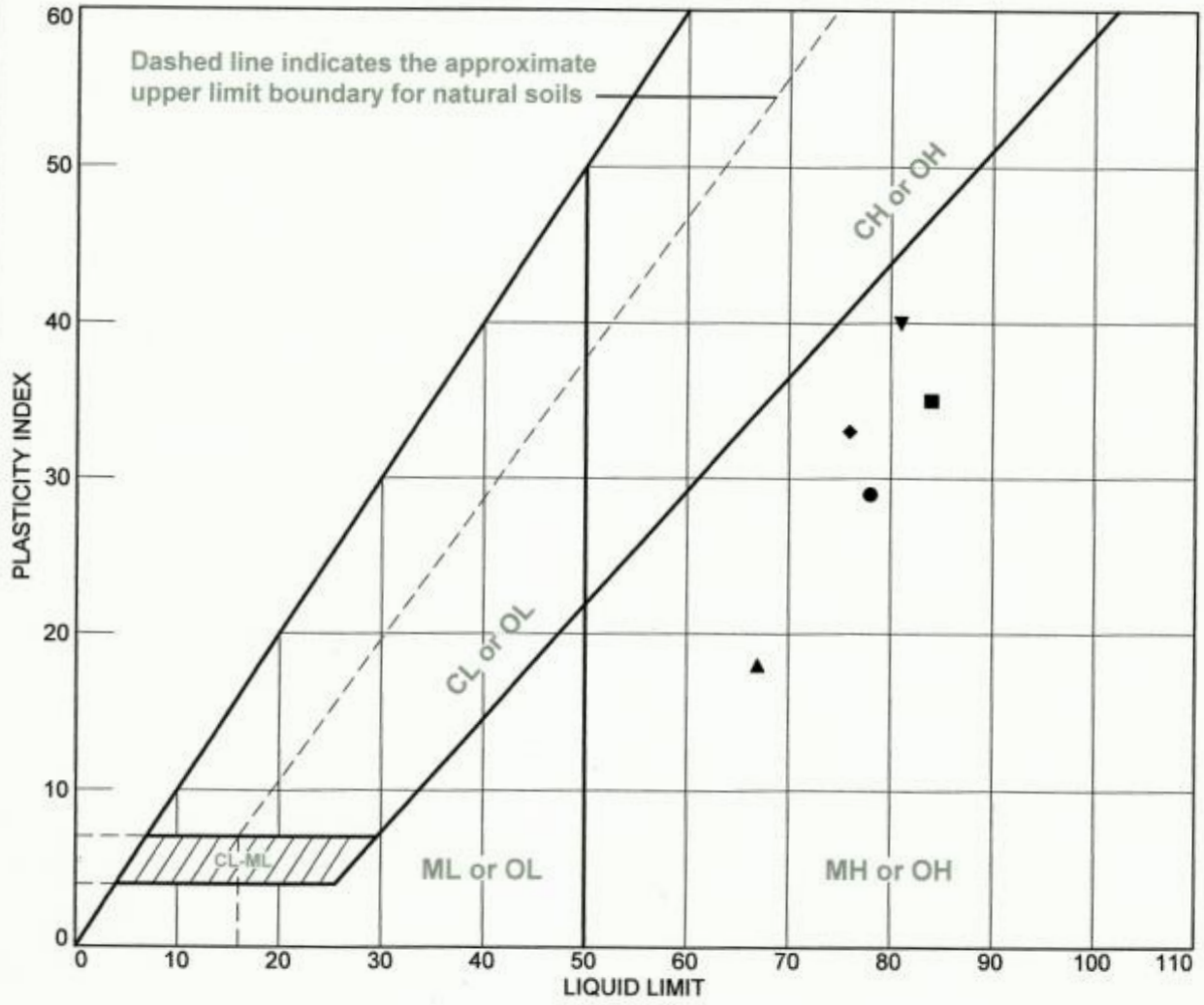

SOIL DATA								
SYMBOL	SOURCE	SAMPLE NO.	DEPTH	NATURAL WATER CONTENT (%)	PLASTIC LIMIT (%)	LIQUID LIMIT (%)	PLASTICITY INDEX (%)	USCS
●	BH09-BS-2		4.6m	52.6	49	78	29	
■	BH09-BS-2		6.0m	59.6	49	84	35	
▲	BH09-BS-2		7.6m	50.8	49	67	18	
◆	BH09-BS-2		9.0m	44.4	43	76	33	SM
▼	BH09-BS-2		10.7m	49.9	41	81	40	MH

STRATA ENGINEERING CONSULTANTS LTD.

Client:

Project: Site Investigation, Barre de L'isle Study Site, Saint Lucia, W.I.

Project No.:

Figure 5.1

Tested By: A.Gabriel **Checked By:** R.Isaac

Particle Size Distribution Report

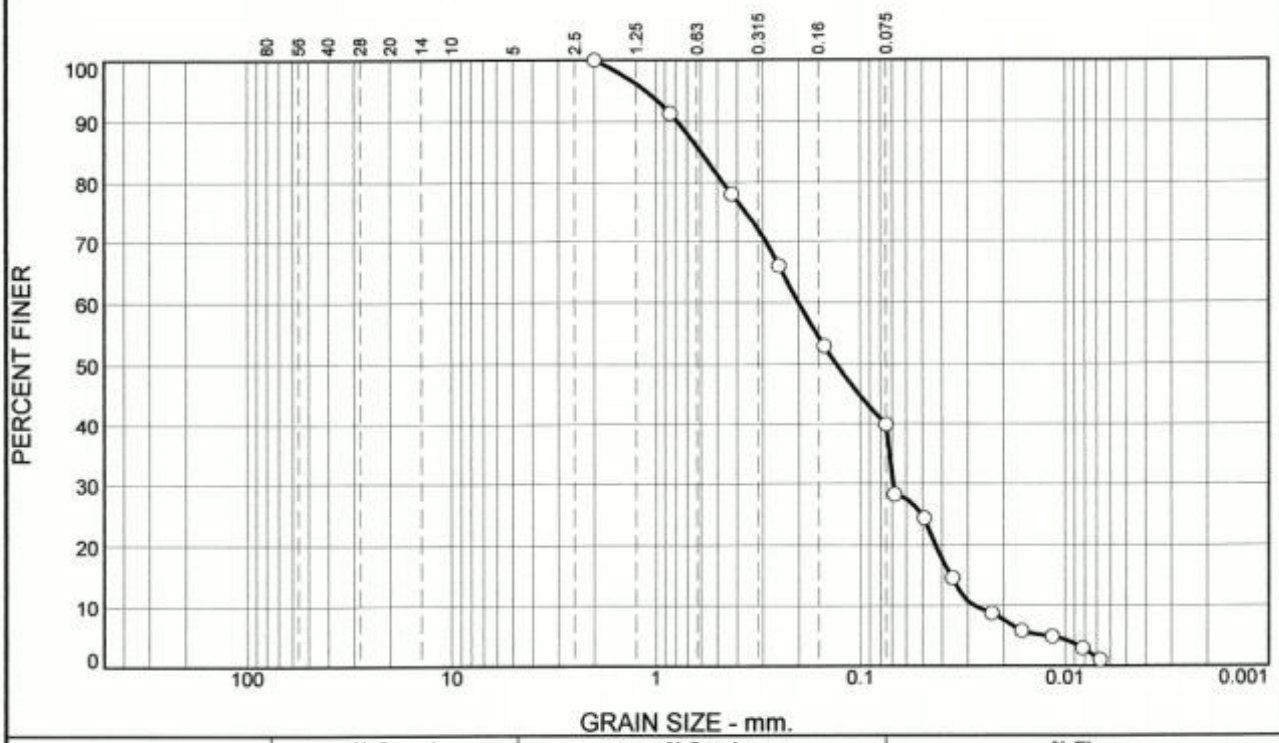

% +3"	% Gravel		% Sand			% Fines	
	Coarse	Fine	Coarse	Medium	Fine	Silt	Clay
0.0	0.0	0.0	0.0	22.0	38.1	39.9	

TEST RESULTS

Opening Size	Percent Finer	Spec.* (Percent)	Pass? (X=Fail)
#10	100.0		
#20	91.3		
#40	78.0		
#60	66.0		
#100	52.9		
#200	39.9		
0.0682 mm.	28.3		
0.0488 mm.	24.4		
0.0355 mm.	14.6		
0.0228 mm.	8.8		
0.0163 mm.	5.9		
0.0115 mm.	4.9		
0.0082 mm.	2.9		
0.0067 mm.	1.0		

* (no specification provided)

Material Description

Atterberg Limits (ASTM D 4318)

PL= LL= PI=

Classification

USCS (D 2487)= AASHTO (M 145)=

Coefficients

D_{90}= 0.7844 D_{85}= 0.6012 D_{60}= 0.2006
D_{50}= 0.1313 D_{30}= 0.0693 D_{15}= 0.0361
D_{10}= 0.0278 C_u= 7.21 C_c= 0.86

Remarks

Date Received: **Date Tested:** 29/01/09

Tested By: A.Gabriel

Checked By: R.Isaac

Title: Managing Director

Source of Sample: BH09-BS-2 **Depth:** 1.5m **Date Sampled:** 12/01/09

STRATA ENGINEERING CONSULTANTS LTD.

Client:

Project: Site Investigation, Barre de L'isle Study Site, Saint Lucia, W.I.

Project No: **Figure** 5.2

Particle Size Distribution Report

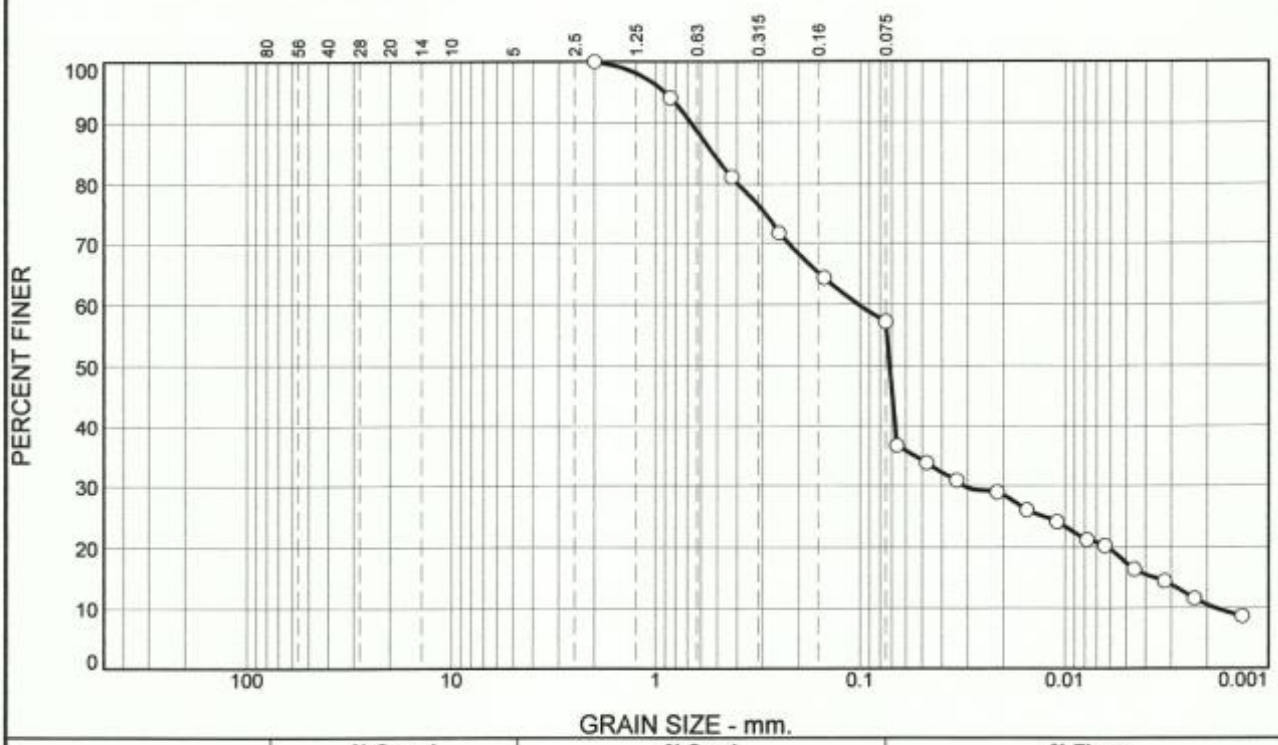

% +3"	% Gravel		% Sand			% Fines	
	Coarse	Fine	Coarse	Medium	Fine	Silt	Clay
0.0	0.0	0.0	0.0	18.9	23.9	46.7	10.5

TEST RESULTS

Opening Size	Percent Finer	Spec.* (Percent)	Pass? (X=Fail)
#10	100.0		
#20	94.1		
#40	81.1		
#60	71.7		
#100	64.4		
#200	57.2		
0.0663 mm.	36.7		
0.0473 mm.	33.8		
0.0338 mm.	30.9		
0.0215 mm.	29.0		
0.0153 mm.	26.1		
0.0109 mm.	24.1		
0.0078 mm.	21.2		
0.0064 mm.	20.3		
0.0046 mm.	16.4		
0.0032 mm.	14.5		
0.0023 mm.	11.6		
0.0013 mm.	8.7		

* (no specification provided)

Material Description

RESIDUAL SOIL - SILT,some clay,little sand,medium plasticity,excessive oxidation,white specks,firm to stiff,wet, rusty brown

Atterberg Limits (ASTM D 4318)

PL= LL= PI=

Classification

USCS (D 2487)= MH AASHTO (M 145)=

Coefficients

D_{90}= 0.6716 D_{85}= 0.5235 D_{60}= 0.1023
D_{50}= 0.0719 D_{30}= 0.0315 D_{15}= 0.0036
D_{10}= 0.0018 C_u= 56.15 C_c= 5.31

Remarks

Date Received: **Date Tested:** 29/01/09

Tested By: A.Gabriel

Checked By: R.Isaac

Title: Managing Director

Source of Sample: BH09-BS-2 **Depth:** 3.0m **Date Sampled:** 12/01/09

STRATA ENGINEERING CONSULTANTS LTD.

Client:

Project: Site Investigation, Barre de L'isle Study Site, Saint Lucia, W.I.

Project No: **Figure** 5.3

Particle Size Distribution Report

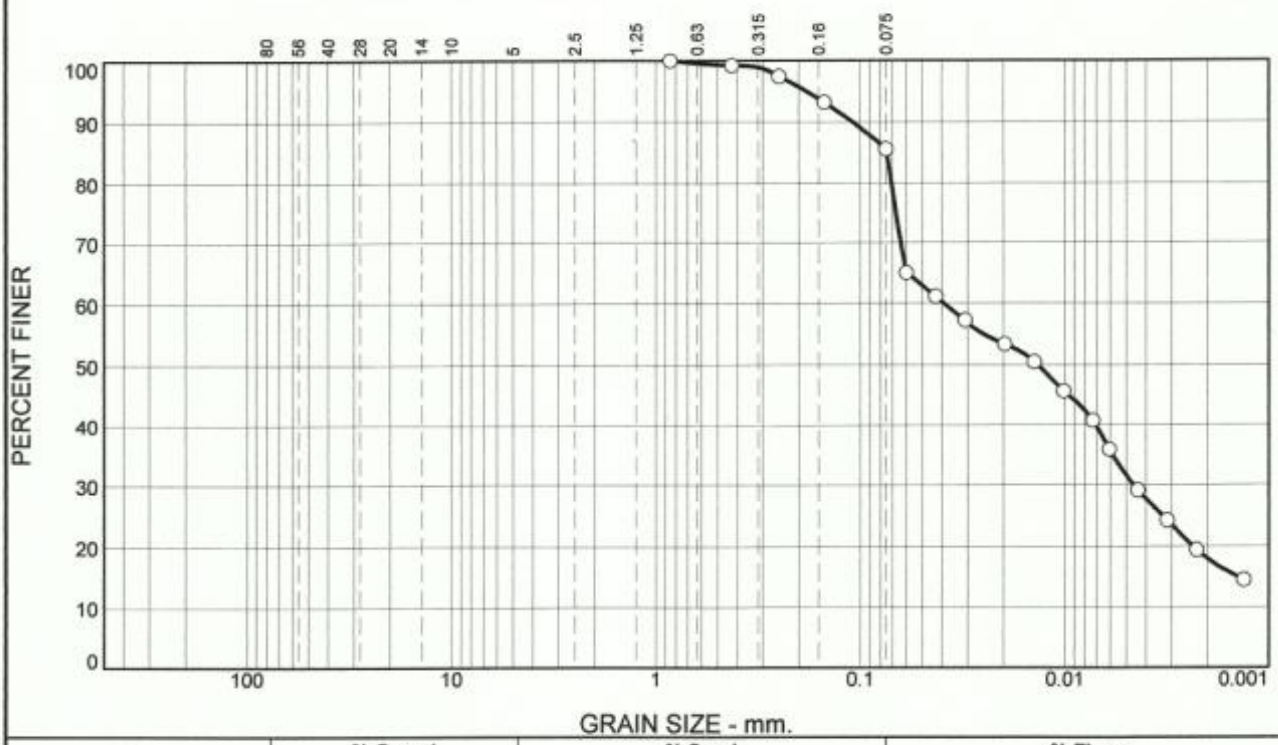

% +3"	% Gravel		% Sand			% Fines	
	Coarse	Fine	Coarse	Medium	Fine	Silt	Clay
0.0	0.0	0.0	0.0	0.8	13.6	67.6	18.0

TEST RESULTS

Opening Size	Percent Finer	Spec.* (Percent)	Pass? (X=Fail)
#20	100.0		
#40	99.2		
#60	97.4		
#100	93.2		
#200	85.6		
0.0597 mm.	65.0		
0.0429 mm.	61.2		
0.0308 mm.	57.3		
0.0198 mm.	53.4		
0.0141 mm.	50.5		
0.0102 mm.	45.6		
0.0073 mm.	40.8		
0.0061 mm.	35.9		
0.0044 mm.	29.1		
0.0031 mm.	24.3		
0.0023 mm.	19.4		
0.0013 mm.	14.6		

* (no specification provided)

Material Description

Atterberg Limits (ASTM D 4318)

PL= 49 LL= 78 PI= 29

Classification

USCS (D 2487)= AASHTO (M 145)= A-7-5(33)

Coefficients

D_{90}= 0.1094 D_{85}= 0.0745 D_{60}= 0.0391
D_{50}= 0.0136 D_{30}= 0.0046 D_{15}= 0.0014
D_{10}= C_u= C_c=

Remarks

Date Received: **Date Tested:** 29/01/09

Tested By: A.Gabriel

Checked By: R.Isaac

Title: Managing Director

Source of Sample: BH09-BS-2 **Depth:** 4.6m **Date Sampled:** 12/01/09

STRATA ENGINEERING CONSULTANTS LTD.

Client:

Project: Site Investigation, Barre de L'isle Study Site, Saint Lucia, W.I.

Project No: **Figure** 5.4

Particle Size Distribution Report

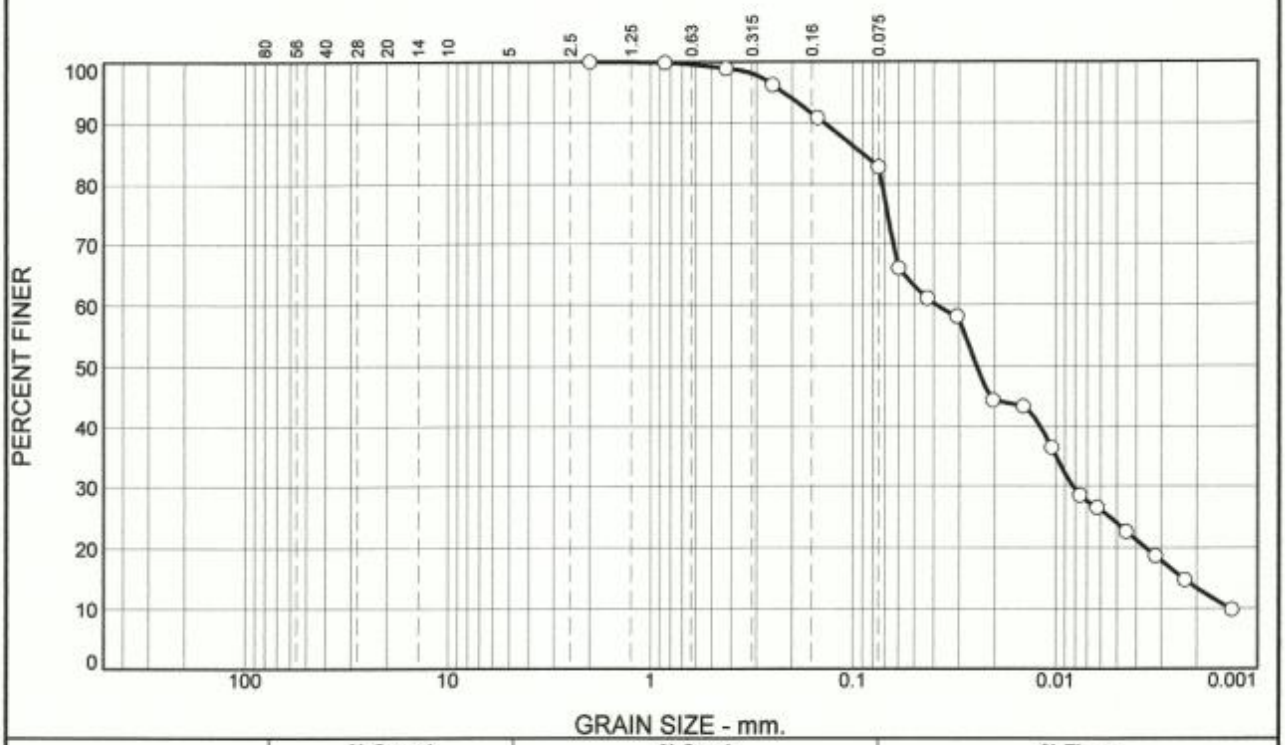

% +3"	% Gravel		% Sand			% Fines	
	Coarse	Fine	Coarse	Medium	Fine	Silt	Clay
0.0	0.0	0.0	0.0	1.1	16.1	69.4	13.4

TEST RESULTS

Opening Size	Percent Finer	Spec.* (Percent)	Pass? (X=Fail)
#10	100.0		
#20	99.9		
#40	98.9		
#60	96.3		
#100	90.9		
#200	82.8		
0.0597 mm.	66.0		
0.0431 mm.	61.1		
0.0308 mm.	58.1		
0.0205 mm.	44.3		
0.0145 mm.	43.3		
0.0105 mm.	36.4		
0.0076 mm.	28.6		
0.0063 mm.	26.6		
0.0045 mm.	22.7		
0.0032 mm.	18.7		
0.0023 mm.	14.8		
0.0013 mm.	9.8		

* (no specification provided)

Material Description

Atterberg Limits (ASTM D 4318)

PL= 49 LL= 84 PI= 35

Classification

USCS (D 2487)= AASHTO (M 145)= A-7-5(37)

Coefficients

D_{90}= 0.1383 D_{85}= 0.0897 D_{60}= 0.0391
D_{50}= 0.0246 D_{30}= 0.0082 D_{15}= 0.0023
D_{10}= 0.0014 C_u= 28.64 C_c= 1.27

Remarks

Date Received: **Date Tested:** 29/01/09

Tested By: A.Gabriel

Checked By: R.Isaac

Title: Managing Director

Source of Sample: BH09-BS-2 **Depth:** 6.0m **Date Sampled:** 12/01/09

STRATA ENGINEERING CONSULTANTS LTD.

Client:

Project: Site Investigation, Barre de L'isle Study Site, Saint Lucia, W.I.

Project No: **Figure** 5.5

Particle Size Distribution Report

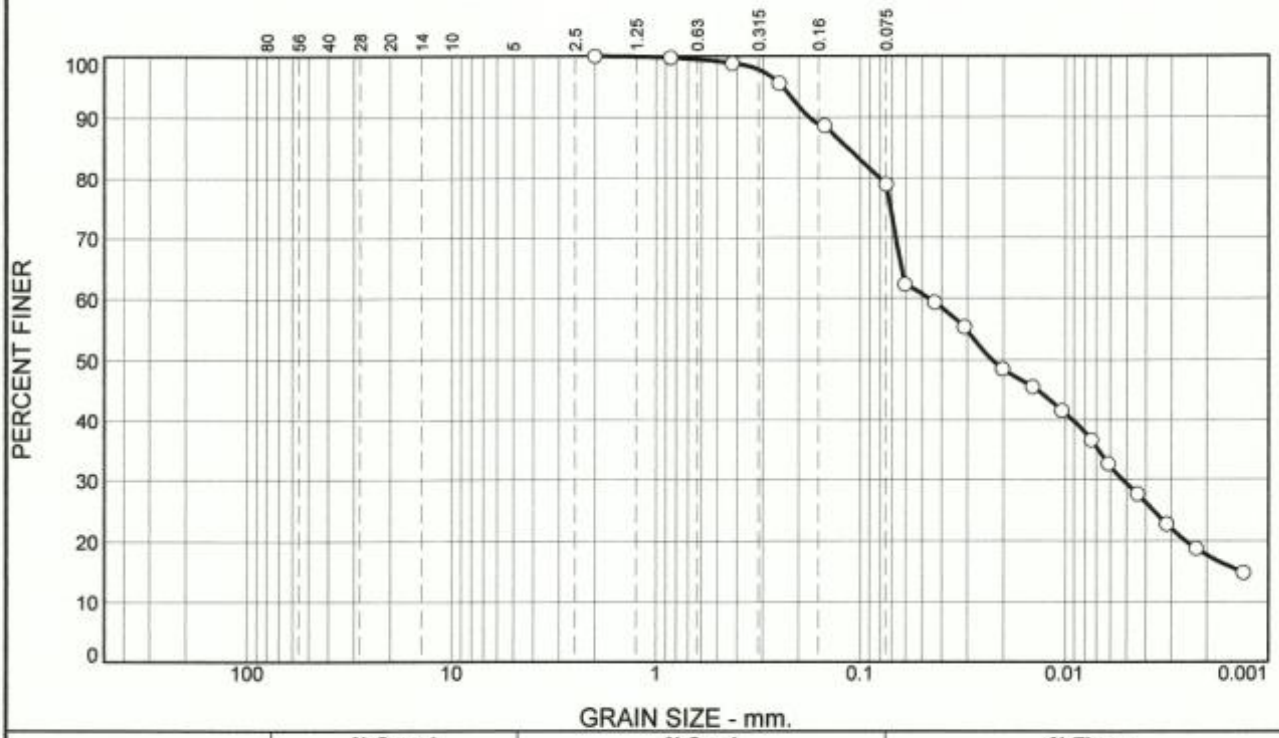

% +3"	% Gravel		% Sand			% Fines	
	Coarse	Fine	Coarse	Medium	Fine	Silt	Clay
0.0	0.0	0.0	0.0	1.1	19.9	61.3	17.7

TEST RESULTS

Opening Size	Percent Finer	Spec.* (Percent)	Pass? (X=Fail)
#10	100.0		
#20	99.8		
#40	98.9		
#60	95.5		
#100	88.6		
#200	79.0		
0.0607 mm.	62.3		
0.0434 mm.	59.4		
0.0311 mm.	55.4		
0.0202 mm.	48.5		
0.0144 mm.	45.5		
0.0103 mm.	41.6		
0.0074 mm.	36.6		
0.0061 mm.	32.6		
0.0044 mm.	27.7		
0.0032 mm.	22.8		
0.0023 mm.	18.8		
0.0013 mm.	14.8		

* (no specification provided)

Material Description

Atterberg Limits (ASTM D 4318)

PL= 49 LL= 67 PI= 18

Classification

USCS (D 2487)= AASHTO (M 145)= A-7-5(20)

Coefficients

D_{90}= 0.1786 D_{85}= 0.1154 D_{60}= 0.0462
D_{50}= 0.0227 D_{30}= 0.0052 D_{15}= 0.0014
D_{10}= C_u= C_c=

Remarks

Date Received: **Date Tested:** 30/01/09

Tested By: A.Gabriel

Checked By: R.Isaac

Title: Managing Director

Source of Sample: BH09-BS-2 **Depth:** 7.6m **Date Sampled:** 12/01/09

STRATA ENGINEERING CONSULTANTS LTD.

Client:

Project: Site Investigation, Barre de L'isle Study Site, Saint Lucia, W.I.

Project No: **Figure** 5.6

Particle Size Distribution Report

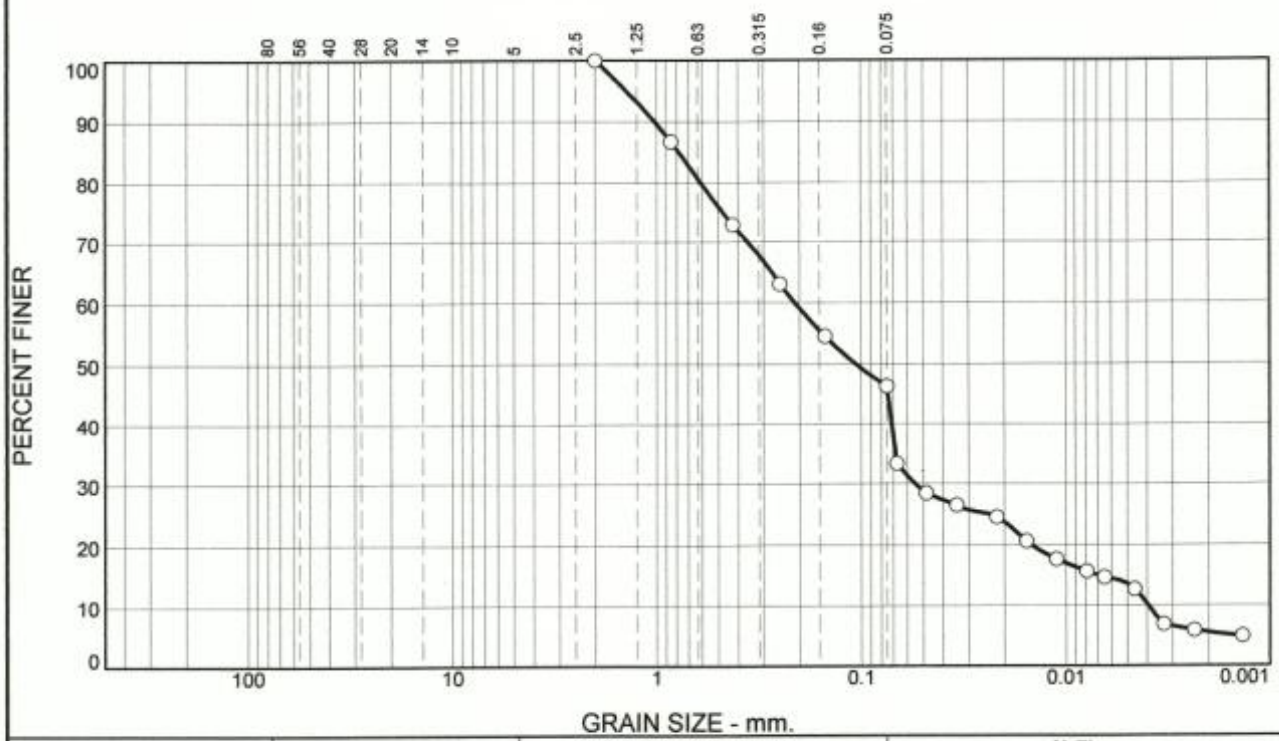

% +3"	% Gravel		% Sand			% Fines	
	Coarse	Fine	Coarse	Medium	Fine	Silt	Clay
0.0	0.0	0.0	0.0	27.1	26.6	32.7	13.6

TEST RESULTS

Opening Size	Percent Finer	Spec.* (Percent)	Pass? (X=Fail)
#10	100.0		
#20	86.7		
#40	72.9		
#60	63.0		
#100	54.5		
#200	46.3		
0.0671 mm.	33.4		
0.0482 mm.	28.5		
0.0343 mm.	26.5		
0.0218 mm.	24.6		
0.0156 mm.	20.6		
0.0111 mm.	17.7		
0.0079 mm.	15.7		
0.0065 mm.	14.7		
0.0046 mm.	12.8		
0.0033 mm.	6.9		
0.0023 mm.	5.9		
0.0014 mm.	4.9		

* (no specification provided)

Material Description

RESIDUAL SOIL - SAND,some silt,little clay,low plasticity, compact,excessive oxidation,wet,rusty brown

Atterberg Limits (ASTM D 4318)

PL= 43 LL= 76 PI= 33

Classification

USCS (D 2487)= SM AASHTO (M 145)= A-7-5(11)

Coefficients

D_{90}= 1.0198 D_{85}= 0.7770 D_{60}= 0.2112
D_{50}= 0.1064 D_{30}= 0.0547 D_{15}= 0.0069
D_{10}= 0.0040 C_u= 53.40 C_c= 3.58

Remarks

Date Received: **Date Tested:** 30/01/09

Tested By: A.Gabriel

Checked By: R.Isaac

Title: Managing Director

Source of Sample: BH09-BS-2 **Depth:** 9.0m **Date Sampled:** 12/01/09

STRATA ENGINEERING CONSULTANTS LTD.

Client:

Project: Site Investigation, Barre de L'isle Study Site, Saint Lucia, W.I.

Project No: **Figure** 5.7

Particle Size Distribution Report

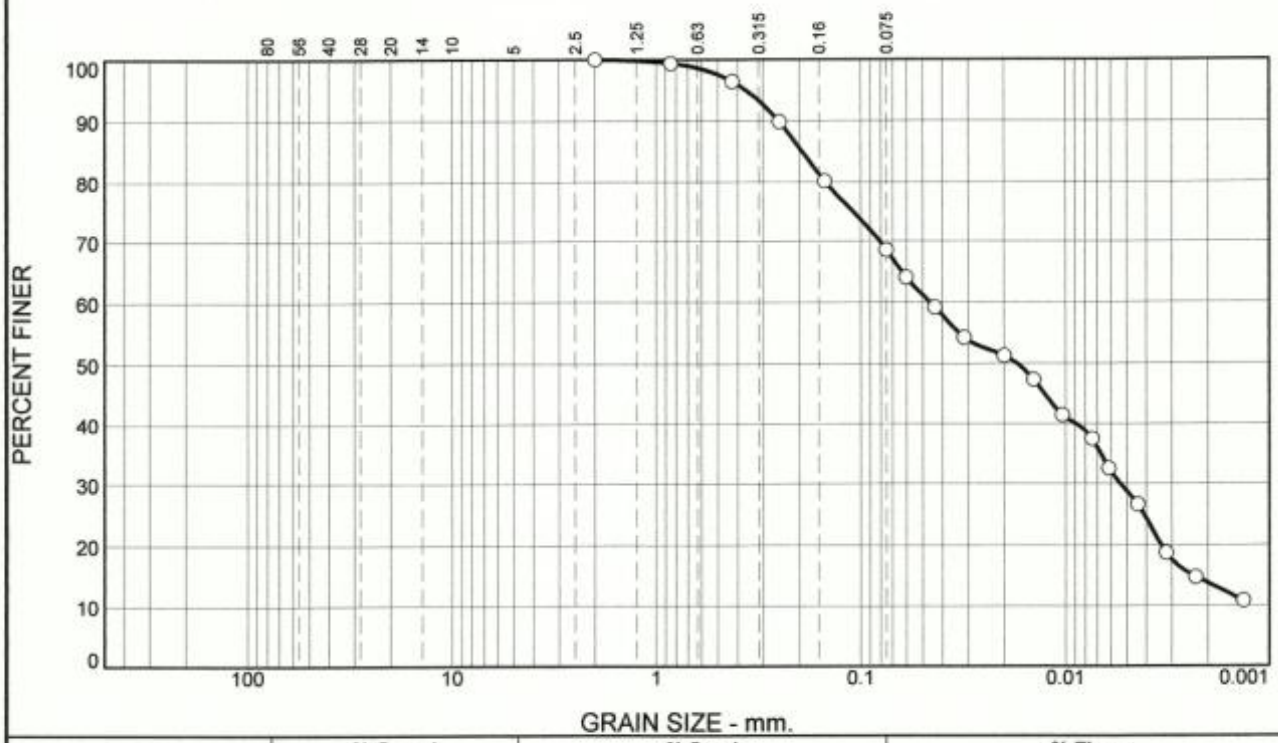

% +3"	% Gravel		% Sand			% Fines	
	Coarse	Fine	Coarse	Medium	Fine	Silt	Clay
0.0	0.0	0.0	0.0	3.6	27.8	54.8	13.8

TEST RESULTS

Opening Size	Percent Finer	Spec.* (Percent)	Pass? (X=Fail)
#10	100.0		
#20	99.4		
#40	96.4		
#60	89.9		
#100	80.1		
#200	68.6		
0.0602 mm.	64.1		
0.0434 mm.	59.2		
0.0313 mm.	54.2		
0.0200 mm.	51.3		
0.0143 mm.	47.3		
0.0103 mm.	41.4		
0.0074 mm.	37.5		
0.0061 mm.	32.5		
0.0044 mm.	26.6		
0.0032 mm.	18.7		
0.0023 mm.	14.8		
0.0013 mm.	10.8		

* (no specification provided)

Material Description

RESIDUAL SOIL - SILT,some sand,some clay,medium plasticity,stiff to very stiff,excessive oxidation,wet,rusty brown

Atterberg Limits (ASTM D 4318)

PL= 41 LL= 81 PI= 40

Classification

USCS (D 2487)= MH AASHTO (M 145)= A-7-5(30)

Coefficients

D_{90}= 0.2520 D_{85}= 0.1932 D_{60}= 0.0460
D_{50}= 0.0173 D_{30}= 0.0054 D_{15}= 0.0024
D_{10}= C_u= C_c=

Remarks

Date Received: **Date Tested:** 30/01/09

Tested By: A.Gabriel

Checked By: R.Isaac

Title: Managing Director

Source of Sample: BH09-BS-2 **Depth:** 10.7m **Date Sampled:** 12/01/09

STRATA ENGINEERING CONSULTANTS LTD.

Client:

Project: Site Investigation, Barre de L'isle Study Site, Saint Lucia, W.I.

Project No: **Figure** 5.8

Particle Size Distribution Report

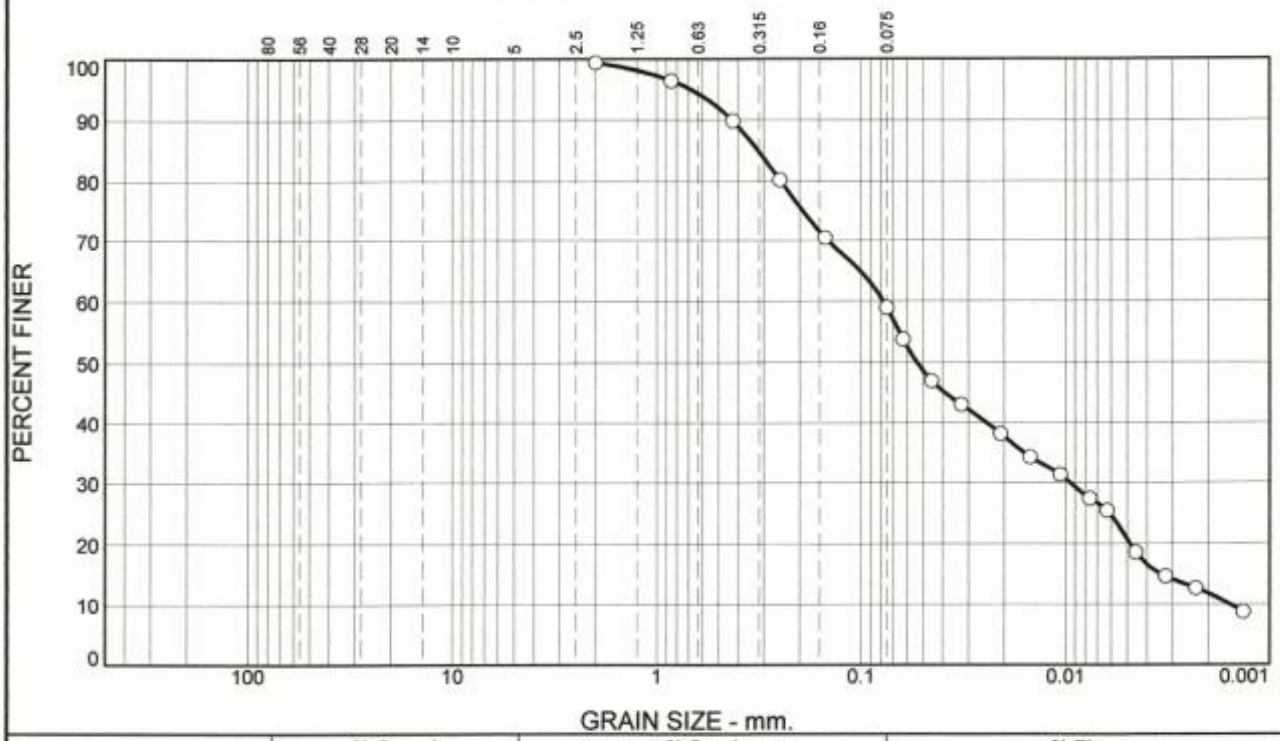

% +3"	% Gravel		% Sand			% Fines	
	Coarse	Fine	Coarse	Medium	Fine	Silt	Clay
				9.5	30.9	47.2	11.8

TEST RESULTS

Opening Size	Percent Finer	Spec.* (Percent)	Pass? (X=Fail)
#10	99.4		
#20	96.4		
#40	89.9		
#60	80.2		
#100	70.5		
#200	59.0		
0.0625 mm.	53.8		
0.0453 mm.	46.9		
0.0325 mm.	43.0		
0.0209 mm.	38.1		
0.0150 mm.	34.2		
0.0107 mm.	31.3		
0.0076 mm.	27.4		
0.0063 mm.	25.4		
0.0045 mm.	18.6		
0.0032 mm.	14.7		
0.0023 mm.	12.7		
0.0013 mm.	8.8		

* (no specification provided)

Material Description

Atterberg Limits (ASTM D 4318)

PL= LL= PI=

Classification

USCS (D 2487)= AASHTO (M 145)=

Coefficients

D_{90}= 0.4284 D_{85}= 0.3189 D_{60}= 0.0782
D_{50}= 0.0535 D_{30}= 0.0096 D_{15}= 0.0034
D_{10}= 0.0016 C_u= 49.93 C_c= 0.75

Remarks

Date Received: **Date Tested:** 30/01/09

Tested By: A.Gabriel

Checked By: R.Isaac

Title: Managing Director

Source of Sample: BH09-BS-2 **Depth:** 12.2m **Date Sampled:** 12/01/09

STRATA ENGINEERING CONSULTANTS LTD.

Client:

Project: Site Investigation, Barre de L'isle Study Site, Saint Lucia, W.I.

Project No: **Figure** 5.9

Particle Size Distribution Report

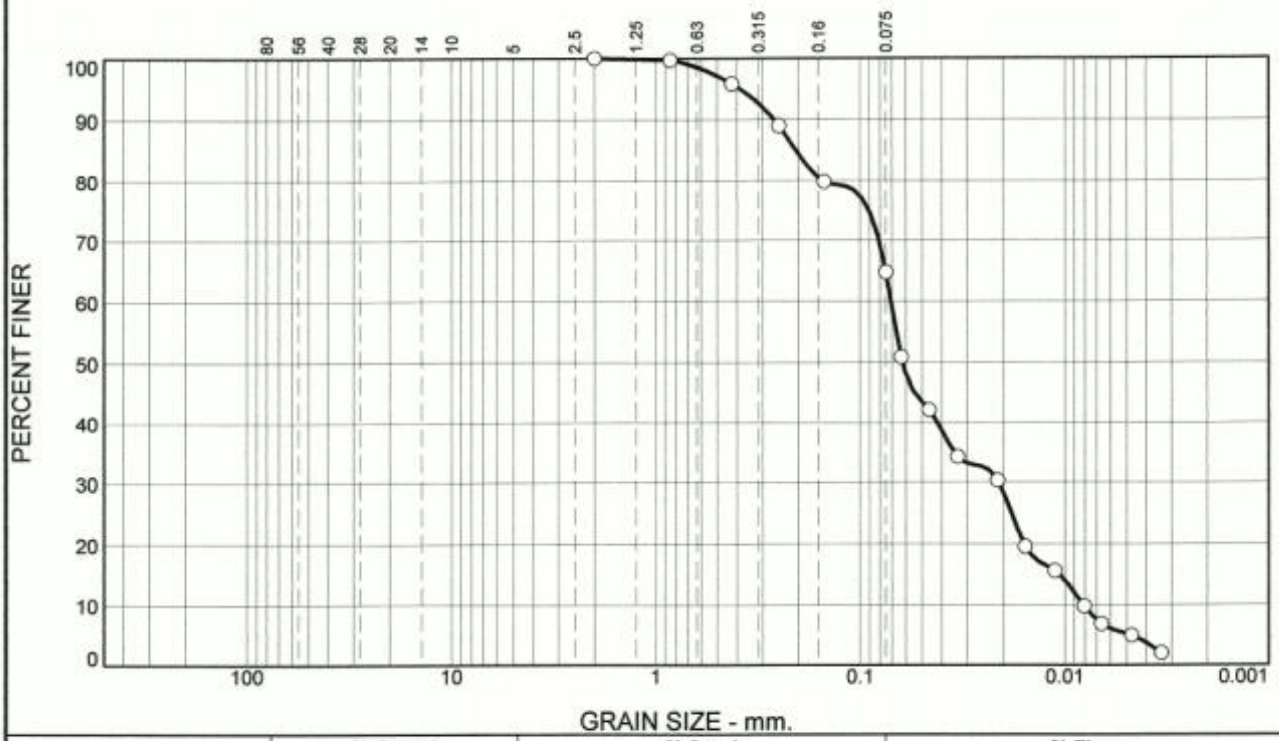

% +3"	% Gravel		% Sand			% Fines	
	Coarse	Fine	Coarse	Medium	Fine	Silt	Clay
0.0	0.0	0.0	0.0	4.2	31.0	64.8	

TEST RESULTS

Opening Size	Percent Finer	Spec.* (Percent)	Pass? (X=Fail)
#10	100.0		
#20	99.7		
#40	95.8		
#60	89.0		
#100	79.8		
#200	64.8		
0.0632 mm.	50.9		
0.0461 mm.	42.1		
0.0334 mm.	34.3		
0.0214 mm.	30.4		
0.0157 mm.	19.6		
0.0112 mm.	15.7		
0.0081 mm.	9.8		
0.0066 mm.	6.9		
0.0047 mm.	4.9		
0.0034 mm.	2.0		

* (no specification provided)

Material Description

RESIDUAL SOIL - SILT,some sand,trace of clay,low to non plastic,compact,excessive oxidation,wet,rusty brown

Atterberg Limits (ASTM D 4318)

PL= LL= PI=

Classification

USCS (D 2487)= MH AASHTO (M 145)=

Coefficients

D_{90}= 0.2636 D_{85}= 0.2061 D_{60}= 0.0708
D_{50}= 0.0622 D_{30}= 0.0211 D_{15}= 0.0106
D_{10}= 0.0081 C_u= 8.70 C_c= 0.77

Remarks

Date Received: **Date Tested:** 30/01/09

Tested By: A.Gabriel

Checked By: R.Isaac

Title: Managing Director

Source of Sample: BH09-BS-2 **Depth:** 13.7m **Date Sampled:** 12/01/09

STRATA ENGINEERING CONSULTANTS LTD.

Client:

Project: Site Investigation, Barre de L'isle Study Site, Saint Lucia, W.I.

Project No: **Figure** 5.10

Particle Size Distribution Report

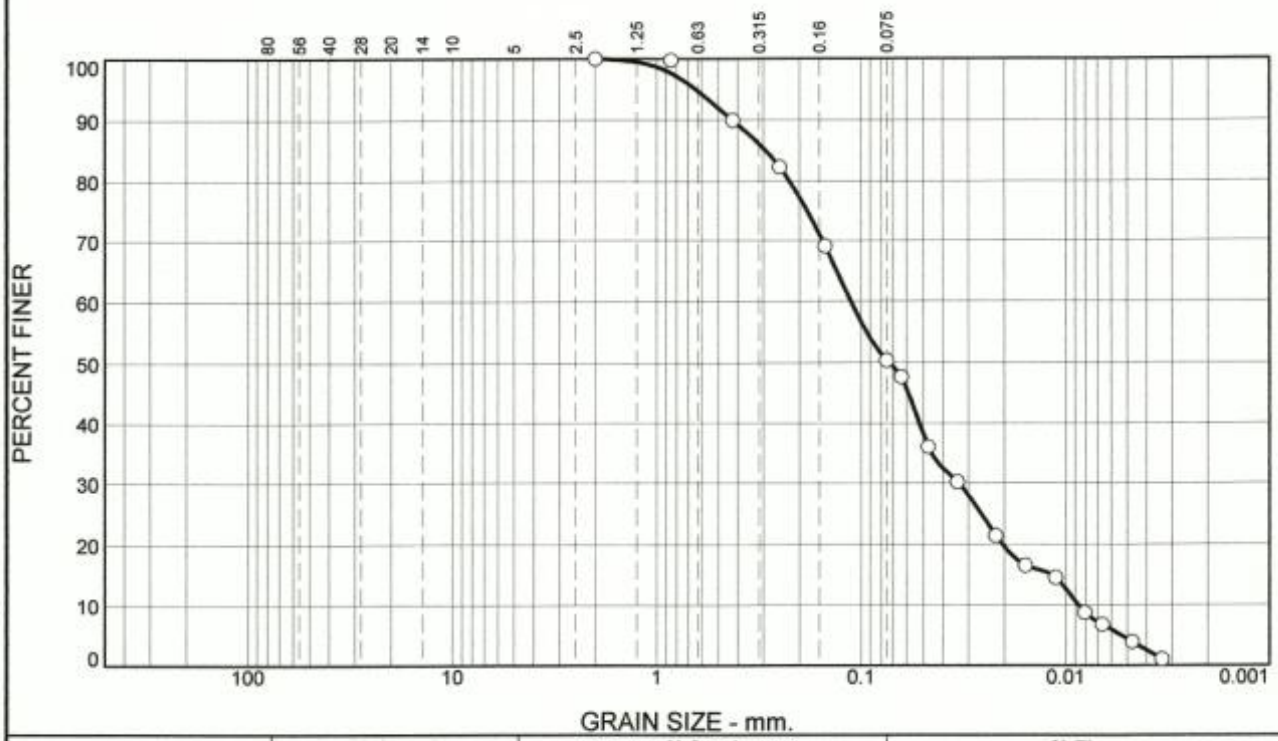

% +3"	% Gravel		% Sand			% Fines	
	Coarse	Fine	Coarse	Medium	Fine	Silt	Clay
0.0	0.0	0.0	0.0	10.0	39.6	50.4	

TEST RESULTS

Opening Size	Percent Finer	Spec.* (Percent)	Pass? (X=Fail)
#10	100.0		
#20	97.6		
#40	90.0		
#60	82.3		
#100	69.1		
#200	50.4		
0.0639 mm.	47.7		
0.0470 mm.	36.0		
0.0339 mm.	30.2		
0.0220 mm.	21.4		
0.0158 mm.	16.5		
0.0112 mm.	14.6		
0.0081 mm.	8.8		
0.0066 mm.	6.8		
0.0047 mm.	3.9		
0.0034 mm.	1.0		

* (no specification provided)

Material Description

HIGHLY WEATHERED ANDESITE - dense to very dense, moist to wet,brown

Atterberg Limits (ASTM D 4318)

PL= LL= PI=

Classification

USCS (D 2487)= ROCK AASHTO (M 145)=

Coefficients

D_{90}= 0.4259 D_{85}= 0.2915 D_{60}= 0.1122
D_{50}= 0.0730 D_{30}= 0.0335 D_{15}= 0.0117
D_{10}= 0.0087 C_u= 12.90 C_c= 1.15

Remarks

Date Received: **Date Tested:**

Tested By: A.Gabriel

Checked By: R.Isaac

Title: Managing Director

Source of Sample: BH09-BS-2 **Depth:** 15.2m **Date Sampled:** 12/01/09

STRATA ENGINEERING CONSULTANTS LTD.

Client:

Project: Site Investigation, Barre de L'isle Study Site, Saint Lucia, W.I.

Project No: **Figure** 5.11

COMPACTION TEST REPORT

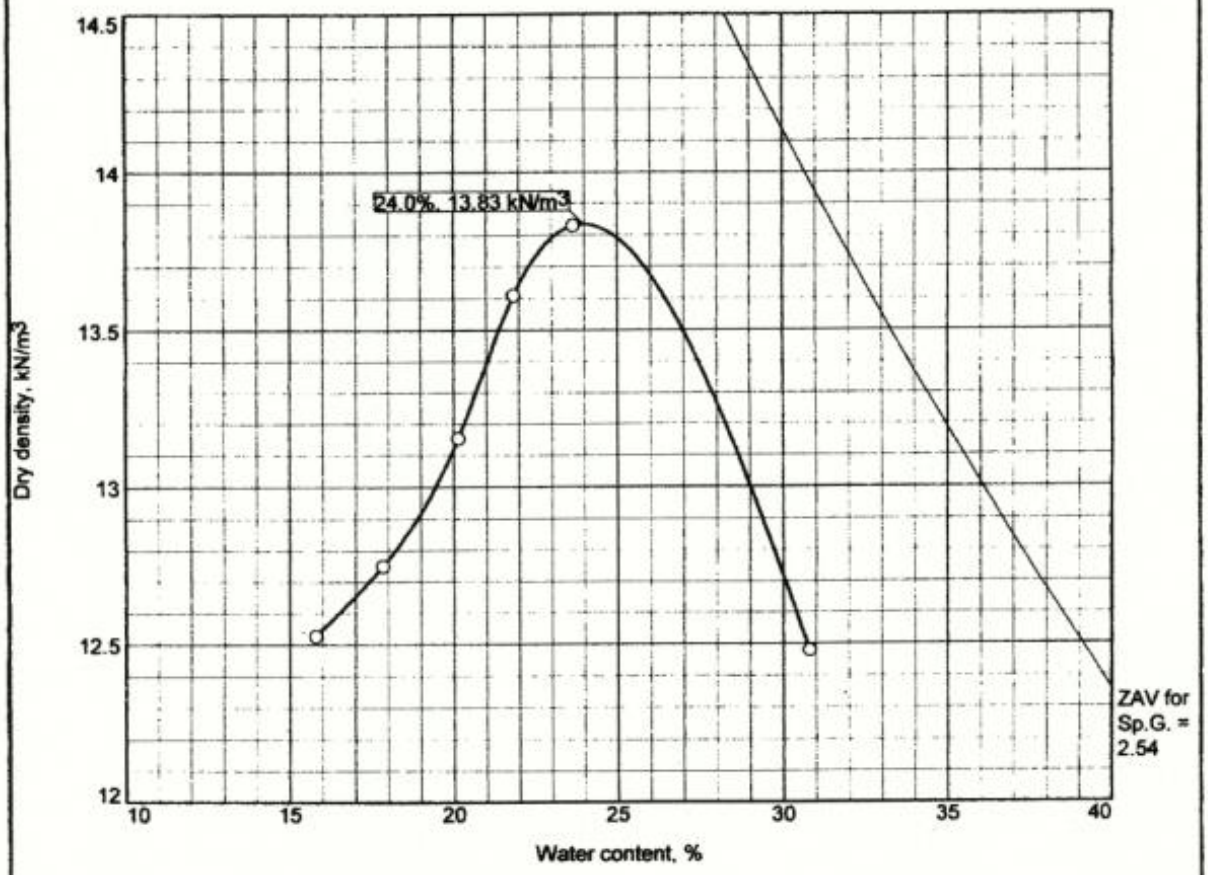

Test specification: ASTM D 698-91 Procedure A Standard

Elev/ Depth	Classification		Nat. Moist.	Sp.G.	LL	PI	% > #4	% < No.200
	USCS	AASHTO						
	MH	A-7-5(35)		2.54	78	38	0.0	78.9

TEST RESULTS	MATERIAL DESCRIPTION
Maximum dry density = 13.83 kN/m3 Optimum moisture = 24.0 %	
Project No. **Client:** **Project:** Site Investigation, Barre de L'isle Study Site, Saint Lucia, W.I. **Location:** Barre D'Isle Hills **Sample Number:** 1	**Remarks:**
STRATA ENGINEERING CONSULTANTS LTD.	**Figure** 5.12

Tested By: A.Gabriel **Checked By:** R.Isaac

Figure 5.12 Moisture-Density Relationship Curve for Residual soil at the Barre de L'isle Study Site

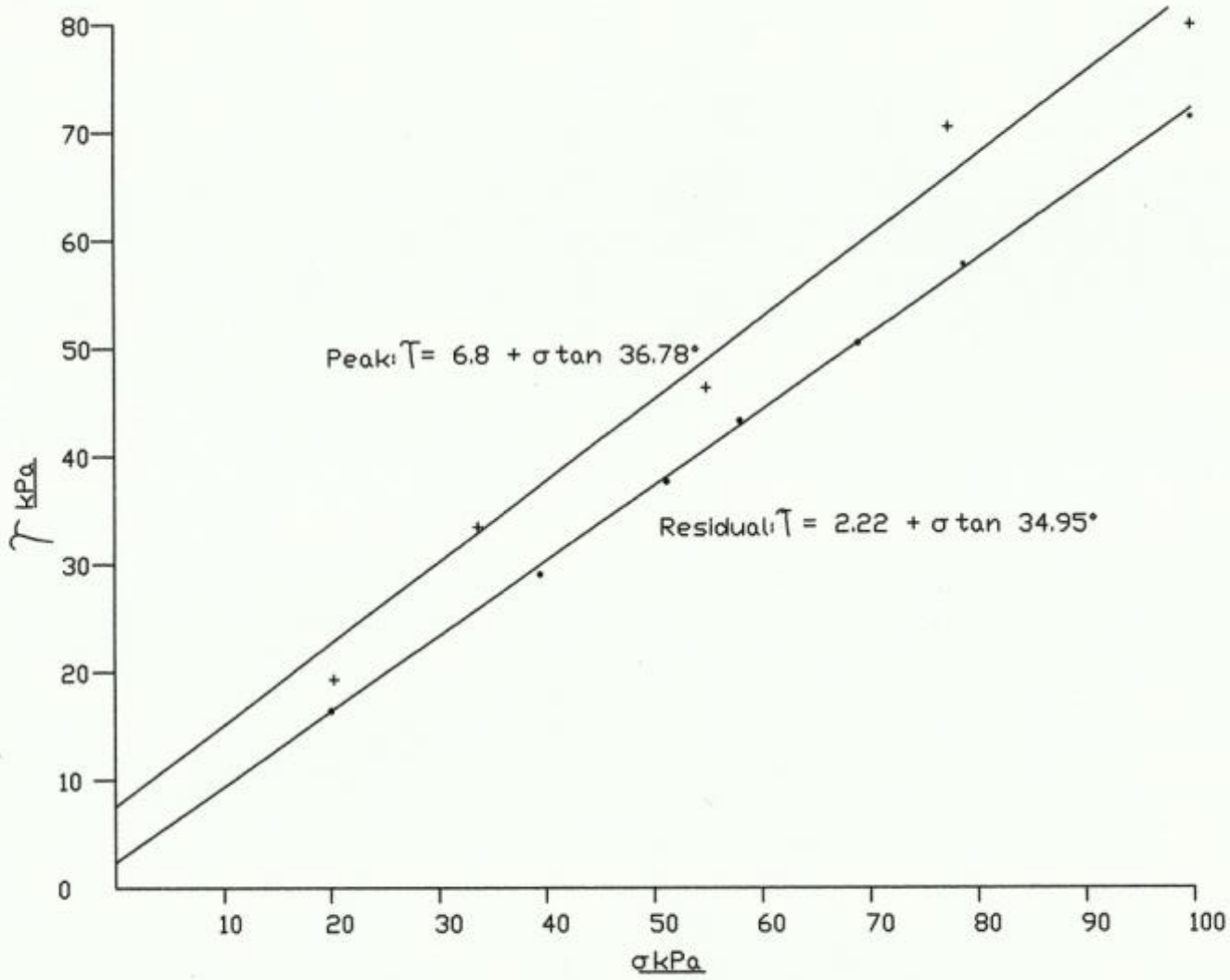

Figure 5.13 Mohr - Coulomb Envelope for Residual soil from site 3 (After Anderson & Kemp, 1985)

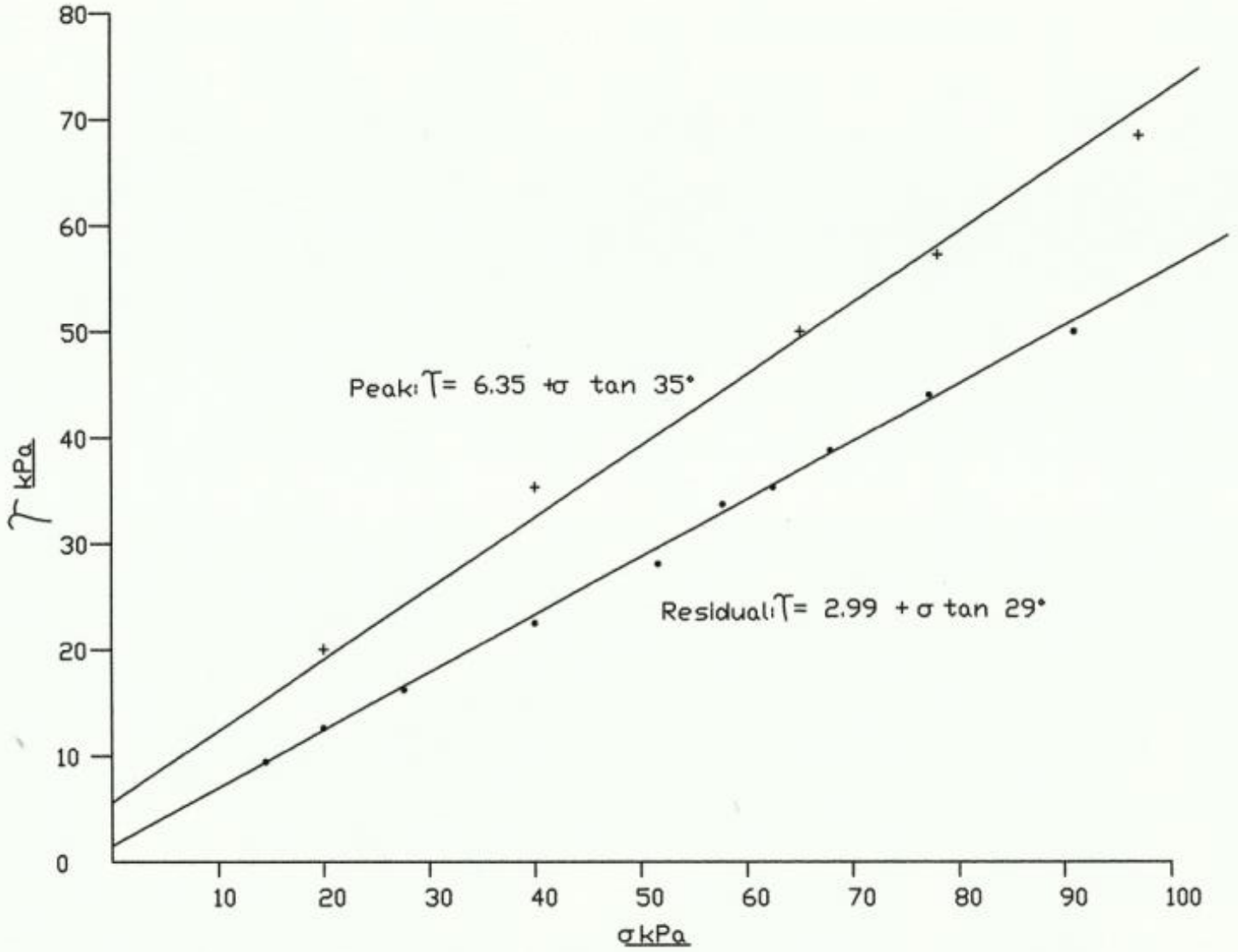

Figure 5.14 Mohr - Coulomb Envelope for Residual soil from site 5 (After Anderson & Kemp, 1985)

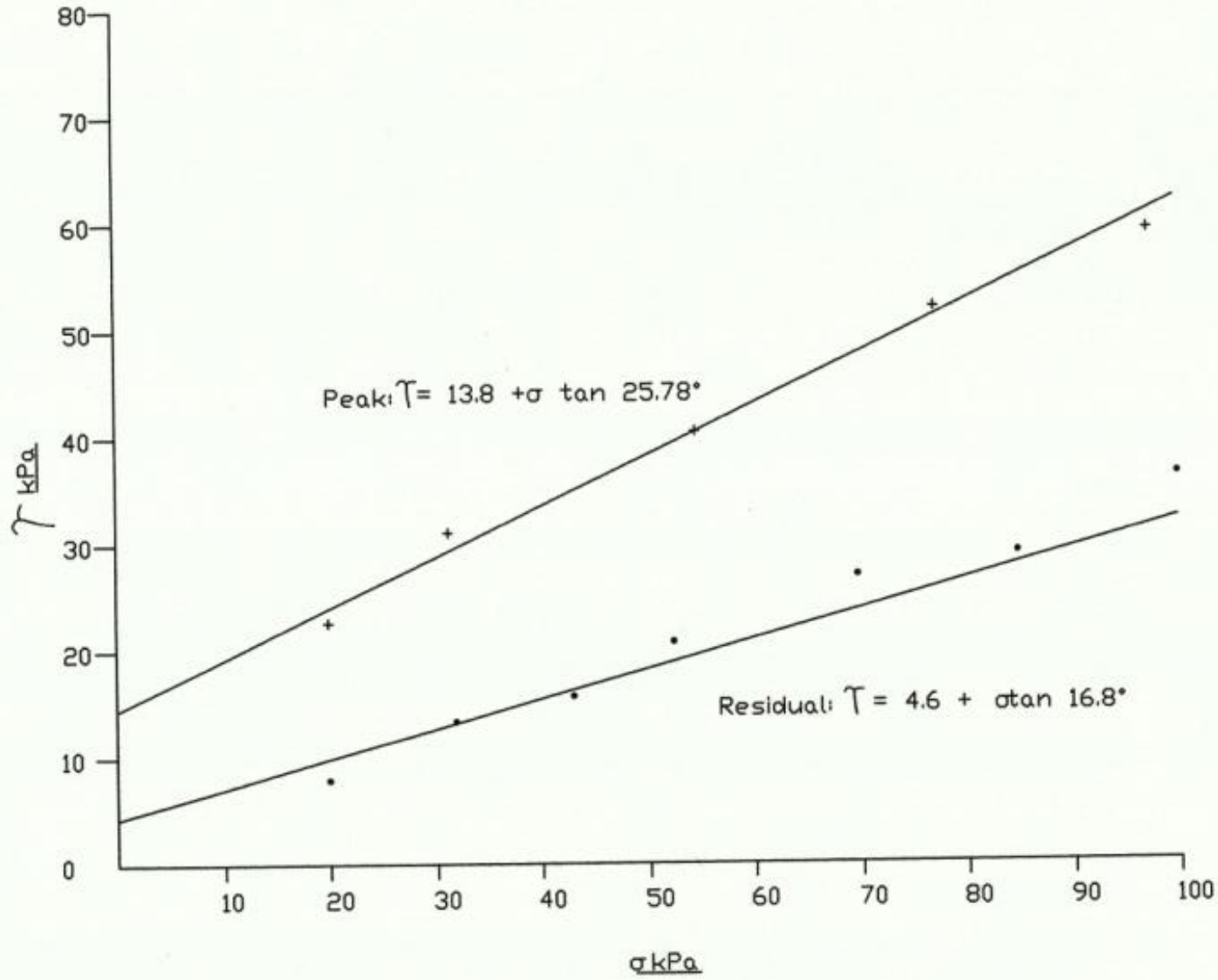

Figure 5.15 Mohr - Coulomb Envelope for Residual soil from site 7 (After Anderson & Kemp, 1985)

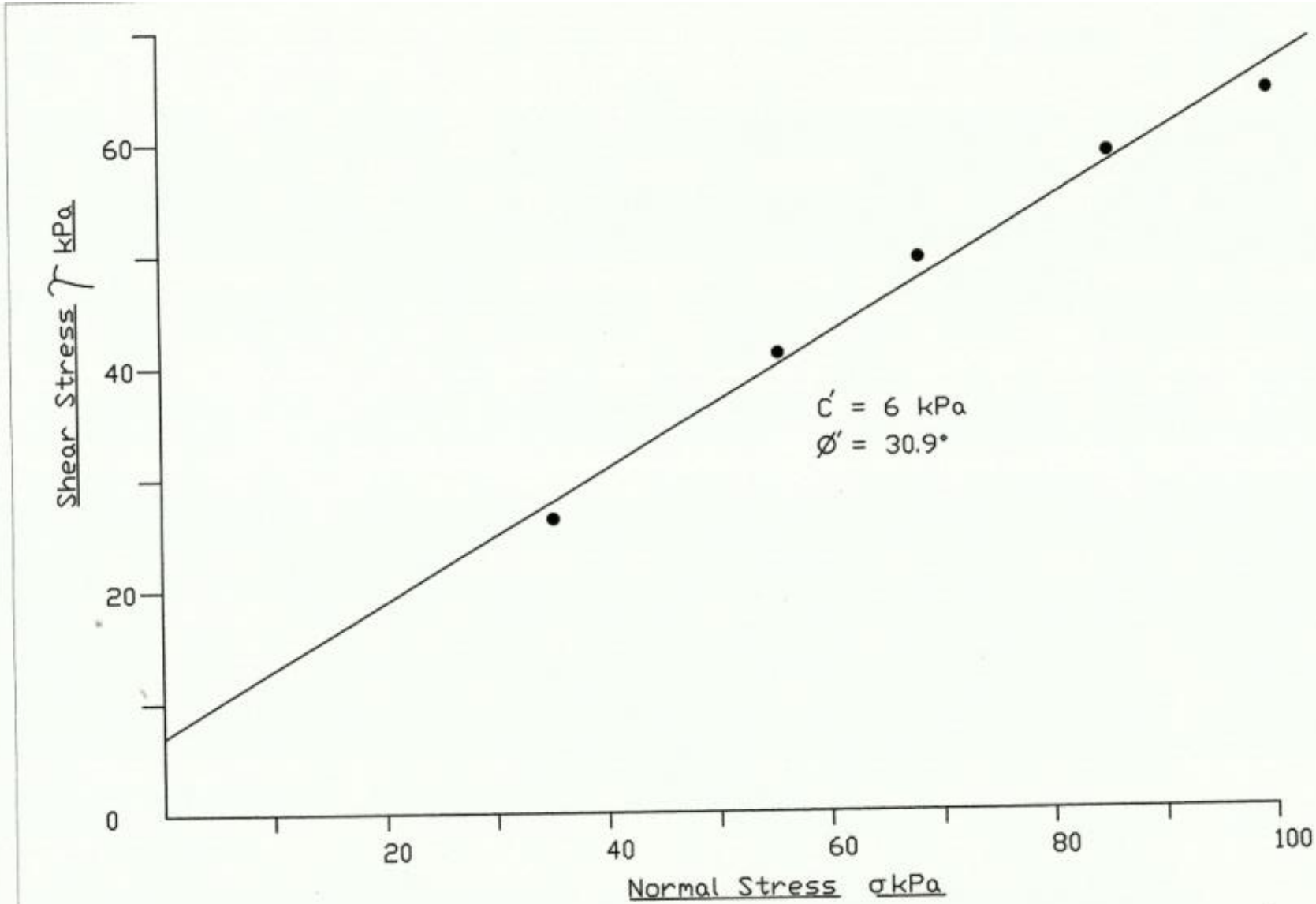

Figure 5.16 Shear Strength envelope for site 10 (After Anderson & Kemp, 1985)

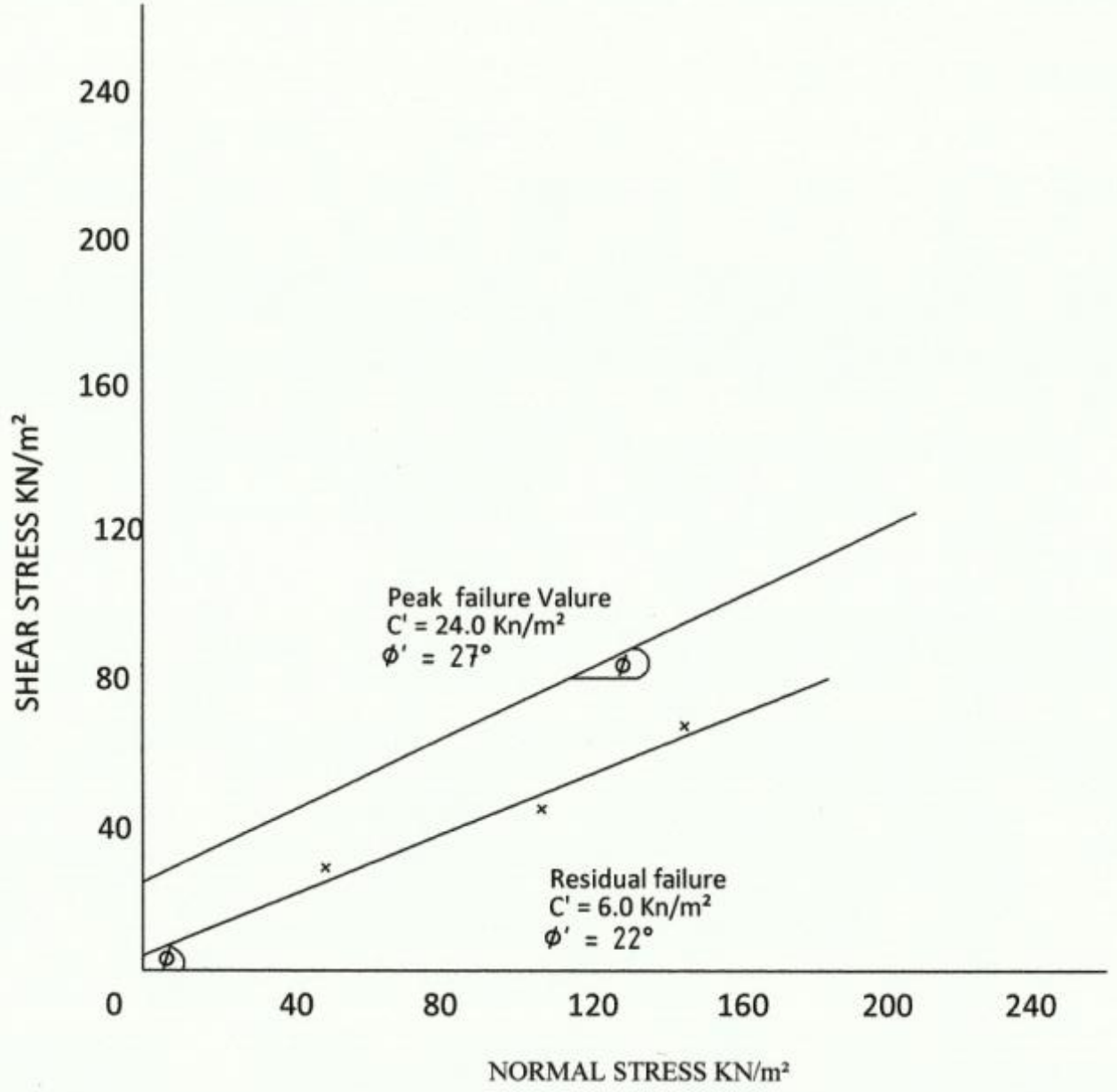

Figure 5.17 Mohr - Coulomb Envelope for Residual Soil from the Barre de L'isle Study Site

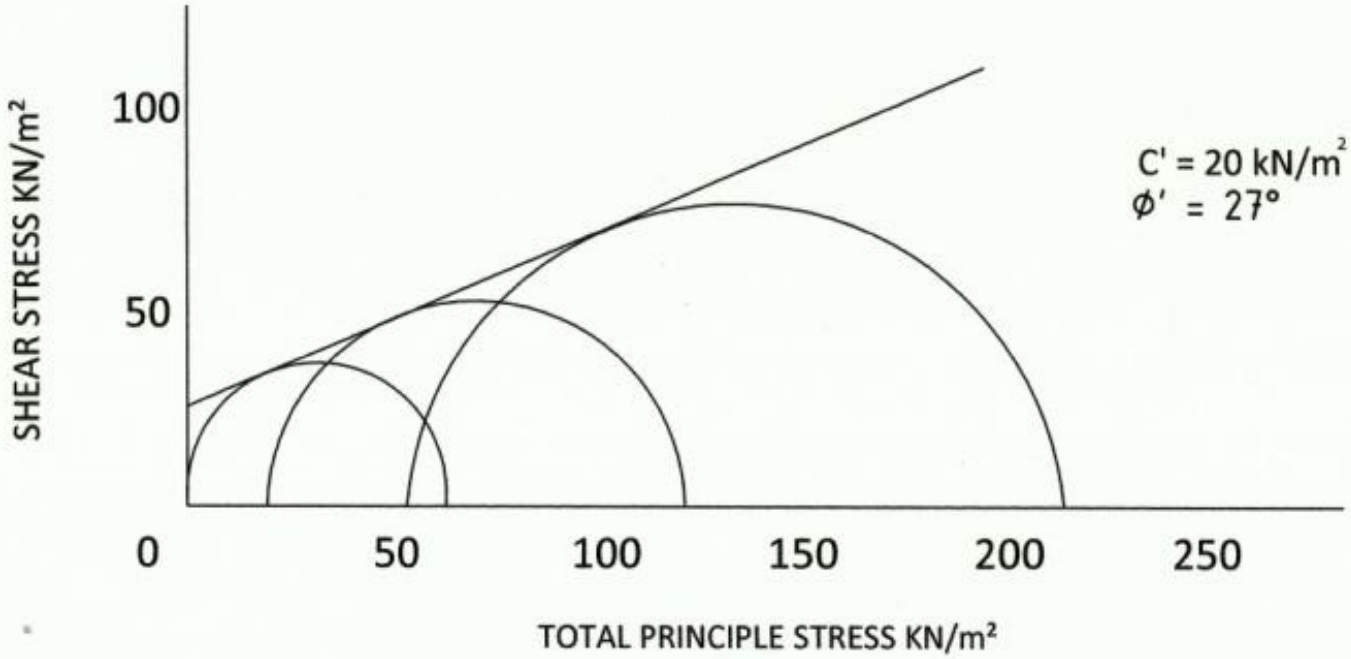

Figure 5.18 Mohr - Coulomb Envelope for Residual Soil from LUCELEC unstable slope on the Barre de L'Isle Ridge

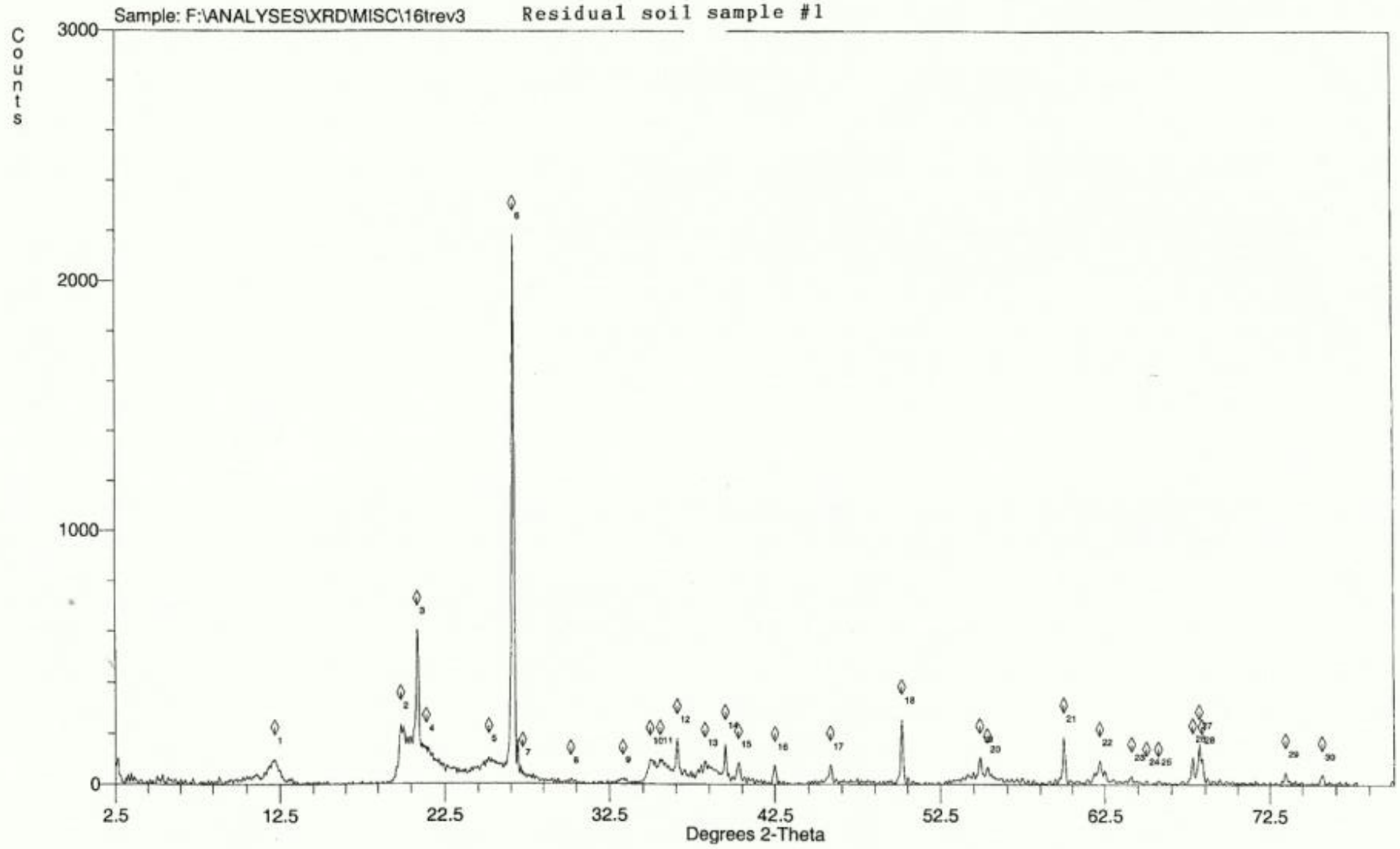

Figure 5.19 X-Ray Diffraction peaks for a Residual soil sample from the Barre de L'isle Study Site (Sample #1)

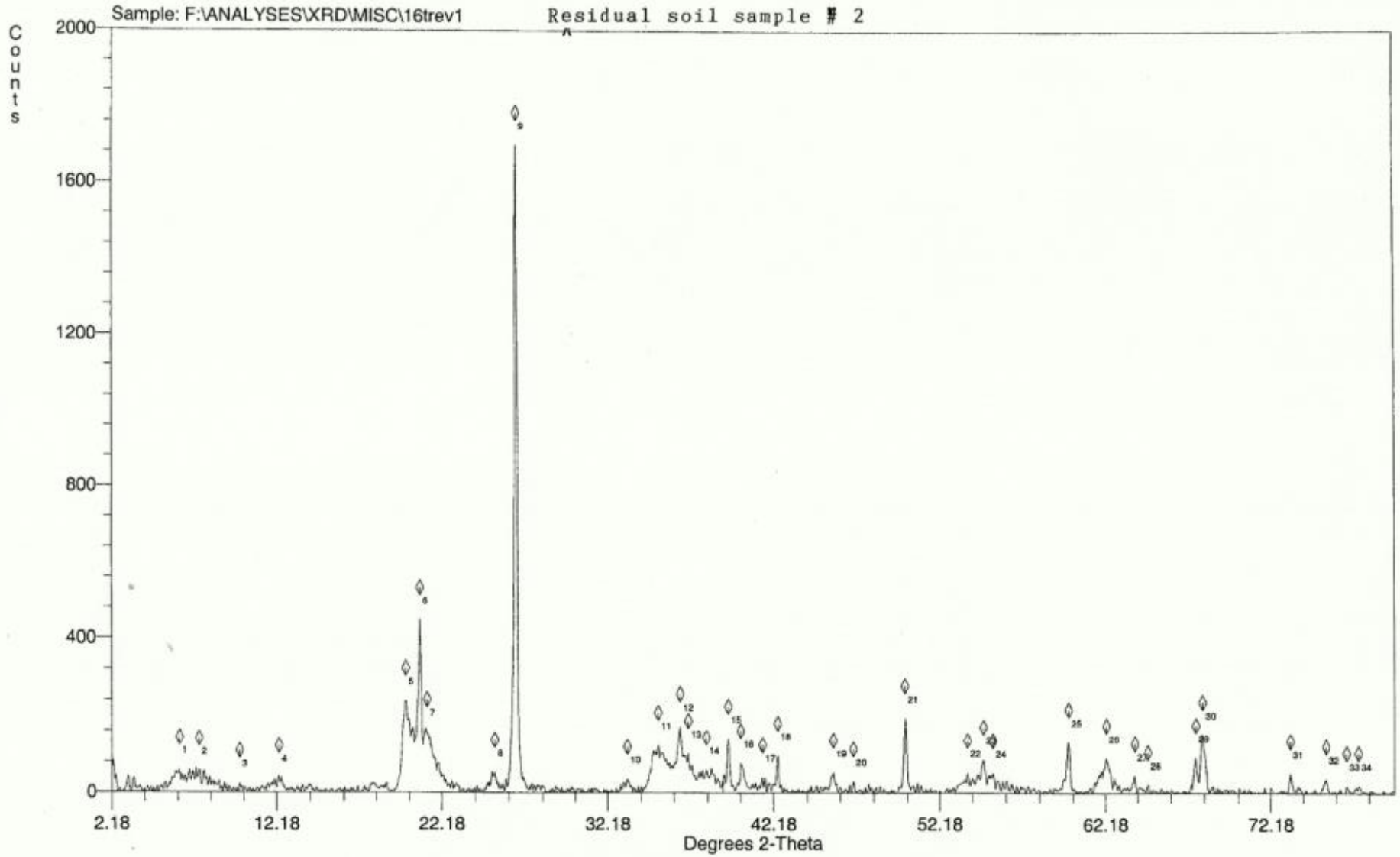

Figure 5.20 X-Ray Diffraction peaks for a Residual Soil sample from the Barre de L'isle Study Site (Sample #2)

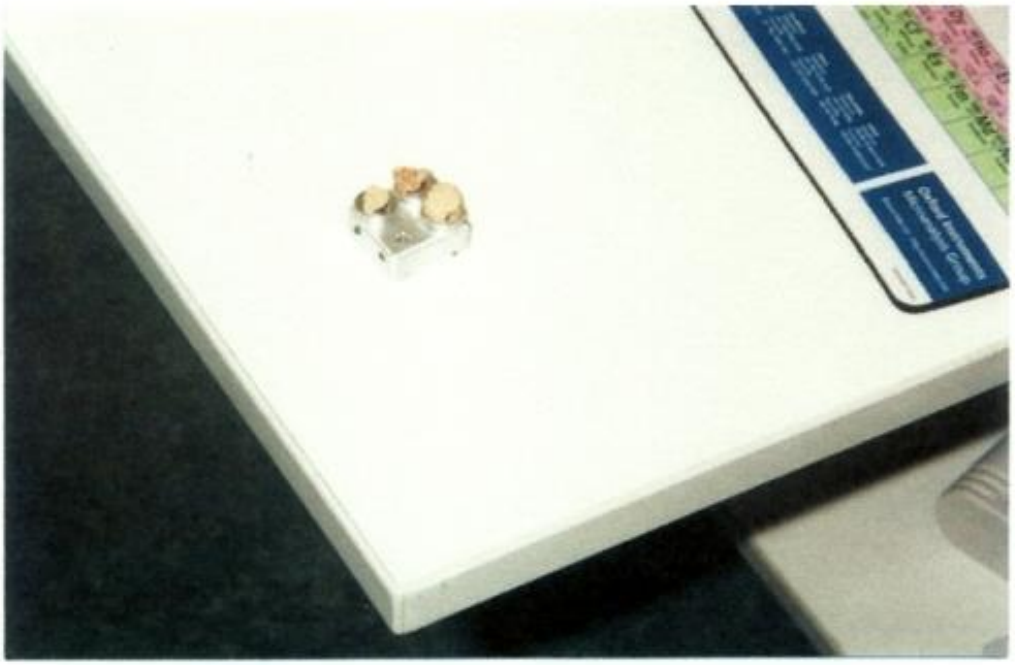

Figure 5.21 Residual soil samples from Barre de L'isle Study Site prepared for SEM Analysis at the University of Newcastle-upon-Tyne laboratory

Figure 5.22 JEOL Scanning Electron Microscope at the University of Newcastle-upon-Tyne

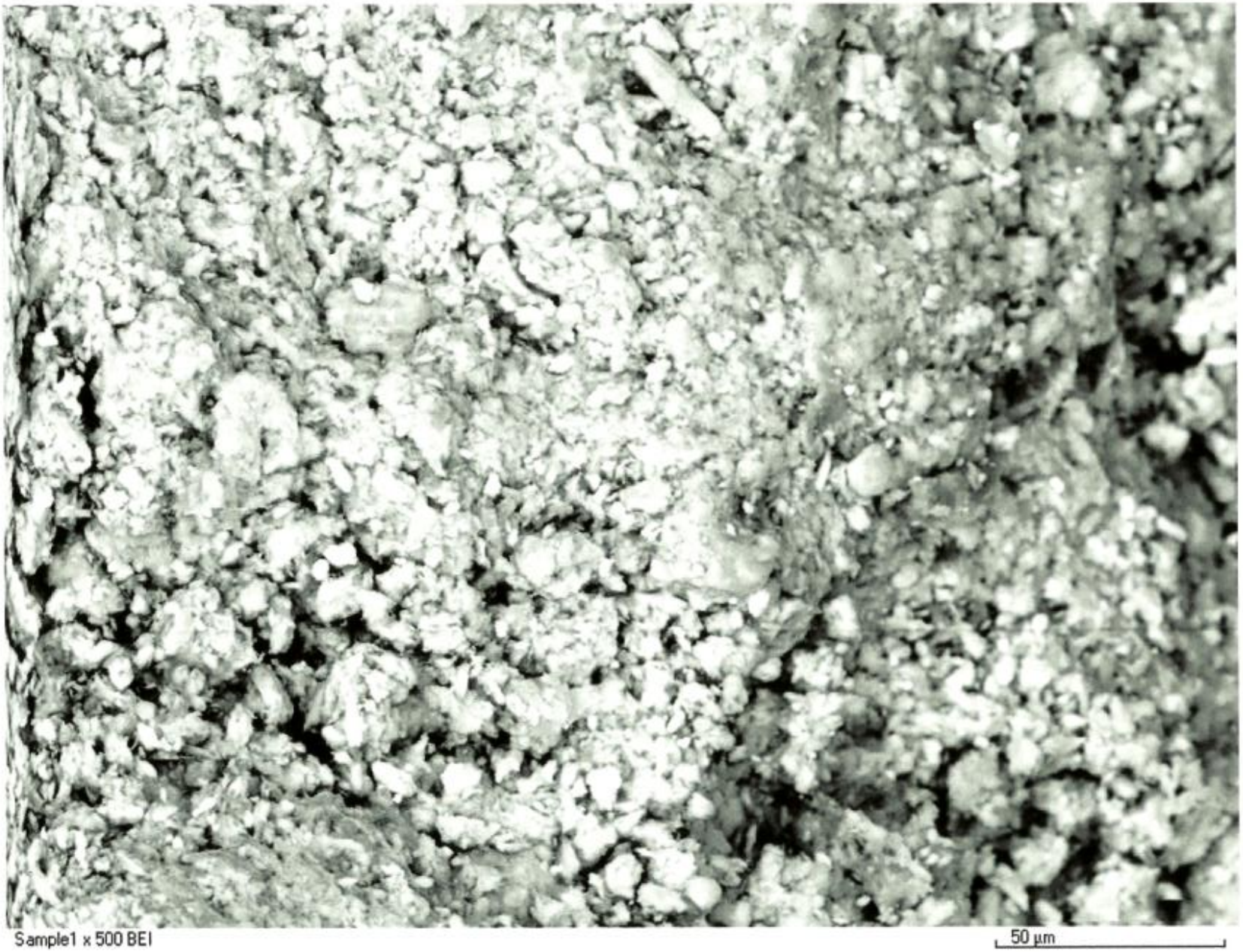

Figure 5.23 SEM Image (x500) of residual soil from Barre de L'isle Study Site

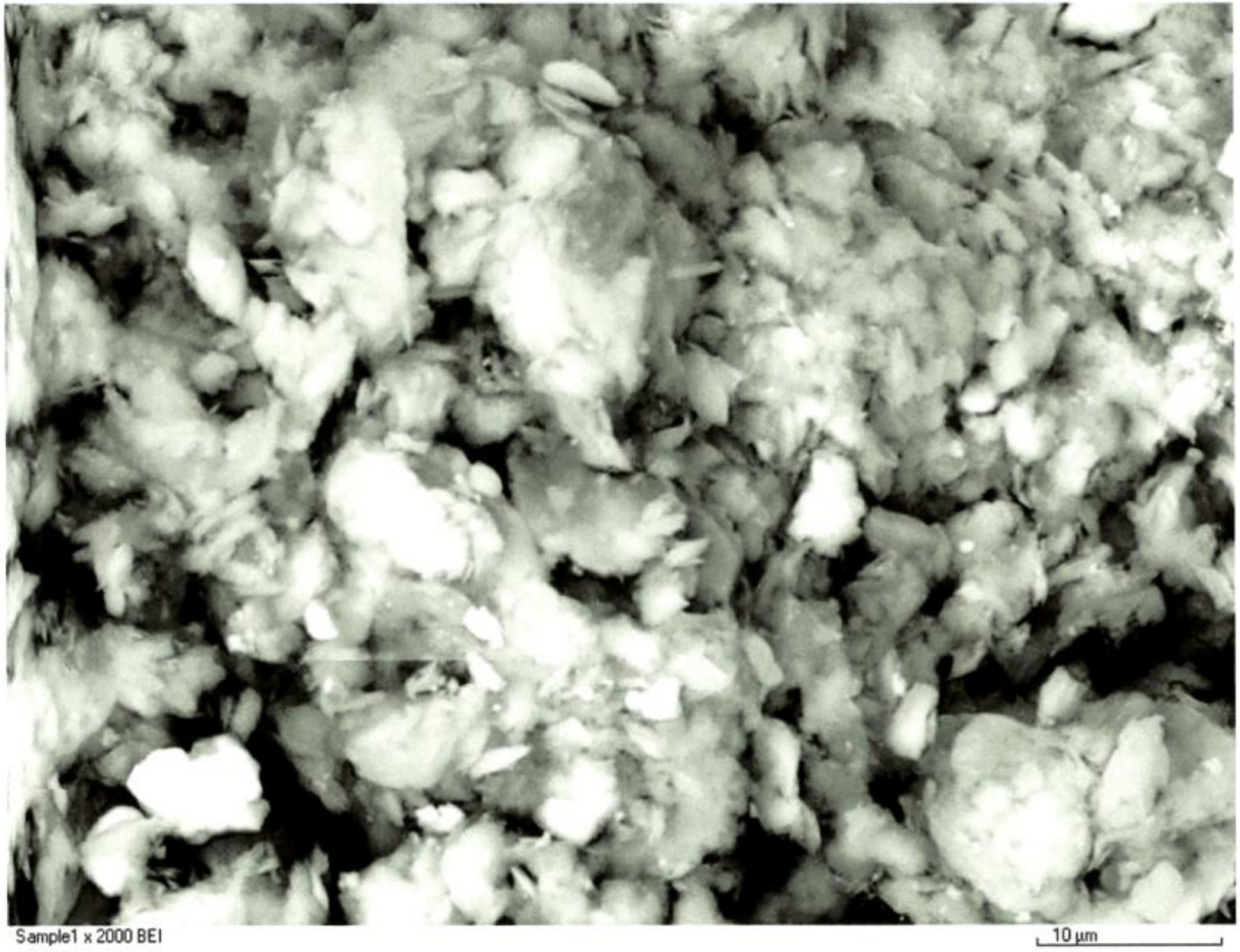

Figure 5.24 SEM Image (x2000) of residual soil from the Barre de L'isle Study Site

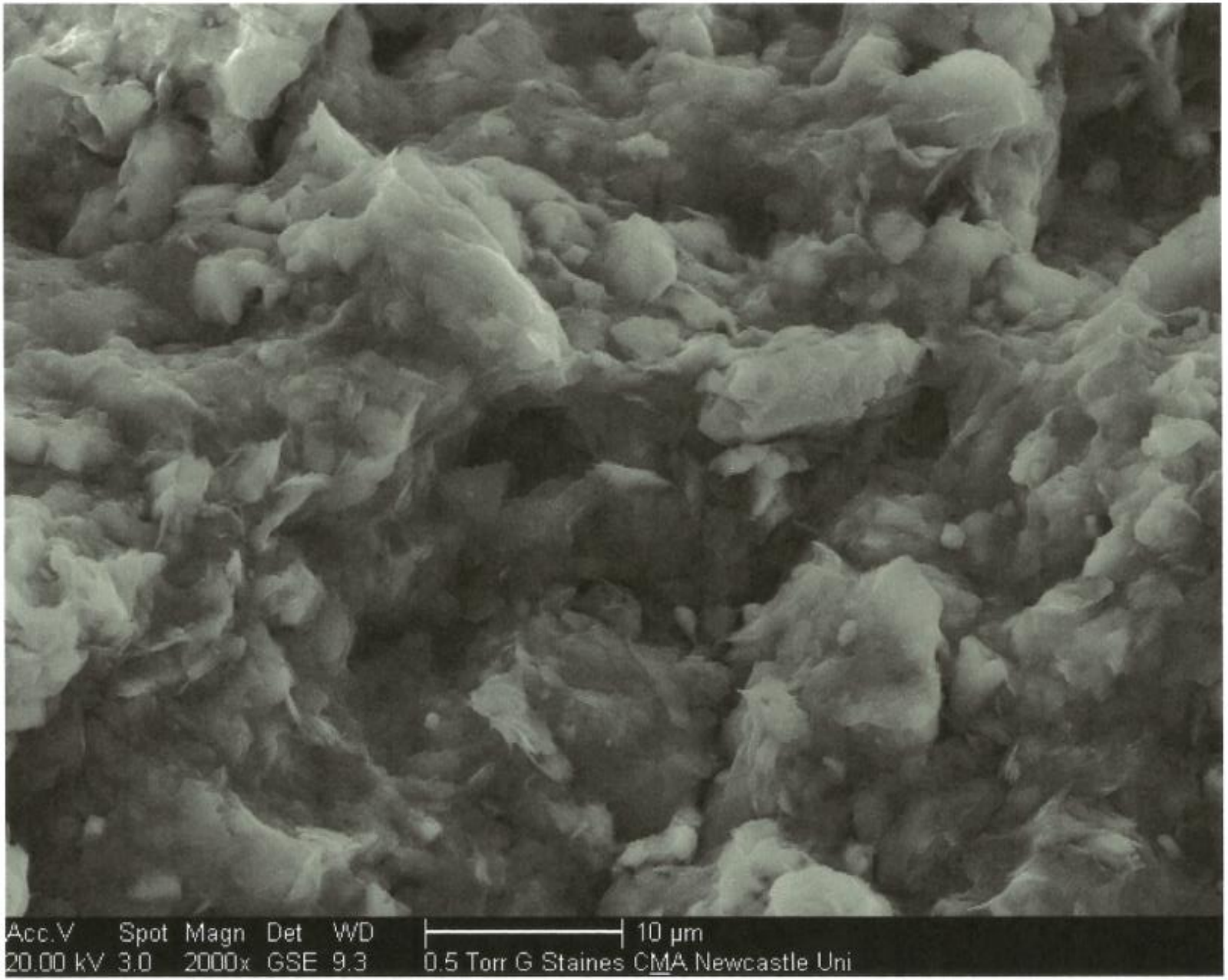

Figure 5.25 SEM Image (x2000) saturated) of residual soil from the Barre de L'isle Study Site

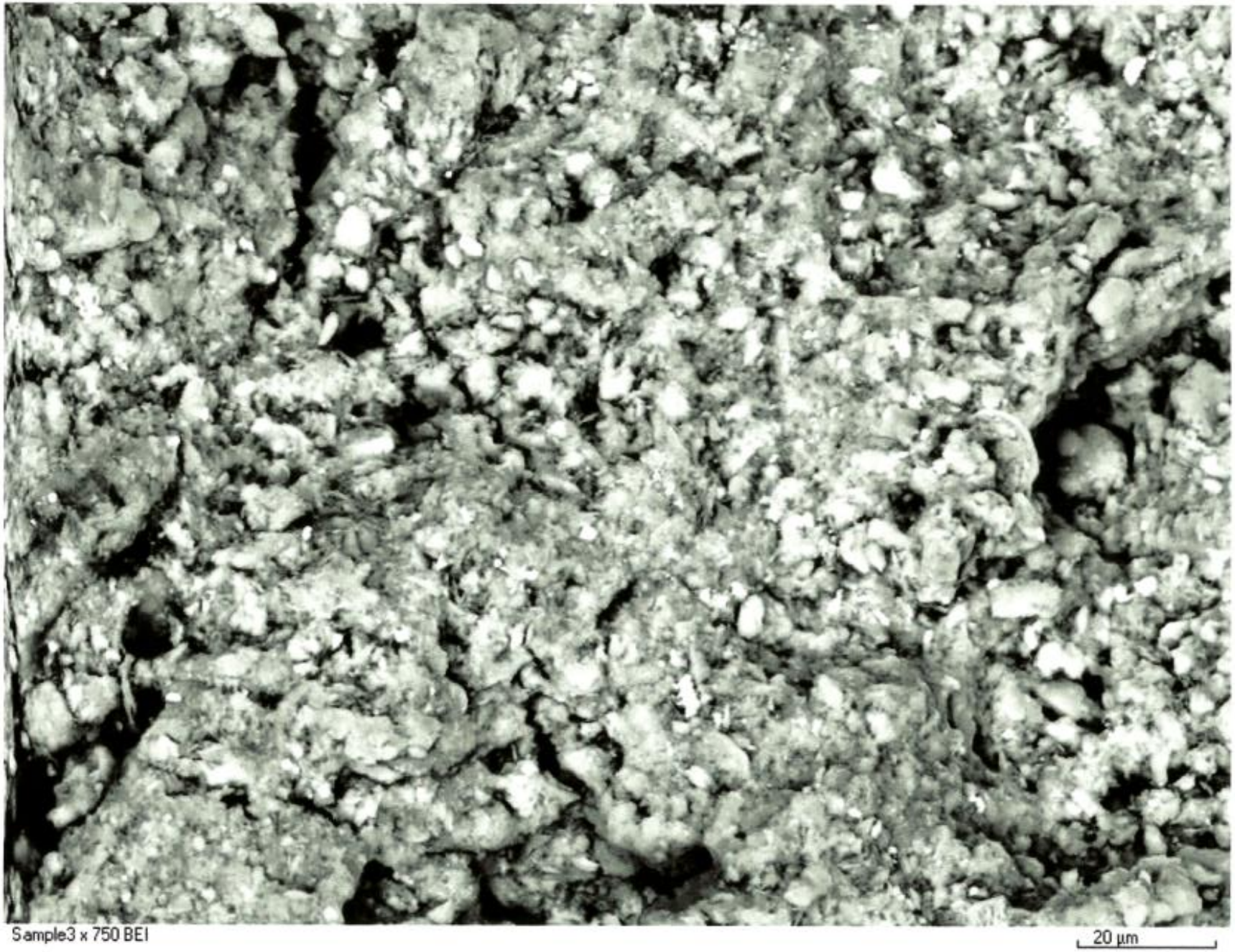

Figure 5.26 SEM Image (x750) of residual soil from RG Quarry

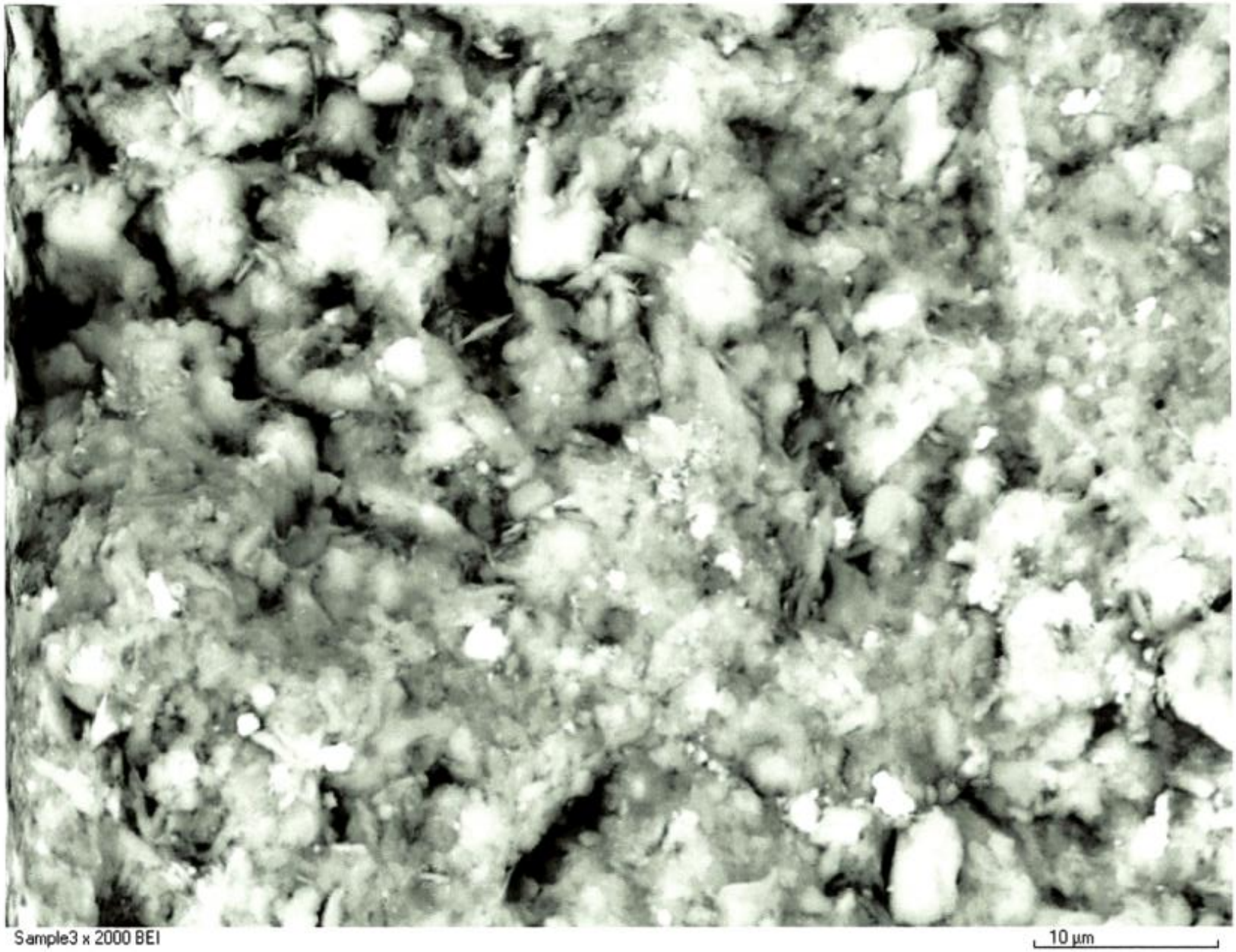

Figure 5.27 SEM Image (x2000) of residual soil from RG Quarry

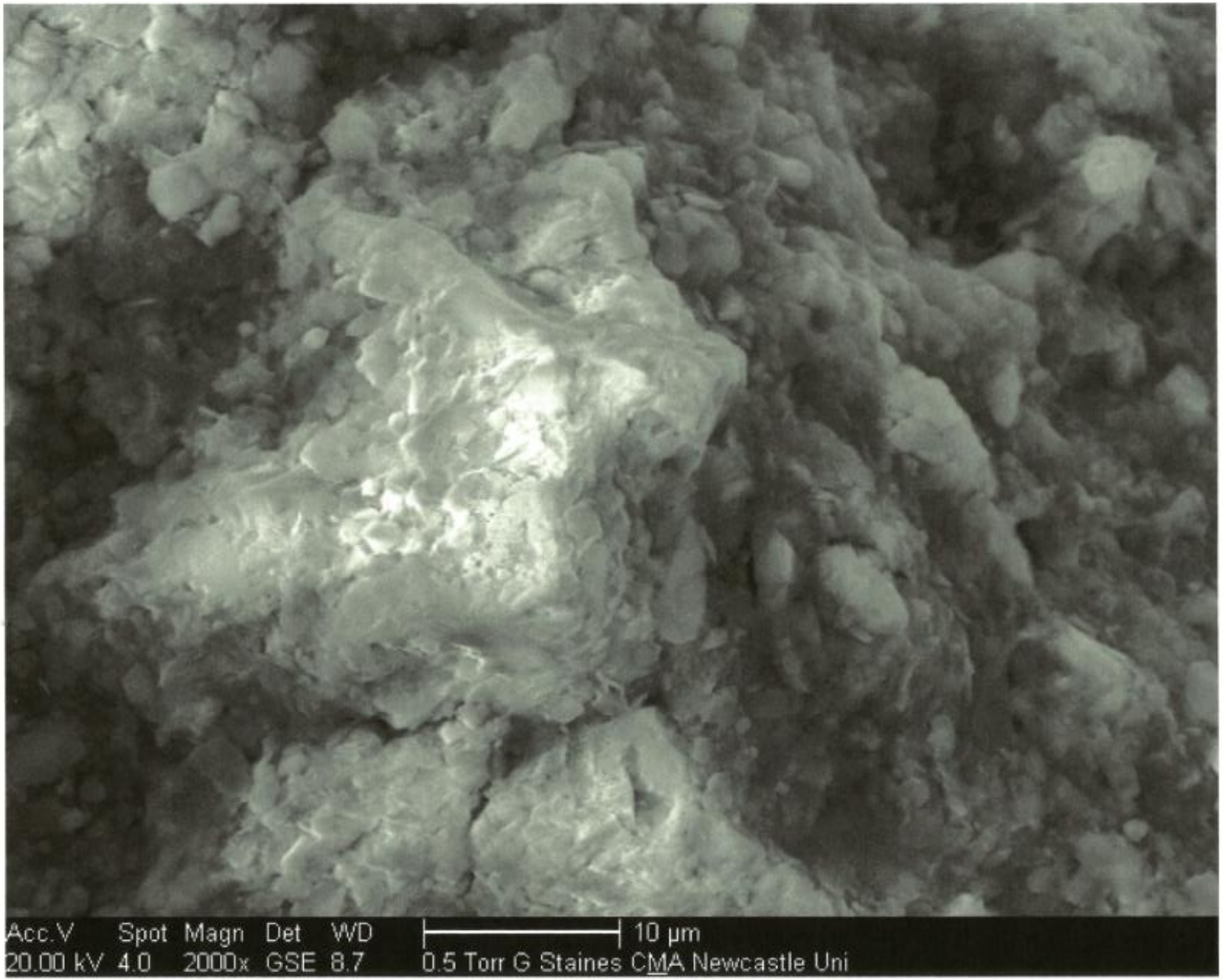

Figure 5.28 SEM Image (x2000 saturated) of residual soil from RG Quarry

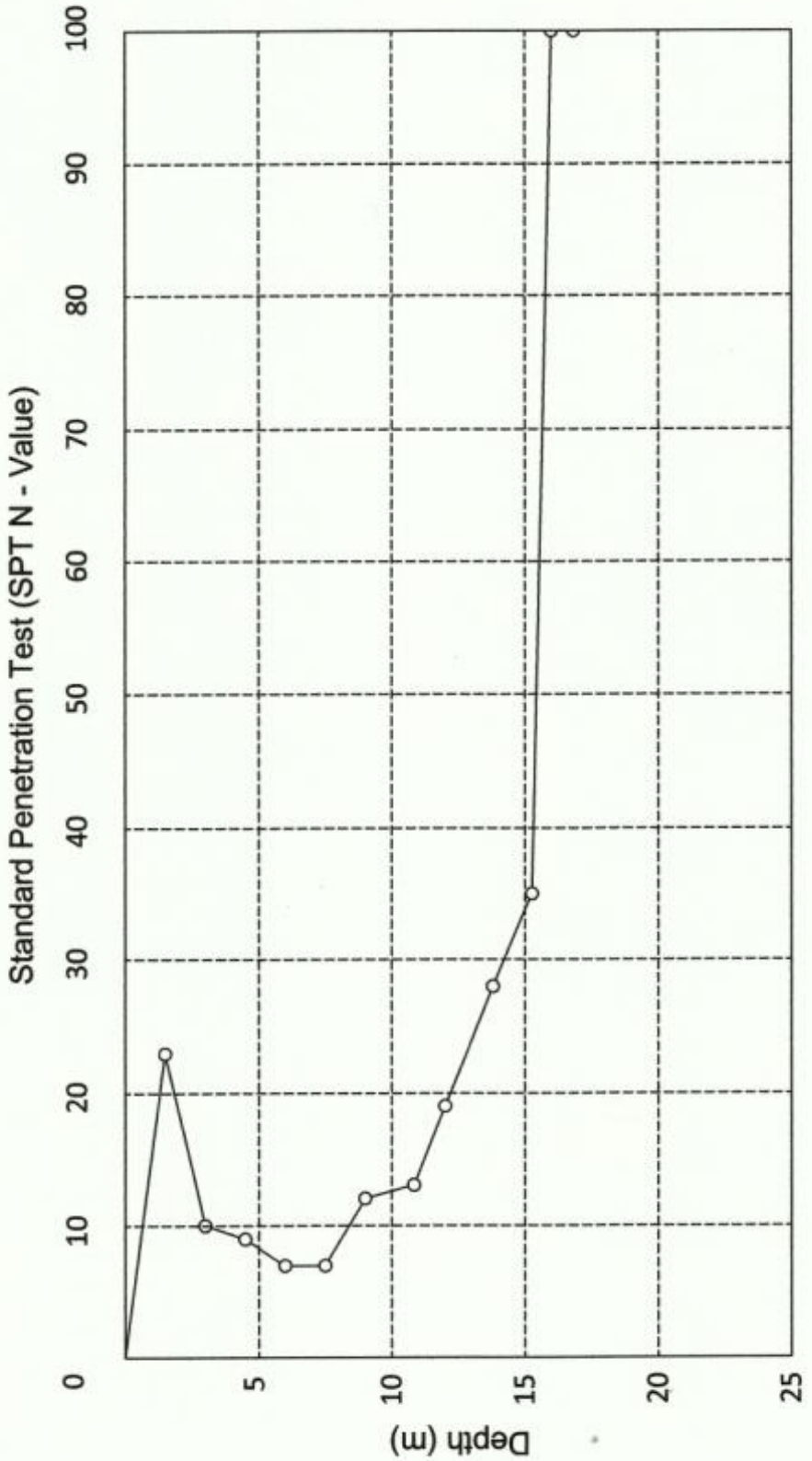

Figure 5.28a Graph of SPT vs Depth for Residual Soils for BH09-BS-2 at the Barre de L'Isle Study Site

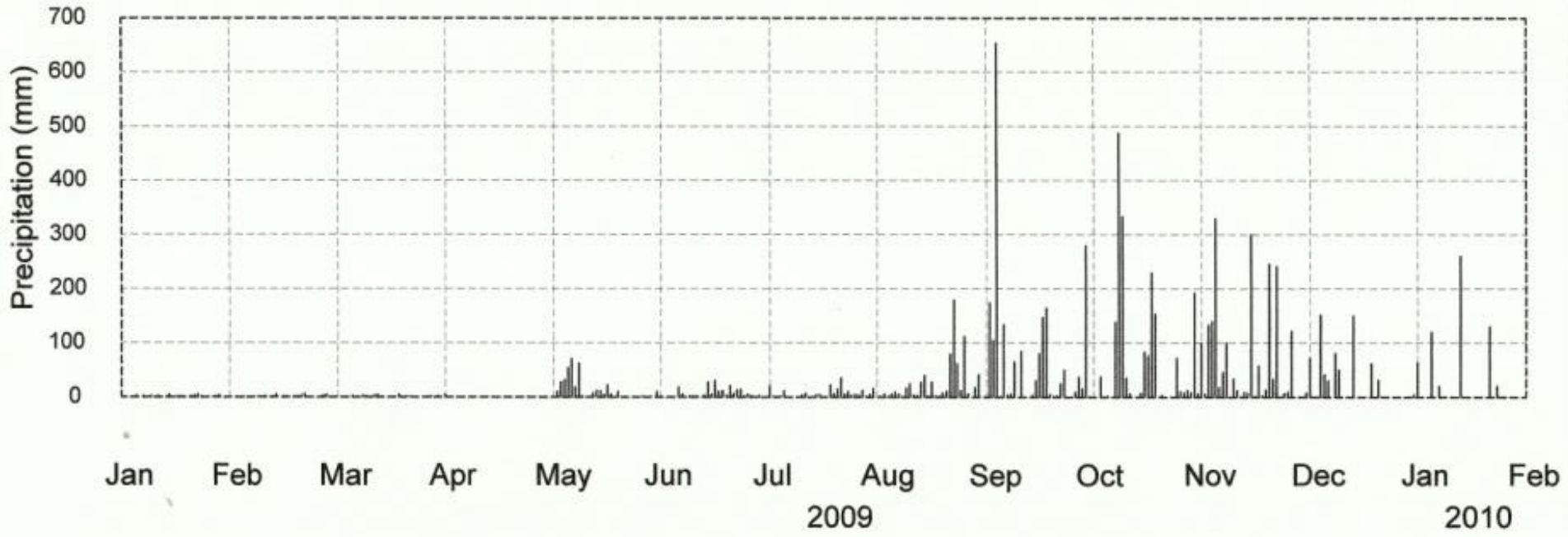

Figure 5.28b Graph of Rainfall for the period of January 1st, 2009 to January 22, 2010 at the Barre de L'Isle Study Site

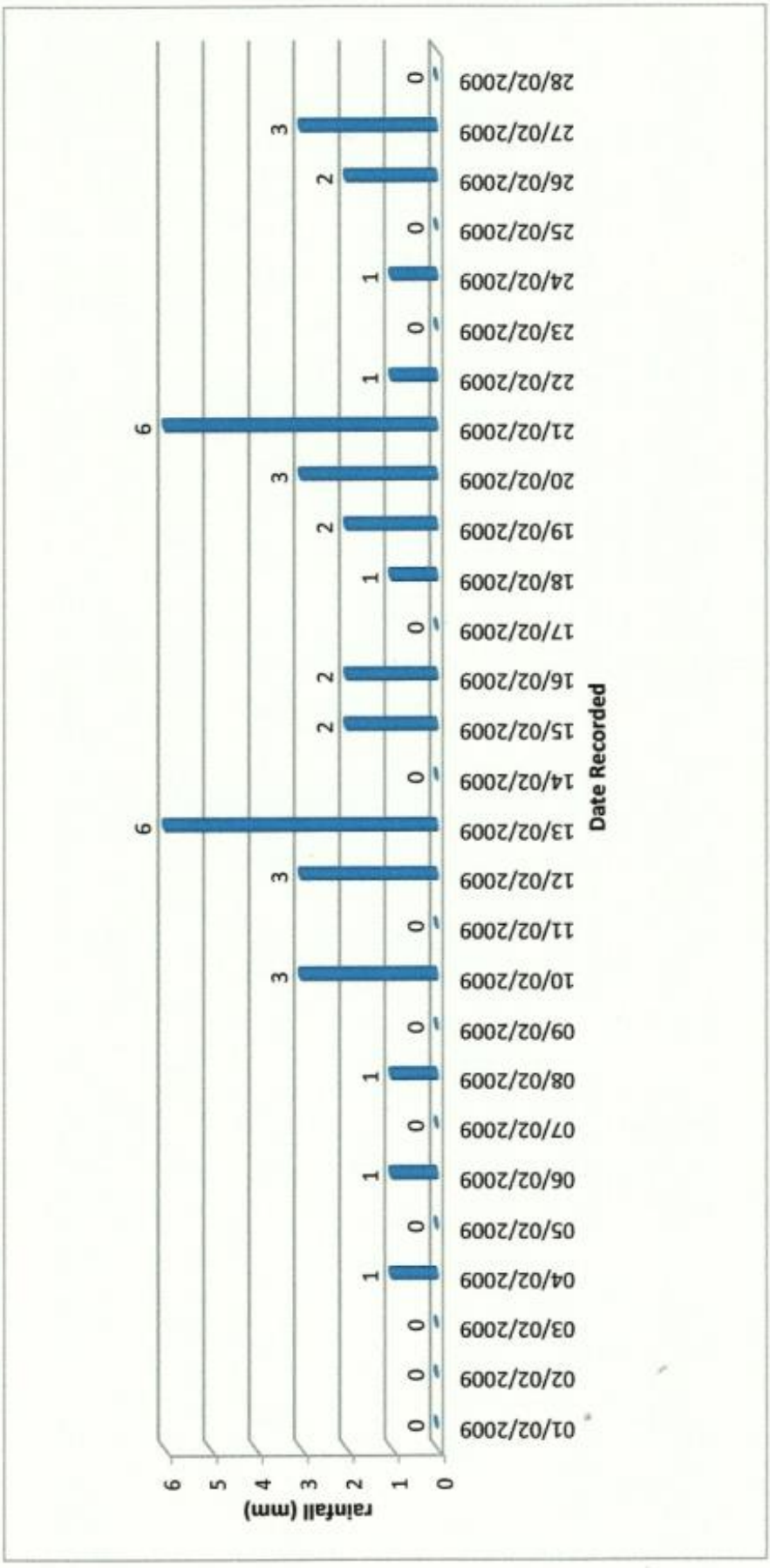

Figure 5.29 Daily Rainfall Graph for February 2009 for the Barre de L'isle Study Site

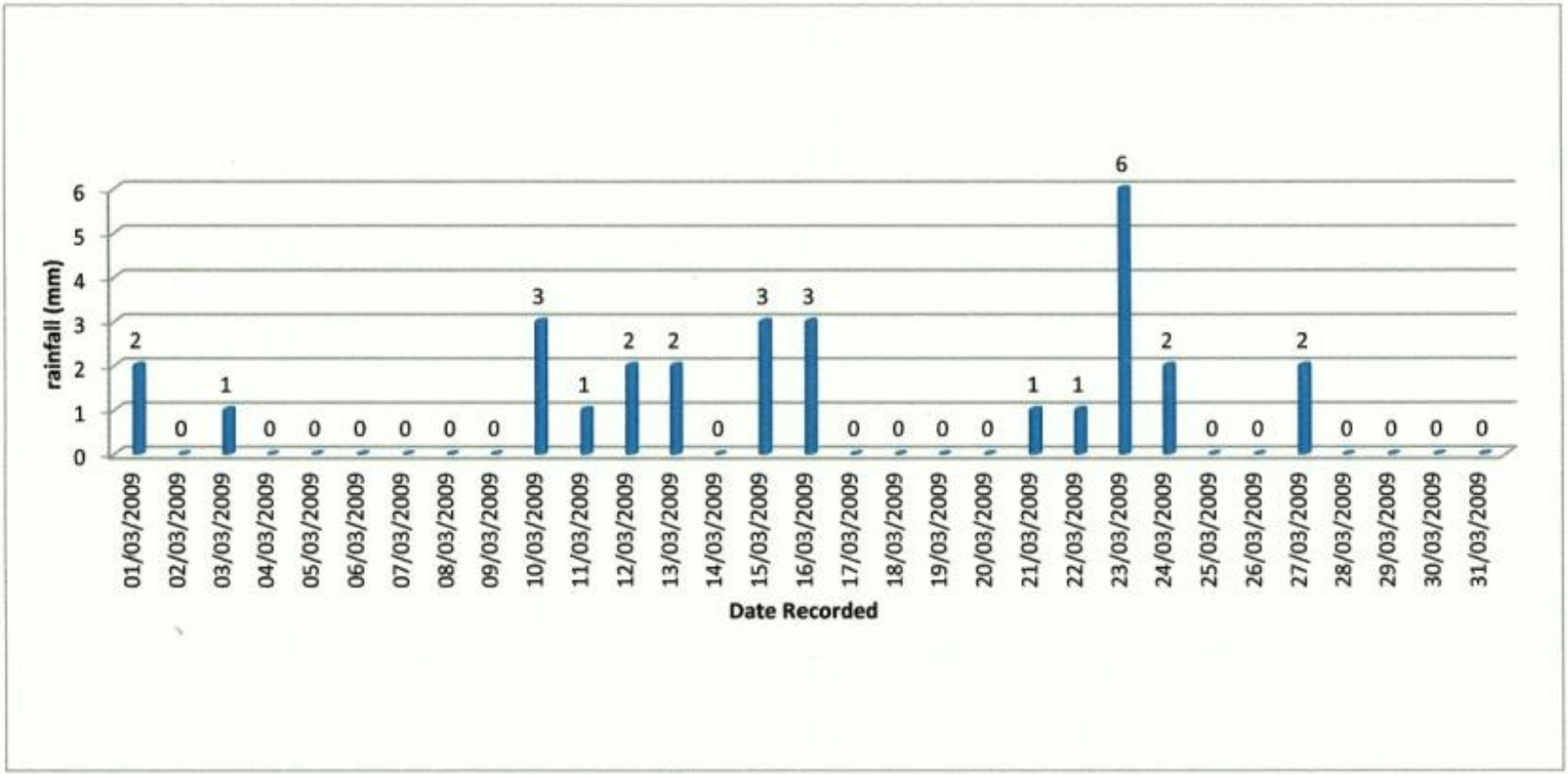

Figure 5.30 Daily Rainfall Graph for March 2009 for the Barre de L'isle Study Site

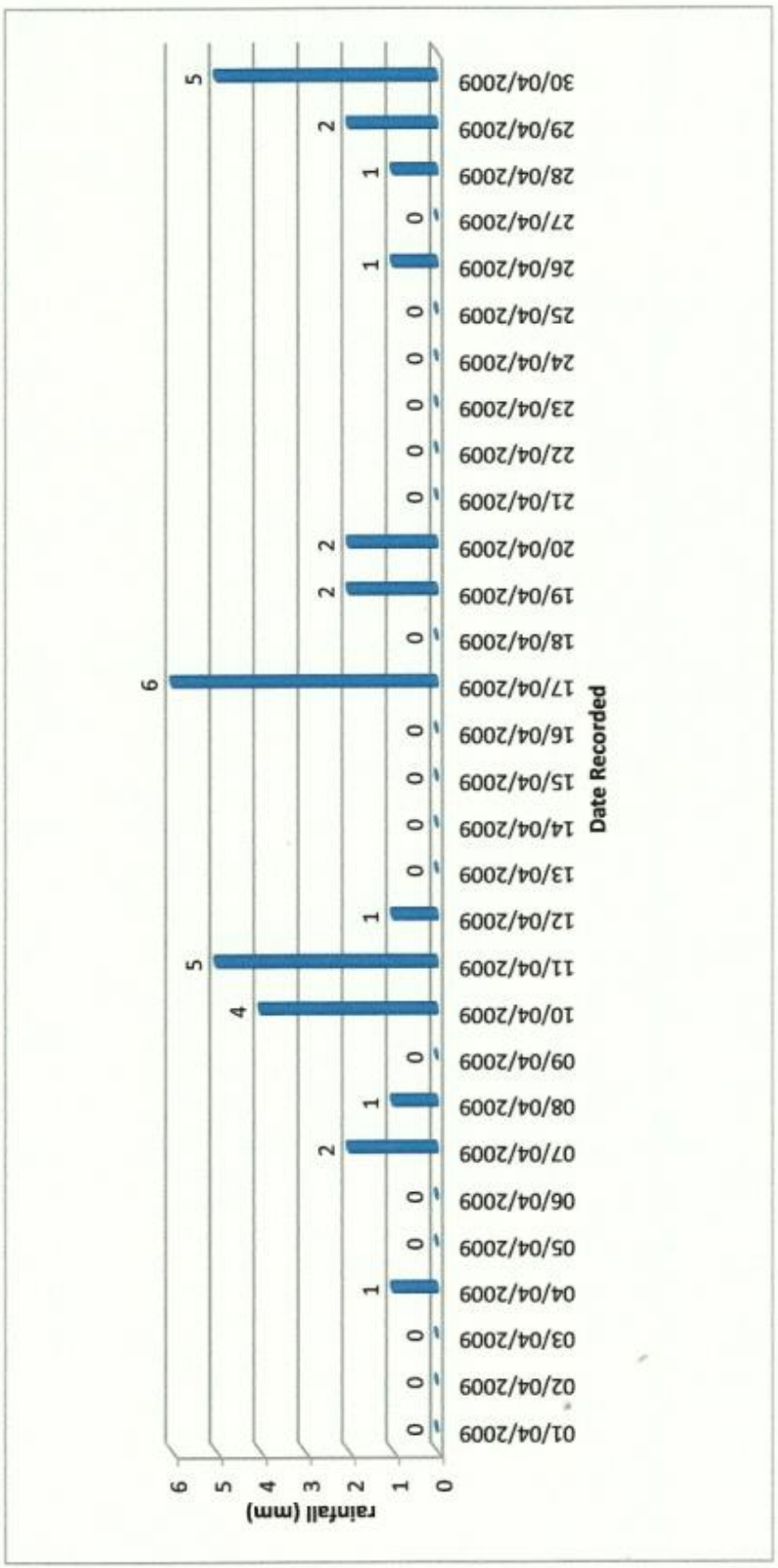

Figure 5.31 Daily Rainfall Graph for April 2009 for the Barre de L'isle Study Site

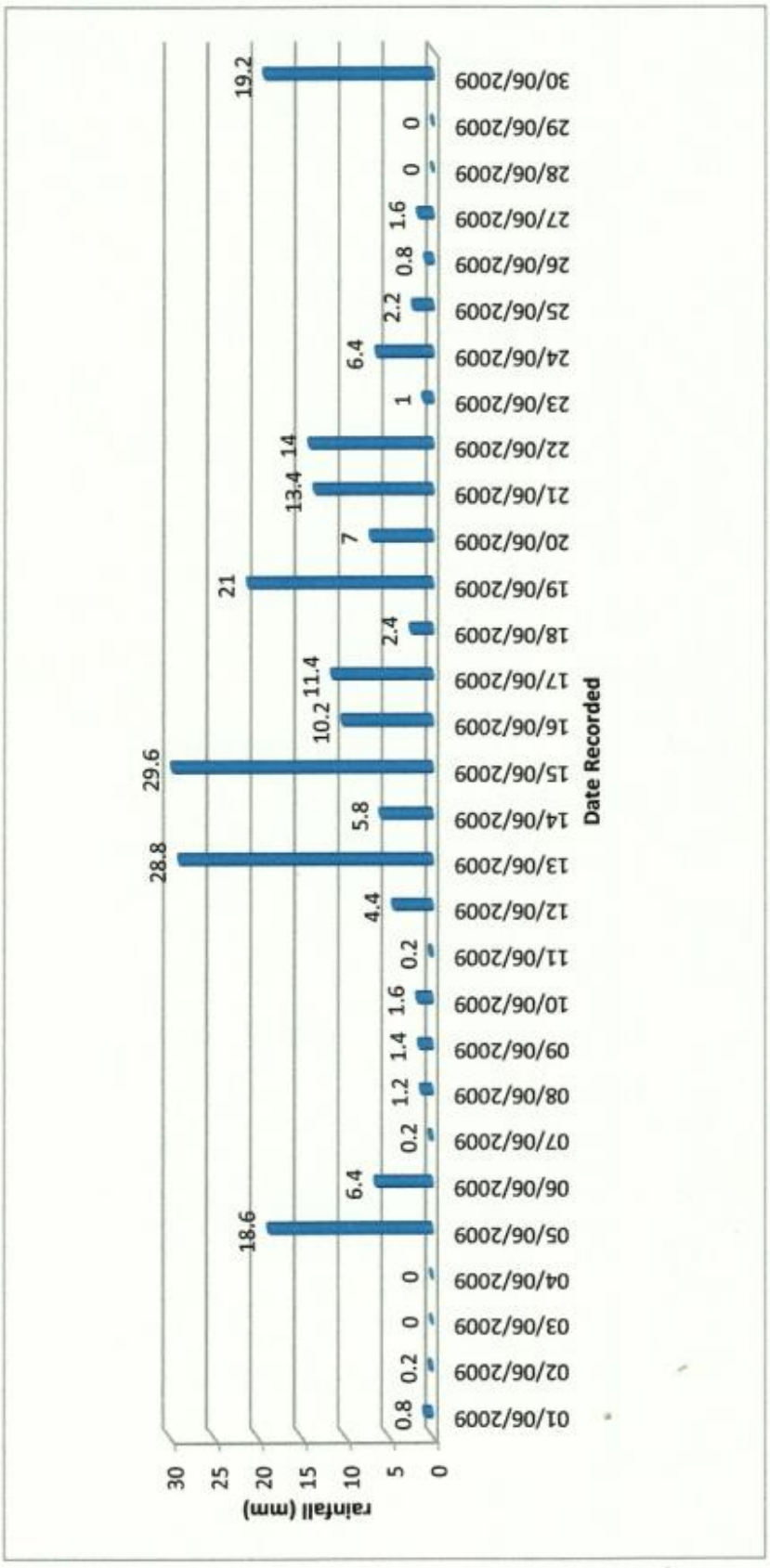

Figure 5.32 Daily Rainfall Graph for June 2009 for the Barre de L'isle Study Site

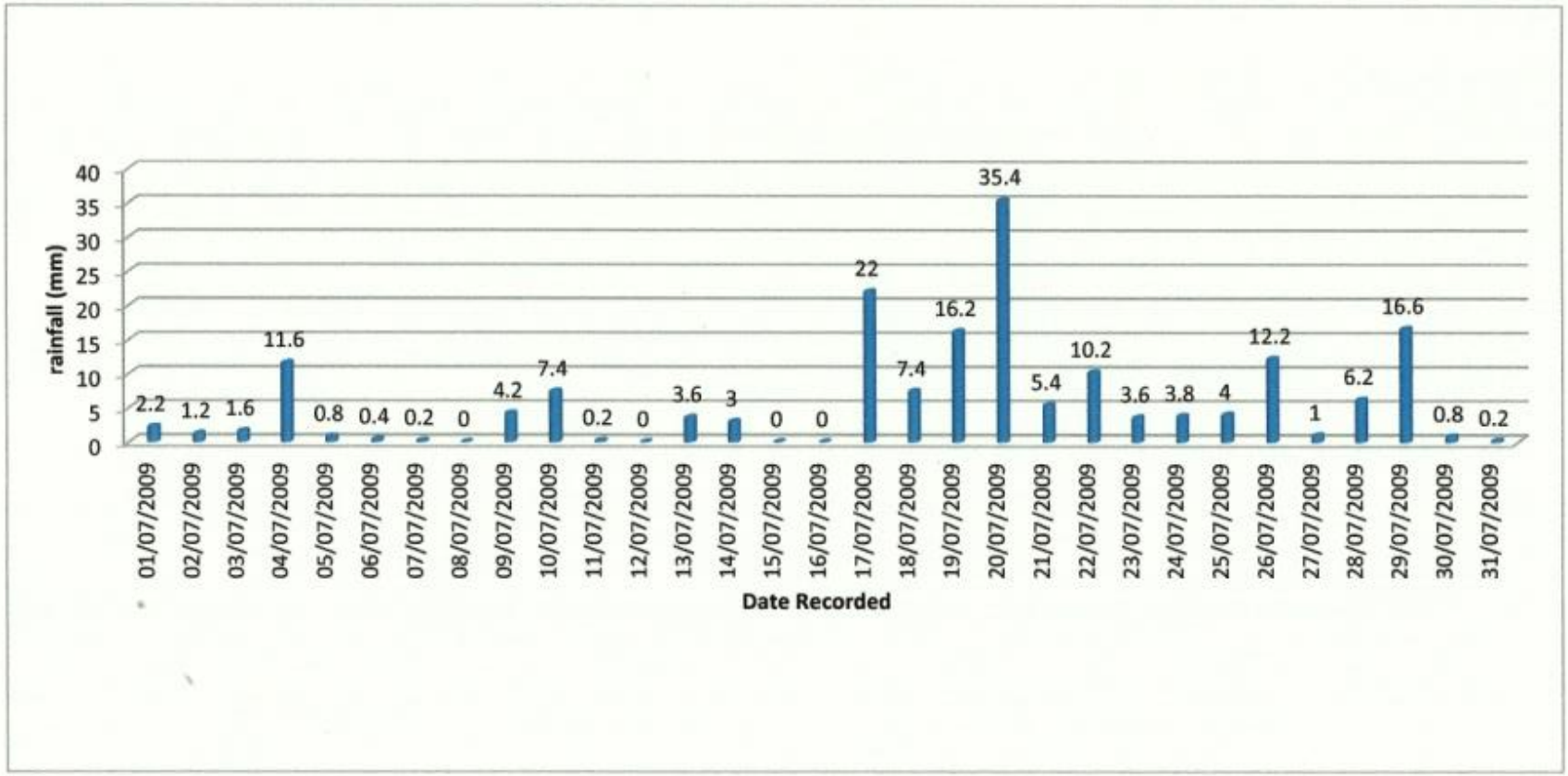

Figure 5.33 Daily Rainfall Graph for July 2009 for the Barre de L'isle Study Site

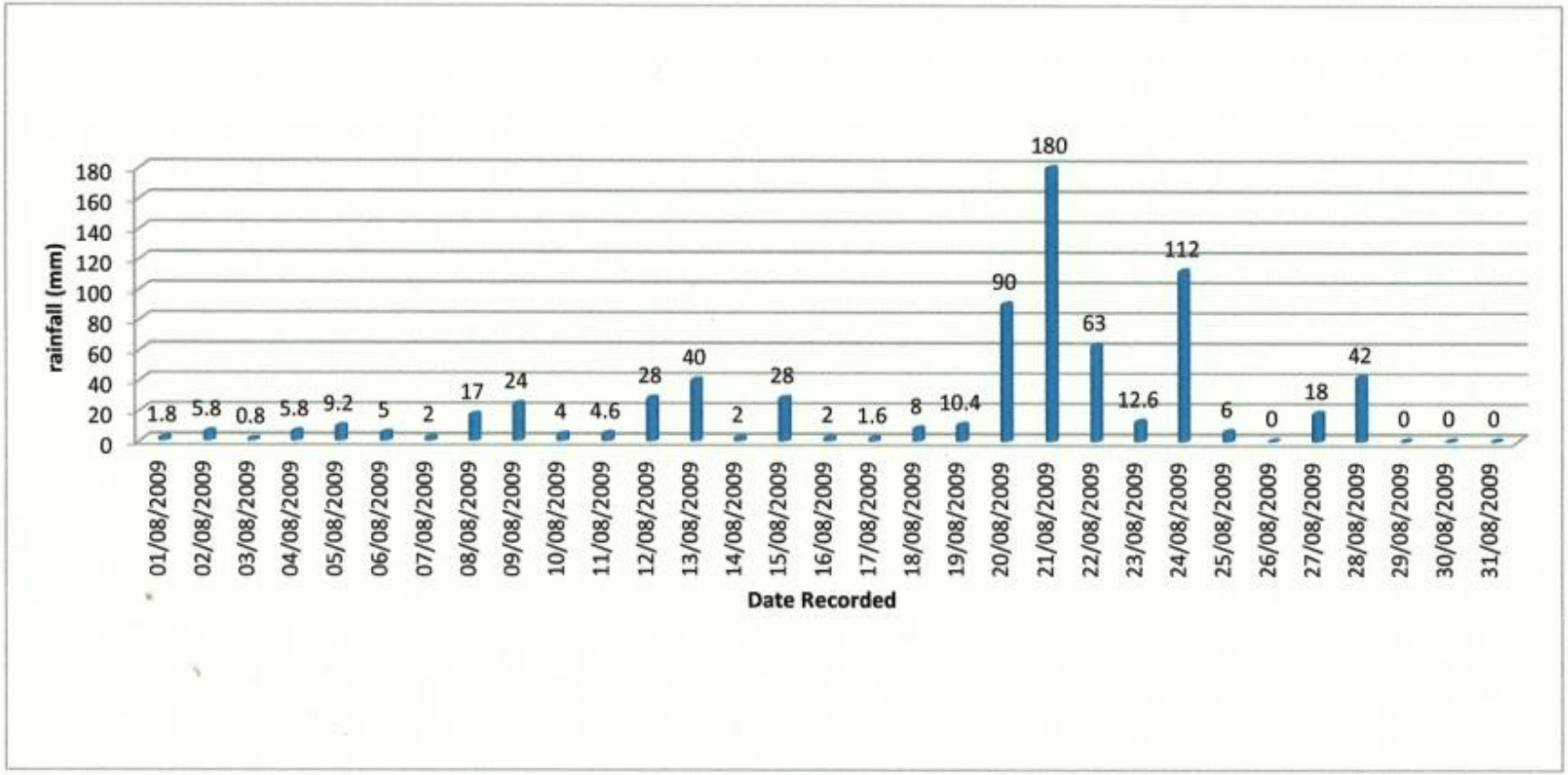

Figure 5.34 Daily Rainfall Graph for August 2009 for the Barre de L'isle Study Site

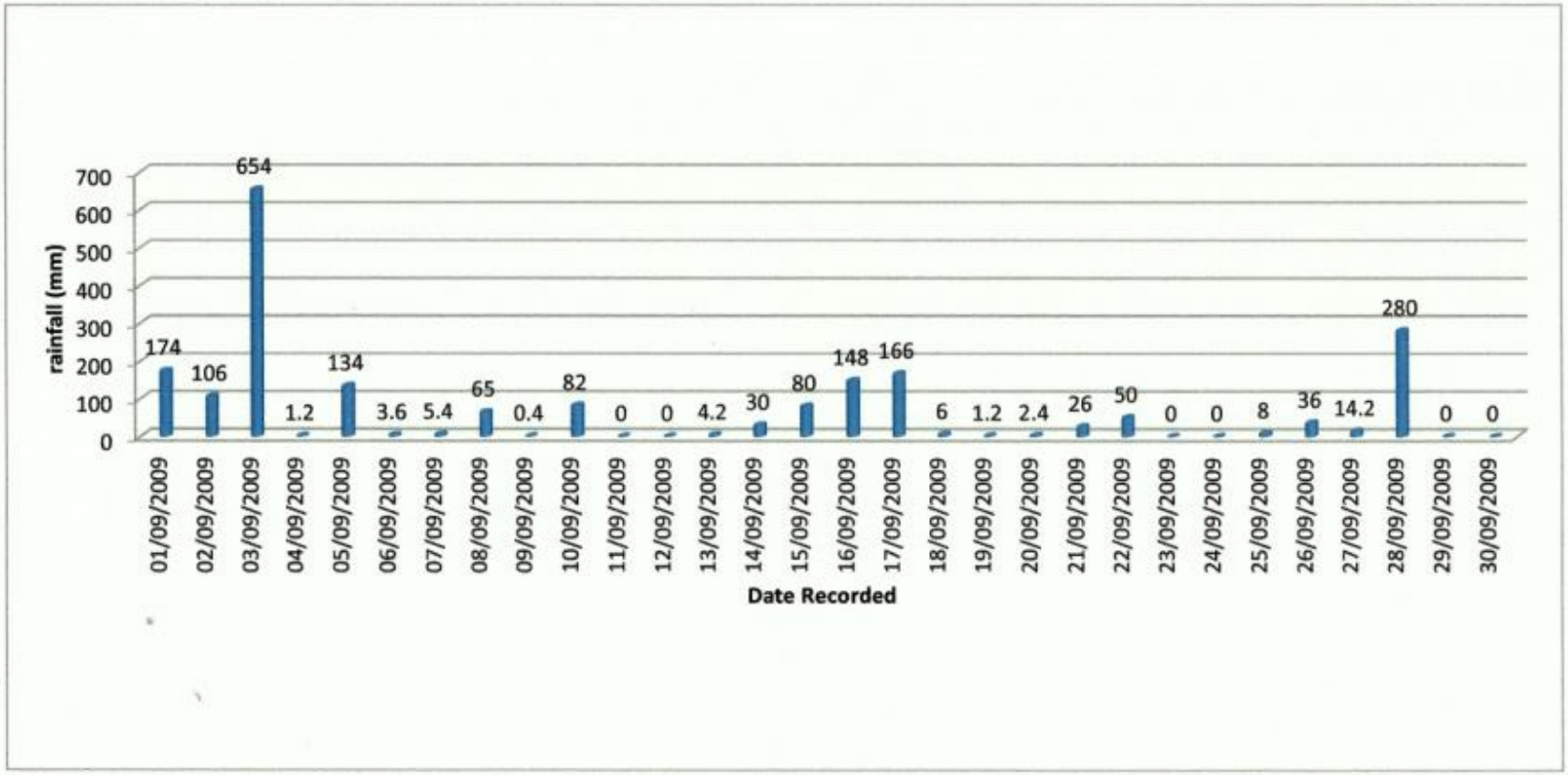

Figure 5.35 Daily Rainfall Graph for September 2009 for the Barre de L'isle Study Site

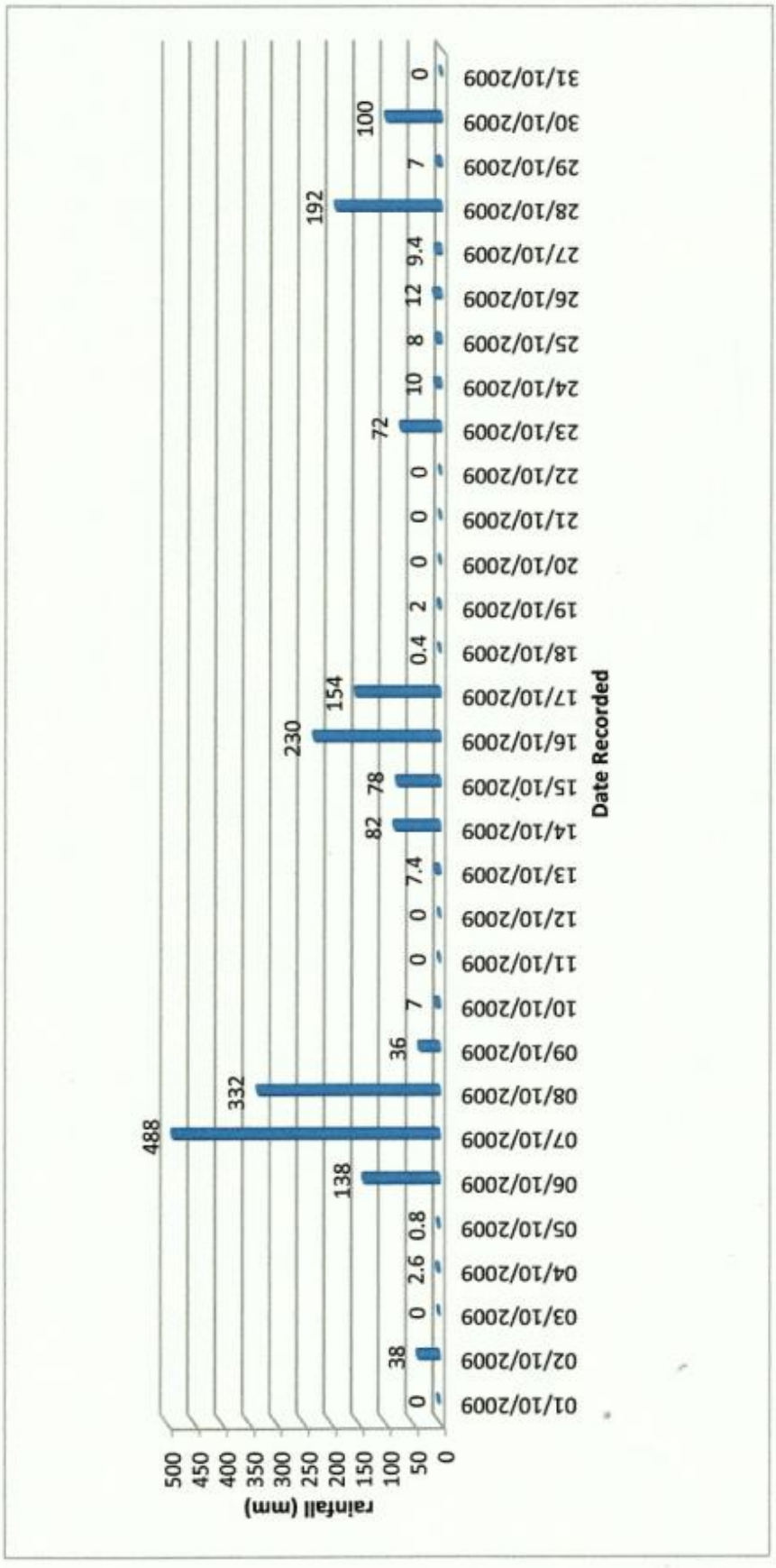

Figure 5.36 Daily Rainfall Graph for October 2009 for the Barre de L'isle Study Site

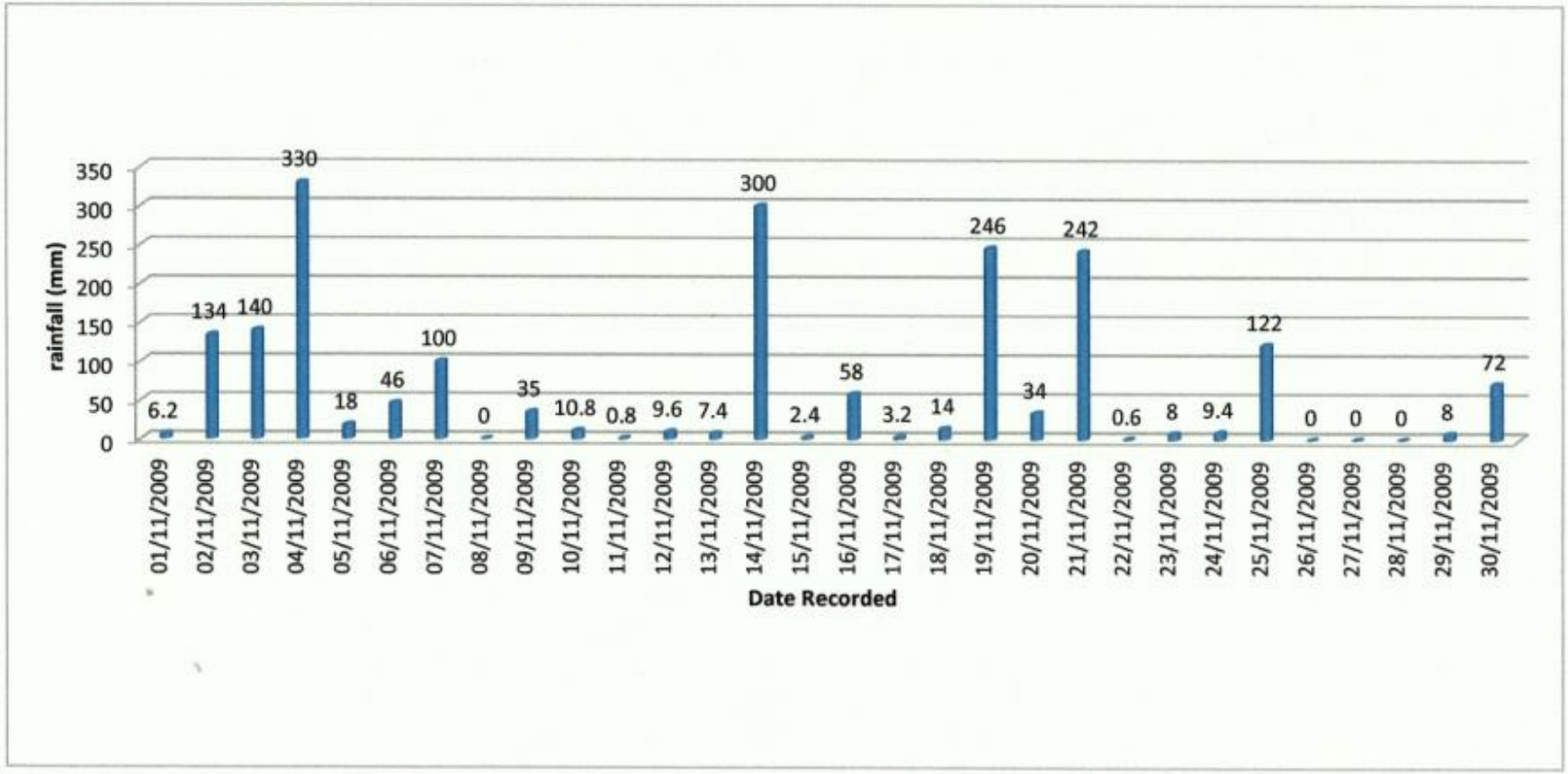

Figure 5.37 Daily Rainfall Graph for November 2009 for the Barre de L'isle Study Site

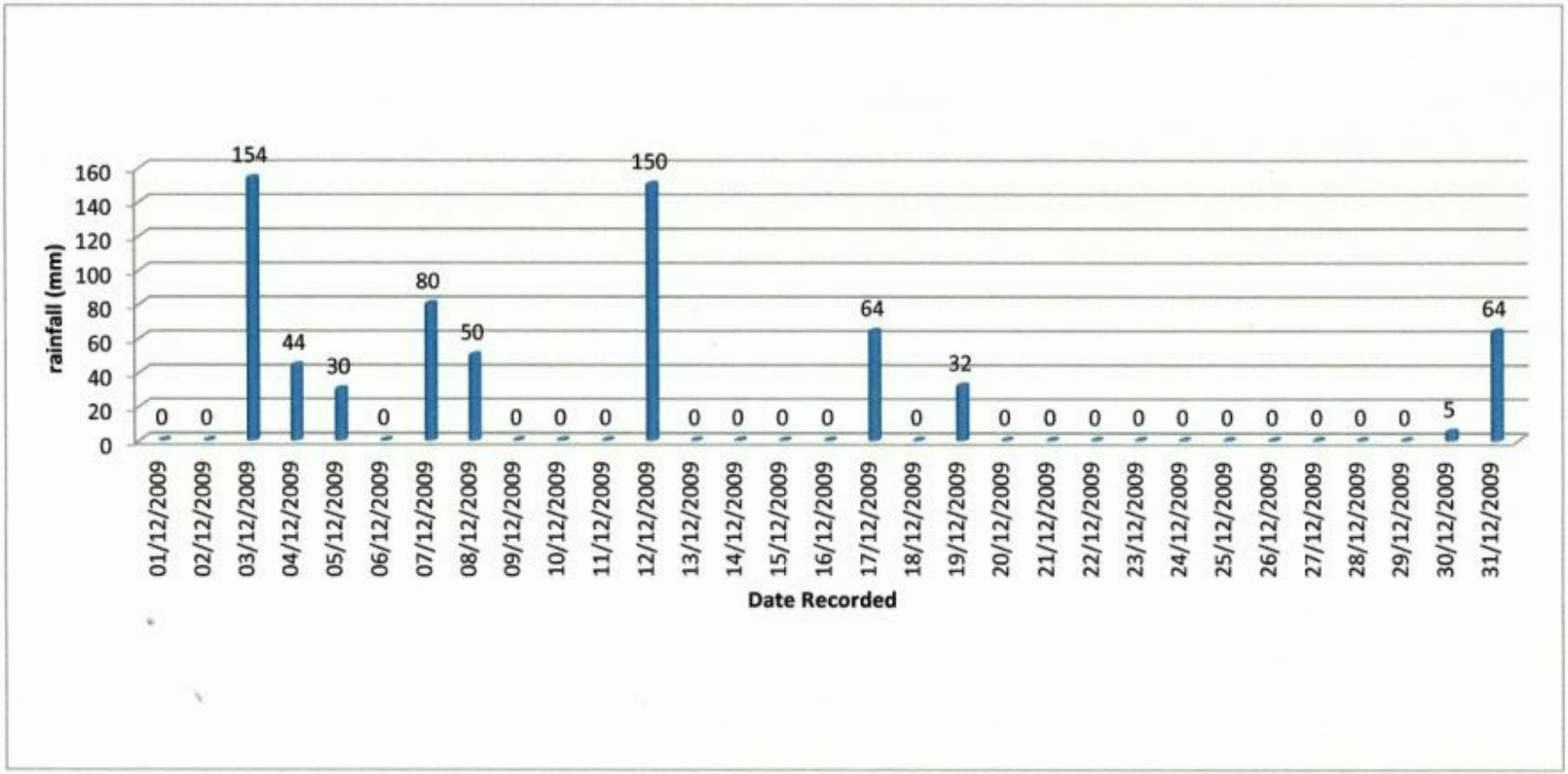

Figure 5.38 Daily Rainfall Graph for December 2009 for the Barre de L'isle Study Site

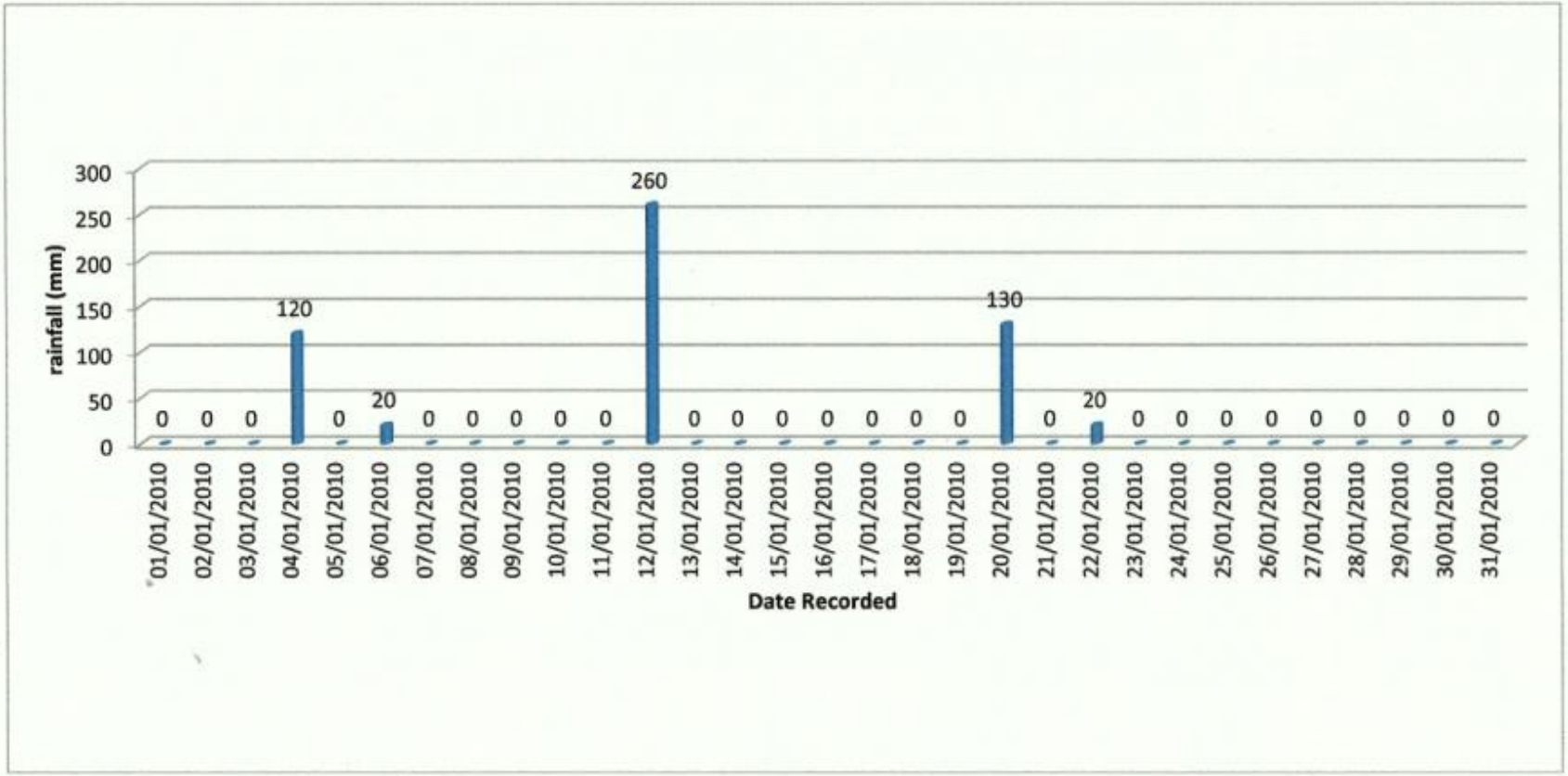

Figure 5.39 Daily Rainfall Graph for January 2010 for the Barre de L'isle Study Site

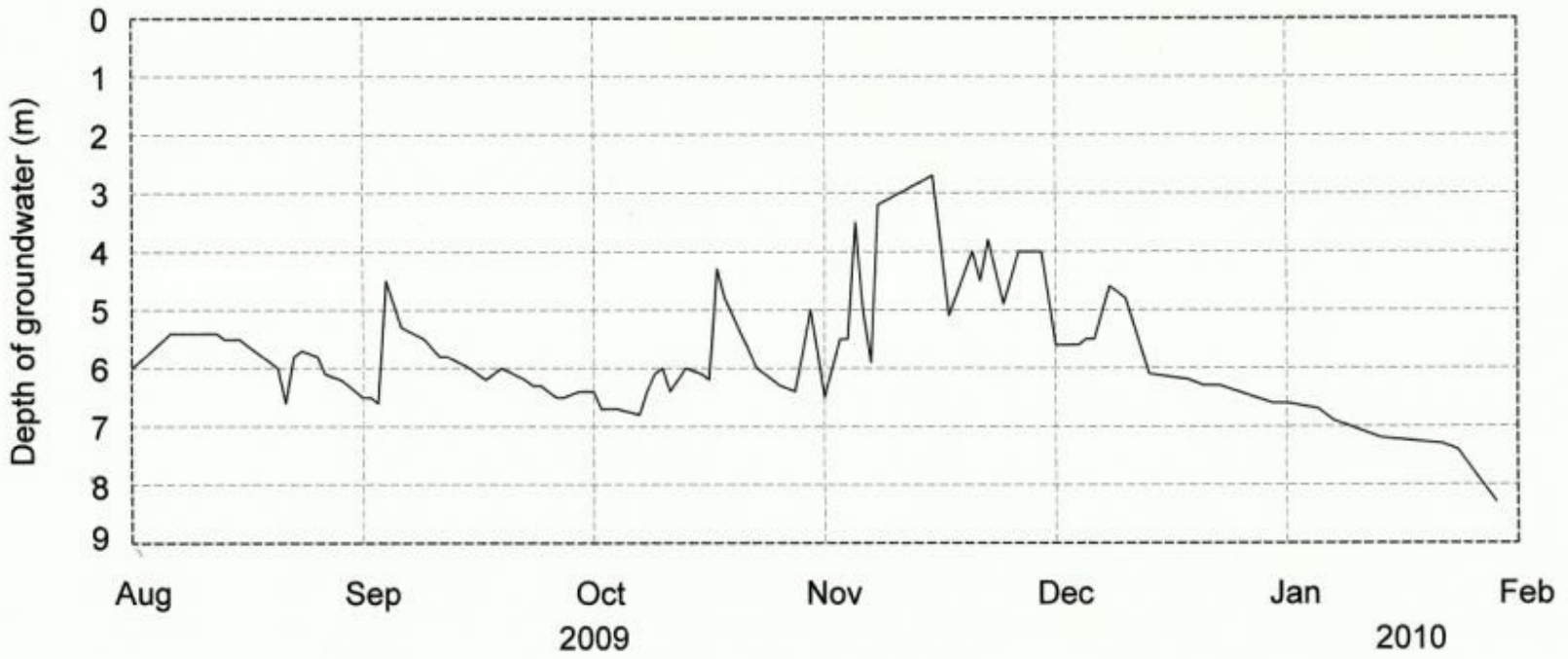

Figure 5.40 Graph of Standpipe Piezometer Readings for the period August 1st, 2009 to January 31st, 2010 at the Barre de L'Isle Study Site

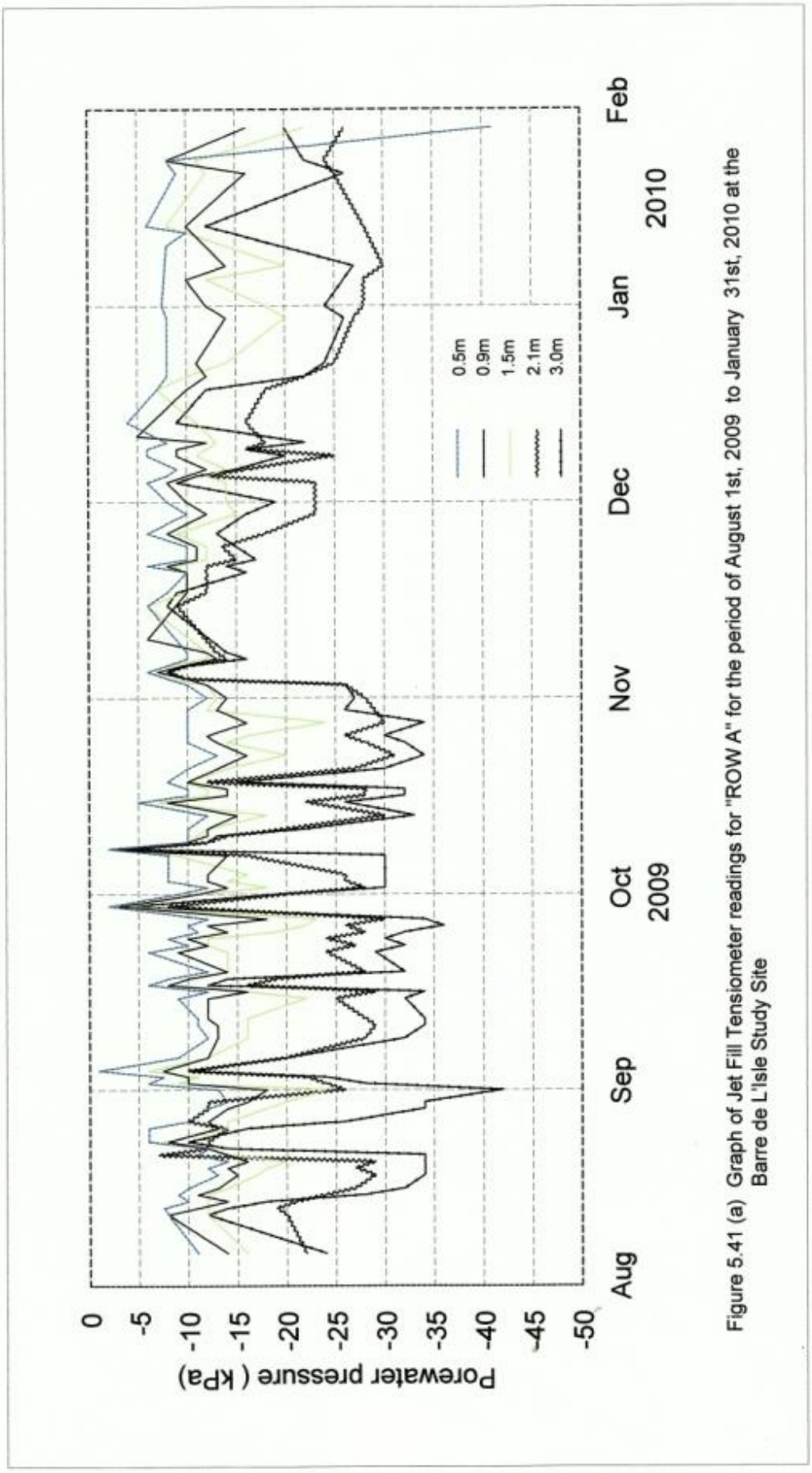

Figure 5.41 (a) Graph of Jet Fill Tensiometer readings for "ROW A" for the period of August 1st, 2009 to January 31st, 2010 at the Barre de L'Isle Study Site

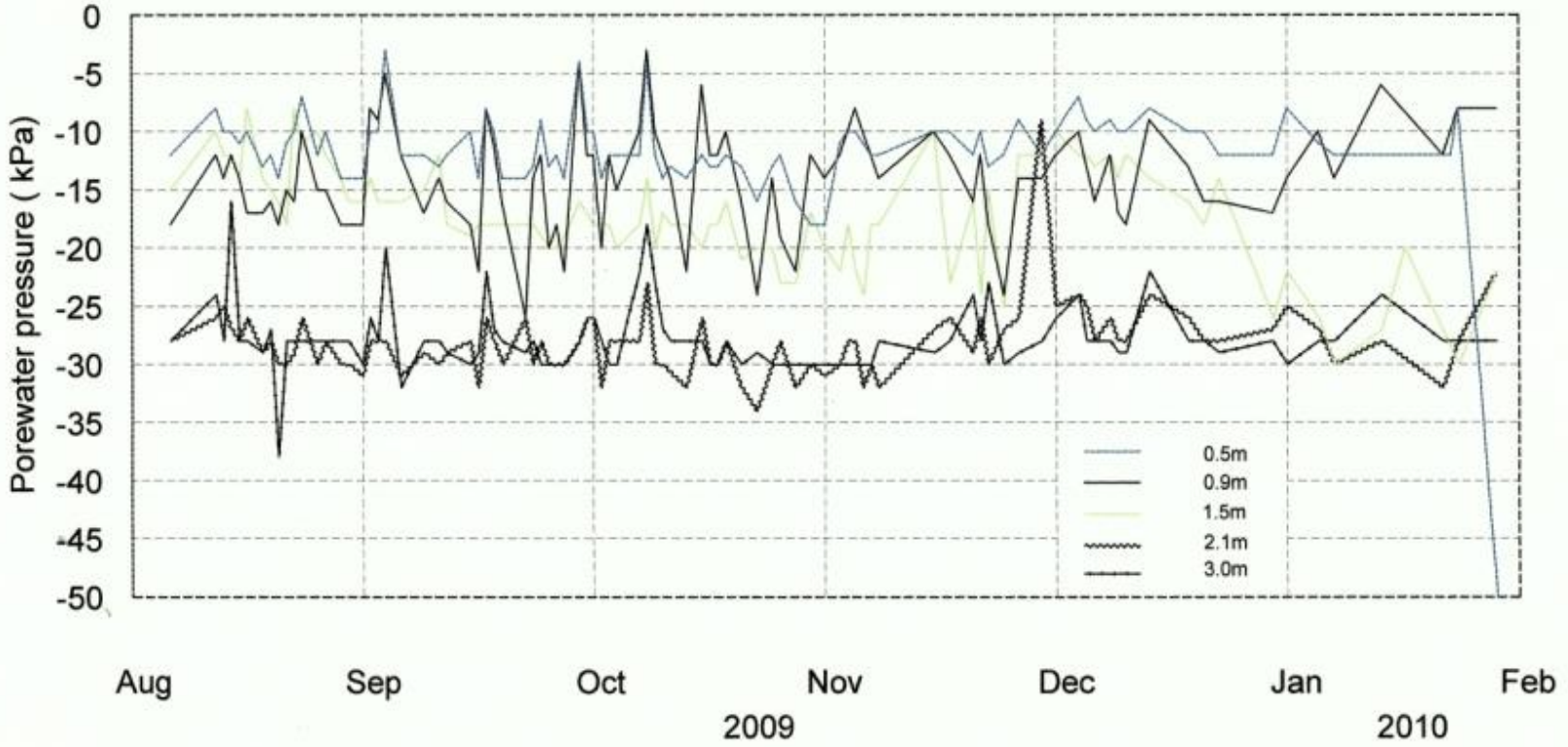

Figure 5.41 (b) Graph of Jet Fill Tensiometer readings for "ROW B" for the period of August 1st, 2009 to January 31st, 2010 at the Barre de L'Isle Study Site

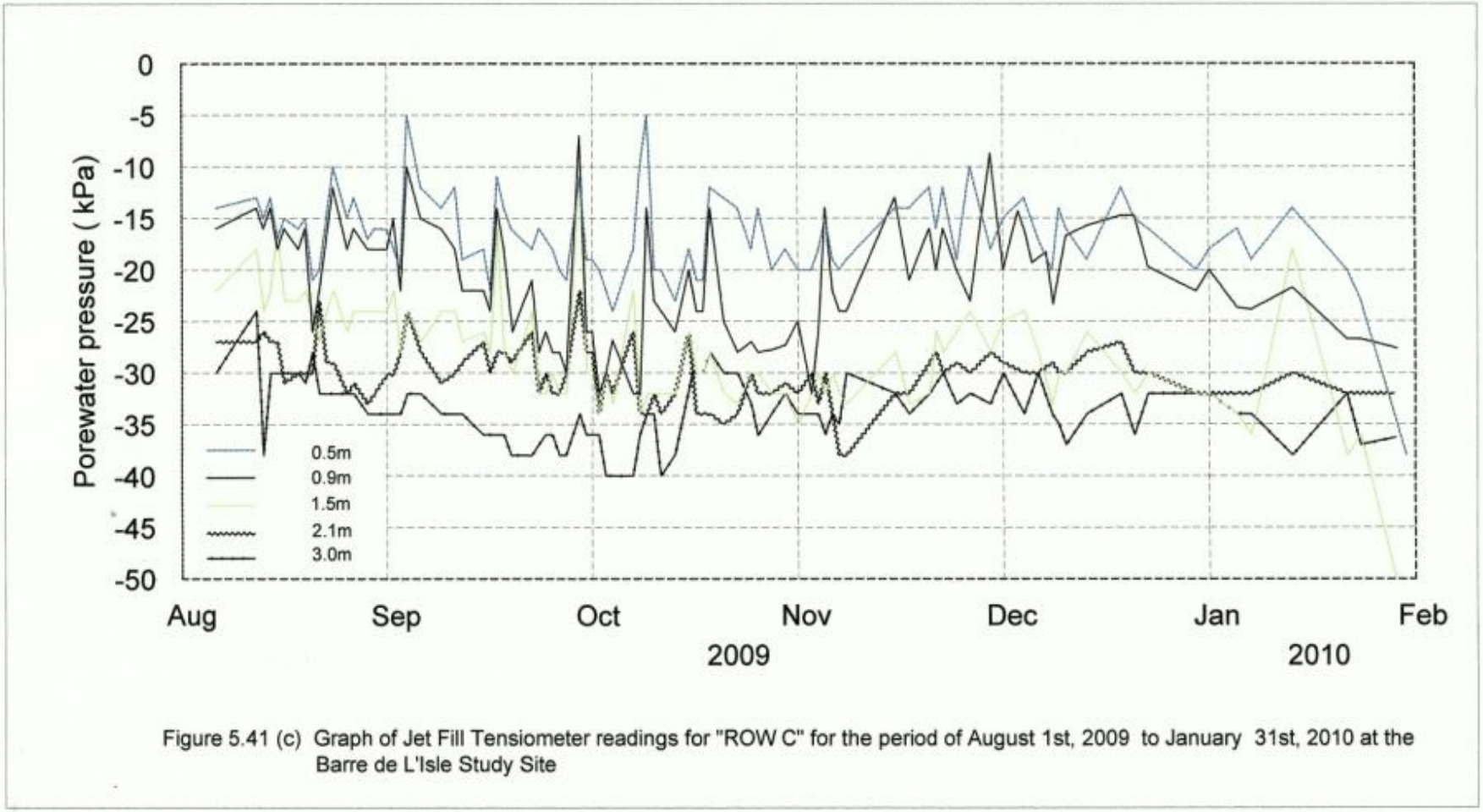

Figure 5.41 (c) Graph of Jet Fill Tensiometer readings for "ROW C" for the period of August 1st, 2009 to January 31st, 2010 at the Barre de L'Isle Study Site

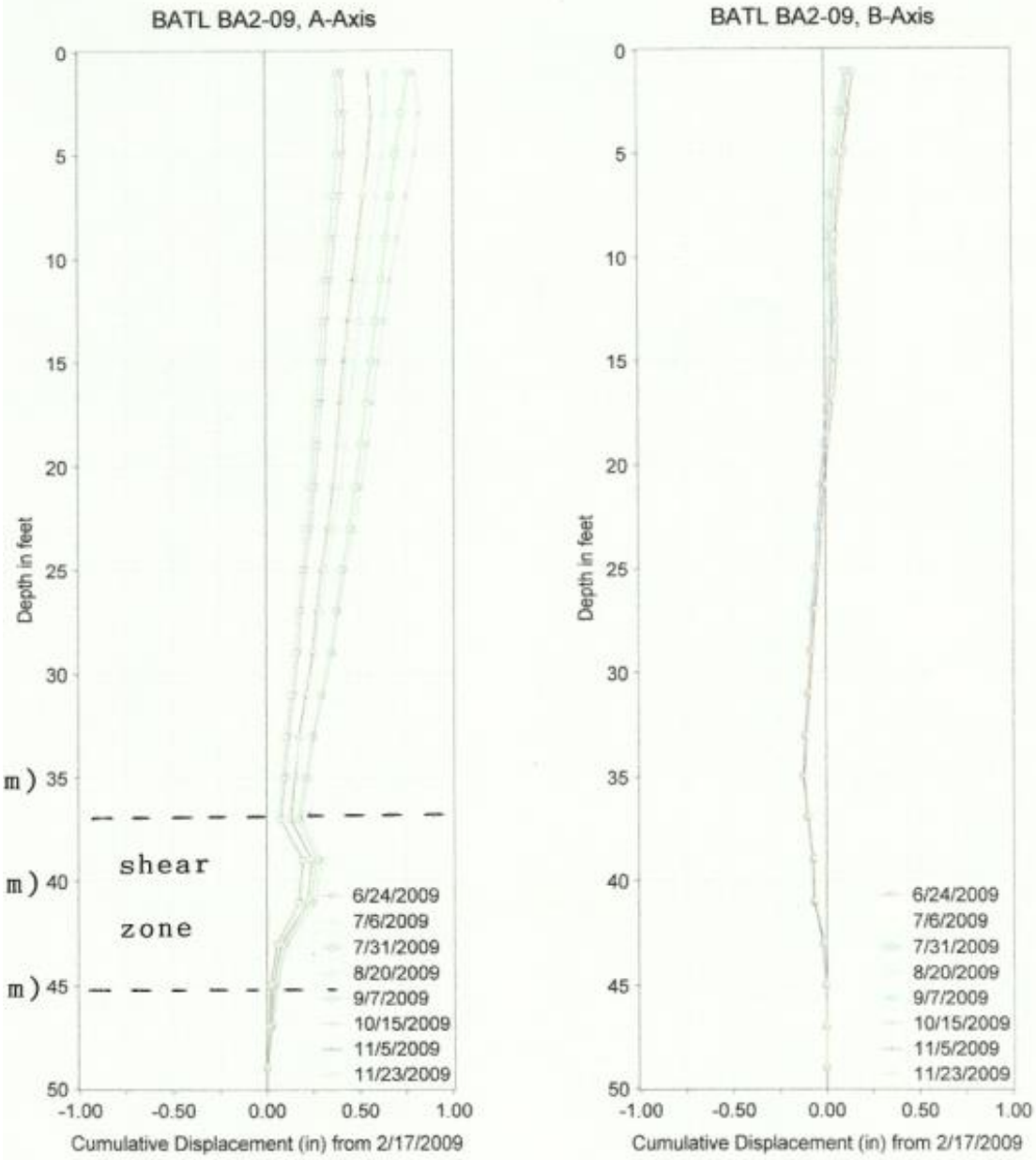

Figure 5.42 Horizontal displacement in inclinometer at Barre de L'isle Study Site

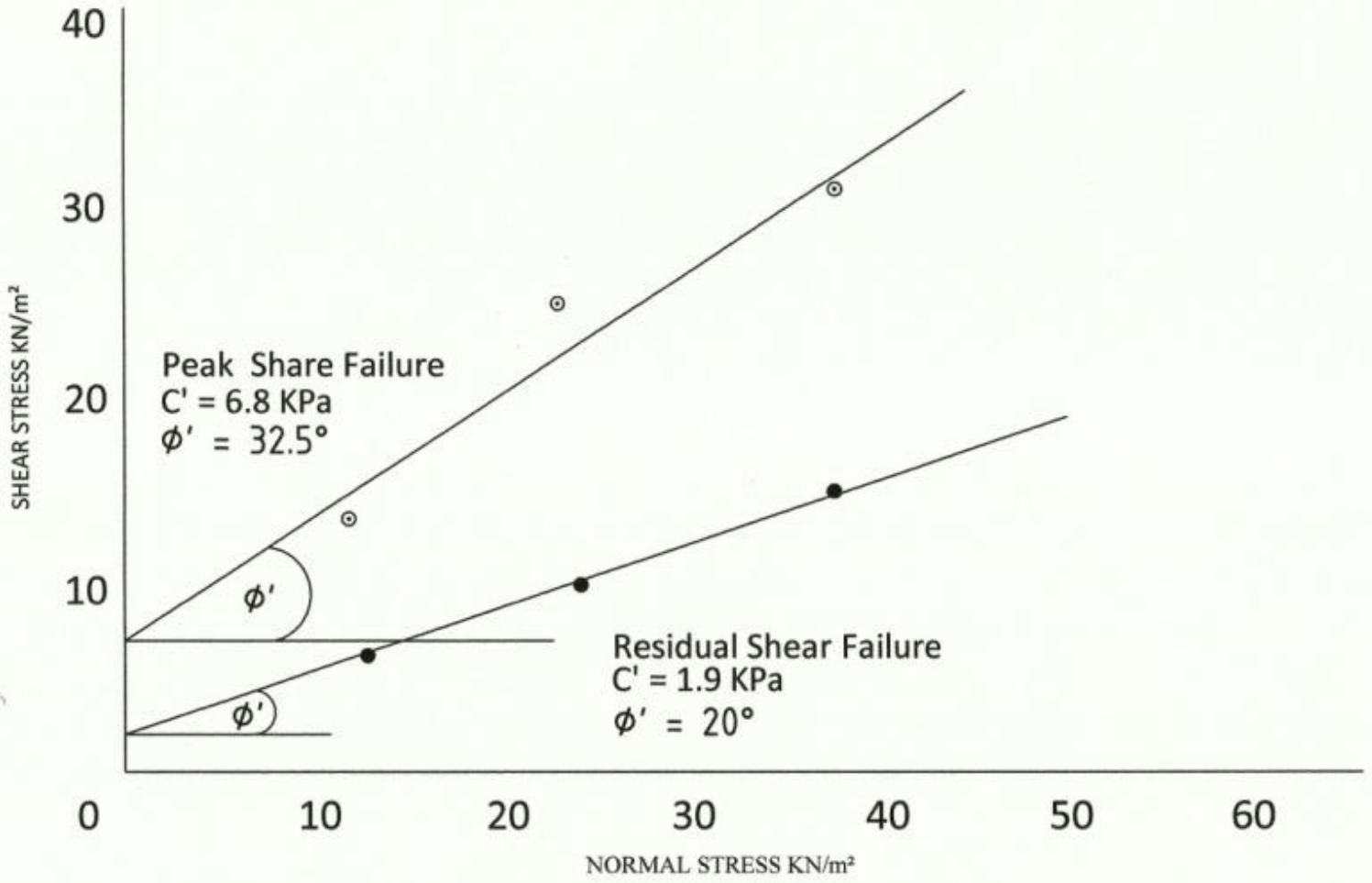

Figure 5.43 Shear Strength envelope for Colluvium at Villa 43

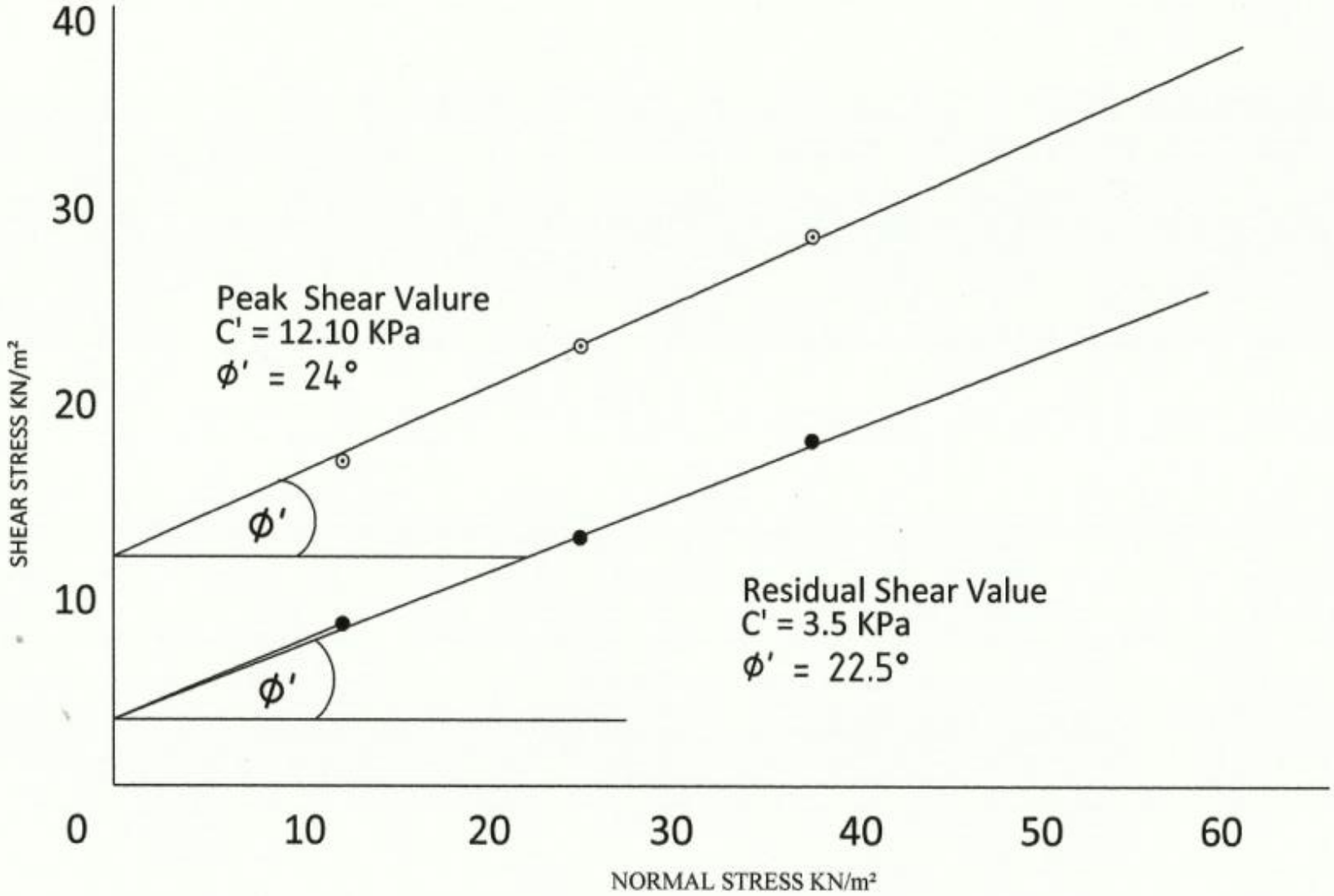

Figure 5.44 Shear Strength envelope for Colluvium at Villa 45

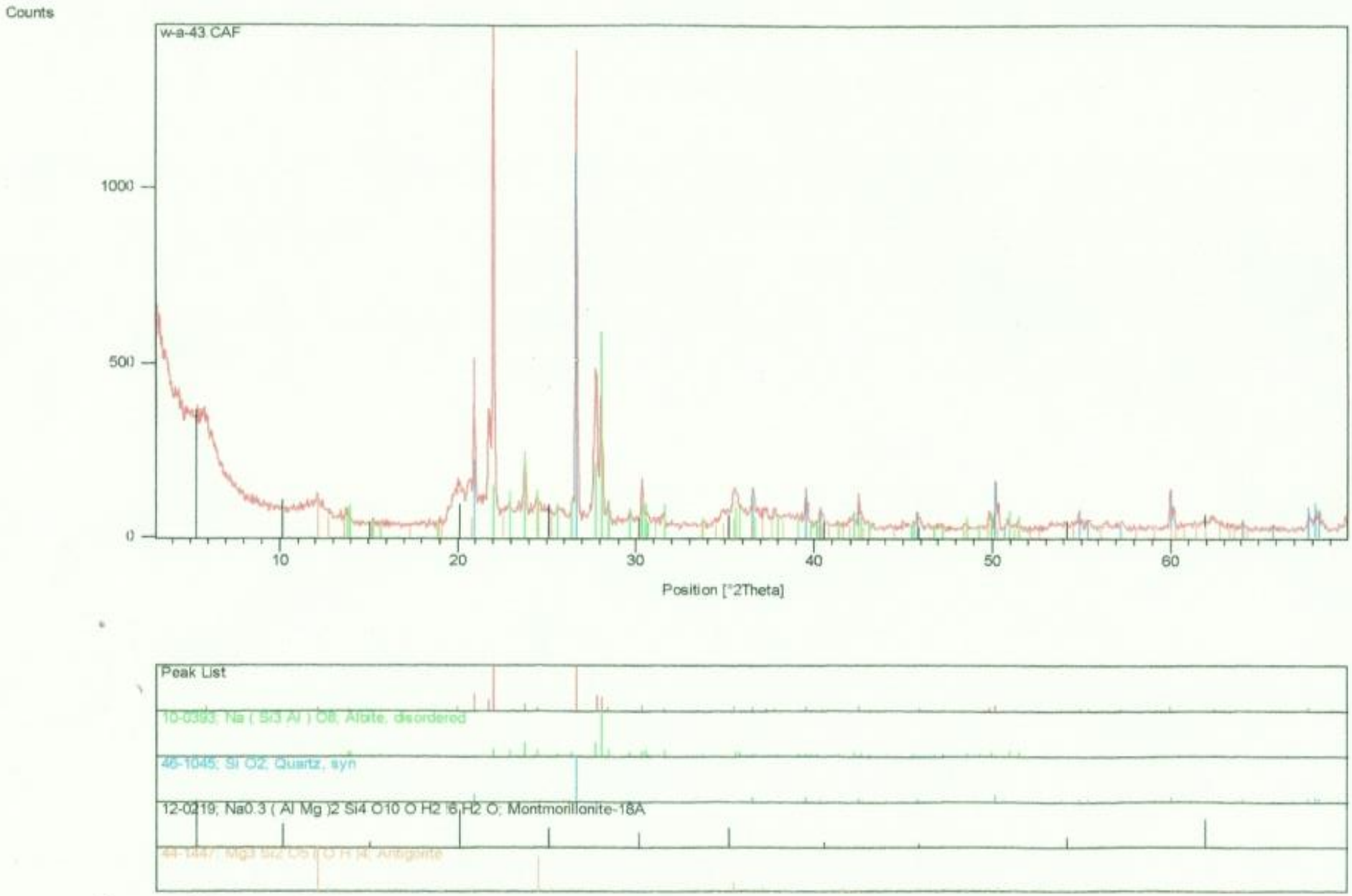

Figure 5.45 X-Ray Diffraction Peaks for Colluvium from borehole SP05-STA-1 at the 2005 Landslide at Windjammer Landing Beach Resort

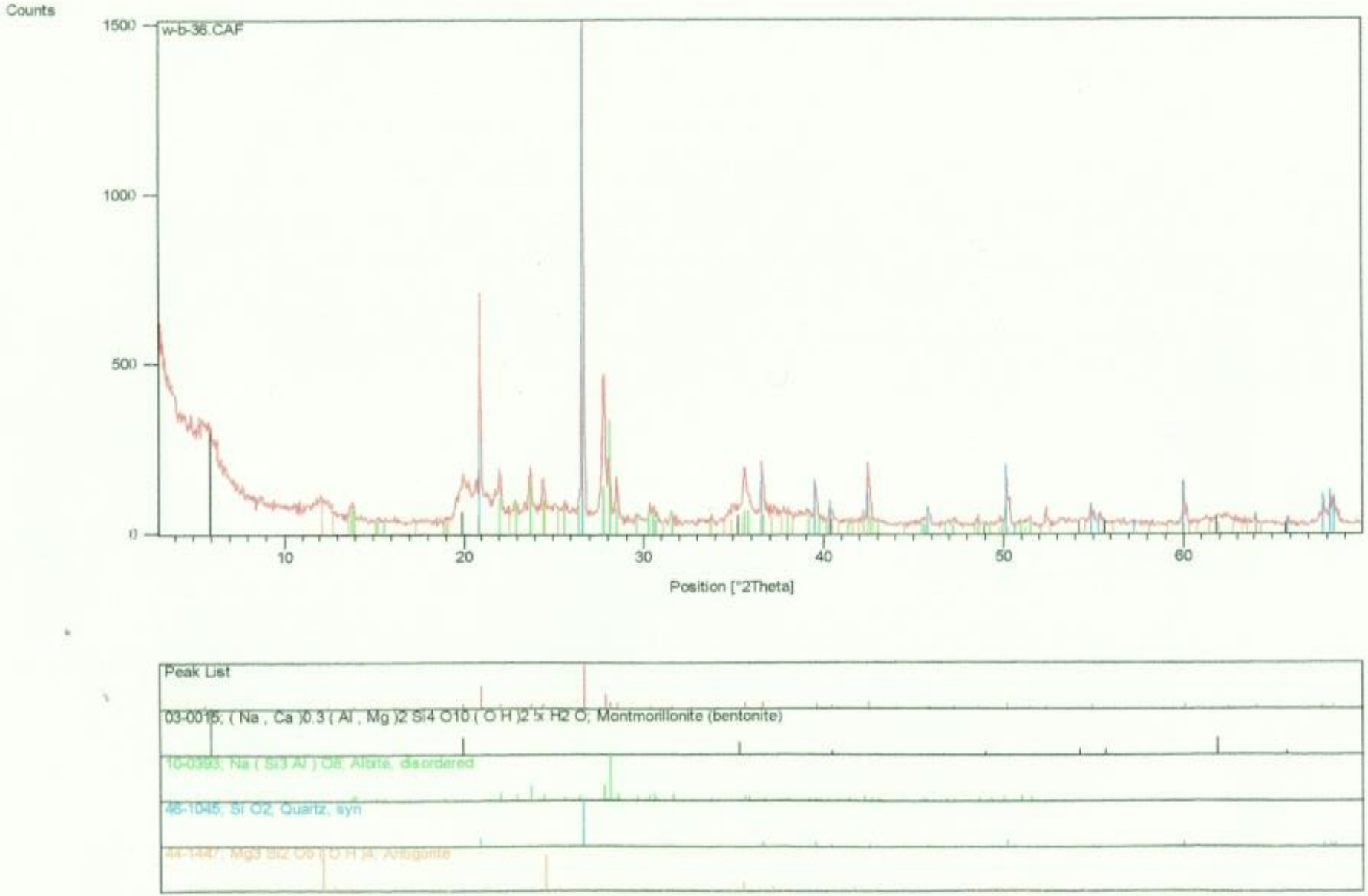

Figure 5.46 : X-Ray Diffaction Peaks for Colluvium from borehole SP05-STB-1 at the 2005 Landslide Area at the Windjammer Landing Beach Resort

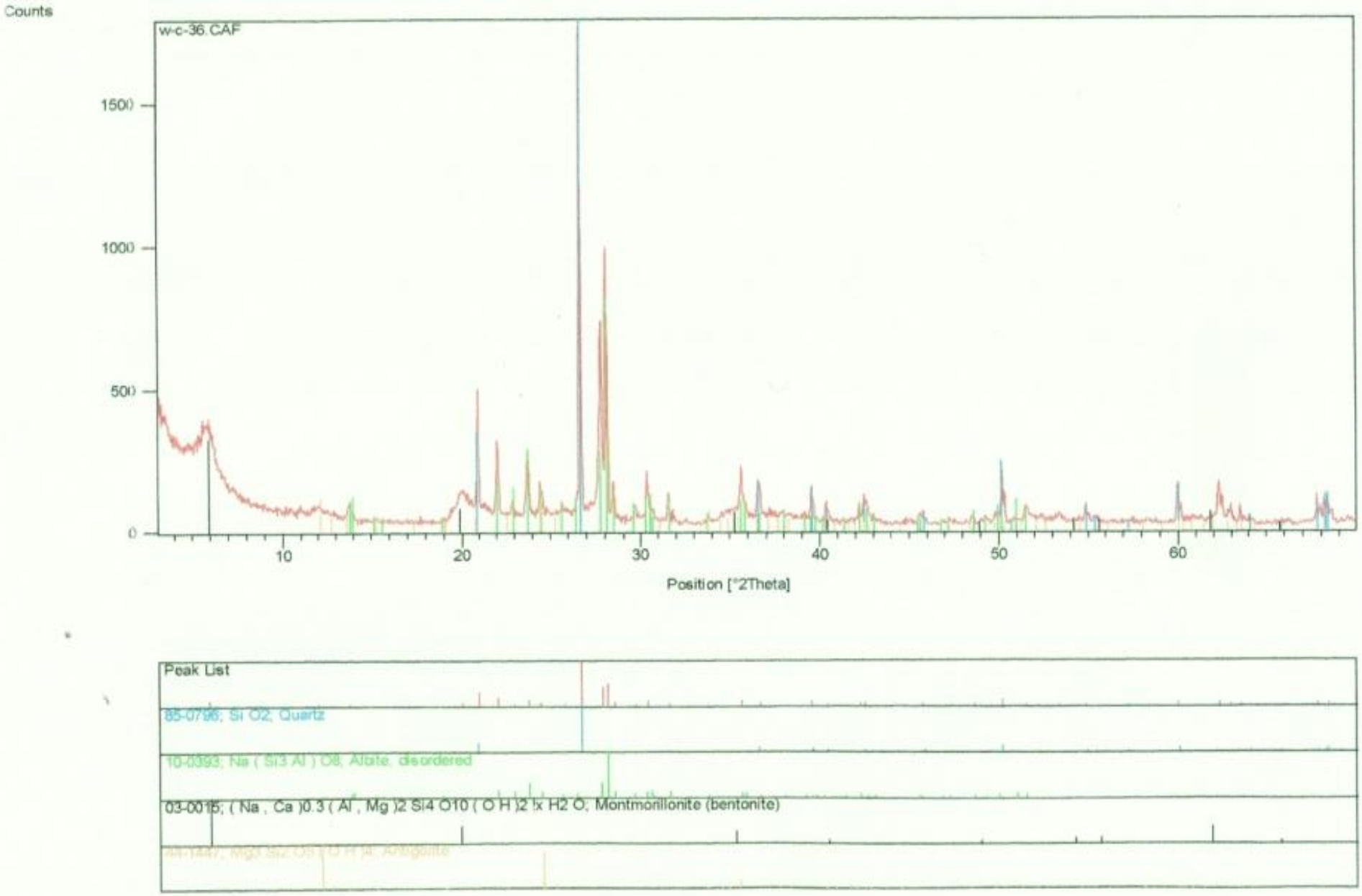

Figure 5.47 X-Ray Diffraction Peaks for Colluvium fromborehole SP05-STC-1 at the 2005 Landslide Area at the Windjammer Landing Beach Resort

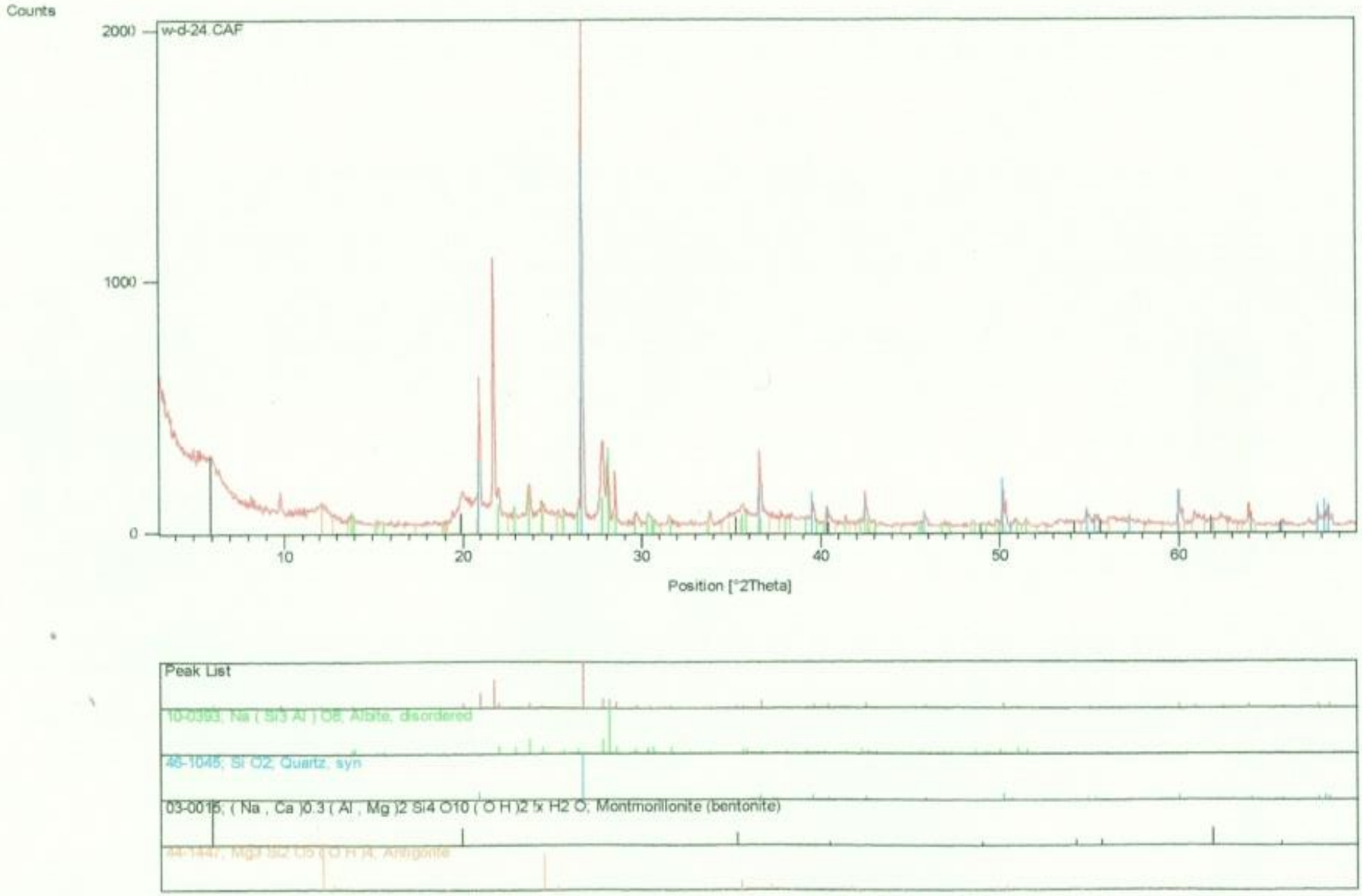

Figure 5.48 X-Ray Diffraction Peaks for Colluvium from borehole SP05-STD-1 at the 2005 Landslide Area at the Windjammer Landing Beach Resort

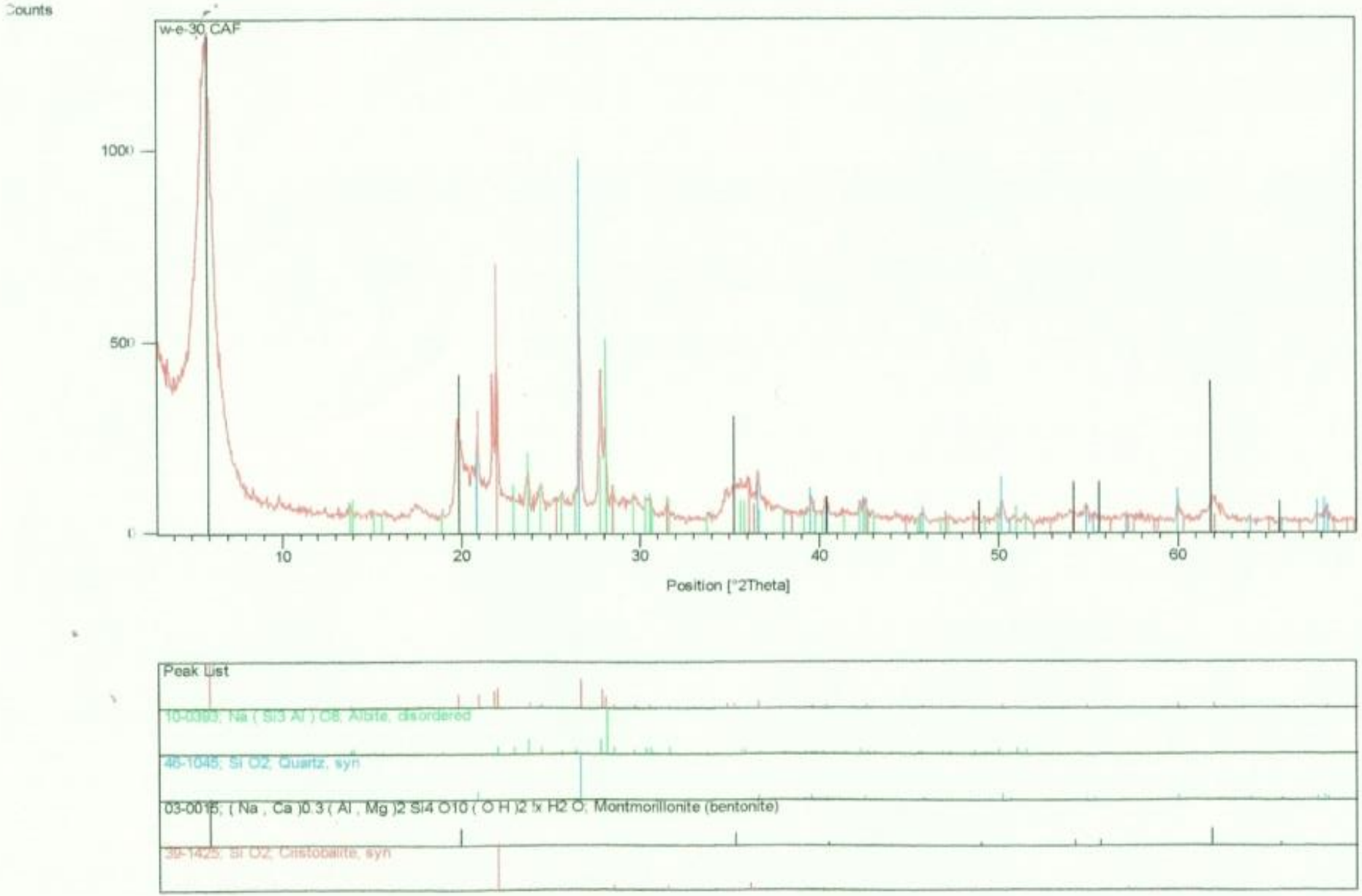

Figure 5.49 X-Ray Diffraction Peaks for Colluvium from borehole SP05-STE-1 at the Landslide Area at the Windjammer Landing Beach Resort

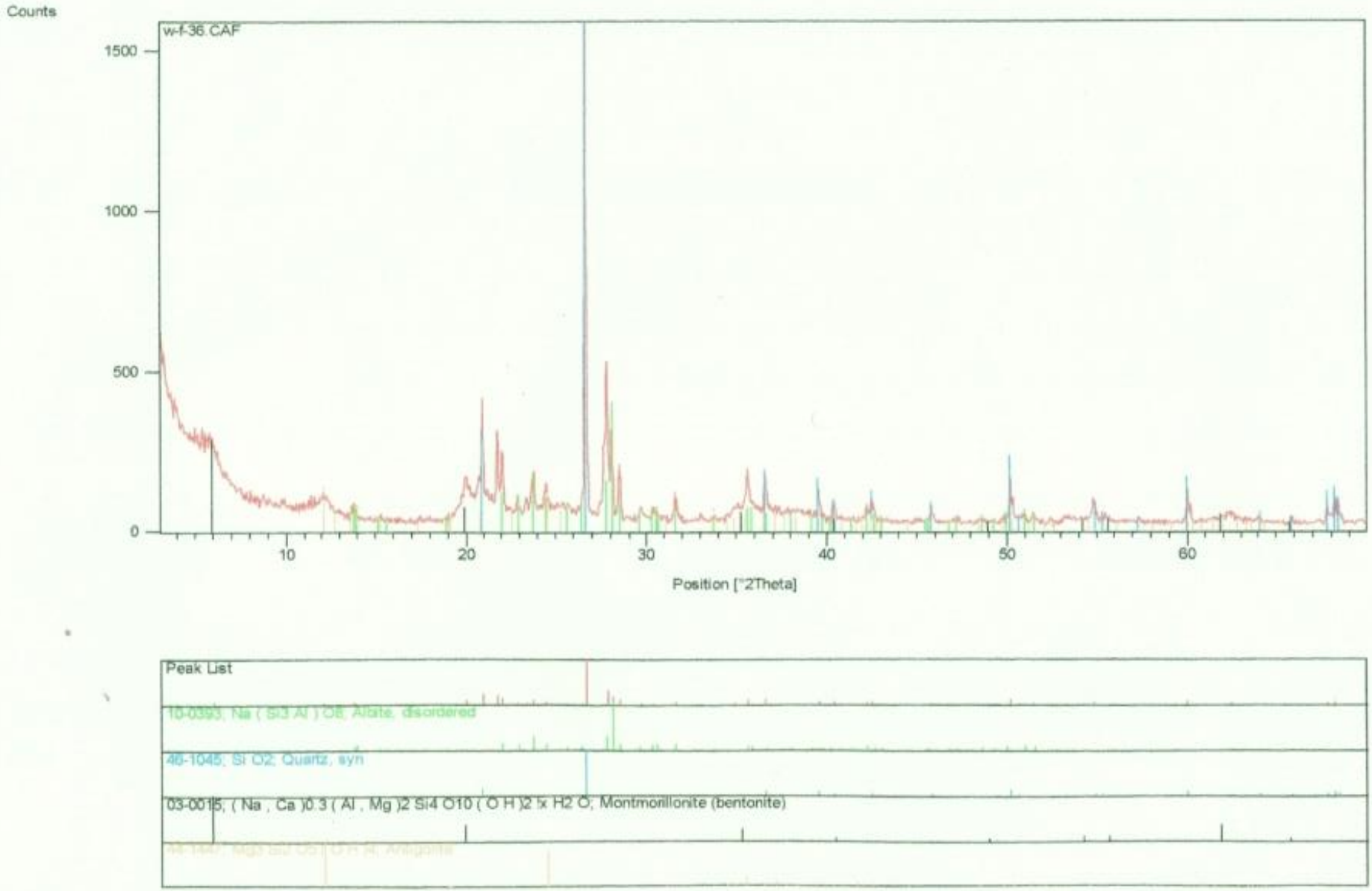

Figure 5.50 X-Ray Diffraction Peaks for Colluvium from borehole SP05-STF-1 at the 2005 Landslide Area at the Windjammer Landing Beach Resort

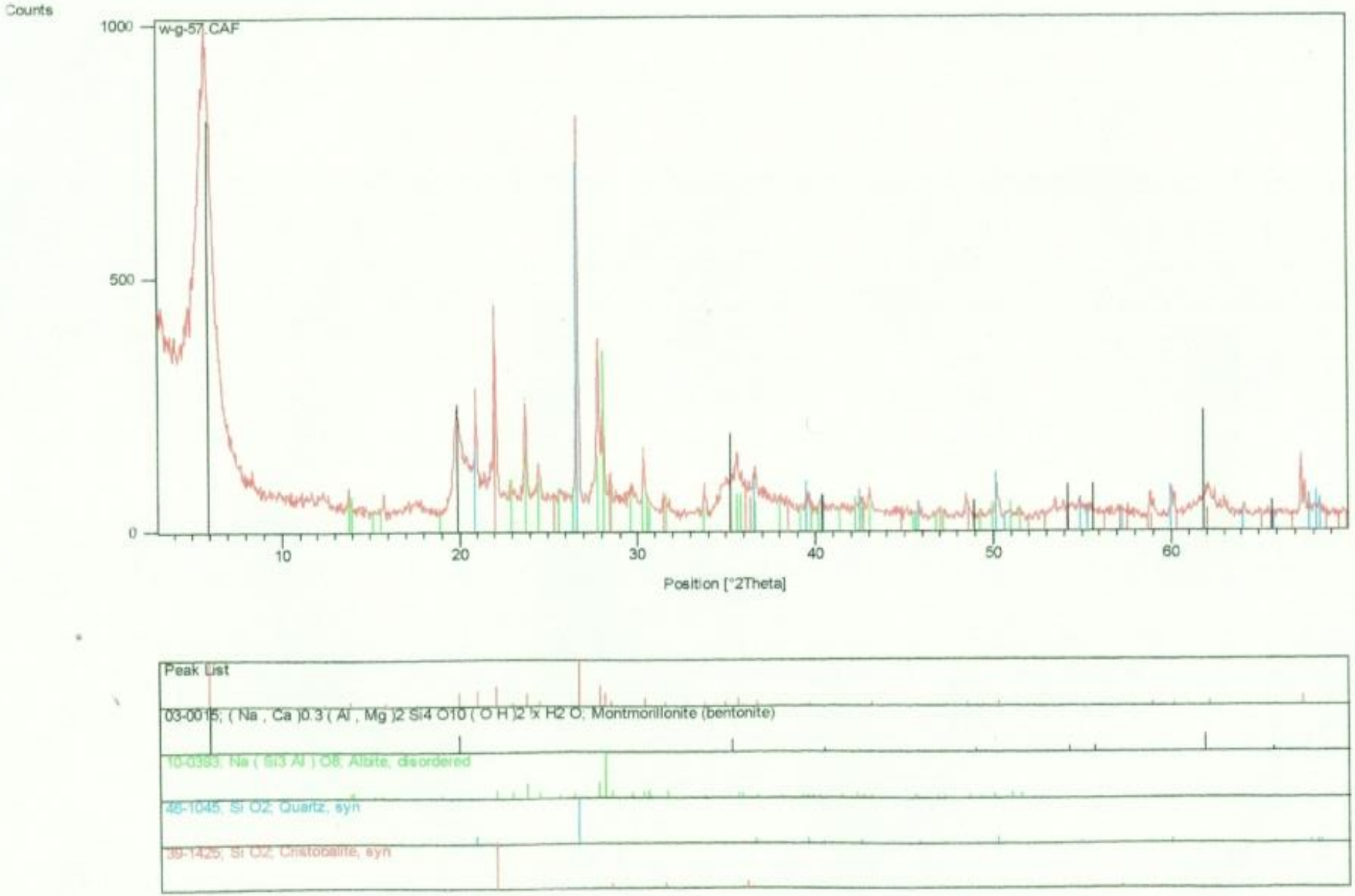

Figure 5.51 X-Ray Diffraction Peaks for Colluvium from borehole SP05-STG-1 at the 2005 Landslide Area at the Windjammer Landing Beach Resort

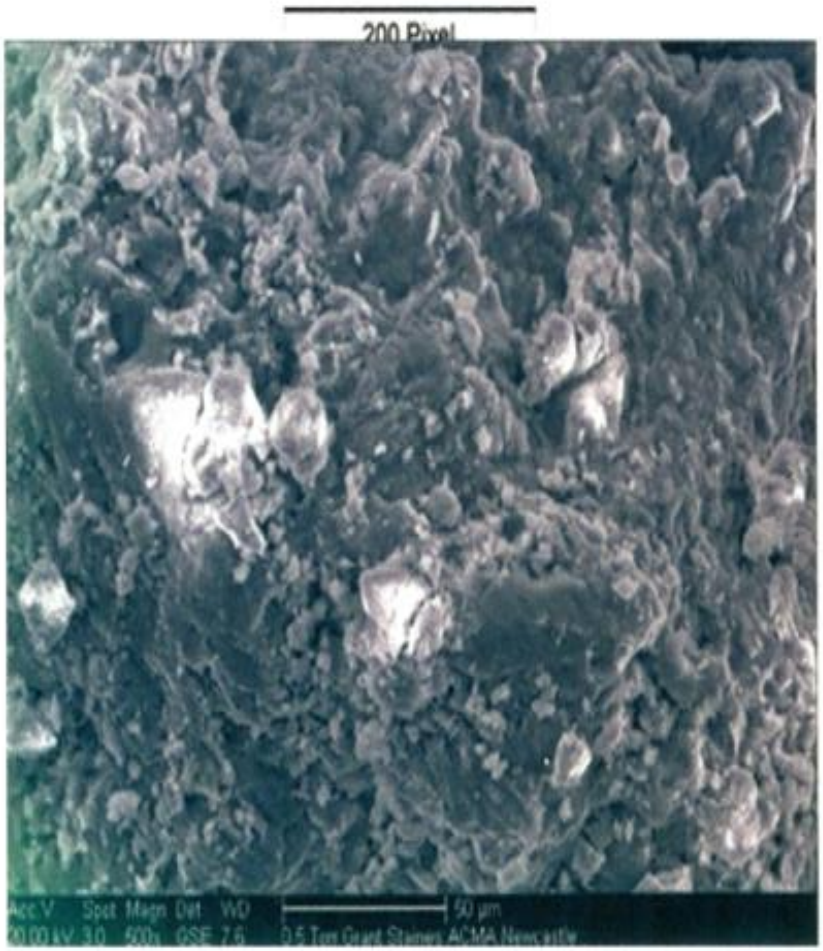

Figure 5.52

ESEM Image (x500) of colluvium from SP05-STA-1 2005 landslide at Windjammer Landing Beach Resort

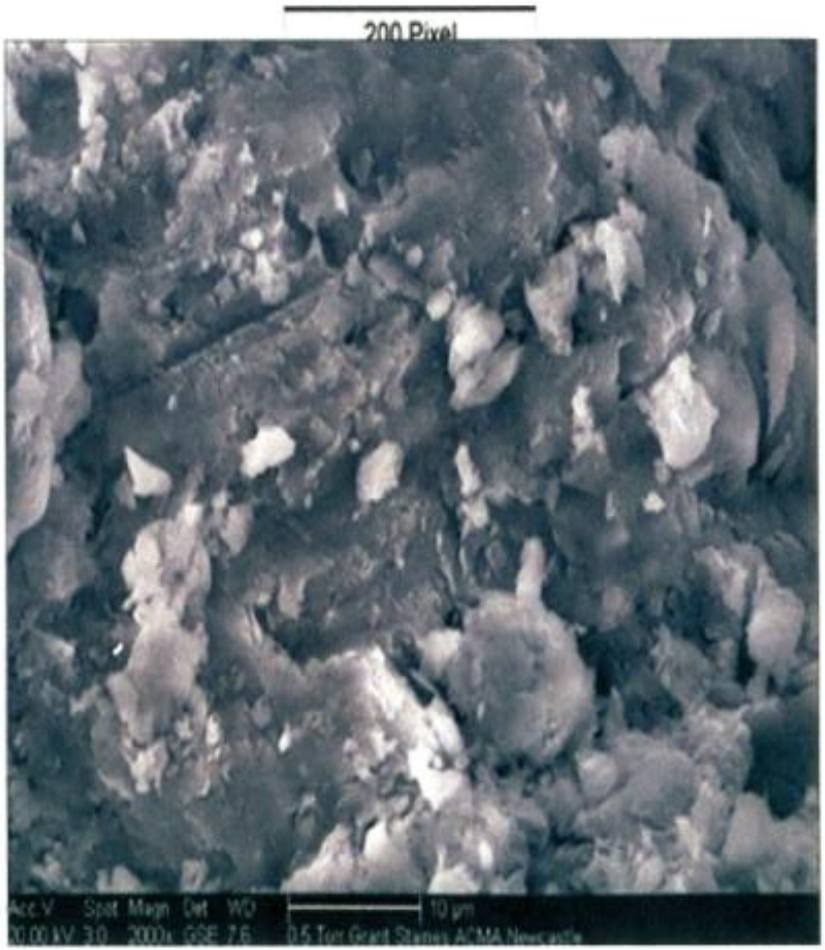

Figure 5.53

ESEM Image (x2000) of colluvium from SP05-STA-1 2005 landslide at Windjammer Landing Beach Resort

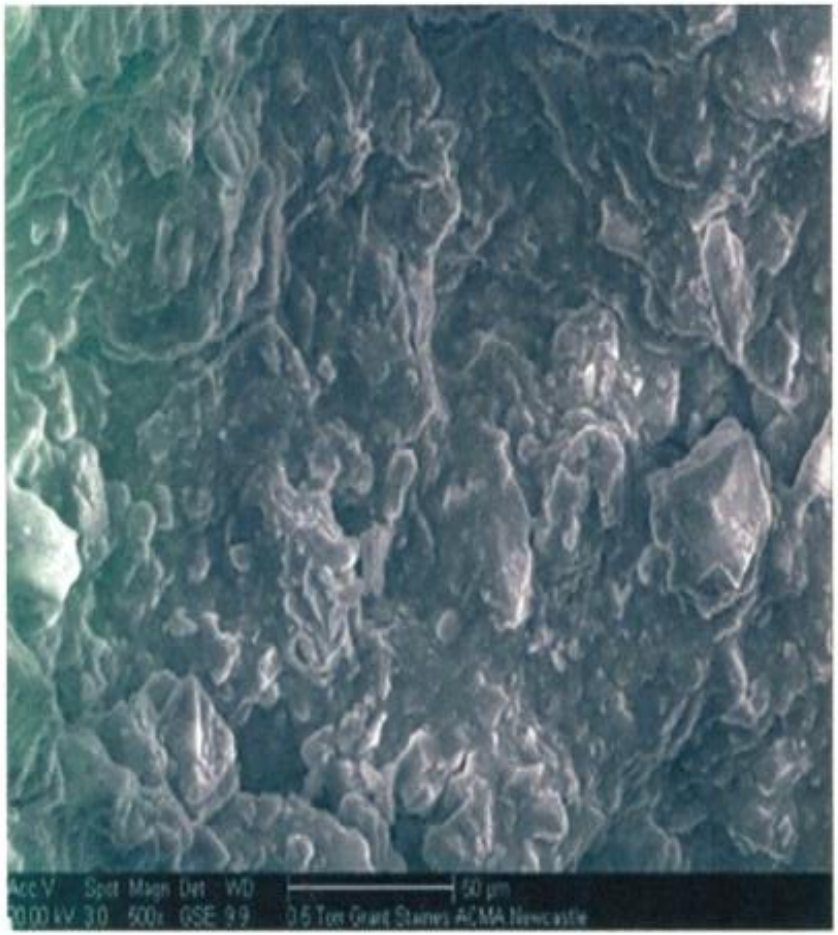

Figure 5.54

ESEM Image (x500) of colluvium from SP05-STB-1 2005 landslide at Windjammer Landing Beach Resort

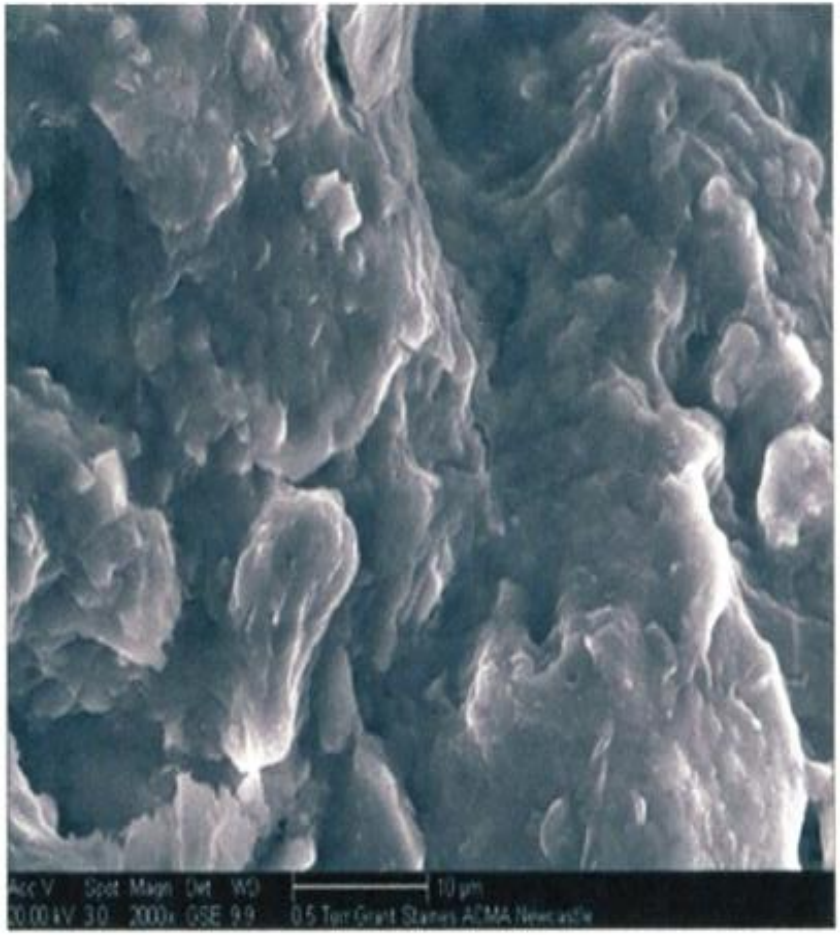

Figure 5.55

ESEM Image (x2000) of colluvium from SP05-STB-1 2005 landslide at Windjammer Landing Beach Resort

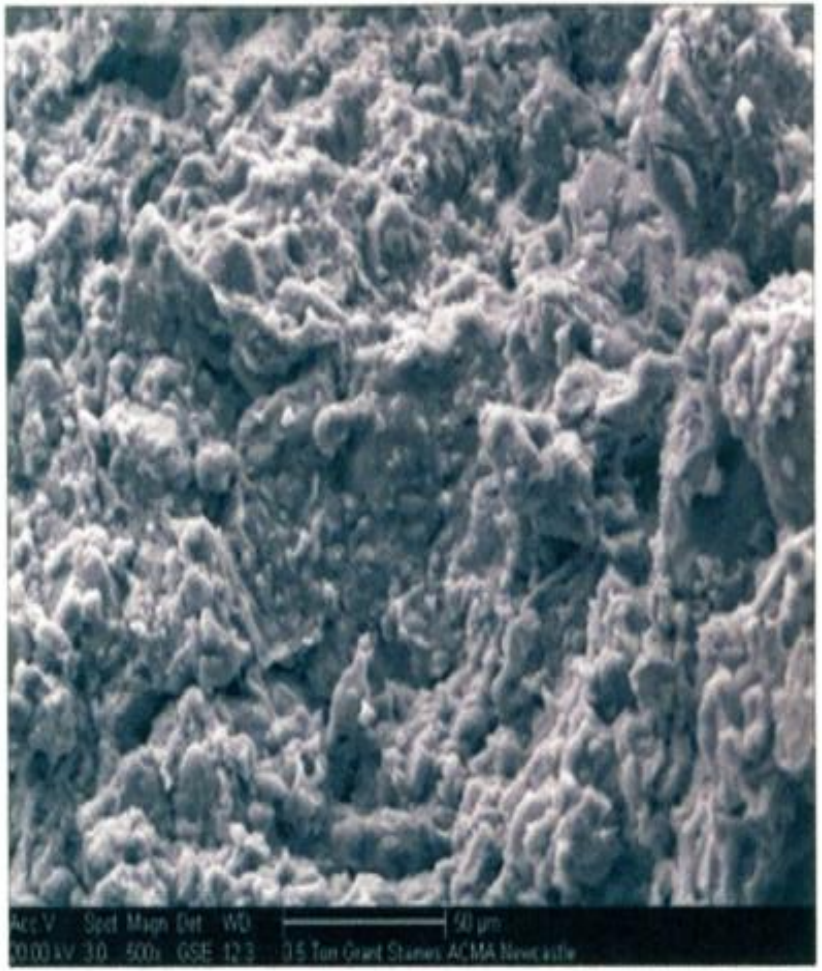

Figure 5.56

ESEM Image (x500) of colluvium from SP05-STC-1 2005 landslide at Windjammer Landing Beach Resort

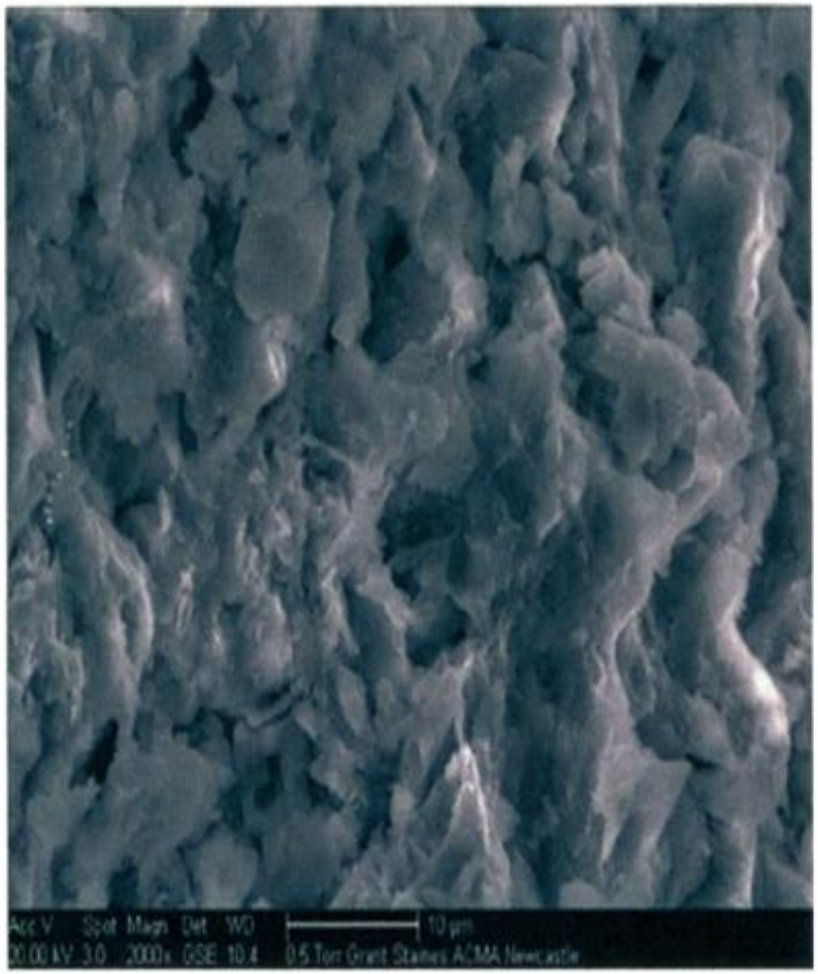

Figure 5.57

ESEM Image (x2000) of colluvium from SP05-STC-1 2005 landslide at Windjammer Landing Beach Resort

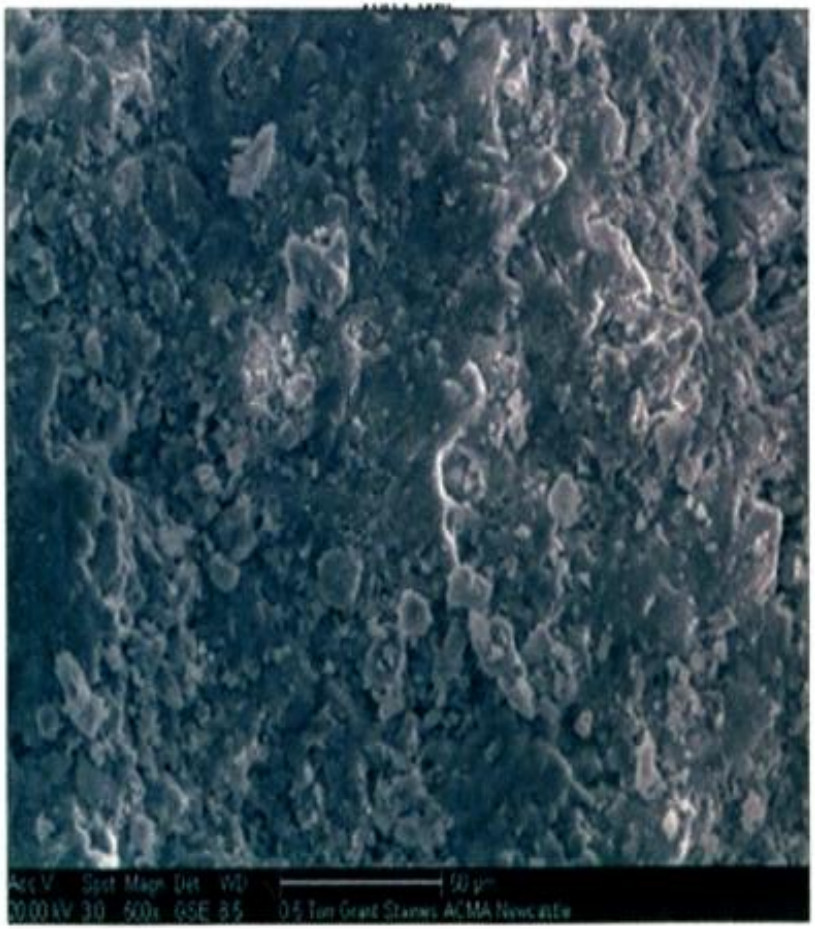

Figure 5.58

ESEM Image (x500) of colluvium from SP05-STD-1 2005 landslide at Windjammer Landing Beach Resort

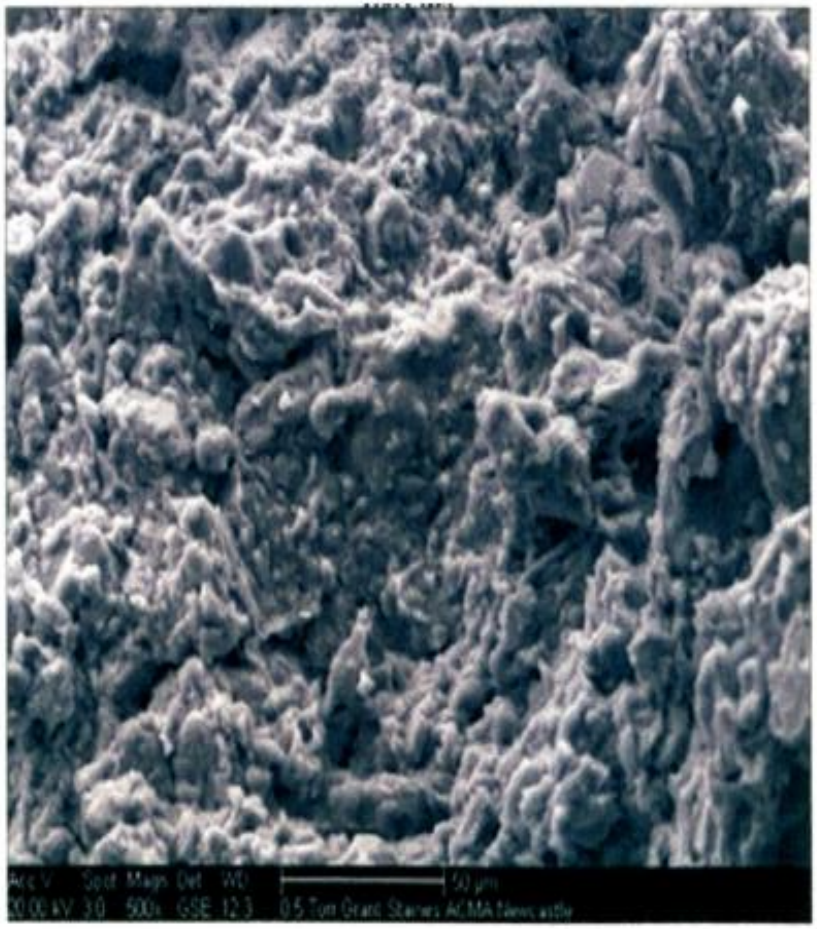

Figure 5.59

ESEM Image (x2000) of colluvium from SP05-STD-1 2005 landslide at Windjammer Landing Beach Resort

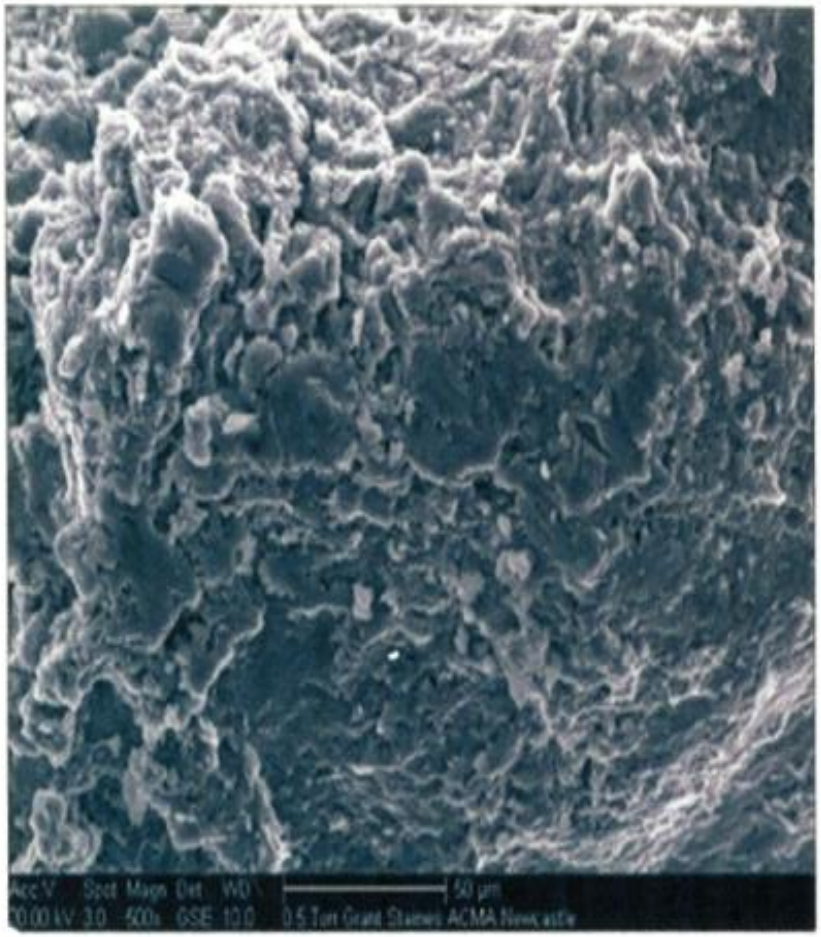

Figure 5.60

ESEM Image (x500) of colluvium from SP05-STE-1 2005 landslide at Windjammer Landing Beach Resort

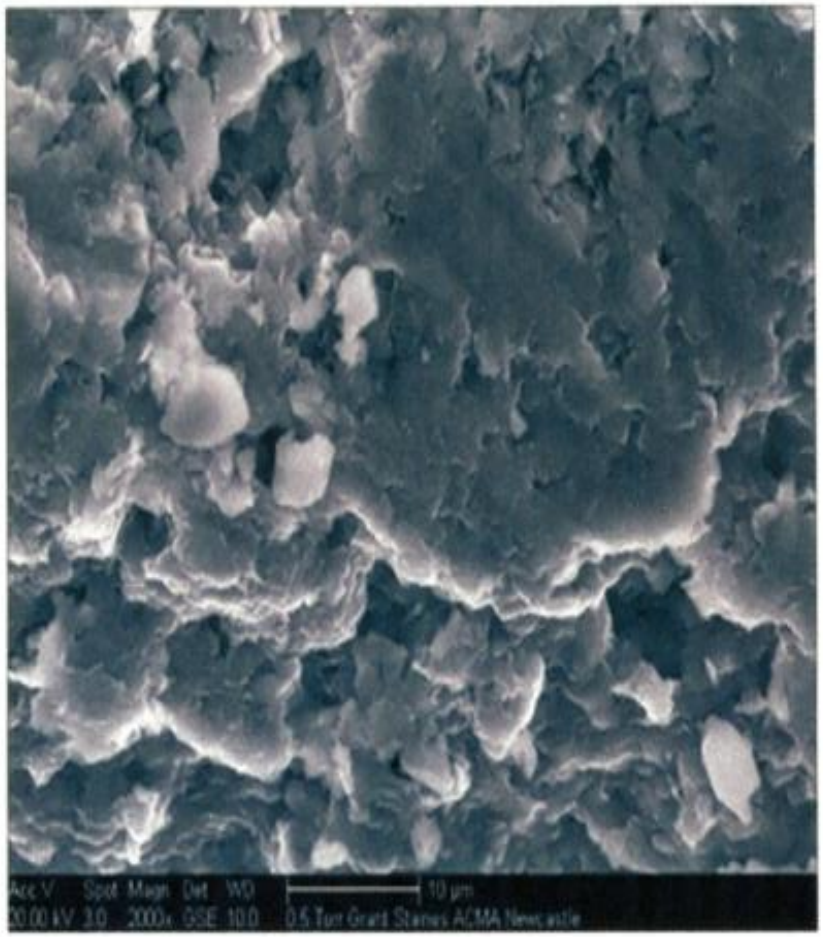

Figure 5.61

ESEM Image (x2000) of colluvium from SP05-STE-1 2005 landslide at Windjammer Landing Beach Resort

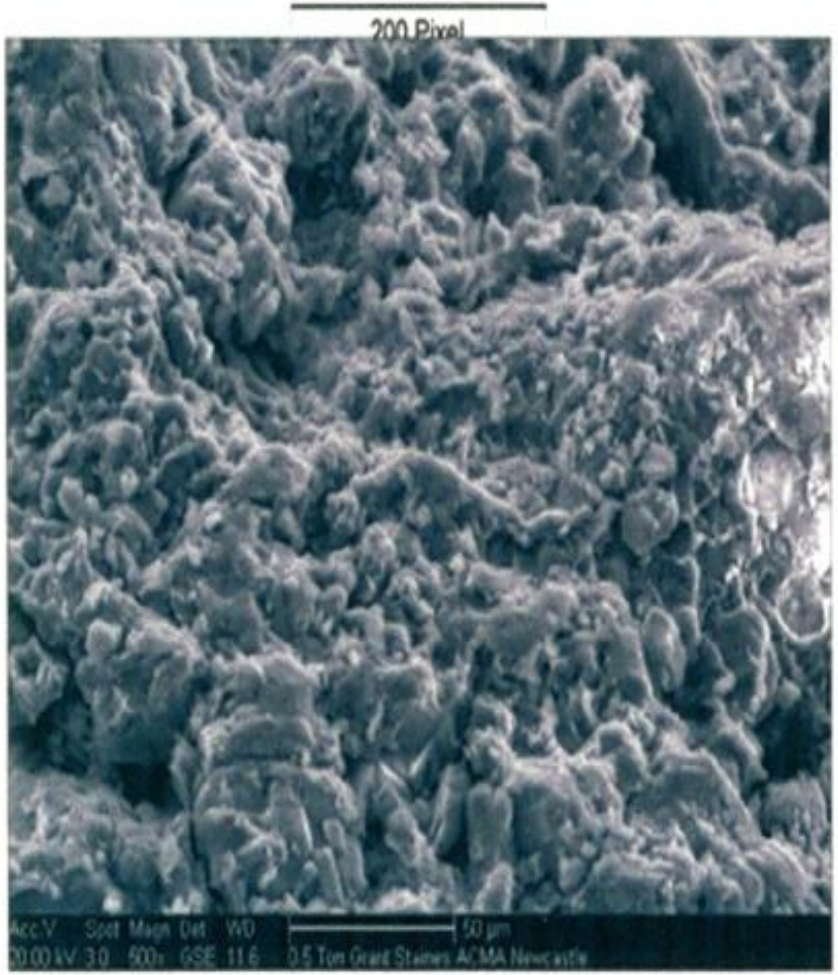

Figure 5.62

ESEM Image (x500) of colluvium from SP05-STF-1 2005 landslide at Windjammer Landing Beach Resort

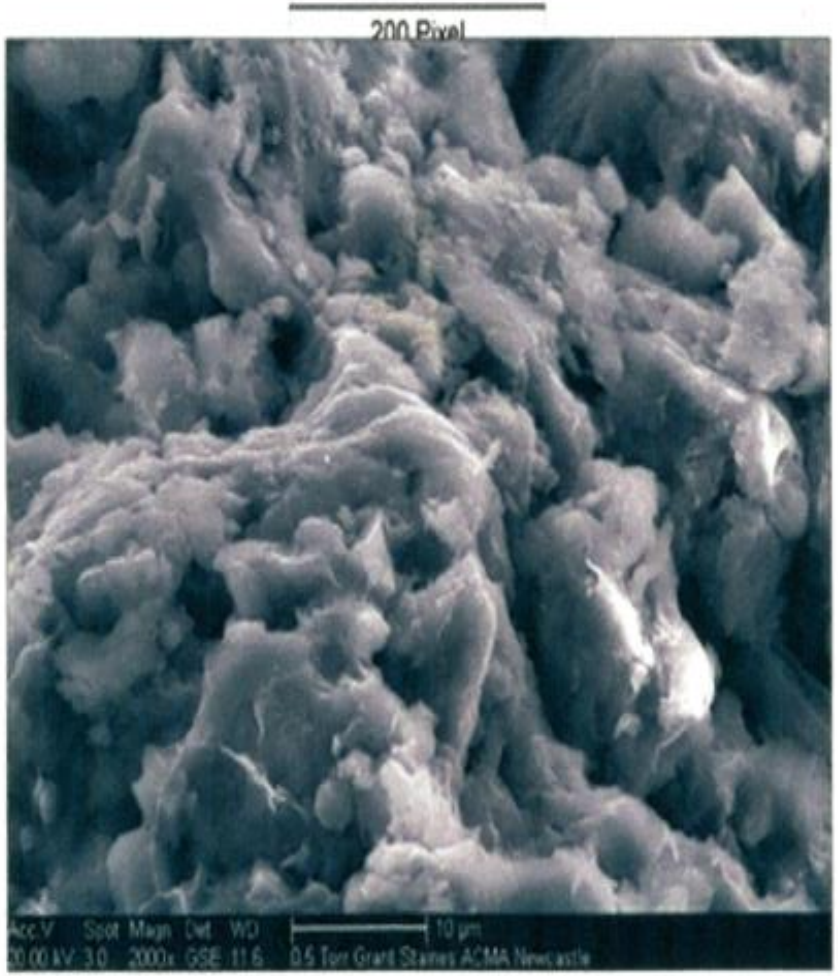

Figure 5.63

ESEM Image (x2000) of colluvium from SP05-STF-1 2005 landslide at Windjammer Landing Beach Resort

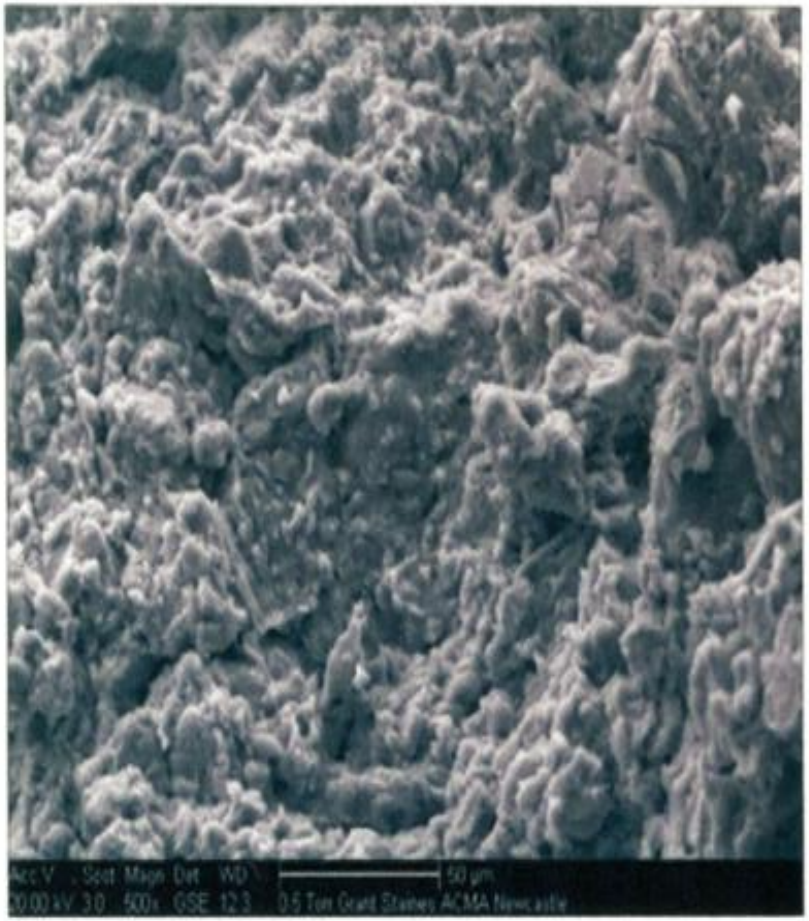

Figure 5.64

ESEM Image (x500) of colluvium from SP05-STG-1 2005 landslide at Windjammer Landing Beach Resort

Figure 5.65

ESEM Image (x500) of colluvium from SP05-STG-1 2005 landslide at Windjammer Landing Beach Resort

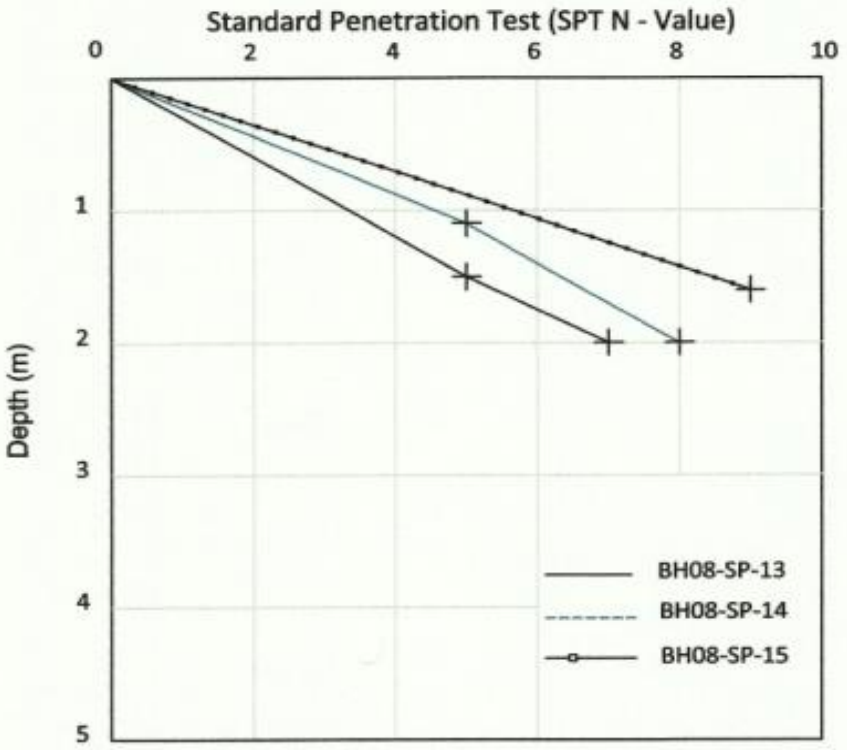

Figure 5.66 Graph of SPT vs Depth for Colluvium at the Windjammer Landing Beach Resort Study Site

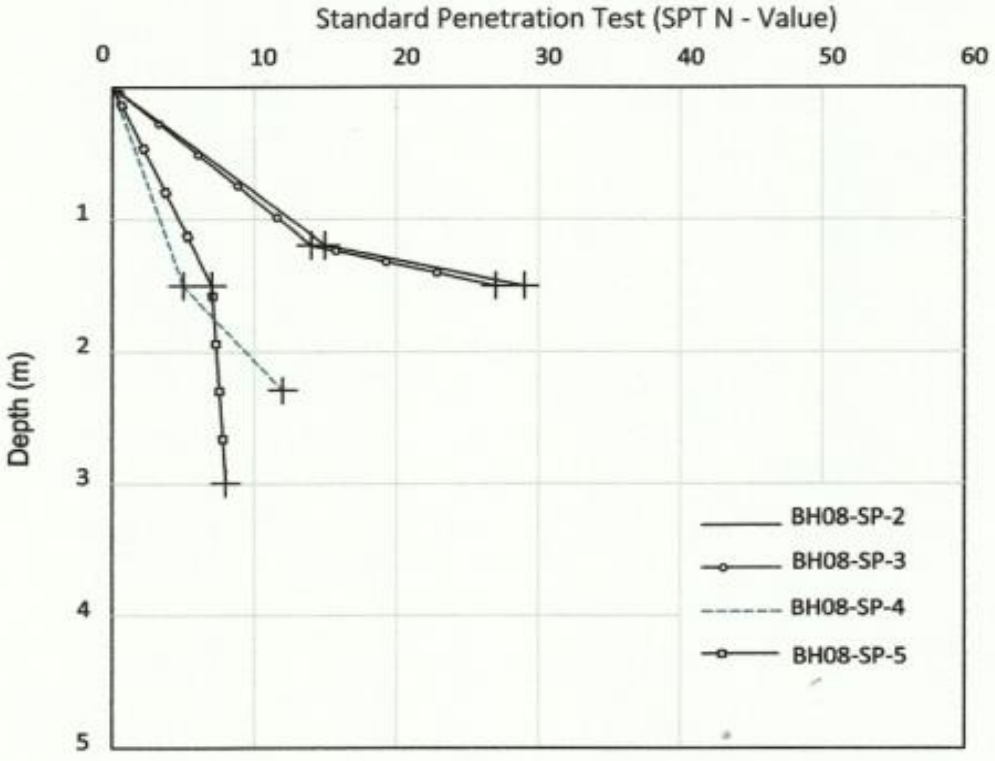

Figure 5.67 Graph of SPT VS Depth for Colluvium samples recovered during the 2008 Supplementary Field Instrumentation Programme

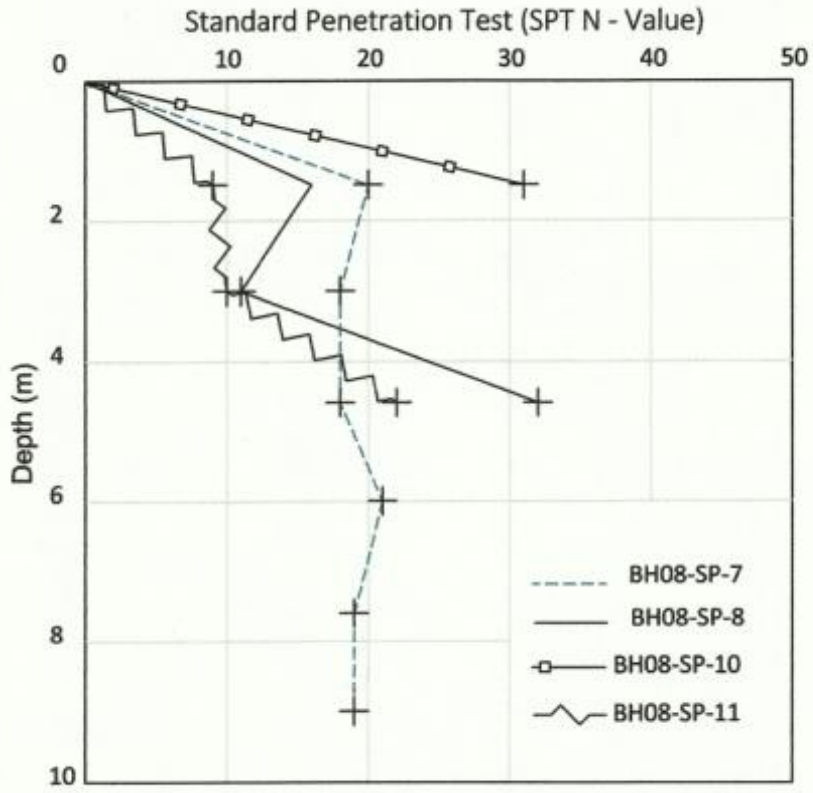

Figure 5.68 Graph of SPT VS Depth for Colluvium samples recovered during the 2008 Supplementary Field Instrumentation Programme

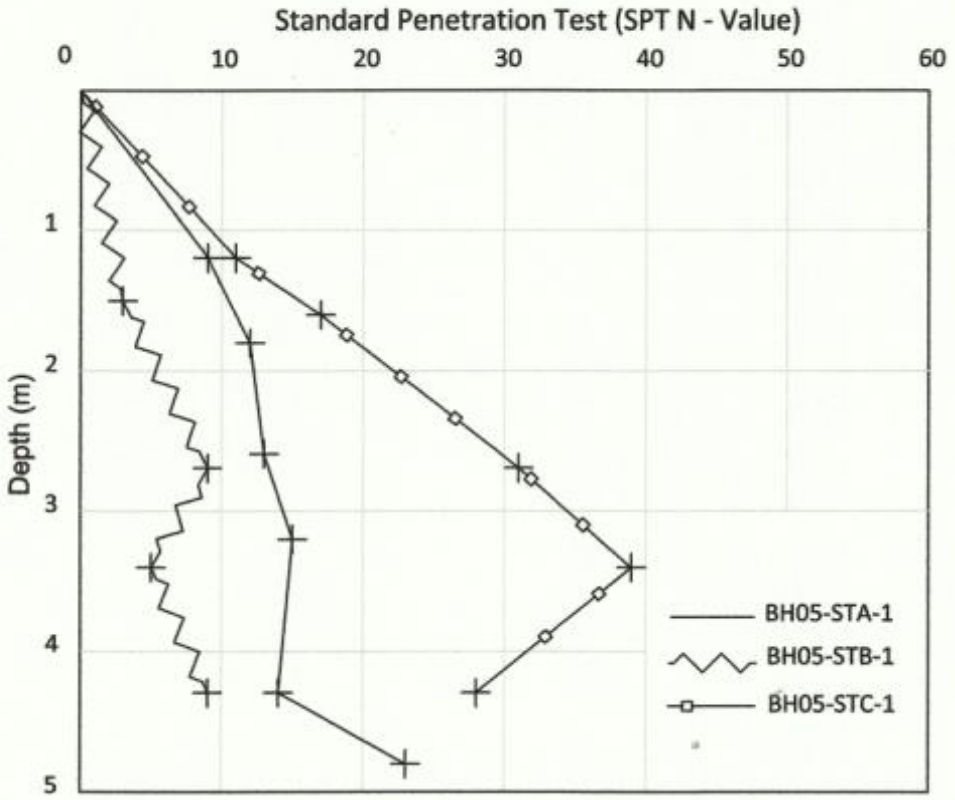

Figure 5.69 Graph of SPT vs Depth for Colluvium at the 2005 Landslide at Windjammer Landing Beach Resort

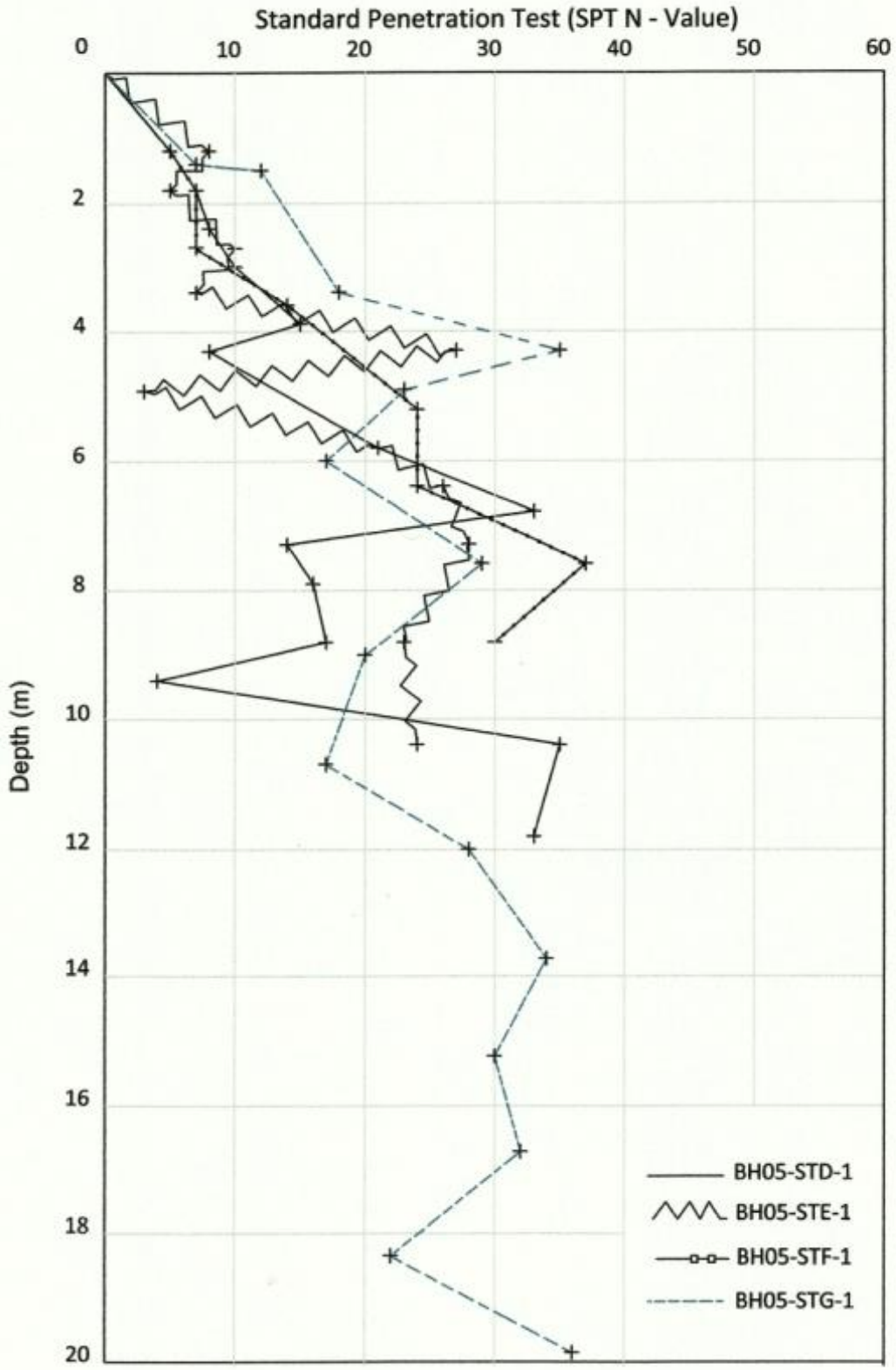

Figure 5.70 Graph of SPT vs Depth for Colluvium at the 2005 Landslide at Windjammer Landing Beach Resort

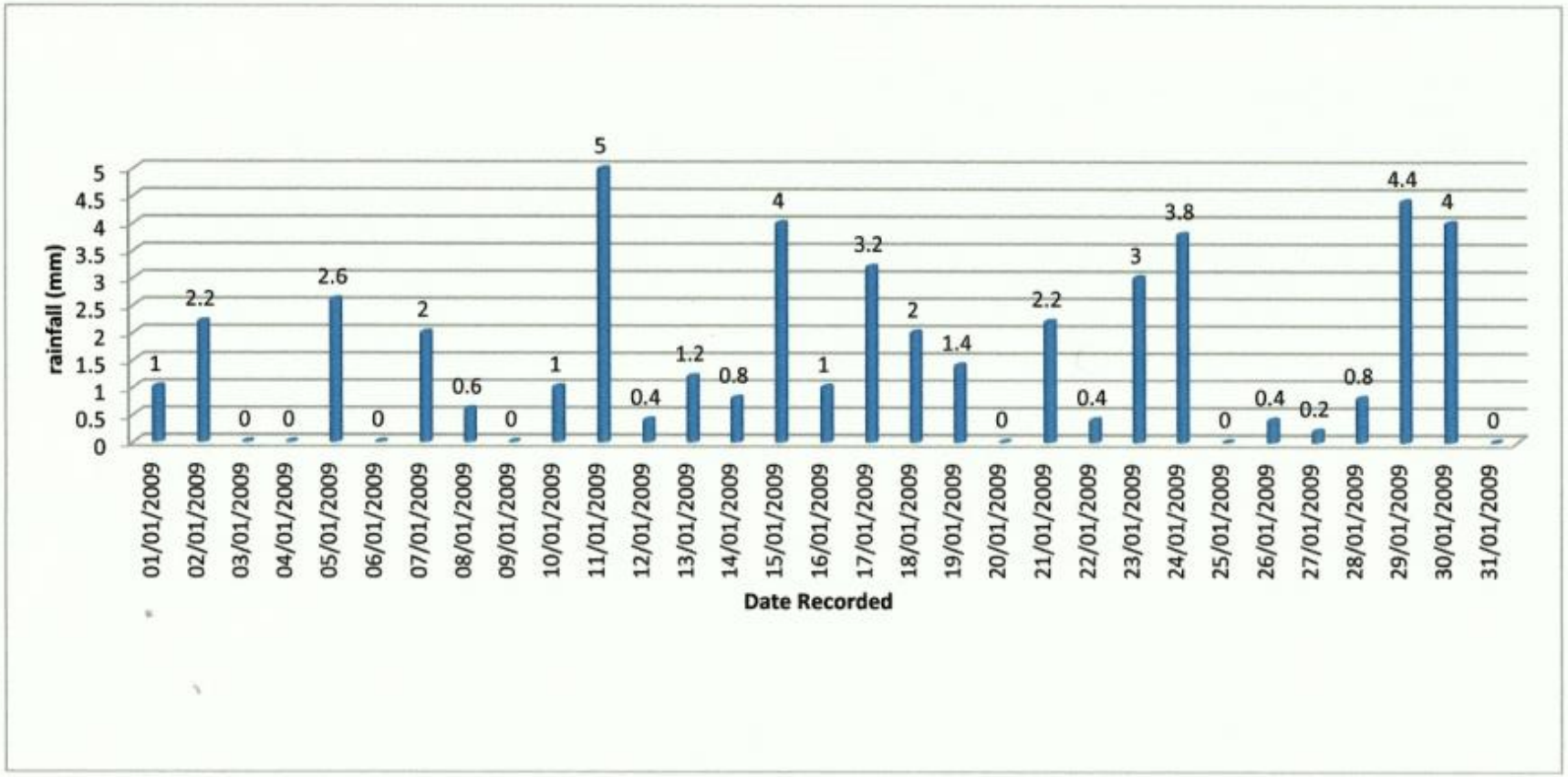

Figure 5.71 Daily rainfall for January 2008 at the Trouya Rain Gauge Station

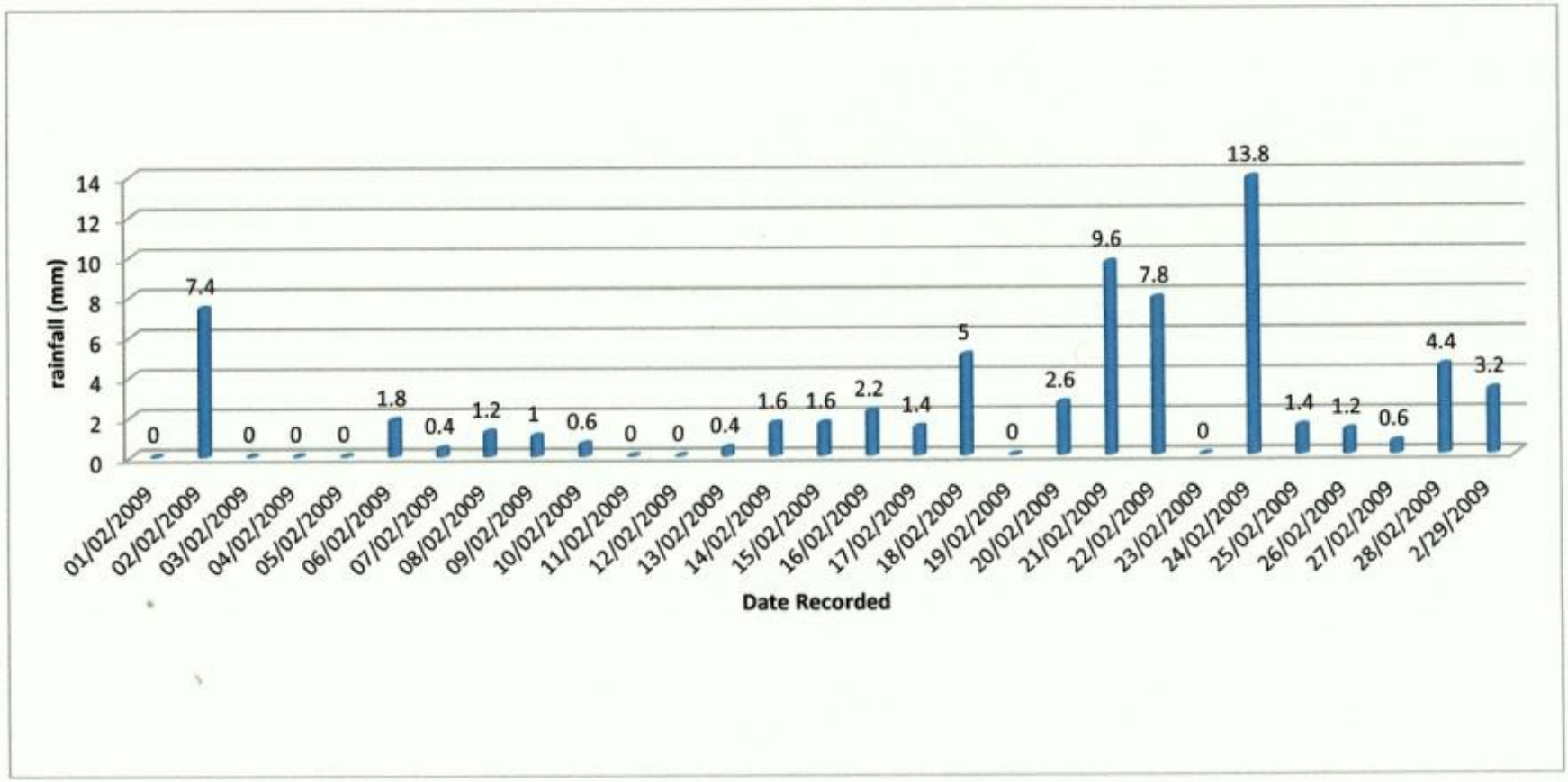

Figure 5.72 Daily rainfall for February 2008 at the Government Weather Station at Trouya

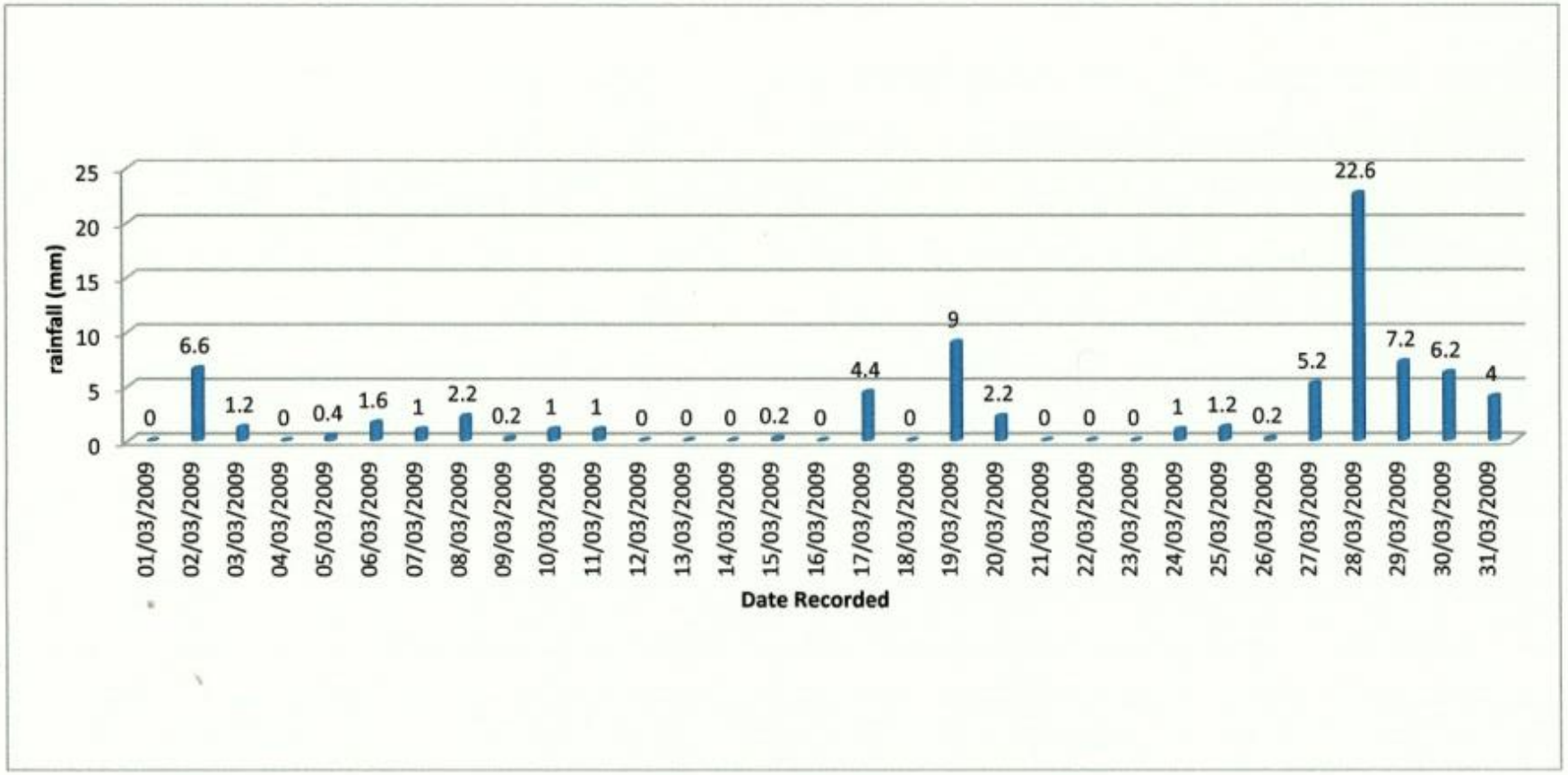

Figure 5.73 Daily rainfall for March 2008 at the Government Weather Station at Trouya

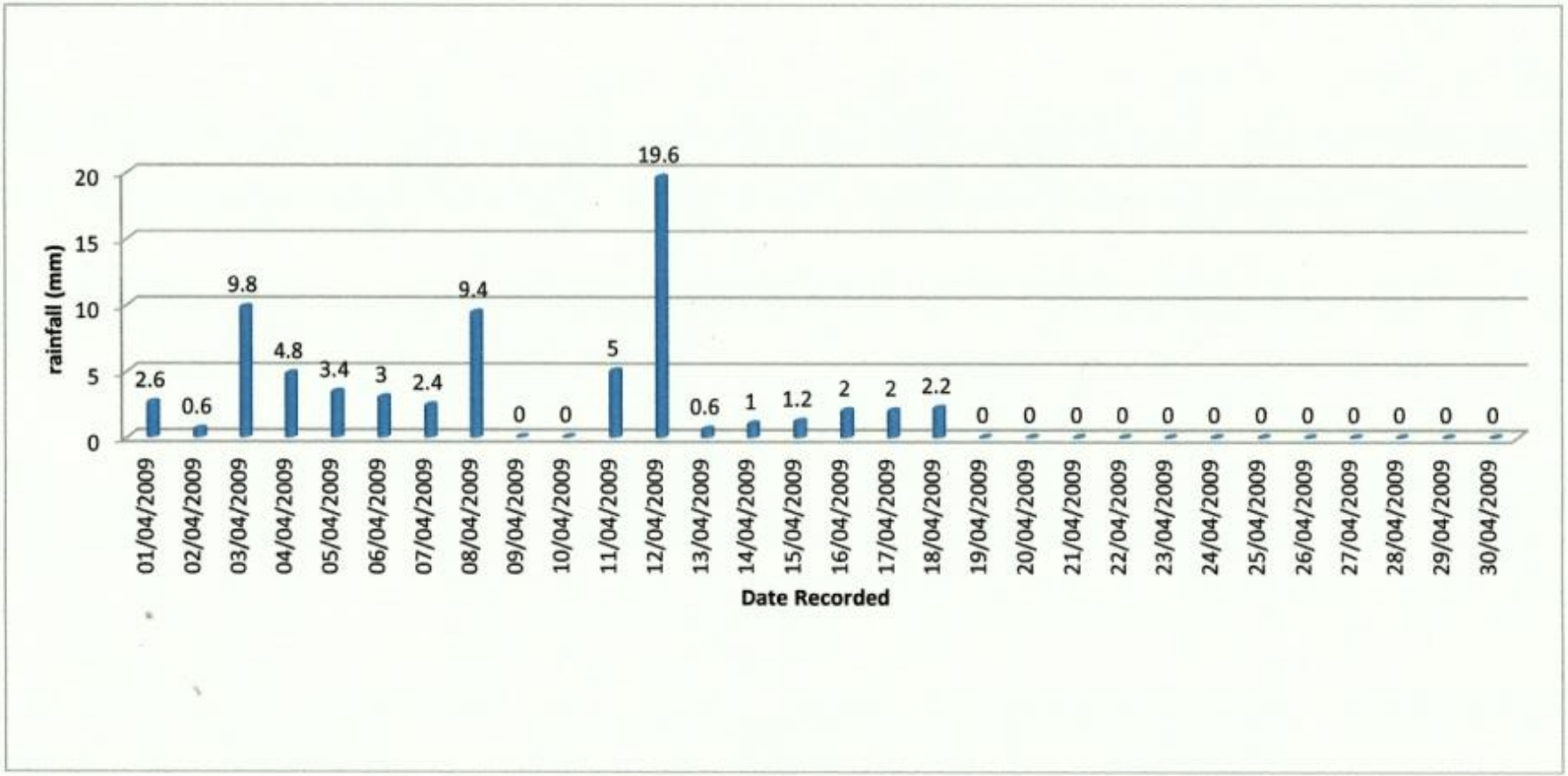

Figure 5.74 Daily rainfall graph for April 2008 at the Government Weather Station at Trouya

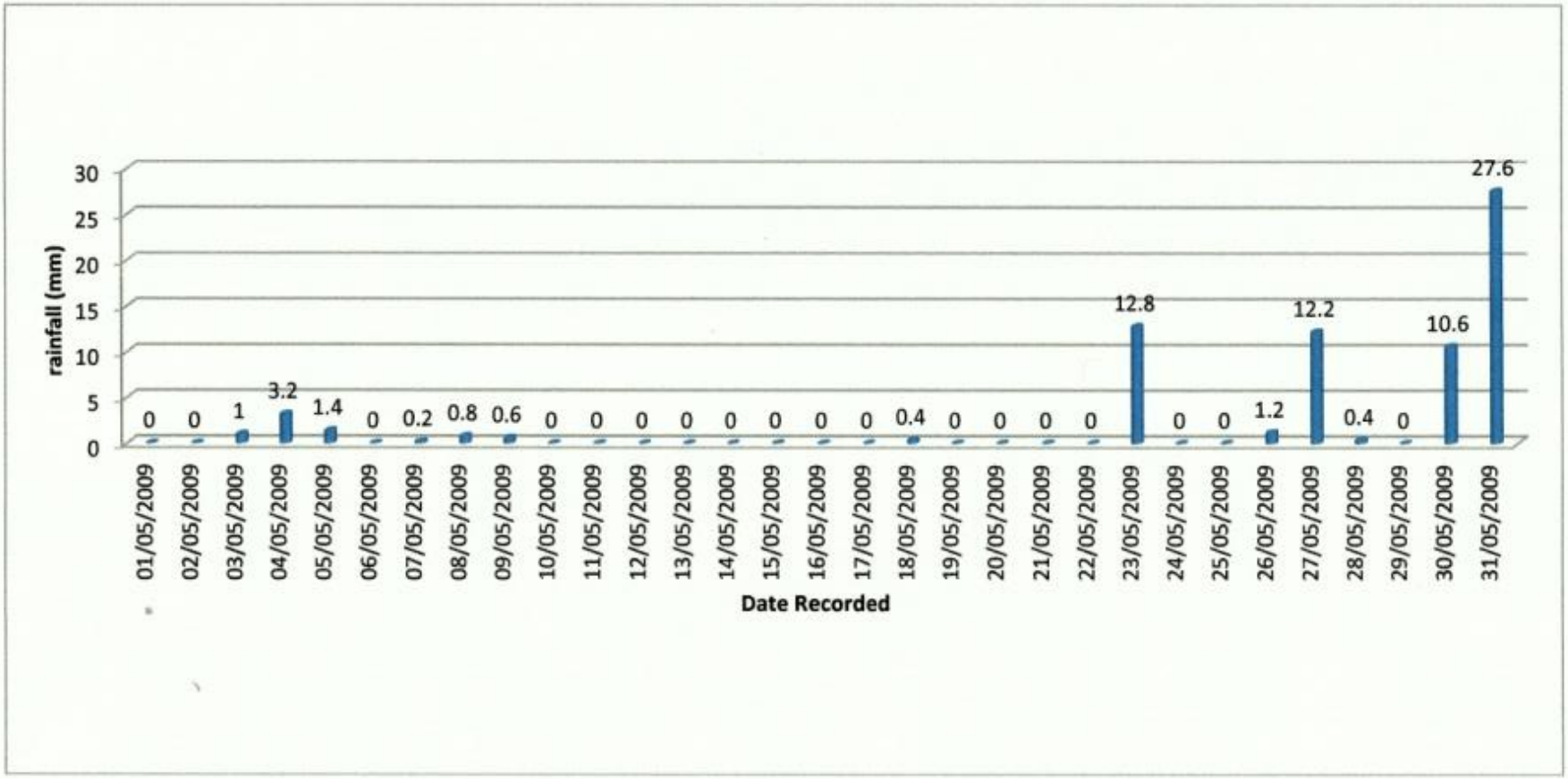

Figure 5.75 Daily rainfall graph for May 2008 at the Government Weather Station at Trouya

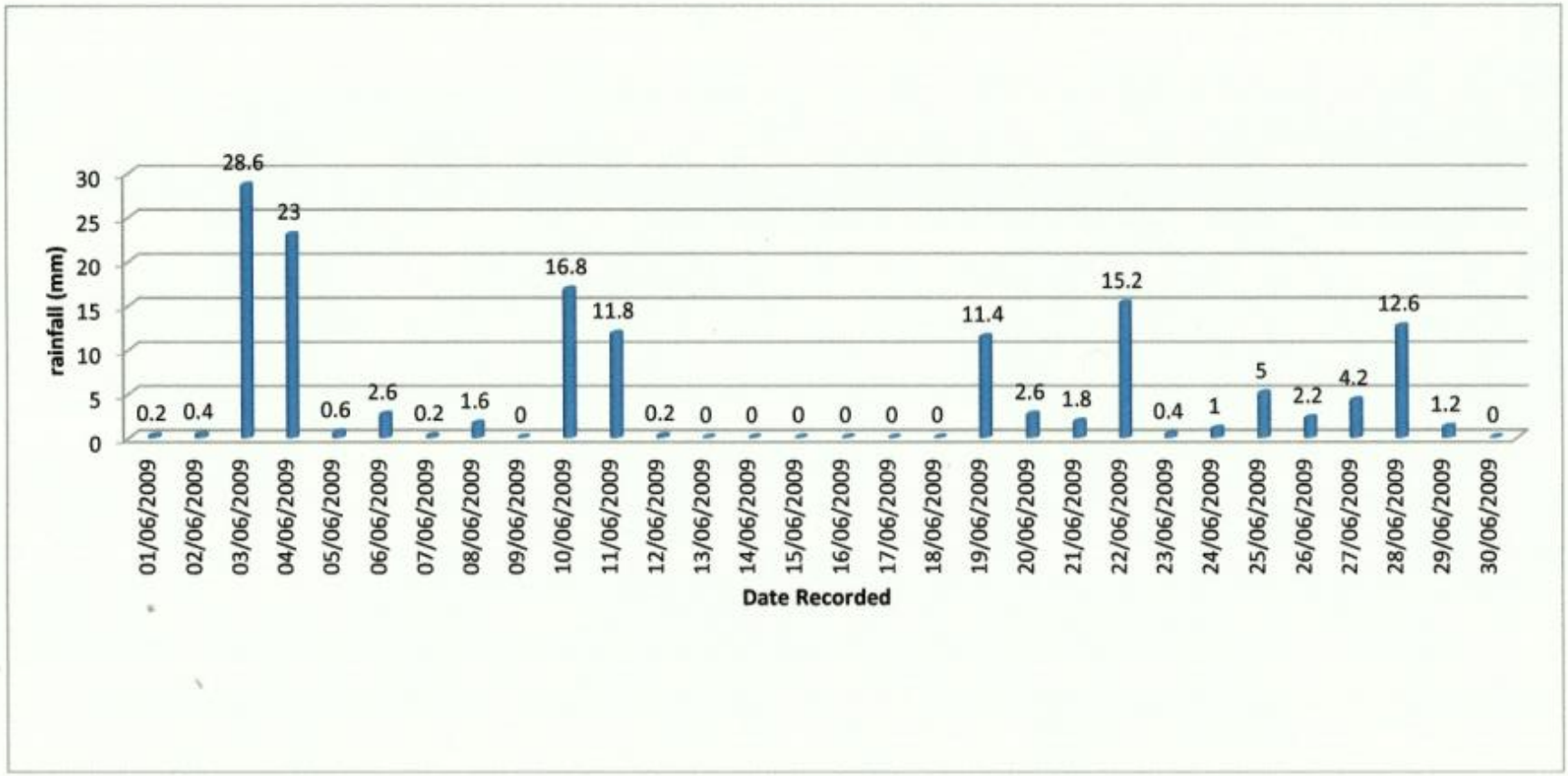

Figure 5.76 Daily rainfall graph for June 2008 at the Government Weather Station at Trouya

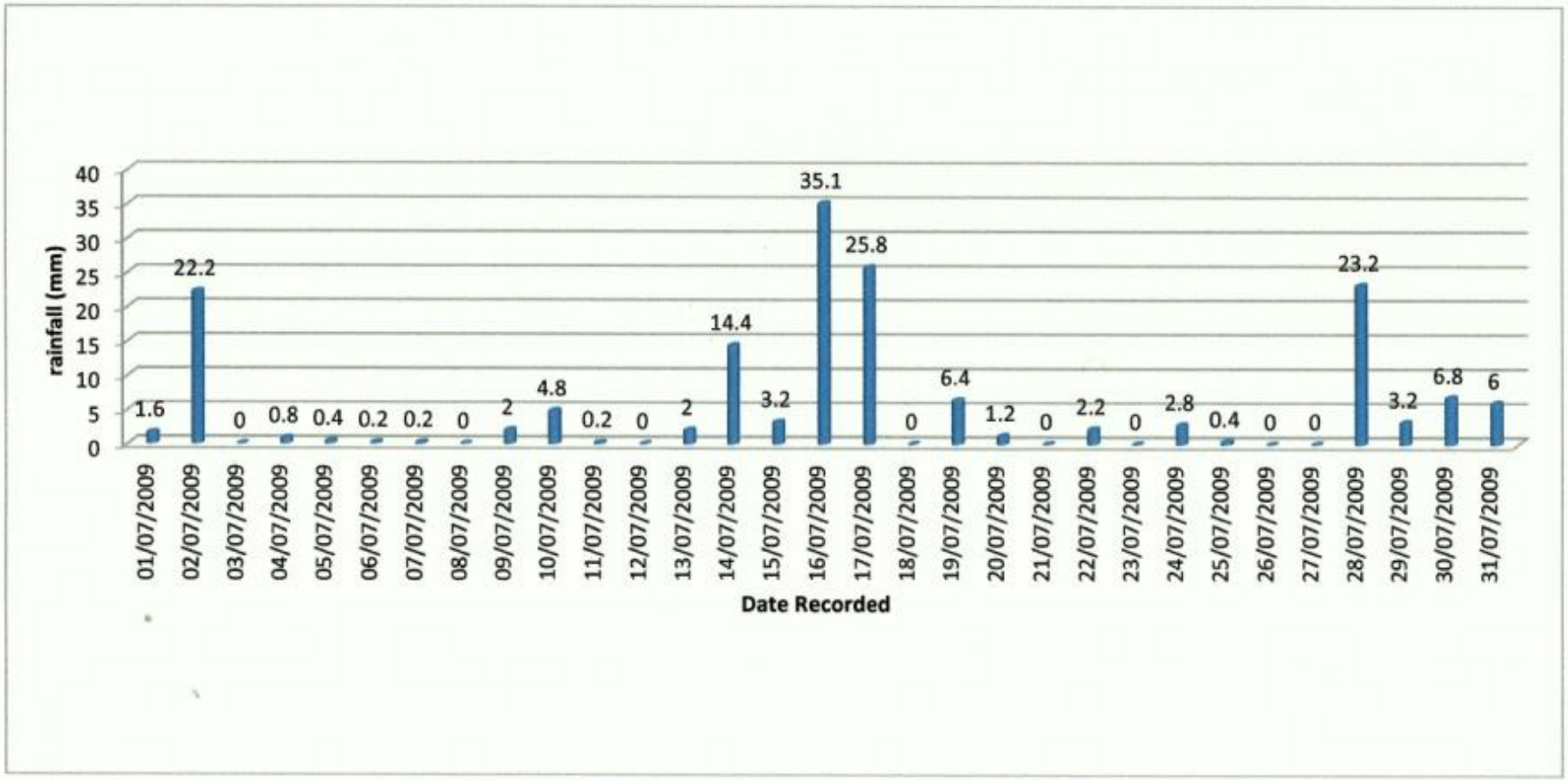

Figure 5.77 Daily rainfall graph for July 2008 at the Government Weather Station at Trouya

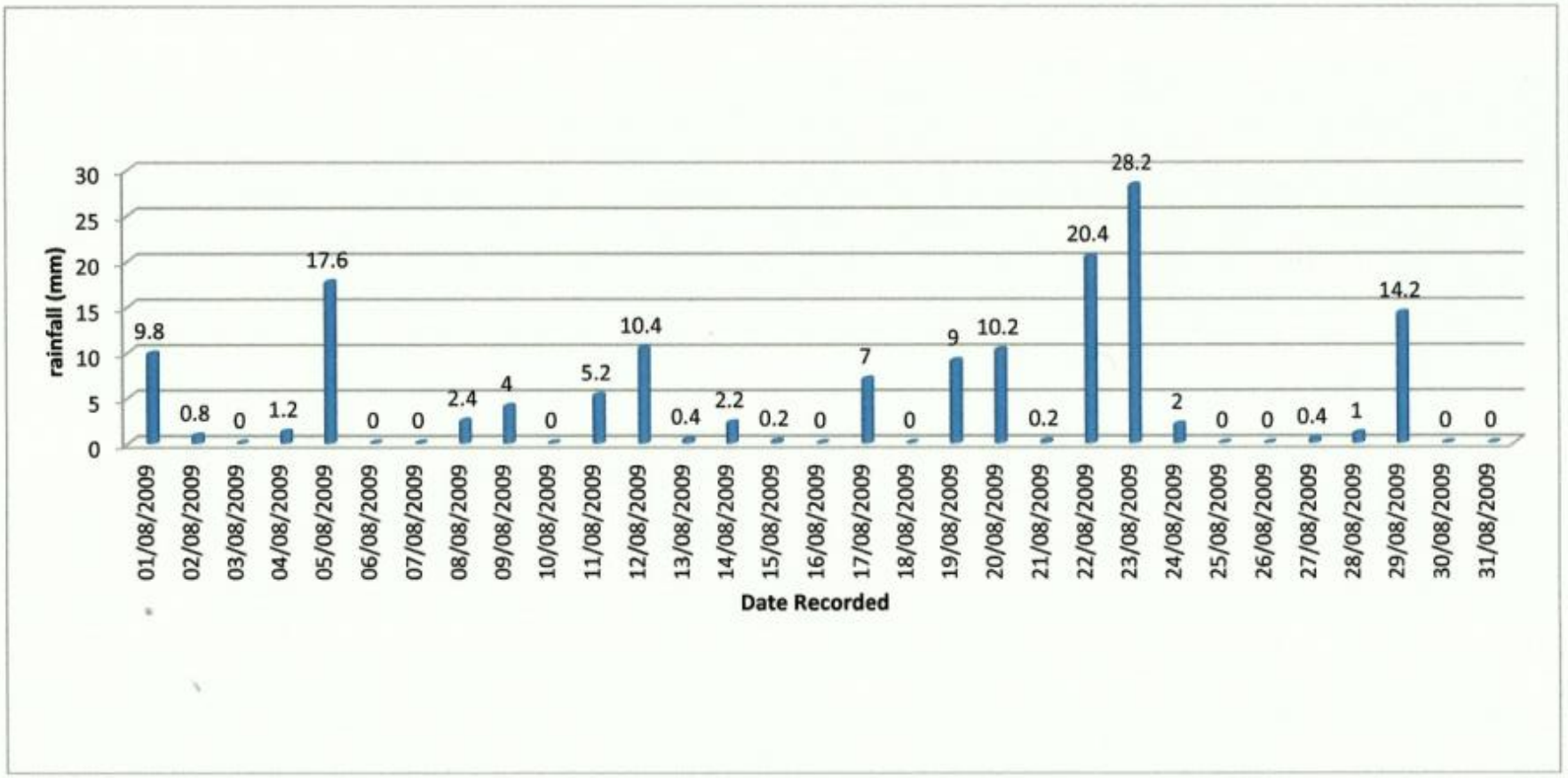

Figure 5.78 Daily rainfall graph for August 2008 at the Government Weather Station at Trouya

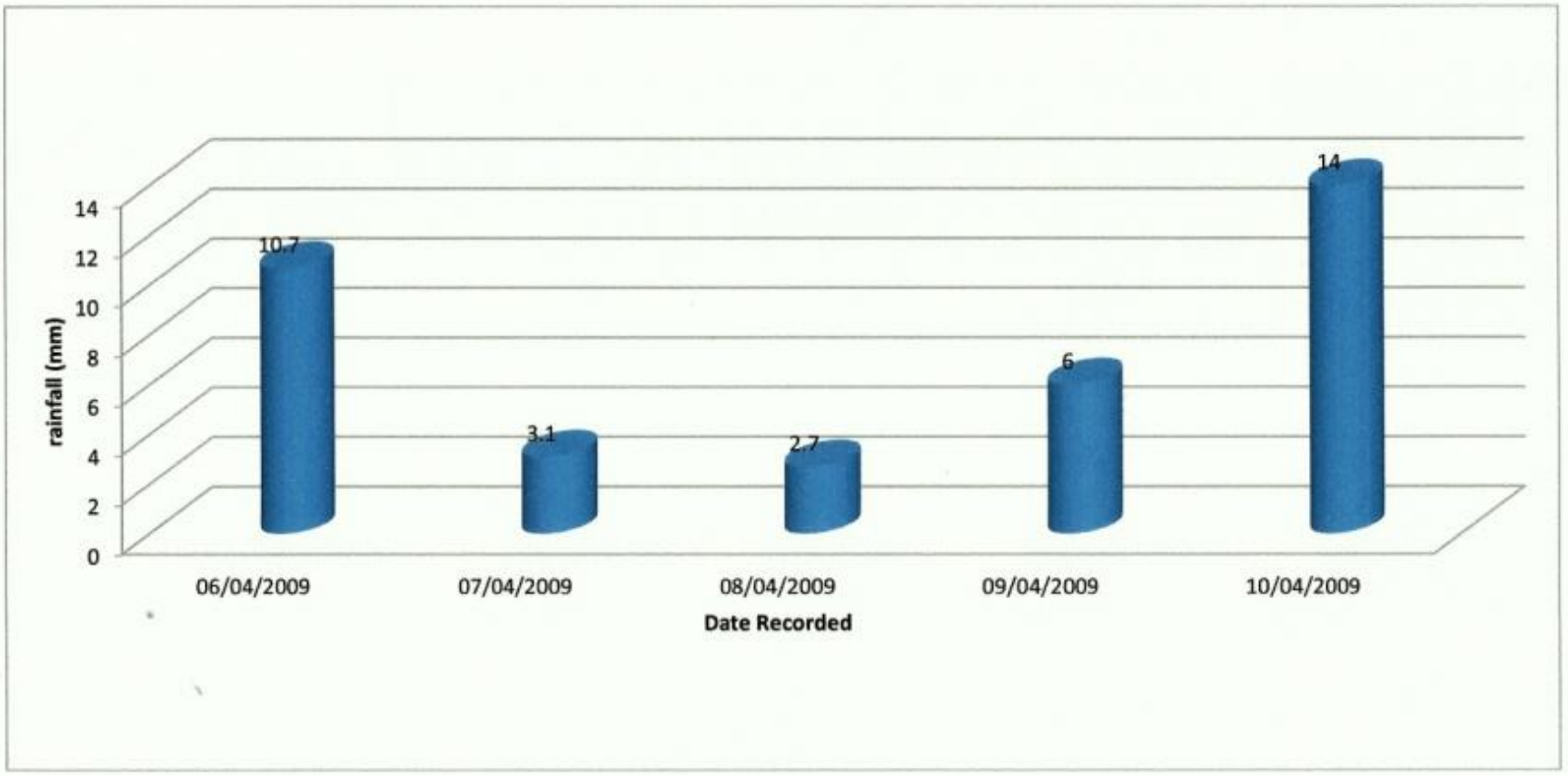

Figure 5.79 Daily rainfall graph for April 2009 from the rain gauge station at the Windjammer Landing Beach Resort

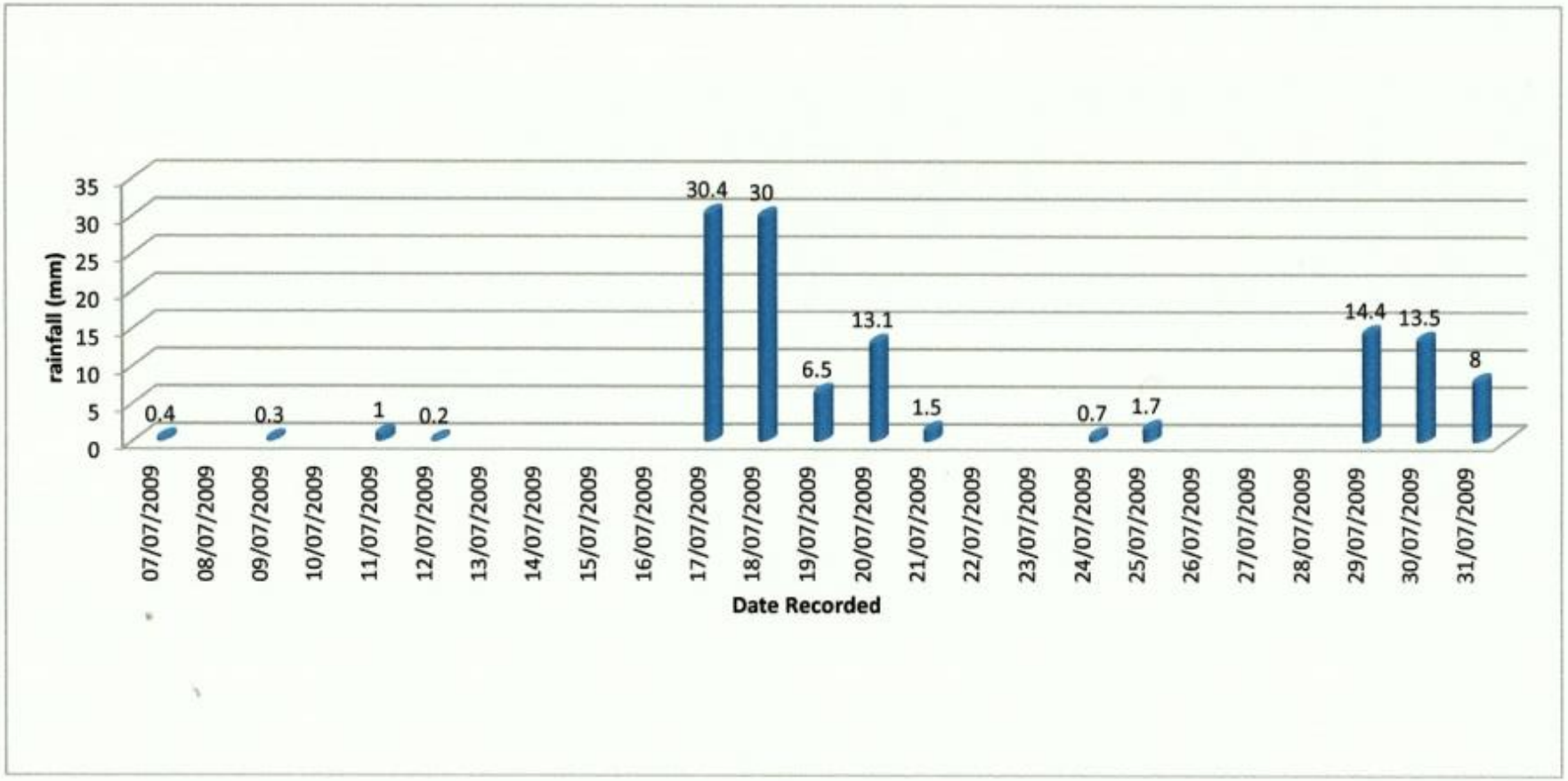

Figure 5.80 Daily rainfall graph for July 2009 at the rain gauge station at the Windjammer Landing Beach Resort

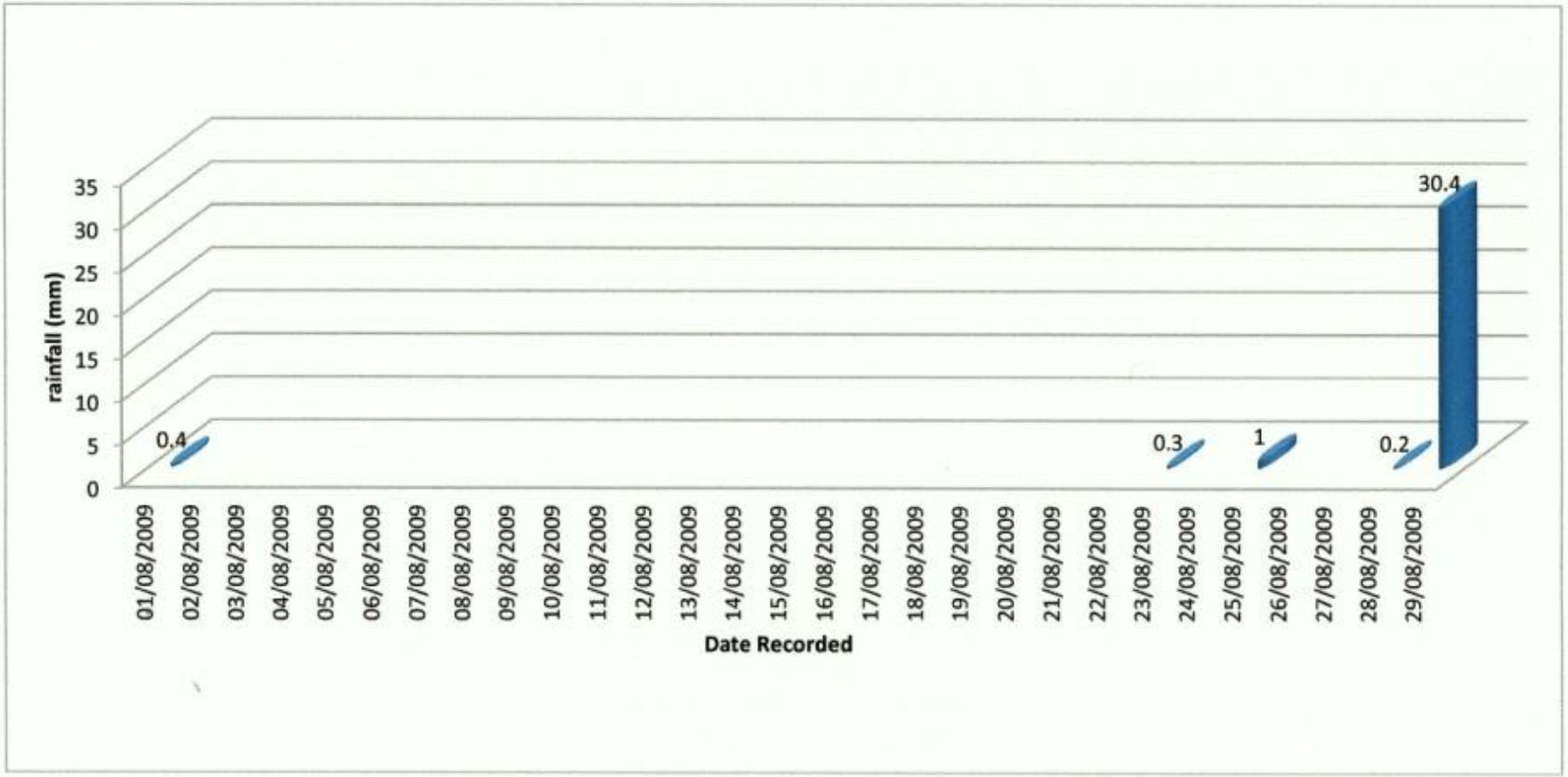

Figure 5.81 Daily rainfall graph for August 2009 at the rain gauge station at the Windjammer Landing Beach Resort

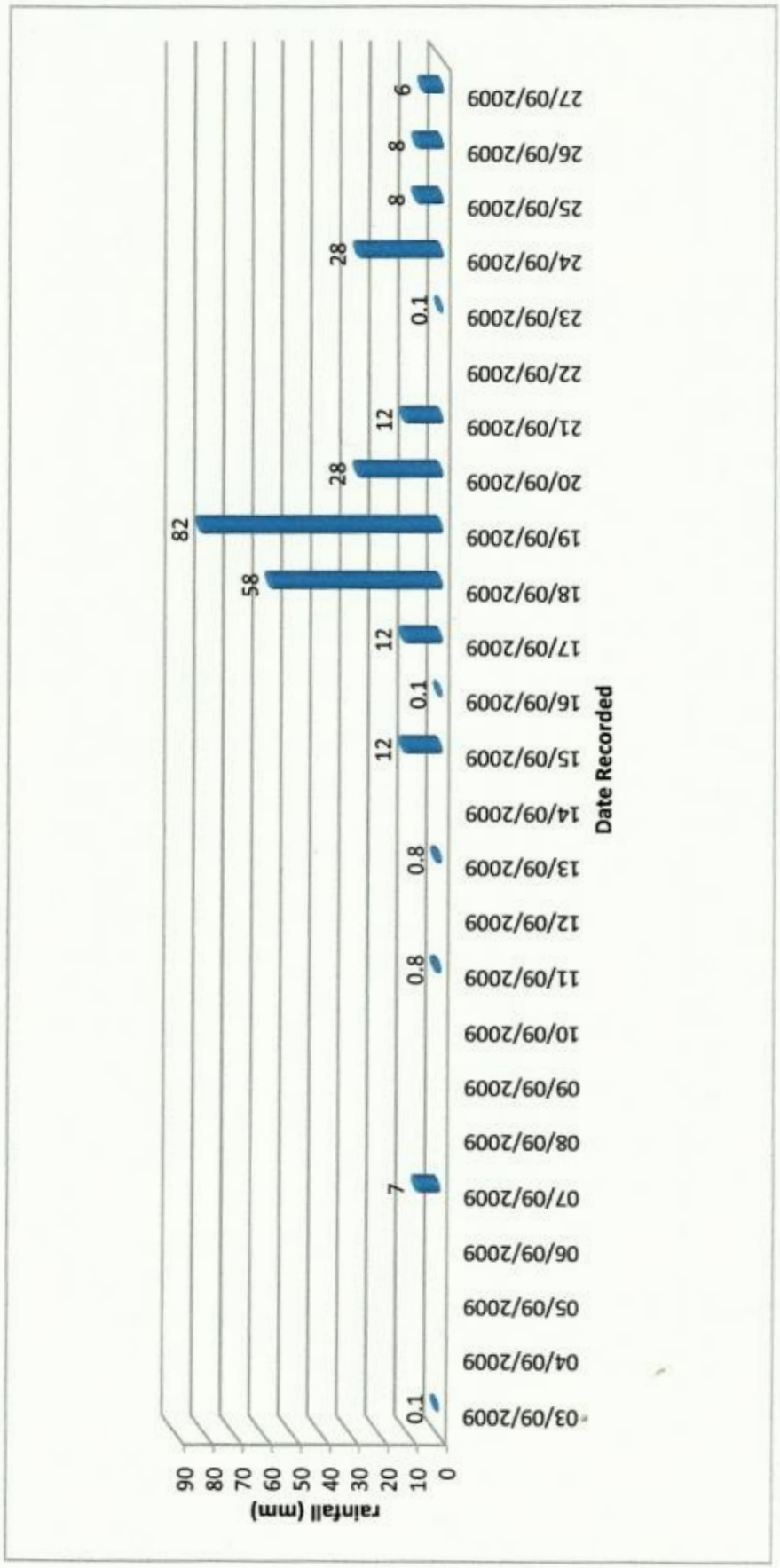

Figure 5.82 Daily rainfall graph for September 2009 at the rain gauge station at the Windjammer Landing Beach Resort

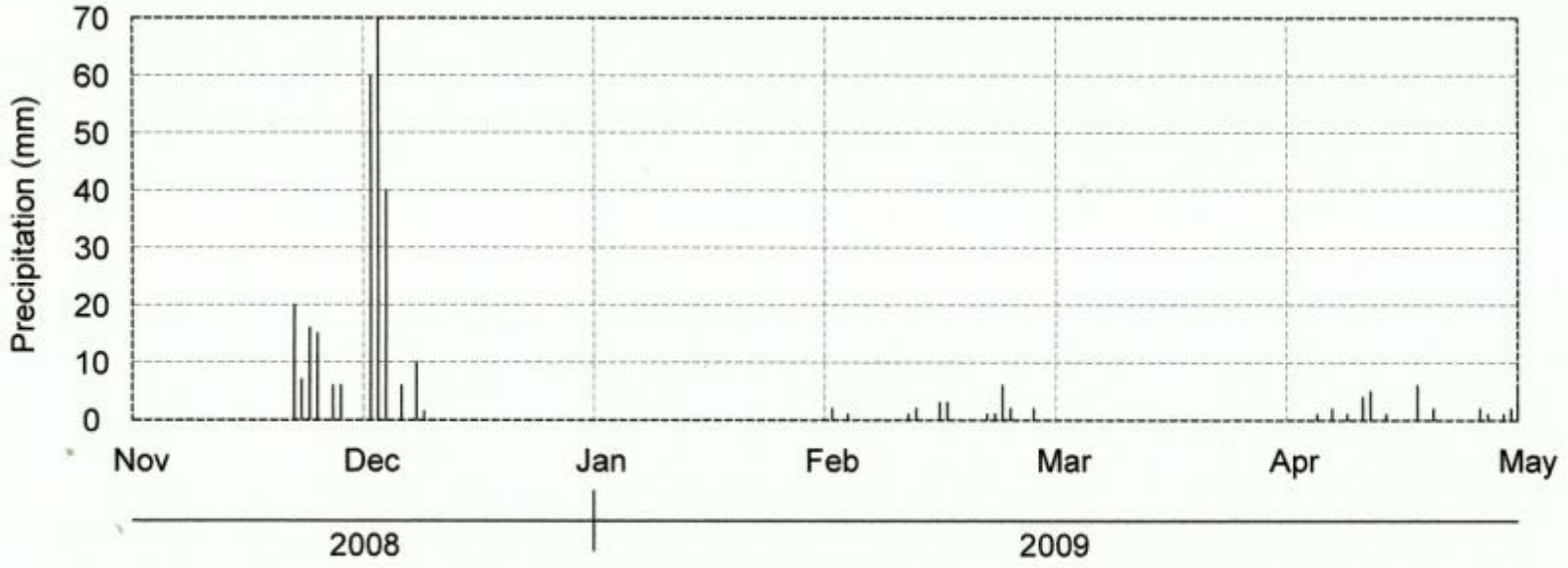

Figure 5.82a Graph of monthly rainfall for November 1st, 2008 to April 30th, 2009 at the Windjammer Landings Beach Resort Study Site

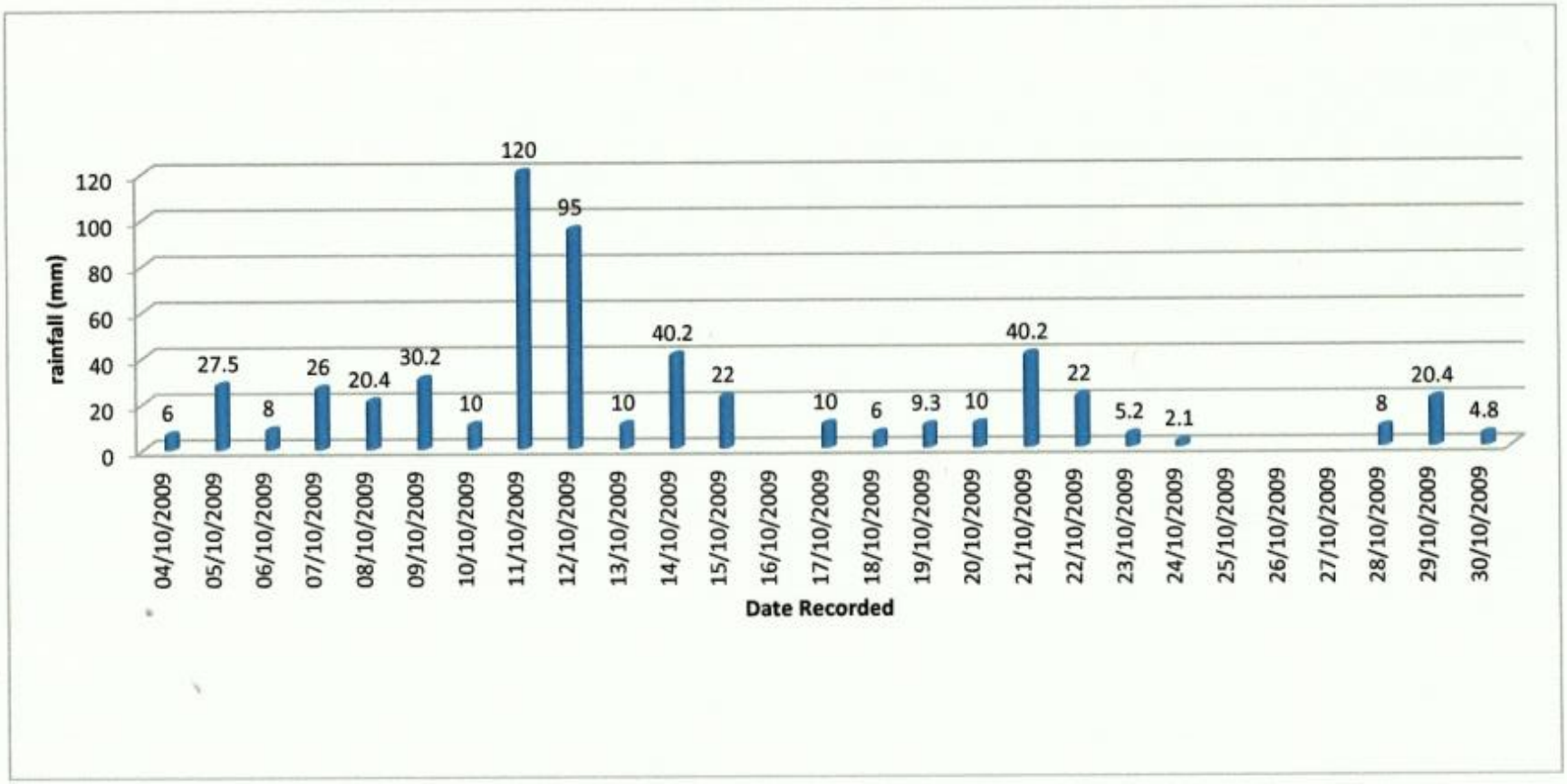

Figure 5.83 Daily rainfall graph for October 2009 at the rain gauge station at the Windjammer Landing Beach Resort

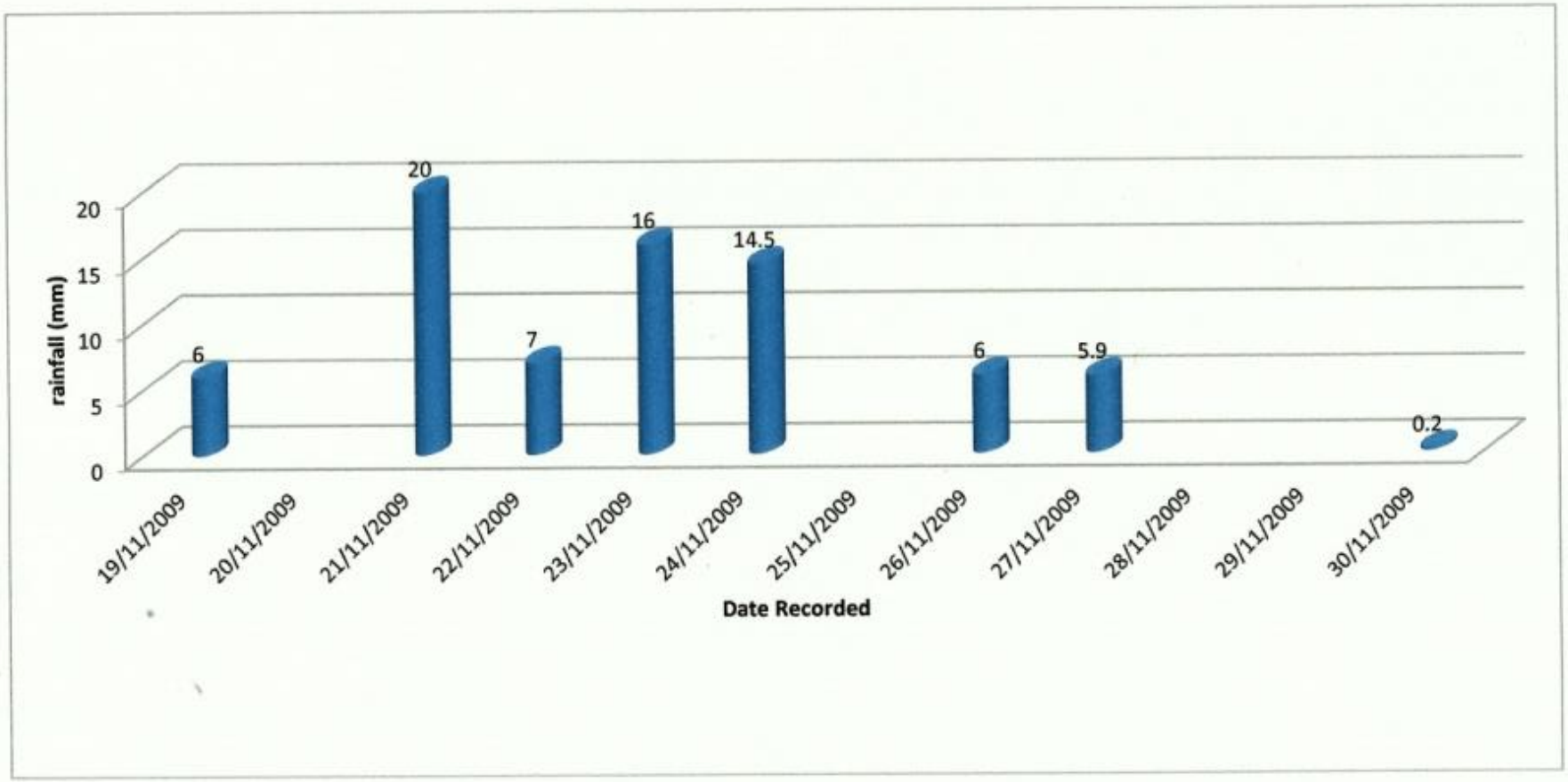

Figure 5.84 Daily rainfall graph for November 2009 at the rain gauge station at the Windjammer Landing Beach Resort

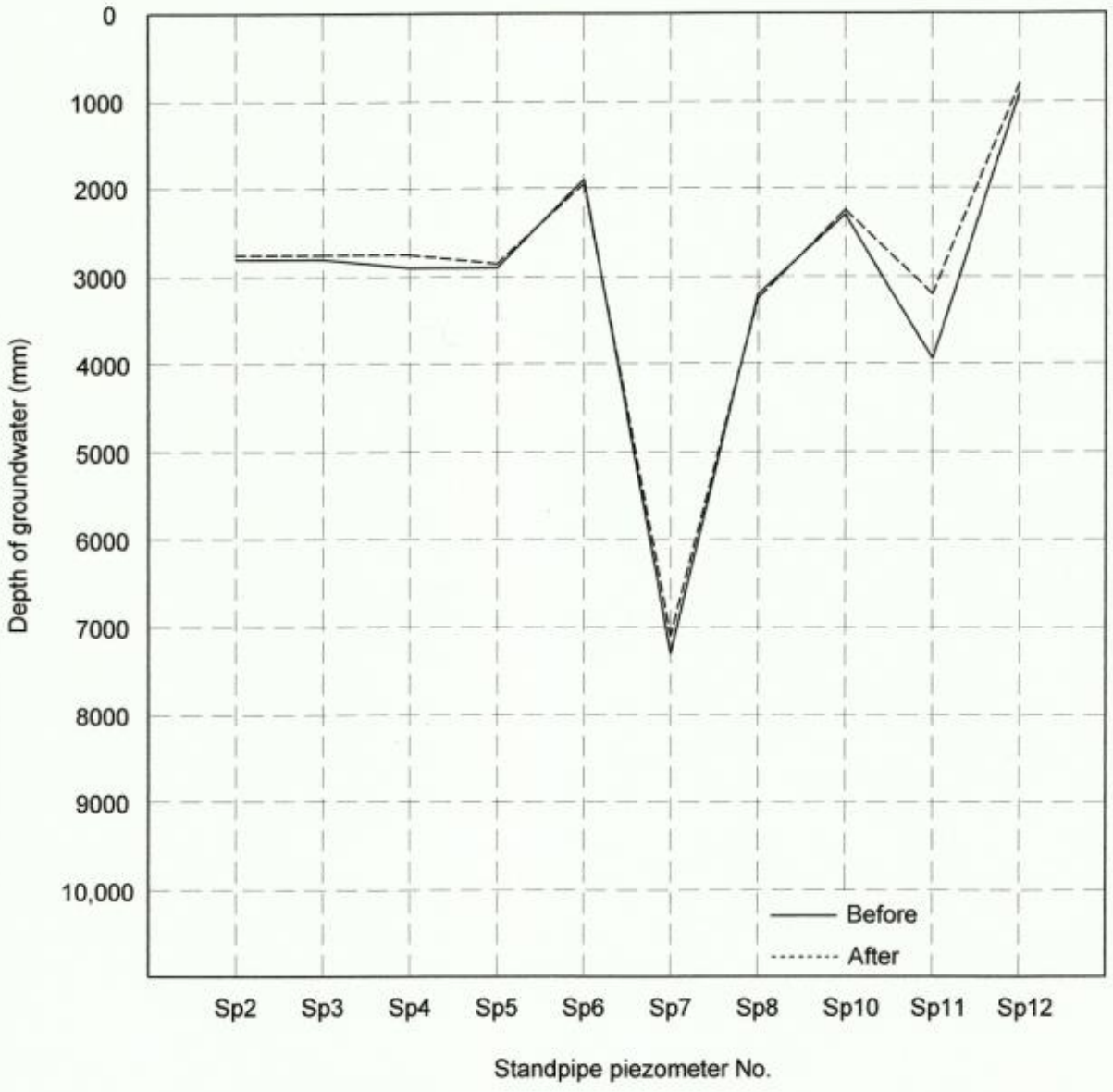

Figure 5.86 Pore Water Response to a Rainfall Event 120mm on October 11, 2008 in the 2005 Landslide Study Area at the Windjammer Landing Beach Resort

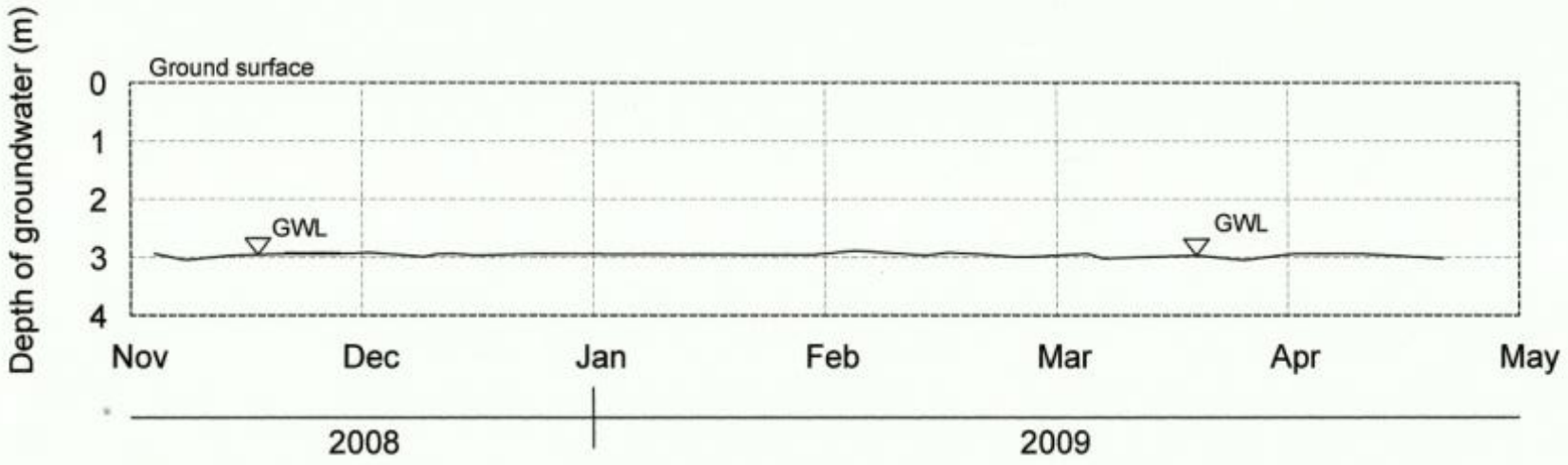

Figure 5.86a Piezometer Readings for November 1st, 2008 to April 30th, 2009 for the Windjammer Landing Beach Resort Study Site

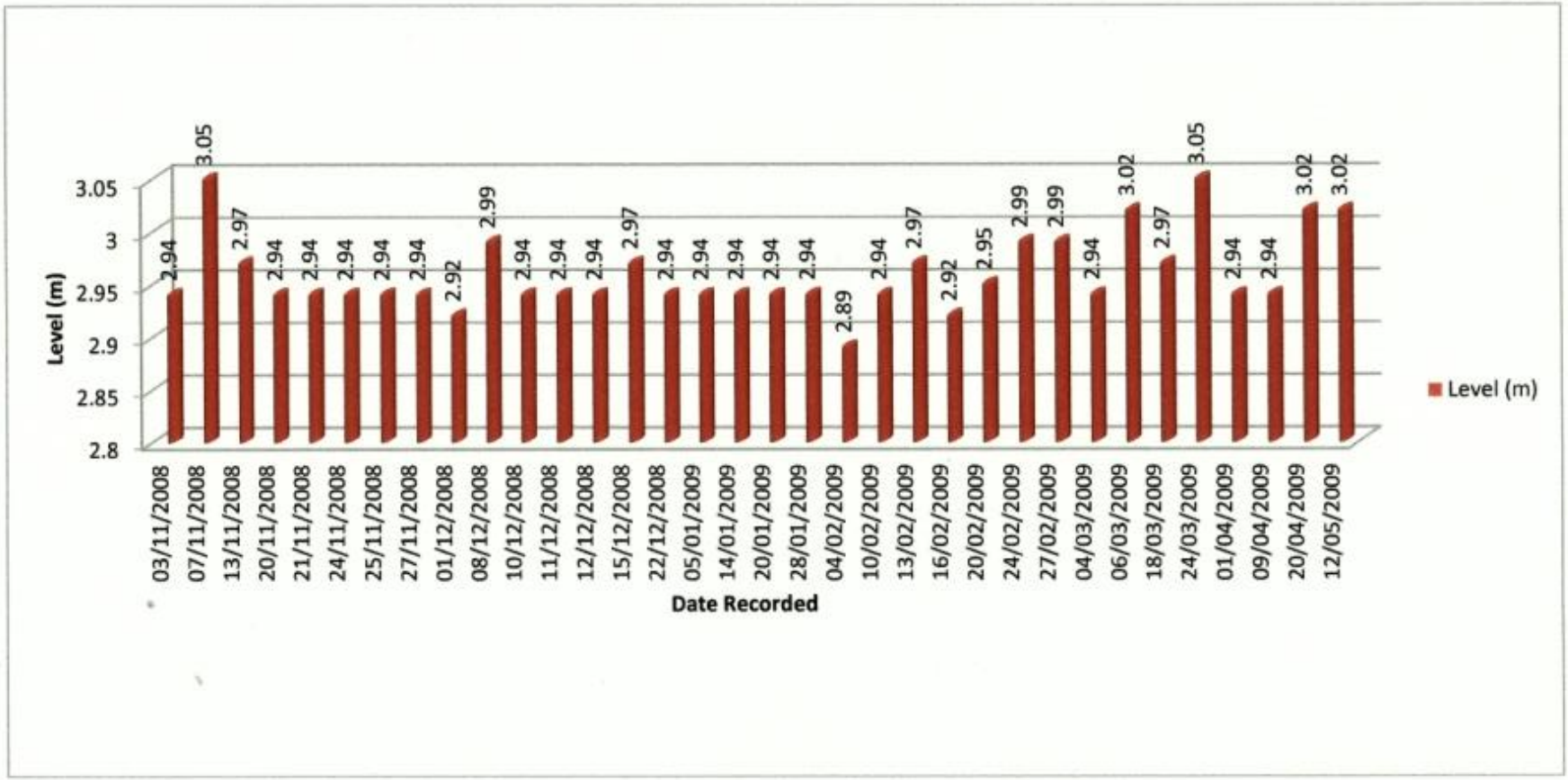

Figure 5.87 Piezometer levels in BH08-SP-13 at the Windjammer Landing Beach Resort Study Site for the period November 2008 – May 2009

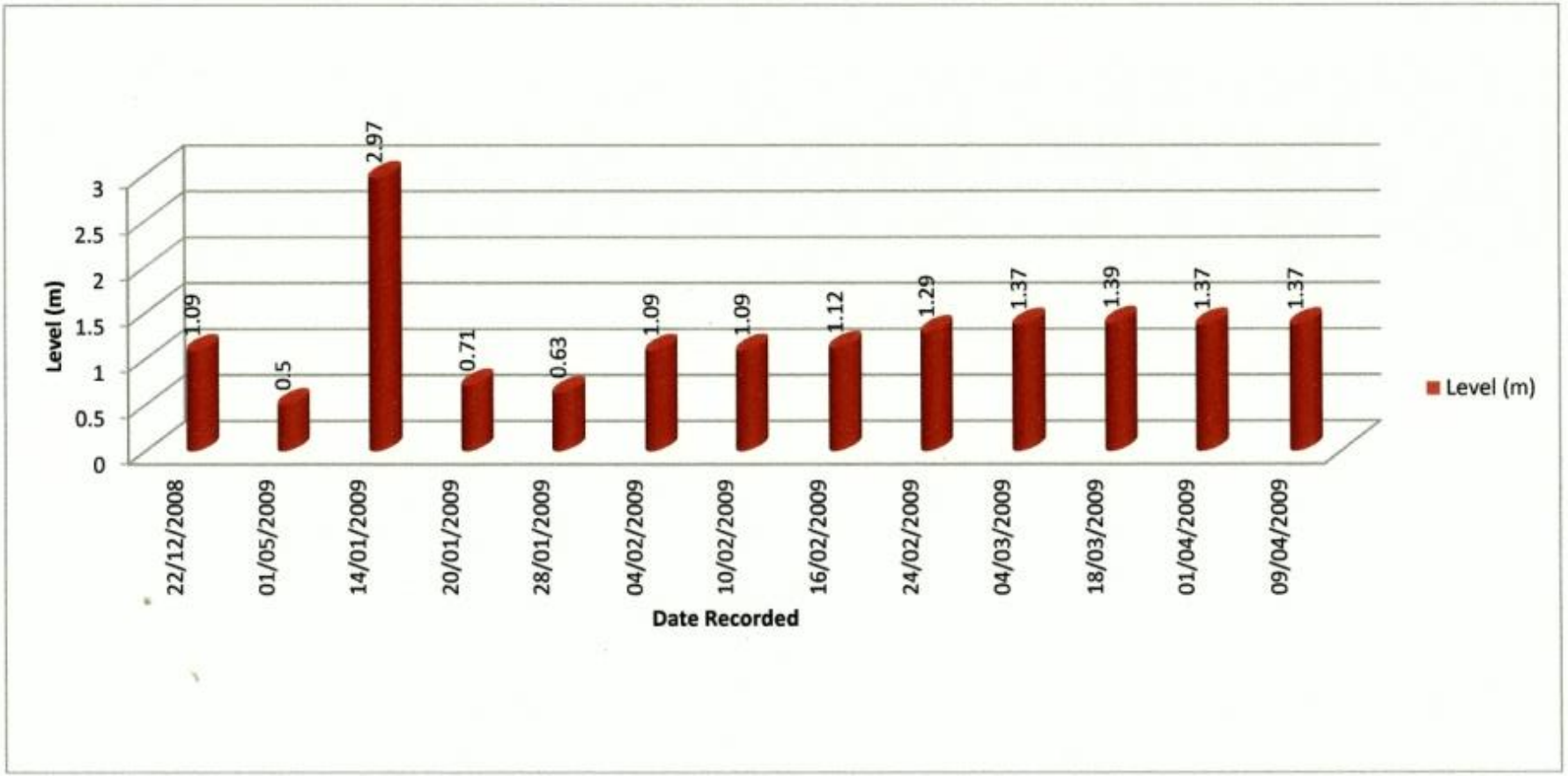

Figure 5.88 Piezometer levels in BH08-SP-14 at the Windjammer Landing Beach Resort Study Site for the period December 2008 – April 2009

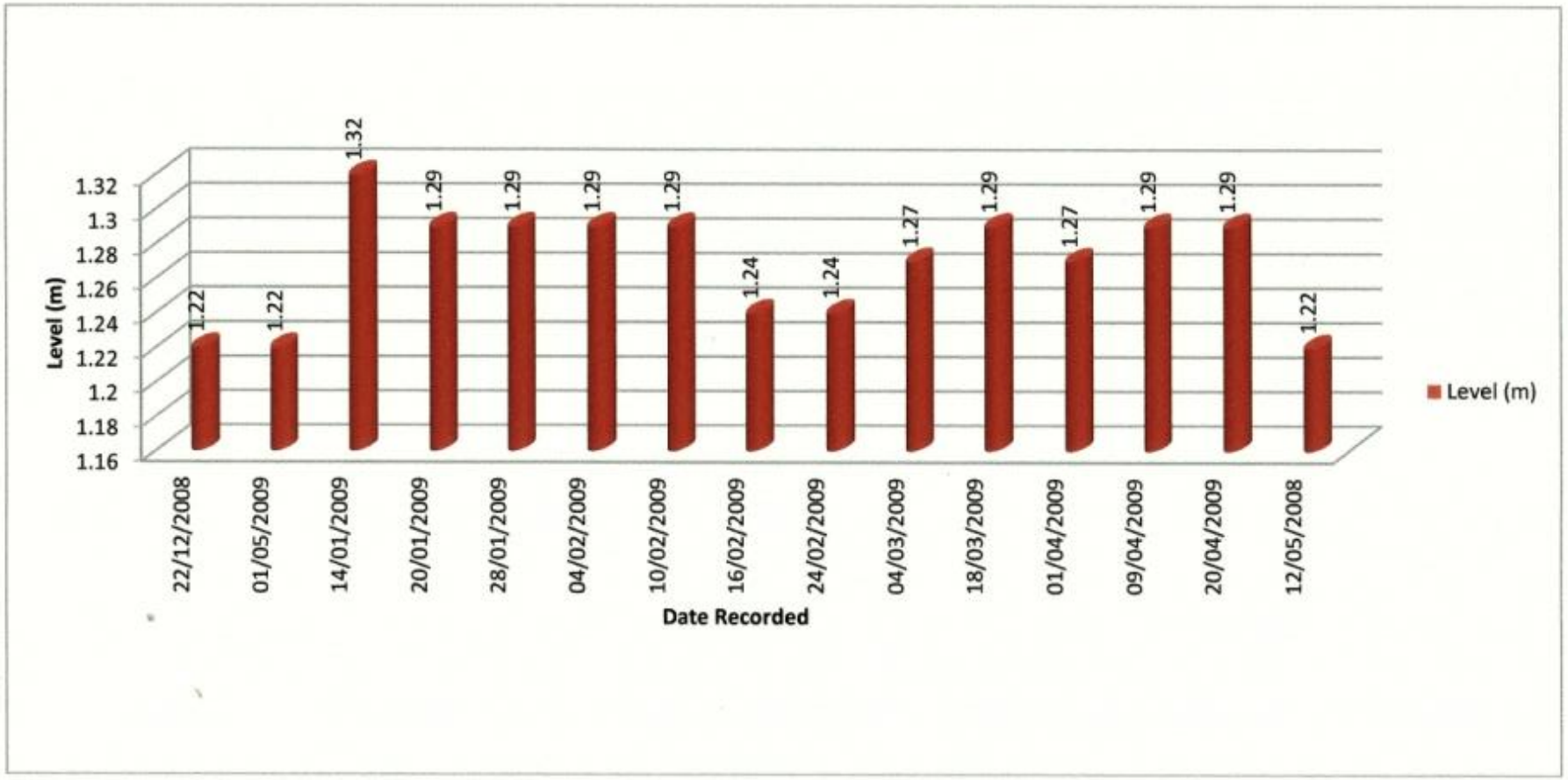

Figure 5.89 Piezometer levels in BH08-SP-15 at the Windjammer Landing Beach Resort Study Site for the period December 2008 – May 2009

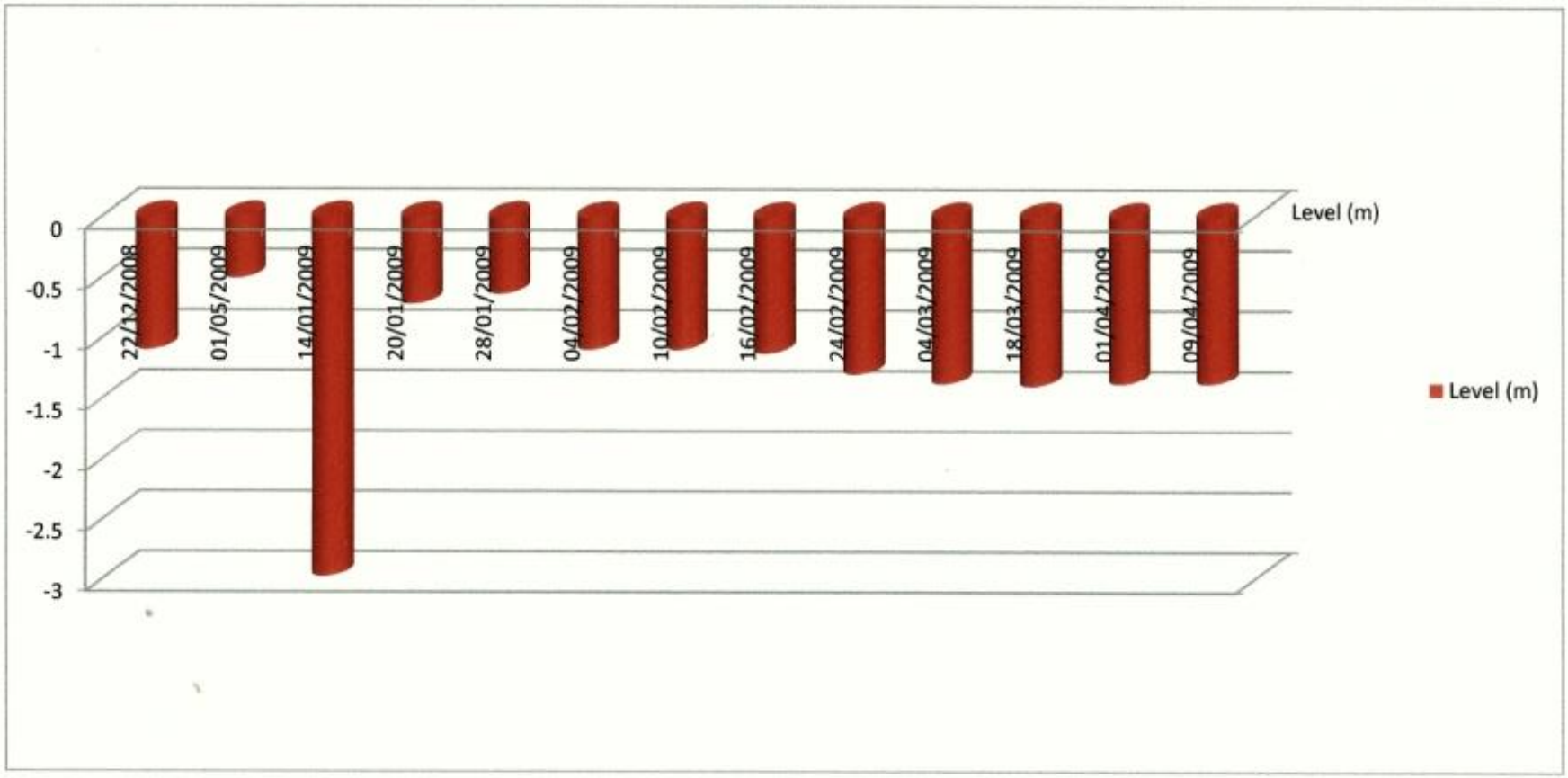

Figure 5.90 Inverted piezometer groundwater levels in BH08-SP-14 at the Windjammer Landing Beach Resort Study Site for the period December 2008 – April 2009

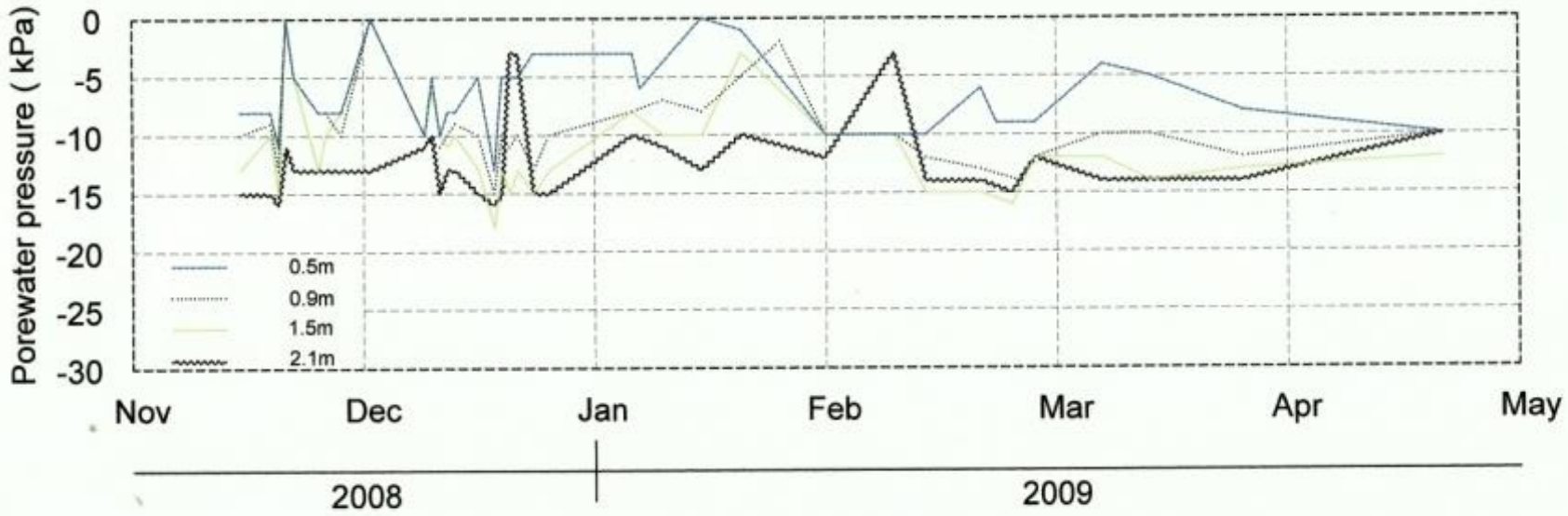

Figure 5.91 Graph of the Pore Water Pressure response to rainfall in Tensiometer "ROW A" at the Windjammer Landings Beach Resort Study Site

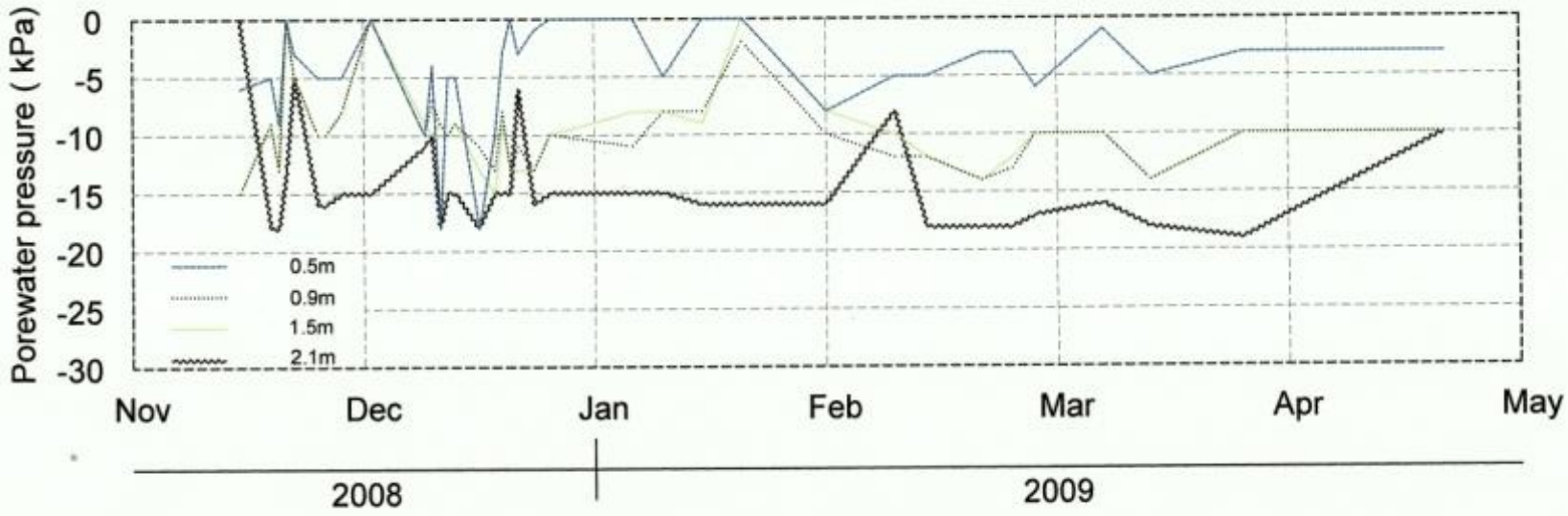

Figure 5.92 Graph of the Pore Water Pressure response to rainfall in Tensiometer "ROW B" at the Windjammer Landings Beach Resort Study Site

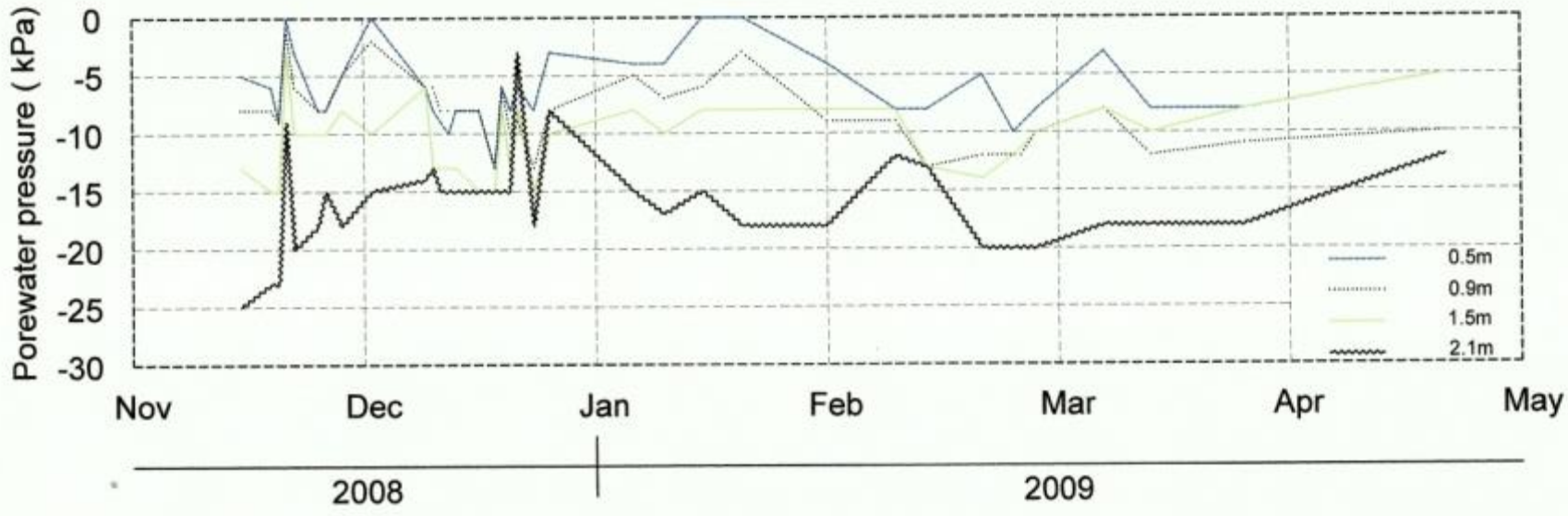

Figure 5.93 Graph of the Pore Water Pressure response to rainfall in Tensiometer "ROW C" at the Windjammer Landings Beach Resort Study Site

CHAPTER 6

Analysis of the Field Monitoring Results

6.1 Introduction

This chapter deals with the analysis of the field data collected at the Barre de L'isle and Windjammer Landing Beach Resort study sites and explains the effect of rainfall intensity on infiltration and pore water pressure response in an unsaturated residual soil and a colluvial deposit.

The residual soil at the Barre de L'isle study site is the weathered residue of parent andesite rock formation of which the entire mountain ridge is composed. The colluvium deposit at the Windjammer Landing Beach Resort study site is from parent basalt rock that traveled downslope and formed a ridge at the toe of the slope overlooking Labrelotte Bay thus providing a scenic and breathtaking view of the Caribbean Sea. High scale villas were constructed on this ridge and in 2005 a landslide occurred after a period of heavy rainfall and three of the villas were destroyed.

In 2008, a smaller landslide occurred on the north slope of the Windjammer resort after a heavy rainfall event. This area of instability was used as a study site for this project. The site was instrumented with tensiometers, standpipe piezometers and slope inclinometers as explained in Chapter 4.

Details of the field instrumentation of the two study sites are explained in Chapter 4 and field monitoring details are discussed in Chapter 5.

6.2 The Barre de L'isle Study Site

6.2.1 Rainfall Distribution and Pore Water Pressure Measurements for the Barre de L'isle Study Site

The field instrumentation at the Barre de L'isle study site was monitored over a period of thirteen (13) months from January 1, 2009 to January 31, 2010 excluding the month of April 2009. However, not all instruments were installed at the beginning of the monitoring period, resulting in some missing data for correlation. The field monitoring consisted of pore water pressure measurements in response to rainfall, runoff and infiltration, subsurface displacements and groundwater level fluctuations.

In order to show proper correlation between rainfall, pore water pressure response and slope deformation, it was necessary to select a period of time when all the field instrumentation was installed and monitored simultaneously and data collected. As a result, the period of August 1, 2009 to January 31, 2010 was selected for this study.

The heaviest rainfall event at the study site occurred on September 3, 2009 with 654 mm of rainfall measured in the rain gauge over a 24 hour period. The second heaviest rainfall event occurred on October 7, 2009 with 488 mm over a 24 hour period. The average antecedent rainfall for both events for a period of 3 days prior to the main event was 93 mm and 47 mm, respectively.

6.2.2 Instrumentation Response to Rainfall during the period of August 2009 to January 2010.

The field instrumentation response to rainfall from August 1st, 2009 to January 31st, 2010 for the Barre de L'isle Study Site is presented in Figure 6.1 to Figure 6.3.

6.2.2.1 Standpipe Piezometer

The Casagrande type standpipe piezometer used at the study site was installed between Row A and Row B tensiometers to a depth of 10.5m below existing ground surface. At this depth, the tip of the piezometer was located in the confined silty sand layer to monitor groundwater level fluctuations. Static groundwater level was recorded at 5.0m. The piezometer was monitored concurrently with the tensiometers and the rain gauge.

The highest significant water level of 3.2m was recorded on November 7, 2009 after a rainfall event of 100mm. However, between the period of November 2 – 6, there was a total of 668mm of antecedent rainfall. The groundwater level increased 3.4m over the period of November 2 -7, 2009. This indicates a time lag before the highest groundwater level was recorded on November 7, 2009. This time lag may in part, due to the low transmissivity of the sand layer and the low permeability of the residual soils at the study site.

The piezometer response to rainfall was not always consistent as shown in the graphs in Figure 6.1 to Figure 6.3**.** It is this author's belief that the piezometer response to rainfall was not totally a result of infiltration but also due to recharging of the confined sand layer identified at a depth of 9.0m in the borehole during the field investigation. The source of the groundwater recharge was not identified but is assumed to be somewhere upslope from the study site.

In some cases, such as for the rainfall event of 654 mm on September 3, 2009 it can be seen from the graphs in Figure 6.1 to Figure 6.3 that the piezometer response of 2100 mm occurred within 48 hours after antecedent rainfalls of 174 mm and 106 mm. Likewise, the rainfall event of 488 mm which occurred on October 7, 2009 resulted in a piezometer response of 400 mm following a 24 hour antecedent rainfall period of 138 mm.

The rainfall event of 230 mm on October 16, 2009 resulted in a piezometer response of 1900 mm over a 48 hour antecedent rainfall periods of 82 mm and 78 mm.

The piezometer response to rainfall events of 330 mm, 100 mm and 242 mm for November 4,7,21 respectively all occurred after periods of antecedent rainfall. This would imply that intensive antecedent rainfall has a greater influence on deep-seated landslides than immediate rainfall.

It appears to this author that the piezometer response to rainfall at the study site is not immediate, but there is a time lag following a period of antecedent rainfall events. This may be due in part to the low permeability of the subsoils and also to the high hydraulic conductivity of the rechargeable confined sand aquifer during rainfall events. The groundwater level in the piezometer decreased slowly after reaching its highest level.

6.2.2.2 Tensiometers

All of the tensiometers installed at the site responded readily to rainfall events. Some more so than others. The pore-water pressure response to rainfall varied with depth in rows A to C during the study period as indicated in the graph**.** The rainfall and pore-water pressure response for the following periods were selected for this analysis:

The data collected from the tensiometers was deemed to be reliable since they all responded to rainfall events recorded during the monitoring period. The graphs in Figure 6.1 to as Figure 6.3 show the variation in pore water pressures and rainfall recorded during the monitoring period of nine (9) months. The tensiometers installed at 0.5m depth in Rows A and B responded quickly to rainfall and to evaporation during dry periods. Row C was slow to respond even to the heaviest rainfall. This may have been due to the fact that Row C was located on a small mound of soil with a shallow drain at the upslope toe. Surface water may have rolled off the mound and removed from Row C by the shallow drain before any infiltration could take place.

The dynamic response of the tensiometers to rainfall and dry periods was due to infiltration during rainfall and evaporation during the drier periods. During rainfall periods the pore water pressures rose quickly at shallow depths and dissipated significantly during dry periods. At greater depths, the tensiometer response was slower during rainfall periods except during the heavy rainfall period of September 3, 2009 (654mm) and October 7, 2009 (488mm) when all the tensiometers responded quickly up to 2.3m depth.

<u>Row 'A' Tensiometers</u>

Figure 6.1 shows the graphs for pore-water pressure response to rainfall for Row 'A' at the top of the slope as recorded in the tensiometers installed at the Barre de L'isle study site.

For August 31, 2009 with no rainfall, the pore-water pressure at 0.5m was – 13.0 kPa and at 3.0m the pore-water pressure was lower at – 42.0 kPa

During the heavy rainfall event of 654 mm on September 3, 2009 the pore-water response was dynamic in all the tensiometers. The pore-water pressure at 0.5m depth was - 1.0 kPa and at 3.0m depth the pore-water pressure was at -10.0 kPa. This is a drastic increase in pore-water pressure compared to the previous recording on August 31. This shows that the heavy rainfall event of September 3 caused rapid infiltration and saturation of the slope over a 24 hour period up to at least a 3.0m depth.

The plot for September 24, 2009 shows the pore-water pressure at 0.5m to be - 11.0 kPa and at 3.0m the pore-water pressure was at - 32.0 kPa for no rainfall on that day. However, the antecedent rainfall for three (3) days prior to this event was 76.0mm.

The tensiometer readings for September 29, 2009 shows the pore-water pressure in the slope at a depth of 0.5m was - 9.0 kPa and at a depth of 3.0m the pore-water pressure was – 20 kPa. There was no rain on that day but the antecedent rainfall recorded for three (3) days prior to this recording was 324 mm.

The rainfall event of October 7, 2009 was measured at 488 mm. The response of the tensiometers to this event was dynamic in that all the readings gravitated toward equilibrium (zero), an indication of almost complete saturation of the slope. At 0.5m the pore-water pressure recorded was – 2.0 kPa and at 3.0m depth the pore-water pressure was recorded at - 4.0 kPa.

Row 'B' Tensiometers

Figure 6.2 contains the graphs for pore-water response to rainfall for Row 'B' which is located in the middle of the slope.

The pore-water pressure recorded for August 31, 2009 at a depth of 0.5m was -14.0 kPa and at 2.75m the pore-water pressure was -30.0 kPa.

The pore-water pressure reading for September 3, 2009 after the heavy rainfall of 654 mm was -2.5 kPa at 0.5m and -20.0 kPa at a depth of 2.75m. This indicates that the pore-water pressure in Row 'B' was lower for the same rainfall event than those in Row 'A' at shallow and greater depths. This also shows that infiltration was greater at the crest than in the middle of the slope for this rainfall event.

The plot for September 24, 2009 show the pore water pressure at 0.5m to be – 13.0 kPa and – 30.0 kPa at 2.75m. There was no rainfall on that day but the antecedent rainfall was 76.0mm.

The pore-water pressure recorded on September 29, 2009 at a depth of 0.5m was - 10.0 kPa and - 26.0 kPa at 2.75m for no rainfall on that day and an antecedent rainfall of 324 mm.

The heavy rainfall of 488 mm on October 7, 2009 caused a drastic increase in the pore-water pressure to – 4.0 kPa at 0.5m and -18.0 kPa at 2.75m.

The pore-water pressures recorded in Row 'B' for the heavy rainfall periods indicate high infiltration rates up to at least 2.75m in the middle of the slope.

Row 'C' Tensiometers

Figure 6.3 shows the graphs of the pore-water pressures in Row 'C' at the toe of the slope. The pore-water pressures at this location were not as dynamic as for the crest or middle of the slope. This was partly due to the presence of a small earth mound on which the instruments were placed and a shallow drain at Row 'C' which removed runoff quickly away from the test site thereby not allowing any meaningful infiltration to take place.

The pore-water pressures at shallow depths ranged between – 16.0 kPa and - 28.0 kPa whereas at 3.0m there was little change throughout the test period with the pore-water pressure ranging between – 32.0 kPa and – 36.0 kPa.

The pore-water pressures recorded for August 31, 2009 at 0.5m was – 21.0 kPa and - 34.0 kPa at 3.0m depth.

The pore-water pressures for September 3, 2009 were recorded at – 16.0 kPa at 0.5m and - 32.0 at 3.0m. There was very little change in the pore-water pressure for the heavy rainfall of 654 mm on this day.

Pore-water pressure readings of – 26.0 kPa and - 36.0 kPa were recorded at depths 0.5m and 3.0m respectfully, for September 24, 2009.

The pore-water pressure readings for September 29, 2009 were -19.0 kPa at 0.5m and - 36.0 kPa at 3.0m depth.

The heavy rainfall of 488 mm on October 7, 2009 caused very little change in the pore-water pressures in Row 'C' much unlike Rows 'A' and 'B'. The pore-water pressure at 0.5m was – 28.0 kPa and the reading at 3.0m was - 36.0 kPa.

6.2.2.3 Slope Inclinometer

The slope inclinometer at the site was installed to monitor horizontal displacements in the subsurface materials. The horizontal displacement measurements were performed with a Digitilt probe manufactured by Slope Indicator Company, Mukilteo, Washington, USA. The horizontal displacement measurements could not be performed simultaneously with the tensiometers and piezometers because of the high cost or rental of the slope inclinometer equipment. Monitoring was conducted on a weekly or bi-weekly basis.
As a result, the variations in horizontal displacement profiles could not be correlated consistently with changes in groundwater levels, rainfall or tensiometer readings.

However, the periodic monitoring of the slope inclinometer over the study period showed that the ground moves in a down-slope direction. There was very little displacement laterally.

Figure 6.4 shows the horizontal displacement of 8.0mm at 12.0m at the Barre de L'isle study site during the monitoring period.

Most of the observed total cumulative displacement of 14.5 mm (0.56 ins) was recorded near the ground surface during the study period. This was most likely caused by wetting and drying (creep) of the soil at the ground surface. The incremental displacements near the ground surface ranged from 0.37 mm to 0.58 mm.

A cumulative horizontal displacement of 8.0 mm was recorded at a depth of 12.0m in the clayey silt residual soil. This zone of movement lies between the sand layer at 9.0m and the weathered bedrock. The incremental displacement at this depth was 0.69 mm. This displacement most likely was generated by high pore water pressures in the sand layer when recharged during heavy rainfall periods. The inclinometer sheared off at a depth of 12.0 m due to accelerated ground movement triggered by heavy rainfall (682 mm) over a 24-hour period during hurricane 'TOMAS' on October 30, 2010.

The horizontal displacement observed near the ground surface may be the result of faulty installation of the inclinometer casing from poor grouting which causes the instrument to shift around when the probe is installed during the survey or from creep initiated from wetting and drying of the surficial soil.

6.2.2.4 Rain Gauge

The rain gauge installed at the study site was read simultaneously with the tensiometers and the standpipe piezometer. The maximum daily rainfall recorded during the nine (9) month study period from February 13, 2009 to December 31, 2009 was 654 mm on September 3, 2009. There were several days of no rainfall. The total amount of rainfall recorded for the study period was 6,983 mm with a daily average of 74 mm.

6.2.2.5 Soil-Water Characteristic Curve (SWCC)

The relationship between moisture content and soil suction is usually expressed in the Soil-Water Characteristic Curve (SWCC). The soil-water characteristic curve can be used to determine the functions of the physical properties of unsaturated soils such as the coefficient of permeability, the coefficient of volume change and the shear strength. Fredlund, 1998 states that the soil-water characteristic curve defines the degree of saturation corresponding to a particular suction in the soil and becomes a measure of the pore size distribution of the soil.

The direct measurement of unsaturated soil property function is usually done through excessive laboratory tests. The laboratory equipment required and the cost of performing these tests are escessive and are not available in Saint Lucia. Fredlund, 2000 suggests the inexpensive use of the grain size distribution curve to estimate the soil-water characteristic curve for unsaturated soils.

Fredlund, 2000 proposed an estimation technique which initiates that the grain size distribution curve is first assumed to estimate an approximate desorption curve for a soil that is initially slurried near the liquid limit. The grain size distribution curve can be viewed as incremental particle sizes from the smallest to the largest. The results from the various particle sizes are then assembled to build the SWCC. Small increments of uniformed-sized particles are transposed to form a SWCC representative of a series of average particle sizes. Once the entire grain-size distribution curve has been incrementally analysed, the individual SWCCs are combined using a superposition technique to give the SWCC for the overall soil. The shape of an estimated SWCC is predominantly controlled by the grain-size distribution and secondarily influenced by the density of the soil.

The determination of the soil property functions of unsaturated soils refers to such relationships such as: 1.) soil suction and shear strength; 2) soil suction and coefficient of permeability and 3) soil suction and soil water retention variable.

The commercially available computer software knowledge-based database system ‘SOILVISION’ manufactured by SoilVision Systems Ltd of Saskatchewan, Canada incorporates the use of the grain-size distribution curve to estimate the soil-water characteristic curve for this study.

The software provides a large database of unsaturated soils information and theoretical methods of estimating the engineering behaviour of unsaturated soils. Fredlund, 1998 theorizes that the soil-water characteristic curve can be used in conjunction with the saturated shear strength of a soil to estimate the relationship between shear strength and matric suction.

He stated that it is possible to use a classification test to estimate the unsaturated soil property function. For example, a grain size analysis may be used to estimate the soil-water characteristic curve which is then used to estimate the unsaturated soil property function. Fredlund, 1998 indicates that a theoretical curve may be combined to the grain size analysis to predict the soil-water characteristic curve.

The software contains a database of information collected from other laboratory studies which are matched with measured soil-water characteristic curves.
The measured soil-water characteristic curves can then be used to generate unsaturated soil property functions or to select unsaturated soil property functions already in the database.

The software may also be used for matching measured soil classification properties with classification properties already in the database. In addition, the grain size distribution curves measured may be compared with grain-size distribution curves already in the database and soil-water characteristic curves can then be generated and compared with soil-water characteristic curves already in the database.

A grain size distribution curve from laboratory tests on soil samples recovered from the Barre de L'isle Study Site was used to generate a soil-water characteristic curve for the soils at this site. Fredlund's theoretical curve was then fitted to the data from the grain size distribution curve using the software 'SOILVISION'. The theoretical grain size curve was then used to predict the soil-water characteristics of the residual soil.

Figure 6.5 shows the grain size distribution curve from laboratory tests on soil samples from the Barre de L'isle study site fitted with Fredlund's theoretical curve.

The volume-mass characteristics derived from the computed data was as follows:

Degree of Saturation, S_r	= 90.7 %
Volumetric water Content, θ	= 41.5 %
Porosity, n	= 45.8 %
Void Ratio, e	= 0.844
Water content, w	= 29.4 %
Dry Density, γ_d	= 13.8 kN/m^3
Bulk Density, γ_b	= 18.0 kN/m^3
Specific Gravity, G_s	= 2.60
Liquid Limit, LL	= 84.0 %
Plastic Limit, PL	= 49.0 %
Plasticity Index, IP	= 35.0 %
Activity	= 2.63
Sand	= 53.7 %
Silt	= 32.7 %
Clay	= 13.6 %

Figure 6.6 contains the Soil-Water Characteristic curve for the Barre de L'isle study site. The SWCC consists of three (3) straight lines with slopes on a logarithmic scale. The first slope represents the curve between the 90.7 % saturated condition of 36.0% gravimetric water content and the low air entry value of 0.5 kPa soil suction.

The second slope refers to the slope of a line between the air entry value and the residual conditions at 6.0 kPa soil suction computed on the gravimetric water content scale at 16.5%. The third slope refers to the slope of a line between the residual water content and completely dry conditions at a soil suction of 1,000,000 kPa at a gravimetric water content of 0 % .

Th air entry value represents the matric suction value that must be exceeded before air receeds into the soil pores. At the residual state condition the water phase is discontinuous and isolated within thin films of water surrounding the soil and air and it becomes very difficult to remove water from the soil with high matric suction values. The increase in soil suction has very little effect on the soil water content.

In general, the soil-water characteristic curve illustrates the following:

i) there is a decrease in moisture content as matric suction increases.
ii) suction approaches 1,000,000 kPa at 0 % water content
iii) the soil changes its water content at a low matric suction i.e, at a low air entry value (0.5 kPa).

Low soil suction values are required to remove water when the soil is saturated.
High soil suction values are required to remove water from the finer soil particles as it dries up.

6.3 Windjammer Landing Beach Resort Study Site

6.3.1 Rainfall Distribution and Pore Water Pressure Measurements for the Windjammer Landing Beach Resort Study Site

Monitoring of the field instrumentation at the Windjammer Landing Beach Resort study site commenced on November 14, 2008 and was completed on May 12, 2009 a period of approximately six (6) months. The instrumentation programme was initiated as a result of a landslide which occurred at the site following a period of intensive rainfall of 120 mm on October 11, 2008. The monitoring programme involved the measurement of pore water pressure response to rainfall in the jet-fill tensiometers, horizontal displacements in the subsoils and groundwater level variations in response to rainfall.

The Windjammer Landing Beach Resort is located at the northern section of the island of Saint Lucia which receives the lowest amount of annual rainfall. The maximum amount of rainfall recorded at the site during the study period was 35.0 mm which occurred on January 14, 2009.

6.3.1.1 Tensiometers

The Windjammer Landing Beach Resort is located at the northern region of Saint Lucia which receives the least amount of annual rainfall. As a result, the response of the tensiometers to rainfall events was not as great as that experienced at the Barre de L'isle study site which is located in an area which receives the heaviest rainfall on the island. However, the pattern of pore-water pressure response to rainfall at the Windjammer study site was almost similar to that observed at the Barre de L'isle site.

The pore-water pressure response to rainfall for six (6) selected days in 2008 and 2009 was used in this analysis. The response of the field instrumentation to rainfall is show on the graphs in Figure 6.7 to Figure 6.9.

'Row A' Tensiometers

Figure 6.7 shows the graphs of the pore-water pressure response to rainfall in the tensiometers in Row A at the top of the slope at the Windjammer Landing Beach Resort study site.

On December 17, 2008 the pore-water pressure recorded at a depth of 0.5m was – 13 kPa and at 2.3m depth the pore-water pressure was higher at – 16 kPa with no rainfall occurring on that day.

The 24 mm of rainfall which occurred on December 24, 2008 caused an increase in the pore-water pressure response to – 2.5 kPa at 0.5m and – 15 kPa at 2.3m. This indicates that the infiltration from this amount of rainfall occurred mainly near the ground surface with very little infiltration to 2.3m.

The plot for the January 14, 2009 shows the pore-water pressure at 0.5m to be 0.0 kPa after 35 mm of rainfall. At a depth of 2.3m the pore-water pressure response was - 10 kPa. This indicates that a rainfall of 35 mm will saturate the ground surface and infiltrate to a depth of at least 2.3 m in the colluvium.

The plot for February 24, 2009 shows the pore-water pressure response to 5.0 mm of rainfall at a depth of 0.5m was – 8 kPa and – 15 kPa at 2.3m, a decrease in pore-water pressure from the response observed on January 14, 2009. This smaller amount of rainfall allows for more rapid evaporation at the ground surface thereby reducing the amount of surface water available for infiltration.

The rainfall event of 15 mm which occurred on February 27, 2009 caused a slight increase in the pore-water pressure to – 7.5 kPa at 0.5m and – 12 kPa at 2.3 m.

The tensiometer readings for May 12, 2009 shows the pore-water pressure response to 30 mm of rainfall at 0.5 m depth to be – 2.5 kPa and – 10 kPa at a depth of 2.3m, a result of ground saturation and infiltration to at least 2.3 m.

All of the tensiometers installed in Row A appear to function appropriately and showed an increase in pore-water pressure in response to rainfall between 5 mm and 35 mm intensity.

Row 'B' Tensiometers

Figure 6.8 shows the graphs for pore-water pressure response to rainfall for Row 'B' located at mid-height of the test area. The pore-water pressure recorded with no rainfall on December 17, 2008 was – 10 kPa at 0.5m depth and - 17.5 kPa at 2.3 m. These values indicate wetter conditions close to the surface than in Row 'A' and less infiltration (drier conditions) at 2.3 m.

The pore-water pressure response to 24 mm of rainfall on December 24, 2008 was 0 kPa at 0.5m and -15 kPa at 2.3m, indicative of surface saturation and some infiltration to at lease 2.3m depth.

The rainfall event of 35 mm on January 14, 2009 resulted in surface saturation with a reading at 0 kPa and – 16 kPa at 2.3m, a condition similar to the results of the rainfall event on December 24, 2008.

The pore-water pressure response to 5 mm of rainfall on February 24, 2009 showed some saturation near the ground surface at -3 kPa with no infiltration occurring to 2.3m which was read at -18 kPa.

On February 27, 2009 15 mm of rainfall occurred at the site and the pore-water pressure response was recorded at - 6 kPa at 0.5m and – 17 kPa at 2.3m. This event did not cause any infiltration to the lower colluvium subsoil.

The 30 mm of rainfall which occurred on May 12, 2009 resulted in surface saturation (-2.5 kPa) and infiltration to depth, a similar response as the instrumentation in Row 'A'. The pore-water pressure response to rainfall as shown by the instrumentation installed in the slope was similar in Rows 'A' and 'B'.

Row 'C' Tensiometers

Figure 6.9 contains the graphs of the pore-water pressure conditions in Row 'C' at the lower section of the slope in the test site. The pore-water pressure responses at this location were almost similar that observed for Rows "A' and 'B'.

The pore-water pressure readings in the tensiometers on December 17, 2008 were - 12.5 kPa near the ground surface and -15 kPa at a depth of 2.3m with no rainfall occurring on that day.

For the rainfall event of 24 mm on December 24, 2008 the pore-water pressure response in Row 'C' was close to that observed for Rows 'A' and 'B' near the ground surface with a reading at – 3 kPa but was wetter at 2.3 m with a reading of 7.5 kPa. This indicates that infiltration occurred to a greater depth in Row 'C' than in Rows 'A' and 'B'.

The pore-water pressure response to 35 mm of rainfall in Row 'C'on January 14, 2009 near the ground surface was 0 kPa which was similar to the readings for Rows 'A' and 'B' for that day and -15 kPa at 2.3m which was close to the other two rows of tensiometers.

The rainfall event of 5 mm on February 24, 2009 generated very little response to the pore-water pressure in Row 'C' which showed drier conditions near the ground surface with a reading of -10 kPa compared to readings of – 8 kPa and -3 kPa for Rows 'A' and 'B' respectively for that day. The pore-water pressure response in the slope to 15 mm of rainfall on February 27, 2009 caused some increase in moisture near the ground surface in the colluvium which showed – 7.5 kPa but no infiltration occurred to 2.3m depth which showed drier conditions at -20 kPa.

A total of 30 mm of rainfall was recorded for May 12, 2009 which resulted in near saturation near the ground surface and to a depth of 1.6 m with a pore-water pressure reading of -2.5 kPa but drier conditions remained at 2.3m with a reading of -18 kPa.

All of the tensiometers in the three rows installed at the site responded to rainfall events showing increases or decreases in pore-water pressures in the colluvium based on rainfall conditions and infiltration.

6.3.1.2 Standpipe Piezometers

Two (2) Casagrande type standpipe piezometers were installed on the slope at the Windjammer study site. Two (2) standpipe piezometers (BH08-SP-13 & BH08-SP-15) were installed at the study site during the period of October 29 to December 18, 2008. BH08-SP-13 was installed at the toe of the slide area near to the damaged retaining wall and BH08-SP-15 was located at the top of the slope in the study area.

Piezometer number BH08-SP-13 was installed to a depth of 3.4m below existing ground surface. At this depth the tip of the piezometer was located near the contact between the colluvium and the weathered basalt bedrock. The groundwater level was at 3.0m below ground surface. BH08-SP-15 was installed to a depth of 2.9m with the tip located near the colluvium contact with the bedrock. The groundwater level was recorded at a depth of 0.8m below ground surface. The monitoring period for the field instrumentation at the study site was from November 3, 2008 to May 12, 2009.

The heaviest rainfall event (35 mm) recorded at this site during the study period occurred on January 14, 2009. The results of the monitoring programme indicates that there was no great response of the groundwater levels in the piezometers to rainfall.The response of the groundwater level to the rainfall event of January 14, 2009 varied in both piezometers installed at the study site. The response in piezometer BH08-SP-13 at the toe of the slope showed an increase in the groundwater level of 30 mm. The groundwater level in BH08-SP-15 showed a negative response of 100 mm to the same rainfall event of January 14, 2009.

The piezometers were installed in a landslide area where ground deformation had taken place and there were several tension cracks visible on the ground surface. The landslide occurred on October 11, 2008 after a rainfall event of 120 mm. At this time there was no monitoring instrumentation in place at the site to record groundwater level response to rainfall. The instrumentation was installed eighteen (18) days after the landslide occurred. It is the author's belief that the presence of the tension cracks in the ground allowed rapid dissipation of any surface infiltration and pore-water pressures did not have time to develop significantly since the colluvium was well drained by the cracks and fissures in the ground.

It should be noted that there were several other landslides reported at other locations on the island as a result of this rainfall event, including the 2008 landslide at the Barre de L'isle study site.

The piezometers installed in the 2005 landslide area located south of the study site did show a response to the 120 mm October 11 rainfall event two to three days after the rainfall. This indicated a time lag before the highest groundwater level was recorded. Two of the piezometers showed a negative response to this rainfall event. The groundwater levels in the piezometers decreased slowly after reaching the highest level.

6.3.1.3 Rain Gauge

The rainfall data used for this study was provided to this author by the maintenance personnel of the Windjammer Landing Beach Resort from their rain gauge installed at the resort. The maximum daily rainfall recorded during the six (6) month monitoring period at the study site was 35.0 mm on January 14, 2009. The total amount of rainfall recorded for the study period was 247 mm with a daily average of 11 mm. The rainfall event of 120 mm that triggered the landslide on October 11, 2008 occurred prior to the installation of the instrumentation at the study site.

6.3.1.4 Slope Inclinometers

Two (2) slope inclinometers were installed in the study area to monitor horizontal displacements in the subsoils. Slope inclinometer SI08-8 was installed at the toe of the slope about 3.0m from the failed retaining wall. SI08-10 was located upslope above the tensiometers. Monitoring of the slope inclinometers was conducted on a weekly basis due to restrictions implemented by the management of the resort.

The slope inclinometers were installed and anchored into the weathered bedrock. SI08-8 was installed to a depth of 3.9m below ground surface. The colluvium was approximately 3.5m thick. Most of the total cumulative horizontal displacement of 75 mm occurred in the upper 1.5m of the inclinometer casing with the critical slip surface established at 1.5m with a cumulative displacement of 65 mm. This slope inclinometer eventually sheared off at due to excessive horizontal displacements and could not be further utilized.

SI08-10 was installed to a depth of 3.3m below ground surface with a casing embedment of 0.4m into the weathered bedrock. A maximum cumulative horizontal displacement of 13 mm was recorded at a depth of 1.8m in the downslope direction with a critical slip surface at 2.4m.

These results indicate that most of the horizontal displacement is taking place at the toe of the slope behind the retaining wall. This could be the result of a build up of pore-water pressures behind the retaining wall during the rainfall event of October 11, 2008 resulting in falure of the retaining wall and the slope.

6.3.1.5 Soil-Water Characteristic Curve (SWCC)

A gravimetric soil-water characteristic curve was generated for a soil sample of colluvium from the Windjammer Landing Beach Resort study site utilizing the grain size distribution curve procedure specified in the commercial software ‘SOILVISION’.

Figure 6.10 shows the grain size distribution curve for colluvium fitted with Fredlund's theoretical curve. The volume-mass characteristics derived from the computed data by 'SOILVISION' were as follows:

Degree of Saturation, S_r	= 83.6 %
Volumetric water content, θ	= 40.4 %
Porosity, n	= 48.3 %
Void ratio, e	= 0.935
Water content, w	= 29.5 %
Dry Density, γ_d	= 13.4 kN/m^3
Bulk Density, γ_b	= 17.4 kN/m^3
Specific Gravity, G_s	= 2.65
Liquid Limit, LL	= 62 %
Plastic Limit, PL	= 32 %
Plasticity index, IP	= 30 %
Activity	= 8.8
Sand	= 32.6 %
Silt	= 64.0 %
Clay	= 3.4 %

Figure 6.11 shows the Soil-Water Characteristic Curve for the Colluvium at the Windjammer Landing Resort study site.

The first slope of the curve represents the slope at 83.6 % saturation with 35.0 % gravimetric water content and a low air entry value of 3.0 kPa. Saturation at residual conditions is 18.0 % and residual suction is 150 kPa.

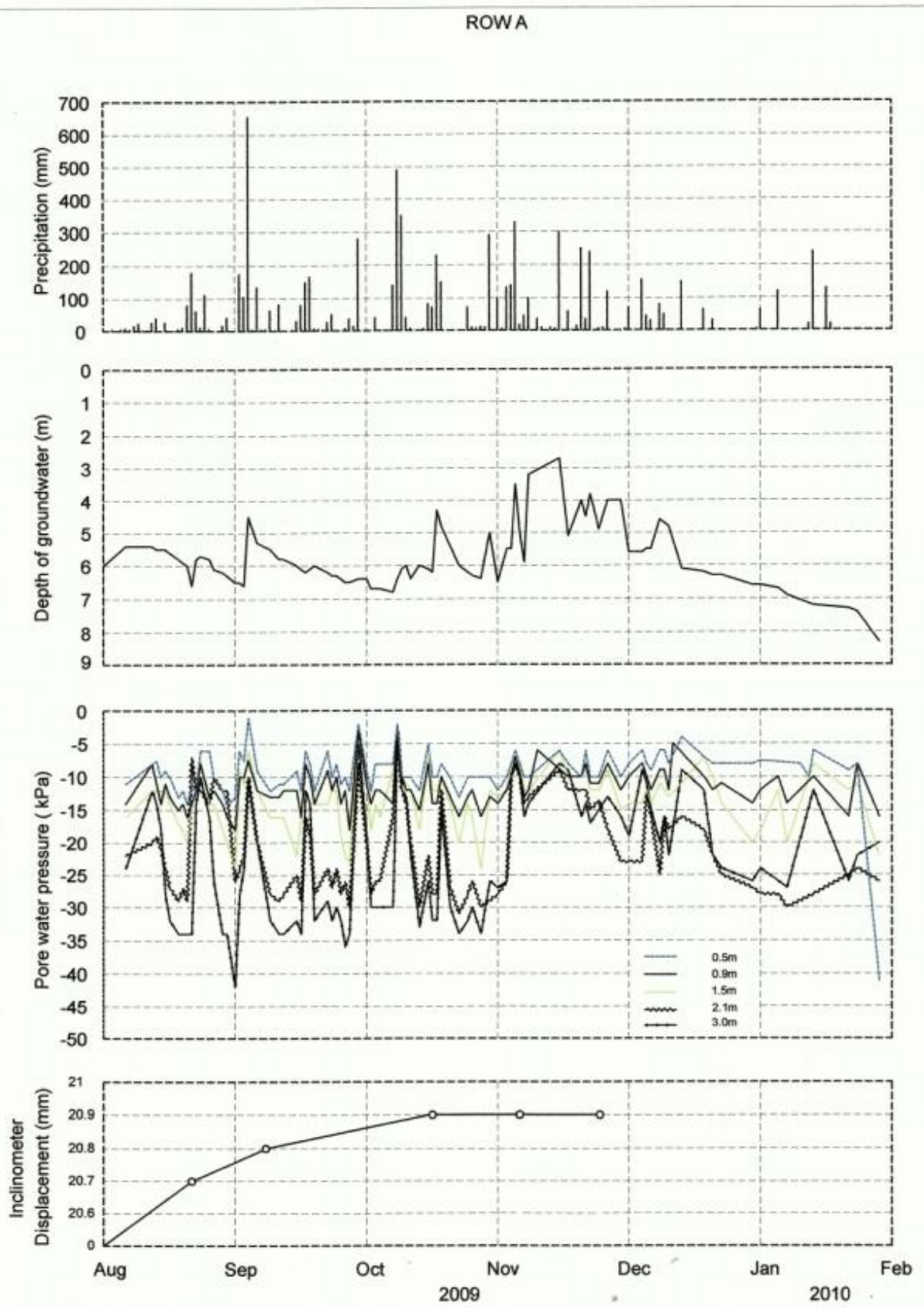

Figure 6.1 Field Instrumentation Response to Rainfall for "Row A" Tensiometers at the Barre de L'Isle Study Site

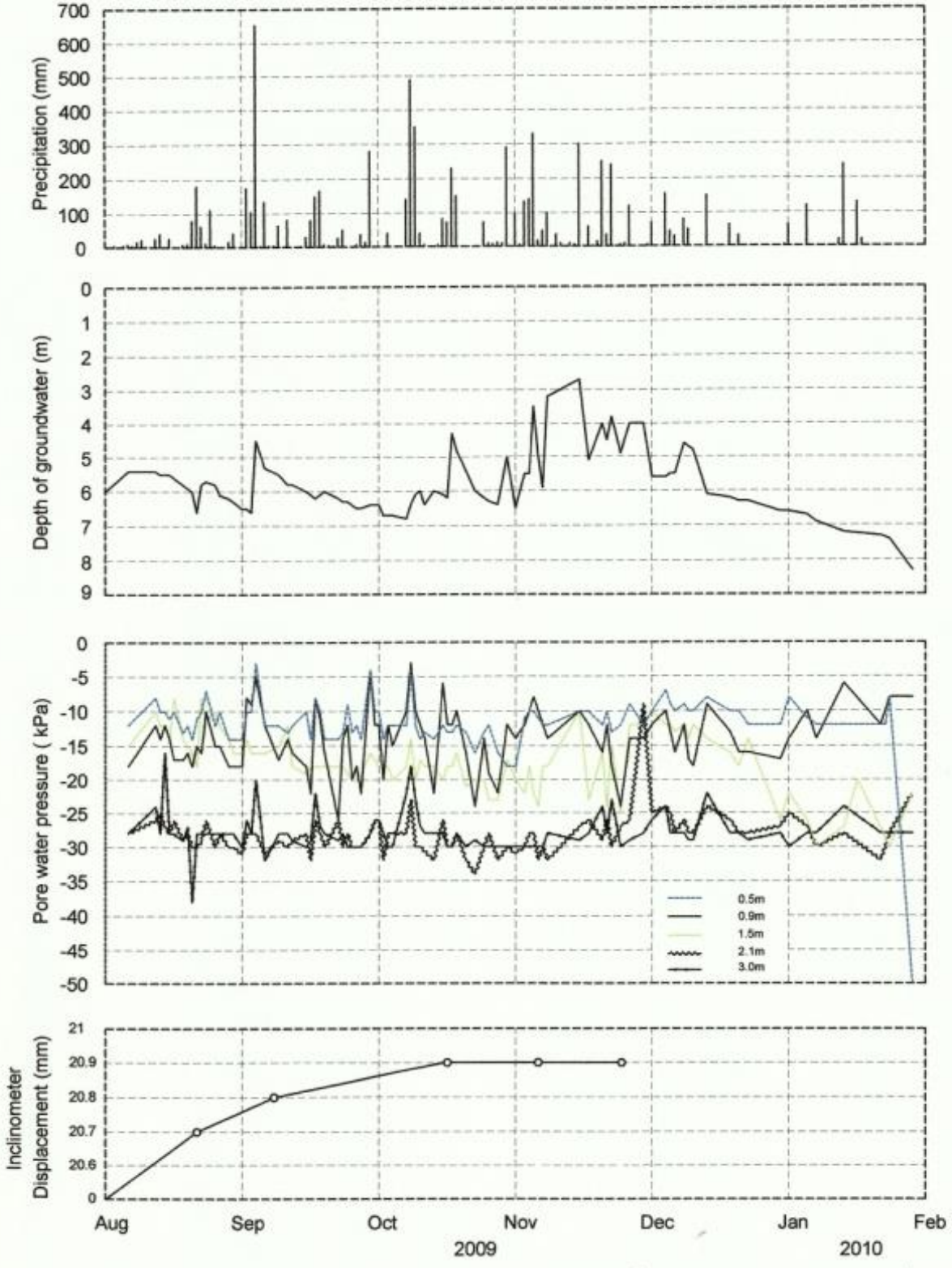

Figure 6.2 Field Instrumentation Response to Rainfall for "Row B" Tensiometers at the Barre de L'Isle Study Site

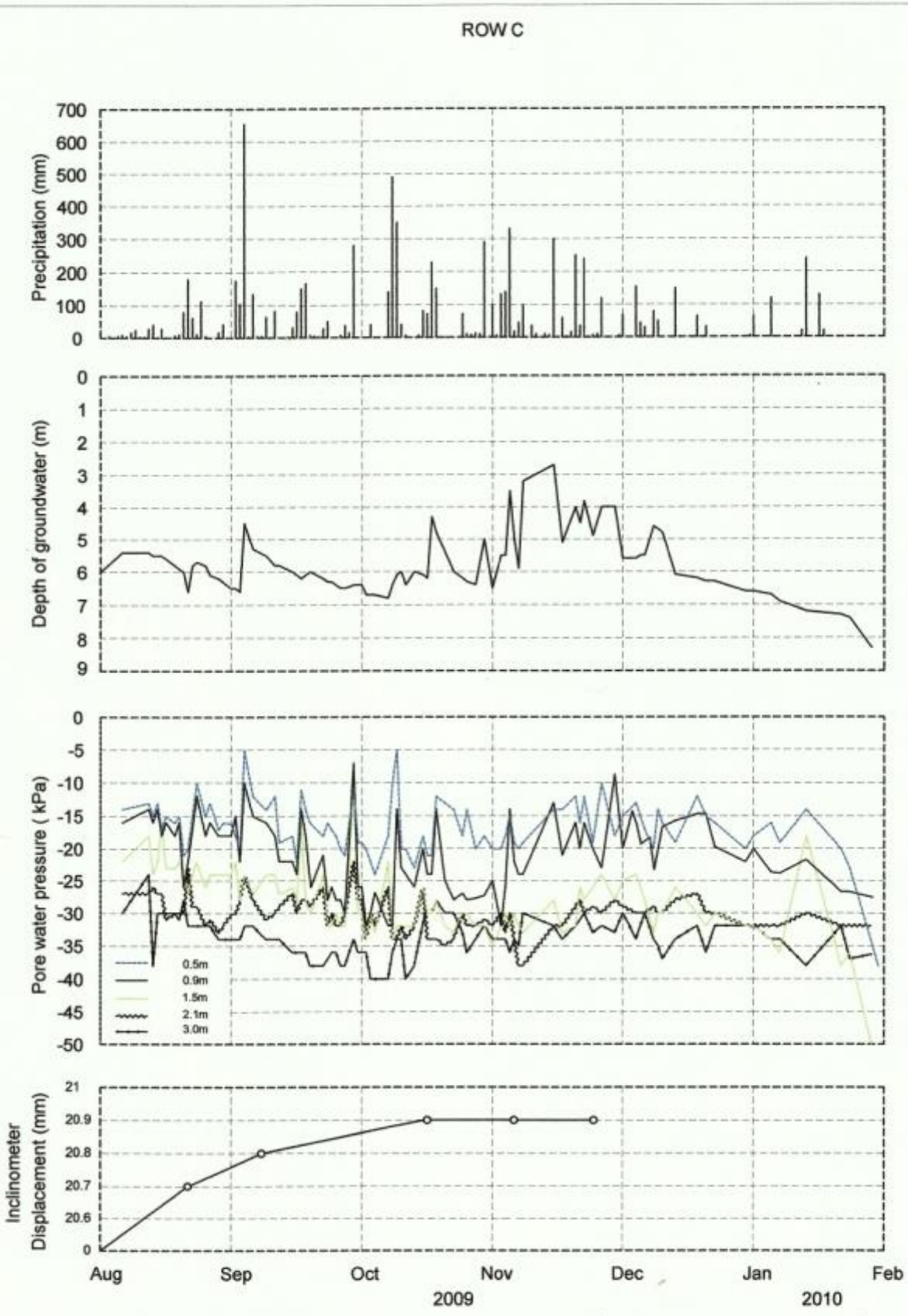

Figure 6.3 Field Instrumentation Response to Rainfall for "Row C" Tensiometers at the Barre de L'Isle Study Site

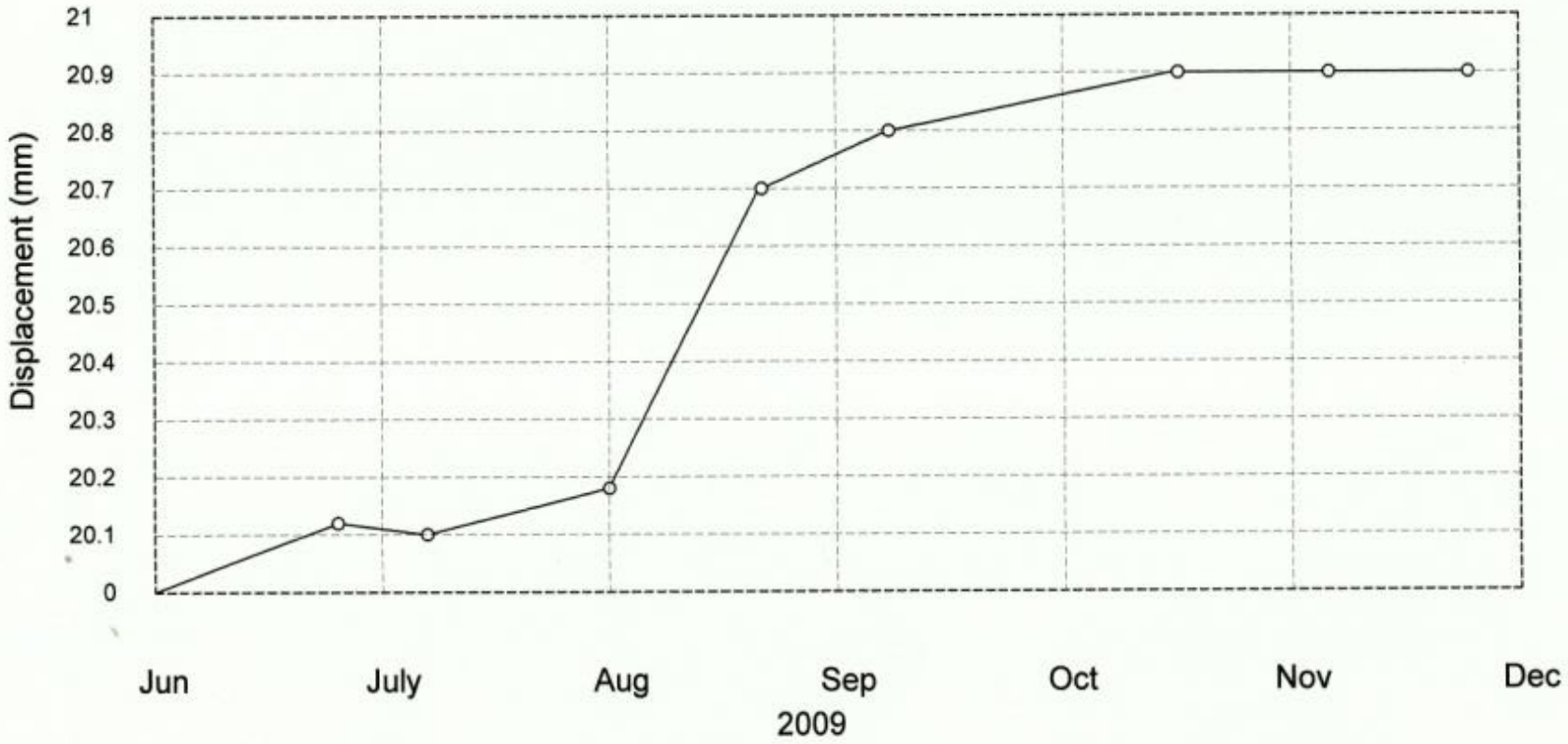

Figure 6.4 Graph of Slope Inclinometer measurement for the period of June 2009 to November 2009 at the Barre de L'Isle Study Site

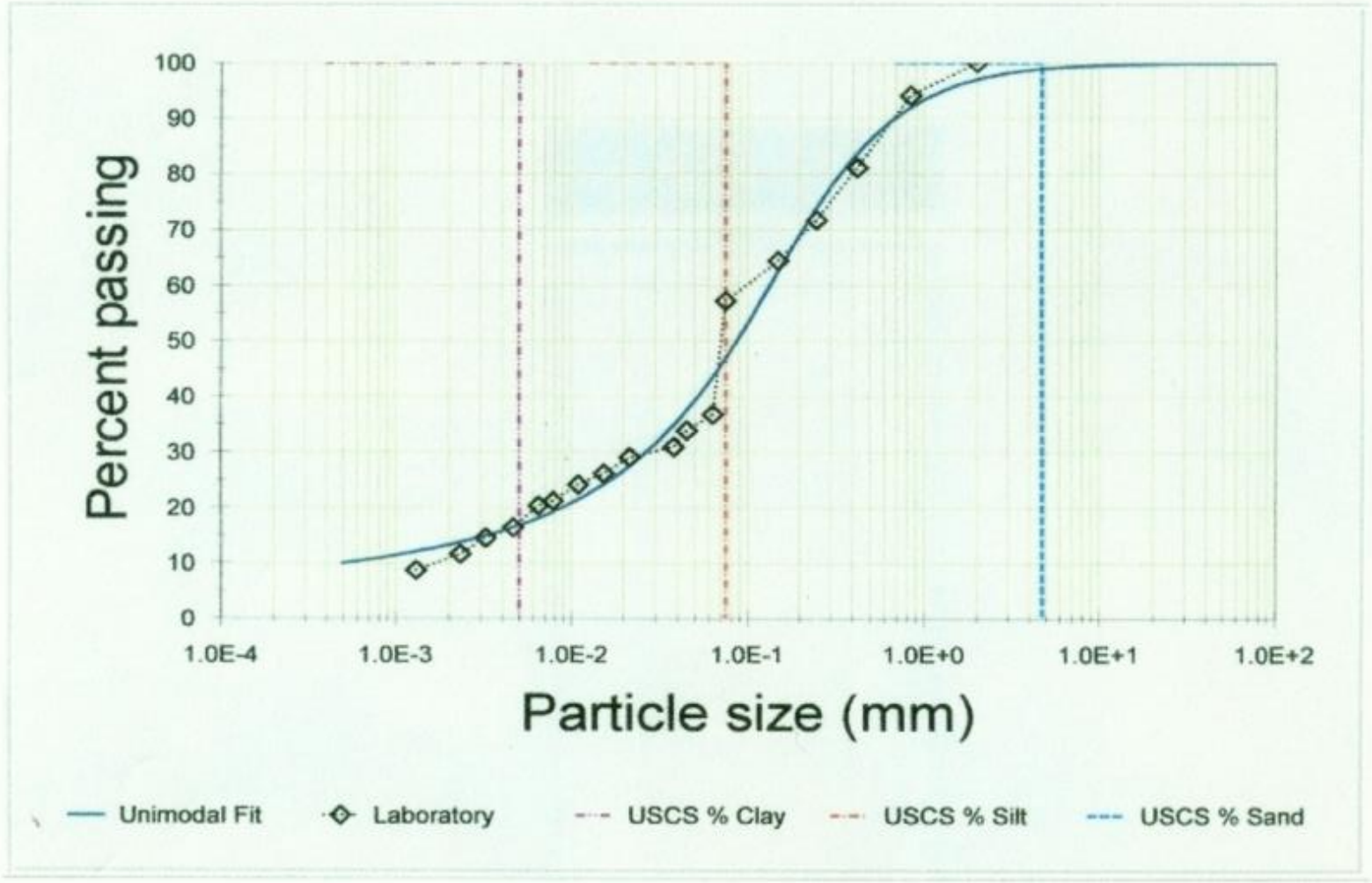

Figure 6.5 Grain size distribution curve from laboratory tests of soil samples from the Barre de L'isle Study Site fitted with Fredlund's Theoretical Curve

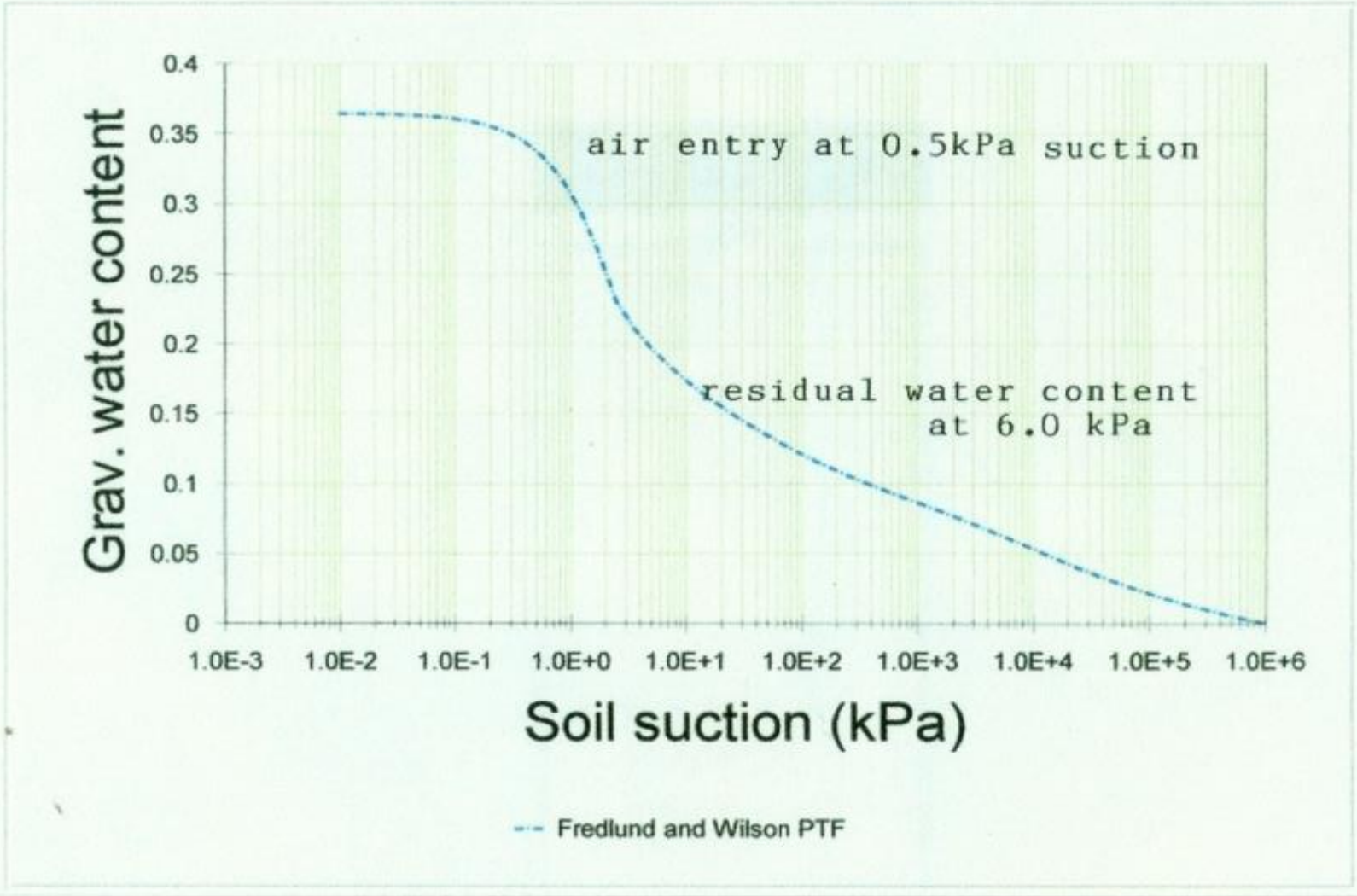

Figure 6.6 Soil-Water Characteristic Curve (SWCC) for residual soil samples from the Barre de L'isle Study Site

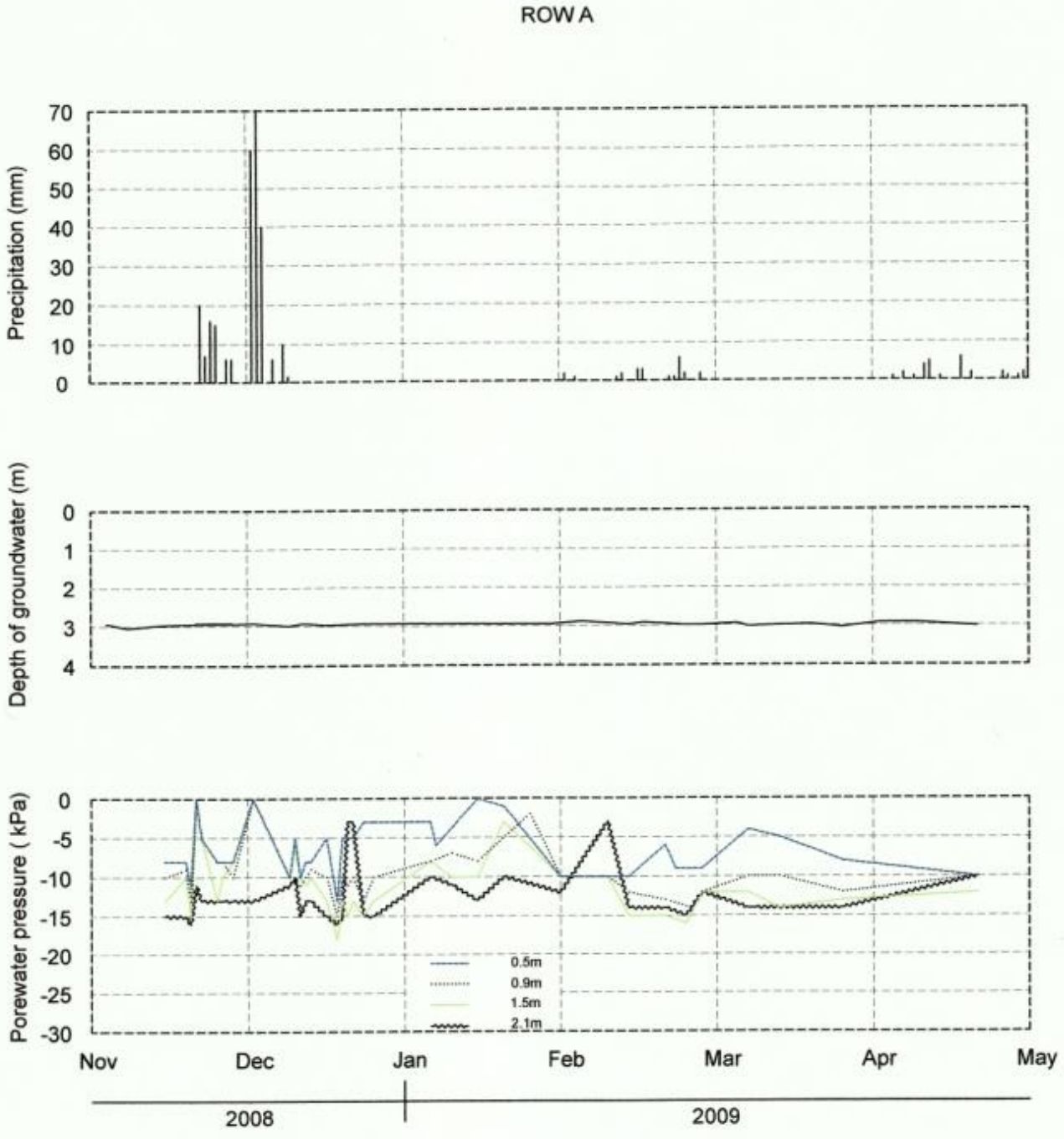

Figure 6.7 Field Instrumentation Response to Rainfall for "Row A" Tensiometers at the Windjammer Landing Beach Resort Study Site

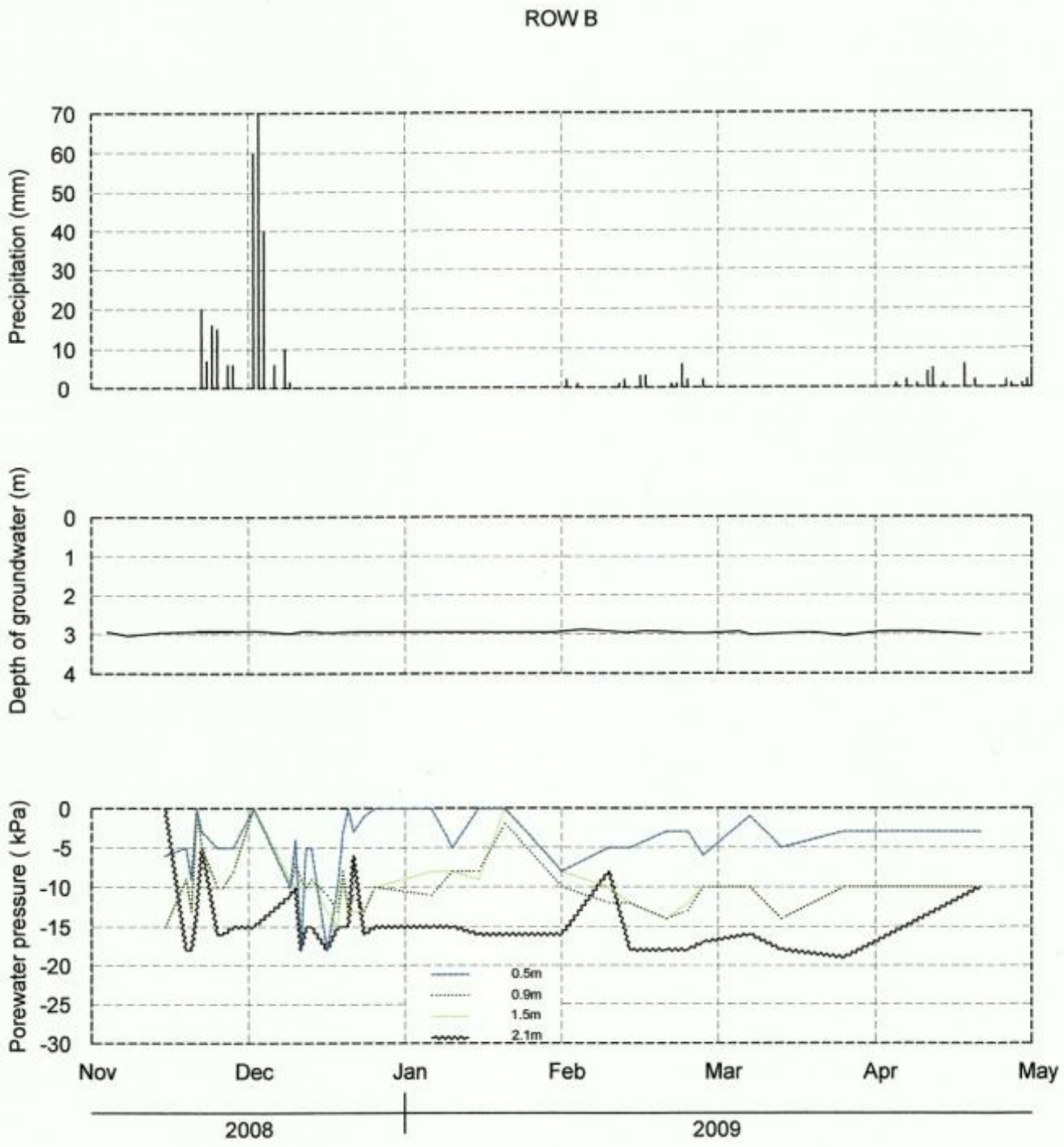

Figure 6.8 Field Instrumentation Response to Rainfall for "Row B" Tensiometers at the Windjammer Landing Beach Resort Study Site

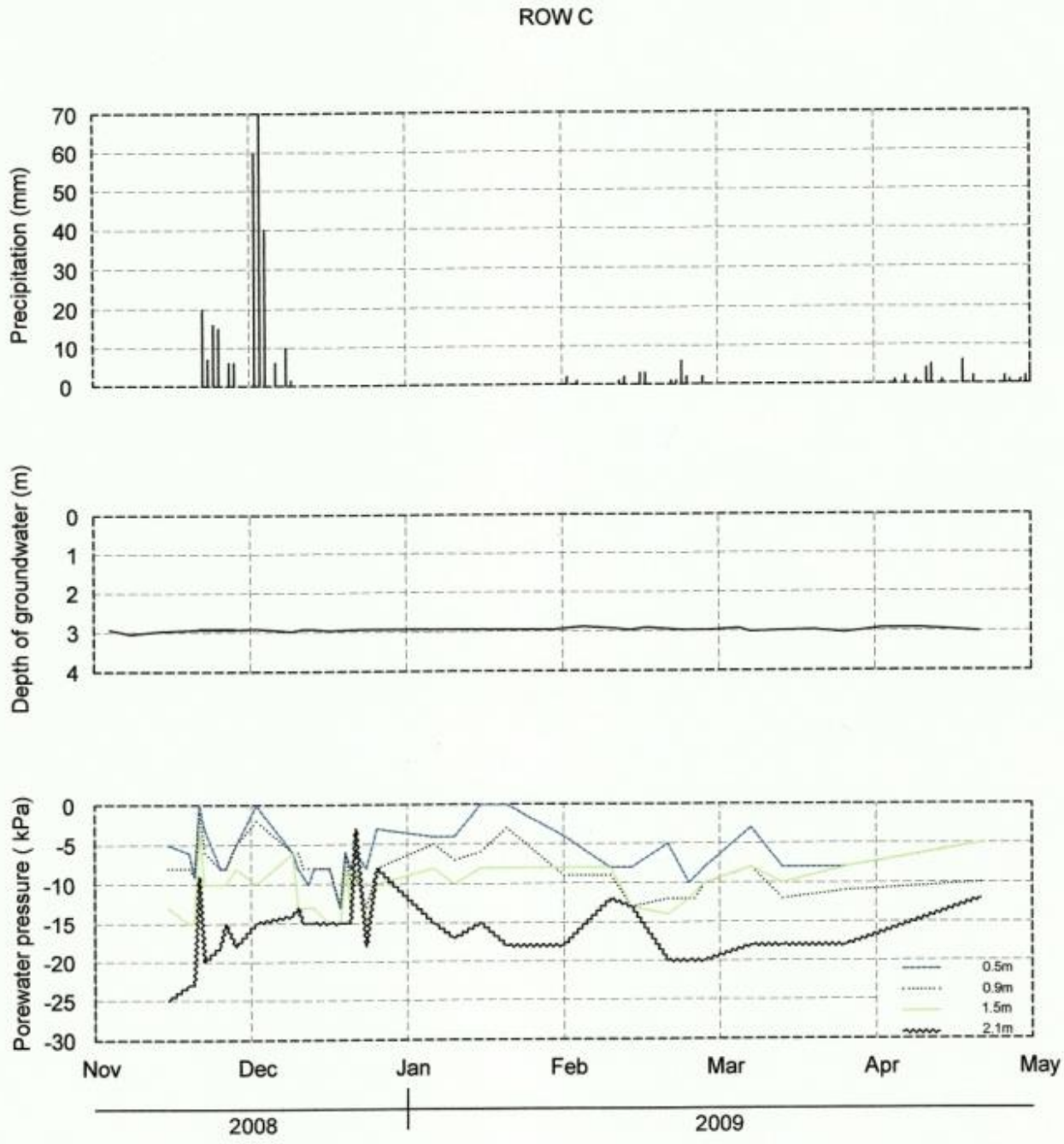

Figure 6.9 Field Instrumentation Response to Rainfall for "Row C" Tensiometers at the Windjammer Landing Beach Resort Study Site

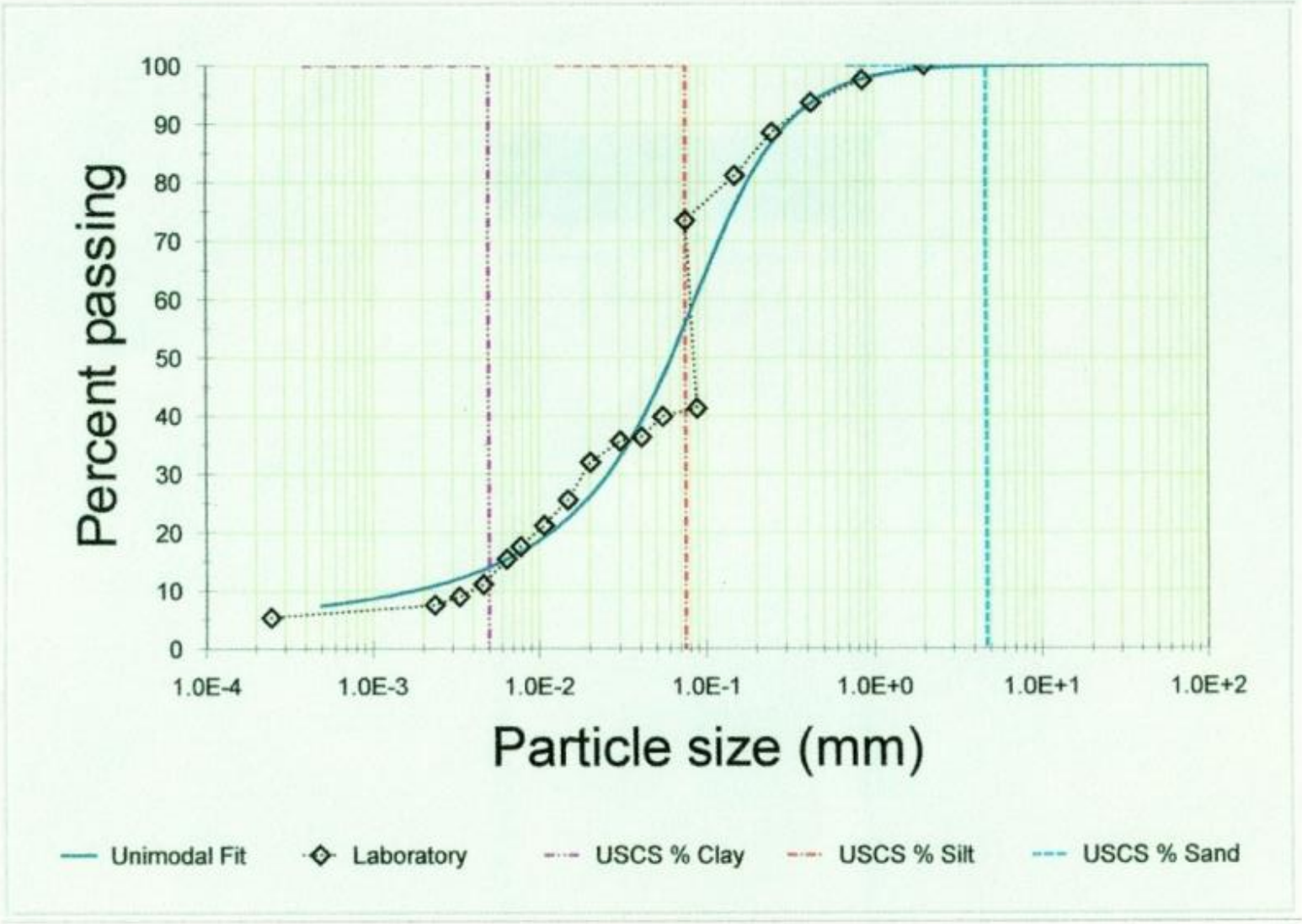

Figure 6.10 Grain size distribution curve from laboratory tests of colluvium from the Windjammer Landing Beach Resort Study Site fitted with Fredlund's Theoretical Curve

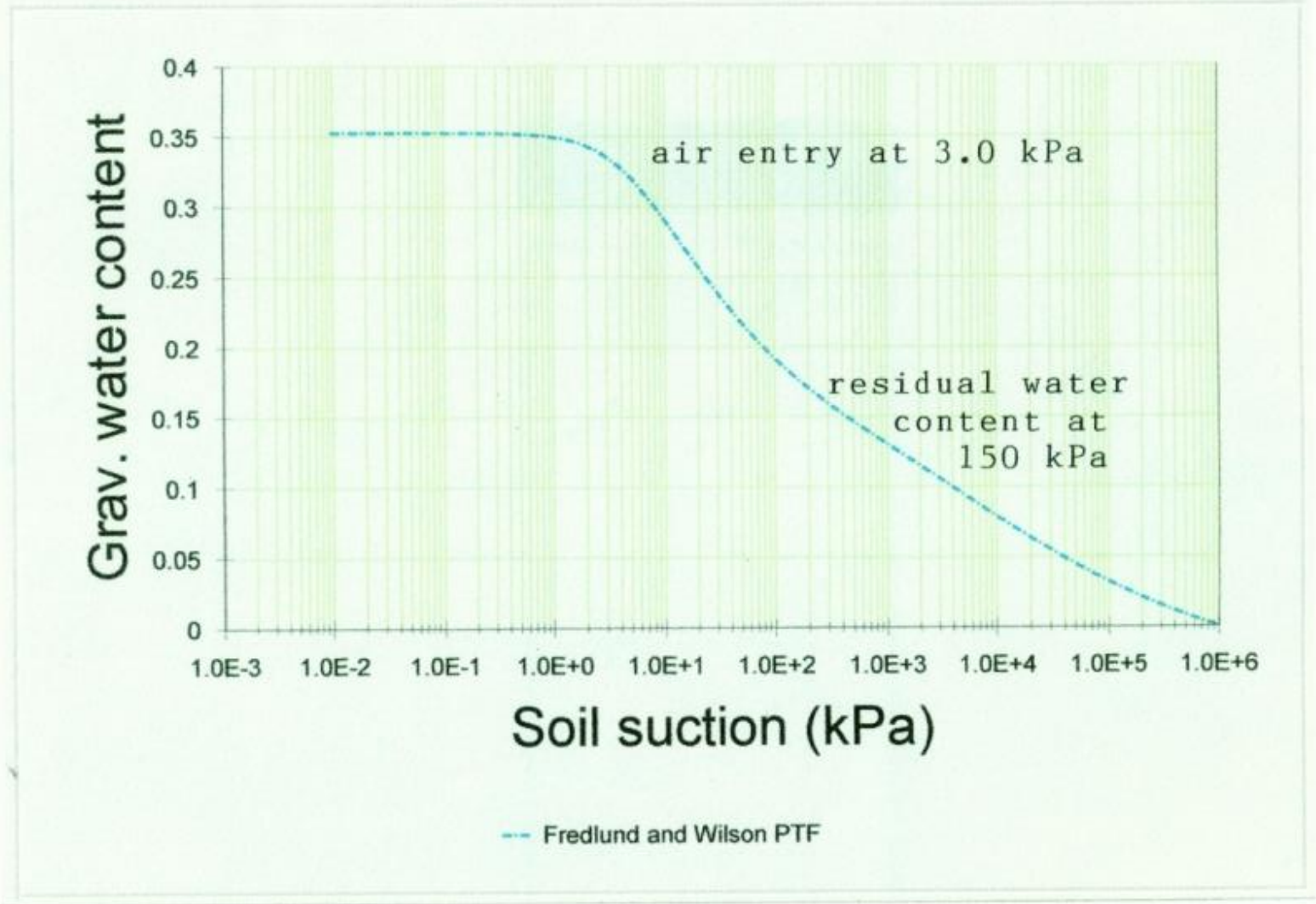

Figure 6.11 Soil-Water Characteristic Curve (SWCC) for colluvium from the Windjammer Landing Beach Resor Study Site

CHAPTER 7

Numerical Analysis of the Barre de L'isle and Windjammer Landing Beach Resort Landslide Study Sites

7.1 Introduction

In order to investigate the effects of rainfall-induced slope instability caused by infiltration into an unsaturated soil slope it is necessary to perform seepage analyses and slope stability analyses under variable climatic conditions. Both of the areas in this study experienced slope instabilities more than once during the wet season which usually occurs between the months of June to December in Saint Lucia. During this period, the heaviest annual rainfall on record has occurred and several hurricanes have been experienced.

This chapter presents a model of the results of the research study and shows how the rate of infiltration, rainfall intensities, and pore-water pressure variation affect the stability of the multi-layered residual soil and colluvial slopes under study. The objective of the numerical modeling is to show how quickly the slopes become saturated and unstable during rainstorms through transient seepage analyses using soil properties, site geometry and boundary conditions to compute the total hydraulic head at nodal points within the modeled cross-sections.

The methodology applied involved creating a saturated-unsaturated flow model for each site with applied boundary conditions and using these models, attempt to predict the pore-water pressure distribution with time during rainstorms and compare the results with actual field measurements. In addition, an assessment of the rate of the response of the pore-water pressures within the slopes to rainfall intensity and infiltration was also made. Finally, the application of the pore water pressures generated in the seepage analyses were used to examine the effect on the stability of the slopes.

The study investigated how variable rainfall patterns, infiltration rates and the existing soil parameters inter-relate to develop instabilities within a multi-layered slope composed of residual soil from parent andesite rock and a slope comprised of colluvium from weathered basalt rock. Also included in the analyses is how the effect of the groundwater response to rainfall contribute to the development of instabilities within the two slopes.

The seepage analyses and the slope stability analyses of the slopes at the two study sites were performed using the commercially available limit equilibrium-based computer software SEEP/W and SLOPE/W from GEO-SLOPE International Ltd of Calgary, Alberta, Canada (Geo-slope 2004). The conventional method of slices was employed to calculate the variation of the factor of safety in response to pore-water pressure variations due to rainfall patterns and groundwater level changes as observed during the monitoring of the field instrumentation. An attempt was made to identify any variable parameters that would influence the development of instabilities within a multi-layered residual soil slope from weathered andesite and a slope composed of colluvial material from weathered basalt, considering the different geological origin, history and composition of these two materials.

Since both the Barre de L'isle and the Windjammer Landing Beach Resort study sites are located on unstable slopes of previous landslide activity, a parametric study of the hydrological conditions that existed in the slopes prior to and during the time of slope failure are examined.

7.1.1 Use of SEEP/W and SLOPE/W in the Numerical Model

The numerical seepage model was developed using SEEP/W, a finite element code tailored for modeling groundwater seepage in soil and rock. SEEP/W utilizes soil properties, site geometry, and boundary conditions provided by the user to compute the total hydraulic head at nodal points within the modeled cross-section. Among other features, SEEP/W includes a graphical user interface, semi-automated mesh generation routines, iterative algorithms for solving unconfined flow problems, specialized boundary conditions (seepage faces etc.), capabilities for steady-state or transient analyses, and features for visualizing model predictions. The code also includes material nodes that allow tracking both saturated and unsaturated flow, including the transition in seepage characteristics for soils that become saturated or unsaturated during the problem simulation.

One (1) cross-section (Figure 6.2) through the slope was modeled with SEEP/W, and then was subsequently evaluated for slope stability analysis (Section 7.2.9). For the numerical analysis, the cross-section was sub-divided into a mesh of elements, consisting of first-order triangular (unstructured) finite elements. For seepage problems, where the primary unknown (hydraulic head) is a scalar quantity, first-order elements provide for efficient, effective modeling. Given appropriate hydraulic conductivity properties and applied boundary conditions, the finite element method (as implemented in SEEP/W code) was then used to simulate steady state and transient seepage across the mesh. The total hydraulic head is computed at each nodal location, from which pore water pressure and seepage gradients can be determined.

The stability of the slope was evaluated using limit equilibrium methods as implemented in the SLOPE/W software. Analyses were completed for static loading, steady state and transient seepage conditions. SLOPE/W is a special-purpose computer code designed to analyze the stability of earth slopes using two-dimensional, limit equilibrium methods. With SLOPE/W, the distribution of pore water pressures within the earth mass can be mapped directly from a SEEP/W solution. In this study, the pore water pressures were obtained from the SEEP/W model described above.

SLOPE/W incorporates various search routines to locate the critical slip surface. For the analyses presented in this thesis, the " Entrance and Exit " method was employed. The soil shear strength parameters from field and laboratory tests were used in the analysis. The stability analyses were performed using the Morgenstern and Price method with circular failure surfaces with optimization.

7.2 Description of the Barre de L'isle Slope for Numerical Analysis

7.2.1 Slope Geometry

The study area extended from the crest of the slope where tension cracks were first observed and includes the main roadway to the toe of the slide area at the active spring source. The slope is approximately 30.0 m high at the crest and is inclined at an overall angle of about 18^{o} (3H : 1V) in a north to south orientation. The areal extent of the failed slope from the crest to the toe is approximately 10 m in length and 77 m at its widest limits. The overall slope length used in the model was 115 m. Figure 6.2 shows a cross-section of the slope with instrumentation and is referred to in Section 6.2.3 of the thesis.

In order to conduct a numerical analysis on the effect of infiltration and seepage on the stability of a multi-layered soil slope it is first necessary to generate a finite element mesh that represents the slope under study. The length of the mesh must be sufficient to ensure that any boundary effects from the sides of the mesh are at a distance from the instrumentation where it will not affect the results of the analysis.

For this analysis, the slope is simplified by assuming that it consists of a residual soil deposit with a silty sand layer sandwiched in between the soil mass. The slope is therefore divided into three (3) material types i.e. clayey sandy silt (residual soil), silty sand and the weathered andesite bedrock. The residual soil is approximately 30.0 m thick at the crest and 7.0m at the toe of the slope.

The confined silty sand layer is approximately 2.0m thick at a depth of 9.0m below ground surface at the location of the instrumentation. Falling head permeability tests were performed to determine the saturated hydraulic conductivity of the silty sand and the clayey silt deposits. The silty sand layer is sandwiched between the clayey sandy silt (residual soil) which has a lower saturated hydraulic conductivity (k_{sat}). For this analysis, it was assumed that the silty sand layer extends throughout the length of the slope under study.

7.2.2 Groundwater Regime

Surface water infiltrates into the soil through the residual soil which has a saturated hydraulic conductivity (k_{sat}**)** of 9.0 x 10^{-5} m/sec and through the silty sand layer which has a greater saturated hydraulic conductivity (k_{sat}) of 1 x 10^{-3} m/sec. It was assumed that the silty sand layer is being recharged at a location upslope from the study area and groundwater is channeled through the silty sand confined aquifer and is discharged in an active spring at the toe of the slope at a rate of 20 litres per minute. The farmer at the site confirms that this spring source is productive both during the wet and dry seasons and is used for farm irrigation. This confirms that there is a recharge area upslope which has a high storage capacity.

Groundwater levels fluctuations were monitored and recorded periodically in the piezometer installed at the study site. The recorded data indicate that the groundwater level normally varied between 5.0 and 6.0m below ground surface and increased during rainfall periods. Piezometer readings were recorded as high as 0.5m below ground surface during rainstorms. For the numerical analysis the groundwater level was inclined parallel to the slope.

7.2.3 Volumetric Water Content

At the heart of of the numerical seepage analysis is the volumetric water content function (VWC function). This function describes the soils ability to store and release water. It is this property that makes a problem potentially transient. Under transient conditions, flow in does not equal flow out of the system. The difference is in the storage or release of water. Under steady state conditions flow in equals flow out and consequently there is no storage.

The volumetric water content used for the transient seepage analysis in the numerical model was 0.415 which was derived from grain size distribution curves from the residual soil fitted to Fredlund's theoretical curve using the commercial software
'SOIL VISION' 2009.

The volume-mass characteristics derived from the computed data residual soil layer to be composed of 13.6 % clay, 32.7 % silt and 53.7 % sand and a Plasticity Index of 35.0 %.

7.2.4 Infiltration Rate

The infiltration rate applied in the transient seepage analysis is 5.6×10^{-6} m/sec as measured in the field during a period of 488 mm of rainfall during one rainstorm on October 7, 2009 as mentioned in Section 5.2.2.6 of the thesis. This infiltrate rate could increase significantly during periods of greater rainfall intensity such as during hurricane 'TOMAS" on October 30, 2010 when 682 mm of rainfall was recorded over a 24 hour period. During that time period the inclinometer installed at the site sheared off at a depth of 12.0m due to accelerated ground movement on the slip surface which was triggered by the intensive rainfall. This occurance could be considered as a worst case scenario. This amount of deformation resulted in the development of tension cracks and some displacement in the pavement of the main road which caused some discomfort to motorists. The road was later resurfaced with an overlay of asphaltic concrete.

7.2.5 Design of the Finite Element Mesh

Meshing for seepage analysis is one of the three fundamental aspects of finite element modeling. The other two are defining boundary conditions and material properties. The two basic mesh patterns are structured and unstructured.

7.2.5.1 Structured Finite Element Mesh

Structured or quadrilateral meshing involves using triangular and rectangular regions to represent the model. The elements within the mesh are ordered in a consistent pattern.
In structured meshing a transition can be made from a fine mesh at the ground surface to a coarser mesh for region below the ground surface. Unstructured meshing does not allow this transition. An initial attempt was made to use a structured mesh pattern for the model in this analysis using a fine 4-noded quadrilaterals elements of 0.25m x 0.25m for the upper 3.0m at the ground surface and 0.5m x 0.5m for the remaining subsoil. Due to the large size of the model this produced a mesh with a very large number of nodes.

Since there is one finite element equation written at every node the computer demand to integrate the constitutive models, assemble the global matrices, factorize the equations, modify the equation for boundary conditions and finally solve the equation was huge.

In the solution for the two-dmentional transient seepage analysis, the SEEP/W software was extremely slow taking 17 hours to complete a one hour time step and would not converge during the iterative process. This resulted in changing the mesh design to an unstructured pattern.

7.2.5.2 Unstructured Finite Element Mesh and Boundary Conditions

The unstructured mesh divides the slope into four (4) segments. The upper and lower soil layers represents the residual soil. The intermediate layer is the silty sand material and the bedrock lies at the base of the lower residual soil layer. The overall slope gradient used appears to be typical of the slope and the bedrock gradient was simplified for the analysis. The finite element mesh shown in Figure 7.1 consists of a total of 4,215 triangular elements and 2,235 nodes. The figure also includes the initial groundwater condition and the location and variable depths of the tensiometers installed in the field. The residual soil and silty sand strata are also included.

7.2.6 'Steady State' Seepage Analysis

A 'steady state' seepage analysis was performed to establish the initial conditions in the slope. The initial groundwater level was established from piezometer readings. The left and right boundaries of the mesh were established as constant head boundaries below the water table and a zero flux boundary above the water table. The constant head boundary below the water table is equal to the initial groundwater elevation, i.e 34.0m on the left boundary of the mesh and 7.0 m on the right boundary. A zero flux boundary condition was assumed along the ground surface. A small surface flux boundary condition of 3.9×10^{-8} m/sec was applied to the model to represent the average daily rainfall recorded (3.4 mm/day) during the drought period of January to June, 2008.

The saturated hydraulic conductivity function, k_{sat}, for the residual soil and silty sand layer was defined over a reasonable suction range of 0.01kPa and 1000 kPa, to reflect the decrease in hydraulic conductivity as the soil becomes unsaturated. The saturated hydraulic conductivity used in the model for steady state seepage analysis of the residual soil and silty sand layer was 9×10^{-5} m/sec and 1×10^{-3} m/sec, respectively. Figure 7.2a and Figure 7.2b illustrate the hydraulic conductivity function graphs for the two materials.

For the residual soil in Figure 7.2a, air begins to enter the soil or start desaturation at about 0.4 kPa. In the silty sand layer air entry into the soil starts at 1.0 kPa as shown in Figure 7.2b.

SEEP/W contains an iterative scheme to solve the finite element equations by computing the total head at each node to determine the material hydraulic conductivity. The iterative process utilizes a repeated substitution technique in which the initial heads are used to define the material hydraulic conductivity which is updated in subsequent iterations using the computed head from the previous iteration.

The process continues until a convergence criteria is achieved. Convergence occurs when the computed solution does not change by more than a specified number of successive iterations. During the iterative process, SEEP/W calculates the residual which represents the total difference in the total head at all the nodes between two consecutive iterations. During the converging process, the residual will fluctuate and become smaller until there is no change in magnitude. The convergence graph for the 'Steady State' seepage analysis for the Barre de L'isle slope is shown in Figure 7.3. The residual converged after 32 iterations.

The initial groundwater level was recorded from the piezometer installed at the study site and was assumed to follow the slope inclination from the crest to the toe as shown in Figure 7.1. In the analysis, the groundwater table or the phreatic line is above the silty sand layer for most of the slope and converges at the top of the silty sand layer at the toe of the slope as a result of the high flow rate in the silty sand layer which reduces the pore-water pressure in the saturated residual soil above the silty sand layer.

Equipotential lines extend almost vertically from the saturated zone to the unsaturated zone above the phreatic line as shown in Figure 7.4. The change in the hydraulic head between equipotential lines indicates that water flows in both the saturated and unsaturated zones. There is capillary flow of water into the unsaturated zone which can be viewed under increased magnification. Thus the unsaturated zone contains water but the pressure is negative since the water is under tension. The reduced rate of flow in the unsaturated zone depends on the rate the hydraulic conductivity changes with respect to matric suction. The hydraulic head ranges from 8.0 m at the toe of the slope to 34.0 m at the crest.

The results of the 'steady state' seepage analysis establishes the initial conditions required for use in the transient seepage analysis i.e, the initial groundwater conditions and the initial hydraulic head. In this analysis a zero flux boundry condition was assigned to the ground suraface used and an infiltration rate of 3.9×10^{-8} m/sec was applied. The saturated hydraulic conductivity of the residual soil used was 9.0 x 10-5 m/sec and a value of 1×10^{-3} m/sec was assigned to the silty sand layer. In the slope geometry, it was assumed that the silty sand layer daylights at the crest of the slope and acts as a recharge zone for the silty sand layer. Figure 7.5 shows the seepage flow paths and flow rate vectors. Flow is generally directed toward the toe of the slope. The amount of water flowing into the unsaturated residual soil layer above the silty sand layer is minimal due to an increase in matric suction in the unsaturated zone.

The flow vectors in this soil layer can only be seen under magnification and are aligned parallel to the phreatic surface. It is evident that the highest flow concentration and velocity is in the saturated silty sand layer due to its greater saturated hydraulic conductivity of 1×10^{-3} m/sec.

At the crest of the slope the flow rate is reduced near the phreatic surface due to matric suction in the silty sand. The flow rate of water in the saturated residual soil below the silty sand layer is less than the flow rate in the silty sand layer due to the lower saturated hydraulic conductivity of 9.0×10^{-5} m/sec of the residual soil. The flow of water from the residual soil layer below the silty sand is directed upward and into the silty sand layer and at greater depths the flow is almost parallel to the phreatic surface.

The pore-water pressure heads at all of the nodes throughout the slope are shown in Figure 7.6. Pore water pressure heads are computed by subtracting the elevation head from the hydraulic head. Contour lines of equal pressure heads are also shown and range from 0.0 m at the phreatic surface to a negative value of -4.0 m in the unsaturated zone. In the saturated zone a maximum positive value of 22.0 m is shown at the base of the left side of the model.

The pore water pressure heads are parallel to the phreatic surface throughout the slope, an indication that the flow of water in the saturated and unsaturated zones is relatively parallel to the phreatic surface as indicated by the flow rate vectors.

Pore water pressures at all the nodes throught the slope are shown in Figure 7.7**.** Pore water pressures range from positive to negative with the phreatic surface representing the zero pressure contour. In the unsaturated zone above the phreatic surface the pore water pressure is at a maximum of -40 kPa due to the effect of matric suction in the capillary zone. In the saturated zone the pore water pressures increases with depth below the phreatic surface from 40 kPa to 220 kPa at the base of the residual soil at the lower left corner of the model.

The flow velocity vectors indicate the direction of flow and the quantity of flow occurring in the subsoils. The magnitude of the velocity flow is depicted in the size and length of the flow vectors. Figure 7.8 shows the flow **v**elocity vectors throughout the slope. The highest flow rate of 1×10^{-4} m/sec is occurring in the silty sand layer because of the higher saturated hydraulic conductivity than the surrounding residual soil.
The magnitude and concentration of the flow velocity vectors are greater in the silty sand layer than in the residual soil. The flow rate of water in the unsaturated residual soil above the phreatic surface is greatly reduced to 1×10^{-12} m/sec due to high matric suction. All flow is finally directed toward the toe of the slope.

The contours for gradient in the slope are shown in Figure 7.9. Gradient varies throughtout the slope with the highest of 0.45 at the crest and lower gradients of 0.2 at the midpoint of the slope. An exit gradient of 0.3 at the toe of the slope and a high gradient of 0.45 at the crest would tend to indicate that the slope is of great concern for slope instability. This would depend, however, on whether there is also high hydraulic conductivity in those areas of the slope.

Figure 7.10 shows the hydraulic conductivity throughout the slope. The hydraulic conductivity is consistantly low at 1×10^{-10} m/sec and 1×10^{-12} m/sec for the surficial residual soil layer because of the high matric suction near the ground surface. At the crest of the slope where the gradient is high at 0.45 for the silty sand layer, the hydraulic conductivity is high at 1×10^{-4} m/sec and the flow rate of water is high in this area as indicated by the larger flow rate vectors. This hydraulic conductivity value is consistent throughout the silty sand layer.

The effects of a flux boundary on the slope during steady state infiltration was examined to assess the seepage conditions in the slope during the dry season. A small surface flux boundary condition of 3.4 mm/day (3.9×10^{-8} m/sec) was applied to the model to represent the average daily rainfall recorded during the drought period of January to June 2008.

This was used as a worst case scenario to examine the seepage conditions in the ground during that period since the discharge at the spring at the toe of the slope remained active throughtout the drought period but at a lower flow rate.

Figure 7.11 shows the flow paths which can be compared with that of Figure 7.5 of zero surface flux. The infiltration rate of 3.9×10^{-8} m/sec is so small that it does not cause any rise in the phreatic surface and there is a small increase in the pore water pressure in the unsaturated zone above the phreatic surface. There is no flow of water in the unsaturated zone. This is expected because in the dry season one would anticipate lowering of the phreatic surface due to evaporation and increased matric suction in the unsaturated zone. Also, the silty sand layer continues to be recharged from upslope at a slower rate and the discharge into the spring at the toe of the slope is reduced. Below the silty sand layer the flow paths in the residual soil are identical in both Figure 7.5 and Figure 7.11.

In Figure 7.12 the equipotential lines are shown to be near vertical in the saturated residual soil below the silty sand layer similar to that observed in Figure 7.4 with the zero surface flux condition. In Figure 7.4 the equipotential lines are near vertical in both the saturated and unsaturated zones in the slope.

In Figure 7.12, however, the small increase in the pore-water pressure in the unsaturated zone with the applied surface flux causes the equipotential lines above the phreatic surface to spread out horizontally and become almost parallel to each other and are aligned parallel to the direction of flow. This occurs because flow is in response to a total head gradient and the gradient is steepest between two parallel equipotential lines.

The pore-water pressure heads below the phreatic surface are shown in Figure 7.13 and do not change with the applied surface flux when compared to the zero surface flux in Figure 7.6. Contour lines of equal pressure head range from zero at the groundwater table to a positive value of 22 kPa at the base of the model. In the capillary zone above the phreatic surface, the soil is saturated by the infiltration but the pressure is negative since water is under tension.

7.2.7 Transient Seepage Analysis

Having carried out a ‘steady state’ seepage analysis using SEEP/W, a transient seepage analysis was performed to show the changes taking place in the saturated and unsaturated areas of the slope with time and the response of the phreatic surface and the hydraulic head to an average daily rainfall of 78 mm for the period of September 1, 2009 to October 10, 2009 (40 days). It was assumed that 44% of this daily rainfall or 34 mm/day infiltrated the soil and this assumption was based on the results of the field run-off/infiltration test outlined in Section 5.2.2.6. This infiltration rate converts to 3.9×10^{-7} m/sec.

When this infiltration rate of 3.9×10^{-7} m/sec was used as a surface boundary flux in the transient numerical analysis simulation, SEEP/W was unable to achieve numerical convergence for the residual after 96 iterations and the analysis was terminated. It was then decided that changing the surface boundary flux by one order of magnitude to 5.6×10^{-6} m/sec (which is the infiltration rate measured in the field) would enable the analysis to be completed.

The surface boundary was specified as a unit flux boundary with an applied surface flux of 5.6×10^{-6} m/sec which is equivalent to 20 mm of rainfall infiltration measured over a 1-hour period during the run-off/infiltration field test as detailed in Section 5.2.2.6. The unit flux was applied over the entire surface of the slope. The remaining boundary conditions applied were similar to that for the ' Steady State' seepage analysis in Section 7.2.5.2.1. The 'no flow' boundary conditions at the sides of the mesh allowed the groundwater table to fluctuate freely in response to rainfall. The soil-water characteristic curve shown in Figure 6.8 was used in the numerical analysis. A volumetric water content of 0.415 was applied in the modeling.

A two-dimensional transient seepage model was used for the slope with a maximum of 150 iterations. The analysis was run using a convergence criteria with the tolerance of vector norms between two successive iterations set at 0.01.

The rate of change of the hydraulic conductivity between each node was set at 1.1 of order of magnitude. The maximum change in the hydraulic conductivity from one iteration to another was set at 1.0 of order of magnitude and a minimum order of 1×10^{-4} m/sec was used. No ponding of water was allowed to occur on the ground surface. An incremental time sequence of 48 hours (172,800 seconds) was used with a total of 20 time steps starting at an elapsed time of zero and saving data from Step 1. The objective was to determine what changes in pore-water pressures are occurring in the slope during the 40 day period of rainfall.

Three major landslides occurred at the study site on the Barre de L'isle ridge during the months July 2005, October 11, 2008 and October 31, 2010. All of the landslides occurred during or immediately following periods of intensive rainfall of 269 mm, 389 mm and 682 mm, respectively over 24 hour duration as reported by the meterological unit of the Government of Saint Lucia.

Anderson and Kemp (1985) reported saturated hydraulic conductivity values ranging between 1×10^{-5} m/sec and 1×10^{-8} m/sec for the residual soil in their study of various sites on the Barre de L'isle ridge as reported in Section 4.4.2.2.

The saturated hydraulic conductivity value of 9.0×10^{-5} m/sec for the residual soil was measured in an insitu falling head field test carried out at the study site. This value is greater than the applied surface flux of 5.6×10^{-6} m/sec used in this analysis as required for simulation in SEEP/W. The infiltration rate must always be less than the saturated hydraulic conductivity for SEEP/W simulation. If the specified per unit area flux rate is higher than k_{sat}, the solution will usually indicate positive pore water pressure development on the ground surface. Water will need to pond on the ground surface to allow the specified flux to enter the ground. The saturated hydraulic conductivity must always be considered when applying ground surface flux rates.The saturated hydraulic conductivity measured for the silty sand layer in a falling head test was 1×10^{-3} m/sec.

It order to assess the sensitivity of changing the saturated hydraulic conductivity k_{sat}, with an applied surface flux boundary condition, ksat values were adjusted in three trial applications to determine the effect of varying the saturated hydraulic conductivity to the applied surface flux.

The objective here is to attempt to predict the pore water pressure variation with time and to compare the results with the actual field data from the tensiometers installed at the study site. It should be kept in mind that the three major ground deformations that occurred at the Barre de L'isle study site as mentioned above occurred during or immediately following a 24-hour period of intensive rainfall. However, there is no available slope inclinometer data for correlation for the periods during which these movements actually occurred.

A review of the response of the pore water pressure in the residual soil to the antecedent and main event rainfall as recorded in the piezometer at the study site is warranted here. Reference is made to the graphs of groundwater levels response to rainfall at the site during the study period as shown in Figure 6.1 to Figure 6.3 in Chapter 6 of the thesis.

The main event of 654 mm of continuous rainfall recorded in the rain gauge at the site on September 3, 2009 was preceded by two days of 174 mm and 106 mm of rainfall on September 1 and 2, 2009 respectively. The response of the groundwater level in the piezometer for the antecedent rainfall was negligible (0.1mm). The initial groundwater level in the piezometer prior to the start of the 654 mm rainfall was 6.5m below existing ground surface.

At the end of the 24-hour rainstorm the groundwater level was recorded at 4.5m below ground surface, which indicated that there was an increase of 2.0m of head in the piezometer at the end of the rainstorm. Figure 7.13a contains a model of the rainfall infiltration and wetting front advance in the residual soil and the increase in pressure head of 2.0m in the standpipe piezometer installed in the silty sand layer during the 654 mm continuous 24-hour rainfall event on September 3, 2009.

A main event rainfall of 488 mm was measured in the rain gauge on October 7, 2009 followed by 332 mm of rainfall on October 8, 2009. The antecedent rainfall was 138 mm. The response of the groundwater level in the piezometer to the antecedent rainfall was negative. For the main event and the follow up rainfall the groundwater level was measured and was found to increase by 0.7m over a 48-hour period.

The rainfall for November 4, 2009 was measured at 330 mm over a 24-hour period. The antecedent rainfall for November 2 and 3, 2009 was 134 mm and 140 mm, respectively. The antecedent rainfall caused an increase of 1.1m in the groundwater level as measured in the piezometer. For the main rainfall event an increase of 2.0 m in the groundwater level was measured.

The effect of the antecedent rainfall on slope instability was included in this study and is included in the average daily rainfall of 78 mm used in the analysis. It has been proven by many researchers (Rahardjo et al, 2001) that the antecedent rainfall plays a major role in landslide occurrence by increasing the pore water pressure in the ground prior to the main rainfall event.

MODEL No.1

For Model No. 1 the saturated hydraulic conductivity, k_{sat} of the residual soil was maintained at 9.0×10^{-5} m/sec and the saturated hydraulic conductivity, k_{sat} of the silty sand layer was increased by one order of magnitude to 1×10^{-3} m/sec. The infiltration rate was kept at 5.6×10^{-6} m/sec.

SEEP /W has the capability of using the specified initial heads to define the material properties and by repeated substitution during the iterative process the material properties are updated in subsequent iterations using the computed head from the previous iteration. Full convergence of the residual was achieved after 96 iterations as shown in Figure 7.14.

Figure 7.15a and Figure 7.15b show the Volumetric Water Content Function Graphs for the residual soil and the silty sand layer, respectively.

The function graphs for the residual soil and the silty sand layer in Figure 7.15a and Figure 7.15b indicate that air will begin to enter and desaturate the soil at about 0.5 kPa for both soils.

During the transient process, infiltration results in a continuous change in flow condition and the transient analysis of seepage is strongly influenced by conditions in the unsaturated zone. The applied surface boundary flux causes the inflow of water to advance downwards through the residual soil causing an increase in the degree of saturation of the residual soil and an increase in the pore water pressure. Movement of water continues downward through the residual soil until it merges with the initial phreatic surface.

At a time assumed to be equal to zero, water begins to infiltrate vertically downward through the overlying residual soil but has not yet reached the water table to cause any increase in the water level. Perched water tables were formed within the residual soil within the next few days and after 4 days (time step 2) of rainfall, the phreatic surface is raised to the level shown in Figure 7.16. For subsequent time steps, for example No.15 and No. 20 as shown in Figure 7.17, there is a very small increase in the level of the phreatic surface because the silty sand layer is so permeable that it carries away essentially all the infiltration. However, during a heavy rainstorm, if the infiltration rate exceeds the discharge capability or hydraulic conductivity of the silty sand layer it is predicted that there will be a back-up or 'overcharge' of inflow into the silty sand layer resulting in a rapid rise in the phreatic surface possibly above the level of the ground surface and an increase in pore water pressures which may trigger instability in the slope.

During antecedent rainfall events when the infiltration rate is nominal, the silty sand layer provides a drainage path for groundwater, thereby controlling any excess pore water pressure generation and there is no rise in the phreatic surface. Infiltration above the raised phreatic surface is vertical into the residual soil and silty sand layer in the area near the crest of the slope.

Further downslope infiltration is also vertical into the residual soil. The flow rate above the phreatic surface is less than below the phreatic surface as indicated by the greater magnitude of the flow rate vectors, due to high matric suction which impedes infiltration.

The flow rate is increased in the residual soil below the phreatic surface and the direction of flow is almost parallel to the phreatic surface, but with a small dip toward the silty sand layer. This occurs because of the greater hydraulic conductivity of the silty sand layer which allows increased inflow of water from the surrounding residual soil.

The silty sand layer is so pervious that it carries away almost all of the infiltration. Flow is parallel to the slope and is directed toward the toe of the slope where it discharges into a spring at the ground surface. The flow rate vectors are of greater magnitude in the silty sand layer than that observed in the residual soil above or below the raised phreatic surface.

In the upper left side of the model, flow in the residual soil below the silty sand layer is directed upward into the silty sand layer where flow is increased as indicated in the increased magnitude of the flow rate vectors. The flow in the residual soil at greater depths below the silty sand layer is parallel to the slope inclination and is directed toward the toe of the slope.

The equipotential lines extend almost vertical in the saturated zone from the base of the model to the silty sand layer where they curve slightly to the right up to the raised phreatic surface as shown in Figure 7.18. Infiltration caused a rise in the phreatic surface and also results in an increase in the pore water pressure in the unsaturated zone with time. The equipotential lines advance into the unsaturated zone where water is in tension and is aligned almost parallel to the phreatic surface.

Contour lines of equal pressure heads ranging from zero at the raised phreatic surface to 22.0m at the base of the model are shown in Figure 7.19. The contour lines are parallel to the phreatic surface from the crest to the toe of the slope as indicated by the flow vectors.

During the transient process infiltration results in raising the phreatic surface thereby increasing the pore water pressure in the previously unsaturated zone. Above the raised phreatic surface water is held in tension initially then the wetting front advances until it meets the phreatic surface causing it to rise above its initial position. In Figure 7.20 the pore water pressure ranges from zero at the raised phreatic surface to 220 kPa at the base of the model.

Infiltration resulted in an increase in the flow velocity in the saturated and unsaturated zones by two to six orders of magnitude as shown in Figure 7.21 when compared to Figure 7.8 for the steady state condition**.** Near the crest of the slope the difference in velocity is six orders of magnitude in the unsaturated zone and further downslope the velocity is greater by five orders of magnitude.

At the toe of the slope the velocity is increased by three orders of magnitude in the unsaturated zone. The flow velocity in the silty sand layer is the same at 1×10^{-4} m/sec for both the steady state and the transient conditions.

The exit gradient in the silty sand layer for the transient state is one order of magnitude greater than the exit gradient for the steady state condition in response to infiltration as shown in Figure 7.9 and Figure 7.22. The hydraulic gradient in the unsaturated zone is as high as unity during the transient process compared to a maximum of 0.45 for the steady state condition. In the saturated zone below the silty sand layer the hydraulic gradient is somewhat lower at 0.2 for the transient compared to 0.35 for the steady state condition.

The saturated hydraulic conductivity of the residual soil above the phreatic surface varies from 3.16×10^{-7} m/sec to 3.16×10^{-8} m/sec as illustrated in Figure 7.23 and is controlled by the high suction present in the soil. The rate of infiltration into the residual soil is controlled the amount of negative pore water pressure or suction present. As the soil becomes saturated by infiltration matric suction is reduced and water flows easily through the residual soil. This results in an increase in the hydraulic conductivity as compared to the steady state condition in Figure 7.10. In the silty sand layer the saturated hydraulic conductivity is consistent over time at 1×10^{-3} m/sec. Below the silty sand layer the saturated hydraulic conductivity is consistent at 1×10^{-4} m/sec.

The volumetric water content contours are presented in Figure 7.24. At the crest of the slope the volumetric water content ranges from 0.25 to 0.35. Further downslope the volumetric water content is lower between 0.2 and 0.3.

7.2.8 Review of The Results of the Transient Seepage Analysis Barre de l'isle Study Site

7.2.8.1 Variation in Total Head in the Residual Soil at the Ground Surface and at 1.5m depth

During the transient process, infiltration results in an increase in the pore water pressure in the residual soil near the ground surface which in turn causes changes in the total head as controlled by matric suction. The changes in the total head as predicted in the model were monitored from the nodes located at the ground surface and at a depth of 1.5m in the slope at the location of the tensiometers installed at variable depths. The graphs in Figure 7.25 represent the changes taking place in the total head during the transient process over a period of 4 days when the phreatic surface rose to a final steady state condition.

Figure 7.26 contains graphs that show the changes in pore water pressure at the ground surface and up to 3.0m depth during the transient process. At node 1666 the total head decreased from 22.2m at the commencement of the rainfall event to 21.7m after 4 days of rainfall during which time the phreatic surface rose to a steady state condition. At the start of the rainfall event water ponded at the ground surface initially and a superficial head was formed and with time the water slowly infiltrated the residual soil as air was removed from the pores within the soil.

The hydraulic conductivity of an unsaturated residual soil is lower than when it is in a saturated state. Since water flows more freely through a saturated soil than through an unsaturated soil the wetting front advanced into the soil and the total head at the ground surface decreased until the initial phreatic surface was encountered.

This decrease in total head at the ground surface from the start of the rainfall event to the end can also be observed occurring at nodes 1699, 1731 and 1760 in Figure 7.26**.** At a depth of 1.5m there is an increase in total head from time zero to the end of the rainfall event, i.e. 4 days as shown at nodes 1667 and 1722. At node 1667 there is an increase in total head of 1.1m from the start of the rainfall to the end of the event. At node 1722 the increase in total head is 0.7m.

The increase in total head at 1.5m depth during the established time period of 4 days is predicted in the model since above the raised phreatic surface capillary water is held in tension and is not susceptible to evaporation at that depth compared to water held in tension near the ground surface which is susceptible to atmospheric conditions.

More water is held in tension near the phreatic surface than at the ground surface as indicated by the increased magnitude of the flow vectors near the phreatic surface in the unsaturated zone. Infiltration results in the advancement of the wetting front downwards to the phreatic surface causing an increase in total head in time during the transient process.

The difference in total head at the ground surface at node 1666 and at 1.5m depth at node 1667 at the start of the rainfall is 2.0m. This initial difference is considered to be high and results in a high hydraulic gradient which generates a high infiltration rate. At the end of the rainfall event the difference between the total head at nodes 1666 and 1667 is less at 0.4m. Infiltration results in a decrease in the difference in total head at the nodes as the soil becomes saturated and this results in a decrease in hydraulic gradient and the infiltration rate is reduced.

At nodes 1699 and 1722, located at the ground surface and at 1.5m depth respectively, a similar pattern is observed. The initial difference in total head is 1.9m and at the end of the rainfall event the difference in total head after 4 days of rainfall is 0.8m. Thus, at the ground surface and at shallow depths, the difference in total head at the start of the rainfall event is high resulting in a high hydraulic gradient which in turn generates rapid infiltration into the soil. As the soil becomes saturated by infiltration, the difference in total head decreases at depth and the hydraulic gradient is reduced resulting in a reduction in the infiltration rate into the residual soil.

7.2.8.2 Variation in the Pore Water Pressure During the Transient Process

The applied surface boundary flux of 5.6×10^{-6} m/sec in the transient process was measured as the infiltration rate into the residual soil during a heavy rainfall event of 488mm on October 7, 2009. Details of the results of the field instrumentation monitoring of the tensiometers installed at the site for that day are presented in the graphs in Figure 6.1 to Figure 6.3.

Pore water pressure readings from the tensiometers for Rows A, B and C for that rainfall event are also illustrated in Figure 6.3 to Figure 6.5. The layout of the tensiometers is shown in Figure 4.2. Row A is located at the top of the drawing and Rows B and C are in the middle and at the bottom of the drawing respectively. The tensiometers in Row A were the most responsive to rainfall events.

The antecedent rainfall from September 29, 2009 to October 5, 2009 averaged about 6.0mm. The pore water pressure measurements in Row A at depths of 0.5m, 0.9m, 1.5m, 2.1m, and 3.0m were -9.0 kPa, -11.0 kPa, -11.0 kPa, -20.0 kPa, and -20.0 kPa respectively. On October 6, 2009 there was a rainfall event of 138.0mm followed by the main event of 488.0mm on October 7, 2009.

For the antecedent rainfall of October 6 there was an increase in the pore water pressure in the tensiometers at all depths in Rows A and B and to a lesser degree in Row C as shown in Figure 6.1 to Figure 6.3.

For the main event on October 7 there was quick response to the rainfall which resulted in an increase in the pore water pressure at all depths in Row A. Pore water pressure readings of -2.0 kPa, -2.0 kPa, -2.0 kPa, -3.0 kpa, and -4.0 kPa were recorded in the tensiometers at depths of 0.5m, 0.9m, 1.5m, 2.1m, and 3.0m respectively.

When a surface boundary flux of 5.6×10^{-6} m/sec was applied in the finite element model the predicted pore water pressure at the nodes at the location of the field instrumentation there is a scatter in the results as presented in Figure 7.26. There are no nodes for pore water pressure prediction in the numerical model at depths of 0.5m and 0.9m for comparison with the field measurements.

The predicted pore water pressure at node 1667 at 1.5m increases compared to the field measurement at the end of the rainfall event. At node 1722 the predicted pore water pressure shows a small decrease at 1.5m compared to field measurements. The predicted pore water pressure at node 1798 in the numerical model shows an increase at 1.5m compared to the field measurements. The numerical model is not capable of including the effects of the evaporation rate in the analysis which would affect the pore water pressure measurements in the field. Also, the presents of trees and agricultural plants in the vicinity of the study site would affect the pore water pressure in the soil through transpiration.

At a depth of 2.1m the pore water pressure at node 1744 is considerably higher in the model compared to the pore water pressure from the field measurements. At node 1774 the pattern is the same with the changes at 2.1m depth being quite obvious.

The predicted pore water pressure at 3.0m are consistently higher than that measured in the field at nodes 1670, 1694 and 1720. There is very little difference between the changes in pore water pressure at node 1670 and at node 1720 whereas at node 1694 the difference is much smaller.

The graphs showing the changes taking place in the volumetric water content during the transient process are presented in Figure 7.27.

7.2.9 Slope Stability Analysis

7.2.9.1 Introduction

There is currently very limited data available on the shear strength parameters for the residual soils on the Barre de L'isle ridge. Anderson and Kemp (1980) reported laboratory test results during their investigation as presented in Table 5.1.1. This author also conducted limited laboratory tests on soil samples recovered during this investigation the results of which are discussed in Section 5.2.1.7.

This section of the thesis examines the effect of climatic conditions on the pore water pressures in the multilayered residual soil slope during infiltration and the resulting effect on the stability of the slope. Finally, the results of the analysis show how quickly the unsaturated residual soils become saturated during a rainstorm causing a decrease in the factor of safety of the slope and how the presence of the silty sand layer contributes to the rapid build up of pore water pressures during a rainstorm from a recharge zone at the ground surface near the crest of the slope.

7.2.9.2 Back Analysis of the Barre de L'Isle Slope

For the back analysis of the slope, an effective angle of internal friction for the residual soil and the silty sand of 23 degrees was kept fixed and the effective cohesion was adjusted based on this author's experience with the local soils to expedite the time involved in back analysis. The critical slip surface is located at a depth of 12.0m below ground surface as indicated by the field instrumentation.

The back-analysis procedure resulted in a value of 2.0 kPa being derived for the effective cohesion required to achieve a factor of safety of unity as presented in Figure 7.28.
he residual shear strength value used is in relatively close agreement with the residual shear strength of the soil samples tested in the laboratory by Anderson and Kemp (1980) and by this author as outlined in Table 5.1.1 and in Section 5.2.1.7.

The silty sand was assigned a value of zero for the effective cohesion.The unit weight used for the residual soil and silty sand layer was kept the same at 18.0 kN/m^3. The phreatic surface was assumed to be at a depth of 0.5m below ground surface to represent a worst case scenario for a period of very heavy rainfall.

7.2.9.3 Slope Stability Analysis of the Barre de L'Isle Slope During the Transient Process

The factor of safety of the slope was analysed during the transient process over a 15 day period of 20 mm/hour or 5.6×10^{-6}m/sec of infiltration to evaluate the effect of rainfall on the factor of safety of the slope and the development of instabilities within the slope. The critical slip surface is at a depth of 12.0m as identified by the slope inclinometer installed at the site during the study period. The initial factor of safety of the slope prior to the rainfall event at a time equal to zero was 1.41 as shown in Figure 7.29. After a period of 2 days of rainfall with an infiltration rate of 5.6×10^{-6} m/sec, a perched water table begins to develop in the unsaturated residual soil as the wetting front advances downward toward the phreatic surface.

At this time the phreatic surface begins to rise as shown in Figure 7.30 and the factor of safety of the slope is reduced to 1.32. Figure 7.31 shows further increase of the phreatic surface after 4 days of rainfall as infiltration increases and the wetting front meets the phreatic surface causing it to rise to the grouind surface near the toe of the upper slope. Further downslope the raised phreatic surface is about 1.0m -2.5m below the ground surface. The factor of safety of the slope is further reduced to 1.14. Figure 7.32 shows some fluctuation of the factor of safety of the slope to 1.17 after 6 days of rainfall probably the result of drainage and a some pore water pressure dissipation within the silty sand layer.

The factor of safety of the slope is slightly increased to 1.17 as a result of drainage of the residual soil and a new wetting front is established near the surface as infiltration continues and the excess pore water pressure in the residual soil is reduced by drainage through the silty sand layer which has a much higher saturafed hydraulic conductivity of 1×10^{-3} m/sec compared to a saturated hydraulic conductivity of 9.0×10^{-5} m/sec for the residual soil.

After 8 days of rainfall the factor of safety of the slope is reduced as there is an increase of total head and pore water pressure as infiltration continues. As a result the factor of safety of the slope is reduced to 1.16 as the process of infiltration and drainage through the silty sand layer continues. This fluctuation of the factor of safety of the slope caused by infiltration and drainage of the residual soil can be visualized in Figure 7.33 and Figure 7.34.

As the infiltration rate of 5.6×10^{-6} m/sec continues it can be seen from Table 7.1 that after 4 days of rainfall distribution the factor of safety of the slope fluctuates between 1.16 and 1.17 for the rest of the time period of 15 days. At this time the 20 mm/hour rainfall does not affect the stability of the slope because of the steady drainage of the slope which results in some sort of balance of the inflow and outflow of water from the slope.

Table 7.1. Summary of the Factor of Safety of the Barre de L'isle Slope during the Transient Process

Time Step No.	Time (Days)	Factor of Safety
Initial	0	1.41
1	2.0	1.32
2	4.0	1.14
3	6.0	1.17
4	8.0	1.16
5	10.0	1.17
6	12.0	1.16
7	14.0	1.17
8	16.0	1.16
9	18.0	1.17
10	20.0	1.16
11	22.0	1.17
12	24.0	1.16
13	26.0	1.17
14	28.0	1.16
15	30.0	1.16

The predicted results of the model which indicates that the factor of safety of the slope was not reduced to unity or failure of the slope is in agreement to what was observed in the field during the 488mm rainfall event of October 7, 2009. For this rainfall event there were no noticeable signs of slope deformation taking place at the ground surface or of any tension cracks developing on the surface of the slope.

The results of the stability analysis implies that it would require a rainfall event of great intensity to occur resulting in an increased infiltration rate that would result in a build up of excess pore water pressure within the slope to induce slope failure.

7.3 Description of the Windjammer Landing Beach Resort Slope for Numerical Analysis

7.3.1 Slope Geometry

The overall slope at the Windjammer Landing Resort site is approximately 90.0 m long from the toe to Villa 43c at the crest. The estimated surcharge of the Villa on the slope is about 40.0 kPa. The slide area extends 30.0m downslope from Villa 43c to a retaining wall at the main access road to the resort. The landslide area is approximately 15.0 m wide and dips at 18^{o} to the west. The overall height of the slope is approximately 17.0m from the retaining wall to the crest. Figure 6.9 contains a cross-section of the slope with instrumentation.

The subsoil stratigraphy consist of colluvium overlying highly weathered basalt bedrock. The colluvium layer is about 3.0m thick and consists of a clayey, sandy silt deposit containing weathered rock fragments of variable sizes.

7.3.2 Groundwater Regime

The groundwater regime was monitored with two standpipe piezometers installed in the colluvium at the crest of the slope and at the retaining wall. Twelve tensiometers were installed at variable depths of 0.5m, 1.0m, 1.6m, and 2.3m to monitor the pore water pressure distribution and matric suction measurements within the slope.

The groundwater level at the site ranged from 1.3m at the crest of the slope to 3.0m at the toe near the retaining wall. The location of the standpipe piezometers and the tensiometers are shown in Figure 4.47.

7.3.3 Volumetric Water Content

The volumetric water content used in the numerical analysis for the colluvium was 0.404 which was calculated from the grainsize distribution curves using the commercial software ‘SOILVISION’. The colluvium is composed of 32.6 % sand, 64.0 % silt and 3.4 % clay with a Plasticity Index of 30.0%.

7.3.4 Design of the Finite Element Mesh

A structured finite element mesh was designed for the Windjammer Landing Resort slope using SEEP/W as shown in Figure 7.35. The mesh divides the slope into two distinct materials, namely colluvium and the highly weathered basalt bedrock. The surface boundary is parallel to the base boundary at the same gradient. During the field investigation it was found that the surface gradient is fairly consistant with that of the base boundary throughtout the slope. The finite element mesh consists of 4-noded quadrilateral elements of 0.5m by 0.5m dimensions which was found suitable for the shallow colluvium layer.

This selected size for the mesh would allow a faster solution for each simulation. The mesh consists of a total of 1,800 elements and 1,991 nodes. The initial groundwater level and pore water pressures from the piezometers installed at the site were identified by constant head boundaries of 33.5 m and 8.5 m respectively at the left and right sides of the mesh. The region above the groundwater table at the left and right sides and at the base of the mesh were defined as 'no flow' boundary conditions. A zero flux boundary was assigned along the ground surface and no ponding of water was allowed at the ground surface.

7.3.5 'Steady State' Seepage Analysis

An initial steady state seepage analysis was performed for the slope to establish the existing pore water pressures and total head conditions to be used in the transient seepage analysis. The saturated hydraulic conductivity, $k_{sat,}$ used for the colluvium in the steady state analysis was 6.3×10^{-5} m/sec which was measured in the field in a falling head permeability test performed in borehole BH08-SP-13 at the site. Figure 7.36a shows the hydraulic conductivity graph for the colluvium. The graph indicates that air begins to desaturate the colluvium at 0.9 kPa. It would require an excess of 1,000 kPa of suction to completely desaturate the colluvium. Figure 7.36b is a graph of the volumetric water content for the colluvium. Figure 7.37 contains the convergence graph for the colluvium during the iterative process. The residual converges after 73 iterations.

Equipotential lines of total head extend vertical from the saturated zone to the unsaturated zone of the colluvium as shown in Figure 7.38. This indicates that there is capillary water held in tension in the unsaturated zone. The total hydraulic head ranges from 10.0 m at the toe of the slope to 32.0m at the crest.

The contours of pore water pressure are presented in Figure 7.39. Pore water pressures range from -10.0 kPa in the unsaturated zone caused by matric suction to 35.0 kPa at the base of the colluvium layer. Flow path contours run parallel to the slope inclination and the phreatic surface in both the saturated and unsaturated zones and are directed downslope as shown in Figure 7.40. The pore water pressure heads in the colluvium range from -1.0m in the unsaturated zone as a result of matric suction to 3.5m at the base of the colluvium layer as shown in Figure 7.41. The flow rate vectors and hydraulic gradient for the colluvium are presented in Figure 7.42. The greater volume of flow is in the colluvium as indicated by the magnitude of the flow vectors. Above the phreatic surface the flow vectors are smaller for the capillary flow.

The contours for the hydraulic gradient in the slope are shown to range from 0.2 to 0.3 at the crest and at the toe of the slope. The high gradients at the crest and at the toe indicate that the slope is of great concern in regards to stability. The flow velocity vectors in Figure 7.43 show the direction and quantity of flow in the colluvium. At the crest of the slope the flow is lower at 3.16×10^{-9} m/sec than at 1×10^{-8} m/sec at the toe. All flow is directed toward the toe of the slope.

The saturated hydraulic conductivity of the colluvium in the unsaturated zone above the phreatic surface varies from 3.16×10^{-6} m/sec to 1×10^{-8} m/sec as shown in Figure 7.44. The hydraulic conductivity of the colluvium in the saturated zone is consistant at 1×10^{-4} m/sec. The flow rate of water is highest in the saturated zone as shown by the magnitude of the flow vectors.

7.3.6 Transient Seepage Analysis

There was no field infiltration test data available for the slope at the Windjammer Landing Beach Resort. Therefore, for the transient seepage analysis an infiltration rate of 1.5×10^{-6} m/sec was used based on the assumption that for the 120 mm rainfall event of October 11, 2009 over a 24 hour period, an amount of 10 % of the total rainfall occurred in 1.0 hour as measured during the infiltration test carried out on the Barre de L'isle study site which amounts to approximately 12.0 mm/hour. Runoff was assumed to amount to about 55.0% of this hourly rainfall resulting in an infiltration rate of 5.4 mm/hour.

In the numerical analysis for the transient seepage processes occurring in the slope the ground surface was assigned a unit flux boundary condition with an applied surface flux rate of 1.5×10^{-6} m/sec. The remaining boundary conditions were similar to that specified for the 'steady state' seepage analysis. The soil-water characteristic curve shown in Figure 6.12b was used in the numerical analysis. A volumetric water content of 0.404 was specified for the colluvium.

MODEL No. 2

In SEEP/W the control was set at 2-dimensional for the transient seepage model with a maximum of 180 iterations. The convergence criteria between two successive iterations was set at 0.01 and the rate of change of the hydraulic conductivity between each node was set at 1.1 of order of magnitude. Full convergence of the residual was achieved after 83 iterations as shown in Figure 7.45. The maximum change in the hydraulic conductivity from one iteration to another was 1.0 of order of magnitude with a minimum order of 1×10^{-4} m/sec. No ponding of water was allowed on the surface of the slope. The infiltration rate was set at 1.5×10^{-6} m/sec. The incremental time sequence of 172,800 seconds (2 days) was applied with a maximum of 15 time steps over a period of 30 days.

The saturated hydraulic conductivity k_{sat} used for the colluvium was 6.3×10^{-5} m/sec and the hydraulic conductivity function graph is presented in Figure 7.36a. The volumetric water content graph is shown in Figure 7.36b. Air begins entry into the colluvium at 0.3 kPa and begins to desaturate the soil. Desaturation of the colluvium is completed at about 40.0 kPa of matric suction. During the transient process the applied surface boundary flux resulted in infiltration downwards into the colluvium as the wetting front advanced in the unsaturated or capillary zone and a perched water table was established.

As the colluvium became saturated matric suction decreased until complete saturation of the colluvium occurred when the wetting front reached the phreatic surface. This resulted in a rise in the phreatic surface as shown in Figure 7.46. Figure 7.47 shows the transient positions of the rising phreatic surface. At a time assumed to be equal to zero, the pore water pressure in the unsaturated zone above the phreatic surface increases as water infiltrates the colluvium until the wetting front merges with the phreatic surface causing it to rise to within 0.5 m below the ground surface after two days (Step 1) of rainfall. At time step No. 2 (4 days) the phreatic surface rises to within 0.15 m below the ground surface. After 6 days (time step 3) of rainfall and thereafter the phreatic surface rises to the ground surface and the colluvium becomes fully saturated and very unstable.

The equipotential lines of total head extend vertically through the colluvium with the phreatic line at the ground surface as illustrated in Figure 7.48. This implies that the total head is the same for all points at the ground surface and therefore, the direction of flow is perpendicular to the equipotential lines at all points. The difference in total head is 22.0m.

The pore water pressure heads in the colluvium are positive and range from zero at the phreatic surface to 8.5m at the base of the colluvium layer as shown in Figure 7.49. The contour lines run parallel to the phreatic line. The pore water pressures in the colluvium are positive as a result of saturation by the rising phreatic line. Figure 7.50 shows the the pore water pressure values ranging from zero at the phreatic surface to 85.0 kPa at the base of the colluvium. The increase in pore water pressure results in a decrease in the shear strength of the colluvium causing instabilities in the slope.

The flow velocity increases from 1e x 10^{-6} m/sec at the crest of the slope to 3.16 x 10^{-5} m/sec at the toe and all flow is directed toward the toe of the slope. This is supported by the the increase in magnitude of the flow rate vectors at the toe of the slope as shown in Figure 7.51. The hydraulic gradient is greater at the crest of the slope at 1.4 than the exit gradient of 0.8 at the toe as illustrated in Figure 7.52. At the middle section of the slope the hydraulic gradient is reduced to 0.2 and increases further downslope toward the toe.

During the transient process, the saturated hydraulic conductivity, k_{sat} of the colluvium is lower at the crest at1e x 10^{-6} m/sec whereas saturated hydraulic conductivity at the toe as shown in Figure 7.53. Figure 7.54 shows the volumetric water content of the colluvium ranging from 0.2 to 0.3 at the crest of the slope and increases from 0.35 to 0.4 at the toe.

7.3.7 Review of the Results of the Transient Seepage Analysis Windjammer Landing Beach Resort

7.3.7.1 Variation in Total Head in the Colluvium at the Ground Surface and up to 2.3m Depth

Infiltration caused an increase in the total head in the colluvium as the pore water pressure increased and matric suction decreased. This resulted in changes in total head at the ground surface and at variable depths within the colluvium as predicted by the numerical analysis model. This was confirmed by the total head differences at the nodes located at the surface and at variable depths in the colluvium in the vicinity of the tensiometers in the field. The measurements of total head were recorded after the phreatic surface was raised to ground surface 6 days after the start of the rainfall.

Figure 7.55a – Figure 7.55e show the graphs of changes in total head taking place at variable depths in the colluvium during the transient process.

The increase in total head ranges from 4.0m to 5.0m from the beginning of the rainfall event to the rise of the phreatic surface to ground level 6 days later. The average increase in total head at the ground surface is 4.3m. The difference in total head for the 13 selected nodes at the ground surface is small not exceeding 1.0m. This implies that at the ground surface the saturated hydraulic conductivity of the colluvium is consistant and the inflow of water is more or less evenly distributed in the colluvium during the rainfall event. In addition, the movement of water into the soil at the ground surface is consistant from the start of the rainfall event.

At this depth infiltration is rapid as indicated in the increase in total head of 4.5m to 5.0m from the start of the rainfall event to the termination after 6 days as predicted in the model. The average increase in total head at 0.5m is 4.8m. There is a small increase in total head of 0.5m in comparison to that taking place at the ground surface. This implies that the infiltration rate and the saturated hydraulic conductivity at 0.5m are slightly lower than that taking place at the ground surface.

At a depth of 1.0m, the total head difference is similar to that observed at 0.5m within the range of 4.6m to 5.0m as predicted in the model as shown in Figure 7.6. The saturated hydraulic conductivity and the infiltration rate of the colluvium is consistant at 0.5m and 1.0m depths and allows water to flow through the soil to greater depths at a steady rate.

The average is 4.8m thus, the saturated hydraulic conductivity of the colluvium at 1.6m is consistant with the upper layers at 0.5m and 1.0m of the soil strata. At 2.3 m there is a slight decrease in the changes in total head on the average of 4.6m from the start to the end of the rainfall event as shown in Figure 7.6. One should observe that there is little difference between the average total head at the ground surface of 4.3m to 2.3m where the average total head is 4.6m.

Overall, it appears that the colluvium at the Windjammer Landing site has a consistant saturated hydraulic conductivity and infiltration rate up to at least a depth of 2.3m as predicted in the finite element model and will allow water to flow to greater depths. This would imply that this material will become saturated to greater depths very quickly during heavy rainfall and develop instabilities within the slope which may result in catastrophic slope failures.

7.3.7.2 Variation in Pore Water Pressure During the Transient Process - Windjammer Landing Beach Resort

The infiltration rate of 1.5×10^{-6} m/sec used in the model was assumed based on the rainfall event of 120mm over a 24-hour period on October 11, 2008 at which time there were no field instruments intalled at the study site to monitor infiltration rates or pore water pressures in the colluvium. The field instrumentation was installed during the period of October 29 to December 18, 2008 approximately 18 days following the rainfall event. As a result a correct comparison of the pore pressure response in the field to that rainfall event to the predicted response from the numerical model cannot be made.

However, the heaviest rainfall event recorded at the Windjammer Landing site during the study period was 35 mm on January 14, 2009 at which time the tensiometers and piezometers were in place and were being monitored.

The location of the tensiometers are identified as unit flux sections in the numerical model at depths of 0.5m, 1.0m, 1.6m, and 2.3m as shown in Figure 7.39. Each tensiometer is represented by the node closest to its actual location in the field and the pore water pressures are calculated at the four nodes of each element. The changes in pore water pressure after 6 days of rainfall are shown in the graphs in Figure 7.56a to Figure 7.56c. Figure 7.57a to Figure 7.57c are graphs of changes in pore water pressure at variable depths in the colluvium over a 24-hour period during the transient process.

For the tensiometers in Rows A, B and C the response to the rainfall event of 35mm at 0.5m depth is very positive as it becomes fully saturated with the matric suction measured in the field at 0.0 kPa.

Although the applied daily rainfall of 35 mm is far less than the daily rainfall of 120 mm used in the numerical model, the predicted pore water pressure at 0.5 m depth over a 24 hour period was measured at -5.8 kPa. This implies that the predicted pore water pressure in the numerical model does not correlate with the actual field measurements which was at 0.0 kPa for that rainfall event.

It is the opinion of the author that the field measurements are more realistic than the predictions of the numerical model since one would expect that for a 120 mm daily rainfall the colluvium would be fully saturated at 0.5m as measured in the field. Furthermore, the 120 mm rainfall event was the triggering mechanism that initiated the slope failure on October 11, 2008. One could speculate that for the more intensive rainfall event of 120 mm there would be a higher infiltration rate which would result in an increase in the pore water pressure at greater depths in comparison to a lesser rainfall amount of 35 mm.
At 1.0m depth the pore water pressures measured in the tensiometers were negative for Rows A, B and C ranging from -5.5 kPa to -7.5 kPa for the 35 mm rainfall. The predicted pore water pressure in the numerical model at 1.0m depth for the 120 mm rainfall event showed a slight increase in pore water pressure with depth to -5.1 kPa over a 24 hour period. This is in good agreement with the pore water pressures measured in the field.

At 1.6m the field measurements indicate a small increase in matric suction varying from -7.5 kPa to -10.0 kPa for Rows A, B, and C. Hence there is a decrease in pore water pressure with depth. The numerical model prediction indicates lower matric suction values of -0.17 kPa to -0.19 kPa at 1.6m and an increase in pore water pressure with depth. This is the result of the fact that a 120 mm rainfall event would cause a higher rate of infiltration into the colluvium and generate higher pore water pressures at greater depths than a 35 mm rainfall event.

The results of the measurements from the tensiometers in Rows A, B and C indicate a further increase in matric suction at 2.3m ranging from -12.5 kPa to -15.0 kPa. The numerical model predicted pore water pressure changes at 2.3m depth for a rainfall event of 120 mm to cause an increase in pore water pressure to 9.5 kPa.

This implies that a 35 mm rainfall results in limited infiltration into the colluvium that would generate increased pore water pressure at greater depths whereas for the 120 mm rainfall event the inflow of water into the colluvium is at a higher rate and the saturated hydraulic conductivity of the colluvium assists in the downward flow of water to greater depths causing saturation and a decrease in the shear strength of the colluvium.

These results are supportive of the fact that the higher rainfall event of 120 mm generated higher infiltration rates into the colluvium to greater depth than the lesser rainfall event of 35 mm. The rainfall event of 35 mm on January 14, 2009 did not result in any visible deformation of the slope and there were no visible tension cracks or seepage conditions on the slope at theWindjammer Landing study site. On the contrary, the rainfall event of 120 mm which occurred on October 11, 2009 triggered a landslide that damaged the retaining wall and several buried utility lines and service pipes.

7.3.8 Slope Stability Analysis

7.3.8.1 Introduction

During the investigation of the major landslide that occurred at the Windjammer Landing Beach Resort in July of 2005, laboratory testing of the colluvial material was conducted to determine the shear strength characteristics for slope stability analysis and for remedial slope stabilization measures the results of which are presented in Table 3.1 of the thesis. The results of the laboratory tests indicate a variation of the soil shear strength parameters from the laboratory testing. This is not supprising for colluvium since the material originated as a result of transportation and re-deposition which involved internal erosion and washing out of the finer soil fraction and remoulding of the soil particles during transportation. The results of two additional laboratory shear strength tests on bulk soil samples of colluvium recovered from the study site are presented in Table 5.9 of the thesis. The results of the laboratory also show a wide variation in the strength parameters of the colluvium in direct shear. For the slope stability analysis an average value of the shear strength parameters from the 2005 and 2009 tests was used in the numerical model.

7.3.8.2 Back Analysis of the Windjammer Landing Beach Resort Slope

A back-analysis of the slope was performed to determine the shear strength of the colluvium at the time of the slope failure and for remedial slope stabilization measures. Figure 7.58 presents the results of the back-analysis. An assumed effective angle of internal friction value of 25.5^{o} was held fixed for the colluvium based on the author's experience with local soils and the effective cohesion was adjusted to 3.0 kPa which resulted in a Factor of Safety of 1.008.

7.3.8.3 Slope Stability Analysis of the Windjammer Landing Beach Resort Slope during the Transient Process

The pore water pressures and total head conditions from the transient seepage numerical analysis were transferred into the slope stability model and the factor of safety of the slope was computed for each time step of 24 hours for the rainfall distribution of 120 mm which includes the antecedent rainfall.

The soil parameters used in the slope stability analysis during the transient process were as follows:

Unit weight = 17.5 kN/m^3
Effective cohesion, C' = 6.0 kPa
Effective Friction Angle, ϕ' = 32.5^o
Infiltration rate = 1.5 x 10^{-6} m/sec.

The infiltration rate is controlled by the saturated hydraulic conductivity of the colluvium which regulates the amount of water entering the soil causing an increase in the pore water pressure. An increase in the pore water pressure results in a decrease in the shear strength of the colluvium causing instabilities in the slope. A slope stability analysis was performed for daily distribution of the 120 mm rainfall over a total period of 7 days. The results of the slope stability analysis are shown in Table 7.2. The initial Factor of Safety of the slope at the start of the rainfall event is 2.39 as shown in Figure 7.59. The phreatic surface is approximately 1.5m below the ground surface.

Table 7.2 Summary of the Factor of Safety of the Windjammer Landing Beach Resort Slope During the Transient Process

Time Step No.	Time (Days)	Factor of Safety
Initial	0	2.39
1	1	2.37
2	2	2.35
3	3	2.11
4	4	1.99
5	5	1.02

For the rainfall distribution of 120 mm over a period of 2 days there is very little difference in the decrease in the Factor of Safety for a saturated hydraulic conductivity of 6.3 x 10^{-5} m/sec. After 3 days of rainfall distribution the Factor of Safety is decreased to 2.11 from the initial 2.39. The Factor of Safety of the slope is reduced to 1.02 after 5 days of rainfall distribution.

As can be seen the stability of the slope is severely affected by the rainfall distribution with time**.** Figure 7.60 shows a raised phreatic surface after 3 days of 120 mm rainfall distribution as the pore water pressures in the colluvium is increased by infiltration. The phreatic surface is about 0.7m below the ground surface and the Factor of Safety is 2.11. As shown in Figure 7.61 the phreatic surface has risen to within 0.1m to 0.3m below ground surface after 4 days of rainfall distribution and the Factor of Safety decreased to 1.99. On day 5 the slope is in a critical state as the Factor of Safety is reduced to 1.02 and the phreatic line has risen to the ground surface as shown in Figure 7.62. The saturated hydraulic conductivity of a soil played a vital role in its stability on sloping ground. Typically, a soil with a saturated hydraulic conductivity of higher magnitude than 5.6 x 10^{-5} m/sec would not develop instabilities within such a short time period of 5 days because infiltration would be reduced and it would take a longer time period for any increase in excess pore water pressures to take place that would generate instabilities in the slope.

Figure 7.1 Finite Element Mesh Design For Barre de L'isle Slope

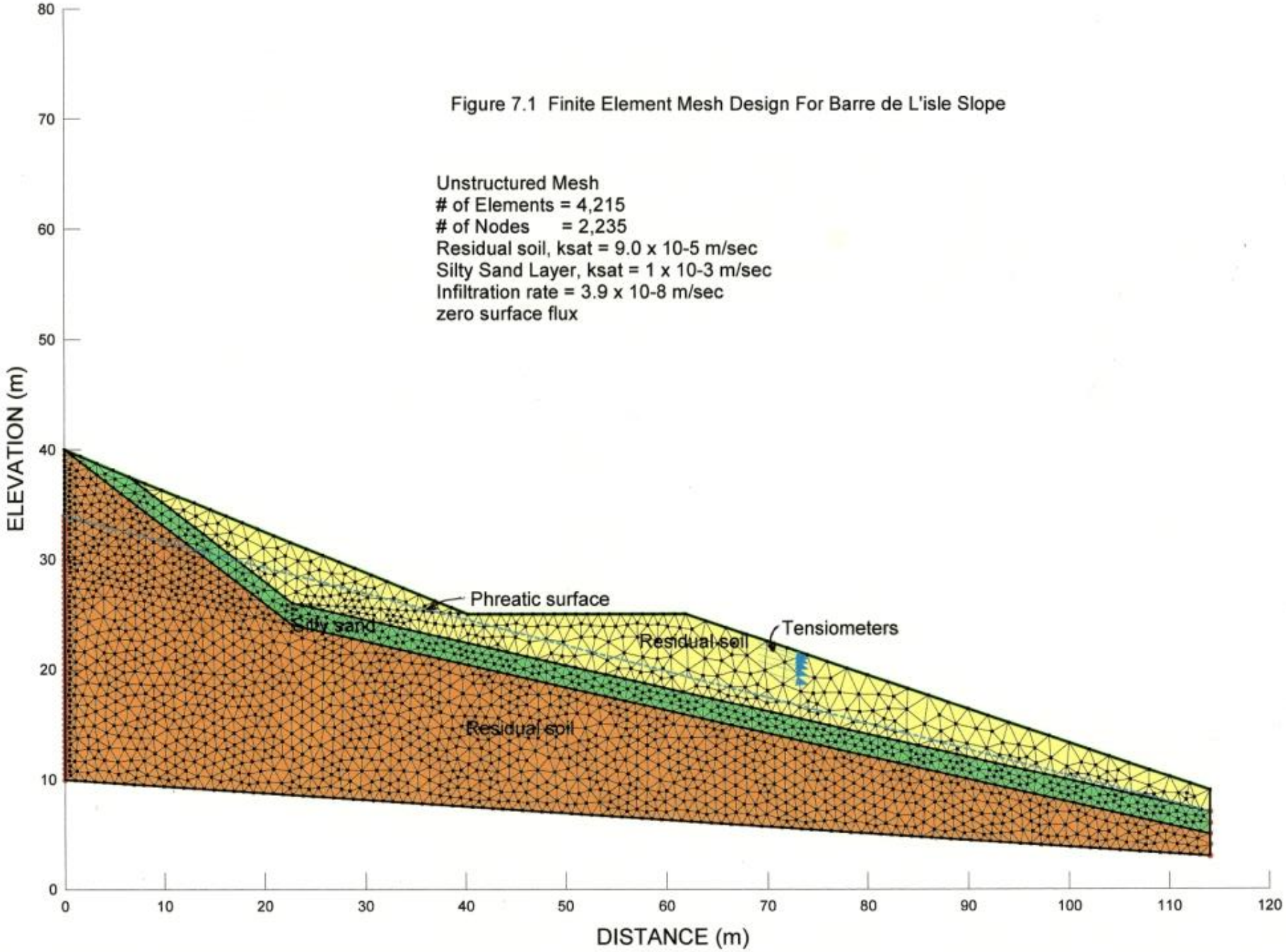

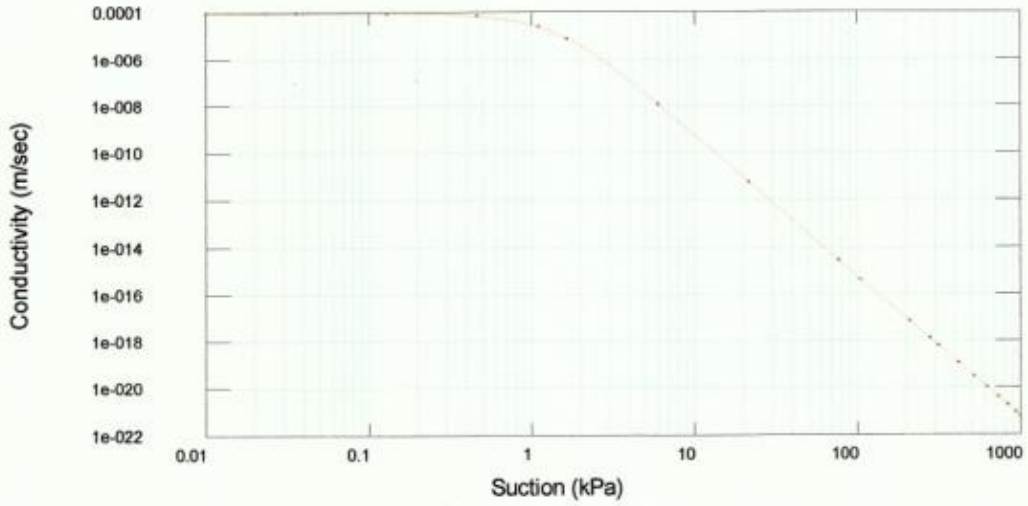

Figure 7.2a Hydraulic Conductivity Function Graph for the Residual Soil Barre de L'isle Study Site – Steady State Seepage Analysis

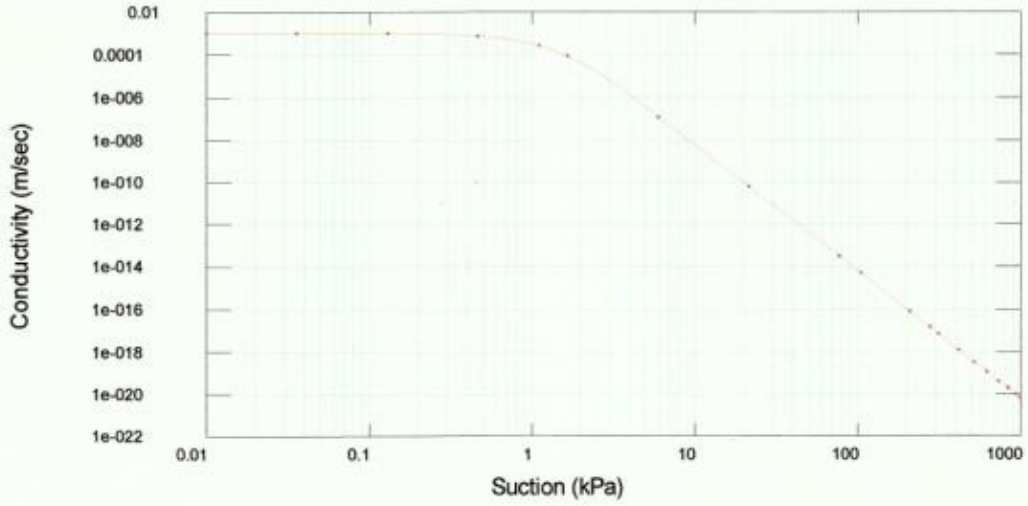

Figure 7.2b Hydraulic Conductivity Function Graph for the Silty Sand Layer Barre de L'isle Study Site – Steady State Seepage Analysis

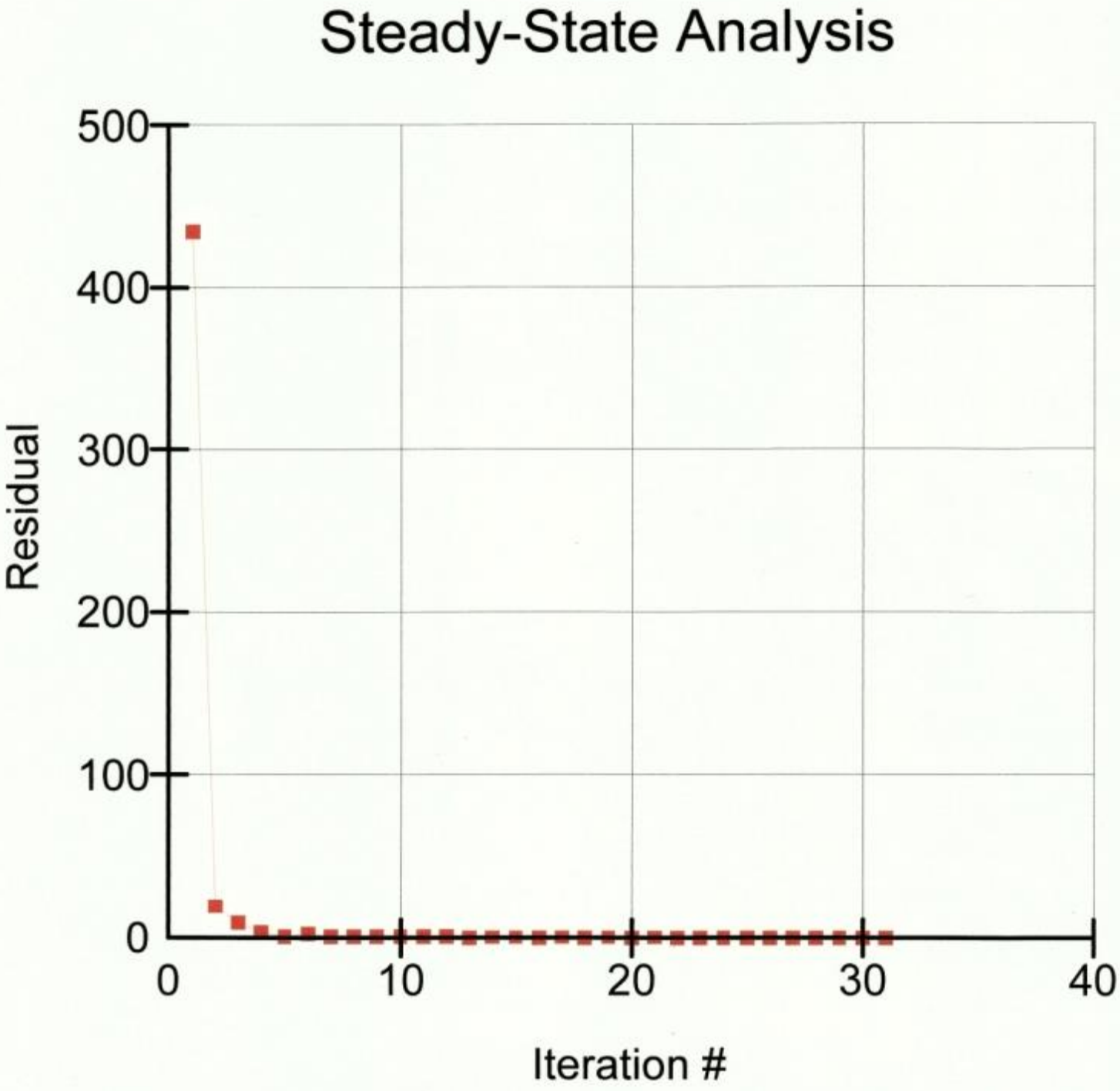

Figure 7.3 : Vector Norm Residual Convergence Graph For Steady State Seepage Analysis For The Barre de Lisle Study Site

Figure 7.4 Total Head for the Steady State Seepage Analysis

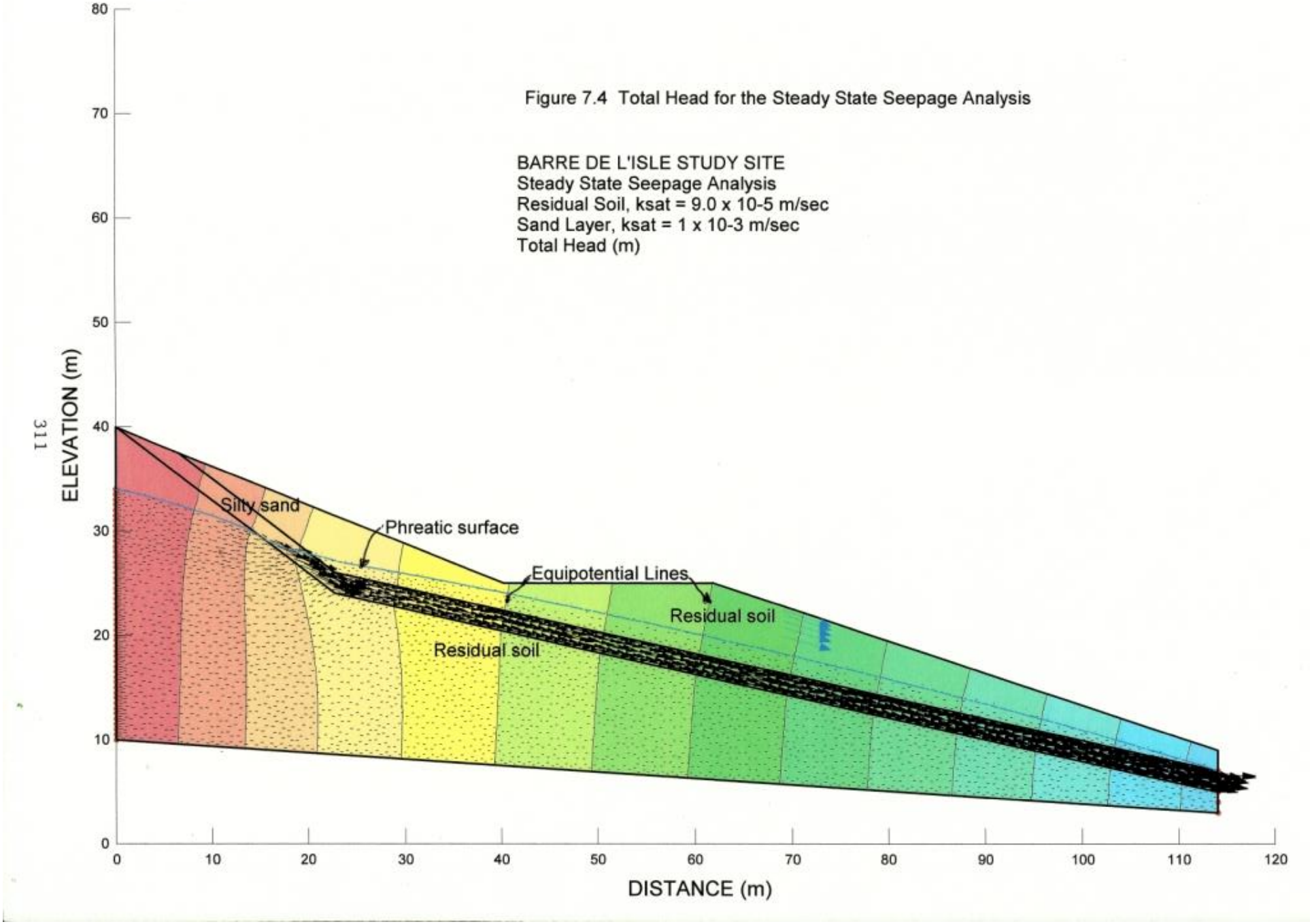

Figure 7.5 Flow Paths for Steady State Condition

BARRE DE L'ISLE STUDY SITE
Steady State Seepage Analysis
Residual Soil, ksat = 9.0 x 10-5 m/sec
Silty Sand Layer, ksat = 1 x 10-3 m/sec
Infiltration Rate = 5.6 x 10-6 m/sec
zero surface flux
Flow Paths

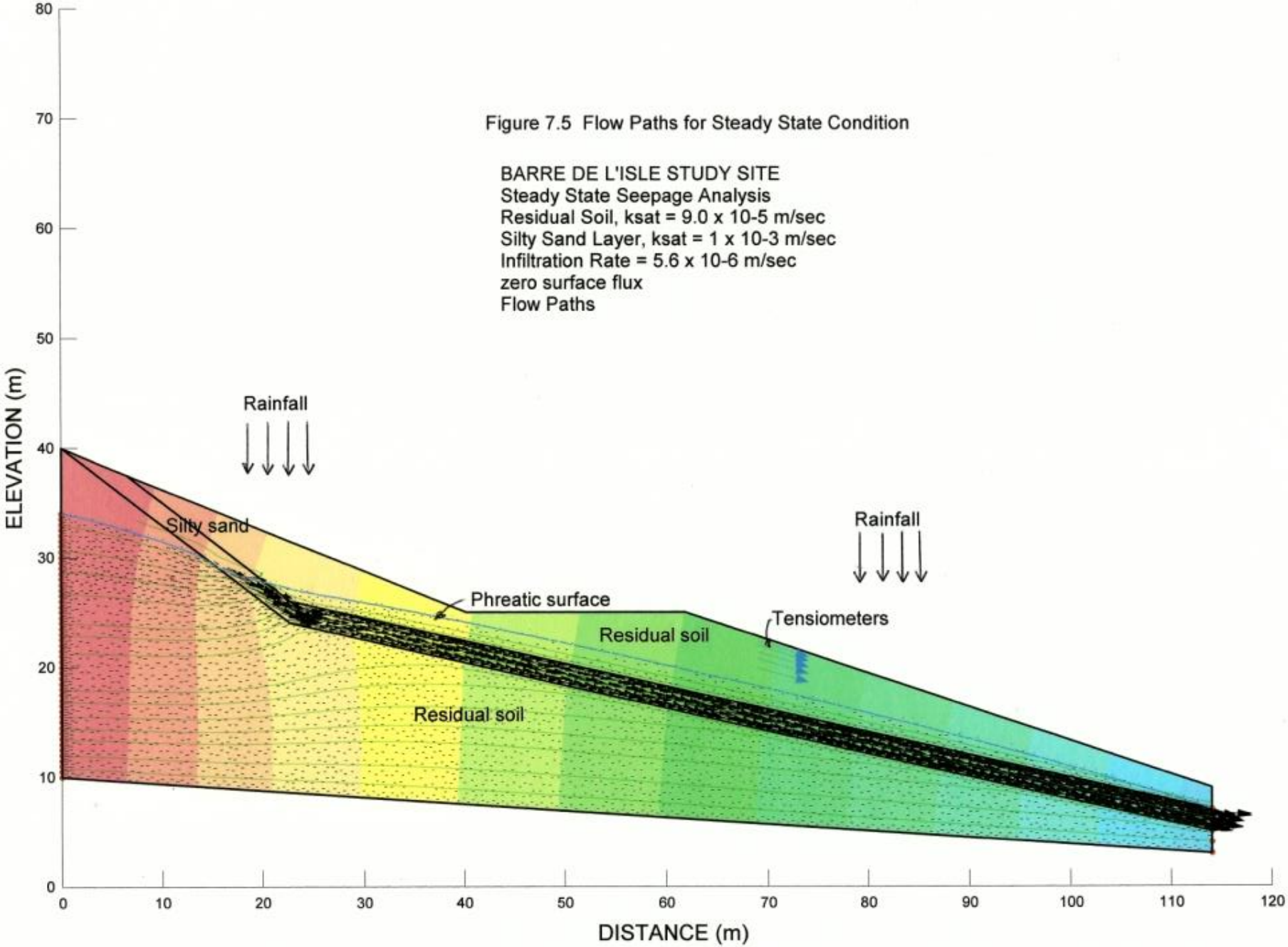

Figure 7.6 Pore Water Pressure Heads for Steady State Condition

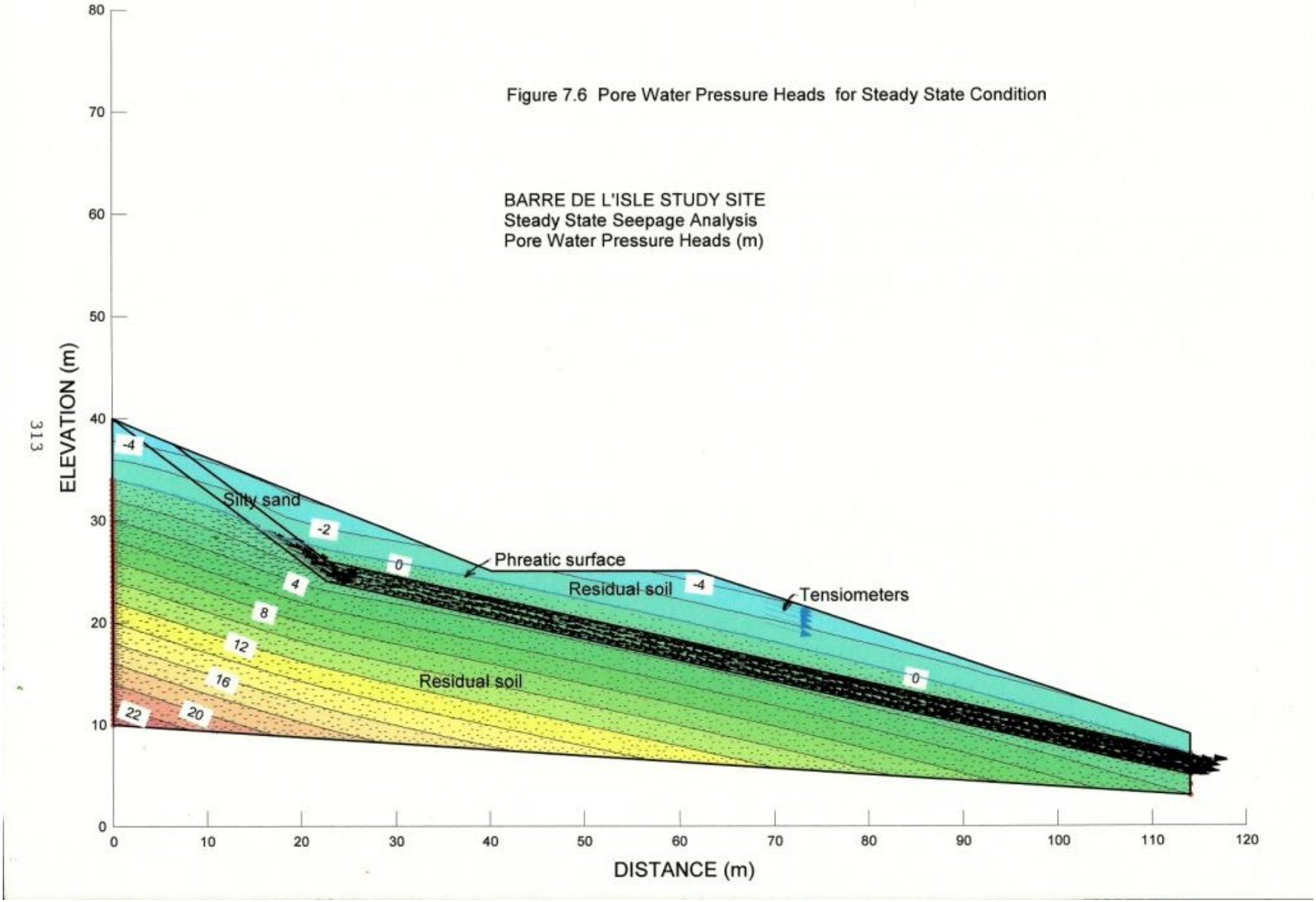

Figure 7.7 Pore Water Pressure for Steady State Condition

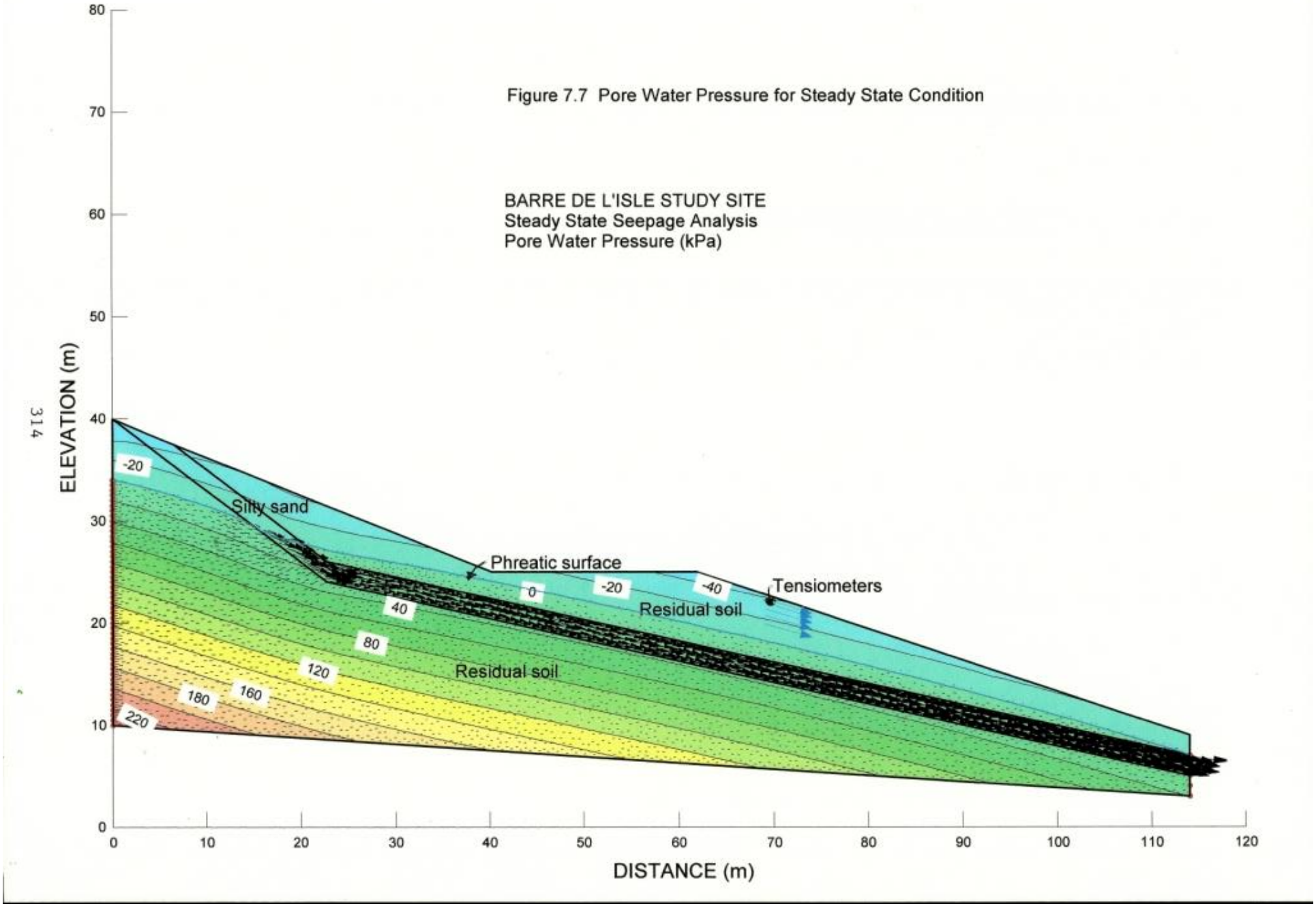

Figure 7.8 XY- Velocity for Steady State Condition

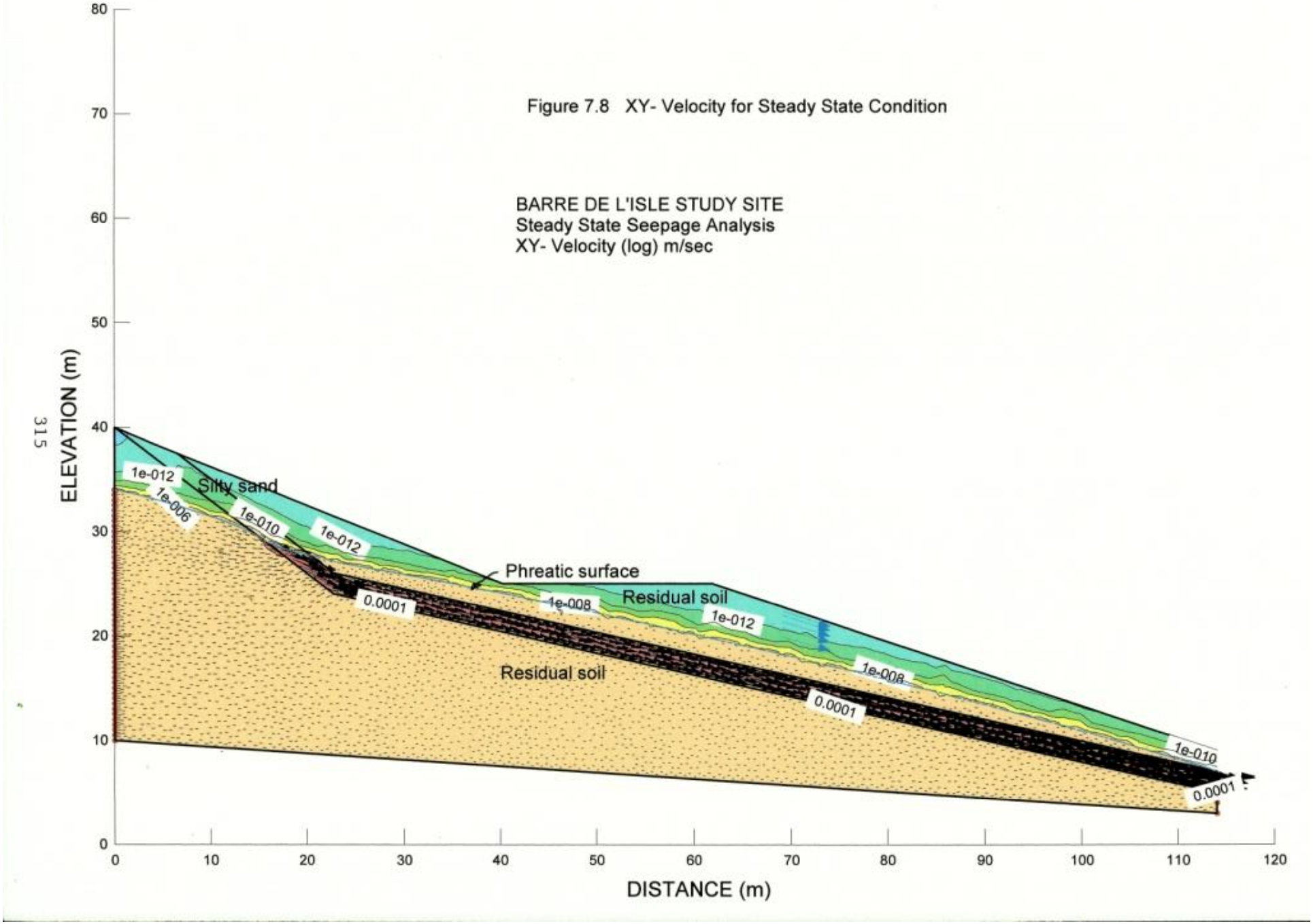

Figure 7.9 XY- Hydraulic Gradient for Steady State Condition

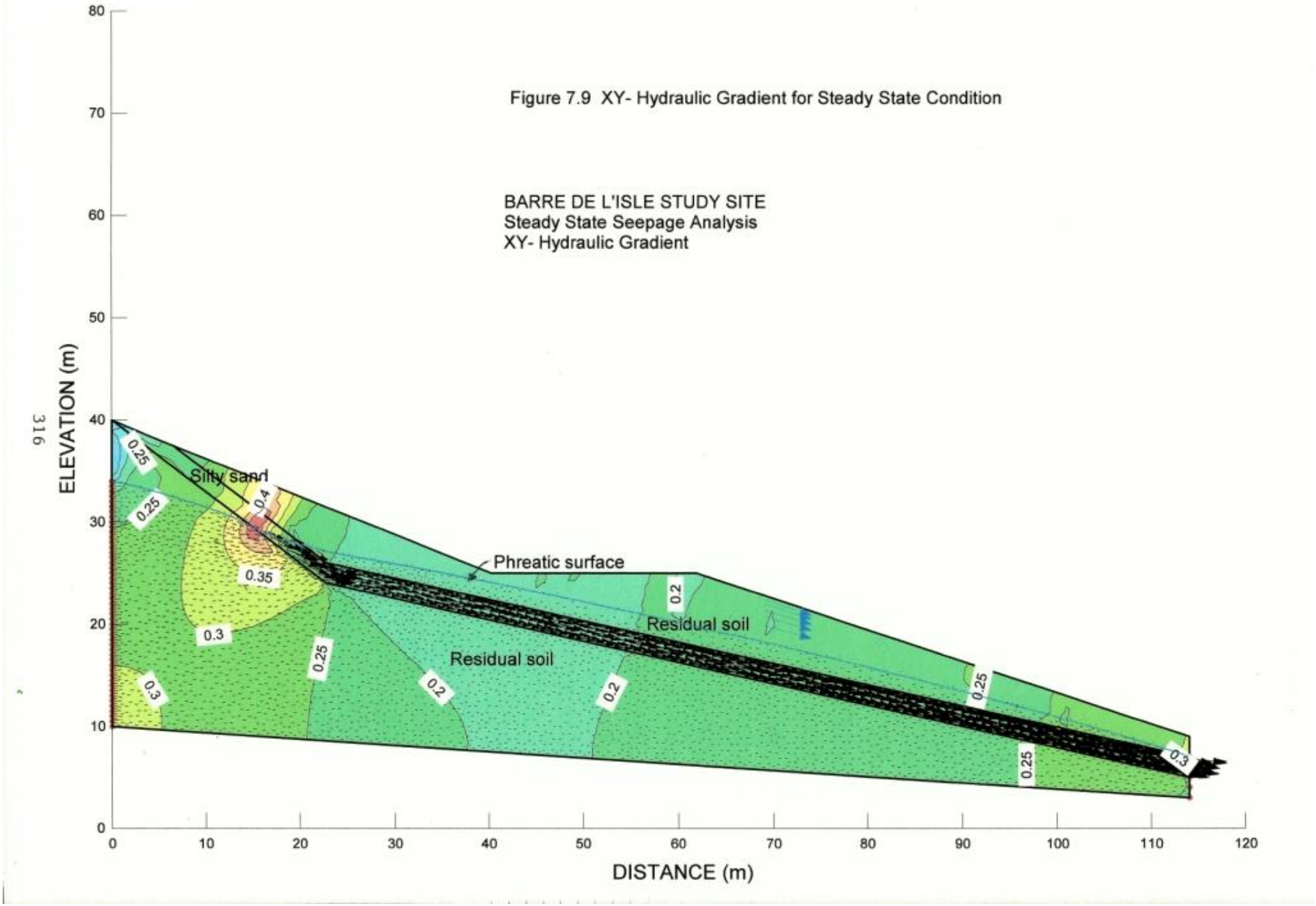

Figure 7.10 X- Hydraulic Conductivity for Steady State Condition

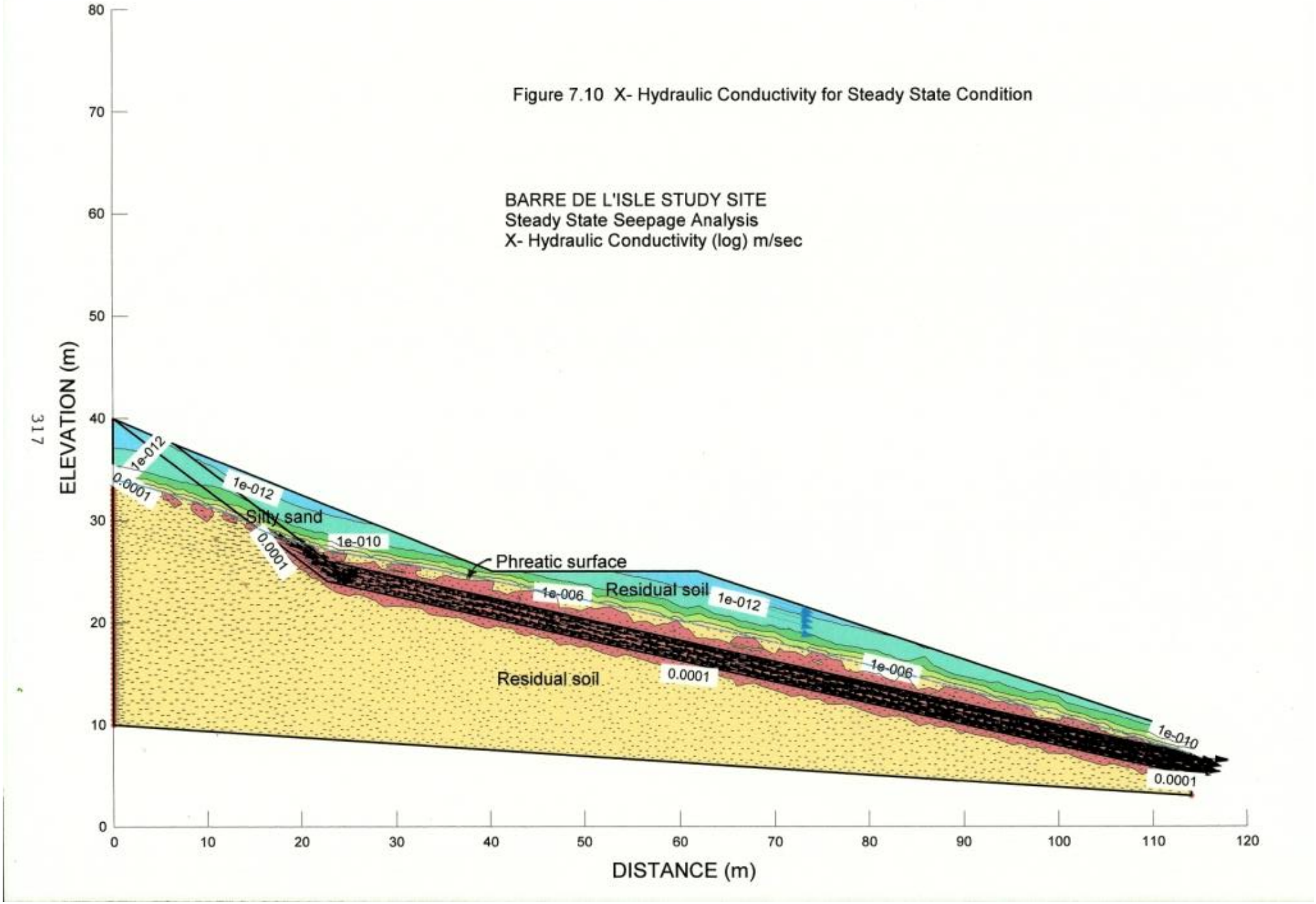

Figure 7.11 Flow Paths For Steady State Surface Boundary Infiltration Condition

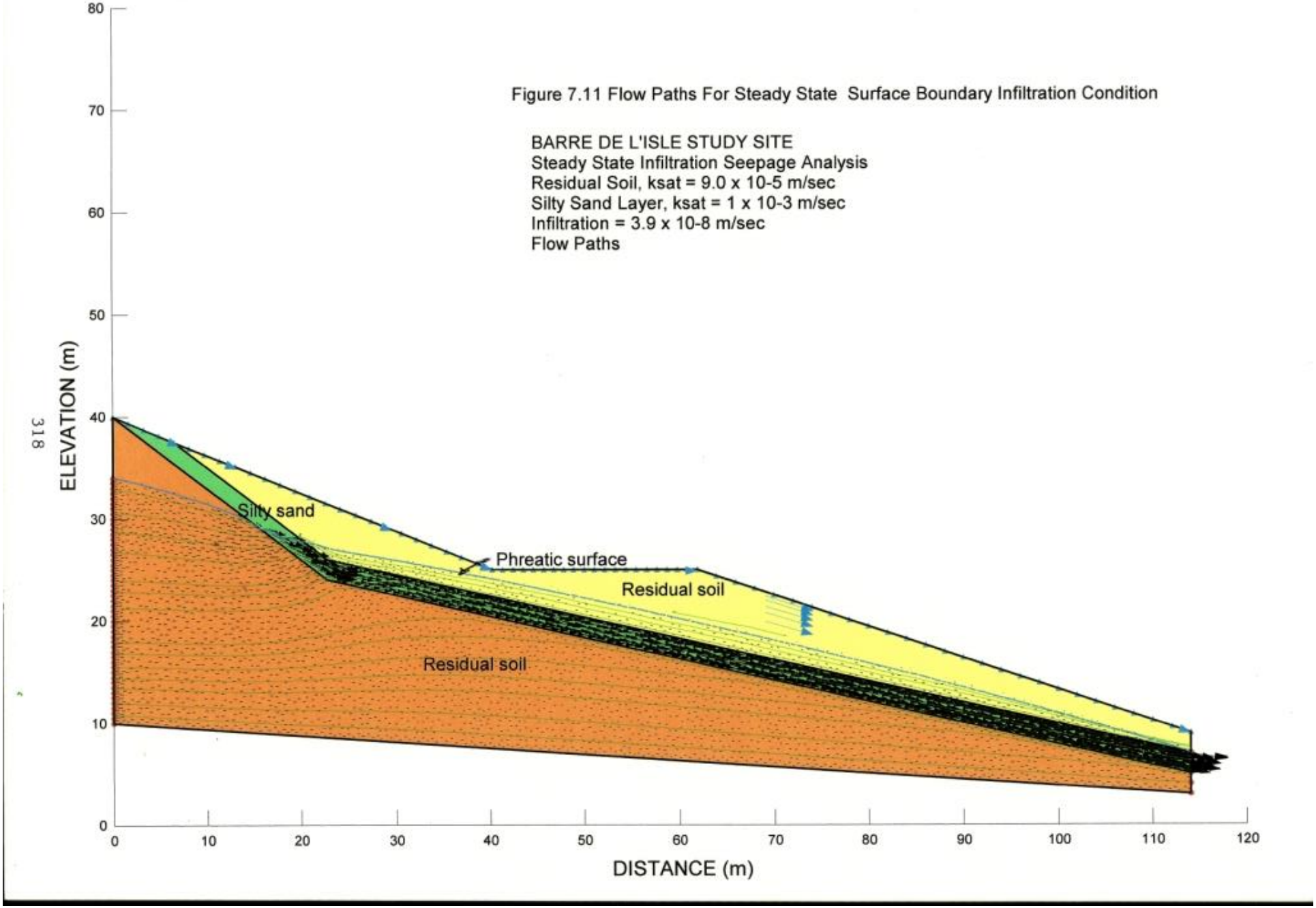

Figure 7.12 Total Head For Steady State Surface Boundary Infiltration Condition

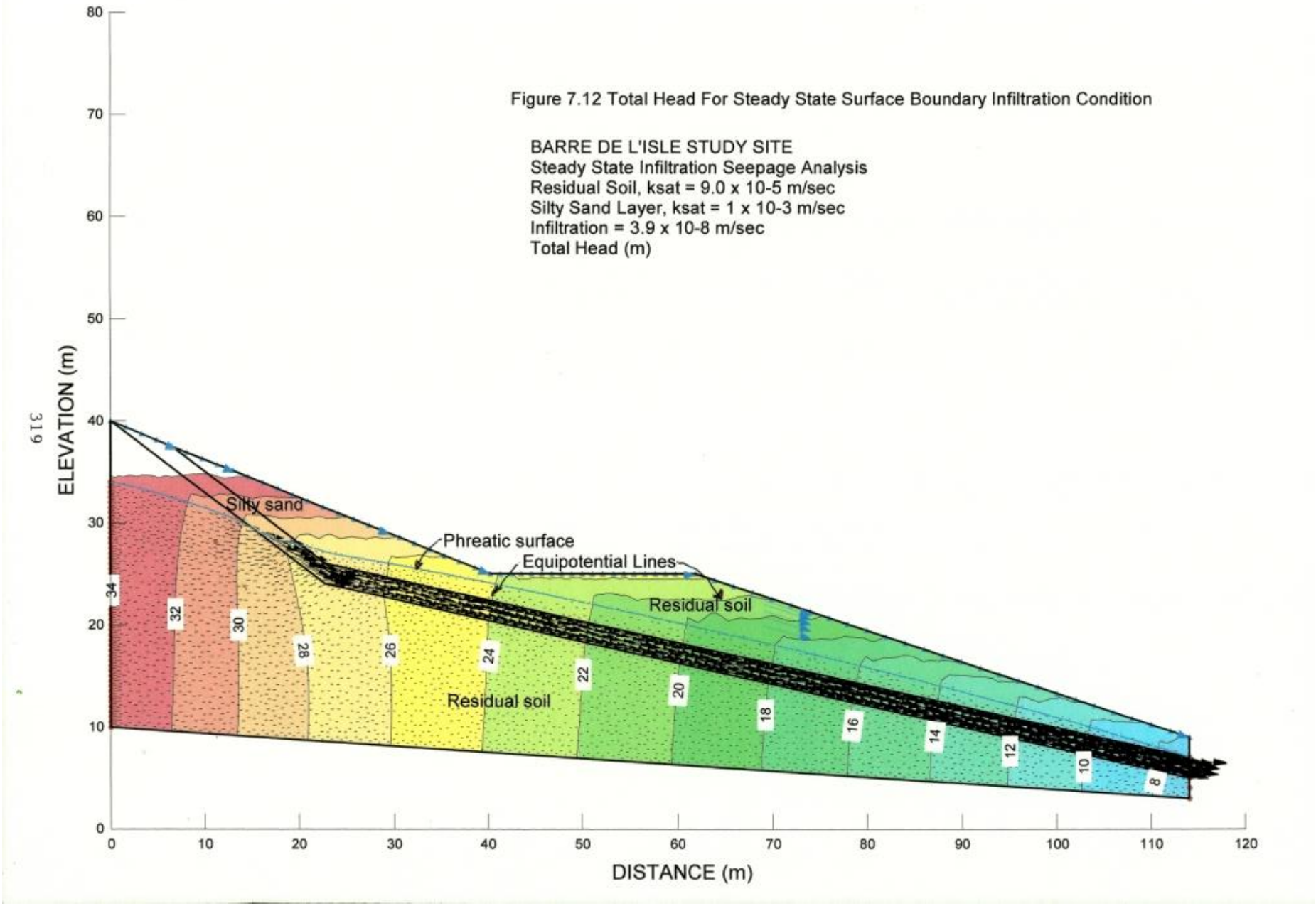

Figure 7.13 Pore Water Pressure Heads For Steady State Surface Boundary Infiltration Condition

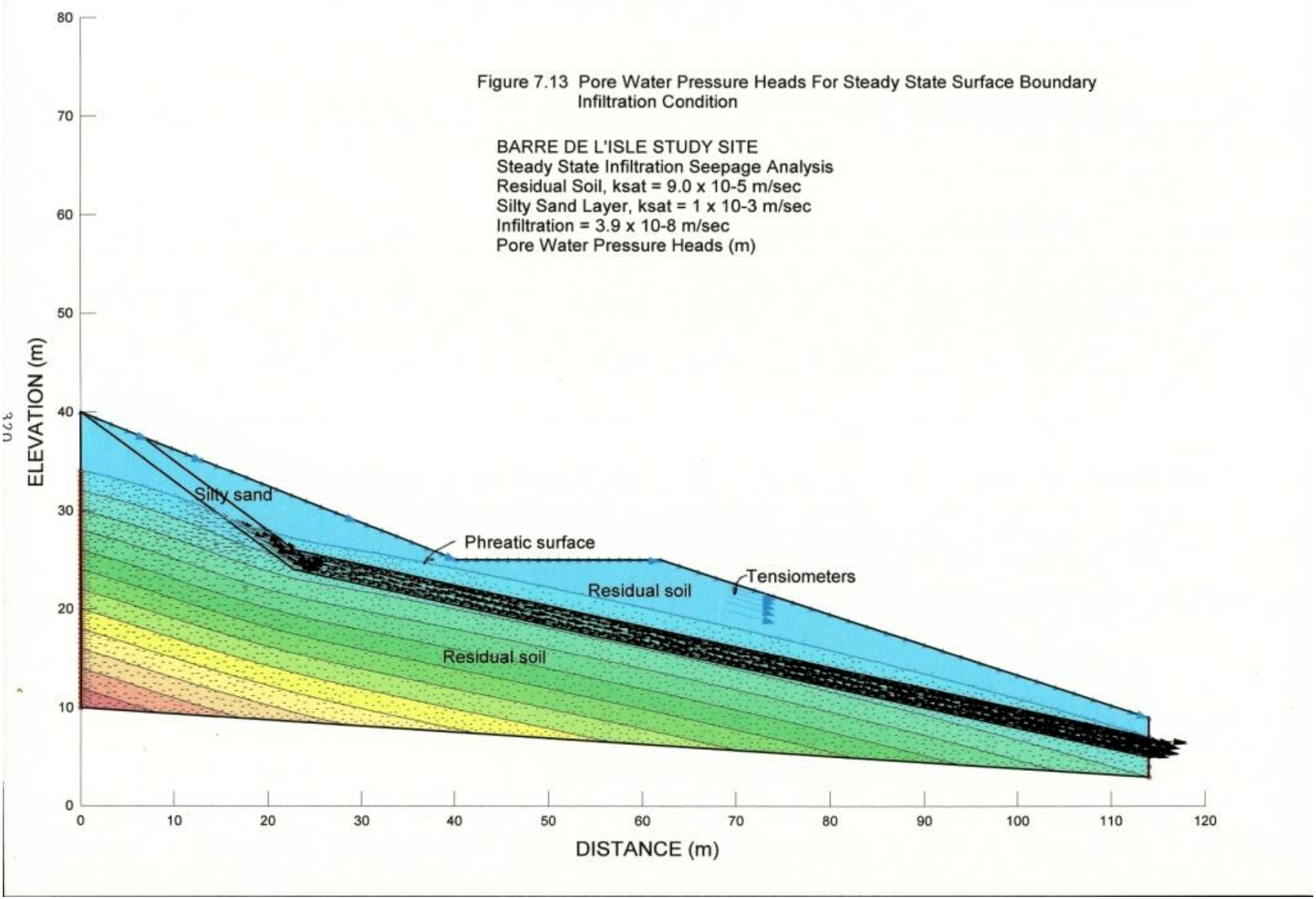

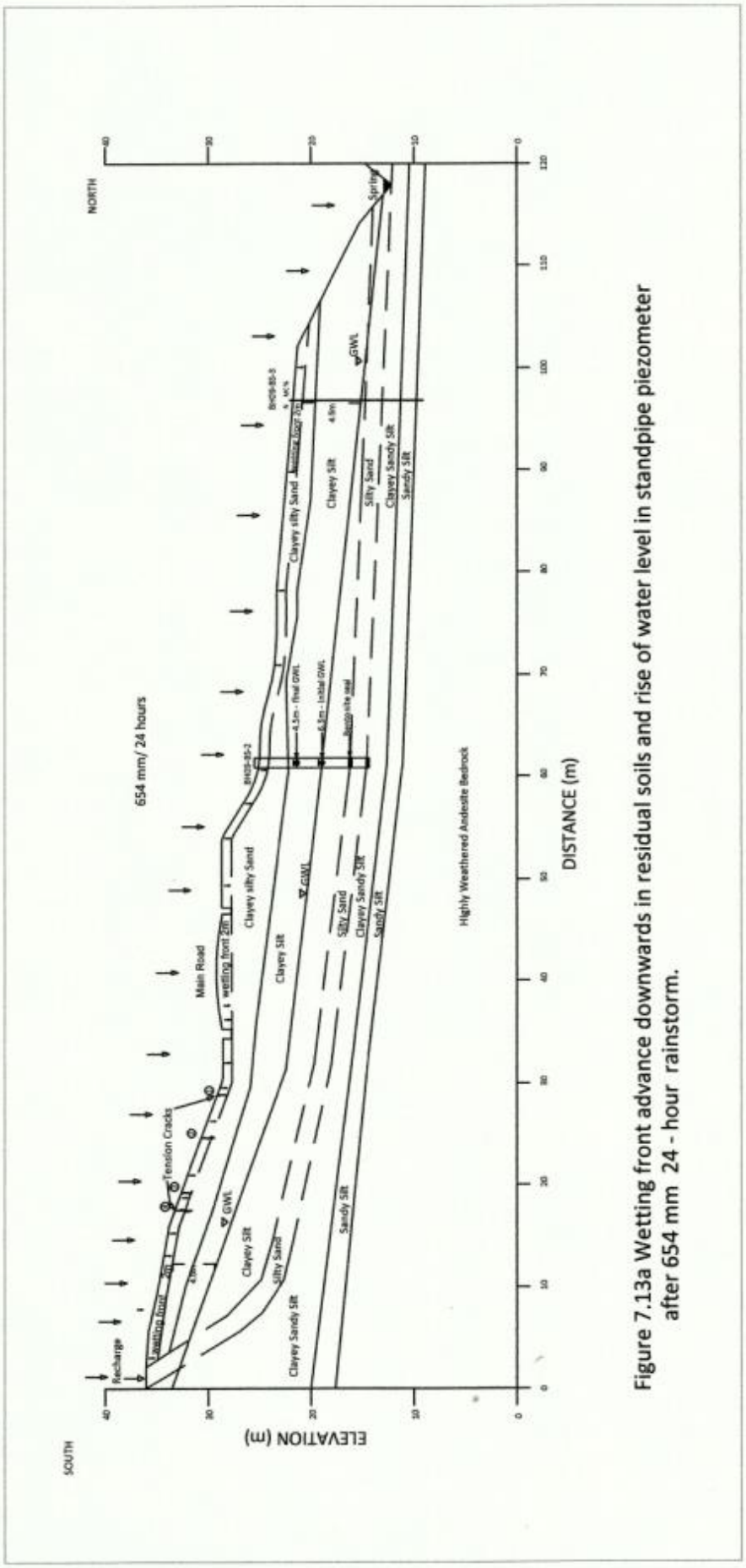

Figure 7.13a Wetting front advance downwards in residual soils and rise of water level in standpipe piezometer after 654 mm 24 - hour rainstorm.

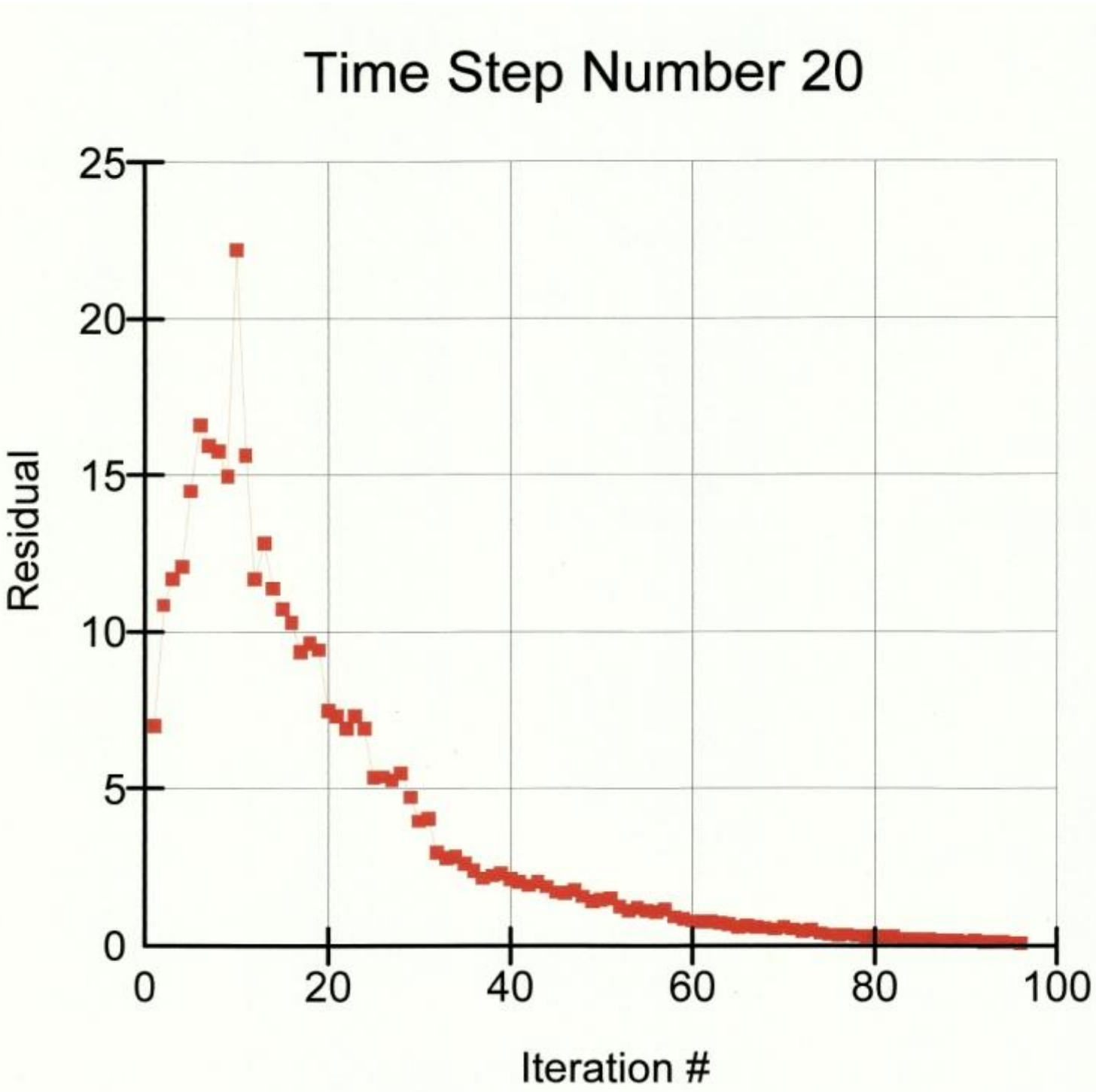

Figure 7.14 : Trial No.3 Vector Norm Residual Convergence Graph For Transient Seepage Analysis For The Barre de Lisle Study Site

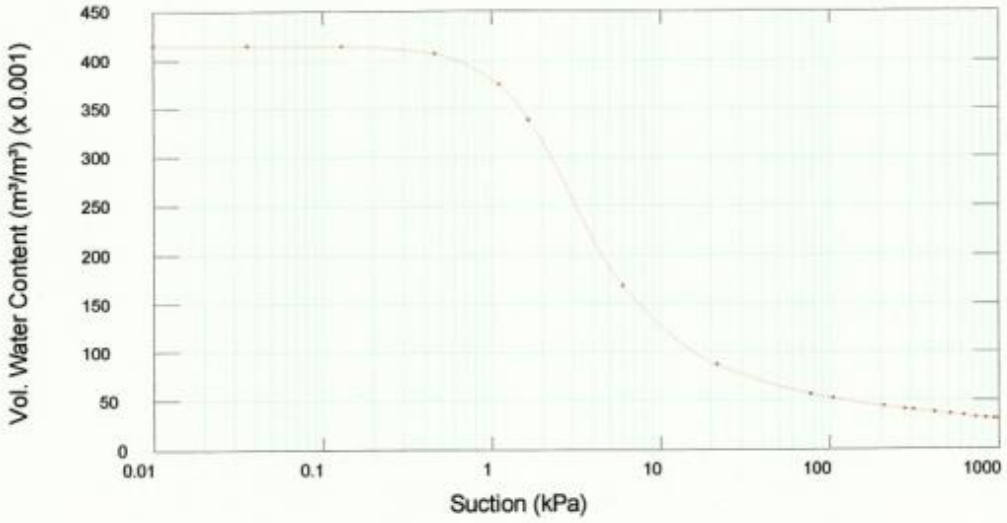

Figure 7.15a Volumetric Water Content Function Graph for the Residual Soil Barre de L'isle Study Site

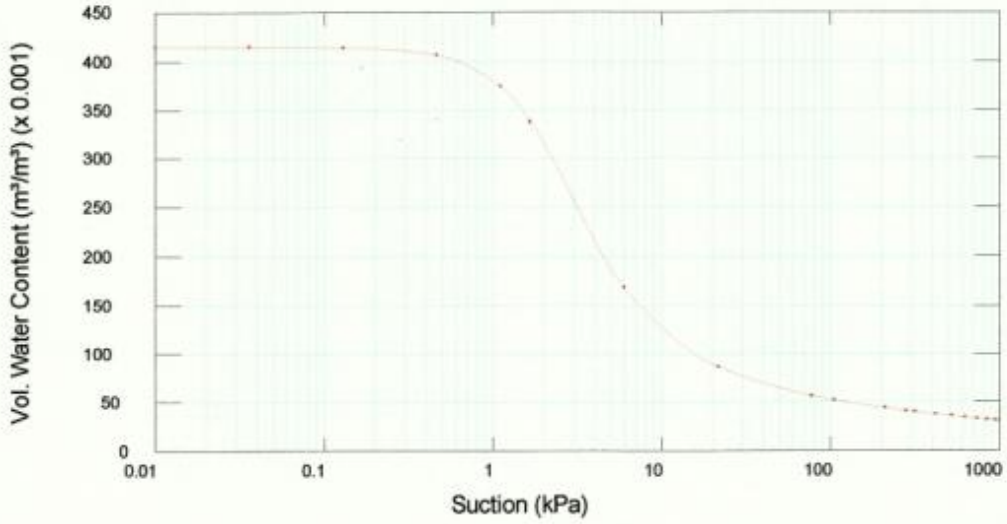

Figure 7.15b Volumetric Water Content Function Graph for the Silty Sand Layer Barre de L'isle Study Site

Figure 7.16 Rise of Phreatic Surface During Transient Seepage

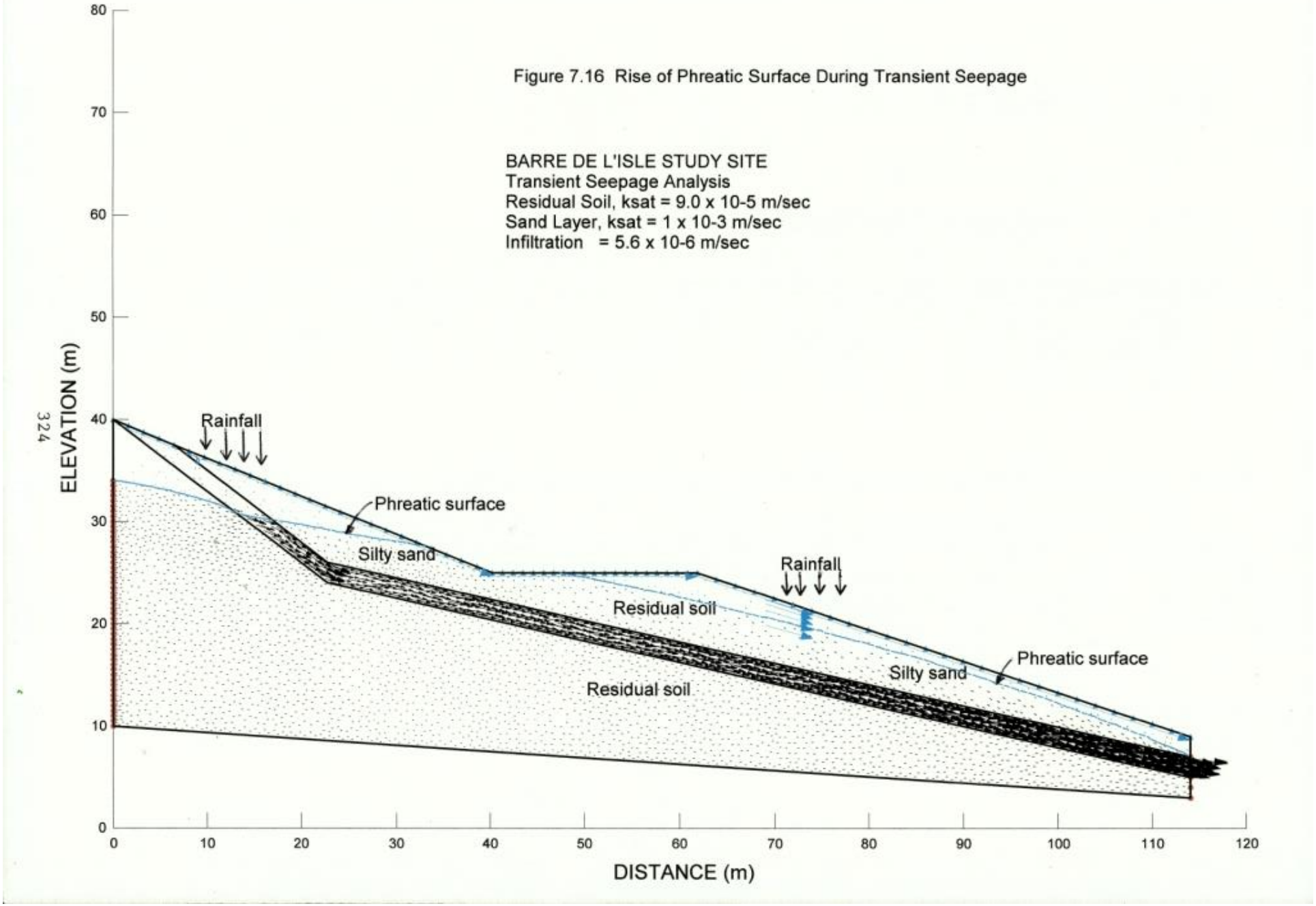

Figure 7.17 Transient Positions of Rising Phreatic Surface

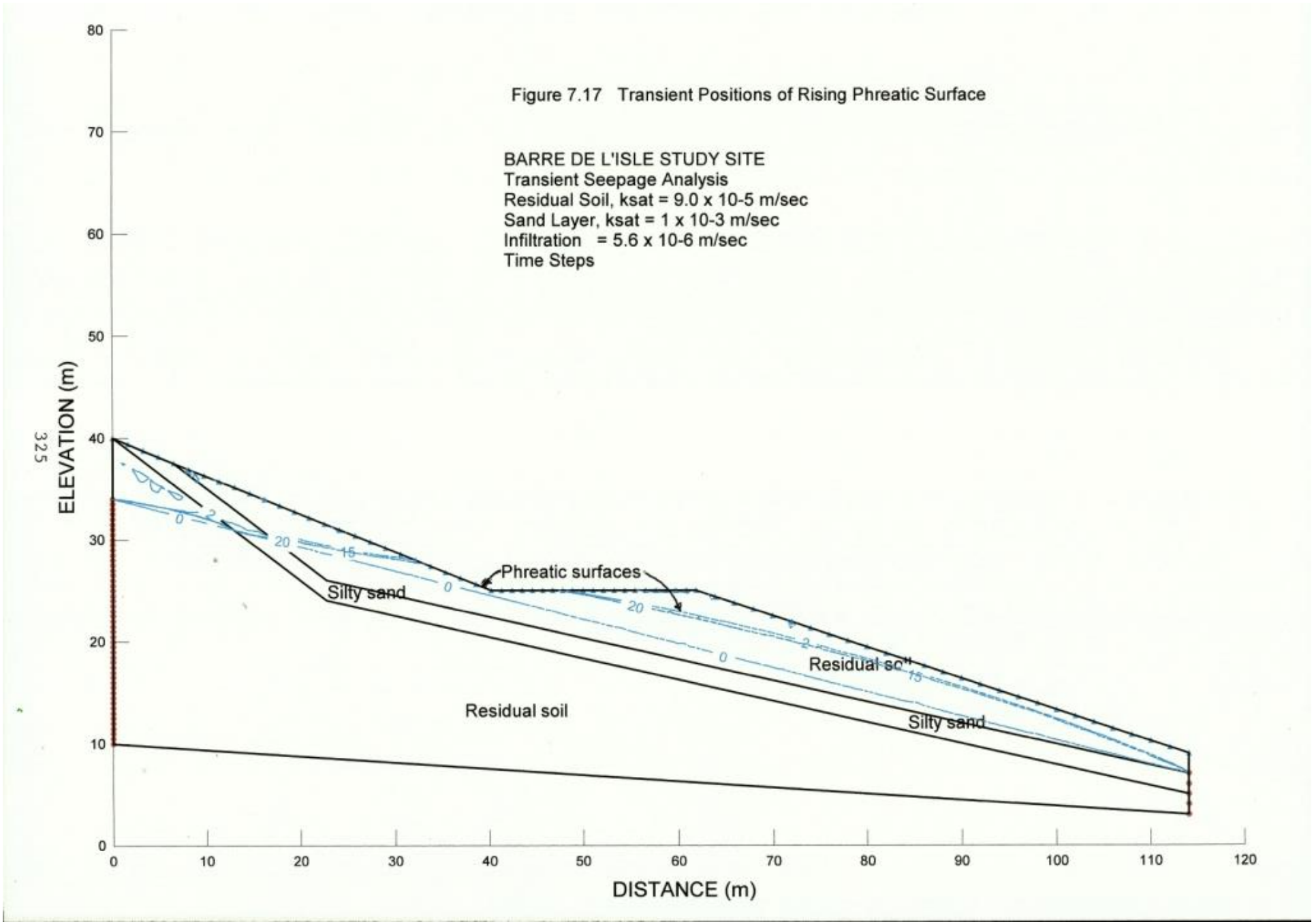

Figure 7.18 Total Head for Transient Seepage Condition

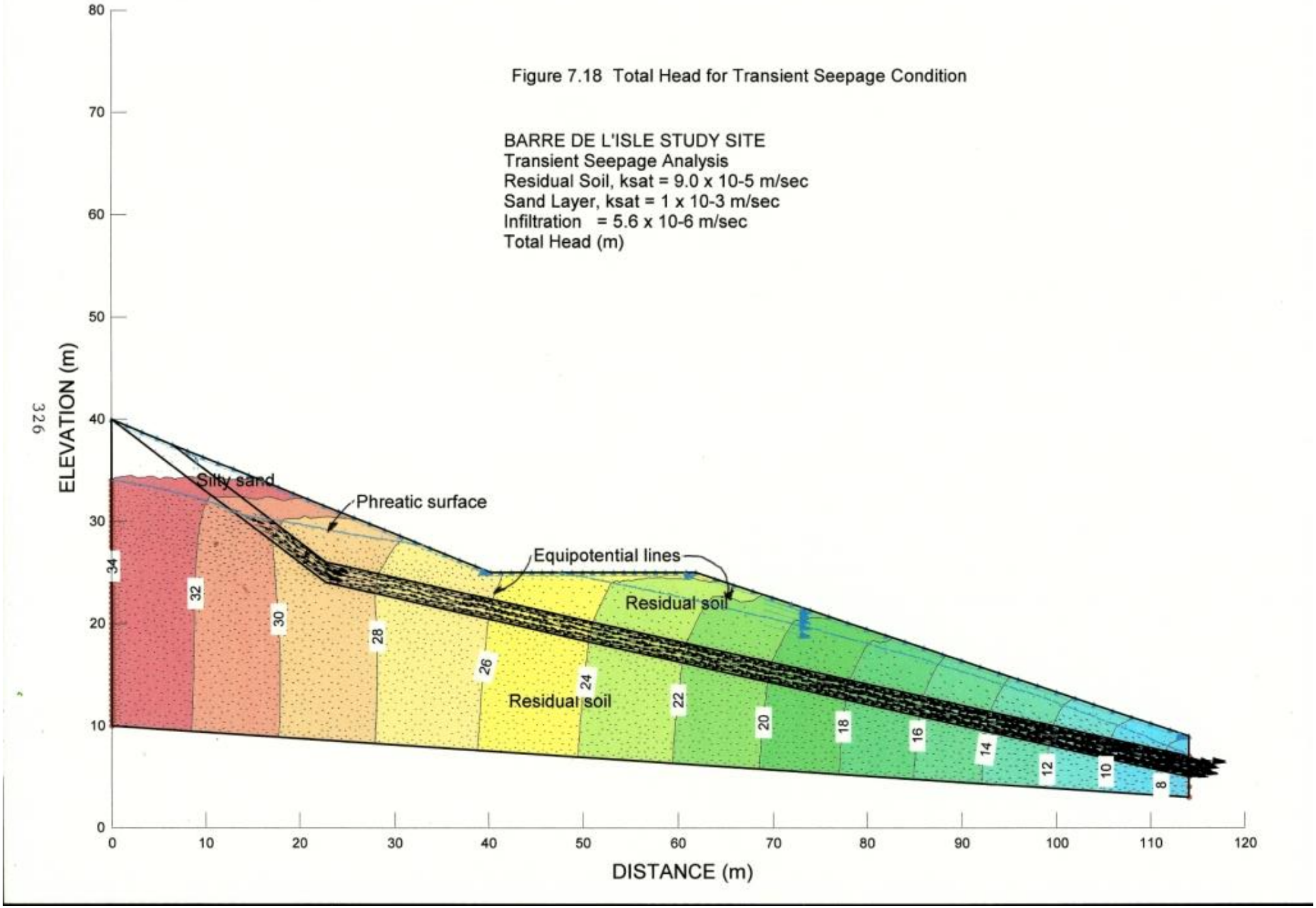

Figure 7.19 Pressure Head for Transient Seepage Condition

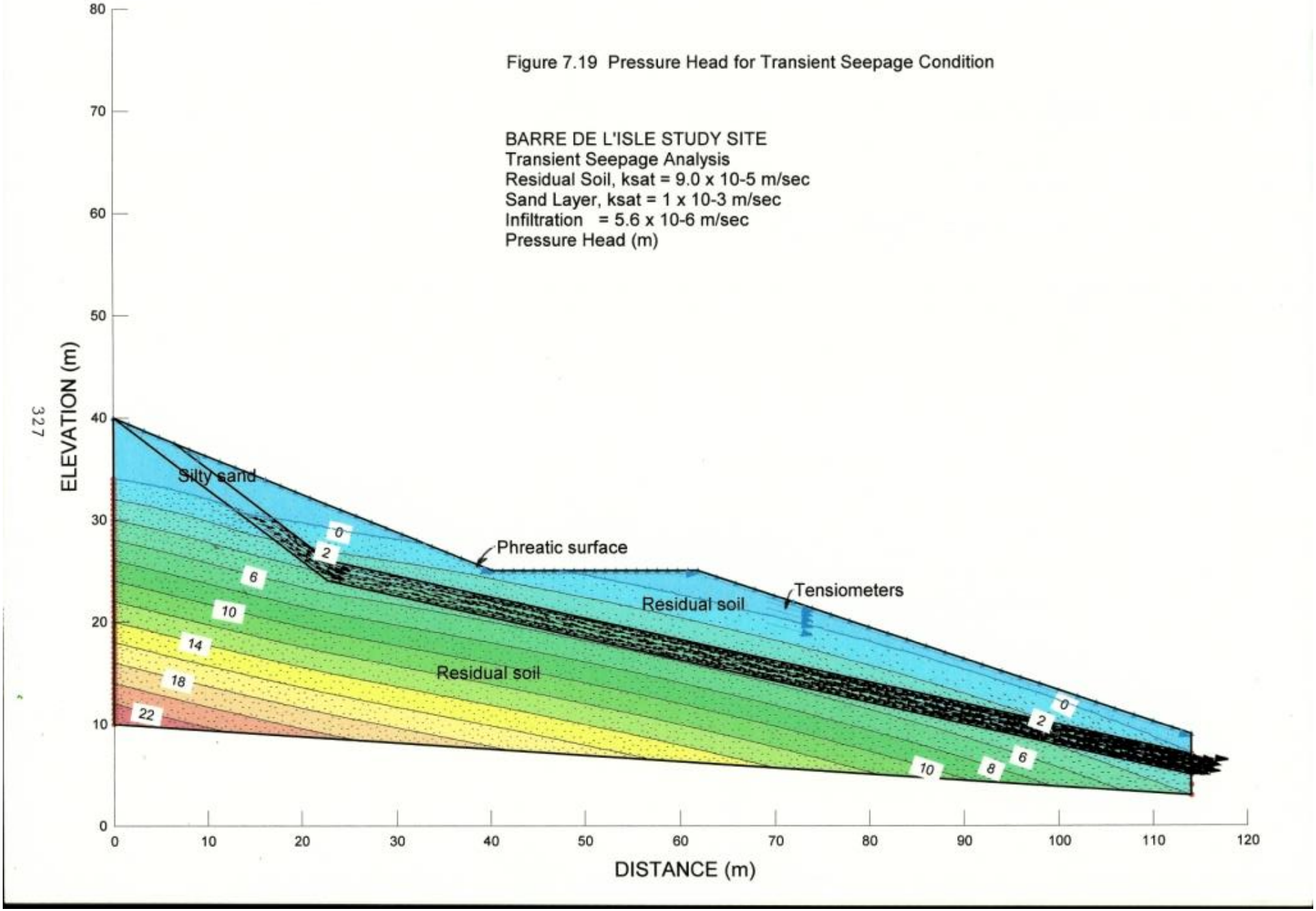

Figure 7.20 Pore Water Pressure for Transient Seepage Condition

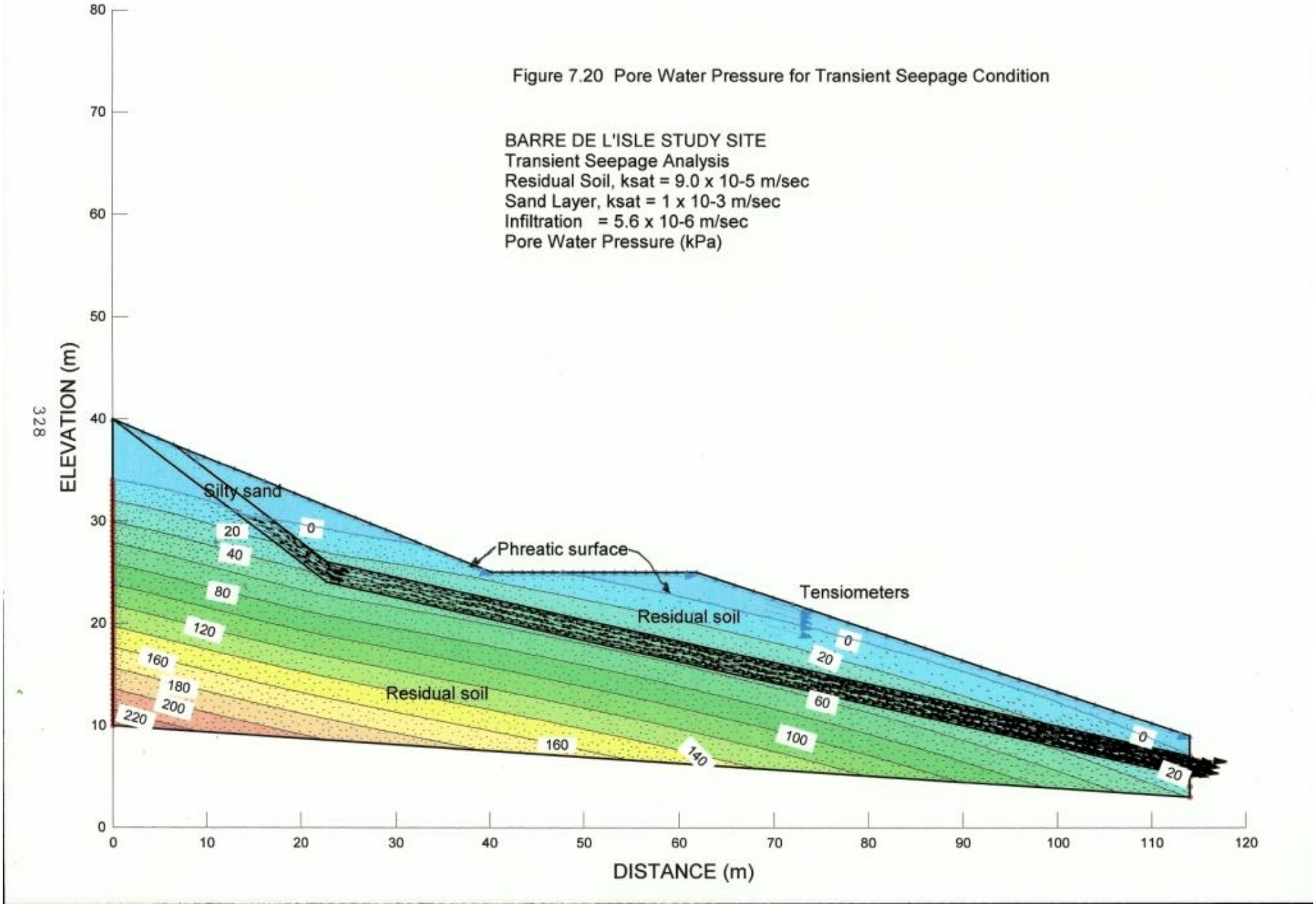

Figure 7.21 XY-Velocity For Transient Seepage Condition

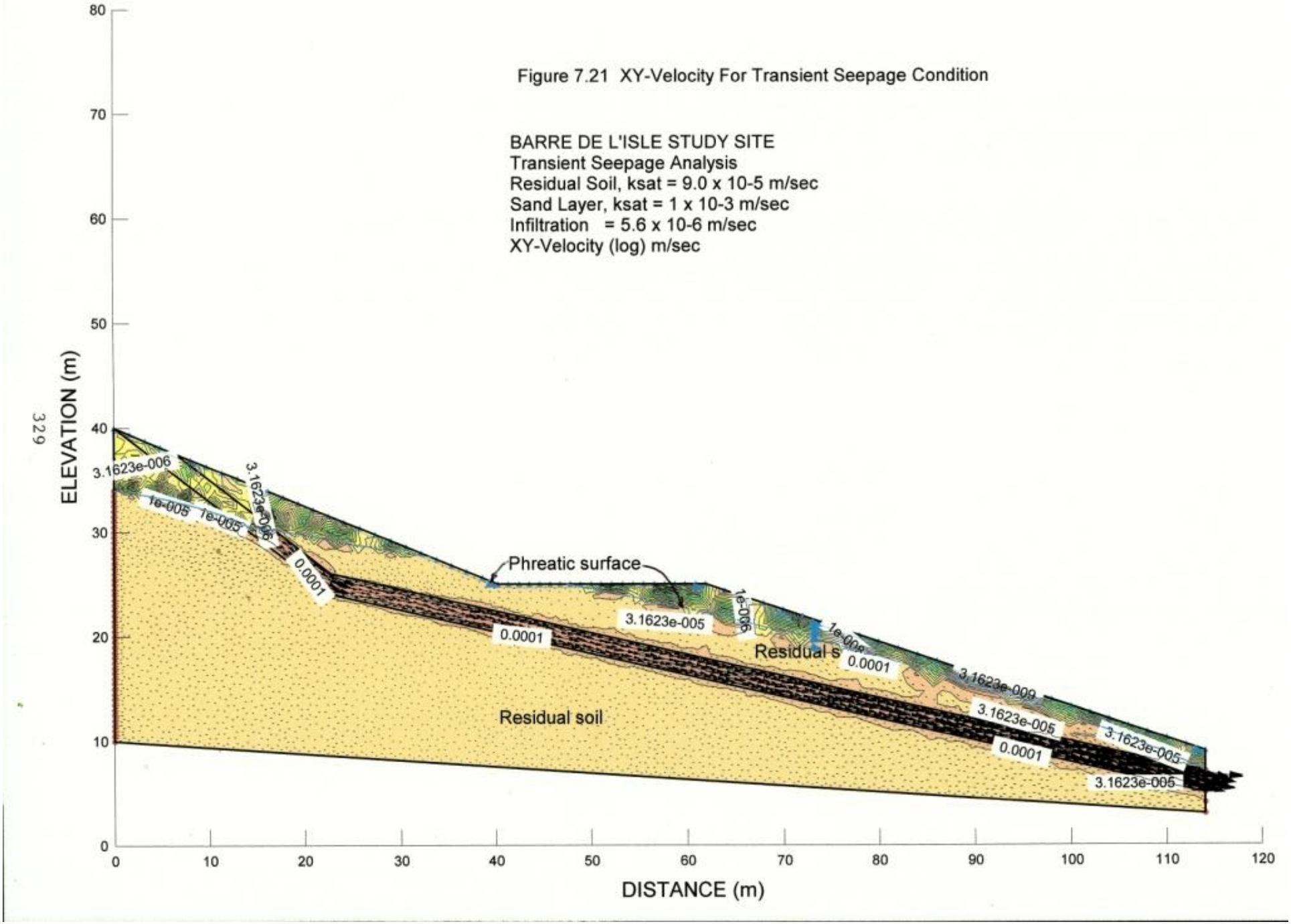

Figure 7.22 XY-Gradient for Transient Seepage Condition

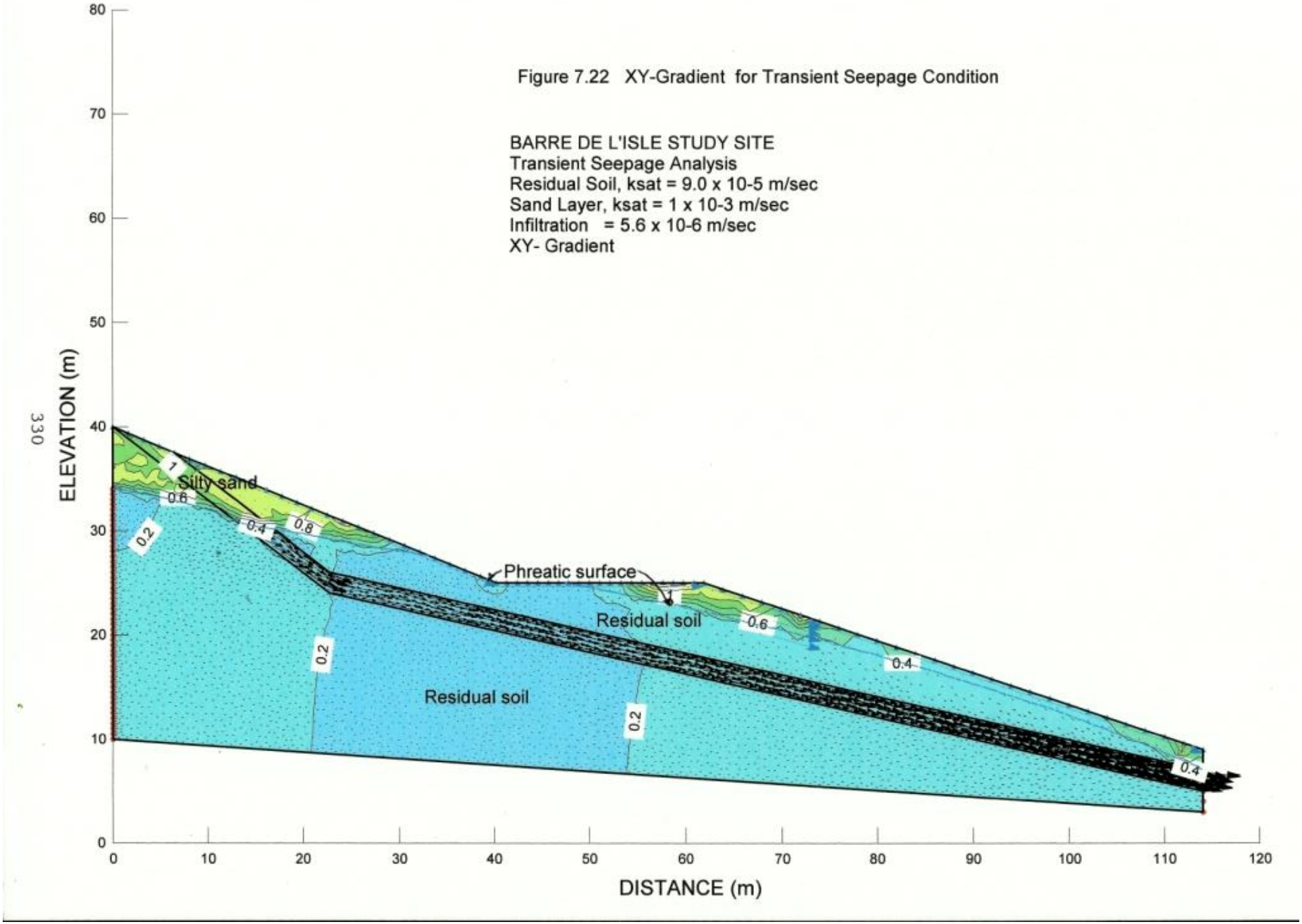

Figure 7.23 X-Hydraulic Conductivity for Transient Seepage Condition

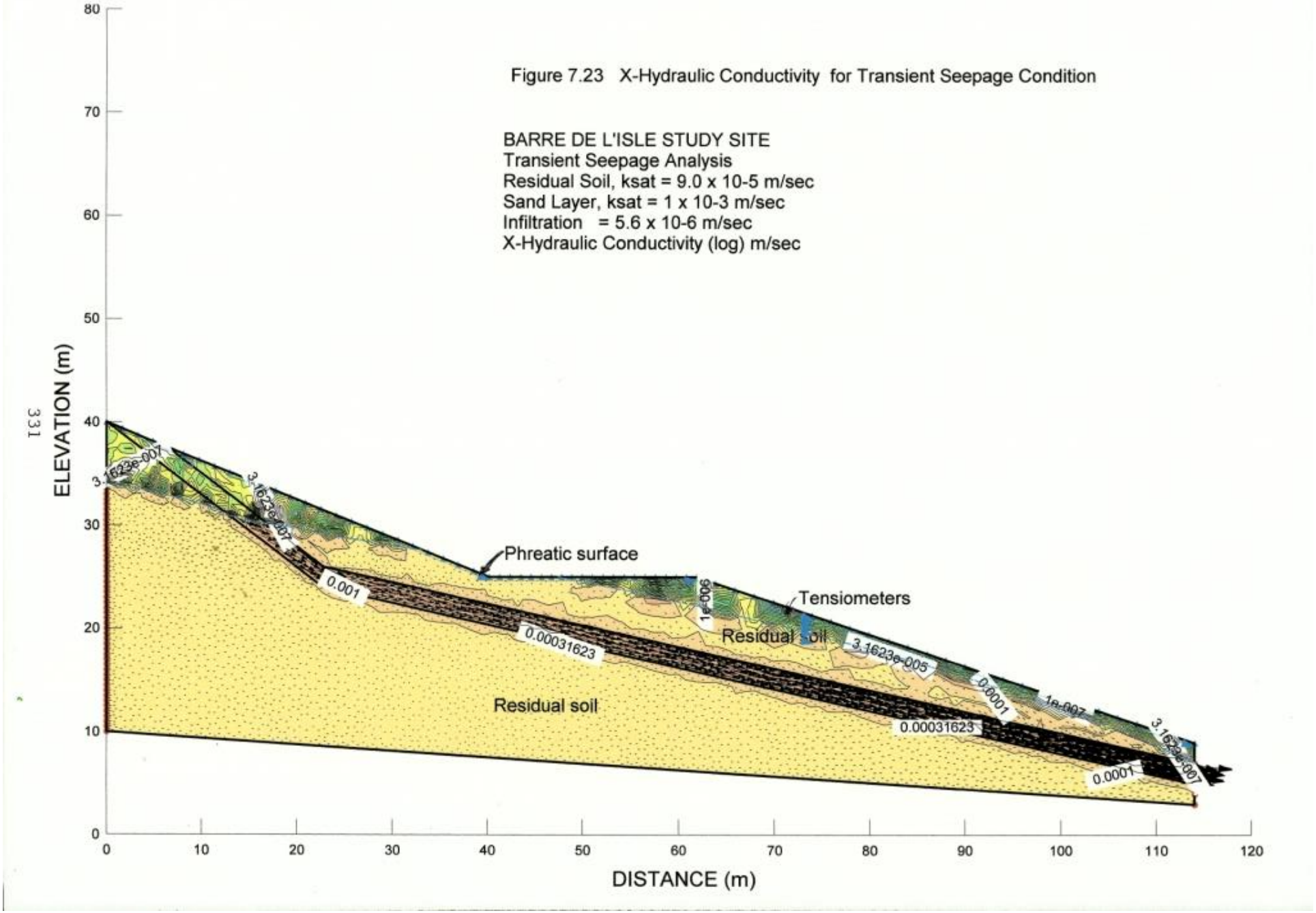

Figure 7.24 Volumetric Water Content for Transient Seepage Condition

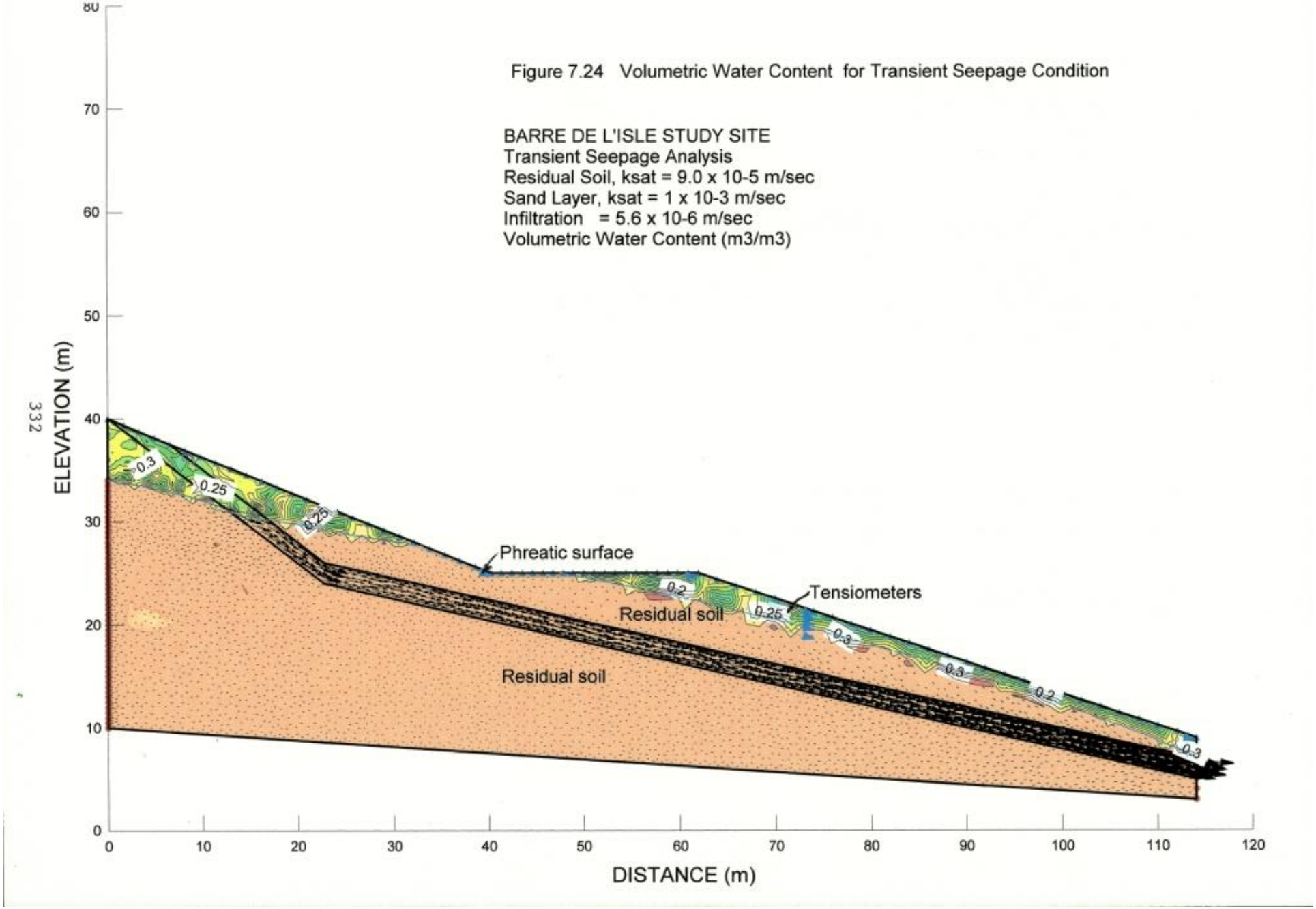

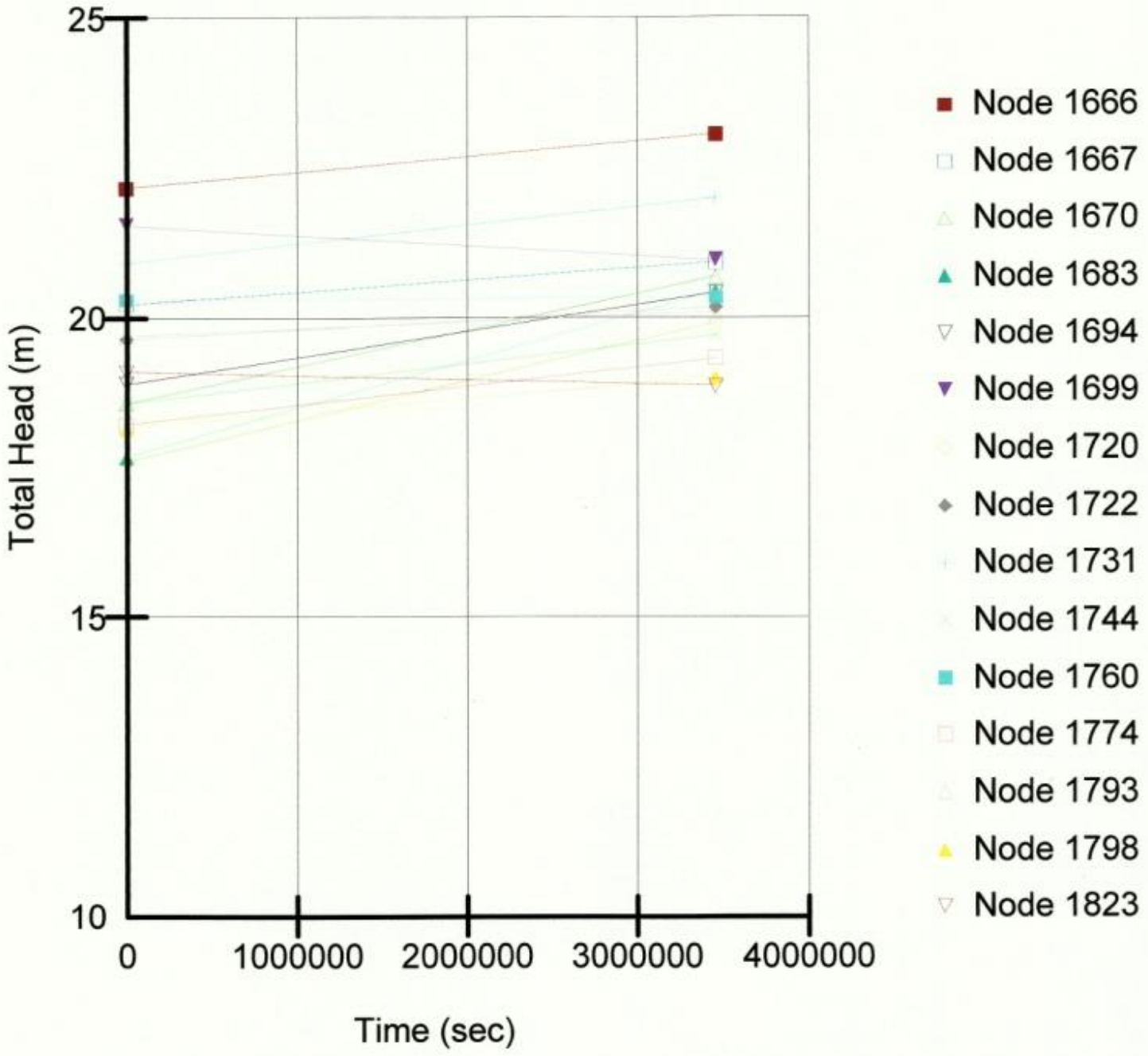

Figure 7.25 : Graph of Changes in Total Head

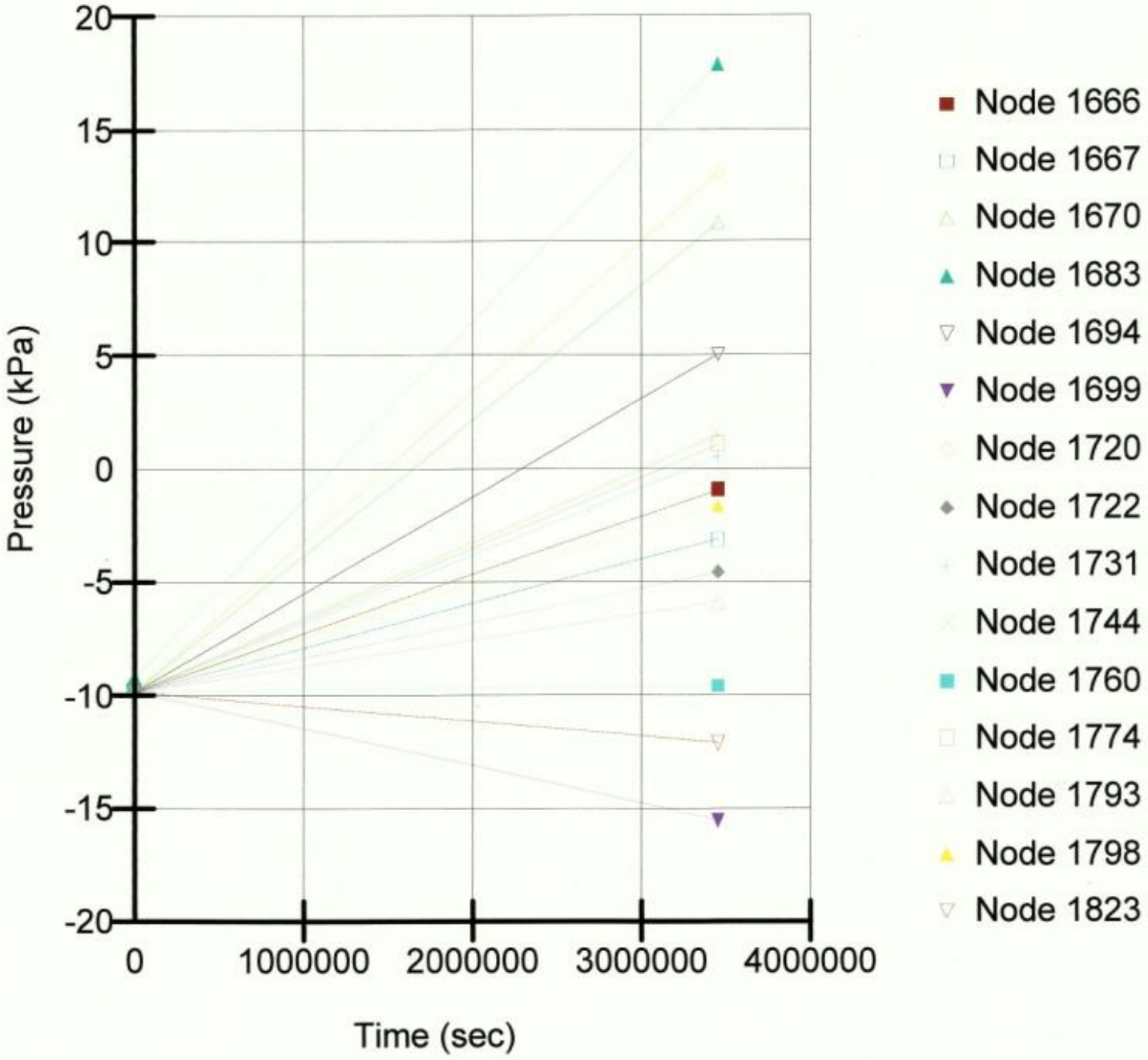

Figure 7.26 : Graph of Changes in Pore Water Pressure at the Ground Surface and up to 3.0m during the Transient Process at the Barre de Lisle Site

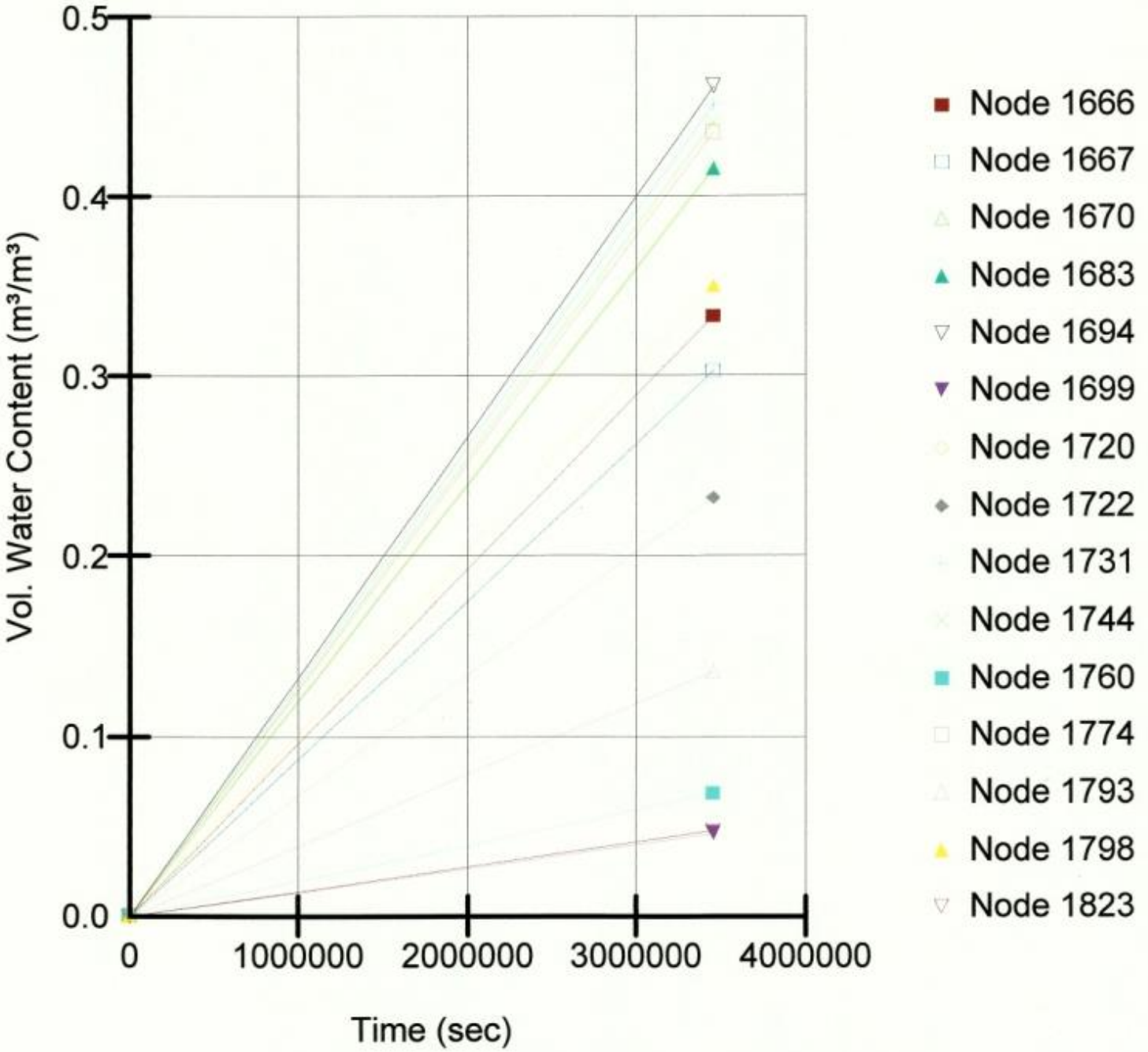

Figure 7.27 : Graph of Changes in the Volumetric Water Content During the Transient Process Barre de Lisle Study Site

Figure 7.28 Back Analysis of Barre de L'isle Slope

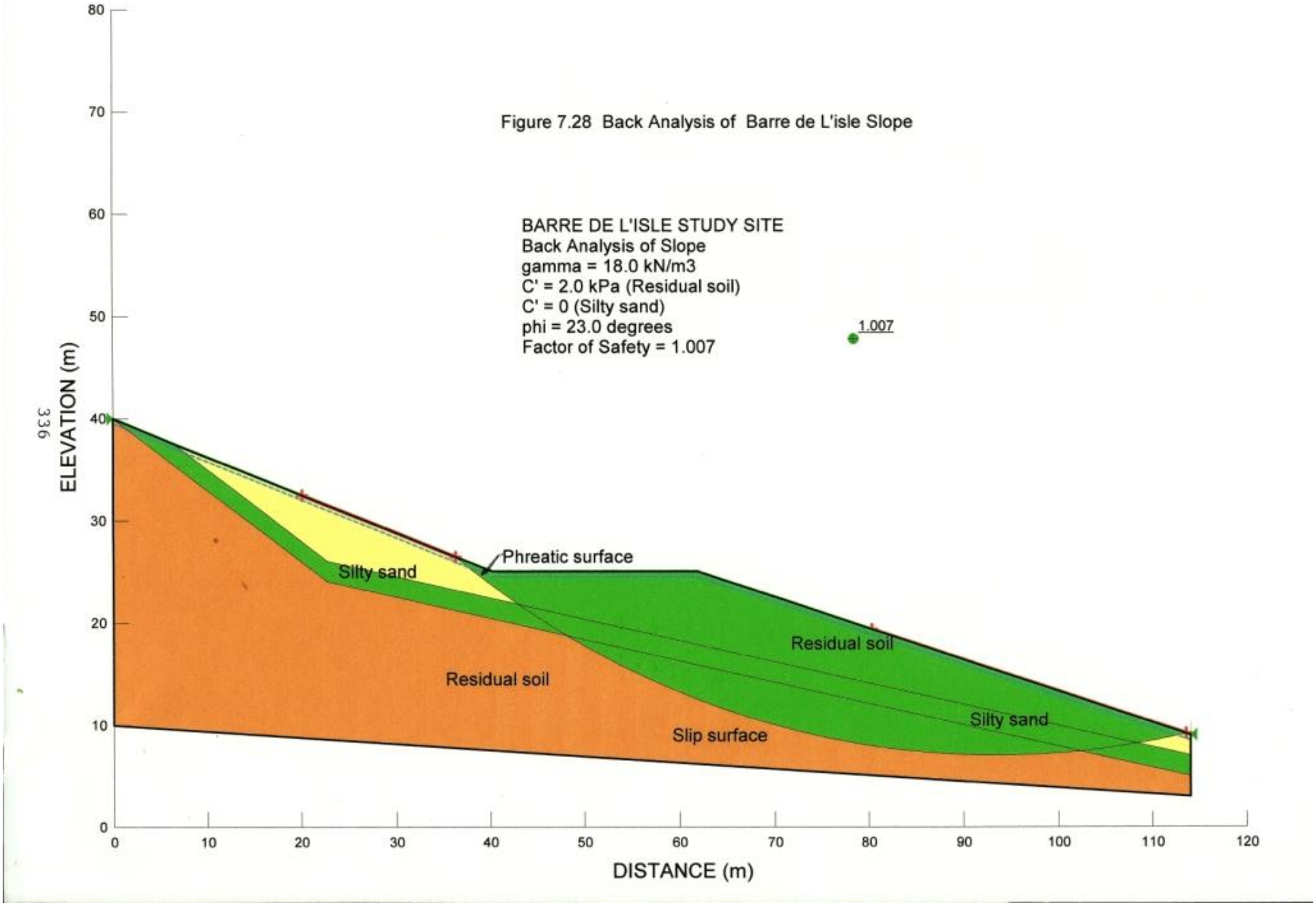

Figure 7.29 Slope Stability Analysis During the Transient Process
Time = 0 (initial) Factor of Safety = 1.414

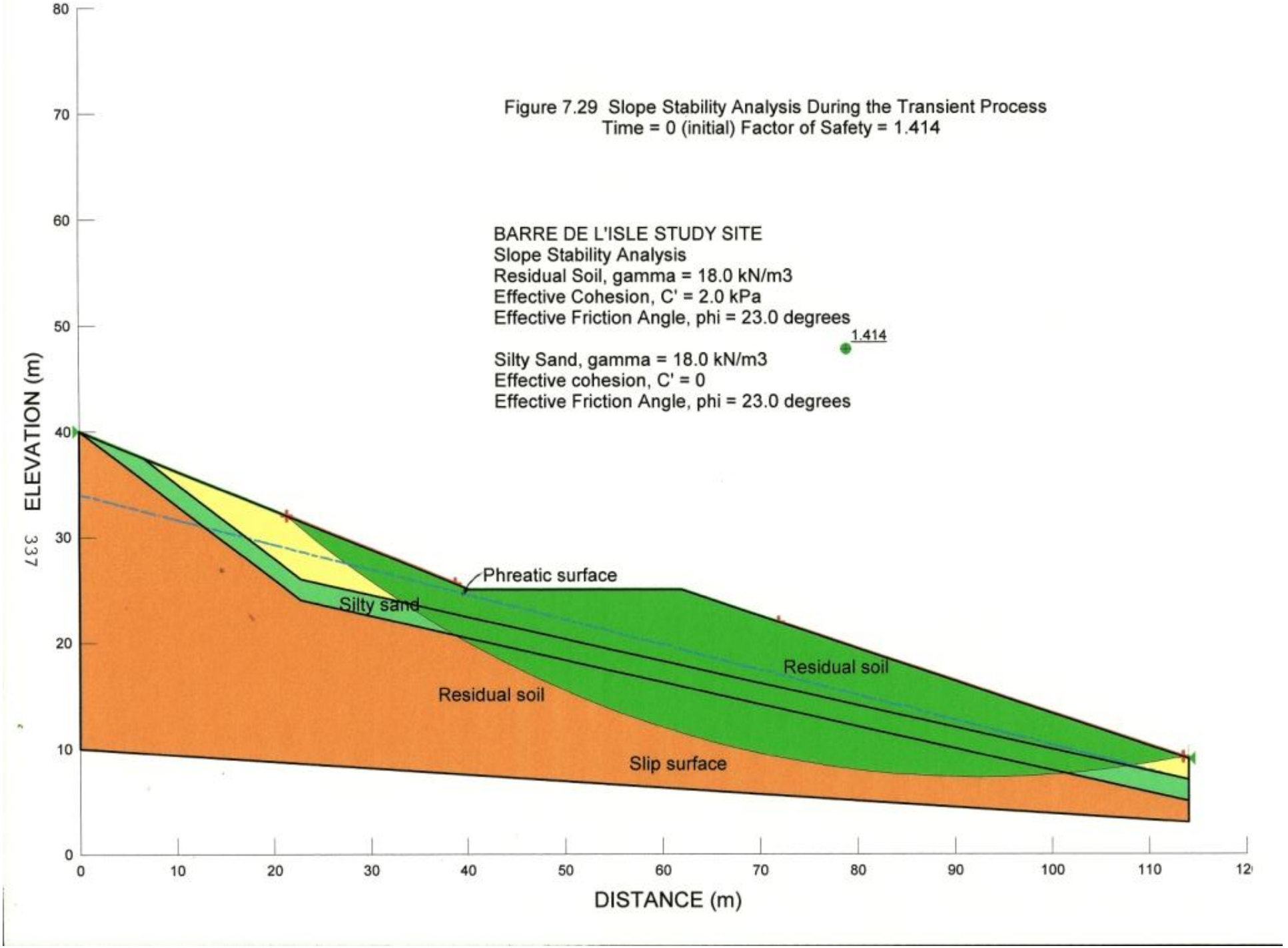

337

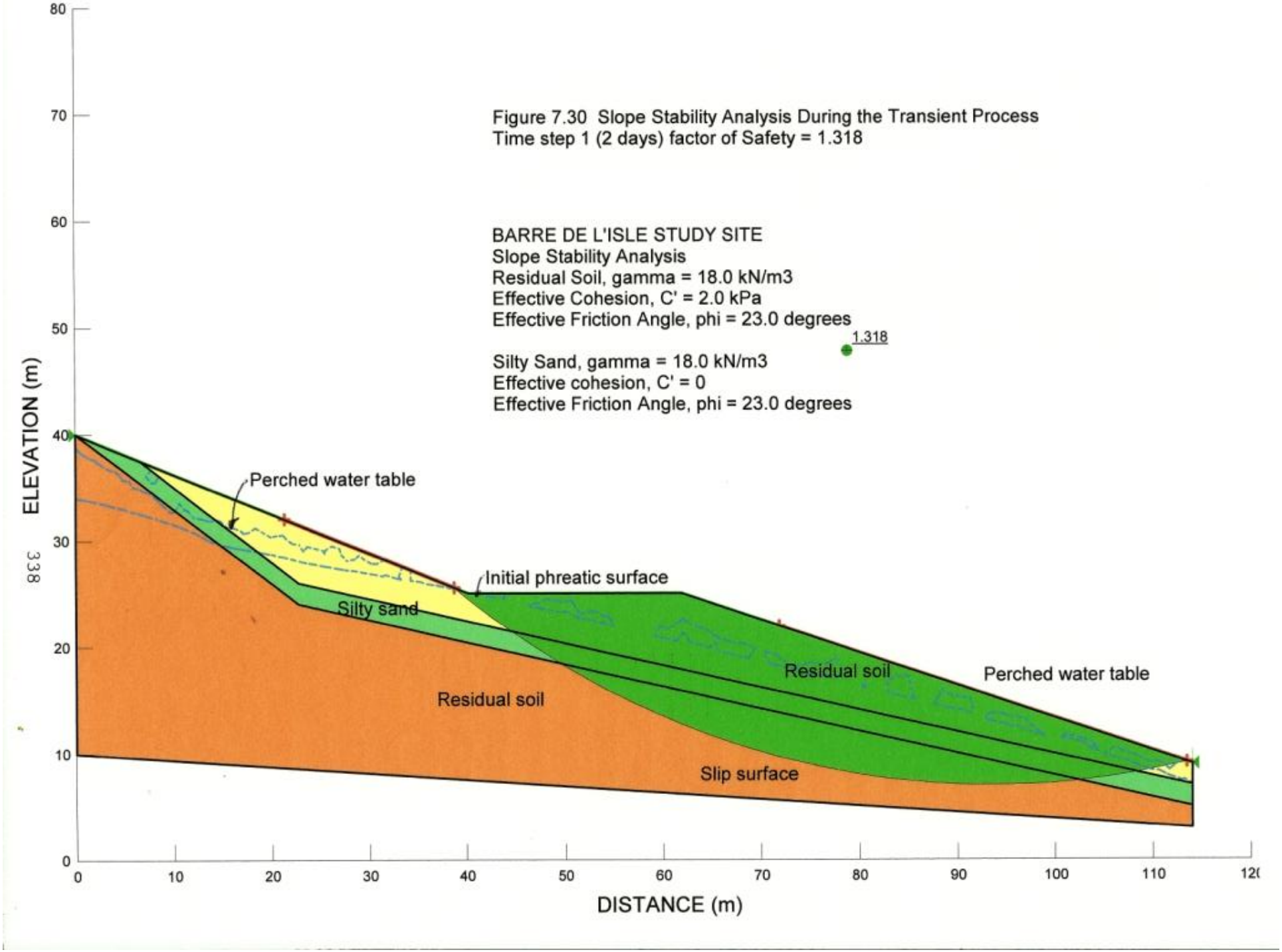
Figure 7.30 Slope Stability Analysis During the Transient Process
Time step 1 (2 days) factor of Safety = 1.318
BARRE DE L'ISLE STUDY SITE
Slope Stability Analysis
Residual Soil, gamma = 18.0 kN/m3
Effective Cohesion, C' = 2.0 kPa
Effective Friction Angle, phi = 23.0 degrees
1.318
Silty Sand, gamma = 18.0 kN/m3
Effective cohesion, C' = 0
Effective Friction Angle, phi = 23.0 degrees
Perched water table
Initial phreatic surface
Silty sand
Residual soil
Residual soil
Perched water table
Slip surface
ELEVATION (m)
DISTANCE (m)
0
10
20
30
40
50
60
70
80
90
100
110
120

Figure 7.31 Slope Stability Analysis During the Transient Process
Time Step 2 (4 days) Factor of Safety = 1.140

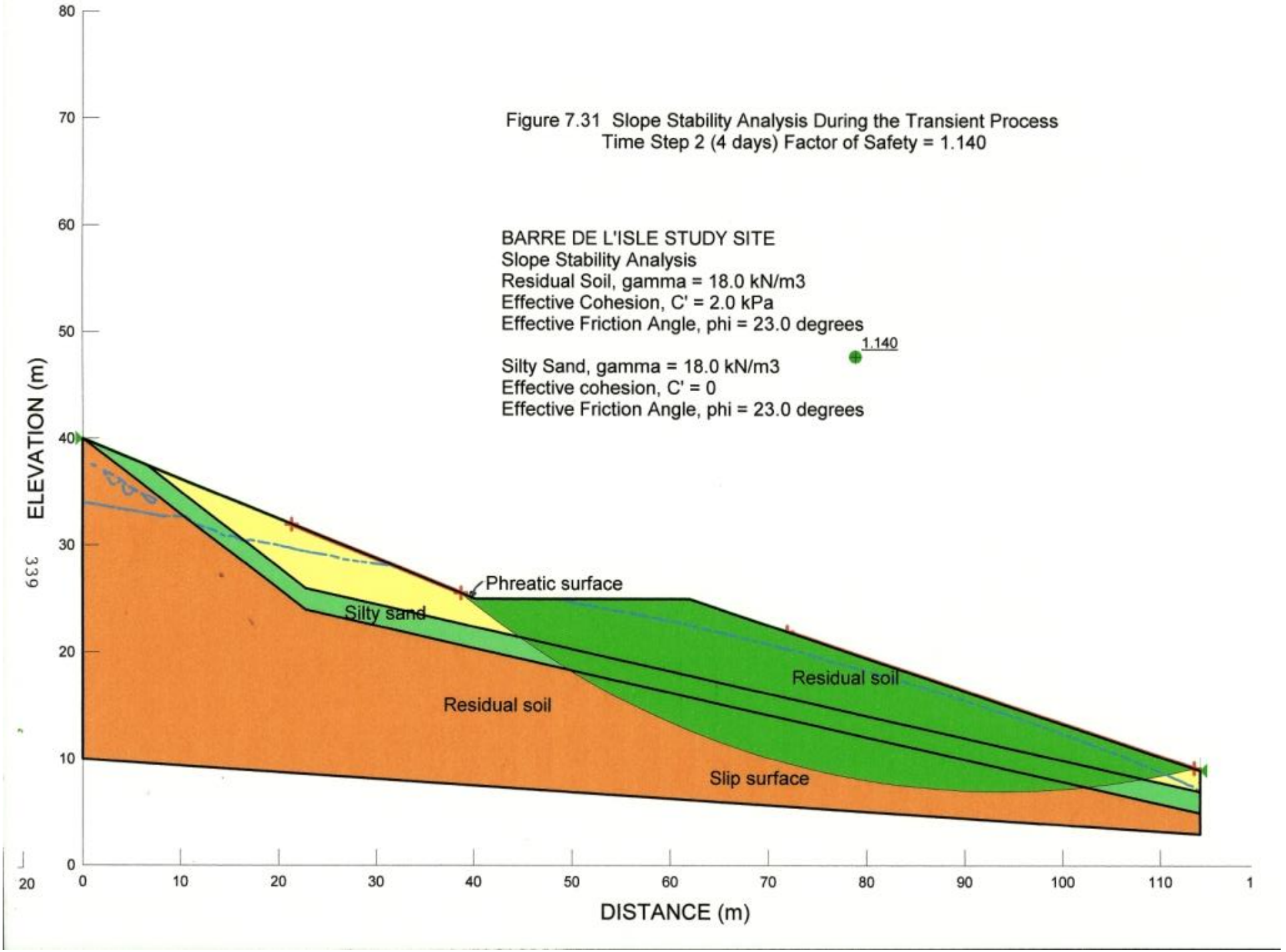

Figure 7.32 Slope Stability Analysis During the Transient Process
Time Step 3 (6 days) Factor of Safety = 1.170

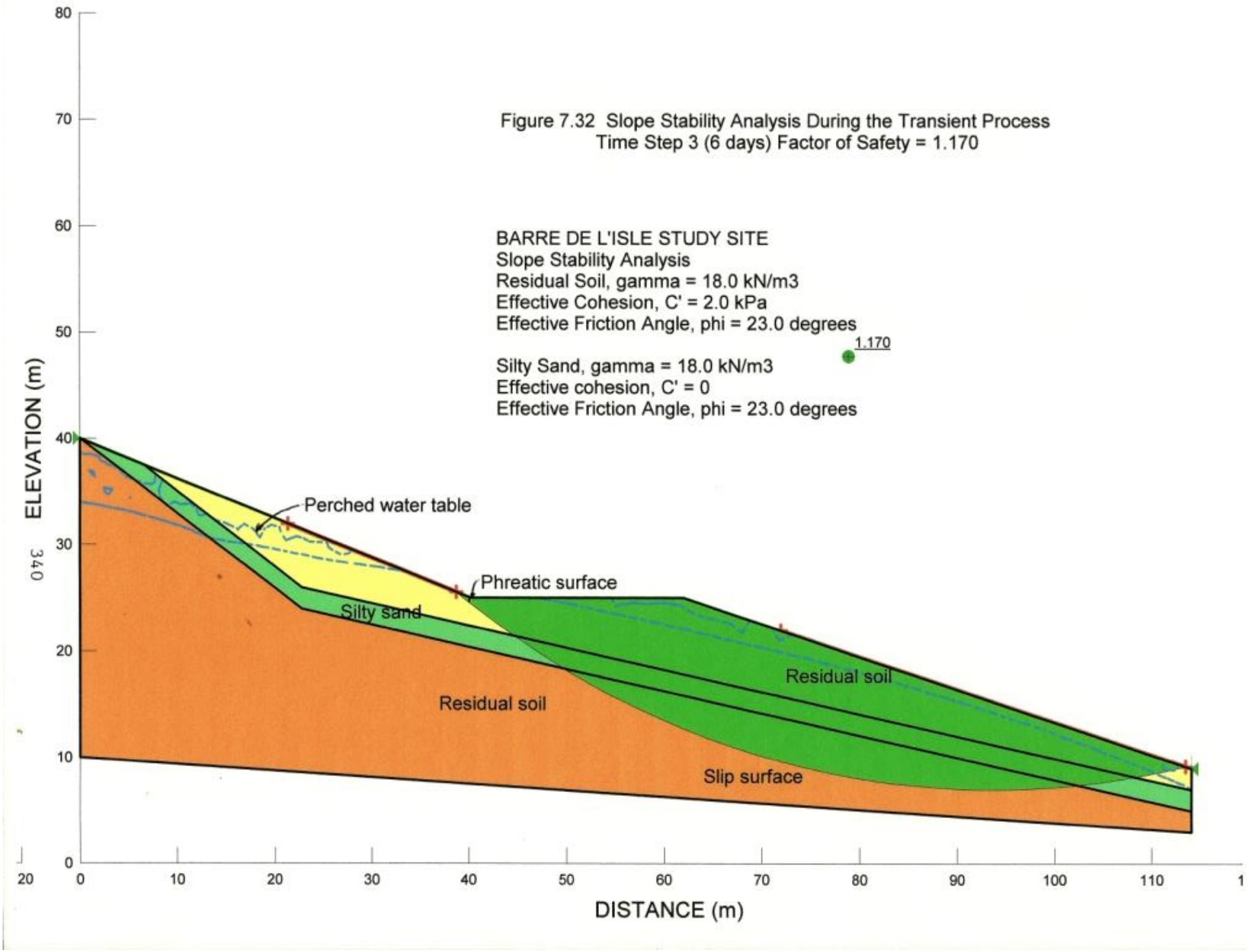

Figure 7.33 Slope Stability Analysis During the Transient Process
Time Step 4 (8 days) Factor of Safety = 1.155

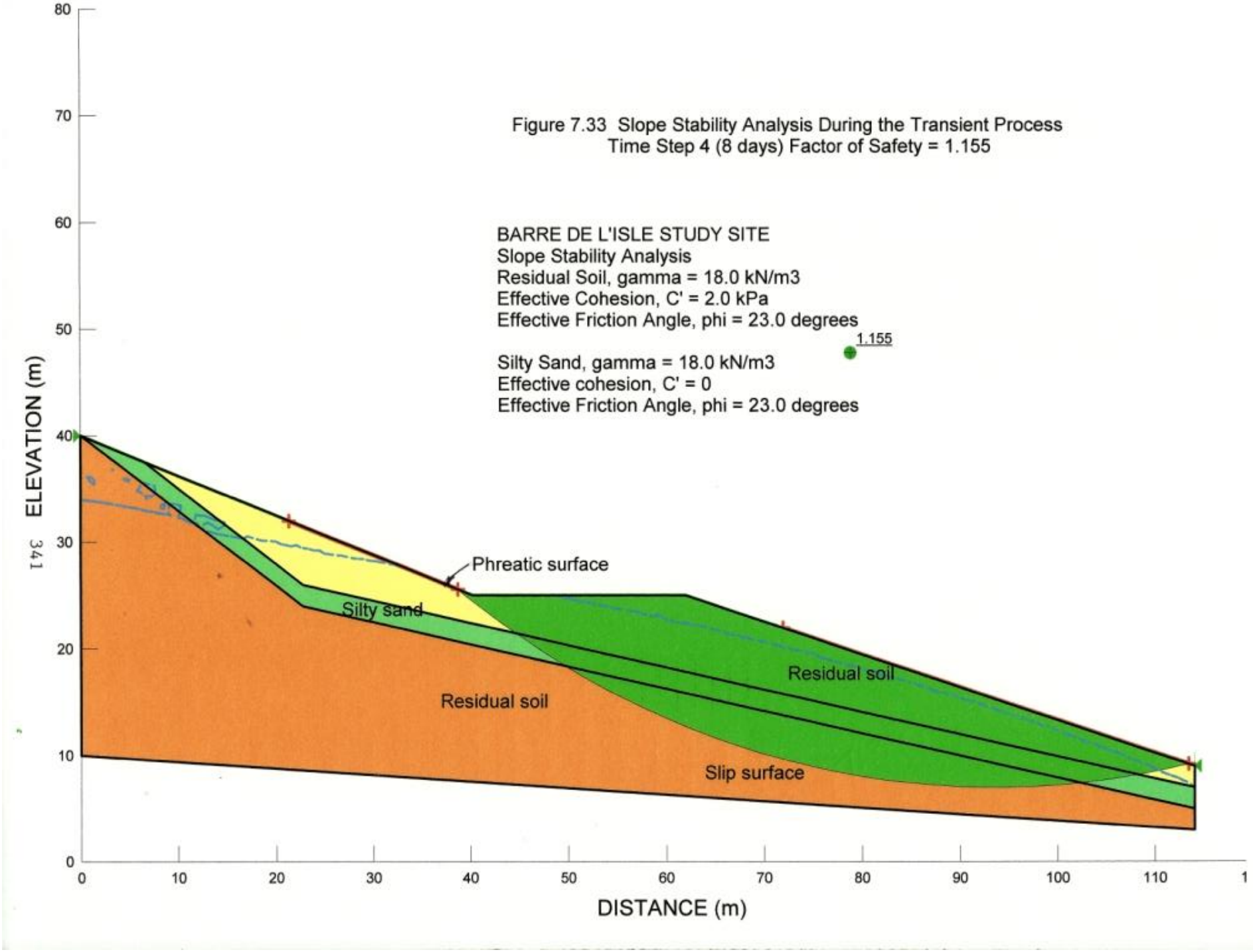

Figure 7.34 Slope Stability Analysis During the Transient Process
Time Step 5 (10 days) Factor of Safety = 1.169

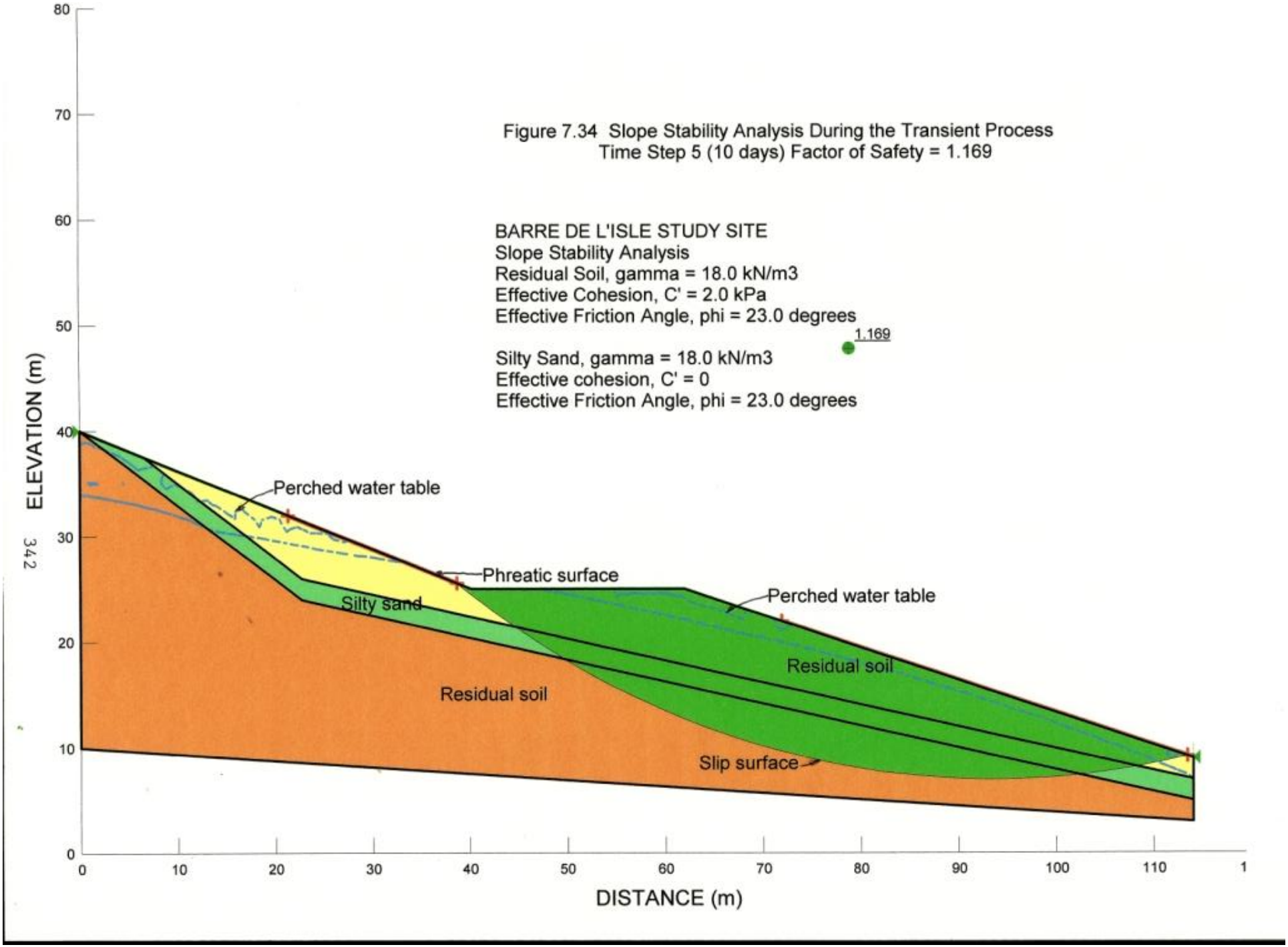

Figure 7.35 Finite Element Mesh Design - Windjammer Landing Beach Resort
Seepage Analysis

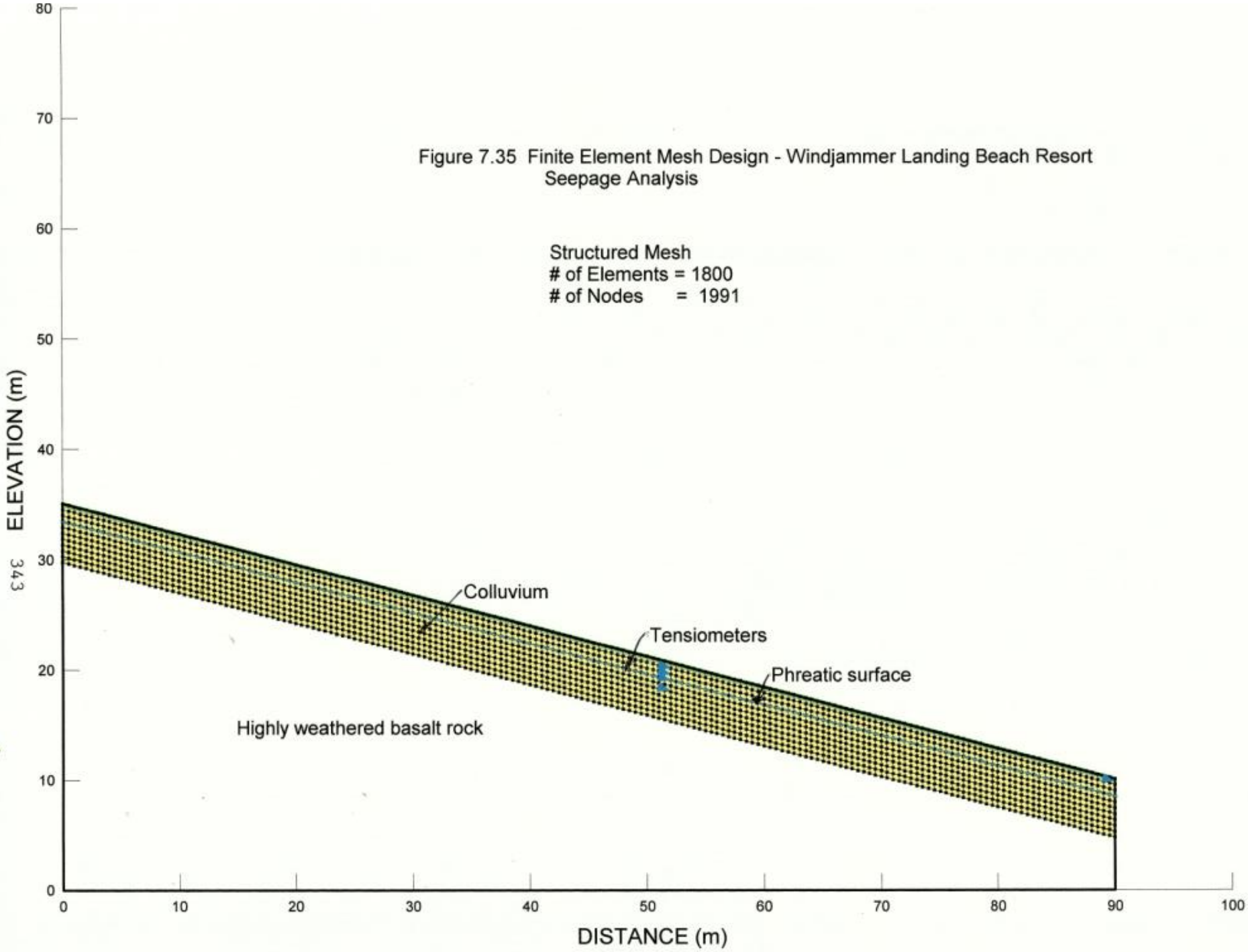

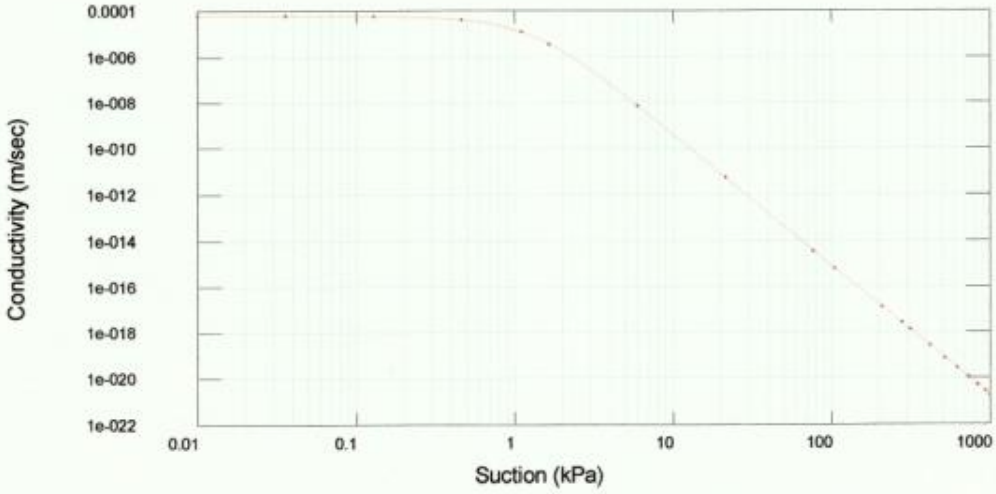

Figure 7.36a Hydraulic Conductivity Function Graph for the Colluvium at the Windjammer Landing Beach Resort

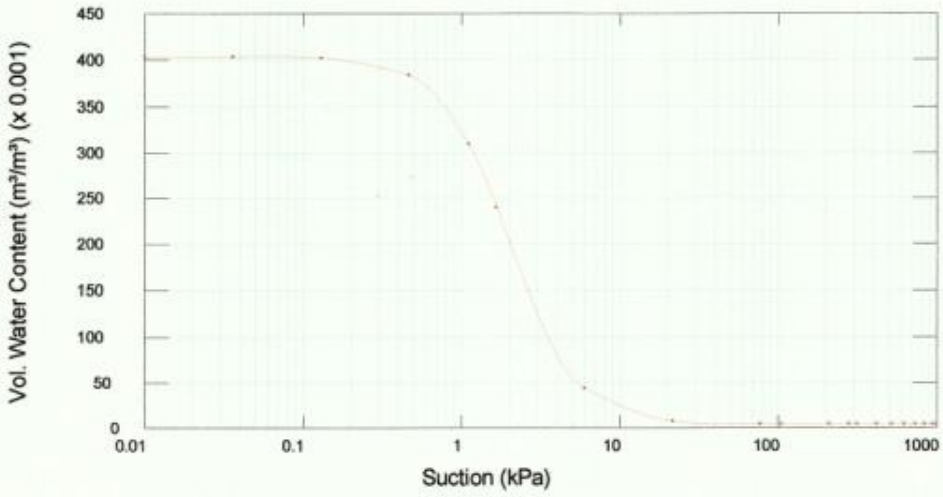

Figure 7.36b Volumetric Water Content Graph for the Colluvium at the Windjammer Landing Landing Beach Resort

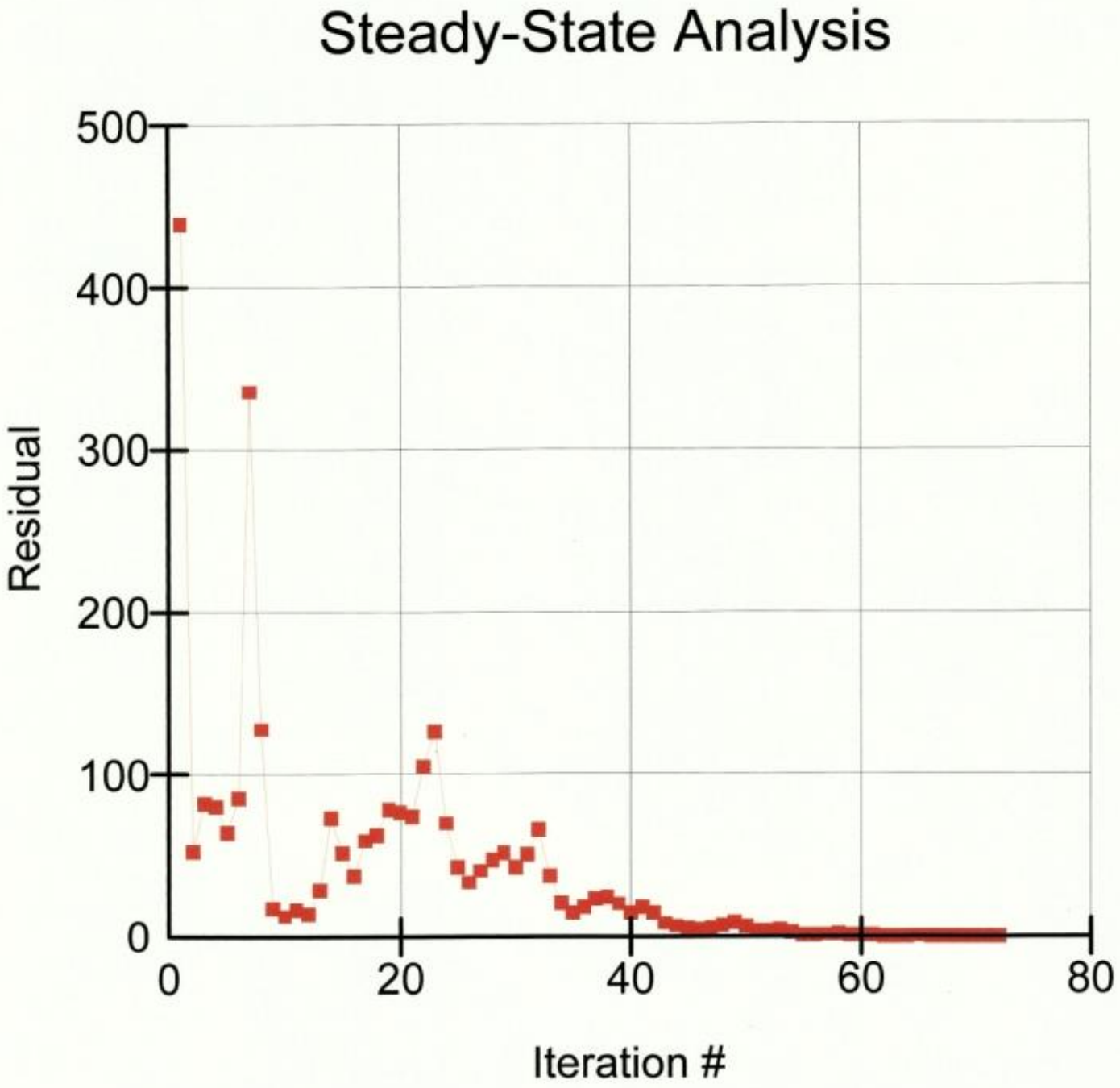

Figure 7.37 : Vector Norm Residual Convergence Graph For Steady State Seepage Analysis Windjammer Landing Beach Resort

Figure 7.38 Total Head for Steady State Seepage Analysis
Windjammer Landing Beach Resort

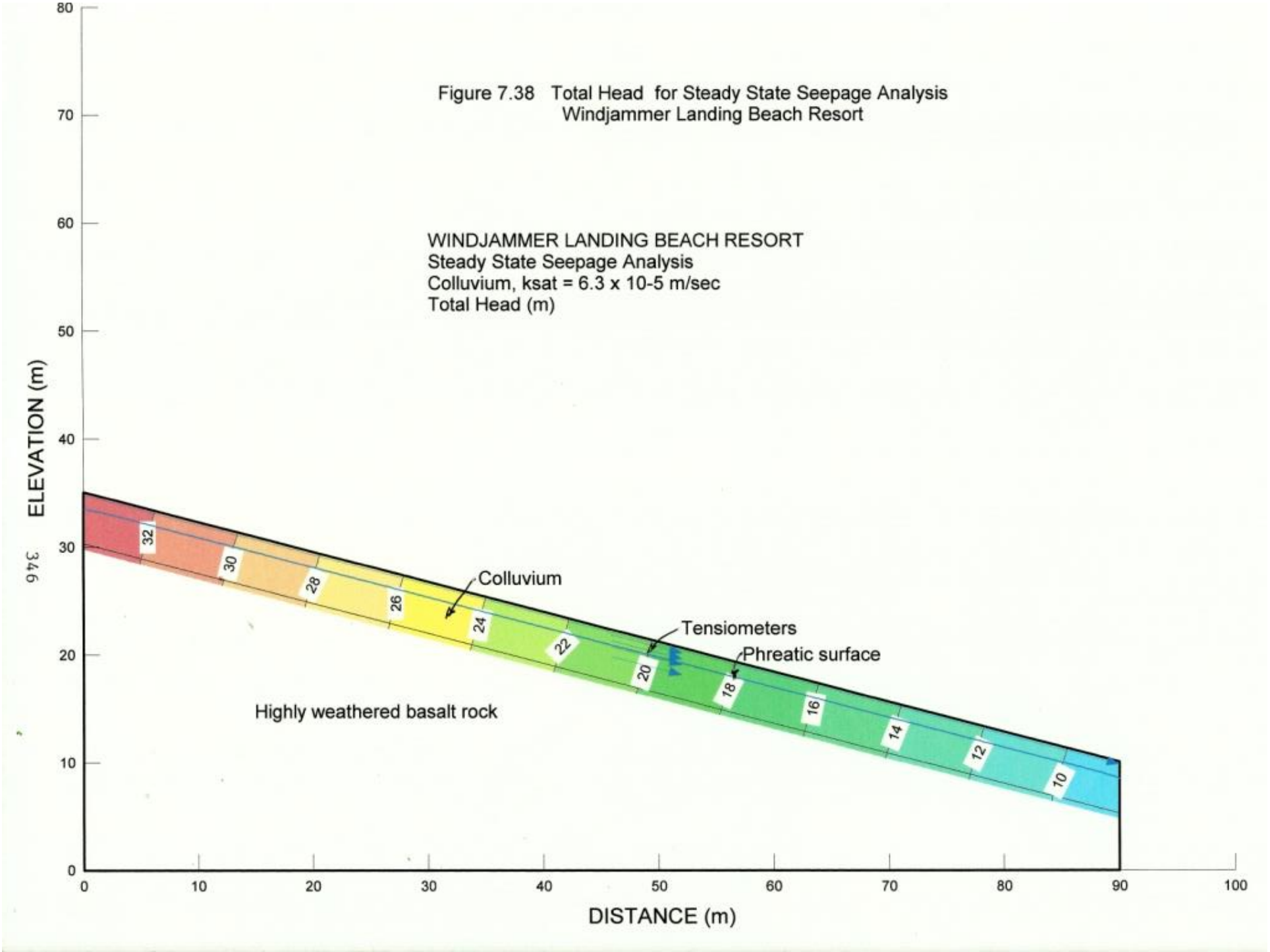

Figure 7.39 Pore Water Pressure for Steady State Seepage Analysis
Windjammer Landing Beach Resort

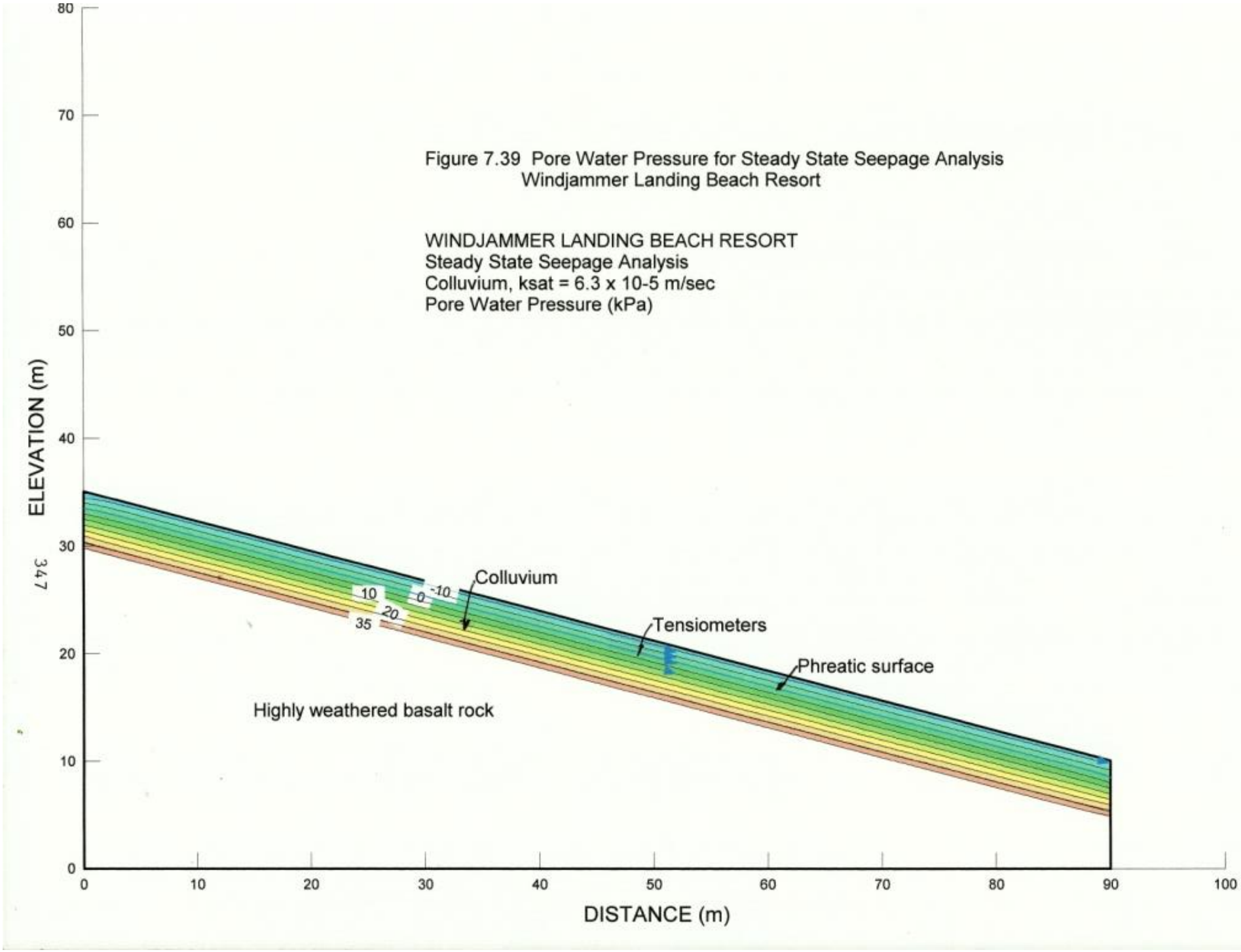

Figure 7.40 Flow Paths for Steady State Seepage Analysis
Windjammer Landing Beach Resort

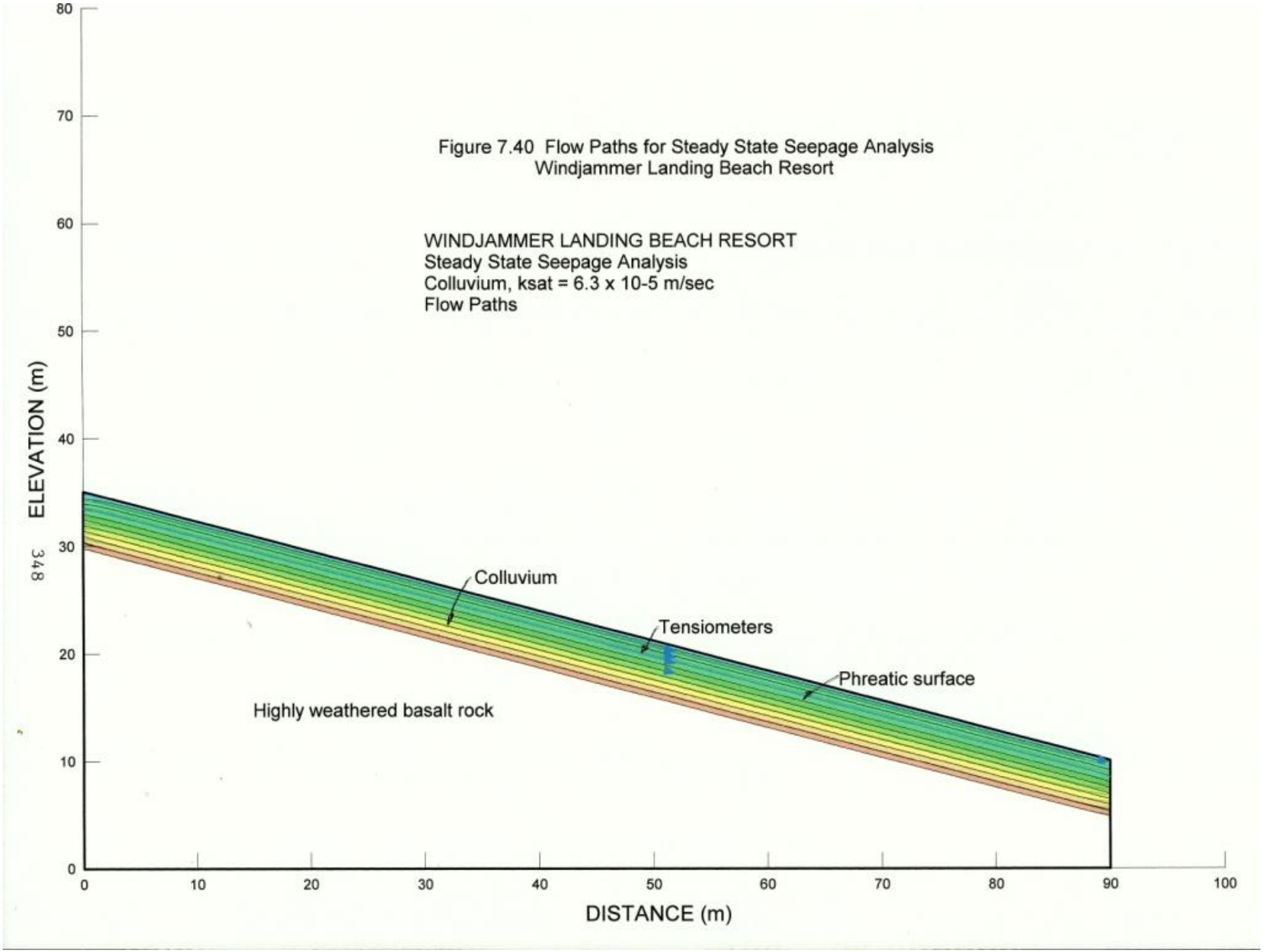

Figure 7.41 Pore Water Pressure Heads for Steady State Seepage Analysis
Windjammer landing Beach Resort

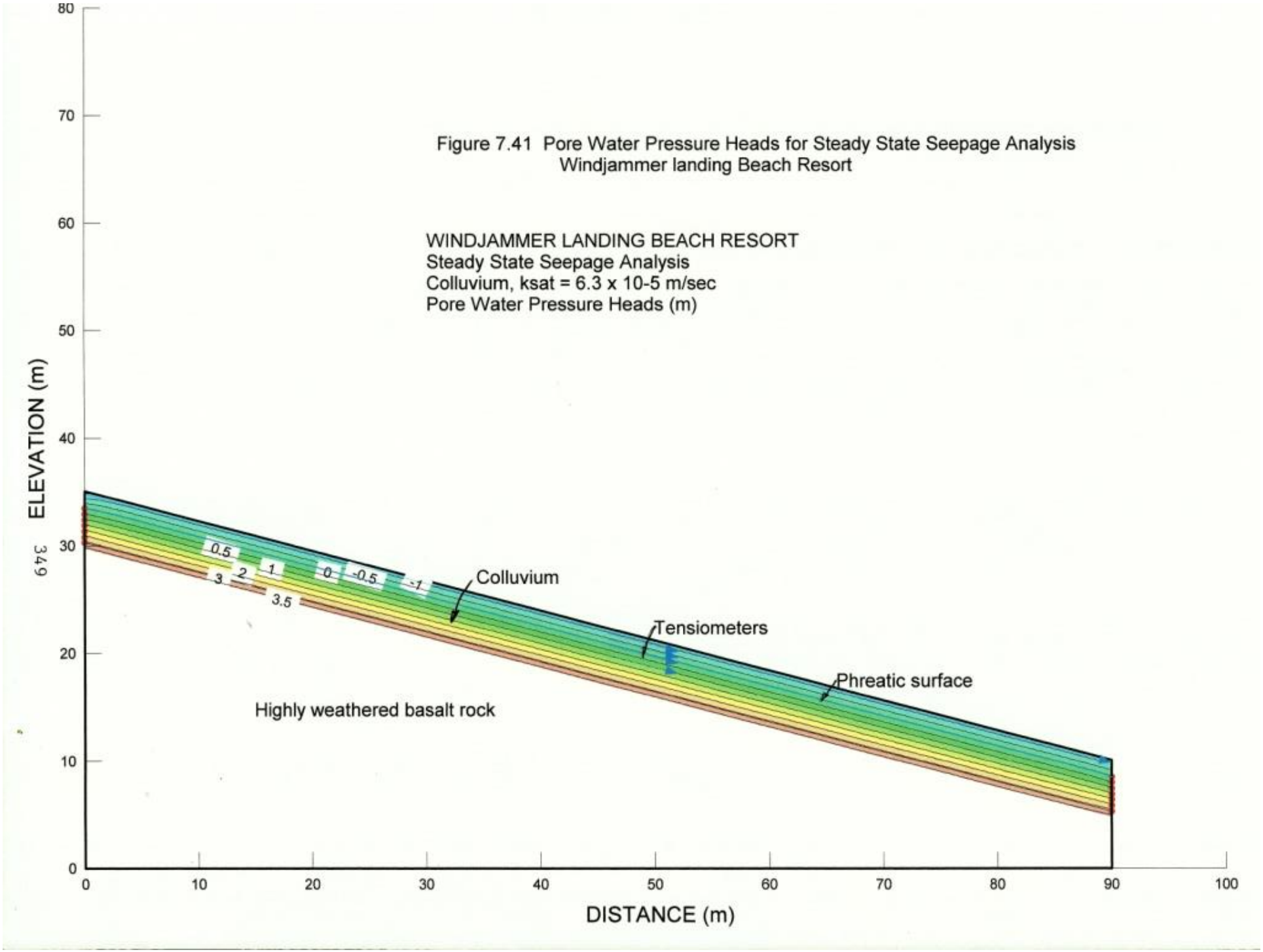

Figure 7.42 Hydraulic Gradient for Steady State Seepage Analysis
Windjammer Landing Beach Resort

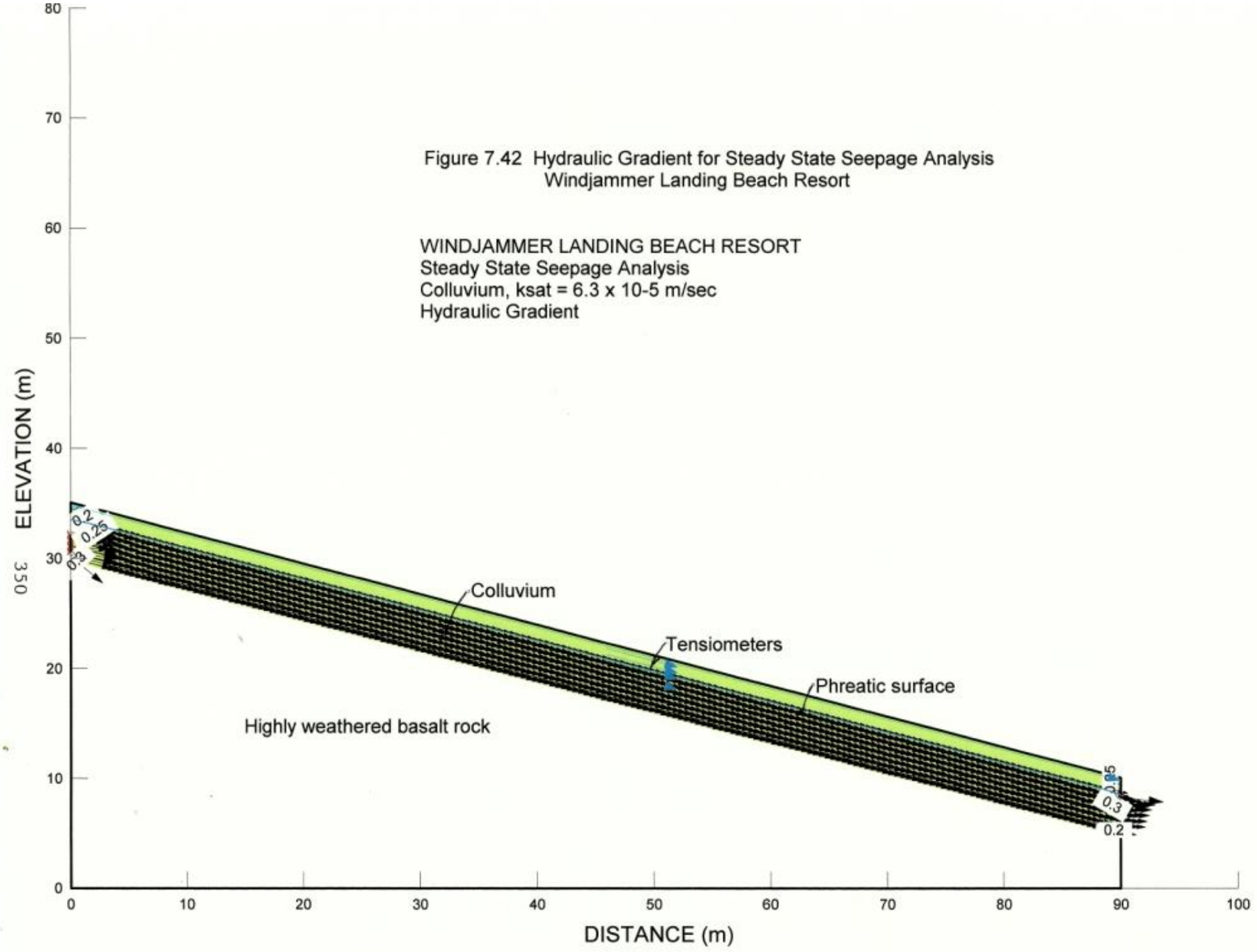

Figure 7.43 XY-Velocity for Steady State Seepage Analysis
Windjammer landing Beach Resort

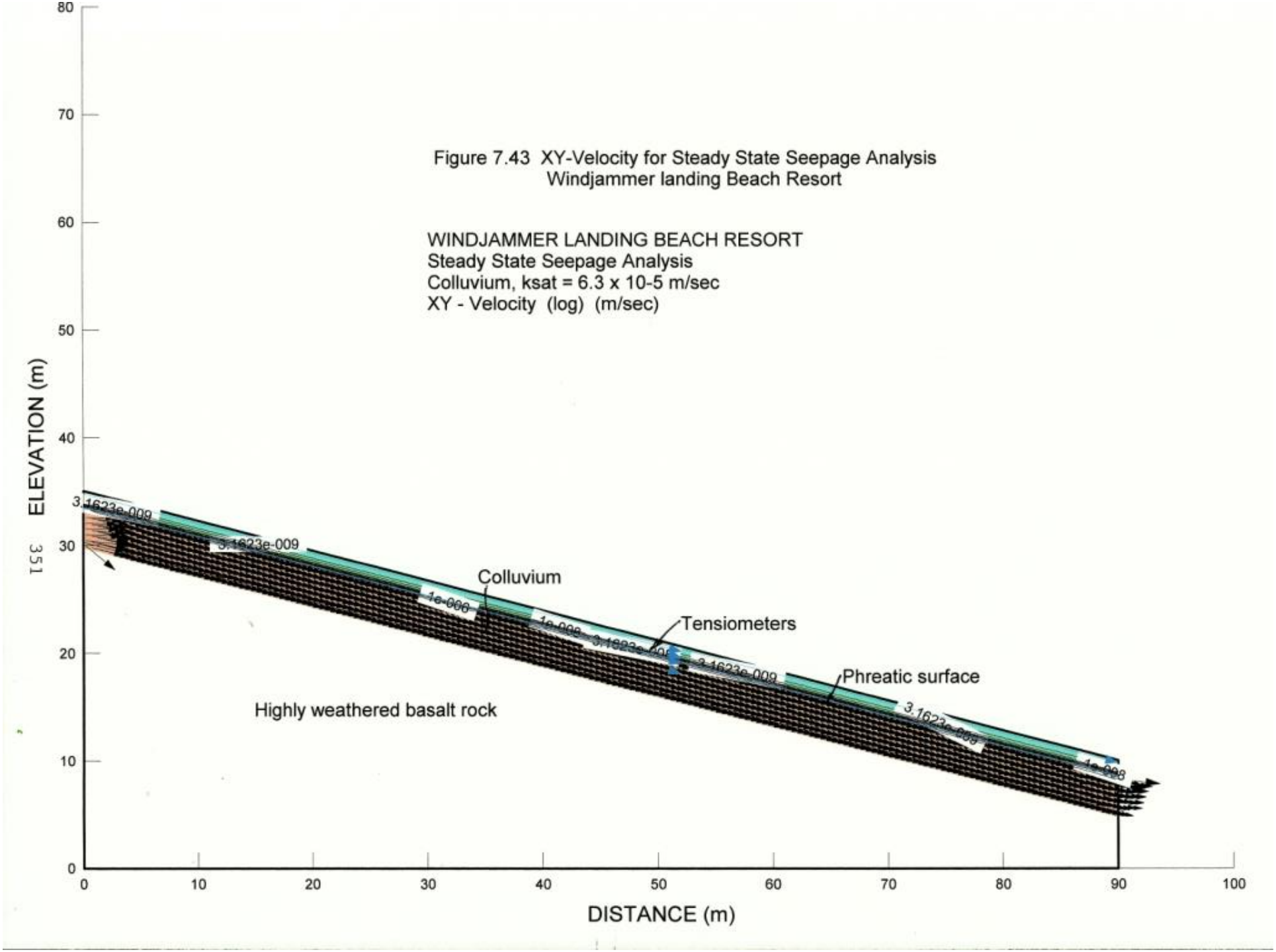

Figure 7.44 X-Hydraulic Conductivity for Steady State Seepage Analysis
Windjammer Landing Beach Resort

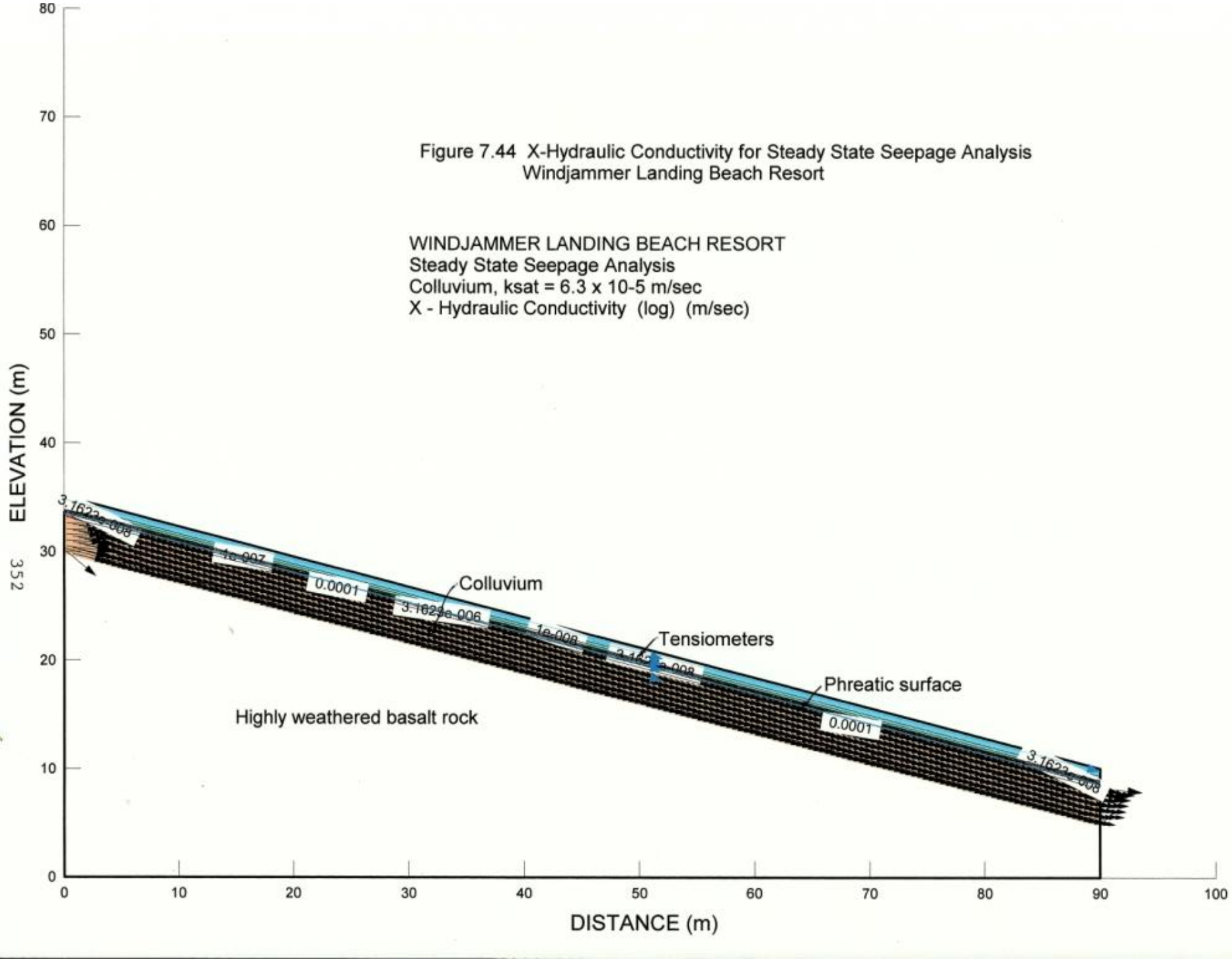

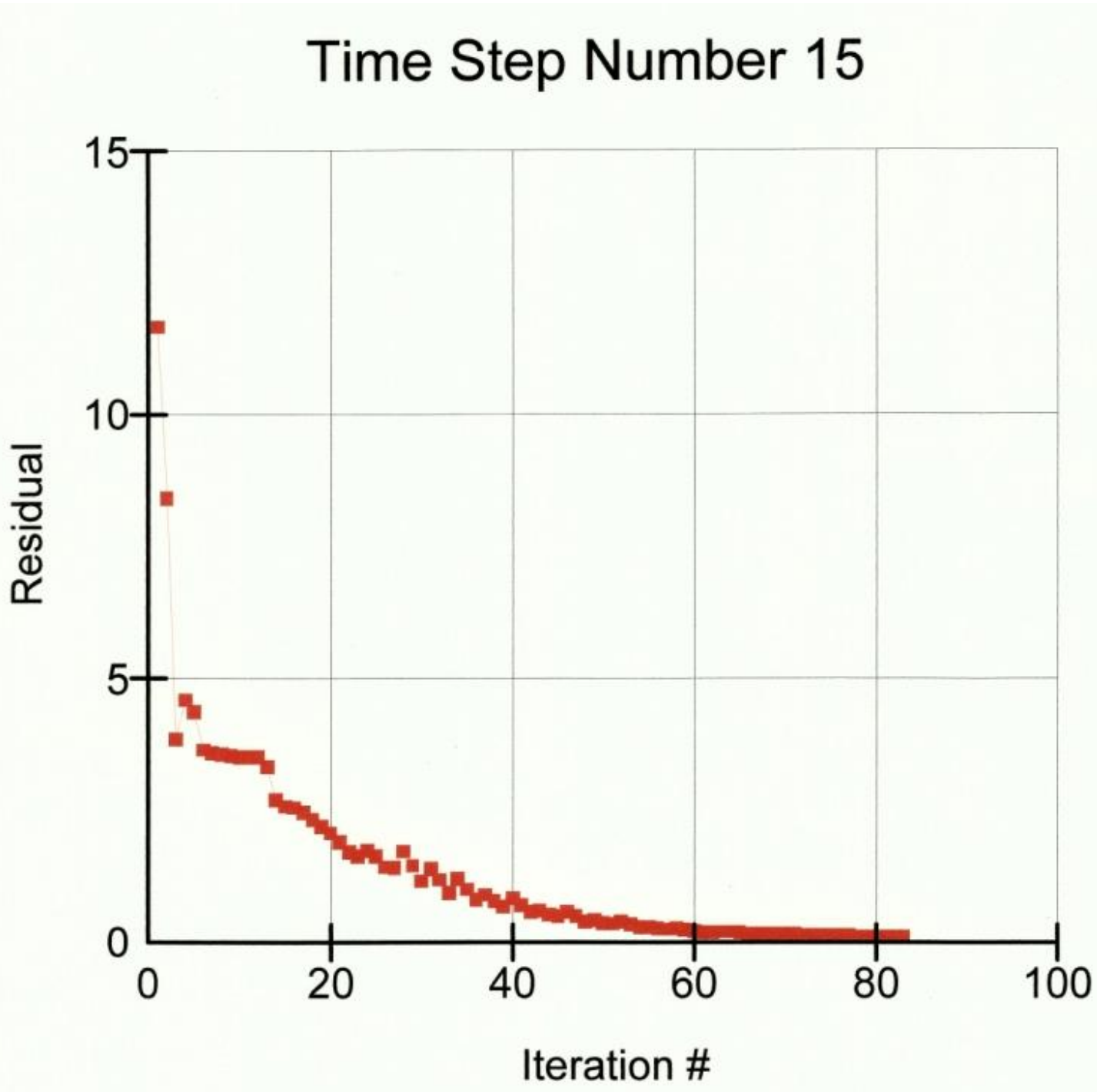

Figure 7.45 : Vector Norm Residual Convergence Graph For Transient Seepage Analysis, Windjammer Landing Beach Resort

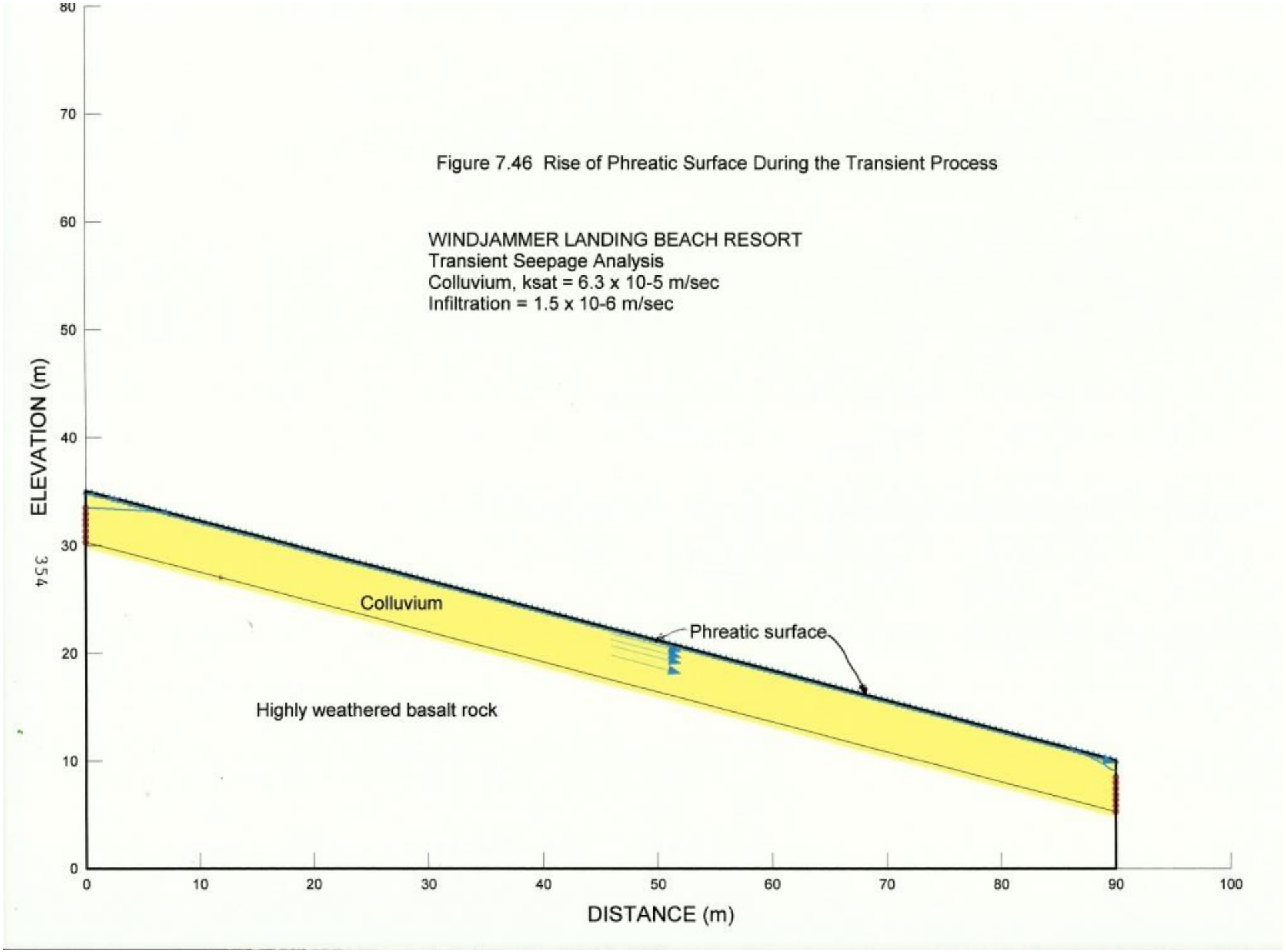

Figure 7.46 Rise of Phreatic Surface During the Transient Process

Figure 7.47 Transient Positions of Rising Phreatic Surface

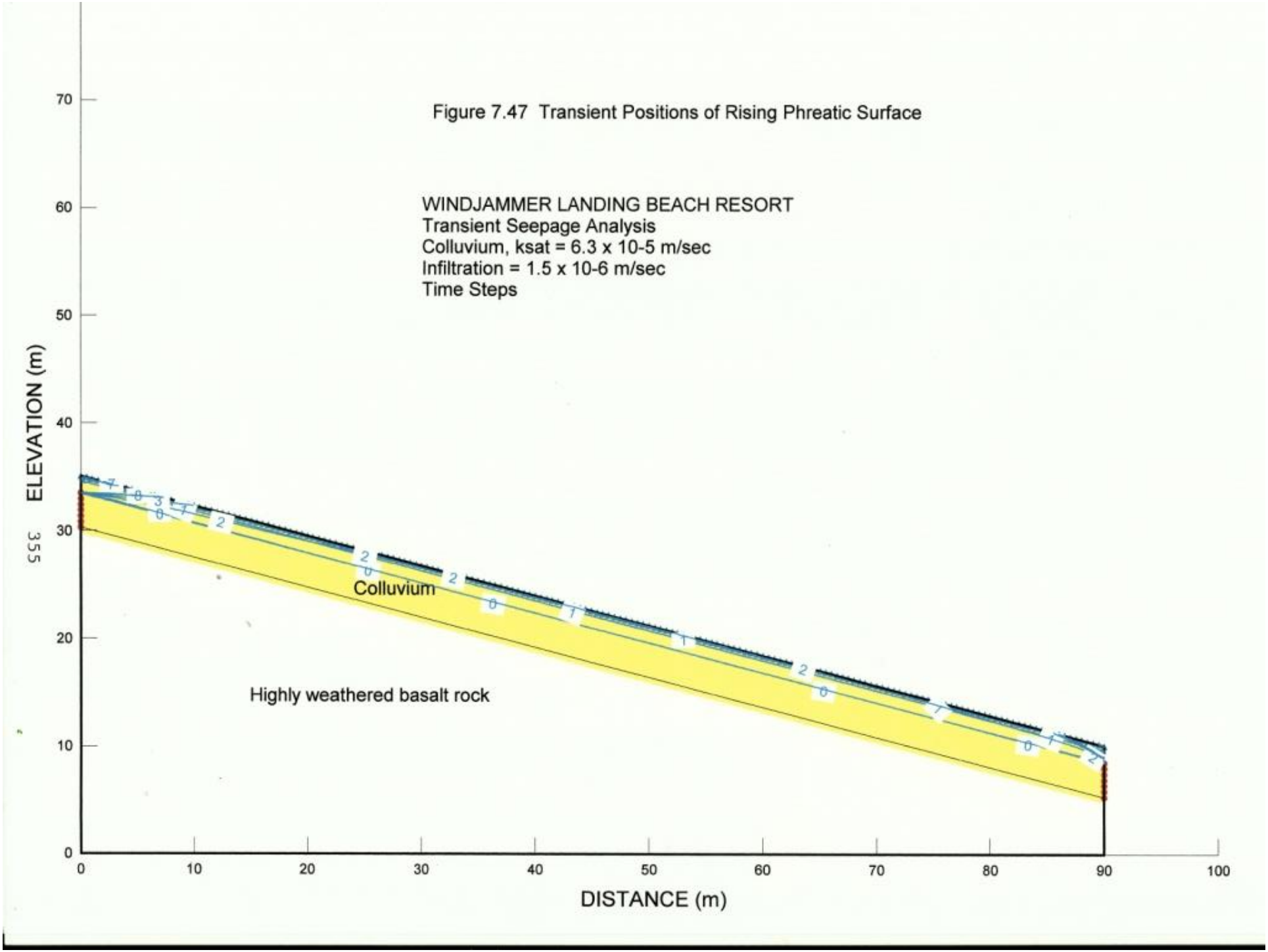

Figure 7.48 Total Head for Transient Seepage Condition

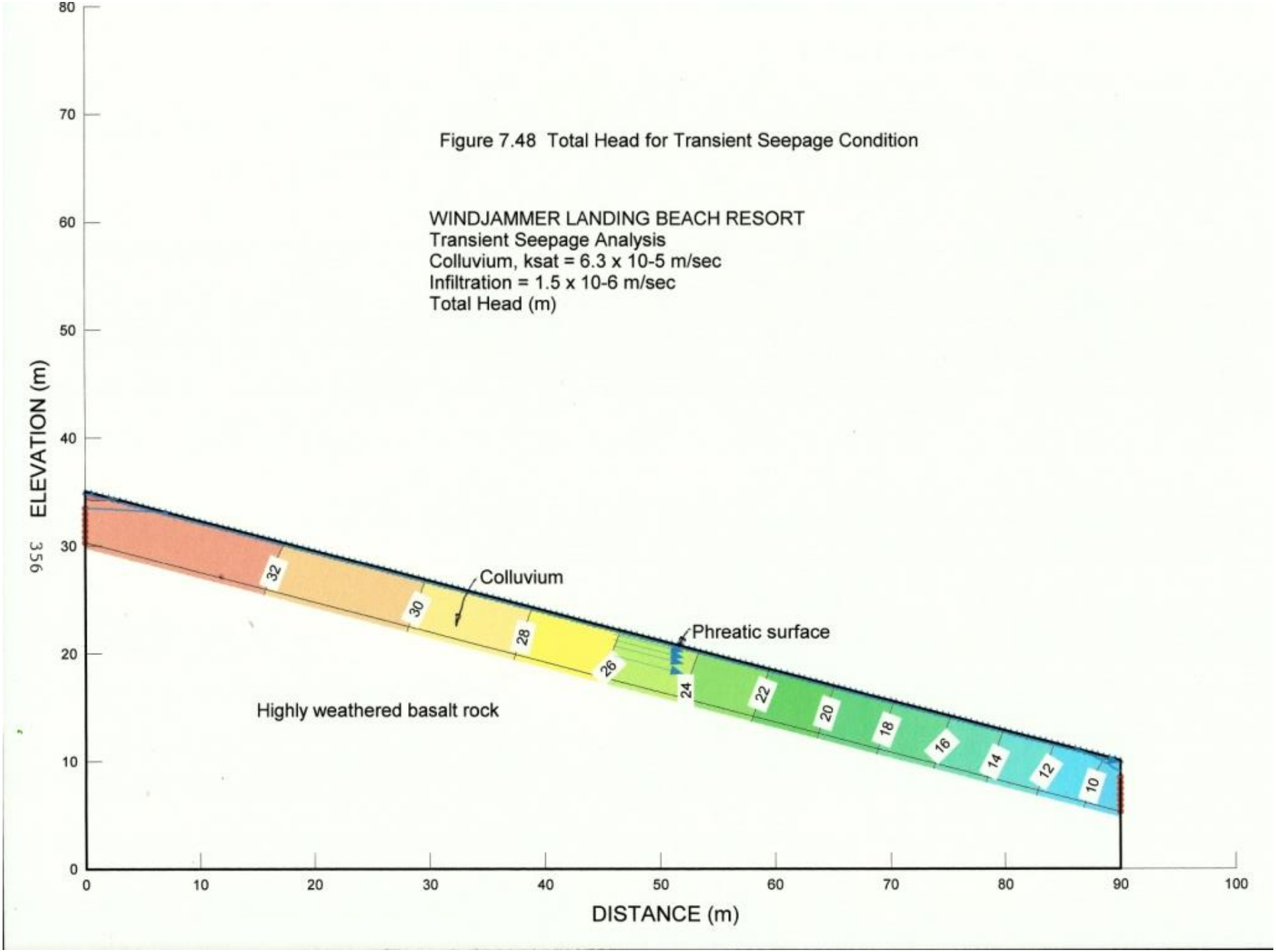

Figure 7.49 Pressure Head for Transient Seepage Condition

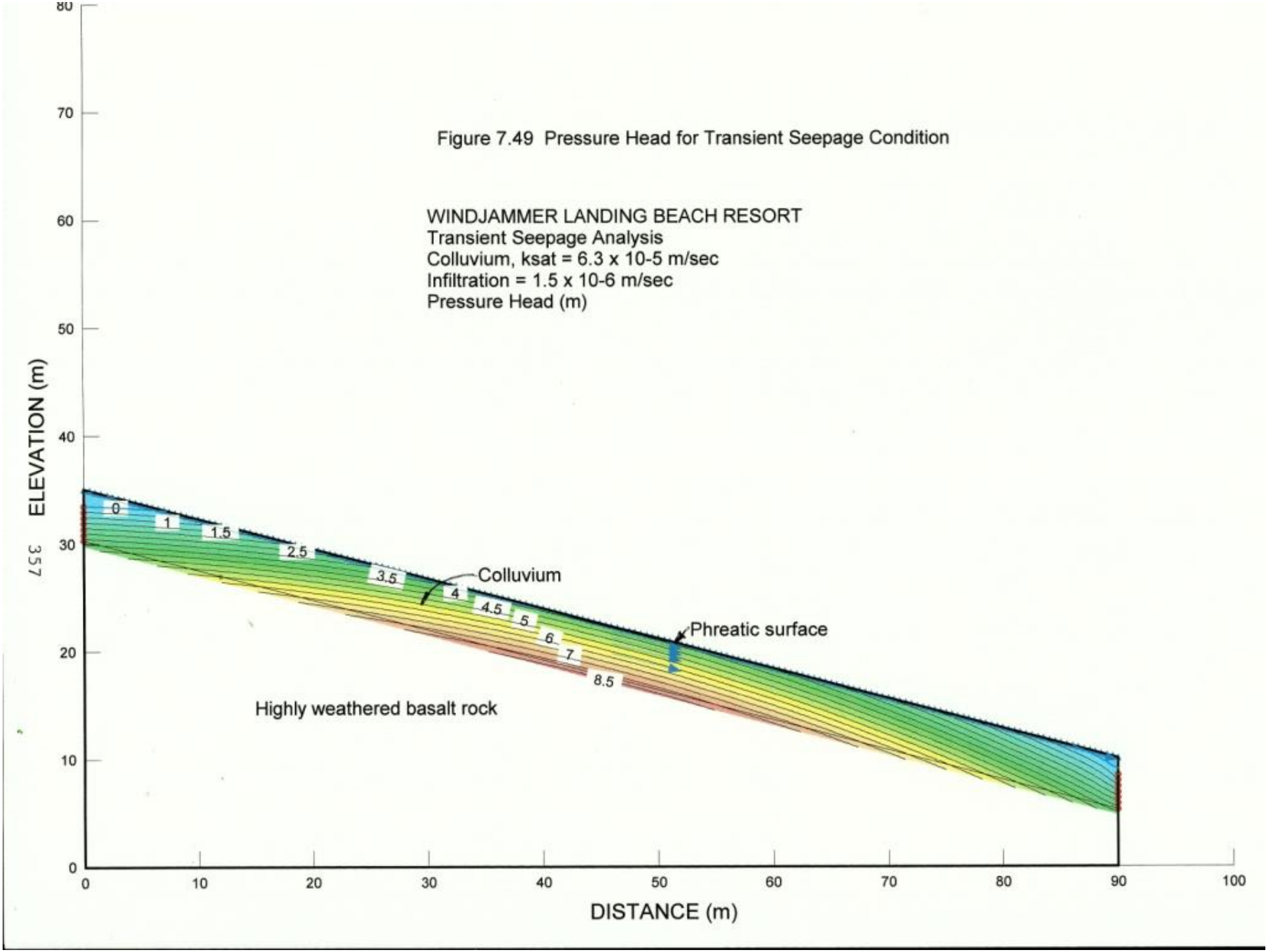

Figure 7.50 Pore Water Pressure During the Transient Seepage Condition

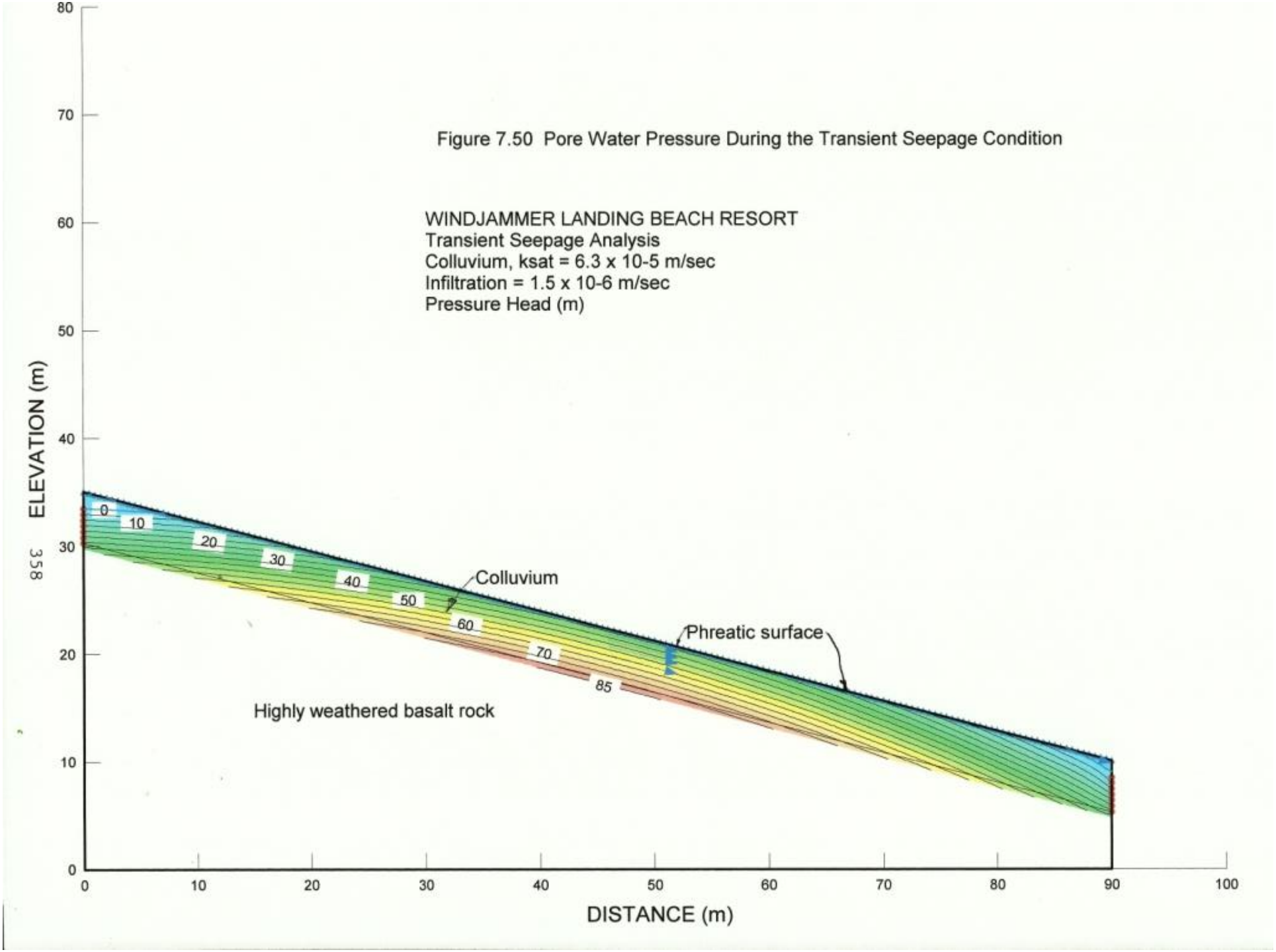

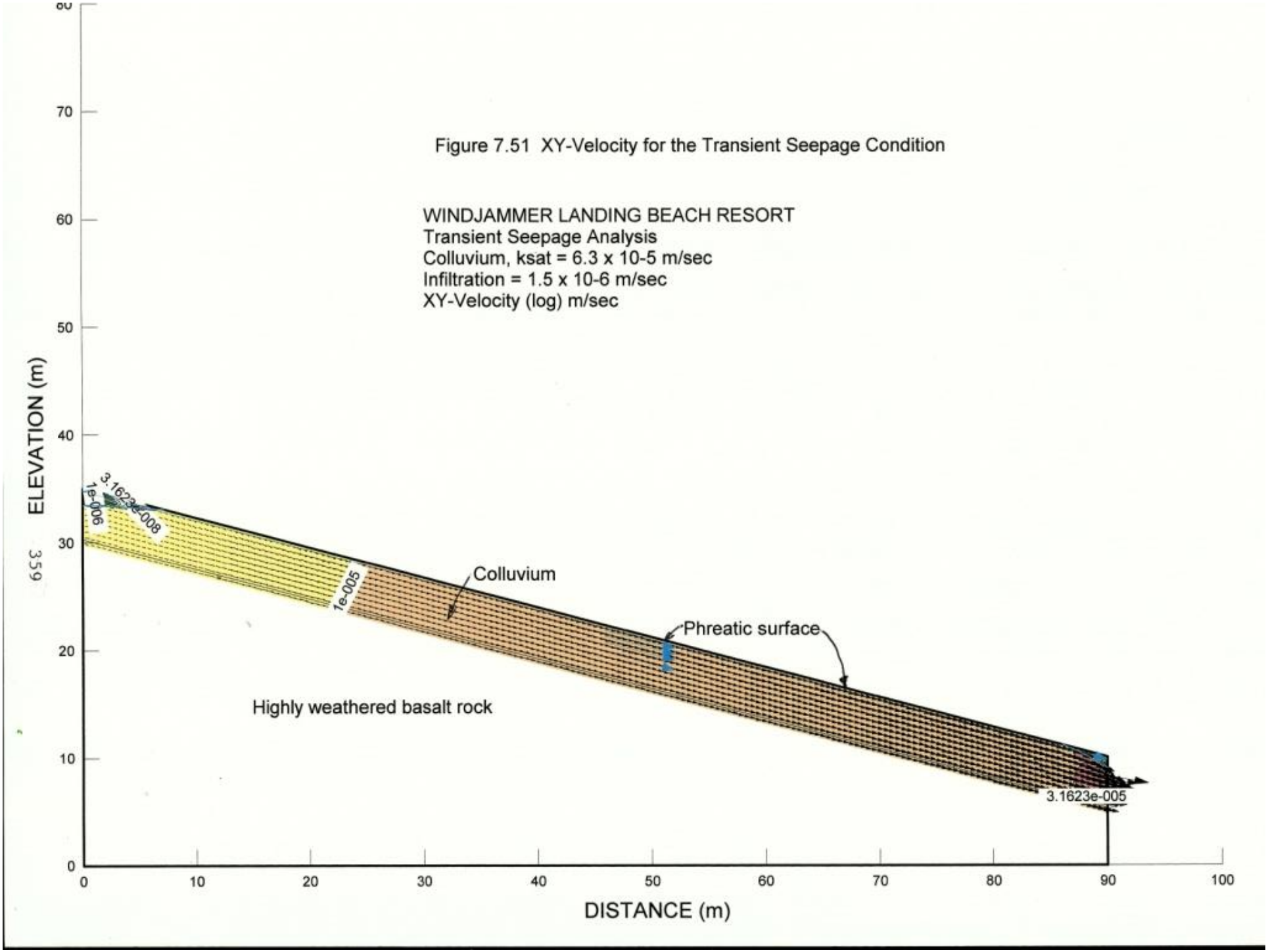

Figure 7.51 XY-Velocity for the Transient Seepage Condition

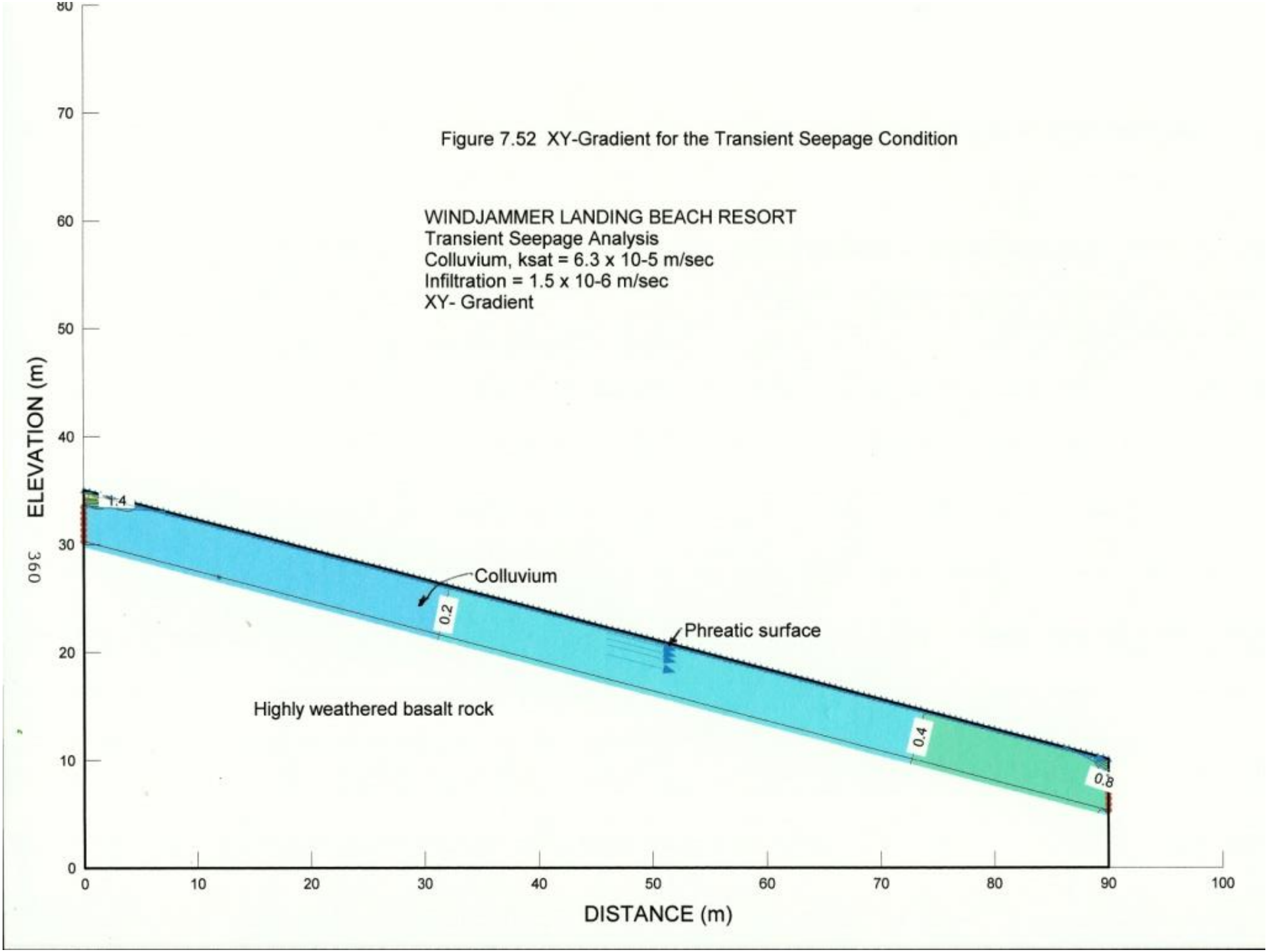

Figure 7.52 XY-Gradient for the Transient Seepage Condition

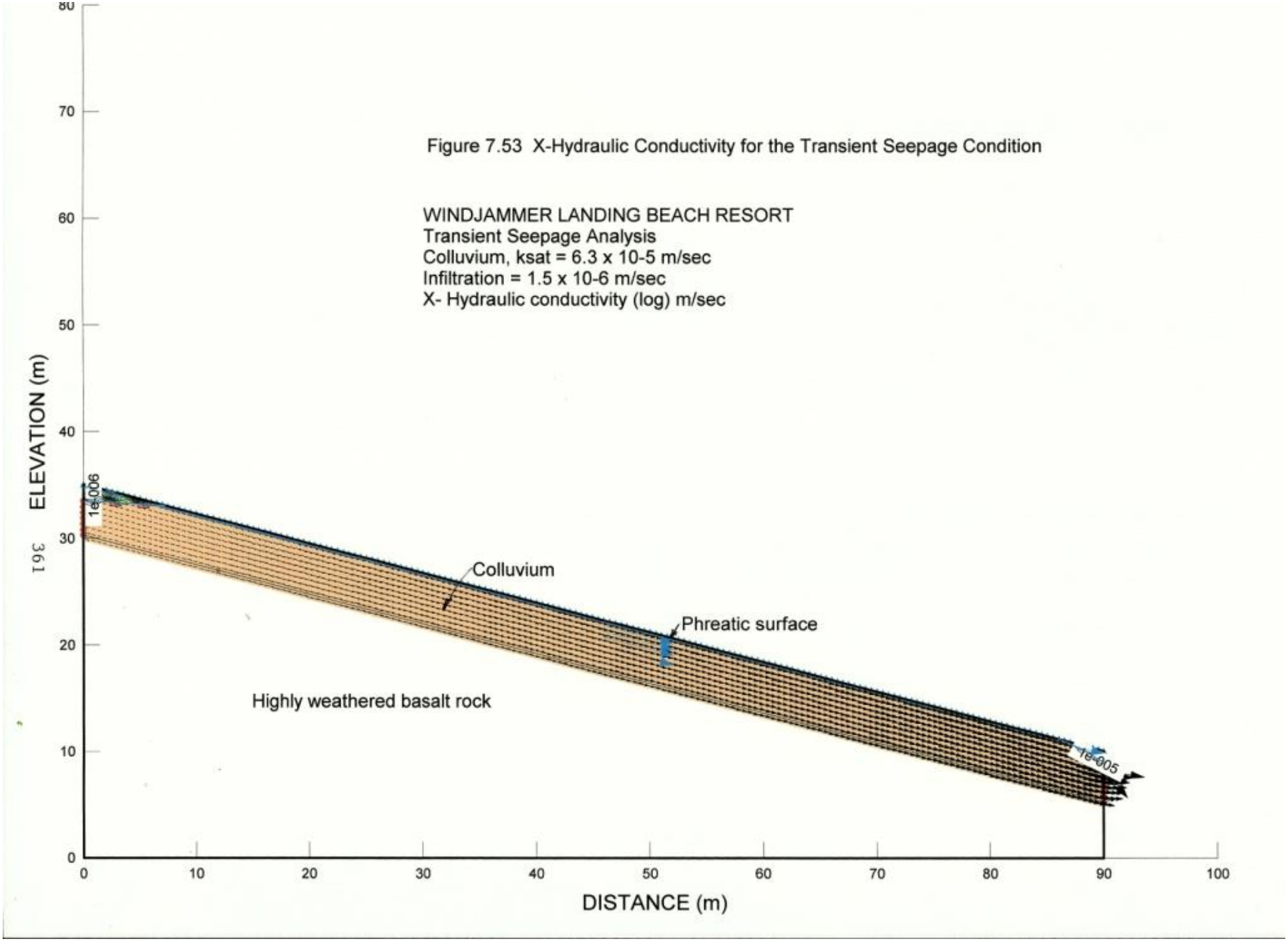

Figure 7.53 X-Hydraulic Conductivity for the Transient Seepage Condition

Figure 7.54 Volumetric Water Content for the Transient Seepage Condition

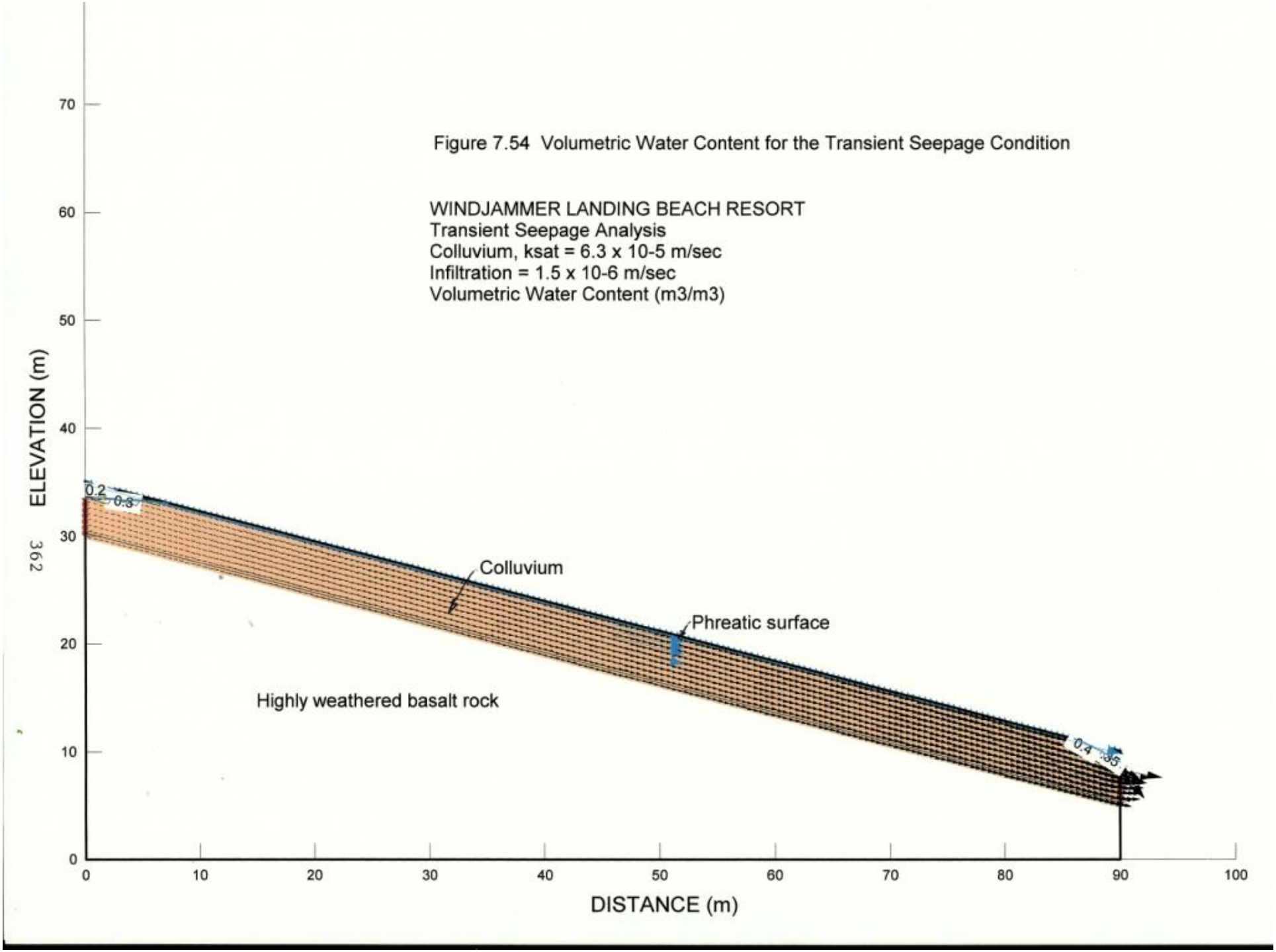

362

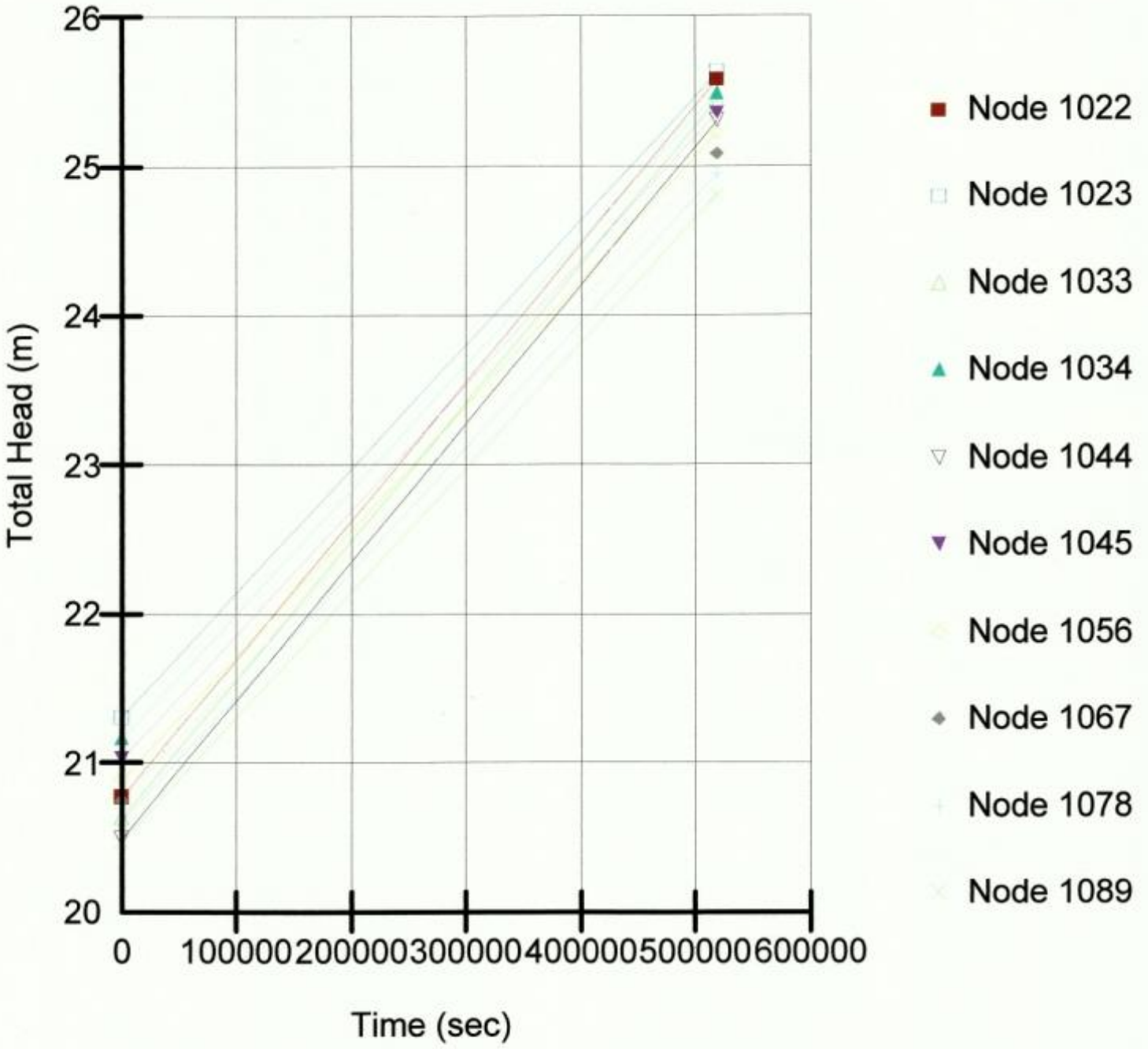

Figure 7.55a : Graph of Changes in Total Head from Ground Surface to 2.3m depth during the Transient Process - Windjammer Landing Beach Resort

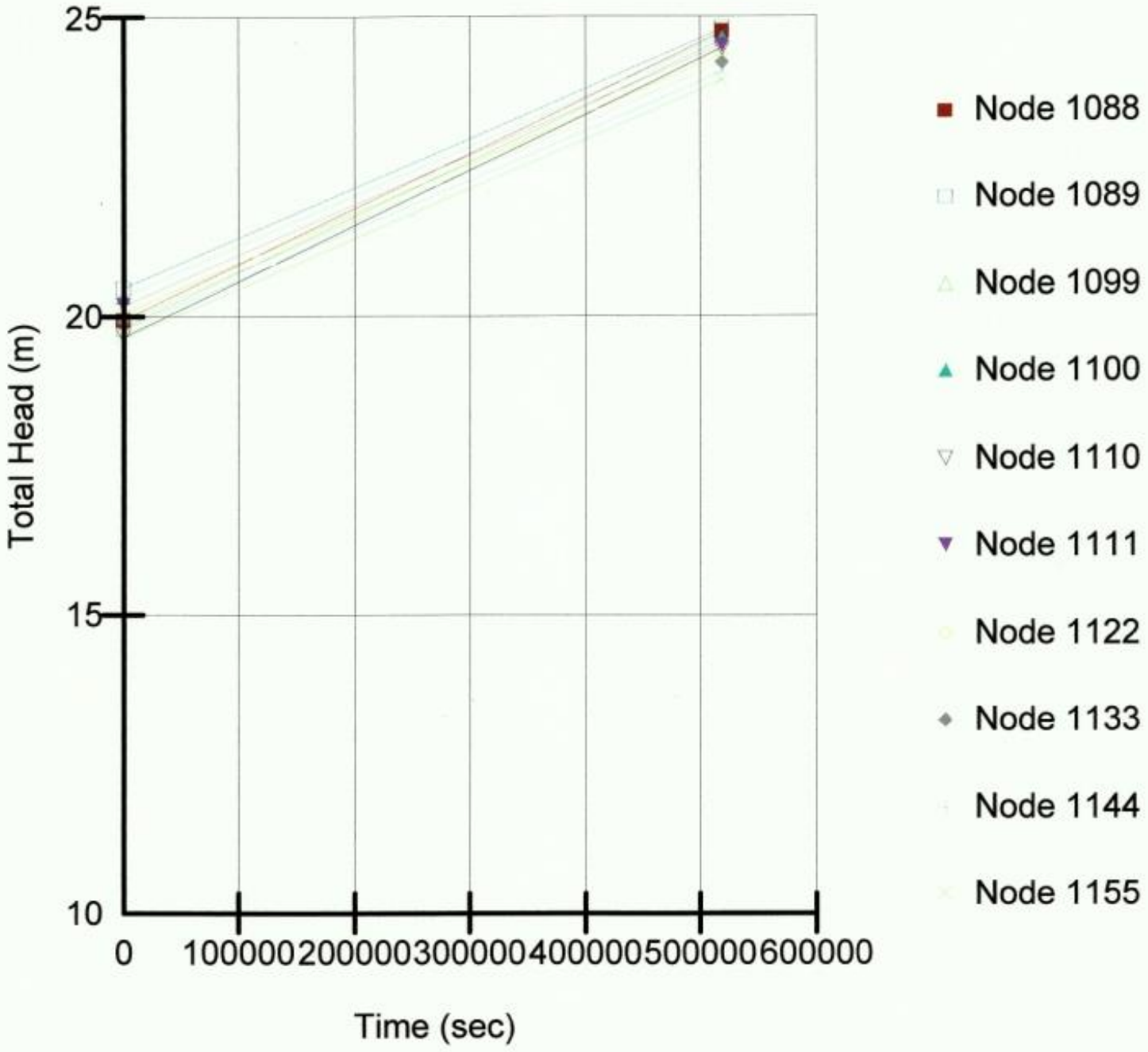

Figure 7.55b : Graph of Changes in Total Head from Ground Surface to 2.3m depth during the Transient Process - Windjammer Landing Beach Resort

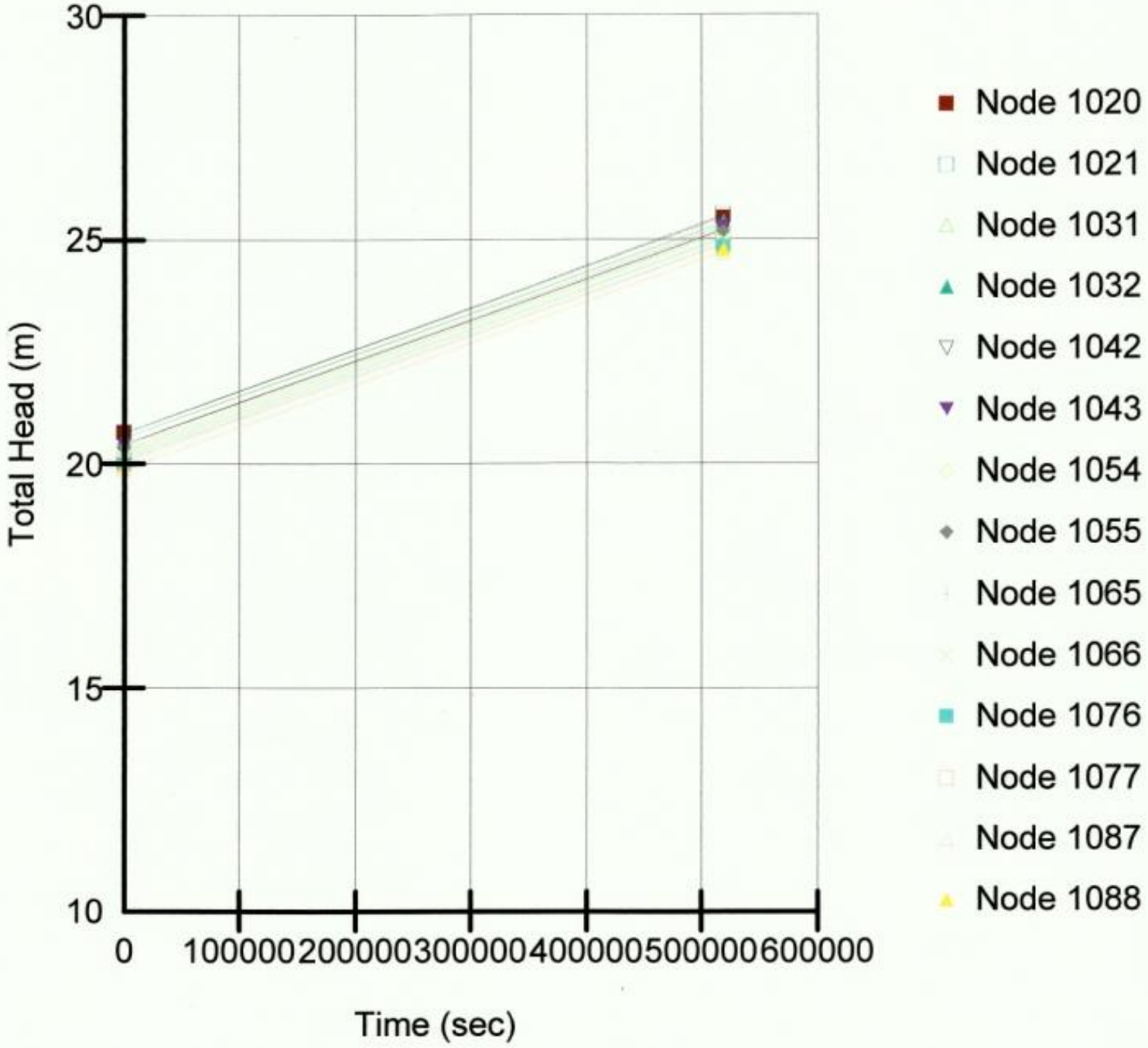

Figure 7.55c : Graph of Changes in Total Head from Ground Surface to 2.3m depth during the Transient Process - Windjammer Landing Beach Resort

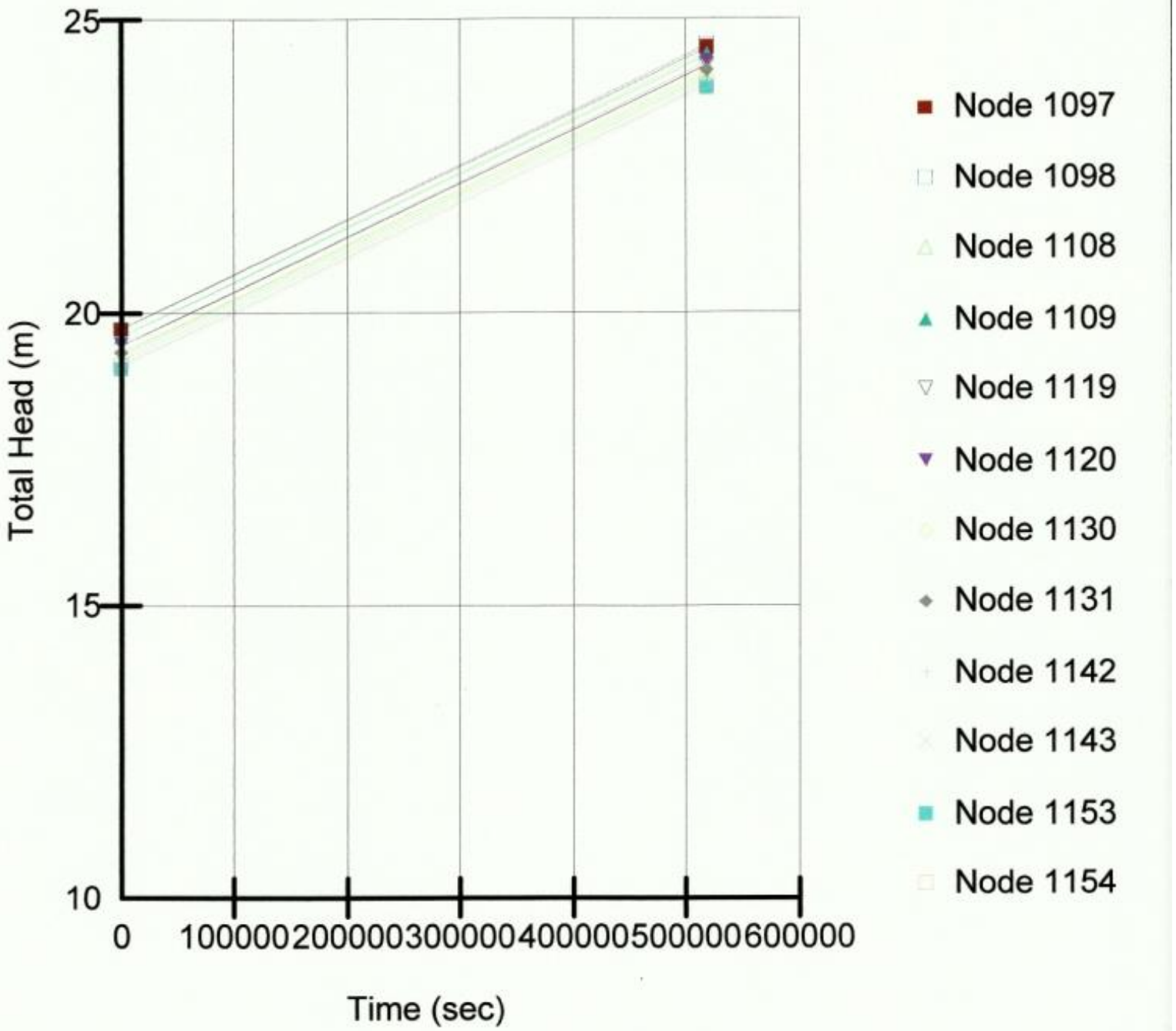

Figure 7.55d : Graph of Changes in Total Head from Ground Surface to 2.3m depth during the Transient Process - Windjammer Landing Beach Resort

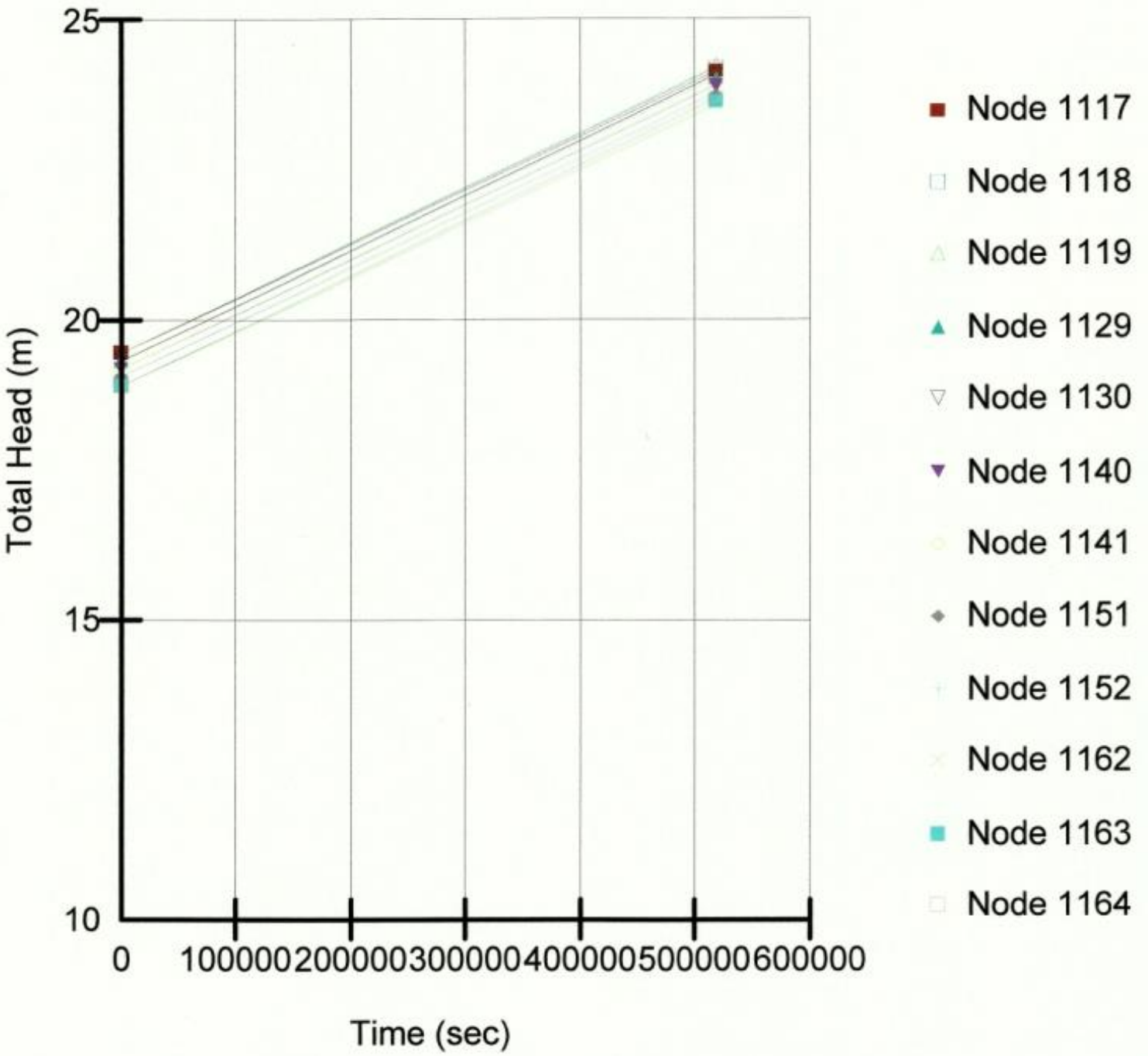

Figure 7.55e : Graph of Changes in Total Head from Ground Surface to 2.3m depth during the Transient Process - Windjammer Landing Beach Resort

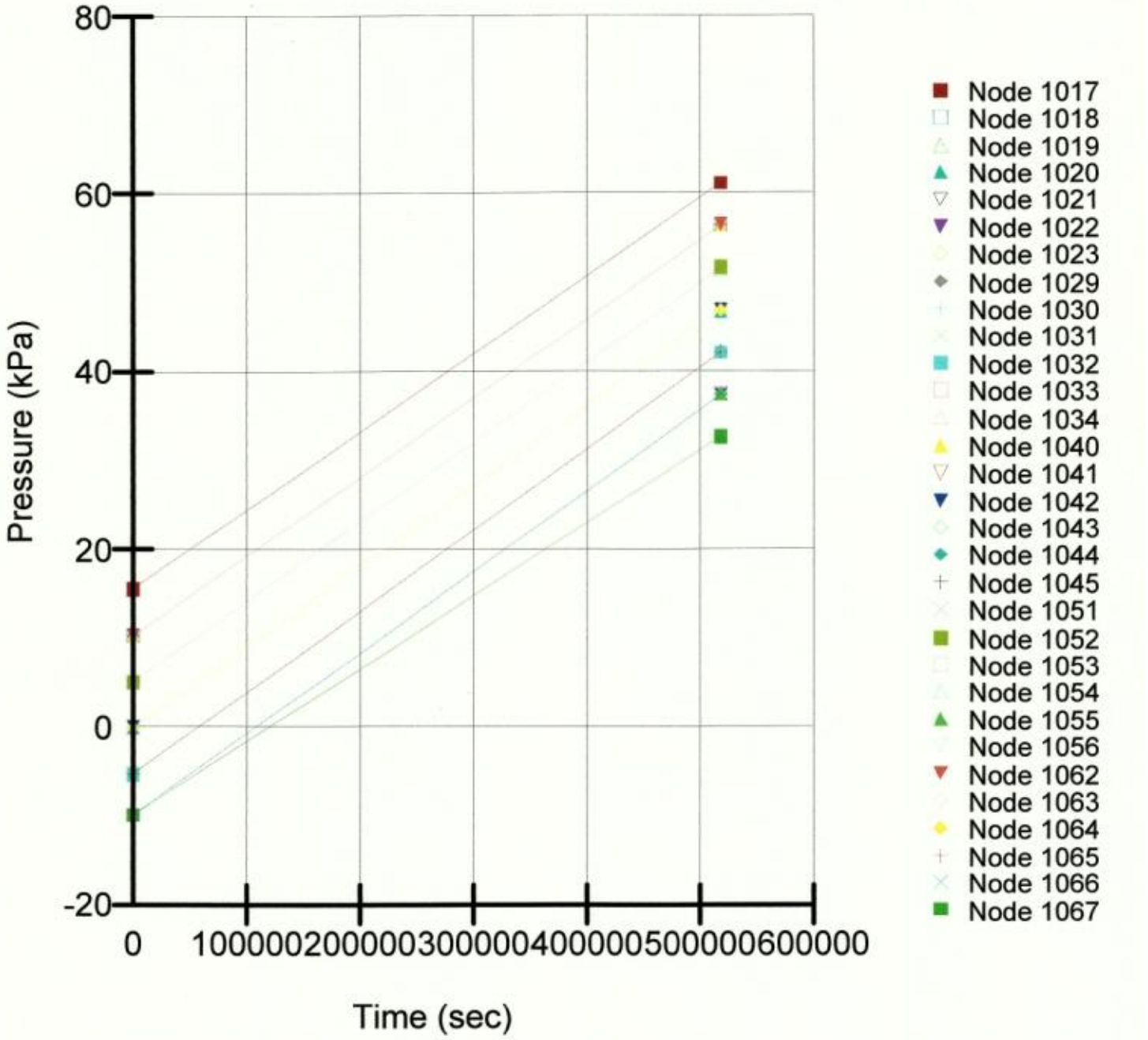

Figure 7.56a : Graph of Changes in Pore Water Pressure from Ground Surface to 2.3m depth during the Transient Process - Windjammer Landing Beach Resort

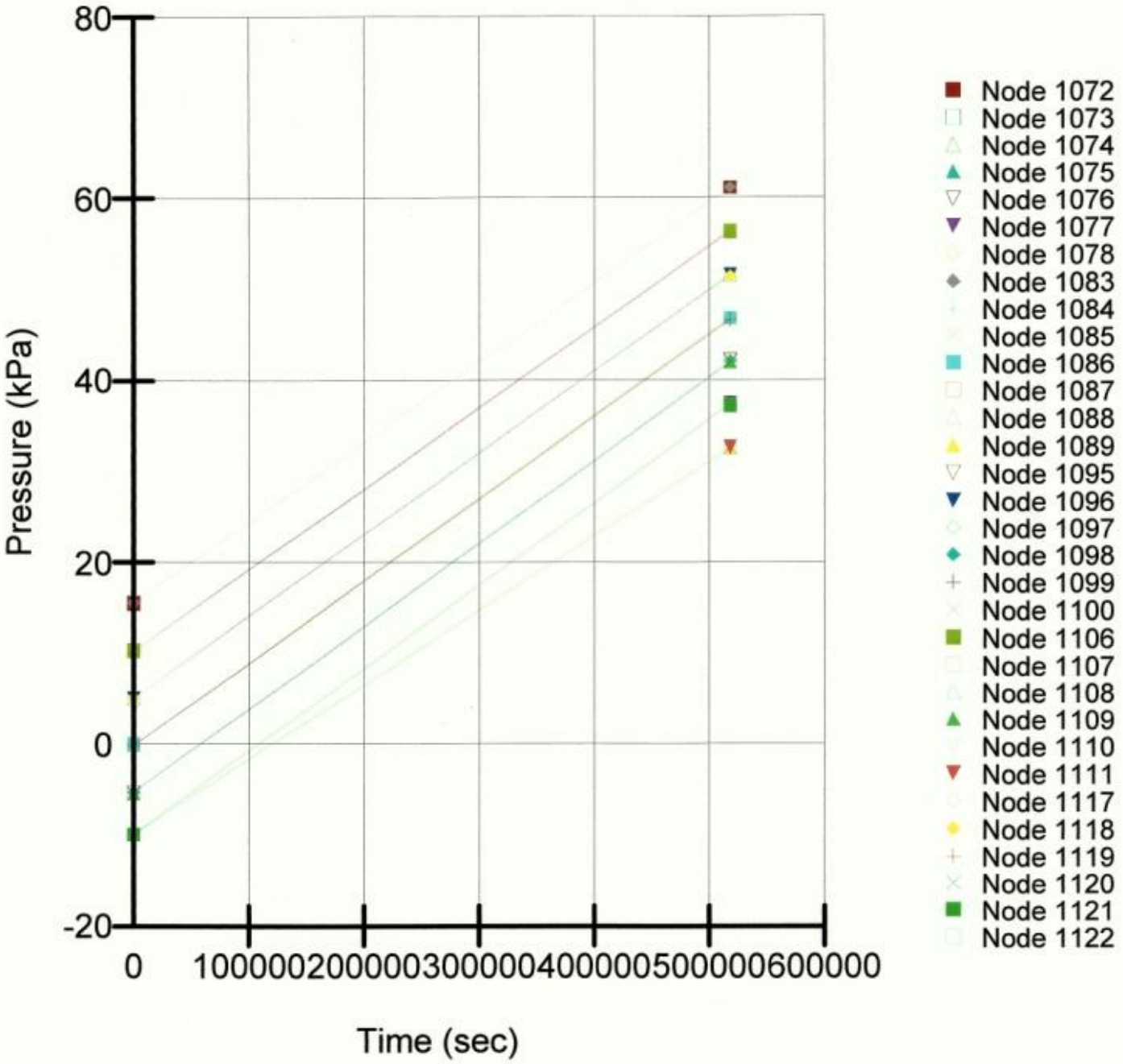

Figure 7.56b : Graph of Changes in Pore Water Pressure from Ground Surface to 2.3m depth during the Transient Process - Windjammer Landing Beach Resort

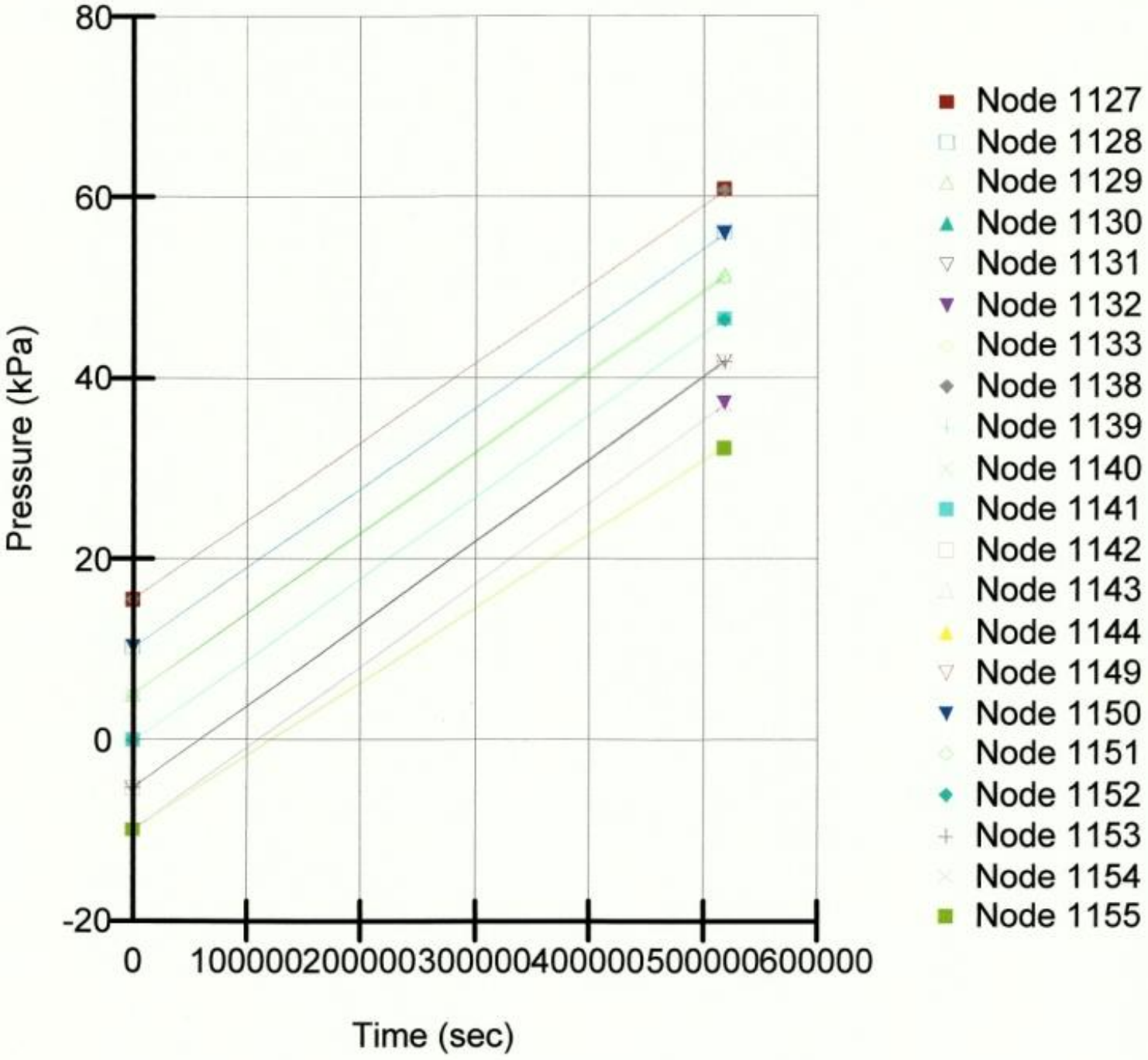

Figure 7.56c : Graph of Changes in Pore Water Pressure from Ground Surface to 2.3m depth during the Transient Process - Windjammer Landing Beach Resort

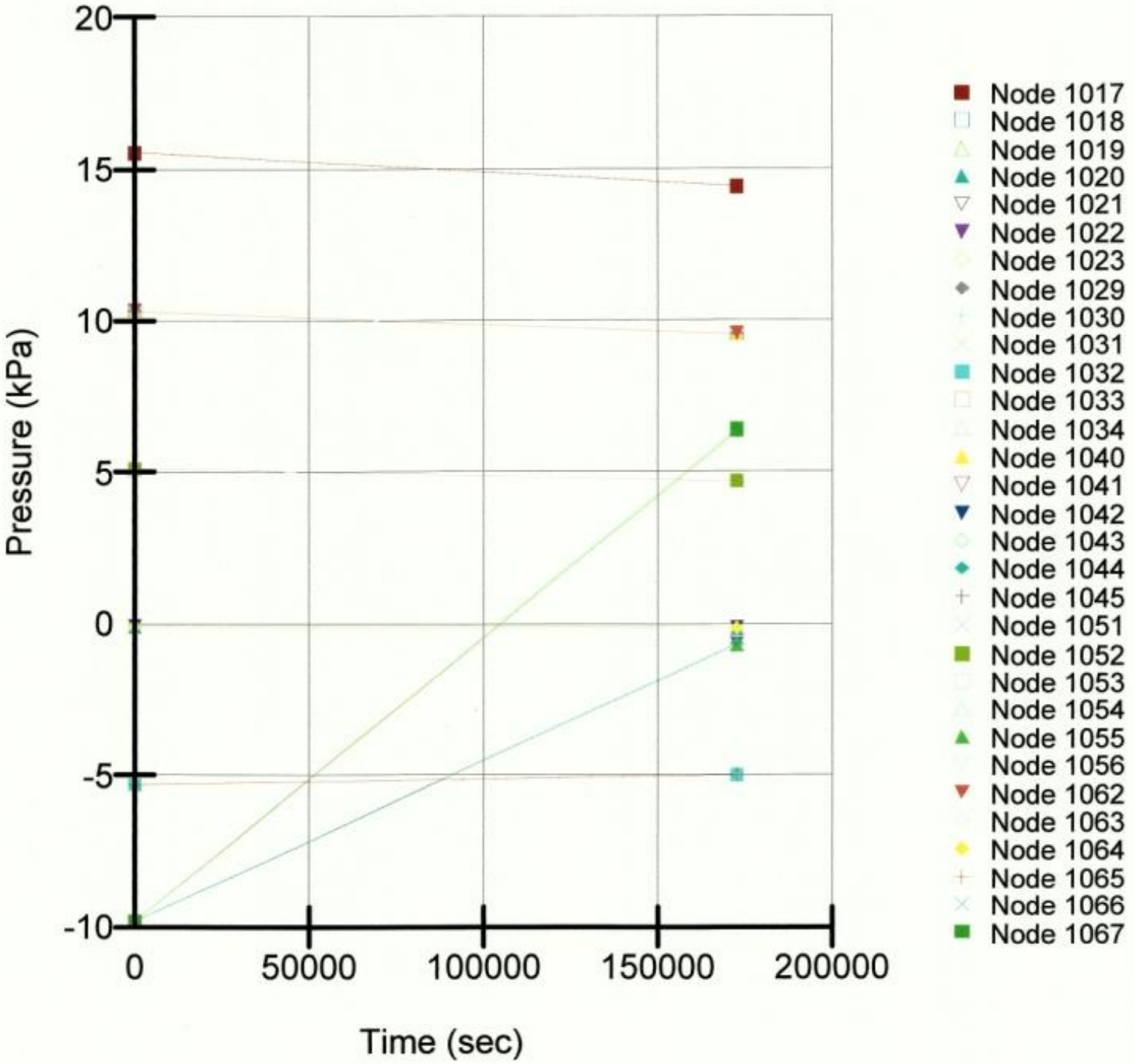

Figure 7.57a : Graph of Changes in Pore Water Pressure at Variable Depths over a 24-hour Period of Rainfall Windjammer Landing Beach Resort

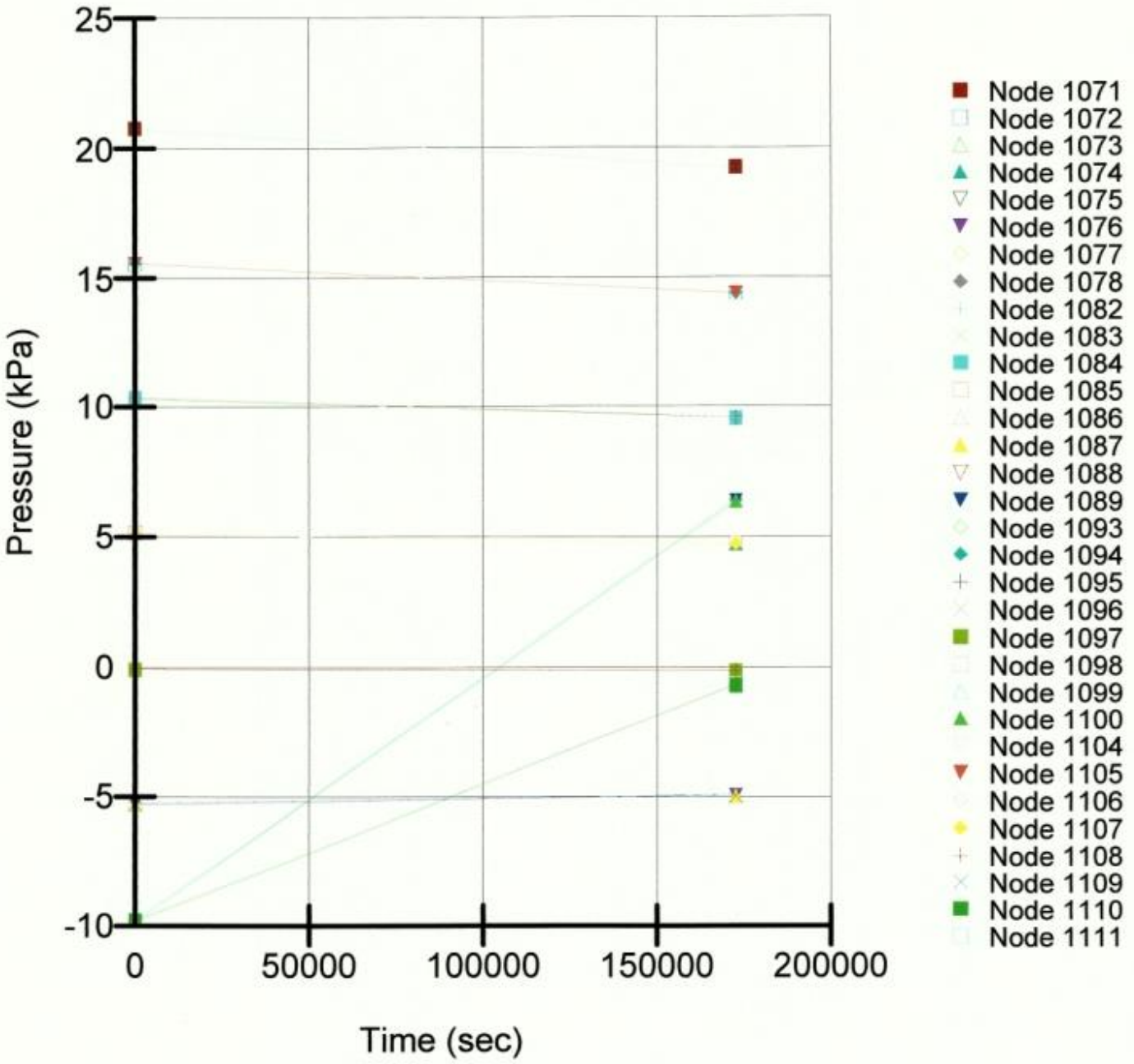

Figure 7.57b : Graph of Changes in Pore Water Pressure at Variable Depths over a 24-hour Periodof Rainfall Windjammer Landing Beach Resort

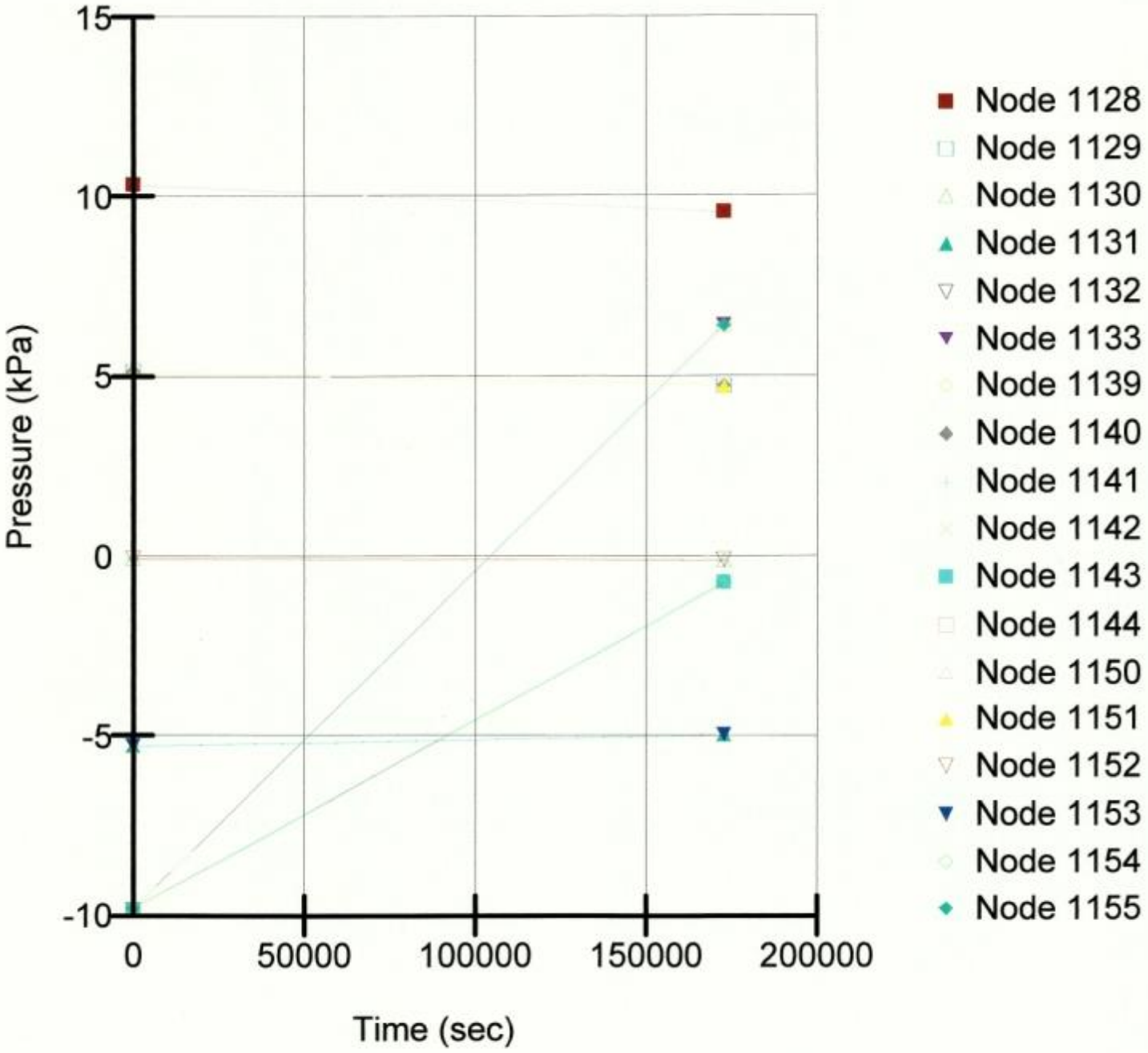

Figure 7.57c : Graph of Changes in Pore Water Pressure at Variable Depths over a 24-hour Period of Rainfall Windjammer Landing Beach Resort

Figure 7.58 Back Analysis of Windjammer Landing Beach Resort Slope

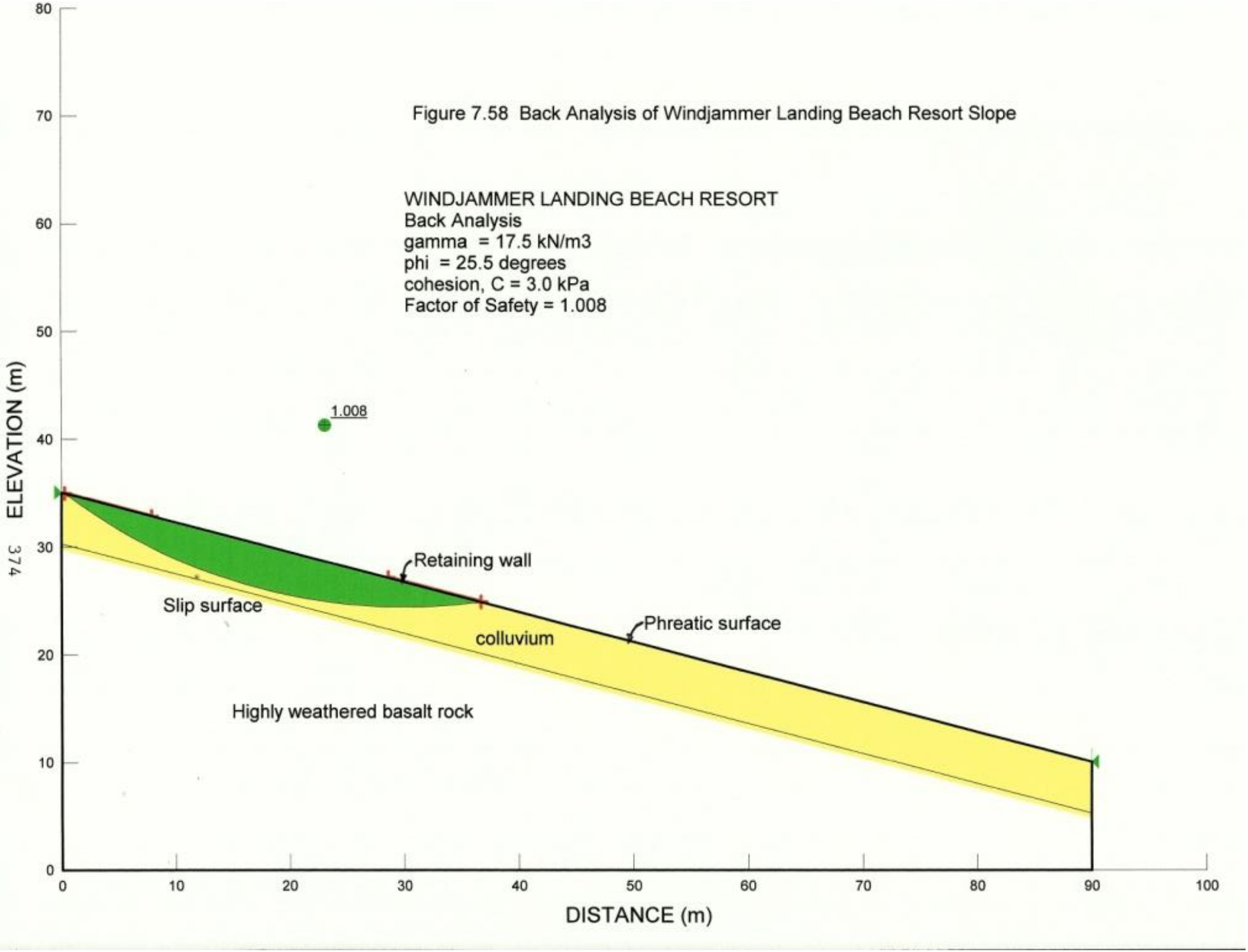

Figure 7.59 Slope Stability Analysis - Windjammer Landing Beach Resort

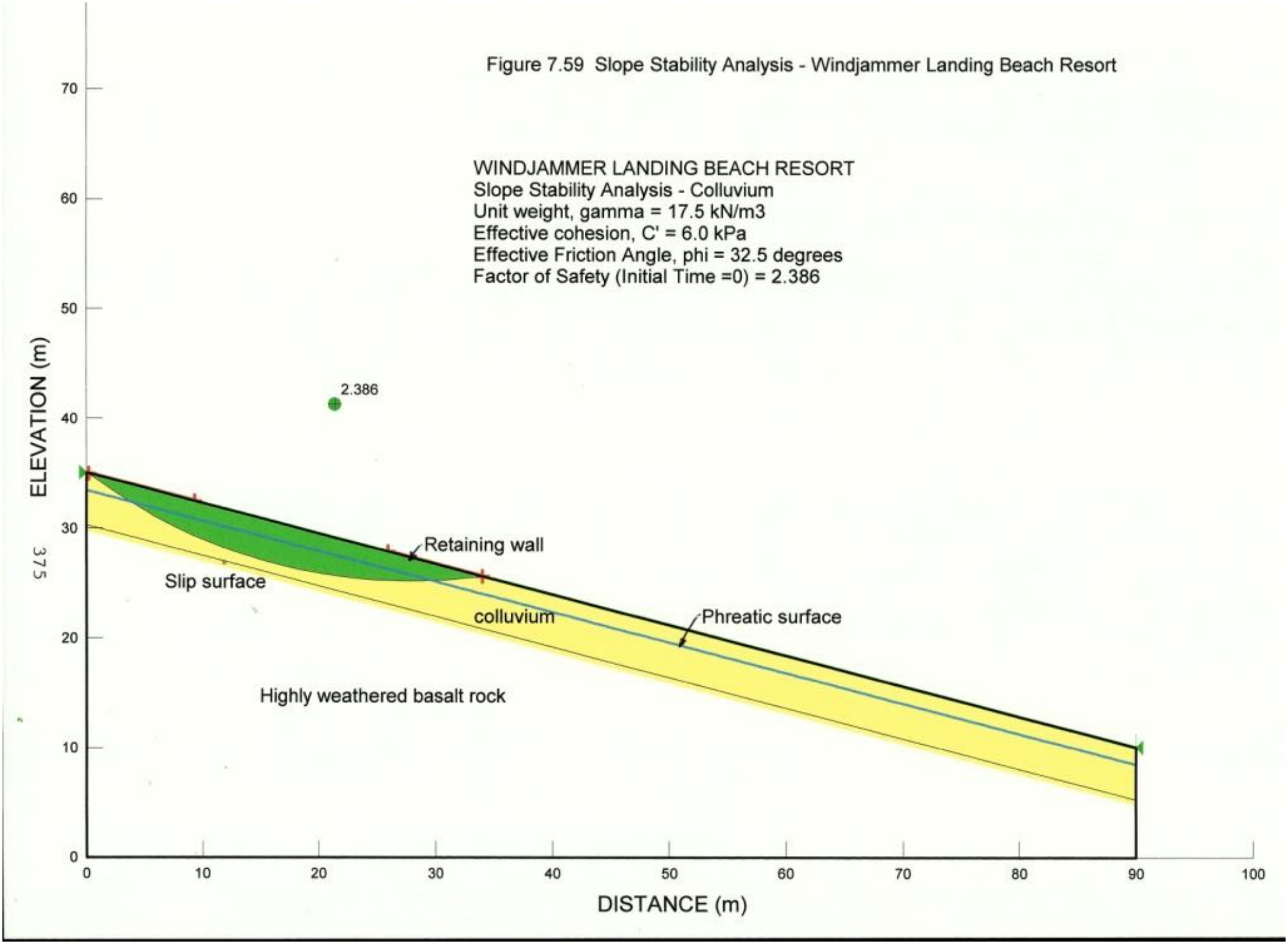

Figure 7.60 Slope Stability Analysis - Windjammer Landing Beach Resort

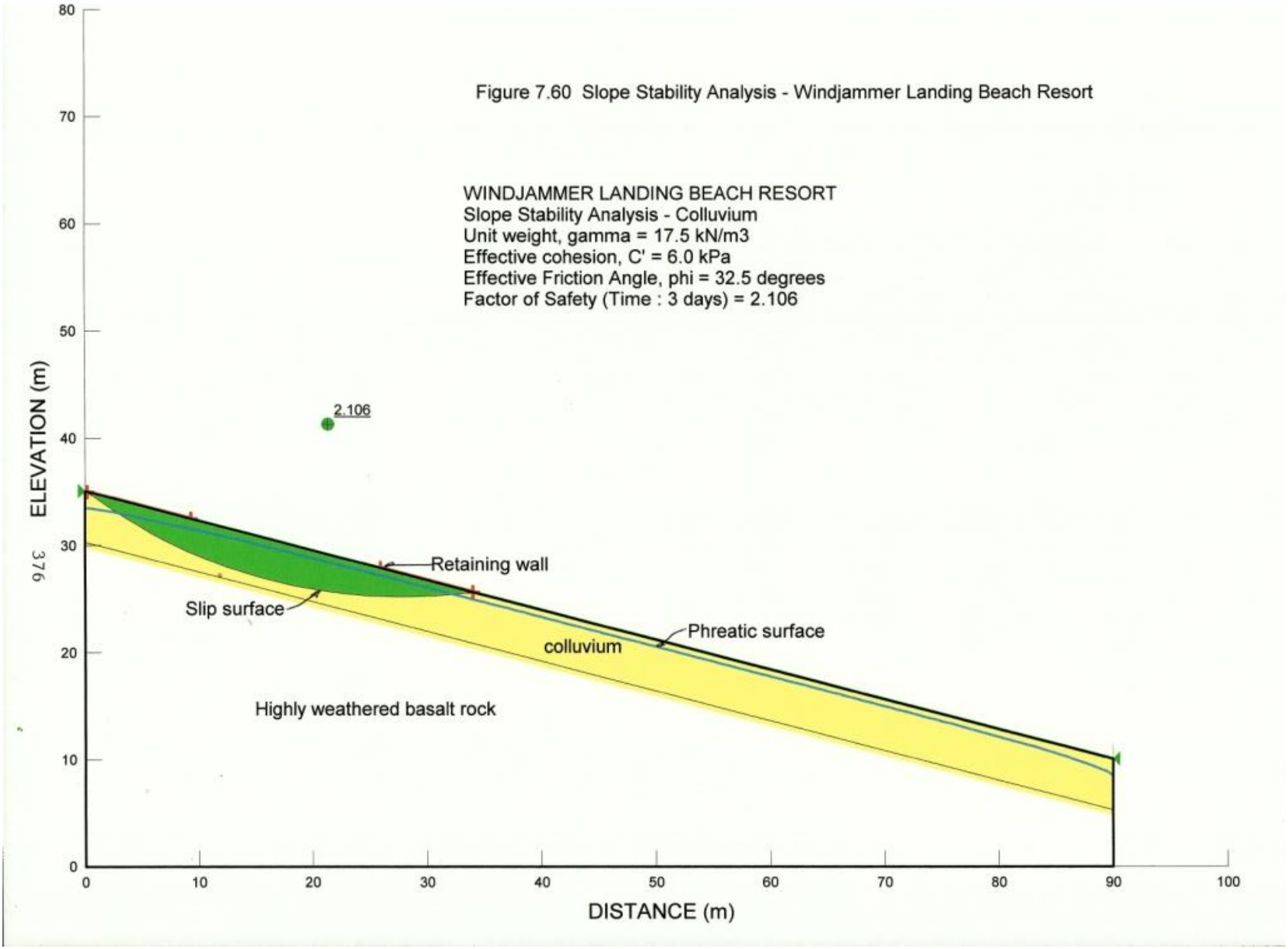

Figure 7.61 Slope Stability Analysis - Windjammer Landing Beach Resort

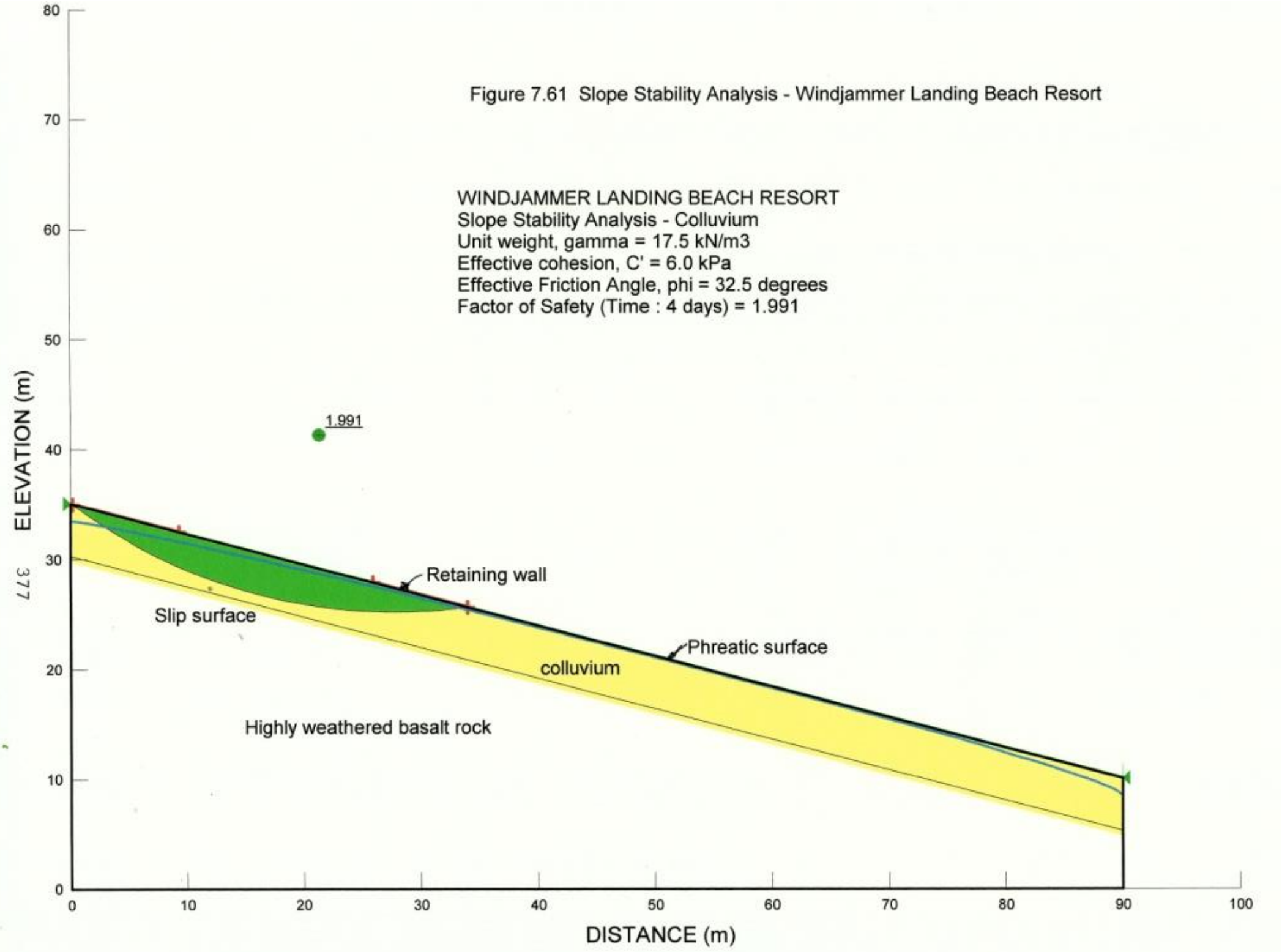

Figure 7.62 Slope Stability Analysis - Windjammer Landing Beach Resort

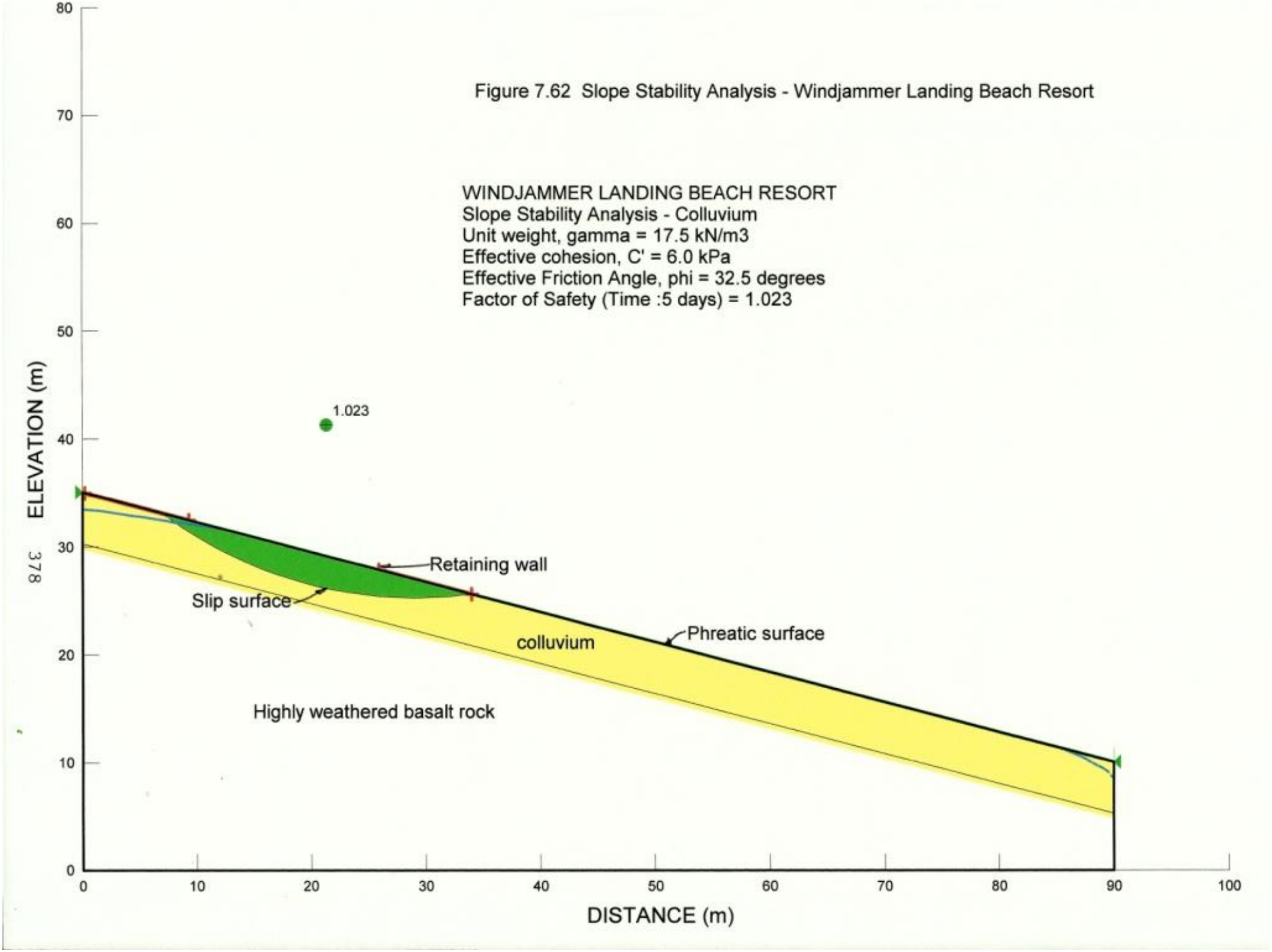

CHAPTER 8

DISCUSSION, CONCLUSIONS AND RECOMMENDATIONS FOR FURTHER RESEARCH WORK

8.1 INTRODUCTION

The prediction of the effect of intensive rainfall and the rate of infiltration and saturation of slopes comprised of unsaturated soil and colluvium is an important aspect of practical engineering since in some cases loss of human life and property are of utmost concern as a result of slope instability.

Given the high cost of damage to structures, roads, public utilities as a result of unexpected ground movements associated with unsaturated soils and colluvium in Saint Lucia, it was considered important to investigate further the behavior of these soil slopes during rainstorms.

The initial part of this final chapter discusses the main themes of the thesis followed by conclusions and recommendations for further research work on the hydrogeological processes taking place in slopes of unsaturated soil and colluvium during a rainstorm of 24-hour duration.

8.2 DISCUSSION

In order to fully understand the engineering properties of a residual soil from parent basalt rock and a colluvium from parent andesite rock, a systematic approach is required which includes their origin, their qualitative and quantitative composition and their microstructure. This involves characterising their material composition and providing a framework to understand their engineering behaviour.

Since residual soils and colluvium are products of weathering during which physical and chemical reactions take place and results in the formation of new minerals, knowledge of the soil parent mineralogy is helpful in understanding its engineering behavior. As new minerals are formed during the weathering process, a new microstructure and microfabric develops and knowledge of the role they play in the engineering behavior of the soil is desirable.

8.2.1 Mineralogy of the Parent Andesite Rock and Microstructure of the Residual Soil

The parent altered andesite rock was observed in petrographic thin section and was found to be composed of a lower silicate mineral and carbonate composition than the basalt rock which may be due to the altered state of the parent rock which had lost some of its original mineralogical composition due to weathering or perhaps as a result of the composition of its magmatic composition. Phenochrysts minerals made up 45% and the finer matrix was 55% of total minerals present.

The larger percentage of matrix material was a result of weathering of the original minerals in the parent andesite rock, hence its altered condition (Figure 2.30 and Figure 2.31, Section 2.3.1.2).

X-ray analysis of residual soil samples show strong peaks of quartz (around 7 angstroms or 12 degrees) and is likely to be of a 1:1 structure, either kaolinite or serpentine (Figure 5.19). The lack of peak definition (excluding peak 3 which is quartz) in the 20-23 degree interval (called the 1st bandhead) suggests that this 1:1 structure is disordered. The 2nd bandhead appears at around 35 degrees and a 3rd bandhead shows at around 55 degrees. Unfortunately, this reflection could also be attributed to the presence of chlorite (phylosilicate - montmorillonite). The chlorite reflection at 14 angstroms isn't recognizable given the scaling of the count rate (vertical axis), but if the chlorite were Fe-rich, then the 14 angstrom reflection could be very low intensity and could be a 1:1 structure reflection at 7 angstroms (near 12 degrees could actually be the chlorite). It may be that both chlorite and a 1:1 structure phase are present.

In Figure 5.20 quartz is also shown to be present in the high peak. The presence of chlorite is suggested by the peak at 14 angstroms. A smectite mineral is suggested by the poorly defined peak 2. Peak 3 is very low intensity and undetermined. Peak 4 could be either chlorite or a 1:1 structure phase such as kaolinite or serpentine or both chlorite and a 1:1 structure phase. Peak 8 is in the vicinity of chlorite and the kaolinite reflections.

SEM peaks for the residual soil are shown in Figure 20a. The mineral composition tend to support the X-ray results which show a high peak for quartz as the dominant mineral present. Chlorite is unrecognized but the products of the weathering process take the form of aluminium, iron, titanium, potassium together with carbon and oxygen.

These results indicate that the mineral composition of the parent andesite rock has been altered by the weathering process and new clay minerals are produced in the soil as shown in the X-ray analyses.

Scanning Electron Microscopic (SEM) analysis was conducted on residual soil samples to examine the fabric of the soil and identify the structural orientation and the presence of possible bonding in its structure. Figures 5.23 to 5.25 show images of the residual soil from the Barre de L'isle Study Site at different magnifications. At low magnification (Figure 5.23) the residual soil grains are angular and moderately compact with variable particle orientation and pore spaces. The clay fraction is not recognizable in the images and the soil appears predominantly composed of silt and sand particles. This is confirmed in the gradation curves and the Atterberg limits which are reviewed below.

At higher magnification (Figure 5.24) individual soil particles are clearly visible and there is some aggregation of particles. The particle orientation is random with some edge to edge and edge to face contact. The soil appears to be composed predominantly of white coloured particles which appear to be quartz minerals as was identified in the parent mineralogy in the petrographic thin sections and verified in the sharp peaks observed in the X-ray and SEM analyses. The rough shape and sharp edges of the soil particles confirms that the soil is composed mainly of silt and sand with a minor clay fraction. The soil has an open structure with pore spaces of variable sizes which contributes significantly to the saturated hydraulic conductivity of the residual soil.

In Figure 5.25 the soil is saturated and under high magnification the pore spaces are shown to be filled with water but the main structure of the dry sample remains. There is no evidence of any decrease in the pore sizes caused by swelling of the clay fraction. This indicates that the quantity of smectite present is small and would not control the engineering behavior of the residual soil. This is verified in the gradation curves and Atterberg limits discussed below.

8.2.2 Index Properties and Saturated Hydraulic Conductivity of the Residual Soil

This section discusses the correlation between the index properties and hydraulic conductivity of the residual soil with the mineral composition of the parent rock and mineralogy and microstructure of the residual soil.

The gradation curves shown in Figures 5.2 to 5.11 represent grain size distribution of the residual soil at the Barre de l'isle study site. The residual soil consists of 19% - 37% sand, 46% - 63% silt and 17% - 18% clay fraction (Section 5.2.1.3). This represents a clayey, sandy silt material. This is in good agreement with the images in the SEM analysis for this soil. The open granular texture observed in Figures 5.23 – 5.25 represents random sorting of the dominant silt and sand particles whereas the clay fraction is unobservable which reflects in a low plasticity texture for this unit. The high peaks of stable quartz and the minor peaks of chlorite and clay minerals observed in the X-ray analysis are also supportive of the granularity of the residual soil.

The natural moisture content (40% - 84%) of the residual soil is above the plastic limit (38% - 49%) which indicates that the soil may undergo plastic deformation. This condition arises because of the open structure of the granular soil becomes filled with infiltrating surface water during rainstorms and the resulting increase in pore water pressure reduces the shear strength of the soil.

The low clay fraction of the residual soil allows rapid infiltration to occur. The saturated hydraulic conductivity of the residual soil was measured at 9.0×10^{-5} m/sec. This value is representative of a silty sand (Cedergren, 1977). This is in close agreement with the gradation curves and the mineralogy and texture of the residual soil. Therefore, it can be seen that there is a strong relationship between the mineralogy of the parent andesite rock and the texture, fabric, gradation, moisture content, plasticity and hydraulic conductivity of the residual soil derived as a result of the weathering process. The nature of the gradation curves is greatly influenced by the degree of leaching taking place during the weathering process.

8.2.3 Mineralogy of the Parent Basalt Rock and the Microstructure of the Colluvium

Petrographic analysis of the parent basalt and andesite rock in thin section was conducted to determine their original mineralogical composition. It was found that the parent basalt rock contained a large amount of silicate minerals some of which were not observed in the altered andesite, together with iron hydroxide and carbonates (Figure 2.28 and Figure 2.29, Section 2.3.1.1). The larger minerals present or phenocrysts made up about 55% and the finer matrix minerals made up 45% of the total minerals present. Most of the less durable silicate minerals present would eventually be transformed to clay minerals namely montmorillonite, illite and kaolinite during the weathering process.

Based on the higher percentage of silicate mineral composition of the parent basalt rock compared to that of the altered andesite, one would expect a higher percentage of clay minerals to be present in the colluvium than in the residual soil from the altered andesite rock. This discussion follows through examination of the soil mineral composition and fabric, Atterberg limits, grain size distribution and the hydraulic conductivity of the two deposits.

X-ray analysis results show strong peaks of predominantly quartz minerals and montmorillonite clay present in the colluvium (Figure 5.45 – Figure 5.51). The amount of montmorillonite clay shown to be present in the colluvium far exceeds that observed in the X-ray diffraction results for the residual soil from altered andesite (Figure 5.19 and Figure 5.20). This is evidenced by the several strong and moderate peaks displayed for all the colluvium samples tested. The presence of montmorillonite clay is well expressed in the colluvium soil fabric and structure as shown in the ESEM images (Figure 5.52 – Figure 5.65).

At low magnification (x500), the ESEM images for the colluvium the soil seems densely packed and randomly orientated. At high magnification (x2000), coarser sand and silt grains are visible embedded mixed within a detrital clay matrix and the pore spaces are visible but not as abundant as in the residual soil. The sand and silt grains appear to be openly arranged in the clay matrix and not tightly compacted within the clay matrix. The disturbed texture of the clay, silt and sand fractions indicate that random sorting and some leaching of fines may have occurred during the downslope transportation of the colluvium. The effect of the presence of montmorillonite clay on the engineering properties of the colluvium are discussed in the following sections.

8.2.4 Index Properties and Saturated Hydraulic Conductivity of Colluvium

The gradation curves for the colluvium at the Windjammer Landing Beach Resort Study Site (Appendix D) indicate an average composition of 26.4% sand, 59.9% silt and a low clay content of 13.7%. Based on the results of the X-ray and ESEM analyses previously discussed, the clay content for this material should be substantially higher. In its intact state, the colluvium has a moisture content almost equal to the plastic limit (Section 5.3.1.1 and Section 5.3.1.2). This indicates a material of a stiff consistency and exhibit brittle deformation contrary to the residual soil which would show plastic deformation. The liquid limit range of 48% - 60% indicates the presence of a small amount of montmorillonite clay although the ESEM and X-ray results tend to show a larger amount of montmorillonite clay present based on the moderate compaction and low pore spaces present in the images.

The low clay content shown in the gradation curves for the colluvium may have resulted from the anomalous behavior of montmorillonite clay in dilute suspension. Rolfe et al (1960) showed in their experiment that when montmorillonite clay is mixed with sodium hexametaphosphate and distilled water in a hydrometer cylinder in the laboratory, the clay particles tend to flocculate instead of settle as discrete particles and based on the concentration of the deflocculent used, the percentage of clay particles remaining in suspension over a 24-hour period could vary between 43% and 77%. This implies that if the zone measured by the hydrometer test is not within the flocculated portion of a cylinder of this suspension it will measure a lower concentration of clay than the original freshly mixed sample contained.

Thus it is possible that this anomalous behaviour of montmorillonite clay in suspension may have been the cause for the low montmorillonite clay content shown in the gradation curves for the colluvium in comparison to the larger amounts shown in the X-ray and ESEM images.

The saturated hydraulic conductivity of the colluvium was measured in the field as 2.0×10^{-6} m/sec and 8.7×10^{-6}m/sec in two falling head tests. In addition, the saturated hydraulic conductivity at the 2008 site investigation ranged from 1.0×10^{-7} m/sec to 6.4×10^{-7} m/sec (Section 5.3.2.6, Tables 5.5 - 5.6). These saturated hydraulic conductivity values for the colluvium are substantially lower than the 9.0×10^{-5}m/sec recorded for the residual soil. The lower saturated hydraulic conductivity value of the colluvium is the direct result of the presence of the increased amount of montmorillonite clay content showed in the X-ray and ESEM images and supported by the index properties of the colluvium.

In summary, analyses of the petrographic, X-ray diffraction, SEM, ESEM images and index properties showed a difference in the characteristics of the parent rock and the resulting products of residual soil and colluvium. The petrographic analysis showed that the original mineral composition of the parent altered andesite rock consisted of a lesser amount of silicate minerals than the parent basalt rock. As a result of the weathering process, the residual soil product from the altered andesite was shown to contain a lesser amount of clay minerals than the colluvium from parent basalt from X-ray diffraction analysis. The colluvium contained a larger amount of montmorillonite clay as identified moderate and strong peaks.

The SEM images showed that the residual soil was moderately compacted and contained angular and randomly sorted grains of silt and sand with visible pore spaces and a low clay content. The gradation curves for the residual soil samples are in good agreement with the images shown in the SEM and X-ray diffraction analysis which are also consistent with the low plasticity results from the Atterberg limits tests.

The ESEM images of the colluvium showed a different fabric structure consisting of silt and sand grains embedded in a clay matrix which is consistent with the X-ray diffraction peaks from samples of this soil. However, the gradation curves for the colluvium were inconsistent with the X-ray and ESEM results which is suspected to be the result of inaccurate laboratory analysis of the soil samples in the hydrometer test.

The saturated hydraulic conductivity of the residual soil is consistent with the X-ray diffraction analysis and SEM analysis and index properties which is representative of a silty sand. The saturated hydraulic conductivity of the colluvium was shown to be of a lower magnitude than the residual soil because of the higher clay content which is consistent with that shown in the X-ray analysis and ESEM images.

8.2.5 Field Measurements and In situ Testing

8.2.5.1 Pore Water Pressure Response to Rainfall at the Barre de L'isle Study Site

The field instrumentation installed at the Barre de L'isle Study Site is discussed in detail in Chapter 4. The objectives of the instrumentation were to measure rainfall, surface runoff, infiltration, pore water pressure changes at variable depths, groundwater response to rainfall and ground deformation in response to an increase in excess pore water pressures. During the monitoring period, the heaviest rainfall event of 654 mm occurred over a 24-hour period on September 3, 2009 with an average intensity of 27 mm/hour. This was followed by a lesser amount of 488 mm over a 24-hour period on October 7, 2009. Between these two major events (1 month), the rainfall intensity decreased considerably to an average of 1.7mm/hour, the driest during the study period. This implies that the antecedent rainfall was small and did not contribute significantly to the moisture content in the ground prior to the second event since enough time was allowed for drainage of the soil to take place prior to the second event of 488mm.

Surface runoff and infiltration measurements conducted during a 488mm rainfall event indicated that most of the water was shed as runoff. The amount of surface water infiltration was considered to be moderate and was controlled by the saturated hydraulic conductivity of the soil which in turn was controlled by the amount of the clay fraction of which the soil is composed. For a residual soil with a low clay fraction of 17.0% -18.0% and low plasticity as measured in the laboratory index tests, this moderate infiltration rate is expected for a clayey, silty sand. In addition, the saturated hydraulic conductivity of 9.0×10^{-5} m/sec measured for the residual soil represents a clayey, silty sand which would allow 44% infiltration at a rate of 5.6×10^{-6} m/sec to take place during a 488mm rainstorm of 24-hour duration.

In contrast, Rahardjo et al, (2005) conducted runoff and infiltration measurements on a residual soil slope in Malaysia and found that for a 151mm total rainfall of 4 hours duration and 37 mm/hour intensity, a total of 53.1 % infiltration occurred for a clayey soil with a saturated hydraulic conductivity ranging from 5.18×10^{-6} m/sec to 1.67×10^{-6} m/sec. This implies that a total rainfall of lower intensity and duration will contribute to higher infiltration in a residual soil of lower saturated hydraulic conductivity than that experienced at the study site. This is attributed to the fact that larger total rainfall events contribute mostly to runoff and less to infiltration since as the soil approaches saturation the pore water pressure is at its maximum and any additional rainfall cannot infiltrate and cause any further increase in the pore water pressure.

At the start of the 654 mm rainstorm all of the tensiometers showed negative values (Figure 6.1 – Figure 6.3). As the rainfall intensified the pore water pressures approached saturation near the surface and the clayey, silty sand of moderate saturated hydraulic conductivity allowed infiltration to occur up to at least 3.0m depth. The tensiometers near the ground surface showed a quick response to the rainfall and showed the initial response to the wetting front as a result of infiltration whereas there was a delay in response in the tensiometers at greater depths. It stands to reason that the soil at the ground surface is more easily influenced by rainfall and atmospheric conditions quicker than deeper soil layers.

The changes in the atmospheric conditions in addition to the soil properties and composition stimulated rapid infiltration to occur near the ground surface than at greater depths. As a result, the pore water pressures at shallow depths responded quickly to changes in matric suction whereas the soil layers at greater depths required more time to respond to matric suction recovery and therefore showed a delayed reaction to the rainfall.

The pore water pressure response in the confined silty sand aquifer showed an immediate response to the rainstorm at a greater depth of 10.5m because of a recharge source at or near the ground surface and its higher saturated hydraulic conductivity of 1.0×10^{-3} m/sec and low clay content. This allowed for rapid infiltration and pore water pressure response to occur at greater depths and induce deep-seated slope instability at 12.2m depth. The advancement of the infiltrating surface water to greater depths was controlled by the more permeable silty sand aquifer layer which contains a minimal clay fraction compared to that present in the upper residual soil layer. Therefore, this silty sand layer quickly becomes saturated at the start of the rainstorm and rapidly transfers the surface water to greater depths. This rapid recharging of the silty sand resulted resulted in a buildup of excess pore water pressure because of the confinement of the upper less permeable residual soil and the bedrock below and result in the immediate response as observed in the standpipe piezometer. As the rainfall decreased, recharging of the silty sand layer is reduced and there was a reduction of excess pore water pressure in the aquifer as the recovery of matric suction began and the water level in the standpipe piezometer gradually dissipated as observed in the field at the end of the rainstorm.

The increase in pore water pressure and reduction of matric suction in the silty sand layer at 10.5m resulted in an increase in the soil water content of the clayey silt confining layer below the silty sand at 10.7m depth causing a reduction in shear strength of the clayey silt and induce slope failure at 12.2m during the rainstorm of 24-hour duration. The changes in pore water pressure taking place in the residual soil during the 488mm rainfall event was shown to be dependent on the initial pore water pressure in the subsoil and the rate of infiltration which in itself was controlled by the saturated hydraulic conductivity of the residual soil and silty sand layer.

Near the ground surface (0.5m) the initial pore water pressures were all negative prior to the start of the rainfall. All of the tensiometers at 0.5m responded immediately to the rainfall with pore water pressure increasing up to -2 kPa and -4 kPa for Rows A and B. The tensiometer in Row C was not as responsive as in Rows A and B because of its location in a shallow drain which did not allow ponding of surface water to cause rapid infiltration to occur as most of the rainfall was quickly shed as runoff by the drain. The rainfall was of such intensity however, that it quickly saturated other areas of the site as indicated by the tensiometers.

At greater depths (3.0m) there was also a dynamic response to this rainfall event in all the tensiometers with pore water pressures increasing from an initial -42 kPa to -4 kPa within 24 hours of rainfall. It was also shown that the pore water pressures in the silty sand aquifer increased as a result of intensive recharging during the 488mm rainstorm at a much faster rate than infiltration through the residual soil and induced deep-seated slope movement.

This was as a result of the higher saturated hydraulic conductivity of the silty sand layer (1×10^{-3} m/sec) which allowed more intensive infiltration to take place to greater depths and cause a rapid buildup of excessive pore water pressure because of its confinement between the residual soil layers. This excess pore water pressure was the triggering mechanism that induced slope movement by reducing the shear strength of the residual soil at a depth of 12.2m.

8.2.5.2 Pore Water Pressure Response to Rainfall at the Windjammer Landing Beach Resort Study Site

The annual rainfall distribution at the Windjammer Landing Beach Resort Study Site in the northern part of the island is considerably less than at the Barre de L'isle Study Site because of topographic variations. The results of the monitoring programme at the site showed that the tensiometers near the ground surface (0.5m) showed a decrease in response to decreasing rainfall because of the effects of atmospheric conditions on small amounts of rainfall particularly because of the effects of rapid evaporation at the ground surface which had an adverse effect on infiltration. During the monitoring period, it was observed that the pore water pressure in the colluvium near the ground surface showed a quick response to rainfall amounts between 5mm and 15mm but did not result in infiltration to 2.3m. It should be remembered that the saturated hydraulic conductivity of the colluvium varied from 1×10^{-6} m/sec to 6.4×10^{-7} m/sec which controlled the rate of infiltration in the colluvium and in this case the rainfall amount was too small to cause infiltration to greater depths. It was also observed that for a rainfall amount of 24mm to 35mm, surface water will infiltrate to a depth of 2.3m in the colluvium within a 24-hour period.

It was also shown that the changes in the pore water pressure in the slope is directly related to the initial pore water pressures at variable depths in the colluvium at the start of the rainfall. Prior to the start of the rainfall event of 24mm on December 24, 2008 the initial pore water pressures were negative at 0.5m depth and were recorded at -13 kPa, -10 kPa and -12.5 kPa respectively in the tensiometers in Rows A, B and C as a result of antecedent rainfall (Section 6.2.2.2 and Figures 6.7 – 6.9). At the end of the 24-hour rainfall event the pore water pressures increased to -2.5 kPa, 0 kPa and -3 kPa in the respective tensiometers.

This showed that infiltration occured quickly in the colluvium near the ground surface and resulted in an immediate increase in the pore water pressure and a reduction in matric suction at the start of the rainfall. It also showed that the increase in the pore water pressure at the end of the 24 mm rainfall ranged from -9.5 kPa to -10.5 kPa within 24 hours of rainfall.

At a depth of 2.3m the tensiometers indicated lower initial pore water pressures than near the ground surface. The tensiometers in rows A, B and C showed initial pore water pressures of -16 kPa, -17.5 kPa and -15 kPa, respectively. Following the 25mm rainfall, there was little change in the pore water pressure in Rows A and B from the initial values to -15 kPa, -15 kPa, and Row C at -7.5 kPa. This implies that infiltration was greater in Row C than in rows A and B.

This could be a result of an increase in the saturated hydraulic conductivity of the colluvium due to higher moisture contents in the subsoils ahead of the advancing wetting front as a result of antecedent rainfall at the location of Row C.

The advancement of the wetting front is controlled by the degree of saturation of the soil ahead of the wetting front. It this case it can be stated that there was an increase in the moisture content of the colluvium as a result of antecedent rainfall to a depth of 2.3m than at the location of Rows A and B which allowed more rapid infiltration to take place within a 24-hour period as a result of a reduction in matric suction.

A combination of the antecedent rainfall and the 24 mm rainfall on December 24, 2008 did not result in a significant increase in the pore water pressure that caused any decrease in the factor of safety of the slope and did not result in any instabilities developing in the colluvial slope within a 24 hour period of rainfall. The slope failed during a 120 mm rainstorm of 24 hour duration on October 11, 2008.

The relationship of pore water pressure and the factor of safety of the slope is established from seepage and slope stability numerical analyses which are discussed in the following section.

8.2.6 Numerical Modeling of the Barre de L'isle and Windjammer Landing Beach Resort Slopes

In order to successfully conduct numerical seepage and slope stability analyses of the residual and colluvium slopes under study, it was first necessary to assimilate the field and laboratory information into a numerical model to better understand the mechanics of infiltration and seepage and their effect on the factor of safety of the two slopes. The numerical modeling of the slopes provided valuable information on the seepage and deformation characteristics of the slopes. The effect of a 24-hour intensive rainfall event on the pore water response and slope deformation was shown by both field measurements and the predicted numerical model results. The changes in pore water pressure with depth during a rainstorm showed that near the ground surface the pore water pressures increased rapidly at the start of the rainfall event and little change occurred at greater depths. As the rainfall continued infiltration and pore water pressure changes at greater depths were minimal.

It was also shown that the total hydraulic head near the ground surface increased at the start of the rainfall event compared to the total hydraulic head at greater depths resulting in higher hydraulic gradients and infiltration rates near the ground surface. Also, the total hydraulic head below the ground surface was shown to increase as the rainfall continued, causing a decrease in the hydraulic gradient and infiltration rate. The saturated hydraulic conductivity was shown to increase with an increase in the difference in total hydraulic head near the ground surface and at depth due to an increase in the hydraulic gradient.

The numerical analysis indicated that the factor of safety of the slopes decreased with time as infiltration and pore water pressures increased.

8.2.6.1 The Barre de L'isle Slope

8.2.6.1.1 Predicted Pore Water Pressure Response to Rainfall

During the 24-hour rainfall event of 654mm on September 3, 2009 it was shown that there was a quick response in pore water pressure in the field at depths of 0.5m, 0.9m, 1.5m, 2.1m and 3.0m. This would suggest that for this rainstorm infiltrated water reached to at least 3.0m depth thereby causing a decrease in the negative pore water pressure at this depth. This was the result of an increase in total hydraulic head near the ground surface at the start of the rainfall which caused an increase in the difference in total hydraulic head at greater depths. This resulted in a higher hydraulic gradient and therefore an increase in saturated hydraulic conductivity in the clayey silt residual soil which allowed the rapid flow of water to greater depths within a 24-hour period. Figure 7.26 shows the changes in the predicted pore water pressure at the ground surface and up to 3.0m in the residual soil.

It was shown that in a surface run-off and infiltration test at the site that 56 % of surface water was run-off and 44 % infiltrated the ground. This indicated that the infiltration rate was greater than the saturated hydraulic conductivity of the soil near the ground surface resulting in a large amount of the surface water being shed as run-off. Darcy's law states that the rate of flow through a soil can be expressed as the hydraulic gradient multiplied by the permeability of the soil. If the hydraulic gradient exceeds unity then the flow rate of water can be greater than the permeability of the soil. For sandy soils a hydraulic gradient greater than unity can result in internal erosion and cause 'piping' of cohesionless materials since a hydraulic gradient greater than unity will result in an increase in the saturated hydraulic conductivity of the soil.

Generally, it was shown that when a surface flux of 5.6×10^{-6} m/sec was applied in the numerical model there was an increase of 1.5m in the predicted pore water pressure response at greater depths in excess of field measurements. This was because the numerical model SEEP/W is not capable of including the effects of evaporation in the analysis which would affect the outcome of the pore water pressure measurements in the field. The effect of tree roots and agricultural plants at the site would play a key role in reducing the pore water pressure in the field through evapo-transpiration.

The pore water pressure changes in the confined silty sand aquifer at 10.5m depth in the slope showed an increase in total hydraulic head of 2.0 m in the confined silty sand aquifer during a 654mm rainfall of 24-hour duration. This increase in total hydraulic head could have been greater since there was a time lag between the end of the rainstorm and the monitoring of the standpipe piezometer and some dissipation of pore water pressure may have taken place prior to monitoring. Usually, the worst case scenario for slope instability is to assume that the groundwater table rises to ground surface in an unconfined aquifer. However, in this case of a confined silty sand aquifer it is possible that the groundwater table may rise above the ground surface at some point during the rainstorm, especially if the confined aquifer becomes "overcharged" with infiltrating surface water. In this case, the total hydraulic head difference may increase and cause an increase in the hydraulic gradient greater than unity which would result in an increase in the saturated hydraulic conductivity of the silty sand. As a result, internal erosion of the silty sand could take place and cause 'piping' of the fines and generate slope instability.

This quick, positive pore water pressure response in the confined silty sand aquifer at a depth of 10.5m below ground surface indicated that the aquifer was being rapidly recharged by a source or sources at or near the ground surface. This indicated that the capacity of the silty sand layer is such that it could not channel the flow of the recharge surface water efficiently for discharge in the spring at the toe of the slope which caused a 'backup' or overflow in the aquifer which generated artesian pressure and an increase in total hydraulic head in the standpipe piezometer.

Keeping in mind that during the 654 mm rainstorm the maximum depth of the wetting front in the numerical model was observed to be no more than 2.0m depth during the 24-hour rainstorm, it would be impractical to suggest that the rapid increase of the total hydraulic head in the confined silty sand aquifer in such a short period of time was as a result of infiltration of water through the overlying residual soils. This increase in the pore water pressure in the confined silty sand layer was a direct result of the rapid recharging of the aquifer which caused increased lateral flow of groundwater in the confined silty sand layer during the rainstorm.

The predicted pore water pressures in the numerical analysis were in fair agreement with the field measurements at shallow depths but varied considerably at greater depths. The predicted pore water pressures results were shown to be greatly dependent on the saturated hydraulic conductivity of the residual soil and the Soil Water Characteristic Curve (SWCC) selected. The parameters used for soil-water retention characteristics of the residual soil did not affect the pore water pressure under saturated conditions because the volumetric water content of the residual soil remained at a constant value under saturated conditions.

The results of the numerical analysis also showed that the rainfall distribution played a significant role in the predicted results. It was shown that infiltration to greater depths was heavily dependent on the duration of the rainfall event and not solely on the amount of rainfall. This is because during a short period of heavy rainfall the ground surface became saturated quickly but most of the the rainfall was shed as run-off and there was insufficient time for infiltrate to occur to displace the suction at greater depths.

In the numerical analysis, it was also shown that at a time assumed to be equal to zero, water began to infiltrate vertically downward through the overlying residual soil layers but had not yet reached the water table to cause any increase in the water level. Perched water tables were formed within the residual soil layers within the next few days and after 4 days (time step 2) of rainfall, the phreatic surface was raised close to the ground surface. Thus, it was shown that the pore water pressure response to rainfall near the ground surface took a very short time to occur whereas at greater depths there was a much longer time lag for infiltration to occur and cause the groundwater table to rise.

Figure 7.25 shows the changes in total hydraulic head taking place near the ground surface and at 1.5m as predicted in the numerical model. The difference in the initial total hydraulic head near the ground surface and at 1.5m depth at the start of the rainstorm is 2.0m. This difference in total hydraulic head resulted in a high hydraulic gradient and therefore increased the saturated hydraulic conductivity near the ground surface which generated higher infiltration.

As the rainstorm continued and the ground surface became saturated, this caused a decrease in the hydraulic gradient to decrease and also a decrease in the saturated hydraulic conductivity and infiltration capacity of the residual soil. Hence the reason why infiltration into the residual soil decreased with depth. The infiltration of surface water caused an increase in the pore water pressure at depth which in turn increased the total hydraulic head at 1.5m and the difference between the total hydraulic head at the ground surface and at 1.5m decreased and as a result infiltration to greater depths also decreased regardless of the rainfall intensity since most of the surface water was shed as run-off.

8.2.6.1.2 Slope Stability

The instability factors taken into account in this study included: i) reduction in soil shear strength during saturation, ii) increased driving forces of the saturated soil and, iii) the decrease in effective stress as a result of saturation. The results of the numerical analysis indicated that for a rainfall distribution of 5.6×10^{-6} m/sec the initial computed factor of safety was 1.41 at the start of the rainfall event. A perched water table was established at a shallow depth after 2 days of rainfall distribution. The phreatic surface continued to rise with time until it reached the ground surface after 6 days of rainfall distribution at which time the computed factor of safety of the slope decreased to 1.14. The increase in the pore water pressure in the residual soil caused a considerable decrease in the computed factor of safety of the slope.

The model predicted that the computed factor of safety of the slope decreased to unity after 6 days of rainfall at which time the groundwater table was raised to the ground surface in the overlying residual soil. This is in conflict with field observations since subsidence and deformation at the ground surface was observed at the end of the 24-hour rainfall event. This would imply that failure of the slope occurred within the 24 hours of rainfall and not 6 days after the completion of the rainfall.

The total hydraulic head in the residual soil responded quickly to positive values during surface water infiltration. This hydrological response supports the concept of pore water transmission associated with normal surface water infiltration. It also supports the concept that steady state seepage is not appropriate to analyse landslide activity particularly for deep-seated landslides.

The total hydraulic head difference of 2.0m in the residual soil was not enough to generate shallow failure in a slope of 21.0^{o} gradient with an angle of internal friction of 23.0^{o}. Shallow slope failures up to 3.0m depth are common on steeper slopes on the Barre de L'isle ridge during rainstorms of lesser intensity. Thus, the wetting front migration downwards in the soil in this case was insignificant in causing slope failure of the slope even with positive pore water pressures dominating. In addition, there was no indication of deformation in the slope inclinometer at the site except at a depth of 12.0m below ground surface.

8.2.6.2 The Windjammer Landing Beach Resort Slope

8.2.6.2.1 Predicted Pore Water Pressure Response to Rainfall

The saturated hydraulic conductivity of the colluvium was measured at 6.3 x 10^{-5} m/sec in a falling head test. In the numerical analysis a rainfall distribution of 1.5 x 10^{-6} m/sec was applied as a simulated surface boundary flux for the colluvium for the 120 mm rainstorm which caused the slope to fail. The predicted pore water pressure response of -5.8 kPa to a 120 mm rainfall event bore little resemblance to the actual field measurements of 0.0 kPa or full saturation near the ground surface for the 35 mm 24-hour rainstorm. There is, however, some trend to the predictions reflecting the precipitation rates which the field data showed. This was partly due to the number of assumptions that were necessary to determine run-off and infiltration rates since these field tests were not performed at this site due to restrictions by the resort management personnel.

However, the trend showed a resulting increase in total hydraulic head near the ground surface at the start of the 35 mm rainfall which increased the hydraulic gradient and the infiltration rate in the colluvium. At a depth of 1.0m there was good agreement in the predicted pore water pressure response at -5.1 kPa and the actual field measurements which ranged from -5.5 kPa to -7.5 kPa. The increase in the saturated hydraulic conductivity of the colluvium as a result of the increased total hydraulic head allowed flow of surface water downwards into the soil but not to the point of complete saturation at 1.0m. Graphs of the predicted pore water pressure changes at the ground surface and up to 2.3m are shown in Figures 7.56a to Figure 7.57c.

At greater depths, however, the field measurements showed a decrease in pore water pressure for the 35 mm event whereas the numerical model showed an increase in pore water pressure with depth for the 120 mm rainfall event. This is expected since the more intensive rainstorm of 120 mm would result in a greater increase in total hydraulic head and thus in infiltration rate than a 35 mm rainfall event over a 24-hour period. It is also possible that the effect of evaporation of surface water played a role by reducing the amount of water available for infiltration into the colluvium which would result in a greater amount of available surface water for infiltration from the larger rainfall event. The numerical model SEEP/W is incapable of simulating the effect of evaporation or vegetation.

The predicted conditions in the slope for the 120 mm rainstorm clearly indicated that infiltration of surface water caused the groundwater table to rise to the ground surface and saturated the colluvium causing slope failure. It was shown in the study that the increase in the total hydraulic head during the rainstorm caused an increase in the hydraulic gradient and the saturated hydraulic conductivity as suction decreased which allowed rapid infiltration of the thin layer of colluvium.

It is speculated that the saturation of the colluvium layer caused the excess infiltrating water to travel downslope and lubricating the impermeable bedrock surface thereby exacerbating downward movement of the soil mass. This is supported by the flow velocities generated in the numerical model which show that flow is predominantly in the colluvium and is parallel with the slope gradient as shown in Figure 7.51**.** Graphs of the changes in total hydraulic heads are shown in Figures 7.55a to Figures 7.55e.

8.2.6.2.2 Slope Stability

In the numerical model it was shown that the predicted factor of safety of the slope was shown to decrease significantly from 2.39 prior to the 120 mm rainstorm to 1.02, five (5) days after the start of the rainfall. This was as a result of increased positive pore water pressures in the colluvium due to infiltration to greater depths as predicted in the numerical model. The rainfall intensity and the saturated hydraulic conductivity of the colluvium (6.3 x 10^{-5} m/sec) were shown to be the main controlling parameters during the infiltration process. The critical slip surface was shown to be at the contact between the colluvium and the highly weathered bedrock.

The numerical analysis also showed that the thickness of the colluvium layer played an important role in the quick response in pore water pressure and failure of the slope. This is because of the fact that the colluvium layer of 3.5m thickness overlying bedrock would tend to become saturated and unstable much faster than, for example the colluvium deposit in the 2005 landslide area which is of much greater depth. This is because infiltration and saturation would transpire quicker in the thinner colluvium deposit of a similar saturated hydraulic conductivity value. Therefore, it can be concluded that the critical time for slope failure in the thin colluvium layer was during or immediately after the 24-hour rainfall of 120 mm whereas, for failure at greater depths in the colluvium would occur sometime after the end of the rainfall event.

8.3 CONCLUSIONS

The research presented in this thesis has provided considerable insight into the hydrological processes taking place in two slopes of unsaturated multi-layered residual soil and colluvium during a 24-hour rainstorm and its marked effect on the stability of the slopes. In the following sections, conclusions drawn from various aspects of this research are summarized.

8.3.1 Weathering of Parent Andesite and Basalt Rocks

The parent andesite and basalt rocks have undergone extensive weathering as reflected in their mineral composition and structure resulting in the formation of residual soils and colluvium. The results of the weathering process produced new minerals, fabric and structure in these materials which have great influence on the engineering properties and behavior of the soils.

The mineral composition of the residual soil from parent Andesite rock consist predominantly of weathering resistant quartz together with titanium, magnesium, potassium and iron-oxide which gives the residual soil its reddish colour. Chlorite and kaolinite clays are present with minor amounts of montmorillonite. The microscopic characteristic of the soil is represented by an open heterogeneous structure of mainly silt and sand with pore spaces of variable sizes which contribute significantly to engineering concerns such as design and construction, soil modeling, laboratory testing and the saturated hydraulic conductivity of the soil. The iron oxides act as cementation and aggregation agents which coat the soil particles and may prevent complete dispersion of the soil mass.

The colluvium from parent basalt rock showed the presence of high concentrations of montmorillonite clay and weathering resistant quartz as the dominant components. The structure is densely packed and randomly orientated with the coarse sand and silt fractions embedded in a detrital clay matrix and pore spaces are visible but not as abundant as in the residual soil. The disturbed texture of the soil fractions in the colluvium indicates that random sorting and some leaching of fines may have occurred during the transportation of the soil.

The presence of montmorillonite clay in the colluvium is directly related to the lower saturated hydraulic conductivity value compared to the residual soil. In addition, the index properties of the colluvium showed good correlation with the presence of the montmorillonite clay fraction.

These results imply that the textural characteristics of the parent andesite and basalt rocks are reflected in the soils derived from them as a result of the weathering process. A complete analysis of the residual soil and colluvium using micro-characterization techniques has been conducted in this study to identify the mineralogical composition of the parent rocks and the soils produced as a result of the weathering process.

8.3.2 Field Measurements of Pore Water Pressures at the Barre de L'isle Study Site

It was shown that at the start of the rainfall, infiltration was almost immediate and there was a rapid increase in pore water pressure at the ground surface. The rainfall intensity caused a greater amount of the surface water to be shed as run-off since at the start of the rainfall the total head difference was insufficient to cause an increase in hydraulic gradient that would allow deeper infiltration of water to occur. This was because the matric suction near the ground surface was positive and caused a reduction of the saturated hydraulic conductivity of the residual soil. As the rainfall continued the pore water pressures increased downwards in the soil as matric suction was replaced by the infiltrating surface water as the hydraulic gradient increased and allowed flow to greater depths. It was shown that in a surface run-off and infiltration test in the residual soil with 17% to 18% clay an amount of 56 % of surface water shed as run-off and 44 % infiltrated the ground during a 488 mm rainstorm.

The response to rainfall was quick in the confined aquifer because of the rapid recharging of the more permeable silty sand layer at 10.5m below ground surface. This excessive recharging generated a rapid increase in the pore water pressures in the confined aquifer and caused a 'back-up' of inflowing water greater than the capacity of the aquifer which caused the development of deep-seated instability in the slope.

The research study also showed that the silty sand layer played an important role in controlling the build-up of excess pore water pressure with time during normal rainfall events of longer duration by draining the slope because of its higher saturated hydraulic conductivity compared to that of the residual soil. Therefore, the silty sand layer acted as a natural hydrogeological feature that assisted in stabilizing the slope by reducing the pore water pressure in the residual soil by drainage of the slope during normal periods of rainfall thereby stabilizing the slope. This shows that failure of the slope was triggered by the rapid infiltration of surface water into the confined silty sand aquifer at depth causing saturation and an increase in excess pore water pressure and not as a result of infiltration of surface water which caused rising of the groundwater table to the ground surface.

It should also be noted that the total hydraulic head difference of >2.0m in the silty sand aquifer is greater than the thickness of the silty sand aquifer (1.7m). This would imply that the slope failed under a condition of high pore water pressures in excess of hydrostatic forces generated by the total saturation of the silty sand aquifer. The high pore water pressures in the silty sand aquifer from surface recharging caused mobility of the cohesionless soil particles resulting in a decrease in effective stress and as a result a decrease in shear strength of the silty sand deposit.

This research has shed new light on the fact that deep-seated slope failures can develop in unsaturated residual soils without complete infiltration and saturation of the slope above the groundwater table. It also showed that slope failure can be triggered by excessive recharging of hydrogeological features at depth with the existence of an unsaturated zone between the wetting front and the initial groundwater table.

8.3.3 Field Measurements of Pore Water Pressures at the Windjammer Landing Beach Resort Study Site

The result of the research showed that a colluvium soil from parent basalt rock composed of a moderately closed texture and fabric with a montmorillonite clay fraction of 13.7% and a low saturated hydraulic conductivity will allow infiltration to take place up to a maximum depth of 0.5m during total rainfalls varying from 5mm to 15 mm within a 24-hour period. It also showed that for increased total rainfall amounts of 24mm to 35mm infiltration will advance to a depth of 2.3m in the colluvium.

At the start of the rainstorm, the pore water pressures at the ground surface increased due to saturation and suction decreased. This resulted in an increase in the hydraulic gradient and the saturated hydraulic conductivity of the colluvium which allowed infiltration of surface water to infiltrate, but the movement of surface water downwards into the colluvium was restricted by matric suction. Therefore, the infiltration rate exceeded the saturated hydraulic conductivity at depth due to suction and a state of equilibrium (steady state) was established between the pore water pressures and suction near the ground surface which impeded further infiltration to greater depths.

Thus, it can be concluded that for the 35mm rainstorm of 24-hour duration, the infiltration rate was too low to advance the wetting front sufficiently downward to cause a reduction in matric suction to generate an increase in the pore water pressures to trigger slope failure. In other words, the 35mm rainfall and the resulting infiltration rate was insufficient to cause an increase in total hydraulic head that would increase the hydraulic gradient and saturated hydraulic conductivity of the colluvium significantly to allow the flow of surface water to greater depths and cause instability in the slope. The field measurements showed that infiltration did not exceed 2.3m for this rainfall event.

It would require the wetting front to advance downward to bedrock (3.5m) to cause any significant increase in pore water pressure and hence a reduction in matric suction to trigger slope failure within 24 hours. It is possible that if the duration of the 35mm rainfall was in excess of 24 hours, deeper infiltration of surface water may have occurred and initiate slope failure.

It is not within the scope of this research to determine the threshold of rainfall required to trigger slope failure in colluvium slopes. However, the study showed that a 35mm intensity rainfall will not trigger failure in a 3.5m thick colluvium slope of 18^{o} gradient during a 24-hour rainstorm

8.3.4 Numerical Modeling of the Barre de L'isle Slope

Numerical modeling is a powerful tool for infiltration, seepage and stability analyses in slopes. However, the method itself cannot guarantee the accuracy of the predictions. The proper simulation of non-homogeneity, slope geometry, and boundary conditions of the slope are of major significance. The numerical modeling utilized all the field observations and Soil-Water Characteristic Curves for the analysis.

The predicted pore water pressure in the numerical analysis were in good agreement with the field measurements at shallow depths but varied considerably at greater depths. The predicted pore water pressures results were shown to be greatly dependent on the saturated hydraulic conductivity of the residual soil and the Soil Water Characteristic Curve (SWCC) selected. It was shown that infiltration to greater depths was heavily dependent on the duration of the rainfall event and not solely on the amount of rainfall. This is because during a short period of heavy rainfall the ground surface became saturated quickly but most of the rainfall was shed as run-off and there was insufficient time for infiltrate to occur to displace the suction at greater depths.

The numerical analysis showed that the combined effect of rainfall intensity and duration and the saturated hydraulic conductivity of the residual soil (9.0×10^{-5} m/sec) resulted in an increase in total hydraulic head and were the major governing parameters influencing the increase in the infiltration rate and pore water pressure response.

It was also shown that deep-seated instabilities developed at a depth of 12.0m in the slope within 24 hours of the start of the rainstorm as a result of excessive infiltration through the more pervious silty sand and triggered slope failure at depth with an unsaturated zone established in the residual soil between the wetting front and the initial groundwater table.

The results of the numerical analysis showed that the silty sand layer played an important role in controlling the build up of excess pore water pressure with time during rainfall events of longer duration by draining the slope because of its higher saturated hydraulic conductivity compared to that of the residual soil.

In the slope stability analysis it was shown that the critical slip surface was deep-seated and located below the silty sand aquifer near the contact with the bedrock**.** This is supported by the field instrumentation which showed the critical slip surface at a depth of 12.0m below ground surface**.**

8.3.5 Numerical Modeling of the Windjammer Landing Beach Resort Slope

The numerical model predicted that a 120 mm rainstorm event resulted in complete saturation of the colluvium layer and trigger slope failure within five days after the start of the rainfall by a gradual advancement of the wetting front. However, this is in disagreement with the actual field observations which showed that the slope failed within 24 hours after the start of the rainstorm.

This was partly due to the number of assumptions that were made in the numerical analysis to determine run-off and infiltration rates at the site since these field tests were not performed at this site. Therefore, the infiltration rate assumed in the model may have been inaccurate which led to this vast difference in the time of slope failure. The predicted pore water pressure response to a 120 mm rainfall event in the numerical analysis showed poor correlation with the actual field measurements for full saturation near the ground surface for a 35 mm rainfall event.

This is the result of the fact that a 120 mm rainfall event would generate a higher rate of infiltration than a 35 mm rainfall event and cause an increase in the pore water pressures at greater depths. This is supported by the fact that during a 35 mm rainfall event there were no signs of surface deformation on the slope but the slope failed during the 120 mm rainfall event.

The factor of safety of the slope was shown to decrease significantly five days after the start of the rainfall. This was shown to be the result of increased positive pore water pressures in the colluvium due to rapid infiltration to greater depths as predicted in the numerical model. The critical slip surface was shown to be at the contact between the colluvium and the highly weathered bedrock where the shear strength of the colluvium was at its lowest with the groundwater table at the surface.

The mechanics of the effect of infiltration on the stability of the slope with time was observed during the transient process as the phreatic surface began to rise toward the ground surface in response to infiltration of surface water as controlled by the saturated hydraulic conductivity of the soil. As the phreatic line approached the ground surface, the Factor of Safety of the slope decreased as the excess pore water pressure build-up caused a reduction in the shear strength of the soil and as the soil particles become mobilized the Factor of Safety of the slope was reduced significantly with time as infiltration continued.

Ideally, if the infiltration rate was reduced by the cessation of rainfall and the Factor of Safety of the slope is still greater than unity then the slope would remain stable if the subsoils are stabilised by drainage.

8.4 RECOMMENDATIONS FOR FURTHER RESEARCH WORK

This research study has helped to increase the understanding of the rapid rate at which unsaturated residual soils and colluvium become saturated and unstable during rainstorms. The study in itself is incomplete at this point and further in-depth research is required to determine the threshold of rainfall required to trigger slope failure.

The following areas of recommended for further research:

i) Correlation between Soil Index Properties and Field Measurements with the Mineral Composition of the Parent Rock

The high cost of the complex petrographic, X-ray and SEM analyses makes it virtually impossible for developing nations with fragile economies to thoroughly investigate and understand the relationship between the engineering behaviour of residual soils and colluvium with the mineralogy and texture of the parent rock. Therefore, it is necessary to develop a better understanding of the inter-related elements of soil forming processes, soil composition and microstructure in addition to soil index properties in order to derive a more workable classification system for tropical residual soils.

ii) Mechanism of Rapid Deep-seated Failure in Natural Residual Soil Slopes

A study of deep-seated (>10.0m) slope failures in unsaturated natural residual soil slopes is encouraged based on the experience with such slope failures in Saint Lucia during hurricane 'TOMAS' in October 2010 during a 688 mm, 24-hour rainstorm (Chapter 2, Section 2.2.12). Two areas of concern are the landslides at Colombette (Figure 2.24) and at Fond St. Jacques (Figure 2.25). Both of these landslides were deep-seated and caused casualties and extensive damage to property. Of particular interest is the Colombette landslide which occurred within 14 hours after the start of the rainstorm. Both slides appear to have been triggered by excessive recharging of hydrogeological features such as confined aquifers or springs.

Most of the deep-seated landslide studied or reported in the literature usually occurred several hours after the rainfall event has stopped. There is very little if any, of studies being conducted on the mechanism of rapid infiltration and failure of deep-seated unsaturated residual soil slopes during a 24-hour rainstorm. Such a research study would require detailed field instrumentation and monitoring, laboratory testing and numerical predictions of rapid pore water pressure response and slope failure within a short time period.

iii) A Constitutive Model for the Transition between Unsaturated and Saturated Conditions for Residual Soils

There is need for a constitutive model capable of modeling the mechanical behaviour of residual soils and colluvium during the transition state from the unsaturated to the saturated condition and vice versa. The model should be capable of simulating the influence of the degree of saturation on the mechanical behavior of the soils under changing suction and saturation states which are common under natural conditions in the field.

The study could be initiated by laboratory experimentation by measuring the mechanical behaviour of residual and colluvium soil samples under wetting and drying cycles and applying these results to actual field conditions. Current constitutive models do not correctly model this behavior in residual soils and colluvium.

iv) The Critical State of Residual Soils

Very little is currently known of the relationship between deformation and effective stress in unsaturated residual soils particularly as the unsaturated soil is transformed into a saturated state during a rainstorm. The complex functions of the effective stresses and pore-water pressures cannot be determined independently since current theories are inadequate and can only be obtained by comparing deformation of unsaturated and saturated soils by applying similar stress paths. This phenomenon requires further study. This required research work should address the conditions when the principle of effective stress did not apply when the soil is in an unsaturated state initially to the situation when the soil quickly becomes saturated and the principle of effective stress is applicable. This research work would require experimentation work involving the collection of information from small to very large stresses and incorporating the critical state concept to develop an improved constitutive model.

v) Rainfall Thresholds for Slope Failure in Colluvium

Very little is currently available in the literature on the effect of infiltration on the stability of colluvium slopes during rainstorms. This research study showed that a rainfall intensity of 35mm did not initiate slope failure in a 3.5m thick layer of colluvium within 24 hours. In the predicted analysis it was shown that a 120mm rainfall event would trigger failure of the slope within five days whereas the actual field observations showed failure of the slope within 24 hours of rainfall.

Thus, there is some discrepancy between the time of the predicted failure in the model and the actual time of slope failure in the field. The 2005 landslide at the Windjammer Landing Resort (Chapter 2, Sect. 2.2.10) was triggered by artesian pressure in a 10.5m thick strata of colluvium.

So there is need for further research to clarify the threshold of rainfall required to trigger failure in colluvium slopes of variable thicknesses and gradients. The study should also incorporate the role of the antecedent rainfall in the process. This would require field instrumentation, laboratory testing and numerical analysis of infiltration and pore water pressure response to rainfall at various depths.

APPENDICES

APPENDIX A

Borehole Logs for Windjammer Landing Beach Resort 2005 Landslide

STRATA ENGINEERING CONSULTANTS LTD.
ST. LUCIA, WEST INDIES

TEST HOLE LOG AND LABORATORY TEST DATA

PROJECT: WINDJAMMER LANDSLIDE INVESTIGATION,ST. LUCIA,WEST INDIES

DWN. RJSAAC | CHKD. | JOB NO. | DATE August 8,2005 | HOLE NO. SP05-STA-1

MOISTURE CONTENT & STANDARD PENETRATION NO.

○ NATURAL MOISTURE CONTENT
× STANDARD PENETRATION TEST
PLASTIC LIMIT (PL) ⊢——⊣ LIQUID LIMIT (LL)

10 20 30 40 50 60 70 80 90

SOIL PROFILE			SAMPLES					
DEPTH ELEV. (m)	CLASSIFICATION		SOIL SYMBOL	OTHER TESTS	UNCONFINED COMPRESSIVE STRENGTH kg/cm²	SAMPLE COND.	TYPE	DEPTH SCALE
	DATUM GROUND SURFACE ELEVATION 23.5m							
	FILL - Silt,trace of clay,trace of sand,wood chips, stiff,moist,brown						SPT	0
1.5 22	COLLUVIUM - Silt,some sand,little clay,medium plasticity,rock fragments,organic specks,white specks,oxides,moist,brown						SPT	1
2.7 20.8	COLLUVIUM - Silt & Sand,trace clay,low plasticity,rock fragments,stiff to very stiff,oxides, moist,brown						SPT	2
							SPT	3
							SPT	4
							SPT	5
5.8 17.7	HIGHLY WEATHERED BEDROCK (BASALT) - fractured, very dense,brown						SPT	6
	ROCK CORE (5.8m - 12.2m) TCR = 61.0% SCR = 43.0% RQD = 17.0%						core	7
							core	8
							core	9
								10

PENETRATION RESISTANCE

(N) = No. OF BLOWS OF A 64 KG HAMMER DROPPED 760 mm (FREE FAL) REQUIRED TO DRIVE A 50 mm DIA. O.D. RAYMOND TYPE SAMPLER 300 mm INTO THE SOIL

SOIL TYPES

TOPSOIL, SILT, PEAT, SAND, FILL, GRAVEL, CLAY, BEDROCK

LABORATORY TEST SYMBOLS

UNCONFINED COMP. STR, kg/m²
DRY UNIT WEIGHT kg/m³
C-CONSOLIDATION TEST
MA-GRAIN SIZE ANALYSIS

CONDITIONS

UNDISTURBED
DISTURBED
LOST SAMPLE

SAMPLE TYPES

U-76 mm DIA. SHELBY TUBE
D.S.-DRIVE SAMPLE
M-MOISTURE CONTENT
R.C.-ROCK CORE

STRATA ENGINEERING
CONSULTANTS LTD.
ST. LUCIA, WEST INDIES

TEST HOLE LOG AND LABORATORY TEST DATA

PROJECT: WINDJAMMER LANDSLIDE INVESTIGATION,ST. LUCIA,WEST INDIES

DWN. R.ISAAC | CHKD. | JOB NO. | DATE August 8,2005 | HOLE NO. SP05-STA-1

MOISTURE CONTENT & STANDARD PENETRATION NO.

○ NATURAL MOISTURE CONTENT
× STANDARD PENETRATION TEST
PLASTIC LIMIT (PL) ⊢——⊣ LIQUID LIMIT (LL)

10 20 30 40 50 60 70 80 90

SOIL PROFILE		SAMPLES					
DEPTH ELEV. (m)	CLASSIFICATION	SOIL SYMBOL	OTHER TESTS	UNCONFINED COMPRESSIVE STRENGTH kg/cm²	SAMPLE COND.	TYPE	DEPTH SCALE
	DATUM GROUND SURFACE ELEVATION 23.5m						
	HIGHLY WEATHERED BEDROCK (BASALT) - very dense,brown					core	11
12.2 11.3	END OF BOREHOLE AT 12.2m STANDPIPE PIEZOMETER INSTALLED TO 7.0m GROUNDWATER LEVEL AT 3.0m					core	12 13 14 15 16 17 18 19 20 21

PENETRATION RESISTANCE

(N) = No. OF BLOWS OF A 64 KG HAMMER DROPPED 760 mm (FREE FAL) REQUIRED TO DRIVE A 50 mm DIA. O.D. RAYMOND TYPE SAMPLER 300 mm INTO THE SOIL

SOIL TYPES

TOPSOIL, SILT, PEAT, SAND, FILL, GRAVEL, CLAY, BEDROCK

LABORATORY TEST SYMBOLS

UNCONFINED COMP. STR, kg/m²
DRY UNIT WEIGHT kg/m³
C-CONSOLIDATION TEST
MA-GRAIN SIZE ANALYSIS

CONDITIONS

UNDISTURBED
DISTURBED
LOST SAMPLE

SAMPLE TYPES

U-76 mm DIA. SHELBY TUBE
D.S.-DRIVE SAMPLE
M-MOISTURE CONTENT
R.C.-ROCK CORE

STRATA ENGINEERING CONSULTANTS LTD.
ST. LUCIA, WEST INDIES

TEST HOLE LOG AND LABORATORY TEST DATA

PROJECT: WINDJAMMER LANDSLIDE INVESTIGATION,ST. LUCIA,WEST INDIES

DWN. R.ISAAC | CHKD. | JOB NO. | DATE August 25,2006 | HOLE NO. SP05-STB-1

MOISTURE CONTENT & STANDARD PENETRATION NO.

○ NATURAL MOISTURE CONTENT
× STANDARD PENETRATION TEST
PLASTIC LIMIT (PL) ⊢——⊣ LIQUID LIMIT (LL)

10 20 30 40 50 60 70 80 90

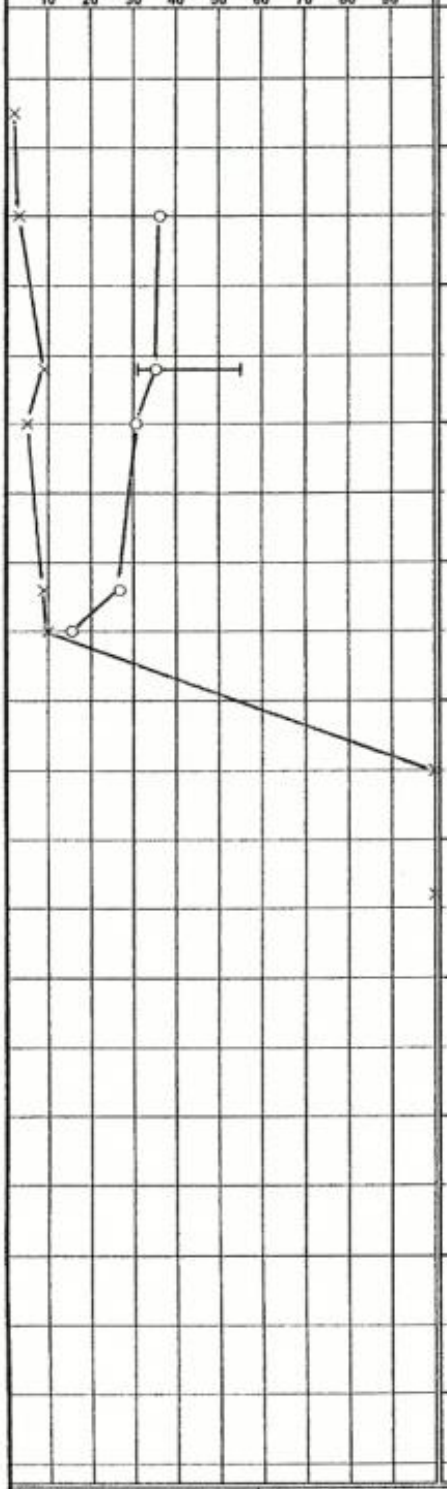

DEPTH / ELEV. (m)	CLASSIFICATION	SOIL SYMBOL	OTHER TESTS	UNCONFINED COMPRESSIVE STRENGTH kg/cm²	SAMPLE COND.
	DATUM GROUND SURFACE ELEVATION 22.9m				
	FILL				
0.8 22.15	COLLUVIUM - SILT,some sand,little clay low to medium plasticity,oxides,organic specks,stiff, moist,brown			0.4 2.0 1.25	
5.5 17.4	HIGHLY WEATHERED BEDROCK (BASALT) - very dense,brown				
6.4 16.5	END OF BOREHOLE AT 6.5m STANDPIPE PIEZOMETER INSTALLED TO 5.2m GROUNDWATER LEVEL AT 0.0m (Artesian pressure) UNCONFINED COMPRESSIVE STRENGTH FROM POCKET PENETROMETER				

PENETRATION RESISTANCE

(N) = No. OF BLOWS OF A 64 KG HAMMER DROPPED 760 mm (FREE FAL) REQUIRED TO DRIVE A 50 mm DIA. O.D. RAYMOND TYPE SAMPLER 300 mm INTO THE SOIL

SOIL TYPES

TOPSOIL, SILT, PEAT, SAND, FILL, GRAVEL, CLAY, BEDROCK

LABORATORY TEST SYMBOLS

UNCONFINED COMP. STR, kg/m²
DRY UNIT WEIGHT kg/m³
C-CONSOLIDATION TEST
MA-GRAIN SIZE ANALYSIS

CONDITIONS

UNDISTURBED
DISTURBED
LOST SAMPLE

SAMPLE TYPE

U-76 mm DIA. SHELBY
D.S.-DRIVE SAMPLE
M-MOISTURE CONTE
R.C.-ROCK CORE

STRATA ENGINEERING CONSULTANTS LTD.
ST. LUCIA, WEST INDIES

TEST HOLE LOG AND LABORATORY TEST DATA

PROJECT: WINDJAMMER LANDSLIDE INVESTIGATION,ST. LUCIA,WEST INDIES

DWN. RJSAAC | CHKD. | JOB NO. | DATE August 30,2005 | HOLE NO. SP05-STC-1

MOISTURE CONTENT & STANDARD PENETRATION NO.

○ NATURAL MOISTURE CONTENT
× STANDARD PENETRATION TEST
PLASTIC LIMIT (PL) ⊢——⊣ LIQUID LIMIT (LL)

10 20 30 40 50 60 70 80 90

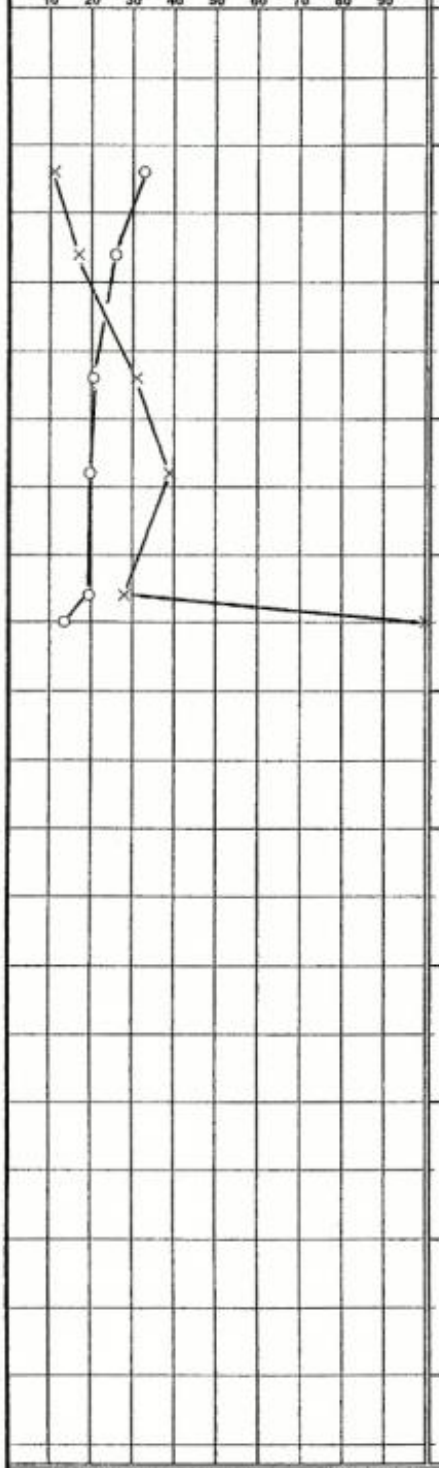

DEPTH ELEV. (m)	CLASSIFICATION	SOIL SYMBOL	OTHER TESTS	UNCONFINED COMPRESSIVE STRENGTH kg/cm2	SAMPLE COND.	TYPE	DEPTH SCALE
	DATUM GROUND SURFACE ELEVATION 17.2m						
	FILL						
1.2 16	COLLUVIUM - SILT,some sand,trace of clay,rock fragments,low plasticity,oxides,very stiff,moist, brown					SPT SPT	
2.7 14.5	COLLUVIUM - SILT,little sand,non plastic,oxides, dense,moist,brown					SPT SPT	
4.5 12.7	HIGHLY WEATHERED BEDROCK (BASALT) - very dense,brown					SPT SPT core	
	ROCK CORE (4.5m - 10.4m) TCR = 38.0% SCR = 23.0% RQD = 5.0%					core	
10.4 6.8						core	

PENETRATION RESISTANCE

(N) = No. OF BLOWS OF A 64 KG HAMMER DROPPED 760 mm (FREE FAL) REQUIRED TO DRIVE A 50 mm DIA. O.D. RAYMOND TYPE SAMPLER 300 mm INTO THE SOIL

SOIL TYPES

TOPSOIL, SILT, PEAT, SAND, FILL, GRAVEL, CLAY, BEDROCK

LABORATORY TEST SYMBOLS

UNCONFINED COMP. STR, kg/m2
DRY UNIT WEIGHT kg/m3
C-CONSOLIDATION TEST
MA-GRAIN SIZE ANALYSIS

CONDITIONS

UNDISTURBED
DISTURBED
LOST SAMPLE

SAMPLE TYPES

U-76 mm DIA. SHELBY TUBE
D.S.-DRIVE SAMPLE
M-MOISTURE CONTENT
R.C.-ROCK CORE

STRATA ENGINEERING CONSULTANTS LTD.
ST. LUCIA, WEST INDIES

TEST HOLE LOG AND LABORATORY TEST DATA

PROJECT: WINDJAMMER LANDSLIDE INVESTIGATION,ST. LUCIA,WEST INDIES

DWN. R.ISAAC | CHKD. | JOB NO. | DATE August 30,2006 | HOLE NO. SP06-STC-1

MOISTURE CONTENT & STANDARD PENETRATION NO.

○ NATURAL MOISTURE CONTENT
× STANDARD PENETRATION TEST
PLASTIC LIMIT (PL) ⊢——⊣ LIQUID LIMIT (LL)

10 20 30 40 50 60 70 80 90

SOIL PROFILE		SAMPLES					
DEPTH ELEV. (m)	CLASSIFICATION	SOIL SYMBOL	OTHER TESTS	UNCONFINED COMPRESSIVE STRENGTH kg/cm2	SAMPLE COND.	TYPE	DEPTH SCALE
	DATUM GROUND SURFACE ELEVATION 17.2m						
	END OF BOREHOLE AT 10.4m STANDPIPE PIEZOMETER INSTALLED TO 9.4m GROUNDWATER LEVEL AT 8.2m						11 12 13 14 15 16 17 18 19 20 21

PENETRATION RESISTANCE

(N) = No. OF BLOWS OF A 64 KG HAMMER DROPPED 760 mm (FREE FAL) REQUIRED TO DRIVE A 50 mm DIA. O.D. RAYMOND TYPE SAMPLER 300 mm INTO THE SOIL

SOIL TYPES

TOPSOIL, SILT, PEAT, SAND, FILL, GRAVEL, CLAY, BEDROCK

LABORATORY TEST SYMBOLS

UNCONFINED COMP. STR, kg/m2
DRY UNIT WEIGHT kg/m3
C-CONSOLIDATION TEST
MA-GRAIN SIZE ANALYSIS

CONDITIONS

UNDISTURBED
DISTURBED
LOST SAMPLE

SAMPLE TYPES

U-76 mm DIA. SHELBY TUBE
D.S.-DRIVE SAMPLE
M-MOISTURE CONTENT
R.C.-ROCK CORE

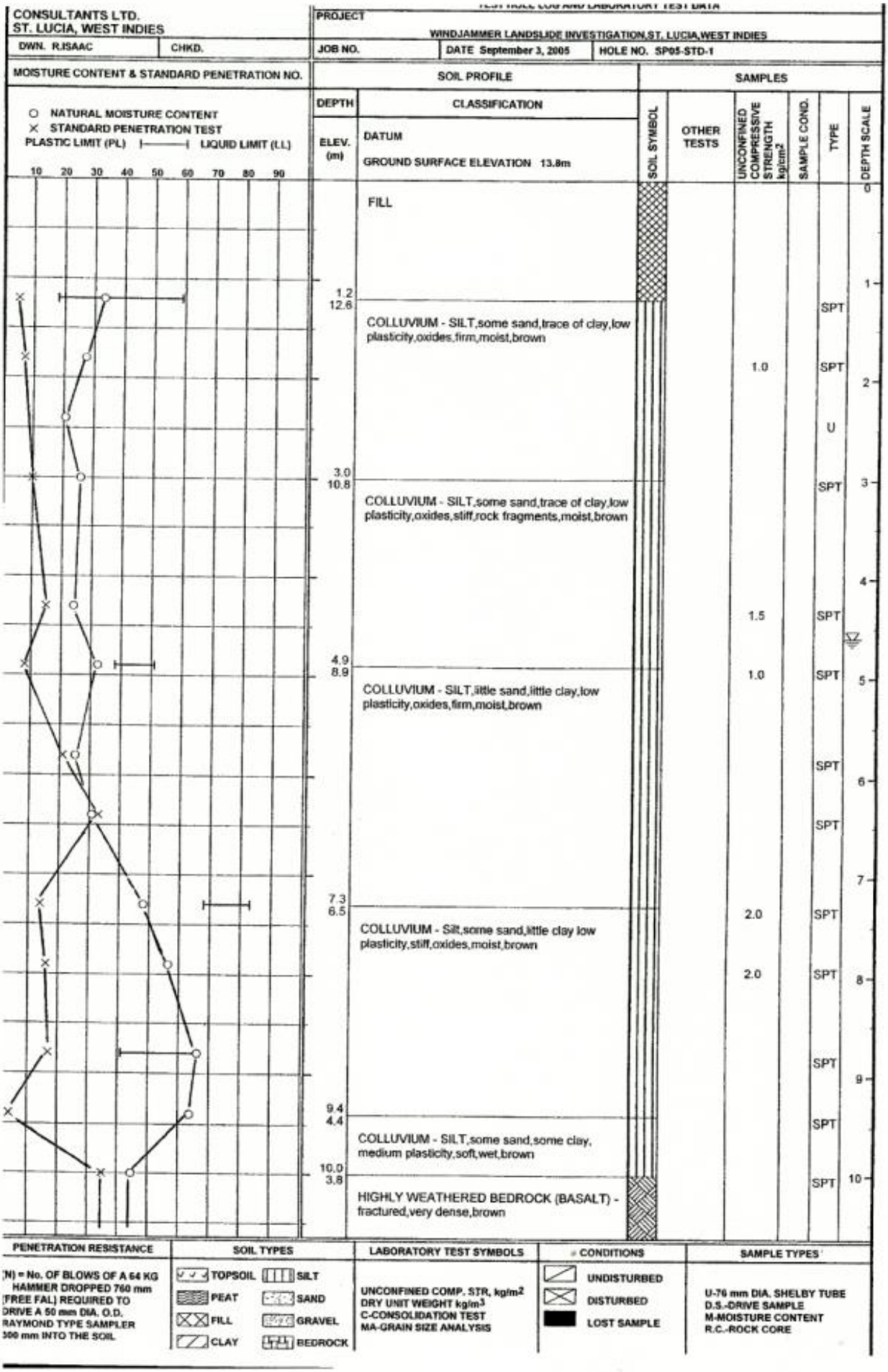
CONSULTANTS LTD.
ST. LUCIA, WEST INDIES
DWN. R.ISAAC
CHKD.
PROJECT
WINDJAMMER LANDSLIDE INVESTIGATION,ST. LUCIA,WEST INDIES
JOB NO.
DATE September 3, 2005
HOLE NO. SP05-STD-1
MOISTURE CONTENT & STANDARD PENETRATION NO.
SOIL PROFILE
SAMPLES
O NATURAL MOISTURE CONTENT
× STANDARD PENETRATION TEST
PLASTIC LIMIT (PL) LIQUID LIMIT (LL)
10 20 30 40 50 60 70 80 90
DEPTH
ELEV. (m)
CLASSIFICATION
DATUM
GROUND SURFACE ELEVATION 13.8m
SOIL SYMBOL
OTHER TESTS
UNCONFINED COMPRESSIVE STRENGTH kg/cm2
SAMPLE COND.
TYPE
DEPTH SCALE
FILL
1.2
12.6
COLLUVIUM - SILT,some sand,trace of clay,low plasticity,oxides,firm,moist,brown
3.0
10.8
COLLUVIUM - SILT,some sand,trace of clay,low plasticity,oxides,stiff,rock fragments,moist,brown
4.9
8.9
COLLUVIUM - SILT,little sand,little clay,low plasticity,oxides,firm,moist,brown
7.3
6.5
COLLUVIUM - Silt,some sand,little clay low plasticity,stiff,oxides,moist,brown
9.4
4.4
COLLUVIUM - SILT,some sand,some clay, medium plasticity,soft,wet,brown
10.0
3.8
HIGHLY WEATHERED BEDROCK (BASALT) - fractured,very dense,brown
1.0
1.5
1.0
2.0
2.0
SPT
U
PENETRATION RESISTANCE
(N) = No. OF BLOWS OF A 64 KG HAMMER DROPPED 760 mm (FREE FAL) REQUIRED TO DRIVE A 50 mm DIA. O.D. RAYMOND TYPE SAMPLER 300 mm INTO THE SOIL
SOIL TYPES
TOPSOIL
SILT
PEAT
SAND
FILL
GRAVEL
CLAY
BEDROCK
LABORATORY TEST SYMBOLS
UNCONFINED COMP. STR, kg/m2
DRY UNIT WEIGHT kg/m3
C-CONSOLIDATION TEST
MA-GRAIN SIZE ANALYSIS
CONDITIONS
UNDISTURBED
DISTURBED
LOST SAMPLE
SAMPLE TYPES
U-76 mm DIA. SHELBY TUBE
D.S.-DRIVE SAMPLE
M-MOISTURE CONTENT
R.C.-ROCK CORE

STRATA ENGINEERING CONSULTANTS LTD.
ST. LUCIA, WEST INDIES

TEST HOLE LOG AND LABORATORY TEST DATA

PROJECT: WINDJAMMER LANDSLIDE INVESTIGATION,ST. LUCIA,WEST INDIES

DWN. R.ISAAC | CHKD. | JOB NO. | DATE September 3, 2005 | HOLE NO. SP05-STD-1

MOISTURE CONTENT & STANDARD PENETRATION NO.

○ NATURAL MOISTURE CONTENT
× STANDARD PENETRATION TEST
PLASTIC LIMIT (PL) ⊢——⊣ LIQUID LIMIT (LL)

10 20 30 40 50 60 70 80 90

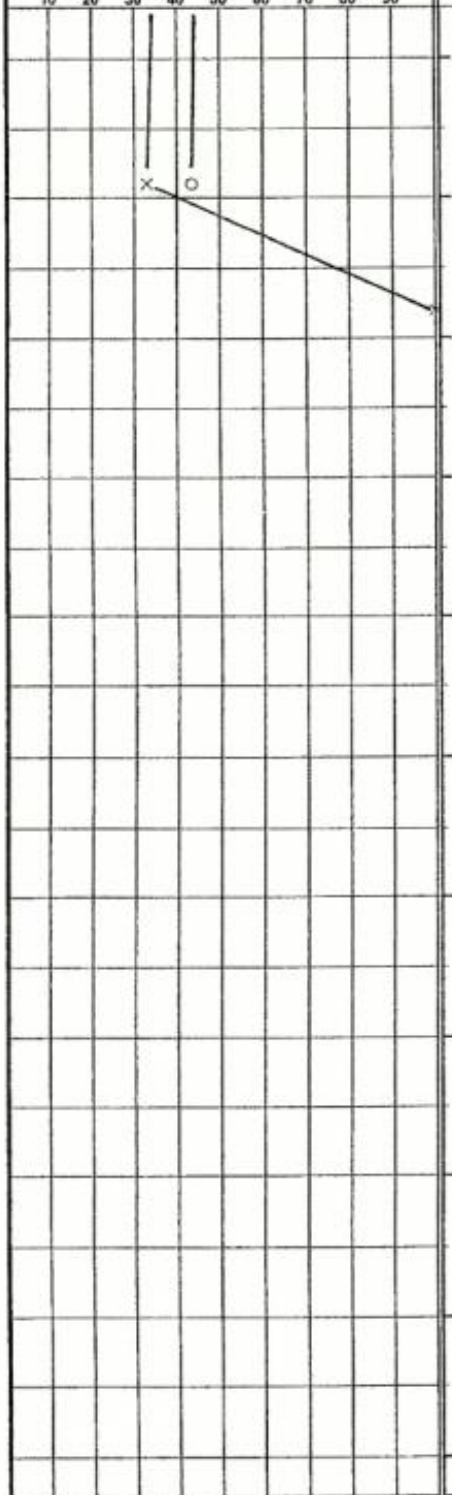

SOIL PROFILE			SAMPLES					
DEPTH ELEV. (m)	CLASSIFICATION		SOIL SYMBOL	OTHER TESTS	UNCONFINED COMPRESSIVE STRENGTH kg/cm²	SAMPLE COND.	TYPE	DEPTH SCALE
DATUM GROUND SURFACE ELEVATION 13.8m								
	HIGHLY WEATHERED BEDROCK (BASALT)- fractured,dense to very dense,brown						SPT	11 12
	(Rock core from 12.8m - 18.5m)						SPT	13
	TCR = 15.0%							14
	SCR = 6.0%							15
	RQD = 0.0						core	16
								17
								18
18.5 -4.7	END OF BOREHOLE AT 18.5m						core	19
	STANDPIPE PIEZOMETER INSTALLED TO 10.7m							20
	GROUNDWATER LEVEL AT 4.6m							
	UNCONFINED COMPRESSIVE STRENGTH FROM POCKET PENETROMETER							21

PENETRATION RESISTANCE	SOIL TYPES	LABORATORY TEST SYMBOLS	CONDITIONS	SAMPLE TYPES
(N) = No. OF BLOWS OF A 64 KG HAMMER DROPPED 760 mm (FREE FAL) REQUIRED TO DRIVE A 50 mm DIA. O.D. RAYMOND TYPE SAMPLER 300 mm INTO THE SOIL	TOPSOIL, SILT, PEAT, SAND, FILL, GRAVEL, CLAY, BEDROCK	UNCONFINED COMP. STR, kg/m² DRY UNIT WEIGHT kg/m³ C-CONSOLIDATION TEST MA-GRAIN SIZE ANALYSIS	UNDISTURBED DISTURBED LOST SAMPLE	U-76 mm DIA. SHELBY TUBE D.S.-DRIVE SAMPLE M-MOISTURE CONTENT R.C.-ROCK CORE

STRATA ENGINEERING
CONSULTANTS LTD.
ST. LUCIA, WEST INDIES

TEST HOLE LOG AND LABORATORY TEST DATA

PROJECT
WINDJAMMER LANDSLIDE INVESTIGATION,ST. LUCIA,WEST INDIES

DWN. R.ISAAC | CHKD. | JOB NO. | DATE September 13, 2005 | HOLE NO. SP05-STE-1

MOISTURE CONTENT & STANDARD PENETRATION NO.

SOIL PROFILE

SAMPLES

○ NATURAL MOISTURE CONTENT
× STANDARD PENETRATION TEST
PLASTIC LIMIT (PL) ⊢——⊣ LIQUID LIMIT (LL)

10 20 30 40 50 60 70 80 90

DEPTH ELEV. (m)	CLASSIFICATION	SOIL SYMBOL	OTHER TESTS	UNCONFINED COMPRESSIVE STRENGTH kg/cm²	SAMPLE COND.	TYPE	DEPTH SCALE
	DATUM GROUND SURFACE ELEVATION 11.2m						
	FILL						0
1.2 10	COLLUVIUM - Silt,some clay,little sand medium to high plasticity,firm to very stiff,rock fragments, oxides,black specks,moist,brown					SPT	1
				1.5		SPT	2
				1.5		SPT	3
						SPT	
						SPT	4
				1.25		SPT	5
						SPT	6
						SPT	
						SPT	7
6.8 2.4	COLLUVIUM - Silt,little clay,little sand,medium plasticity,very stiff,oxides,rock fragments,moist, brown					SPT	8 9 10
						SPT	

PENETRATION RESISTANCE

(N) = No. OF BLOWS OF A 64 KG HAMMER DROPPED 760 mm (FREE FAL) REQUIRED TO DRIVE A 50 mm DIA. O.D. RAYMOND TYPE SAMPLER 300 mm INTO THE SOIL

SOIL TYPES

TOPSOIL, SILT, PEAT, SAND, FILL, GRAVEL, CLAY, BEDROCK

LABORATORY TEST SYMBOLS

UNCONFINED COMP. STR, kg/m²
DRY UNIT WEIGHT kg/m³
C-CONSOLIDATION TEST
MA-GRAIN SIZE ANALYSIS

CONDITIONS

UNDISTURBED
DISTURBED
LOST SAMPLE

SAMPLE TYPES

U-76 mm DIA. SHELBY TUBE
D.S.-DRIVE SAMPLE
M-MOISTURE CONTENT
R.C.-ROCK CORE

CONSULTANTS LTD.
ST. LUCIA, WEST INDIES

PROJECT: WINDJAMMER LANDSLIDE INVESTIGATION,ST. LUCIA,WEST INDIES

DWN. R.ISAAC | CHKD. | JOB NO. | DATE September 13, 2005 | HOLE NO. SP05-STE-1

MOISTURE CONTENT & STANDARD PENETRATION NO.

○ NATURAL MOISTURE CONTENT
× STANDARD PENETRATION TEST
PLASTIC LIMIT (PL) ⊢——⊣ LIQUID LIMIT (LL)

10 20 30 40 50 60 70 80 90

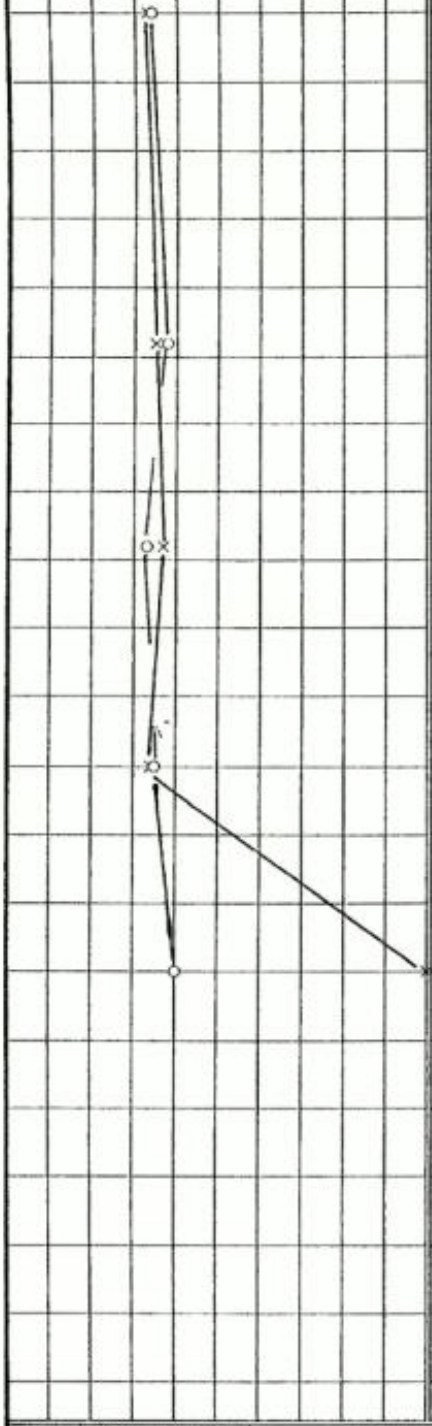

DEPTH ELEV. (m)	CLASSIFICATION	SOIL SYMBOL	OTHER TESTS	UNCONFINED COMPRESSIVE STRENGTH kg/cm²	SAMPLE COND.	TYPE	DEPTH SCALE
	DATUM GROUND SURFACE ELEVATION 11.2m						
11.0 0.2	HIGHLY WEATHERED BEDROCK (BASALT) - fractured,dense to very dense,brown					SPT	11
							12
							13
						SPT	
							14
						SPT	15
							16
						SPT	
							17
						SPT	18
	Rock core (18.0m - 21.3m) TCR = 53.0% SCR = 33.0% RQD = 18.0%						19
							20
						core	21

PENETRATION RESISTANCE

(N) = No. OF BLOWS OF A 64 KG HAMMER DROPPED 760 mm (FREE FAL) REQUIRED TO DRIVE A 50 mm DIA. O.D. RAYMOND TYPE SAMPLER 300 mm INTO THE SOIL

SOIL TYPES

TOPSOIL, SILT, PEAT, SAND, FILL, GRAVEL, CLAY, BEDROCK

LABORATORY TEST SYMBOLS

UNCONFINED COMP. STR, kg/m²
DRY UNIT WEIGHT kg/m³
C-CONSOLIDATION TEST
MA-GRAIN SIZE ANALYSIS

CONDITIONS

UNDISTURBED
DISTURBED
LOST SAMPLE

SAMPLE TYPES

U-76 mm DIA. SHELBY TUBE
D.S.-DRIVE SAMPLE
M-MOISTURE CONTENT
R.C.-ROCK CORE

STRATA ENGINEERING CONSULTANTS LTD.
ST. LUCIA, WEST INDIES

TEST HOLE LOG AND LABORATORY TEST DATA

PROJECT: WINDJAMMER LANDSLIDE INVESTIGATION,ST. LUCIA,WEST INDIES

DWN. R.ISAAC | CHKD. | JOB NO. | DATE September 13, 2005 | HOLE NO. SP05-STE-1

MOISTURE CONTENT & STANDARD PENETRATION NO.

○ NATURAL MOISTURE CONTENT
× STANDARD PENETRATION TEST
PLASTIC LIMIT (PL) |——| LIQUID LIMIT (LL)

10 20 30 40 50 60 70 80 90

SOIL PROFILE			SAMPLES					
DEPTH ELEV. (m)	CLASSIFICATION		SOIL SYMBOL	OTHER TESTS	UNCONFINED COMPRESSIVE STRENGTH kg/cm²	SAMPLE COND.	TYPE	DEPTH SCALE
DATUM GROUND SURFACE ELEVATION 11.2m								
21.3 -10.1	END OF BOREHOLE AT 21.3m STANDPIPE PIEZOMETER INSTALLED TO 17.7m GROUNDWATER LEVEL AT 3.4m UNCONFINED COMPRESSIVE STRENGTH FROM POCKET PENETROMETER						core	22 23 24 25 26 27 28 29 30 31

PENETRATION RESISTANCE

(N) = No. OF BLOWS OF A 64 KG HAMMER DROPPED 760 mm (FREE FAL) REQUIRED TO DRIVE A 50 mm DIA. O.D. RAYMOND TYPE SAMPLER 300 mm INTO THE SOIL

SOIL TYPES

TOPSOIL, SILT, PEAT, SAND, FILL, GRAVEL, CLAY, BEDROCK

LABORATORY TEST SYMBOLS

UNCONFINED COMP. STR, kg/m²
DRY UNIT WEIGHT kg/m³
C-CONSOLIDATION TEST
MA-GRAIN SIZE ANALYSIS

CONDITIONS

UNDISTURBED
DISTURBED
LOST SAMPLE

SAMPLE TYPES

U-76 mm DIA. SHELBY TUBE
D.S.-DRIVE SAMPLE
M-MOISTURE CONTENT
R.C.-ROCK CORE

STRATA ENGINEERING
CONSULTANTS LTD.
ST. LUCIA, WEST INDIES

TEST HOLE LOG AND LABORATORY TEST DATA

PROJECT: WINDJAMMER LANDSLIDE INVESTIGATION,ST. LUCIA WEST INDIES

DWN. RJISAAC | CHKD. | JOB NO. | DATE September 27, 2005 | HOLE NO. SP05-STF-1

MOISTURE CONTENT & STANDARD PENETRATION NO.

○ NATURAL MOISTURE CONTENT
× STANDARD PENETRATION TEST
PLASTIC LIMIT (PL) ⊢——⊣ LIQUID LIMIT (LL)

10 20 30 40 50 60 70 80 90

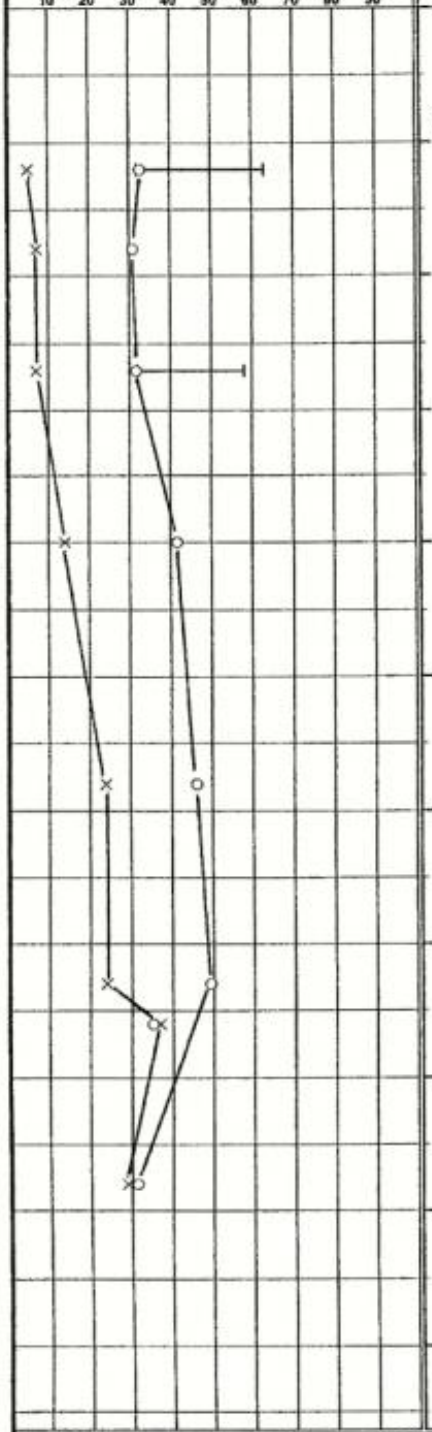

SOIL PROFILE			SAMPLES					
DEPTH ELEV. (m)	CLASSIFICATION DATUM GROUND SURFACE ELEVATION 13.6m		SOIL SYMBOL	OTHER TESTS	UNCONFINED COMPRESSIVE STRENGTH kg/cm²	SAMPLE COND.	TYPE	DEPTH SCALE
	TOPSOIL							0
0.8 12.85	COLLUVIUM - Silt,some clay,little sand,medium plasticity,rock fragments,firm,oxides,moist,rusty brown						SPT	1
					0.8		SPT	2
					1.0		SPT	3
							U	
4.0 9.6					2.5		SPT	4
	COLLUVIUM - Silt,some sand,trace of clay,low plasticity,stiff,rock fragments,oxides,moist, brown							5
5.8 7.8							SPT	6
	HIGHLY WEATHERED BEDROCK (BASALT) - fractured,compact to very dense,brown							7
							SPT	
							SPT	8
							SPT	9
								10

PENETRATION RESISTANCE	SOIL TYPES	LABORATORY TEST SYMBOLS	CONDITIONS	SAMPLE TYPES
(N) = No. OF BLOWS OF A 64 KG HAMMER DROPPED 760 mm (FREE FAL) REQUIRED TO DRIVE A 50 mm DIA. O.D. RAYMOND TYPE SAMPLER 300 mm INTO THE SOIL	TOPSOIL, SILT, PEAT, SAND, FILL, GRAVEL, CLAY, BEDROCK	UNCONFINED COMP. STR, kg/m² DRY UNIT WEIGHT kg/m³ C-CONSOLIDATION TEST MA-GRAIN SIZE ANALYSIS	UNDISTURBED DISTURBED LOST SAMPLE	U-76 mm DIA. SHELBY TUBE D.S.-DRIVE SAMPLE M-MOISTURE CONTENT R.C.-ROCK CORE

STRATA ENGINEERING CONSULTANTS LTD.
ST. LUCIA, WEST INDIES

TEST HOLE LOG AND LABORATORY TEST DATA

PROJECT: WINDJAMMER LANDSLIDE INVESTIGATION,ST. LUCIA,WEST INDIES

DWN. R.ISAAC | CHKD. | JOB NO. | DATE September 27, 2005 | HOLE NO. SP05-STF-1

MOISTURE CONTENT & STANDARD PENETRATION NO.

○ NATURAL MOISTURE CONTENT
× STANDARD PENETRATION TEST
PLASTIC LIMIT (PL) ⊢——⊣ LIQUID LIMIT (LL)

10 20 30 40 50 60 70 80 90

SOIL PROFILE			SAMPLES					
DEPTH ELEV. (m)	CLASSIFICATION DATUM GROUND SURFACE ELEVATION 13.6m	SOIL SYMBOL	OTHER TESTS	UNCONFINED COMPRESSIVE STRENGTH kg/cm²	SAMPLE COND.	TYPE	DEPTH SCALE
	HIGHLY WEATHERED BEDROCK (BASALT) - fractured,very dense,brown					SPT	11
	Rock core (10.7m - 13.7m)						
	TCR = 66.0%						12
	SCR = 55.0%						
	RQD = 55.0%						13
13.7 -0.1						core	
	END OF BOREHOLE AT 13.7m						14
	STANDPIPE PIEZOMETER INSTALLED TO 9.9m						
	GROUNDWATER LEVEL AT 4.6m						15
	UNCONFINED COMPRESSIVE STRENGTH FROM POCKET PENETROMETER						
							16
							17
							18
							19
							20
							21

PENETRATION RESISTANCE

(N) = No. OF BLOWS OF A 64 KG HAMMER DROPPED 760 mm (FREE FAL) REQUIRED TO DRIVE A 50 mm DIA. O.D. RAYMOND TYPE SAMPLER 300 mm INTO THE SOIL

SOIL TYPES

TOPSOIL, SILT, PEAT, SAND, FILL, GRAVEL, CLAY, BEDROCK

LABORATORY TEST SYMBOLS

UNCONFINED COMP. STR, kg/m²
DRY UNIT WEIGHT kg/m³
C-CONSOLIDATION TEST
MA-GRAIN SIZE ANALYSIS

CONDITIONS

UNDISTURBED
DISTURBED
LOST SAMPLE

SAMPLE TYPES

U-76 mm DIA. SHELBY TUBE
D.S.-DRIVE SAMPLE
M-MOISTURE CONTENT
R.C.-ROCK CORE

STRATA ENGINEERING CONSULTANTS LTD.
ST. LUCIA, WEST INDIES

TEST HOLE LOG AND LABORATORY TEST DATA

PROJECT: WINDJAMMER LANDSLIDE INVESTIGATION,ST. LUCIA,WEST INDIES

DWN. R.ISAAC | CHKD. | JOB NO. | DATE October 8, 2005 | HOLE NO. SP05-STG-1

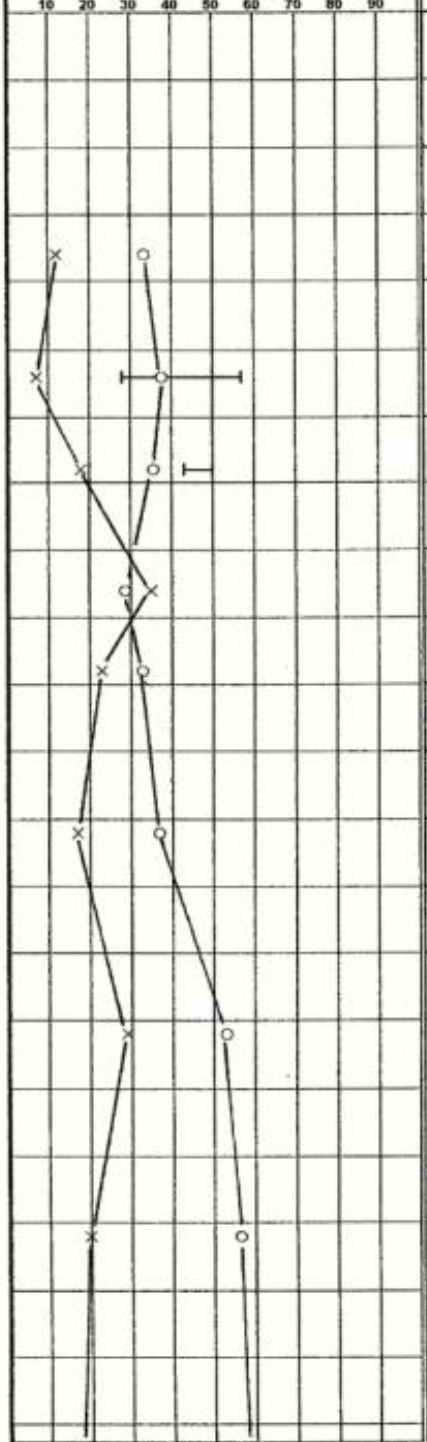

DEPTH ELEV. (m)	CLASSIFICATION (DATUM: GROUND SURFACE ELEVATION 9.6m)	SOIL SYMBOL	OTHER TESTS	UNCONFINED COMPRESSIVE STRENGTH kg/cm2	SAMPLE COND.	TYPE	DEPTH SCALE
	FILL						0
1.8							1
7.8	COLLUVIUM -Silt,some sand,trace of clay, low to non plastic,loose to compact,oxides,black specks,moist,rusty brown					SPT	2
				1.25		SPT	3
				2.5		SPT	
						SPT	4
						SPT	5
						SPT	6
							7
7.6 2	HIGHLY WEATHERED BEDROCK (BASALT) - fractured,compact to dense,brown					SPT	8
						SPT	9
							10

PENETRATION RESISTANCE

(N) = No. OF BLOWS OF A 64 KG HAMMER DROPPED 760 mm (FREE FAL) REQUIRED TO DRIVE A 50 mm DIA. O.D. RAYMOND TYPE SAMPLER 300 mm INTO THE SOIL

SOIL TYPES

TOPSOIL, SILT, PEAT, SAND, FILL, GRAVEL, CLAY, BEDROCK

LABORATORY TEST SYMBOLS

UNCONFINED COMP. STR, kg/m²
DRY UNIT WEIGHT kg/m³
C-CONSOLIDATION TEST
MA-GRAIN SIZE ANALYSIS

CONDITIONS

UNDISTURBED
DISTURBED
LOST SAMPLE

SAMPLE TYPES

U-76 mm DIA. SHELBY TUBE
D.S.-DRIVE SAMPLE
M-MOISTURE CONTENT
R.C.-ROCK CORE

STRATA ENGINEERING CONSULTANTS LTD.
ST. LUCIA, WEST INDIES

TEST HOLE LOG AND LABORATORY TEST DATA

PROJECT: WINDJAMMER LANDSLIDE INVESTIGATION,ST. LUCIA,WEST INDIES

DWN. R.ISAAC | CHKD. | JOB NO. | DATE October 8, 2005 | HOLE NO. SP05-STG-1

MOISTURE CONTENT & STANDARD PENETRATION NO.

○ NATURAL MOISTURE CONTENT
× STANDARD PENETRATION TEST
PLASTIC LIMIT (PL) ⊢——⊣ LIQUID LIMIT (LL)

10 20 30 40 50 60 70 80 90

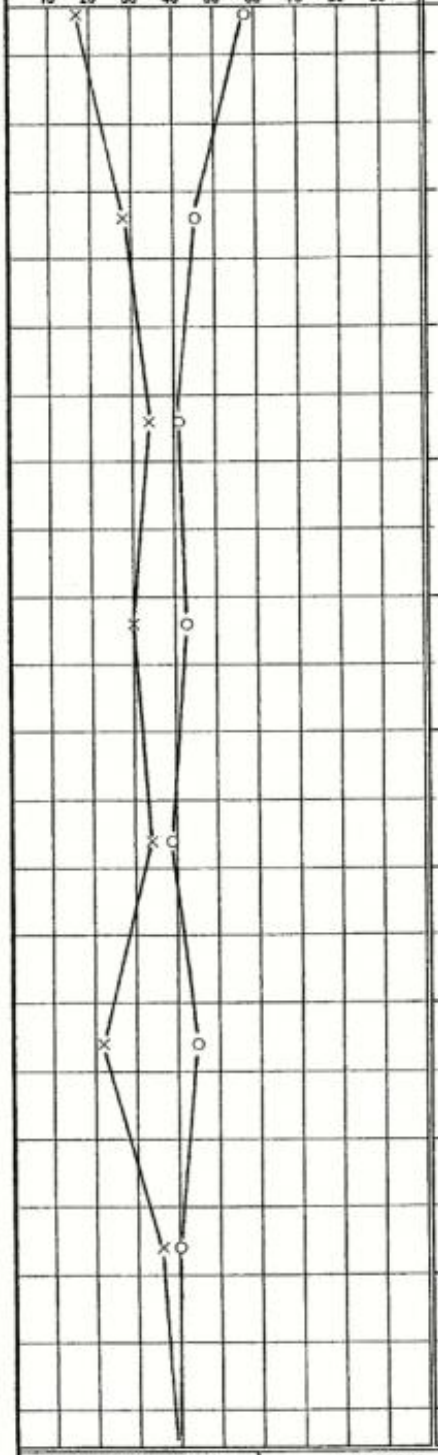

SOIL PROFILE			SAMPLES					
DEPTH ELEV. (m)	CLASSIFICATION	SOIL SYMBOL	OTHER TESTS	UNCONFINED COMPRESSIVE STRENGTH kg/cm2	SAMPLE COND.	TYPE	DEPTH SCALE
DATUM GROUND SURFACE ELEVATION 9.6m	HIGHLY WEATHERED BEDROCK (BASALT) - fractured,compact to dense,oxides,moist, brown					SPT SPT SPT SPT SPT SPT	11 12 13 14 15 16 17 18 19 20 21

PENETRATION RESISTANCE

(N) = No. OF BLOWS OF A 64 KG HAMMER DROPPED 760 mm (FREE FAL) REQUIRED TO DRIVE A 50 mm DIA. O.D. RAYMOND TYPE SAMPLER 300 mm INTO THE SOIL

SOIL TYPES

TOPSOIL, SILT, PEAT, SAND, FILL, GRAVEL, CLAY, BEDROCK

LABORATORY TEST SYMBOLS

UNCONFINED COMP. STR, kg/m2
DRY UNIT WEIGHT kg/m3
C-CONSOLIDATION TEST
MA-GRAIN SIZE ANALYSIS

CONDITIONS

UNDISTURBED
DISTURBED
LOST SAMPLE

SAMPLE TYPES

U-76 mm DIA. SHELBY TUBE
D.S.-DRIVE SAMPLE
M-MOISTURE CONTENT
R.C.-ROCK CORE

STRATA ENGINEERING CONSULTANTS LTD.
ST. LUCIA, WEST INDIES

TEST HOLE LOG AND LABORATORY TEST DATA

PROJECT: WINDJAMMER LANDSLIDE INVESTIGATION,ST. LUCIA,WEST INDIES

DWN. R.ISAAC | CHKD. | JOB NO. | DATE October 8, 2005 | HOLE NO. SP05-STG-1

MOISTURE CONTENT & STANDARD PENETRATION NO.

○ NATURAL MOISTURE CONTENT
× STANDARD PENETRATION TEST
PLASTIC LIMIT (PL) ⊢——⊣ LIQUID LIMIT (LL)

10 20 30 40 50 60 70 80 90

DEPTH ELEV. (m)	CLASSIFICATION DATUM GROUND SURFACE ELEVATION 9.6m	SOIL SYMBOL	OTHER TESTS	UNCONFINED COMPRESSIVE STRENGTH kg/cm²	SAMPLE COND.	TYPE	DEPTH SCALE
	HIGHLY WEATHERED BEDROCK (BASALT) - fractured,dense,brown					SPT	22
23.0 -13.4	END OF BOREHOLE AT 23.0m STANDPIPE PIEZOMETER INSTALLED TO 18.3m GROUNDWATER LEVEL AT 1.2m UNCONFINED COMPRESSIVE STRENGTH FROM POCKET PENETROMETER					SPT	23 24 25 26 27 28 29 30 31

PENETRATION RESISTANCE

(N) = No. OF BLOWS OF A 64 KG HAMMER DROPPED 760 mm (FREE FALL) REQUIRED TO DRIVE A 50 mm DIA. O.D. RAYMOND TYPE SAMPLER 300 mm INTO THE SOIL

SOIL TYPES

TOPSOIL, SILT, PEAT, SAND, FILL, GRAVEL, CLAY, BEDROCK

LABORATORY TEST SYMBOLS

UNCONFINED COMP. STR, kg/m²
DRY UNIT WEIGHT kg/m³
C-CONSOLIDATION TEST
MA-GRAIN SIZE ANALYSIS

CONDITIONS

UNDISTURBED
DISTURBED
LOST SAMPLE

SAMPLE TYPES

U-76 mm DIA. SHELBY TUBE
D.S.-DRIVE SAMPLE
M-MOISTURE CONTENT
R.C.-ROCK CORE

APPENDIX B

Borehole Log for the Standpipe Piezometer at the Barre de L'isle Study Site

STRATA ENGINEERING CONSULTANTS LTD.
ST. LUCIA, WEST INDIES

TEST HOLE LOG AND LABORATORY TEST DATA

PROJECT: Site Investigation, Barre de L'isle Study Site, Saint Lucia, W.I.

DWN. R. ISAAC | CHKD. | JOB NO. | DATE December 18, 2008 | HOLE NO. BH09-BS-2 (North)

MOISTURE CONTENT & STANDARD PENETRATION NO. | SOIL PROFILE | SAMPLES

○ NATURAL MOISTURE CONTENT
× STANDARD PENETRATION TEST
PLASTIC LIMIT (PL) ⊢——⊣ LIQUID LIMIT (LL)

10 20 30 40 50 60 70 80 90

DEPTH ELEV. (m)	CLASSIFICATION DATUM GROUND SURFACE ELEVATION
	RESIDUAL SOIL - SAND and silt,trace of clay, compact,low to non plastic,excessive oxidation, wet,rusty brown
3.0	
	RESIDUAL SOIL - SILT,some clay,little sand, medium plasticity,excessive oxidation,white specks,firm to stiff,wet,rusty brown
4.6	
6.0	
7.6	
9.0	
	RESIDUAL SOIL - SAND,some silt,little clay, low plasticity,compact,excessive oxidation,wet, rusty brown
10.7	
	RESIDUAL SOIL - SILT,some sand,some clay, medium plasticity,stiff to very stiff,excessive oxidation,wet,rusty brown
13.7	
	RESIDUAL SOIL - SILT,some sand,trace of clay,low to non plastic,compact,excessive oxidation,wet,rusty brown
15.2	
	HIGHLY WEATHERED ANDESITE - dense to very dense,moist to wet,brown
16.8	
-16.8	END OF BOREHOLE AT 16.8m STANDPIPE PIEZOMETER INSTALLED TO 10.5m GROUNDWATER LEVEL AT 6.0m

SAMPLES: SOIL SYMBOL | OTHER TESTS | UNCONFINED COMPRESSIVE STRENGTH kg/cm² | SAMPLE COND. | TYPE | DEPTH SCALE

DEPTH SCALE: 0 2 4 6 8 10 12 14 16 18 20 22 24

PENETRATION RESISTANCE	SOIL TYPES	LABORATORY TEST SYMBOLS	CONDITIONS	SAMPLE TYPES
(N) = No. OF BLOWS OF A 64 KG HAMMER DROPPED 760 mm (FREE FAL) REQUIRED TO DRIVE A 50 mm DIA. O.D. RAYMOND TYPE SAMPLER 300 mm INTO THE SOIL	TOPSOIL, SILT, PEAT, SAND, FILL, GRAVEL, CLAY, BEDROCK	UNCONFINED COMP. STR, kg/m² DRY UNIT WEIGHT kg/m³ C-CONSOLIDATION TEST MA-GRAIN SIZE ANALYSIS	UNDISTURBED DISTURBED LOST SAMPLE	U-76 mm DIA. SHELBY TUBE D.S.-DRIVE SAMPLE M-MOISTURE CONTENT R.C.-ROCK CORE

APPENDIX C

Borehole Logs for the Standpipe Piezometers at the Windjammer Landing Beach Resort Study Site

STRATA ENGINEERING CONSULTANTS LTD. ST. LUCIA, WEST INDIES		TEST HOLE LOG AND LABORATORY TEST DATA		
		PROJECT: WINDJAMMER LANDING RESORT INSTRUMENTATION, Labreiotte Bay, St Lucia, W.I.		
DWN. R.ISAAC	CHKD.	JOB NO.	DATE October 29,2008	HOLE NO. BH08-SP-13

MOISTURE CONTENT & STANDARD PENETRATION NO.

○ NATURAL MOISTURE CONTENT
× STANDARD PENETRATION TEST
PLASTIC LIMIT (PL) ⊢——⊣ LIQUID LIMIT (LL)

10 20 30 40 50 60 70 80 90

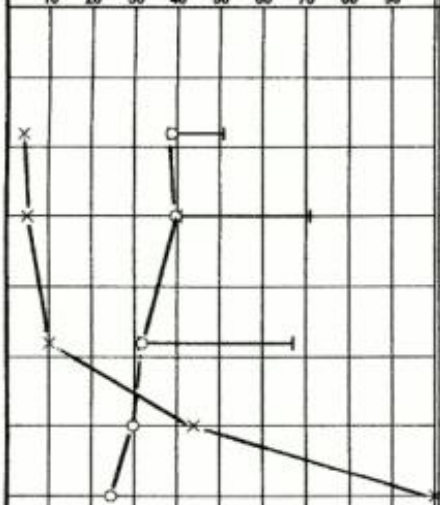

DEPTH ELEV. (m)	CLASSIFICATION DATUM GROUND SURFACE ELEVATION	SOIL SYMBOL	OTHER TESTS	UNCONFINED COMPRESSIVE STRENGTH kg/cm²	SAMPLE COND.	TYPE	DEPTH SCALE
0.3	TOPSOIL						0
	SILT - some sand, little clay,weathered rock fragments,medium plasticity,compact to dense, moist,brown						1
							2
3.0							3
3.5	HIGHLY WEATHERED BASALT BEDROCK - fractured, very dense, brown						
	END OF BOREHOLE AT 3.5m STANDPIPE PIEZOMETER INSTALLED TO 3.2m GROUNDWATER LEVEL AT 3.0m						4
							5
							6
							7
							8
							9
							10

PENETRATION RESISTANCE	SOIL TYPES	LABORATORY TEST SYMBOLS	CONDITIONS	SAMPLE TYPES
(N) = No. OF BLOWS OF A 64 KG HAMMER DROPPED 760 mm (FREE FAL) REQUIRED TO DRIVE A 60 mm DIA. O.D. RAYMOND TYPE SAMPLER 300 mm INTO THE SOIL	TOPSOIL, SILT, PEAT, SAND, FILL, GRAVEL, CLAY, BEDROCK	UNCONFINED COMP. STR, kg/m² DRY UNIT WEIGHT kg/m³ C-CONSOLIDATION TEST MA-GRAIN SIZE ANALYSIS	UNDISTURBED DISTURBED LOST SAMPLE	U-76 mm DIA. SHELBY TUBE D.S.-DRIVE SAMPLE M-MOISTURE CONTENT R.C.-ROCK CORE

STRATA ENGINEERING CONSULTANTS LTD.
ST. LUCIA, WEST INDIES

TEST HOLE LOG AND LABORATORY TEST DATA

PROJECT: WINDJAMMER LANDING RESORT INSTRUMENTATION,Labreiotte Bay,St.Lucia,W.I.

DWN. RJSAAC | CHKD. | JOB NO. | DATE December 16, 2008 | HOLE NO. BH08-SP-14

MOISTURE CONTENT & STANDARD PENETRATION NO.

○ NATURAL MOISTURE CONTENT
× STANDARD PENETRATION TEST
PLASTIC LIMIT (PL) ⊢——⊣ LIQUID LIMIT (LL)

10 20 30 40 50 60 70 80 90

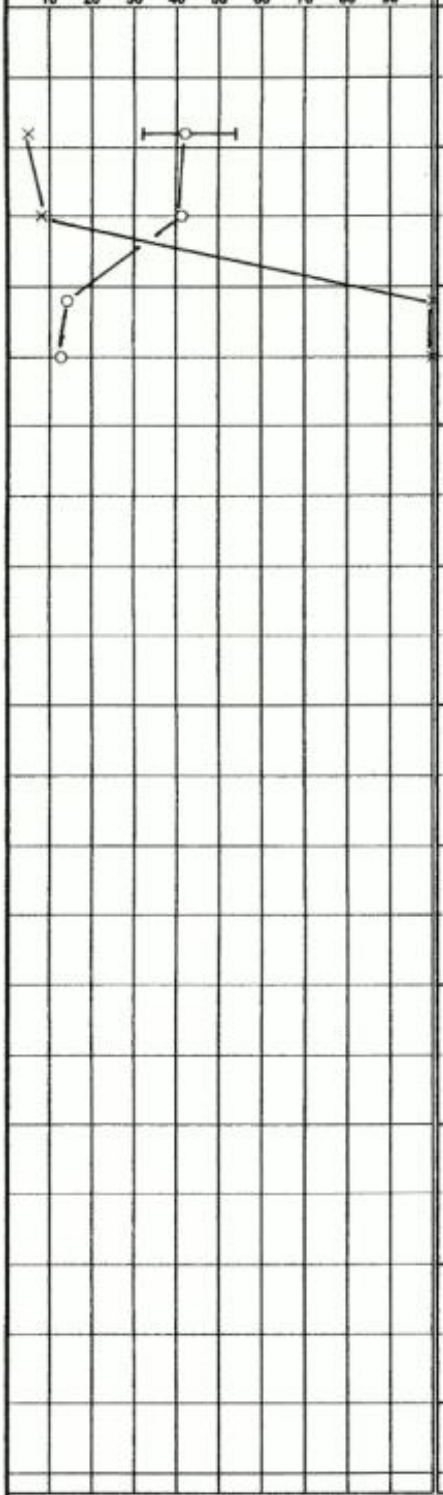

SOIL PROFILE			SAMPLES					
DEPTH ELEV. (m)	CLASSIFICATION DATUM GROUND SURFACE ELEVATION		SOIL SYMBOL	OTHER TESTS	UNCONFINED COMPRESSIVE STRENGTH kg/cm²	SAMPLE COND.	TYPE	DEPTH SCALE
0.3	Topsoil							0
	COLLUVIUM - silt,some clay,little sand,rock fragments,low to medium plasticity,firm,rootlets, oxides,black specks,moist,light brown							1
2.1								2
2.5	HIGHLY WEATHERED BASALT BEDROCK - fractured,very dense,brown							3
	END OF BOREHOLE AT 2.5m							4
	STANDPIPE PIEZOMETER INSTALLED TO 2.1m							5
	GROUNDWATER LEVEL AT 0.5m							6
								7
								8
								9
								10

PENETRATION RESISTANCE	SOIL TYPES	LABORATORY TEST SYMBOLS	CONDITIONS	SAMPLE TYPES
(N) = No. OF BLOWS OF A 64 KG HAMMER DROPPED 760 mm (FREE FAL) REQUIRED TO DRIVE A 50 mm DIA. O.D. RAYMOND TYPE SAMPLER 300 mm INTO THE SOIL	TOPSOIL, SILT, PEAT, SAND, FILL, GRAVEL, CLAY, BEDROCK	UNCONFINED COMP. STR, kg/m² DRY UNIT WEIGHT kg/m³ C-CONSOLIDATION TEST MA-GRAIN SIZE ANALYSIS	UNDISTURBED DISTURBED LOST SAMPLE	U-75 mm DIA. SHELBY TUBE D.S.-DRIVE SAMPLE M-MOISTURE CONTENT R.C.-ROCK CORE

STRATA ENGINEERING CONSULTANTS LTD.
ST. LUCIA, WEST INDIES

TEST HOLE LOG AND LABORATORY TEST DATA

PROJECT: WINDJAMMER LANDING RESORT INSTRUMENTATION,Labrelotte Bay,St.Lucia,W.I.

DWN. R.ISAAC | CHKD. | JOB NO. | DATE December 18, 2008 | HOLE NO. BH08-SP-15

MOISTURE CONTENT & STANDARD PENETRATION NO.

○ NATURAL MOISTURE CONTENT
× STANDARD PENETRATION TEST
PLASTIC LIMIT (PL) ⊢——⊣ LIQUID LIMIT (LL)

10 20 30 40 50 60 70 80 90

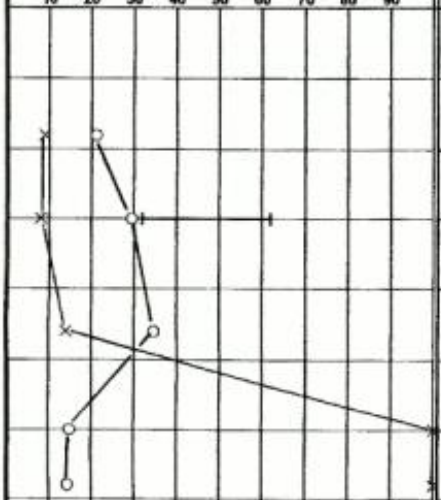

SOIL PROFILE			SAMPLES					
DEPTH ELEV. (m)	CLASSIFICATION DATUM GROUND SURFACE ELEVATION		SOIL SYMBOL	OTHER TESTS	UNCONFINED COMPRESSIVE STRENGTH kg/cm²	SAMPLE COND.	TYPE	DEPTH SCALE
0.3	TOPSOIL							0
	COLLUVIUM - Silt, some sand,little clay,rock fragments,low plasticity,firm, oxides,moist,light brown							1
3.0								2
3.4	HIGHLY WEATHERED BASALT BEDROCK - fractured, very dense, brown							3
	END OF BOREHOLE AT 3.4m							4
	STANDPIPE PIEZOMETER INSTALLED TO 3.4m							5
	GROUNDWATER LEVEL AT 1.2m							6
								7
								8
								9
								10

PENETRATION RESISTANCE	SOIL TYPES	LABORATORY TEST SYMBOLS	CONDITIONS	SAMPLE TYPES
(N) = No. OF BLOWS OF A 64 KG HAMMER DROPPED 760 mm (FREE FAL) REQUIRED TO DRIVE A 50 mm DIA. O.D. RAYMOND TYPE SAMPLER 300 mm INTO THE SOIL	TOPSOIL, SILT, PEAT, SAND, FILL, GRAVEL, CLAY, BEDROCK	UNCONFINED COMP. STR. kg/m² DRY UNIT WEIGHT kg/m³ C-CONSOLIDATION TEST MA-GRAIN SIZE ANALYSIS	UNDISTURBED DISTURBED LOST SAMPLE	U-76 mm DIA. SHELBY TUBE D.S.-DRIVE SAMPLE M-MOISTURE CONTENT R.C.-ROCK CORE

APPENDIX D

Grain Size Distribution Curves for Colluvium at the Windjammer Landing Beach Resort Study Site

Particle Size Distribution Report

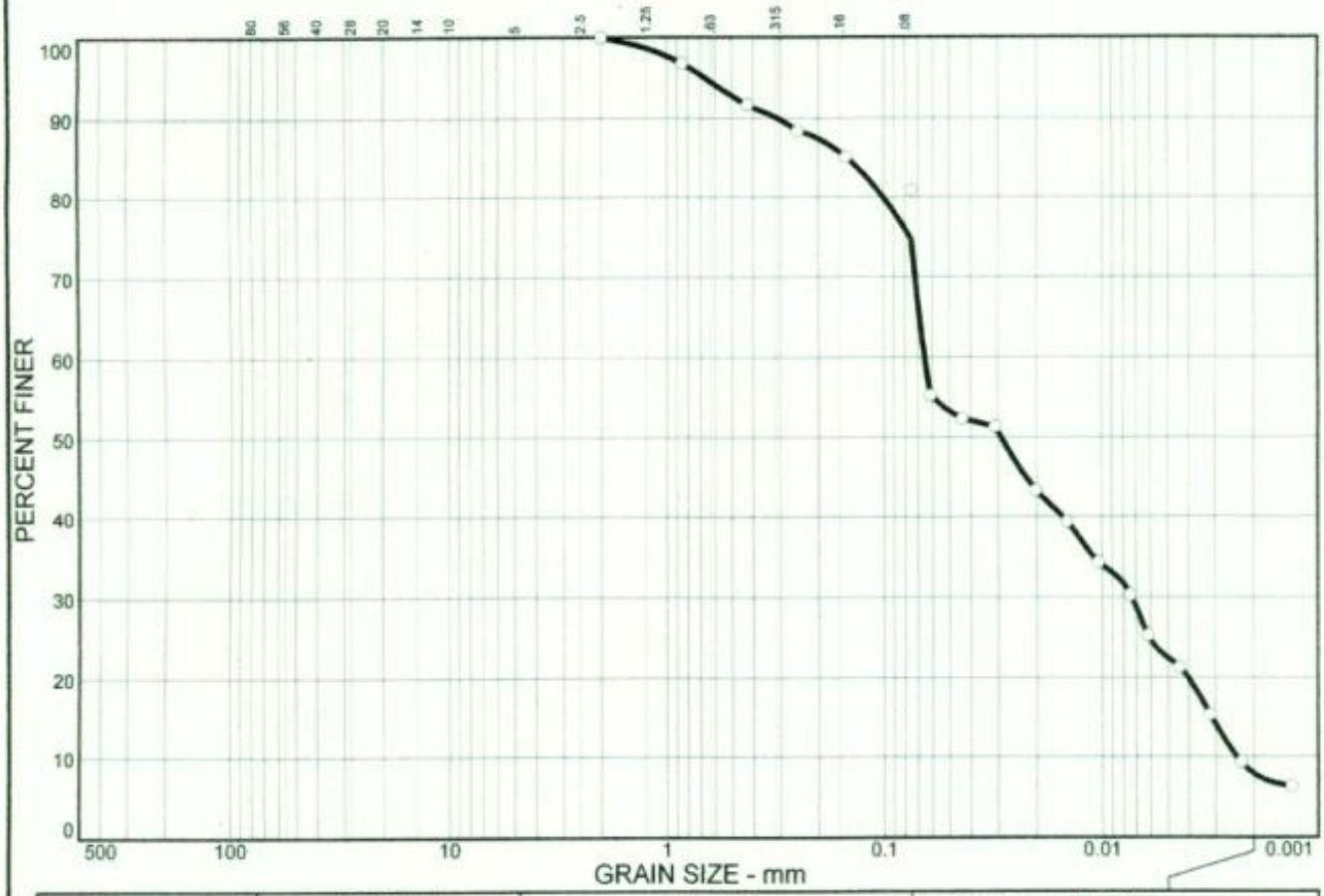

% COBBLES	% GRAVEL		% SAND			% FINES	
	CRS.	FINE	CRS.	MEDIUM	FINE	SILT	CLAY
0.0	0.0	0.0	0.0	8.3	17.1	66.8	7.8

SIEVE SIZE	PERCENT FINER	SPEC.* PERCENT	PASS? (X=NO)
#10	100.0		
#20	96.8		
#40	91.7		
#60	88.4		
#100	85.1		
#200	80.9		

* (no specification provided)

Soil Description

Atterberg Limits

PL= 38 LL= 51 PI= 13

Coefficients

D_{85}= 0.149 D_{60}= 0.0651 D_{50}= 0.0292
D_{30}= 0.0074 D_{15}= 0.0031 D_{10}= 0.0024
C_u= 27.04 C_c= 0.35

Classification

USCS= AASHTO=

Remarks

Sample No.: **Source of Sample:** BH08-SP-13 **Date:** 24/11/08
Location: **Elev./Depth:** 0.9m

STRATA ENGINEERING CONSULTANTS LTD.

Client: WINDJAMMER LANDING RESORT & SPA
Project: WINDJAMMER LANDING RESORT INSTRUMENTATION, Labrelotte Bay,St.Lucia,W.I.
Project No: **Figure**

Particle Size Distribution Report

% COBBLES	% GRAVEL		% SAND			% FINES	
	CRS.	FINE	CRS.	MEDIUM	FINE	SILT	CLAY
0.0	0.0	0.0	0.0	5.5	15.6	65.5	13.4

SIEVE SIZE	PERCENT FINER	SPEC.* PERCENT	PASS? (X=NO)
#10	100.0		
#20	97.2		
#40	94.5		
#60	92.2		
#100	89.6		
#200	86.8		

* (no specification provided)

Soil Description

Atterberg Limits

PL= 41 LL= 71 PI= 30

Coefficients

D_{85}= 0.104 D_{60}= 0.0479 D_{50}= 0.0144
D_{30}= 0.0045 D_{15}= 0.0022 D_{10}= 0.0014
C_u= 33.20 C_c= 0.29

Classification

USCS= AASHTO=

Remarks

Sample No.: **Source of Sample:** BH08-SP-13 **Date:** 24/11/08
Location: **Elev./Depth:** 1.5m

STRATA ENGINEERING CONSULTANTS LTD.

Client: WINDJAMMER LANDING RESORT & SPA
Project: WINDJAMMER LANDING RESORT INSTRUMENTATION, Labrelotte Bay,St.Lucia,W.I.
Project No: **Figure**

Particle Size Distribution Report

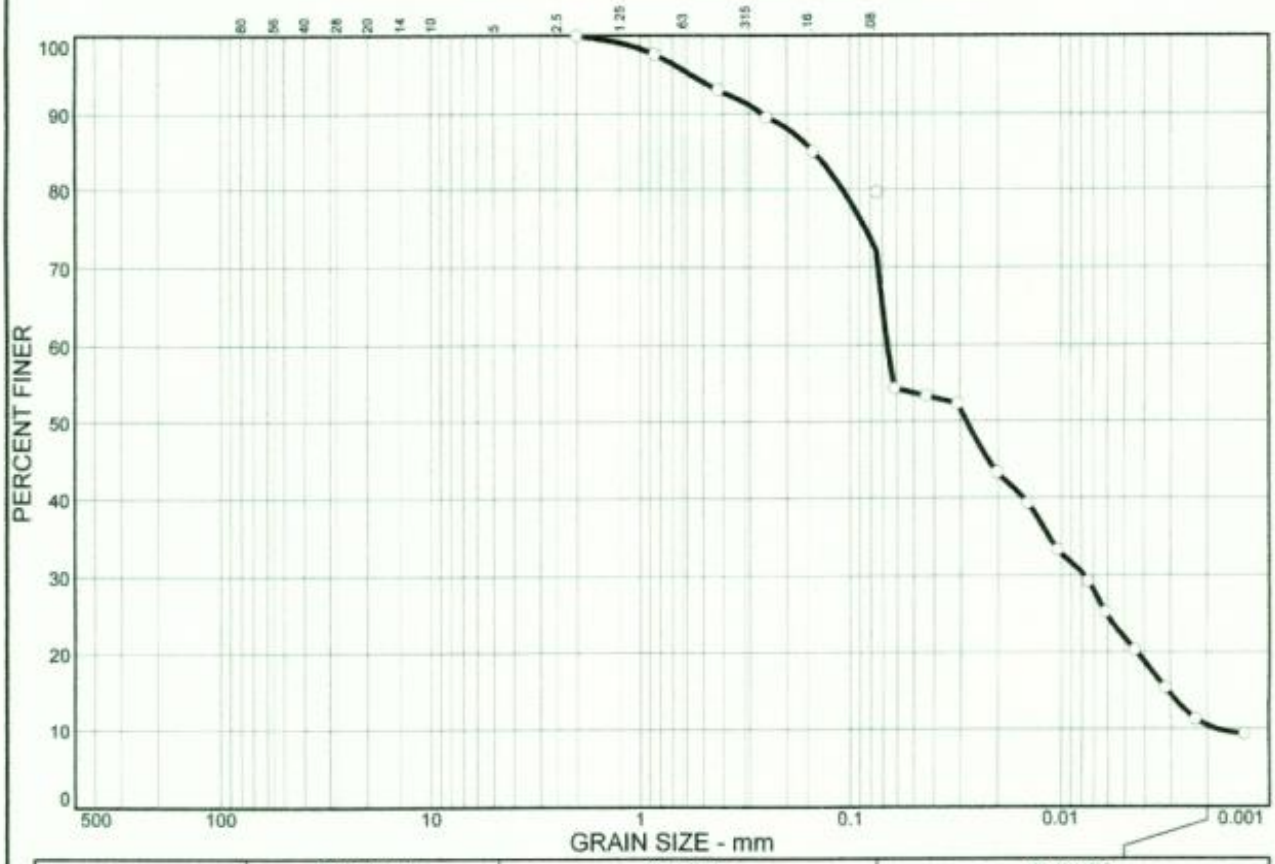

% COBBLES	% GRAVEL		% SAND			% FINES	
	CRS.	FINE	CRS.	MEDIUM	FINE	SILT	CLAY
0.0	0.0	0.0	0.0	6.9	21.0	61.7	10.4

SIEVE SIZE	PERCENT FINER	SPEC.* PERCENT	PASS? (X=NO)
#10	100.0		
#20	97.6		
#40	93.1		
#60	89.5		
#100	85.0		
#200	79.6		

* (no specification provided)

Soil Description

Atterberg Limits

PL= 31 LL= 67 PI= 36

Coefficients

D_{85}= 0.150 D_{60}= 0.0664 D_{50}= 0.0281
D_{30}= 0.0078 D_{15}= 0.0031 D_{10}= 0.0018
C_u= 36.29 C_c= 0.50

Classification

USCS= AASHTO=

Remarks

Sample No.: **Source of Sample:** BH08-SP-13 **Date:** 24/11/08
Location: **Elev./Depth:** 2.4m

STRATA ENGINEERING CONSULTANTS LTD.

Client: WINDJAMMER LANDING RESORT & SPA
Project: WINDJAMMER LANDING RESORT INSTRUMENTATION, Labrelotte Bay,St.Lucia,W.I.
Project No: **Figure**

Particle Size Distribution Report

% COBBLES	% GRAVEL		% SAND			% FINES	
	CRS.	FINE	CRS.	MEDIUM	FINE	SILT	CLAY
0.0	0.0	0.0	0.0	8.5	20.4	66.8	4.3

SIEVE SIZE	PERCENT FINER	SPEC.* PERCENT	PASS? (X=NO)
#10	100.0		
#20	96.9		
#40	91.5		
#60	87.6		
#100	83.2		
#200	78.0		

* (no specification provided)

Soil Description

Atterberg Limits

PL= LL= PI=

Coefficients

D_{85}= 0.176 D_{60}= 0.0659 D_{50}= 0.0260
D_{30}= 0.0098 D_{15}= 0.0044 D_{10}= 0.0034
C_u= 19.53 C_c= 0.43

Classification

USCS= ROCK AASHTO=

Remarks

Sample No.: **Source of Sample:** BH08-SP-13 **Date:** 24/11/08
Location: **Elev./Depth:** 3.0m

STRATA ENGINEERING CONSULTANTS LTD.

Client: WINDJAMMER LANDING RESORT & SPA
Project: WINDJAMMER LANDING RESORT INSTRUMENTATION, Labrelotte Bay,St.Lucia,W.I.
Project No: **Figure**

Particle Size Distribution Report

% COBBLES	% GRAVEL		% SAND			% FINES	
	CRS.	FINE	CRS.	MEDIUM	FINE	SILT	CLAY
0.0	0.0	0.0	0.0	3.3	12.3	61.5	22.9

SIEVE SIZE	PERCENT FINER	SPEC.* PERCENT	PASS? (X=NO)
#10	100.0		
#20	98.0		
#40	96.7		
#60	94.9		
#100	93.0		
#200	90.4		

* (no specification provided)

Soil Description

Atterberg Limits

PL= 32 LL= 54 PI= 22

Coefficients

D_{85}= 0.0775 D_{60}= 0.0201 D_{50}= 0.0119
D_{30}= 0.0032 D_{15}= D_{10}=
C_u= C_c=

Classification

USCS= AASHTO=

Remarks

Sample No.: **Source of Sample:** BH08-SP-14 **Date:** 08/01/09
Location: **Elev./Depth:** 0.9m

STRATA ENGINEERING CONSULTANTS LTD.

Client: WINDJAMMER LANDING RESORT & SPA
Project: WINDJAMMER LANDING RESORT INSTRUMENTATION, Labrelotte Bay,St.Lucia,W.I.
Project No: **Figure**

Particle Size Distribution Report

% COBBLES	% GRAVEL		% SAND			% FINES	
	CRS.	FINE	CRS.	MEDIUM	FINE	SILT	CLAY
0.0	0.0	0.0	0.0	2.4	13.3	56.0	28.3

SIEVE SIZE	PERCENT FINER	SPEC.* PERCENT	PASS? (X=NO)
#10	100.0		
#20	99.0		
#40	97.6		
#60	96.0		
#100	93.6		
#200	90.5		

* (no specification provided)

Soil Description

Atterberg Limits

PL= LL= PI=

Coefficients

D_{85}= 0.0781 D_{60}= 0.0223 D_{50}= 0.0104
D_{30}= 0.0023 D_{15}= D_{10}=
C_u= C_c=

Classification

USCS= AASHTO=

Remarks

Sample No.:
Location:

Source of Sample: BH08-SP-14

Date: 08/01/09
Elev./Depth: 1.5m

STRATA ENGINEERING CONSULTANTS LTD.

Client: WINDJAMMER LANDING RESORT & SPA
Project: WINDJAMMER LANDING RESORT INSTRUMENTATION, Labrelotte Bay,St.Lucia,W.I.
Project No:
Figure

Particle Size Distribution Report

% COBBLES	% GRAVEL		% SAND			% FINES	
	CRS.	FINE	CRS.	MEDIUM	FINE	SILT	CLAY
0.0	0.0	0.0	0.0	10.2	25.4	64.4	0.0

SIEVE SIZE	PERCENT FINER	SPEC.* PERCENT	PASS? (X=NO)
#10	100.0		
#20	96.2		
#40	89.8		
#60	83.5		
#100	75.7		
#200	67.3		

* (no specification provided)

Soil Description

Atterberg Limits

PL= LL= PI=

Coefficients

D_{85}= 0.273 D_{60}= 0.0721 D_{50}= 0.0650
D_{30}= 0.0170 D_{15}= 0.0087 D_{10}= 0.0064
C_u= 11.34 C_c= 0.63

Classification

USCS= AASHTO=

Remarks

Sample No.: **Source of Sample:** BH08-SP-15 **Date:** 13/01/09
Location: **Elev./Depth:** 0.9m

STRATA ENGINEERING CONSULTANTS LTD.

Client: WINDJAMMER LANDING RESORT & SPA
Project: WINDJAMMER LANDING RESORT INSTRUMENTATION, Labrelotte Bay,St.Lucia,W.I.
Project No: **Figure**

Particle Size Distribution Report

% COBBLES	% GRAVEL		% SAND			% FINES	
	CRS.	FINE	CRS.	MEDIUM	FINE	SILT	CLAY
0.0	0.0	0.0	0.0	6.4	26.2	64.0	3.4

SIEVE SIZE	PERCENT FINER	SPEC.* PERCENT	PASS? (X=NO)
#10	100.0		
#20	97.5		
#40	93.6		
#60	88.5		
#100	81.1		
#200	73.4		

* (no specification provided)

Soil Description

Atterberg Limits

PL= 32 LL= 62 PI= 30

Coefficients

D_{85}= 0.205 D_{60}= 0.0692 D_{50}= 0.0603
D_{30}= 0.0154 D_{15}= 0.0063 D_{10}= 0.0048
C_u= 14.44 C_c= 0.71

Classification

USCS= AASHTO=

Remarks

Sample No.:
Location:
Source of Sample: BH08-SP-15
Date: 13/01/09
Elev./Depth: 1.5m

STRATA ENGINEERING CONSULTANTS LTD.

Client: WINDJAMMER LANDING RESORT & SPA
Project: WINDJAMMER LANDING RESORT INSTRUMENTATION, Labrelotte Bay,St.Lucia,W.I.
Project No:
Figure

Particle Size Distribution Report

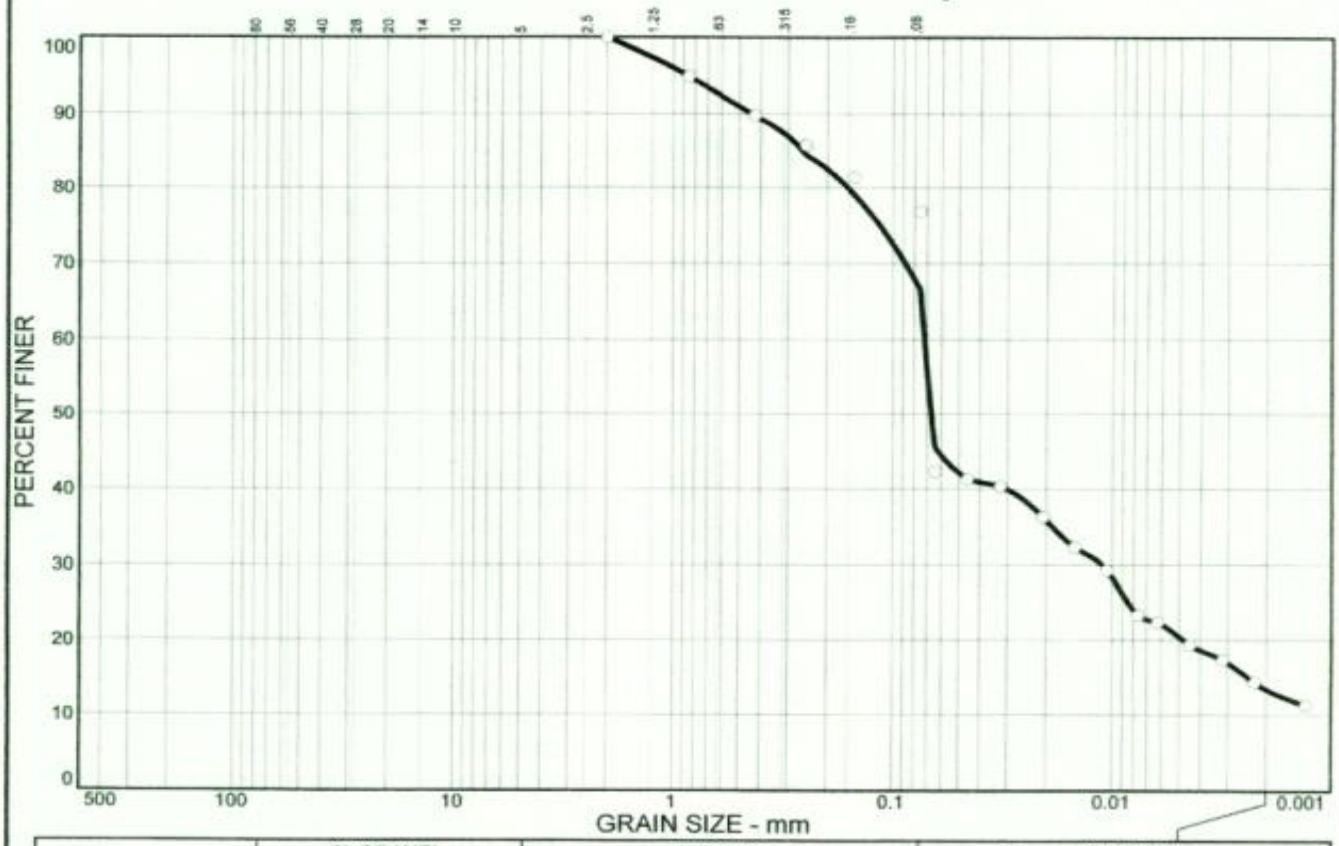

% COBBLES	% GRAVEL		% SAND			% FINES	
	CRS.	FINE	CRS.	MEDIUM	FINE	SILT	CLAY
0.0	0.0	0.0	0.0	10.3	23.2	53.2	13.3

SIEVE SIZE	PERCENT FINER	SPEC.* PERCENT	PASS? (X=NO)
#10	100.0		
#20	94.9		
#40	89.7		
#60	85.7		
#100	81.4		
#200	76.8		

* (no specification provided)

Soil Description

Atterberg Limits

PL= LL= PI=

Coefficients

D_{85}= 0.259 D_{60}= 0.0719 D_{50}= 0.0668
D_{30}= 0.0111 D_{15}= 0.0024 D_{10}=
C_u= C_c=

Classification

USCS= AASHTO=

Remarks

Sample No.:
Location:

Source of Sample: BH08-SP-15

Date: 13/01/09
Elev./Depth: 2.3m

STRATA ENGINEERING CONSULTANTS LTD.

Client: WINDJAMMER LANDING RESORT & SPA
Project: WINDJAMMER LANDING RESORT INSTRUMENTATION, Labrelotte Bay,St.Lucia,W.I.
Project No:
Figure

APPENDIX E

Plasticity Charts for Colluvium at the Windjammer Landing Beach Resort Study Site

LIQUID AND PLASTIC LIMITS TEST REPORT

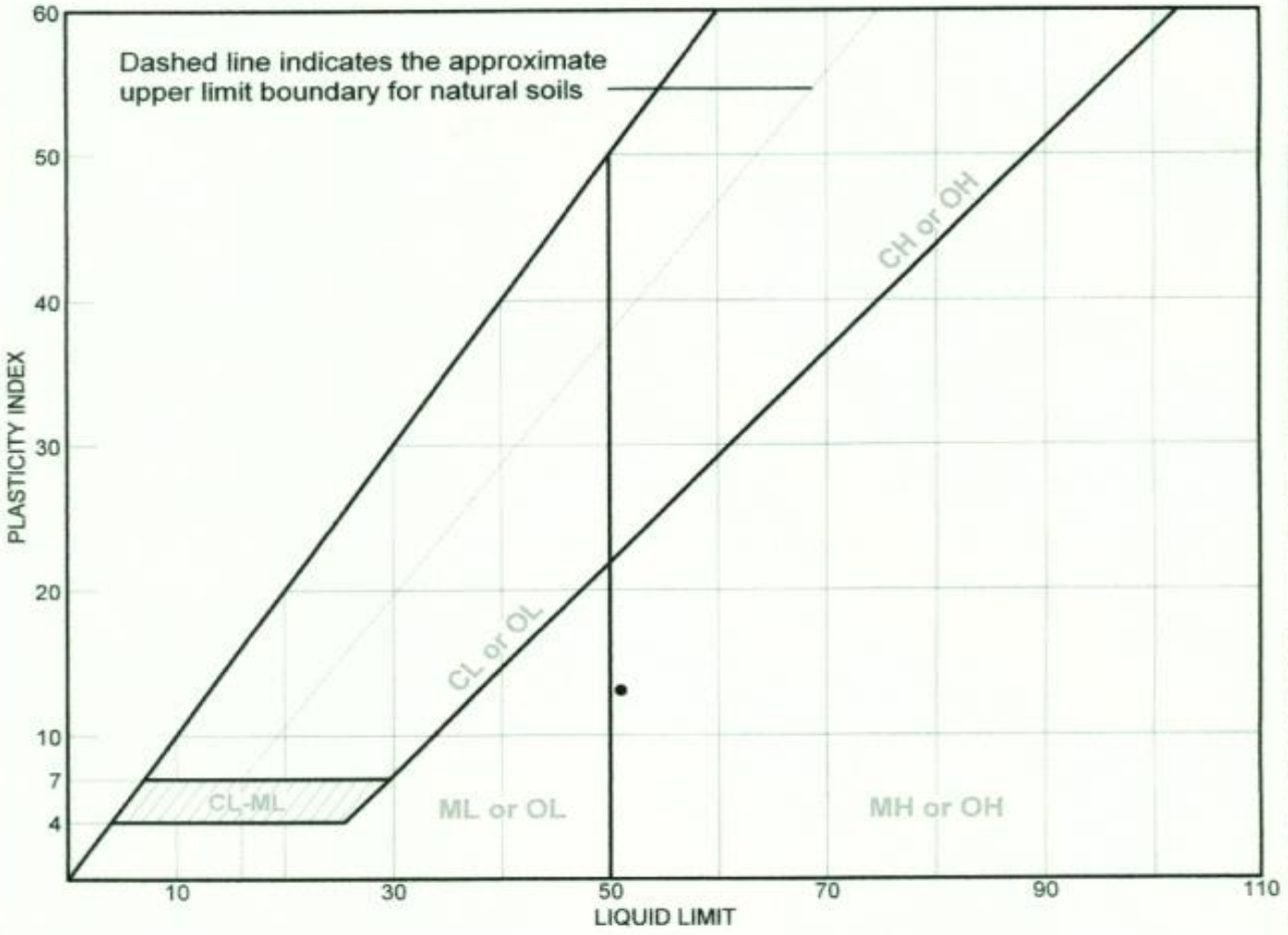

SOIL DATA

SYMBOL	SOURCE	SAMPLE NO.	DEPTH (m.)	NATURAL WATER CONTENT (%)	PLASTIC LIMIT (%)	LIQUID LIMIT (%)	PLASTICITY INDEX (%)	USCS
•	BH08-SP-13		0.9m	38.8	38	51	13	

LIQUID AND PLASTIC LIMITS TEST REPORT

STRATA ENGINEERING CONSULTANTS LTD.

Client: WINDJAMMER LANDING RESORT & SPA

Project: WINDJAMMER LANDING RESORT INSTRUMENTATION,Labrelotte Bay,St.Lucia,W.I.

Project No.:

Figure

LIQUID AND PLASTIC LIMITS TEST REPORT

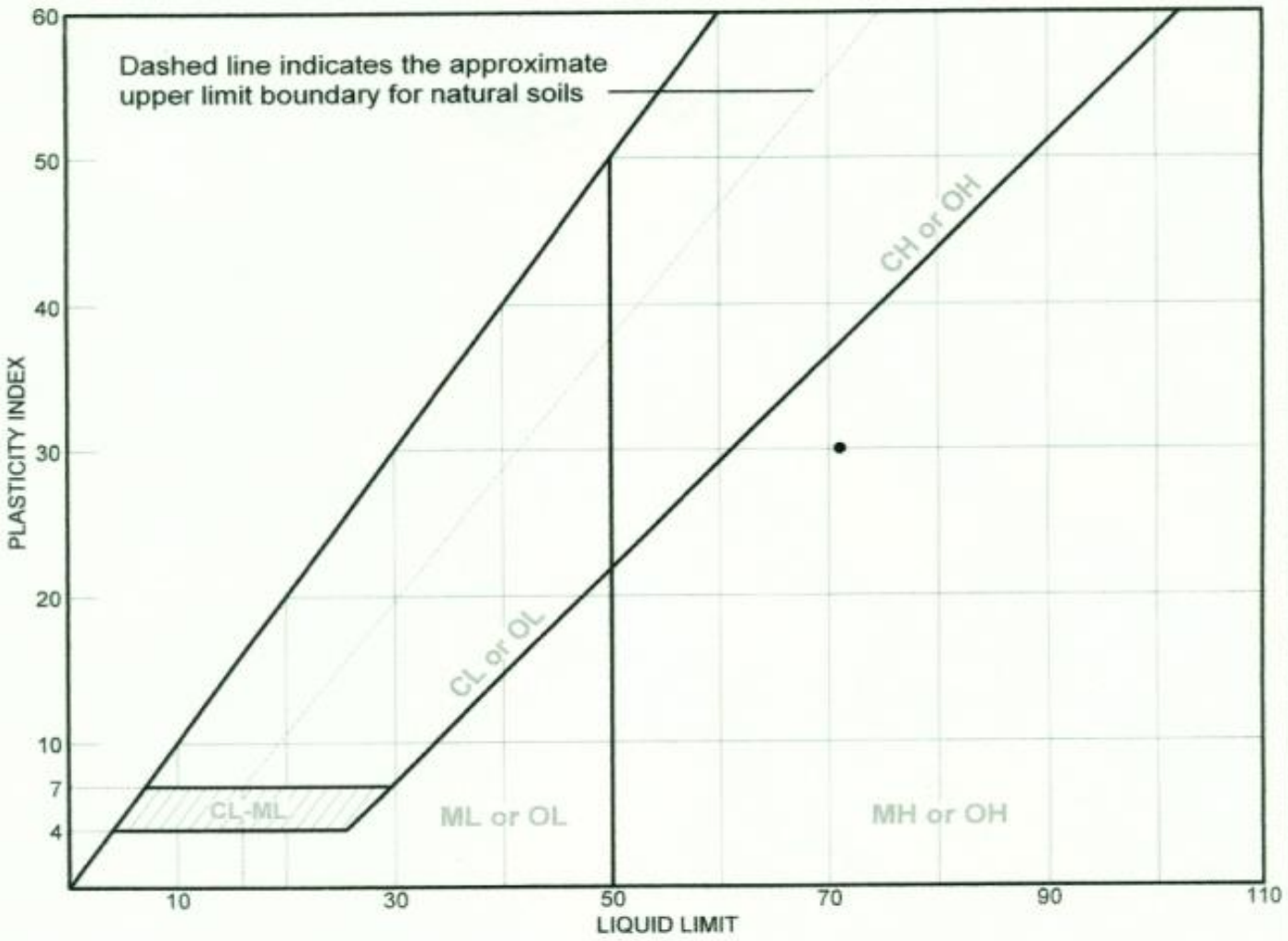

SOIL DATA

SYMBOL	SOURCE	SAMPLE NO.	DEPTH (m.)	NATURAL WATER CONTENT (%)	PLASTIC LIMIT (%)	LIQUID LIMIT (%)	PLASTICITY INDEX (%)	USCS
●	BH08-SP-13		1.5m	39.7	41	71	30	

LIQUID AND PLASTIC LIMITS TEST REPORT

STRATA ENGINEERING CONSULTANTS LTD.

Client: WINDJAMMER LANDING RESORT & SPA

Project: WINDJAMMER LANDING RESORT INSTRUMENTATION,Labrelotte Bay,St.Lucia,W.I.

Project No.:

Figure

LIQUID AND PLASTIC LIMITS TEST REPORT

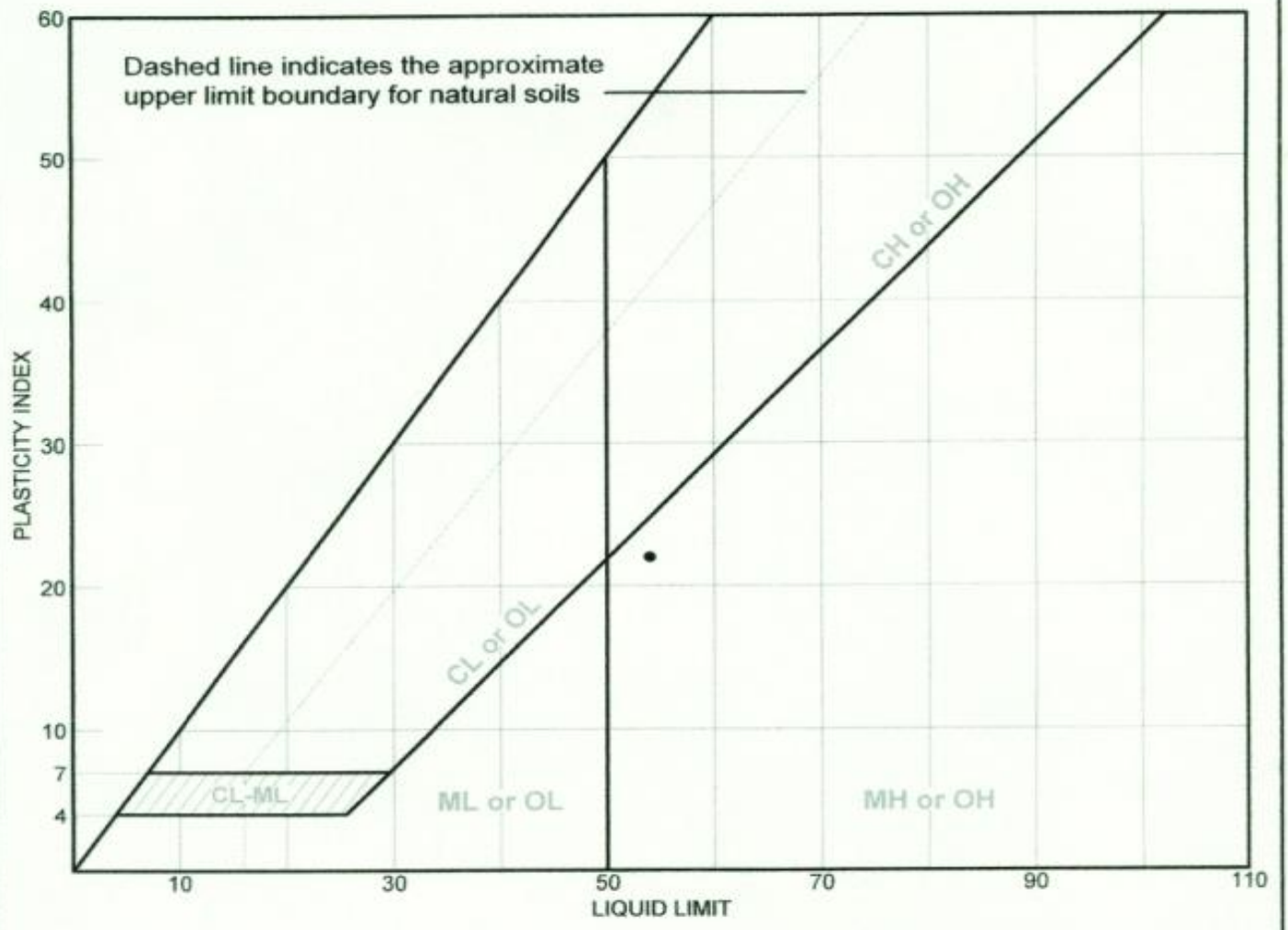

SOIL DATA

SYMBOL	SOURCE	SAMPLE NO.	DEPTH (m.)	NATURAL WATER CONTENT (%)	PLASTIC LIMIT (%)	LIQUID LIMIT (%)	PLASTICITY INDEX (%)	USCS
•	BH08-SP-14		0.9m	42	32	54	22	

LIQUID AND PLASTIC LIMITS TEST REPORT

STRATA ENGINEERING CONSULTANTS LTD.

Client: WINDJAMMER LANDING RESORT & SPA

Project: WINDJAMMER LANDING RESORT INSTRUMENTATION,Labrelotte Bay,St.Lucia,W.I.

Project No.:

Figure

LIQUID AND PLASTIC LIMITS TEST REPORT

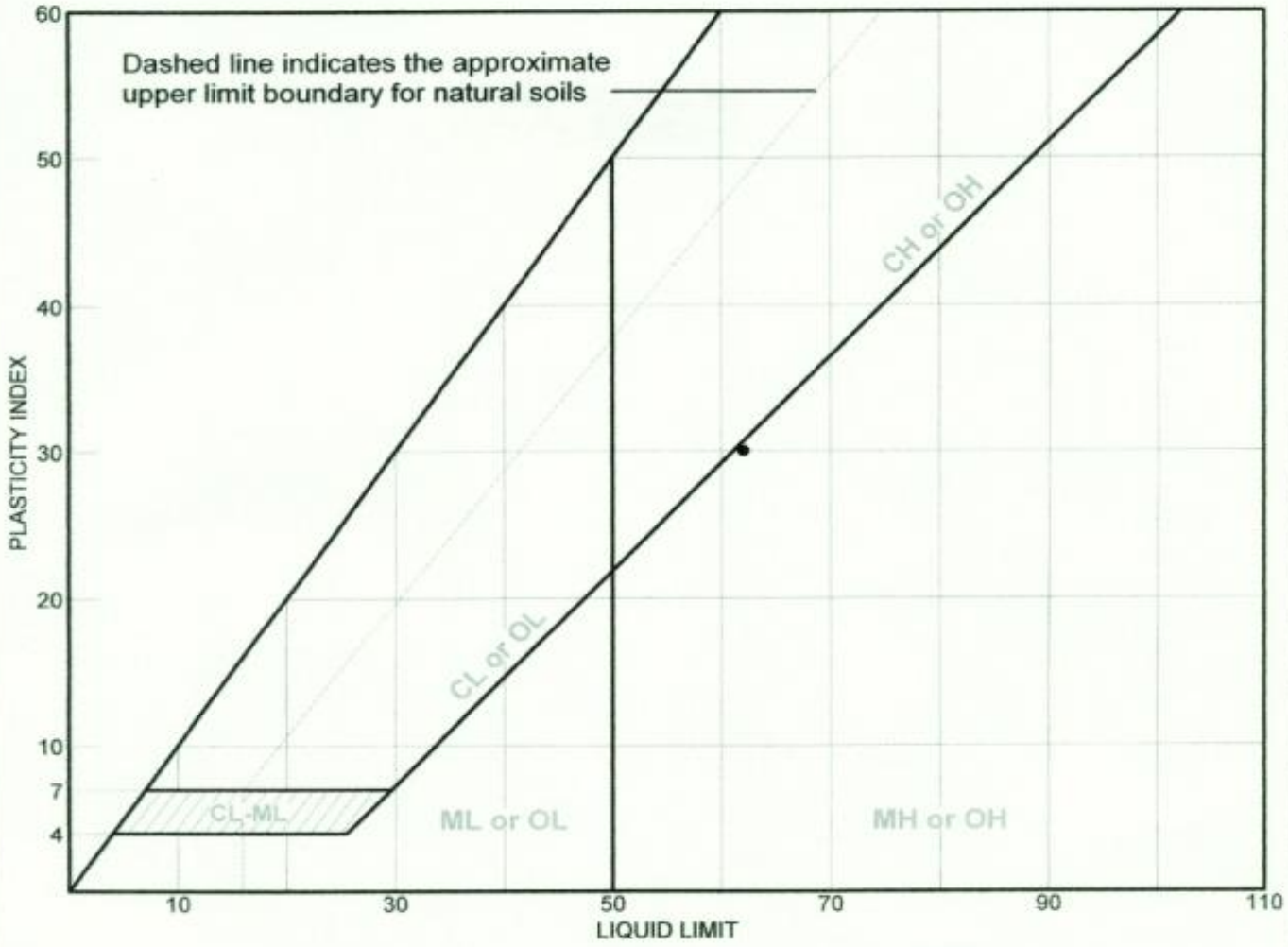

SOIL DATA								
SYMBOL	SOURCE	SAMPLE NO.	DEPTH (m.)	NATURAL WATER CONTENT (%)	PLASTIC LIMIT (%)	LIQUID LIMIT (%)	PLASTICITY INDEX (%)	USCS
●	BH08-SP-15		1.5m	29.5	32	62	30	

LIQUID AND PLASTIC LIMITS TEST REPORT

STRATA ENGINEERING CONSULTANTS LTD.

Client: WINDJAMMER LANDING RESORT & SPA

Project: WINDJAMMER LANDING RESORT INSTRUMENTATION,Labrelotte Bay,St.Lucia,W.I.

Project No.:

Figure

REFERENCES

Ali, F.H., Huat, T., Mariapan, S., ' Measurement of Suction and Infiltration on Slopes of Unsaturated Residual Soil' Project No. 03-02-03-0484, Department of Civil Engineering, University of Malaya, pp 1-4

American Society for Testing and Materials (ASTM) ' The Unified Soil Classification System', Annual Book of ASTM Standards; D2487-93, 2004

American Society for Testing and Materials (ASTM) 'Standard Test Method for Penetration Test and Split-Barrel Sampling of Soils', Annual Book of ASTM Standards; D1586-84, 2004

American Society for Testing and Materials (ASTM) 'Standard Test Method for Particle-Size Analysis of Soils' Annual Book of ASTM Standards; D 422-63, 2004

American Society for Testing and Materials (ASTM) ' Standard Test Method for Laboratory Determination of Water (Moisture) Content of Soil and Rock' , Annual Book of ASTM Standards; D 2216-92, 2004

American Society for Testing and Materials (ASTM) ' Standard Test Method for Liquid Limit, Plastic Limit and Plasticity Index of Soils' Annual Book of ASTM Standards; D 4318-93, 2004

American Society for Testing and Materials (ASTM) ' Standard Practice for Description of Soils (Visual-Manual Procedure)' Annual Book of ASTM Standards; D 2488-93, 2004

Anderson, M.G., Kemp, M.J. (1985) ' The Prediction of Pore Water Pressure 'Conditions in Road Cut Slopes in Saint Lucia, West Indies' Final Technical Report: Overseas Development Administration, London. Research Scheme R3426, pp 17- 200

Anderson, S.A., Sitar, N., (1995) ' Analysis of Rainfall-Induced Debris Flows' Journal of Geotechnical Engineering, Vol. 121, No.7, July 1995, pp 544-551

Anonyomous, (1972) 'The Description of Rock Masses for Engineering Purposes' Quarterly Journal of Engineering Geology, Vol. 10, pp 355-388

Aung, K.K., Rahardjo, H., Toll, D.G., Leong, E.C., (2000) ' Minerology and microfabric of unsaturated residual soils,' : Unsaturated Soils for Asia; Proceedings of the Asian Conference on Unsaturated Soils ; UNSAT-ASIA 2000/SINGAPORE/18-19 May 2000, pp 317-320

Australian Geomechanics Society (2000) " Landslide Risk Management Concepts and Guidelines" Sub-Committee on Landslide Risk Management, Australian Geomechanics, Vol. 35, pp 49-92

Ayalew, L., (1999) 'The effectof seasonal rainfall on landslides in the highlands of Ethiopia' Bulletin of Engineering Geology & the Environment, Springer-Verlag, Vol. 58, pp 9-19

Barata, F.E., (1969) ' Landslides in The Tropical Region of Rio De Janeiro,' Proceedings of the Seventh International Conference on Soil Mechanics and Foundation Engineering, Mexico 1969, pp 507-516

Bishop, A.W., (1959) 'The Principle of Effective Stress,' lecture delivered in Oslo, Norway in 1955; published in Teknisk Ukeblad, Vol. 106, No. 39, pp 859-863

Blatz, J.A., Ferreira, J., Graham, J., (2004) ' Effects of near-surface environmental conditions on instability of an unsaturated soil slope'; Canadian Geotechnical Journal, Vol. 41, 2002, pp 1111-1126

Blight, G.E., (1997) ' Mechanics of Residual Soils' Prepared by Technical Committee 25 on The Preoperties of Tropical and Residual Soils of the International Society for Soil Mechanics and Foundation Engineering: Balkema/Rotterdam/Brookfield pp. 1-230

Bommer, J.J., Rodriguez, C.E., (2002) ' Earthquake-induced Landslides in Central America' Journal of Engineering Geology, Elsevier Science Ltd, Volume 63, pp 189-220

Bommer, J.J, Rolo, R., Mitroulia, A., Berdousis, P., ' Geotechnical Properties and Seismic Slope Stability of Volcanic Soils' 12th European Conference on Earthquake Engineering, Elsevier Science ltd, Paper 695

Brand, E.W., (1984) ' Landslides in Southeast Asia: A State of the Art Report,' Proceedings of the 4th International Symposium on Landslides,' Toronto, Canada, Volume 1, pp 17-59.

British Standards (BS 7755), Section 3.2: 1995, ISO 10390: Soil Quality, Part 3, Chemical Methods, Section 3.2, Determination of pH.

British Standards (BS 7755), Section 3.12, 1996; ISO 13536, 1995; Soil Quality, Part 3; Chemical Methods, Section 3.12; 'Determination of the Potential Cation Exchange Capacity and Exchangeable Cations using Barium Chloride Solution buffered at pH = 8.1'

British Standards (BS 7755), Section 3.11, 1995, ISO 11048: Soil Quality, Part 3, Chemical Methods, Section 3.11, Determination of water soluble and acid soluble sulphate.

British Standards (BS 7755), Section 3.8, 1995, ISO 10694: Soil Quality, Part 3, Chemical Methods, Section 3.8, Determination of organic and total carbon after dry combustion (elementary analysis)

Bronders, J., (1994) ' Hydraulic conductivity of a tropical residual soil prone to landslides' Quarterly Journal of Engineering Geology, Vol. 27, pp 375- 381

Brown, F., Clark, J., (1995) ' The West Coast Road in Saint Lucia, an Approach to Slope Stabilisation' Vegetation and Slopes; Natural Resources Institute, UK pp 172-181

Cai, F., Ugai, K., (2004) ' Numerical Analysis of Rainfall Effects on Slope Stability' International Journal of Geomechanics, Vol. 4, No. 2, 2004, pp 69-78

Castro, G., (1975) ' Liquefaction and Cyclic Mobility of Saturated Sands' Journal of Geotechnical Engineering Division, American Society of Civil Engineers, Vol. 101, No.6, pp. 551-569

Cardinali, M., et al (2002) 'Geomorphological Approach to Estimating Landslide Hazard and Risk in Urban and Rural Areas in Umbria, Central Italy,' NHESS, Volume 2 : 1-2, pp 57-72

Caribbean Group for Cooporation in Economic Development (2002) ' Natural Hazard Risk Management in the Caribbean : Revisiting the Challenge,' Private Sector and Infrastructure Department, Latin America and the Caribbean Region : The World Bank, pp 1-20

Cedergren, H.R., (1977) ' Seepage, Drainage & Flow Nets' Second Edition, John Wiley & Sons, pp 38-40, 497-501

Chamley, H., (1989) ' Clay Sedimentology' Springer-Verlag Berlin Heidelberg Germany, pp 402-405

Chen, H., Lee, C.F., Law, K.T., (2004)' Causative Mechanisms of Rainfall-Induced Fill Slope Failures' Journal of Geotechnical and Geoenvironmental Engineering, Vol. 130, No.6,June 1, 2004. ASCE, ISSN 1090-0241/2004/ 6-593-602, pp 593-601

Cheung, W.M., Shiu, Y.K., (2000) " Assessment of Global Landslide Risk Posed by Man-made Slope Features, Geotechnical Engineering Office, Hong Kong, GEO Report No. 125

Ching-Jiang, J., Chih-Hao, T., Ming-Chien, C., Jiin-Fa, L., (2010), 'Monitoring and Numerical Analysis for Typhoon Morakot Induced Landslide in Cau-Pin Area, Taiwan', 4th Japan-Taiwan Joint Workshop on Geotechnical Hazards from Large Earthquakes and Heavy Rainfalls, 25 – 28 October, 2010, Sendai, Japan.

Cho, S.E., Lee, S.R., (2002) ‘ Evaluation of Surficial Stability for Homogeneous Slopes Considering Rainfall Characteristics’ Journal of Geotechnical and Geoenvironmental Engineering, Vol. 128, No. 9, 2002, pp 756-763

Chowdhury, R., Flentje, P. (2002) ‘ Uncertainties in Rainfall-Induced Landslide Hazards’ Quarterly Journal of Engineering Geology and Hydrology, Volume 35, pp 61-70

Clark, J., Hellin, J., (1996) ‘Bio-Engineering for Effective Road Maintenance in the Caribbean’ Natural Resources Institute; University of Greenwich, U.K, Pp 2-106

Collins, K., (1985) ‘ Towards Characterization of Tropical Soil Microstructure’ : Proceedings of the 1st International Conference on Geomechanics in Tropical Lateritic and Saprolitic Soils’ Brasilia 1, pp. 85-96

Collins, B.D., Znidarcic, D., (2004) ‘ Stability Analyses of Rainfall Induced Landslides’ Journal of Geotechnical and Geoenvironmental Engineering, Vol. 130, No. 4, April 1, 2004. ASCE ISSN 1090-0241/2004/4-362-372 pp 362- 371

Craig, R.F., (2004) ‘Craig’s Soil Mechanics’ Seventh Edition, Spon Press, Taylor & Francis, pp. 299, Figure 8.9

D’Appolonia, E., Alperstein, R., D’Appolonia, D.J., (1967) ‘ Behaviour of a Colluvial Slope’ Journal of Soil Mechanics and Foundation Division, Proceedings of the American Society of Civil Engineers, pp 447-472

DeGraff, J.V., (1985) ‘ Landslide Hazard on St. Lucia, West Indies; Final Report: Washington D.C., Organization of American States

DeGraff, J.V., Bryce, R., Jibson, R.W., Mora, S.,Rogers, C.T., (1989) ‘ Landslides: Their Extent and Significance in the Caribbean,’ Brabb, E.,E., and Harrod (eds) A.A.Balkema, Rotterdam, Netherlands, pp. 51-80

Deschamps, R., Yankey, G., ‘ Limitations in the Back-Analysis of Strength From Failures’, Nicholson Construction Company, Pennsylvania, USA; FMSM Engineers, Lexinton , Kentucky, USA

Deutscher, M.S., Gasmo, J.M., Rahardjo, H., Leong, E.C., ‘ Field measurements of pore-water profiles in residual soil slopes of the Bukit Timah Granite Formation, Singapore’; Unsaturated Soils For Asia, Proceedings of the Asian Conference on Unsaturated Soils, UNSAT-ASIA 2000 SINGAPORE/18-19 May 2000, pp. 777-782

Duncan, J.M., Stark, T.D., (1992) ‘ Soil Strengths from Back-Analysis of Slope Failures,’ Stability and Performance of Slopes and Embankments-11, Volume 2, Proceedings of a Specialty Conference sponsored by the Geotechnical Engineering Division of the American Society of Civil Engineers, Berkeley, California, USA, June 29 – July 1, 1992, pp. 890-904

Economic Commission for Latin America and the Caribbean Sub-regional Headquarters for the Caribbean (ECLAC) (2011) ' Macro-socioeconomic and Environmental Assessment of the Damage and Losses caused by Hurricane 'TOMAS' : A Geo-environmental Disaster' United nations, February 7, 2011

Fabius, M., Matich, M.A.J., Roper, R.J., Maki, G.C., (1999)' Case History of an Unusual Dyke Failure,' Proceedings of the Canadian Dam Association, 2nd Annual Conference, Sudbury, Ontario October 3-7, 1999 pp 1-9

Faisal, H.A., (2000) ' Unsaturated tropical residual soils and rainfall induced slope failures in Malaysia,' ; Unsaturated Soils for Asia; Proceedings of the Asian Conference on Unsaturated Soils, UNSAT-ASIA 2000/SINGAPORE/18-19 May 2000, pp 41-51

Felt, E.J., (1951), ' Soil Series Names as a Basis for Interpretive Soil Classification for Engineering Purposes' American Society for Testing Materials; Specification Technical Publications, 113 pp 62-79.

Fityus, S., Smith, D.W., (2000) ' The influence of fabric and mineralogy on the expansivity of an Australian residual clay soil' Unsaturated Soils for Asia; Proceedings of the Asian Conference on Unsaturated Soils, UNSAT-ASIA 2000/SINGAPORE/18-19, May 2000, pp. 657-662

Fookes, P.G., (1997) ' Tropical Residual Soils' A Geological Society Engineering Group – Working Party Revised Report, Published by The Geological Society, London, pp. 10-147

Fredlund, D.G., Morgernstern, N.R. (1977) ' Stress State Variables for Unsaturated Soils' ASCE Journal of Geotechnical Engineering GT5, Volume 103, pp. 447-466

Fredlund, D.G., Morgernstern, N.R., (1978) Closure to Paper Entitled ' Stress State Variables for Unsaturated Soils,' ASCE Journal of Geotechnical Engineering Division G11, pp. 1415-1416

Fredlund, D.G., Rahardjo, H., (1993) ' Soil Mechanics for Unsaturated Soils' John Wiley & Sons, Inc., New York

Fredlund, D.G., Xing, A., (1994) ' Equations for the Soil-Water Characteristic Curve' Canadian Geotechnical Journal, Vol. 31, No. 3, pp. 521-532

Fredlund, M.D., (1998) ' Unsaturated Seepage Modeling Made Easy'; Geotechnical News Magazine, Bitech Publishers, Vancouver, British Columbia, Canada; June issue, pp. 52-59

Fredlund, M.D., Wilson, G.W., Fredlund, D.G., (2002) ' Use of the grain size distribution for estimation of the soil-water characteristic curve'; Canadian Geotechnical Journal, Vol. 39, No. 5, pp. 1103-1117

Fredlund, M.D., Wilson, G.W., (2000) ‘ Use of Grain-Size Functions in Unsaturated Soil Mechanics’; ASCE Geo-Institute Denver Symposium, Denver, Colorado, USA, August 3-8, 2000, pp. 69-83

Franks, C.A.M., (1999) ‘ Characteristics of some rainfall-induced landslides on natural slopes, Lantau Island, Hong Kong,’ Quarterly Journal of Engineering Geology Vol 32, 247-259

Gasmo , J., Hritzuk, K.J., Rahardjo, H., and Leong, E.C., (1999) **‘**Instrumentation of an Unsaturated Residual Soil Slope,’ Geotechnical Testing Journnal, GTJODI, Vol. 22, No. 2, pp. 134-142.

Gasmo, J.M., Rahardjo, H., Deutscher, M.S., Leong, E,C., (2000) ‘ Preliminary Assessment of Slope Stability with respect to Rainfall-induced Slope Failures’ Unsaturated Soils for Asia, Proceedings of the Asian Conference on Unsaturated Soils, UNSAT-ASIA 2000, SINGAPORE 18-19, May 2000, pp. 783-788

Geocon Inc., (1990) “Report on the Preliminary Geotechnical Recommendations : Proposed Conference Centre, Windjammer Landing Resort’, Saint Lucia’ (not published)

Geocon Inc.,(1991) ‘ Windjammer Landing Company Ltd: Geotechnical Studies –Monitoring Program: Status Report’, February 1991 (not published)

Geocon Inc., (1991) ‘ Drawings and Construction Notes for the Windjammer Landing Resort, Castries, Saint Lucia’, July 1991 (not published)

Geocon Inc., (1992) ‘ Cause of Slide Assessment at Villas 14 & 16; Windjammer Landing Villa Beach Resort, Saint Lucia’, March 1992 (not published)

Geotech Associates Ltd., (1997) ‘ factual Report on Soil Investigation for Windjammer Resort Extension, Saint Lucia’, January 1997 (not published)

Geotech Associates Ltd., (1997) ‘ Report on Soil Investigation for Windjammer Landing Resort Extension, Saint Lucia’ March 1997 (not published)

Geotech Associates Ltd., (2004) ‘ report on Assessment of Slope Instability and Cracking of Units 17-22 at Windjammer Landing Beach Resort, Saint Lucia’ December 2004 (not published)

Geological Society Engineering Group Working Party Report, (1995) ‘ The description and classification of weathered rocks for engineering purposes’ Quarterly Journal of Engineering Geology, Vol. 28, pp 207-227

Geo-Slope International Ltd (2004) Slope/W for Slope Stability Modeling – First Edition, Users Manual. Calgary, Alberta, CANADA

Geo-Slope International Ltd (2004) Seep/W for Seepage Modeling – First Edition, Calgary, Alberta, CANADA

Gidigasu, M.D., (1976) ‘ Laterite Soil Engineering’; Elsevier Scientific Publishing Company, Amsterdam, 1976

Gillott, J.E., (1968) 'Clay in Engineering Geology', Elsevier Publishing Company, Amsterdam, Netherlands

Gjetvaj, V., Znidarcic, D., Nossan, A.S., Popovic, N. (2009) ' Increase of Slope Stability with Time by Drilled Drains'; Proceedings of the 17th International Conference on Soil mechanics and Geotechnical Engineering; IOS Press; Editors : M.Hamza et al, pp 1714-1717.

Gofar, N., Lee, L.M., Asof, M., (2006) ' Transient Seepage and Slope Stability Analysis for a Rainfall Induced Landslide: A Case Study' Malaysian Journal of Civil Engineering, Volume 18, No.1, pp. 1-13.

Government of Saint Lucia – Ministry of Agriculture, Fisheries and Forestry; Department of Water Resources, Union Saint Lucia, West Indies

Griffiths,D.V., Lane,P.A., (1999) ' Slope Stability Analysis by Finite Elements' Colorado School of Mines, Golden, Colarado, U.S.A.; Geotechnique 49, No. 3, pp. 387-403

Grim, R.E., (1968) ' Clay Mineralogy' McGraw-Hill, New York.

Gupta, A.S., Rao, K.S., (1998) ' Index properties of weathered rocks: inter-relationship and applicability' Bulletin of Engineering Geology & the Environment, Vol. 57, pp. 161-172

Guzzetti, F., (2003) ' Landslide Hazard Assessment and Risk Evaluation : Limits and Prospectives' Proceedings of the 4th EGS Plinius Conference held at Mallorca, Spain

Hagerty, D.J., Curini, A., (2004) ' Impoundment Failure Sepage Analysis', The Geological Society of America; The Environmental & Engineering Geoscience, Volume X, No. 1, February 2004, pp 57 - 68

Halcrow & Associates Ltd, (1995) Report on the 'Castries to Cul de Sac Highway – Soils and Rock Investigations'; Saint Lucia ; not published

Hamdham, I. N., Schweiger, H.F., (2011) ' Slope Stability Analysis of Unsaturated Soil with Fully Coupled Flow-Deformation Analysis' IAMG 2011, mathematical Geosciences at the Crossroads of Theory and Practice, University of Salzburg, Austria, pp 1-17

Harrison, B.A., Blight, G.E., (2000) ' A Comparison of in-situ soil suction measurements'; Unsaturated Soils for Asia; Proceedings of the Asian Conference on Unsaturated Soils ; UNSAT-ASIA 2000/SINGAPORE/18-19 May 2000, pp 281-284

Ho, D.Y.F, Fredlund, D. G. (1982) ' Increase in Strength due to Suction for two Hong Kong Soils' Proceedings, ASCE Geotechnical Conference on Engineering and Construction in Tropical and Residual Soils, Honalulu, Hawaii, pp 263-295.

Hoek, E., Bray, (1977) 'Rock Slope Engineering' The Institution of Mining & Metallurgy, London, Revised Second Edition, pp 100 & 132

Hossain, M.K., (2010) ' Effect of Rainfall on Matric Suction and Stability of a Residual Granite Soil Slope,' Dhaka University of engineering & Technology, Gazipur, Bangladesh, DUET Journal, Volume 1, Issue 1, pp 37 - 41

Huang, W.T., (1962) 'Petrology' ; McGraw-Hill Book Company, New York; pp 132, 146-147.

Huat, B.B.K., Ali, F.H., Huat, L.T., Marriappan (2005) ' Infiltration Characteristics of Unsaturated Residual Soils of Various Weathering Grades' Jurnal Teknologi, Vol. 42 (B) pp 45-56

Hurlbut, Jr., C.S., (1971) 'Dana's Manual of Mineralogy'; 18th Edition, John Wiley & Sons, New York, U.S.A.,

Huvaj-Sarihan, N., Stark, T.D., (2008) ' Back-Analysis of Landfill Slope Failures,' 6th International Conference on Case Histories in Geotechnical Engineering, Paper No. 2.34, Arlington, Virginia, USA, pp. 1 - 7

Imaizumi, F., Miyamoto, K. (2012) ' Spartial Distribution of Pore Water Pressure and Effective Stress in Vertical Seepage Flow through Multi-layered Soil Structure,' Journal of Japan Society of Erosion Control Engineering, Volume 65, No.5

International Society for Rock Mechanics (ISRM) 1986 ' Rock Characterization Testing & Monitoring'; Pergamon Press Ltd, pp 5-52

Irfan, T.Y., (1996) ' Mineralogy, fabric properties and classification of weathered granites in Hong Kong' Quarterly Journal of Engineering Geology, Vol. 29, pp 5-35

Irfan, T.Y., (1999) ' Characterization of weathered volcanic rocks in Hong Kong' Quarterly Journal of Engineering Geology, Vol. 32, 317-348

Jiao, J.J., Nandy, S., Malone A., (1999) ' Hydrogeological Studies of the Slope Failure at Tuen Mun Highway Chainage 550, Hong Kong' 2nd International Conference on Landslides, Slope Stability & Safety of Infra-Structures: 27-28 July, 1999 Singapore; pp 177 - 184

Jiao, J.J., Malone, A.W. (2000) ' An Hypothesis Concerning a Confined Groundwater Zone in Slopes of Weathered Igneous Rocks' Symposium on Slope Hazards and Their Preventon, May 8-10, 2000 Hong Kong PRC, pp 165 - 170

Jiao, J.J., (2000) ' A confined groundwater zone in weathered igneous rocks and its impact on slope stability' ; International Symposium on Hydrogeology and the Environment, Wuhan, China, October 17-20, 2000, pp 1-8

Jiao, J.J., Leung,C., Ding, G. (2003) ' Confined Groundwater at No. 52, Holliwood Road, Hong Kong' International Conference on Slope Engineering, December 8-10, 2003, Hong Kong

Jiao, J.J., Wang, X.S., Nandy, S. (2005) ' Confined Groundwater Zone and Slope Instability in Weathered Igneous Rocks in Hong Kong' Elsevier Science Direct; Journal of Engineering Geology Vol. 80, pp. 71-92

Kakou, B.G., Shimizu, H., Nishimura, S., (2001) ' Residual Strength of Colluvium and Stability Analysis of Farmland Slope' Agricultural Engineering International: the CIGA Journal of Scientific Research and Development. Vol. 111. pp 1-10

Karikari-Yeboah, O., Gyasi-Agyei, Y. ‘ Stability of Slopes Characterised by Colluvium: Investigation, Analysis and Stabilisation,’ Polar Technologies International Pty. Ltd, Australia

Kasim, F., Fredlund, D.G., Gan, J.K.N., (1998) ‘The Effect of steady state rainfall on long term matric suction conditions in slopes’ ; Slope Engineering in Hong Kong ; Proceedings of the Annual Seminar on Slope Engineering in Hong Kong; Balkema, Rotterdam/Brookfield; pp 75-82

Khalili, N., Geiser, F., Blight, G.E., (2004) ‘ Effective Stress in Unsaturated Soils: Review with New Evidence’ International Journal of Geomechanics, Vol. 4, No. 2, 2004, pp 115-126

Kim, J., Jeong, S., Park, S., Sharma, J. (2004) ‘ Influence of Rainfall-Induced Wetting on the Stability of Slopes in Weathered Soils,’ Elsevier: Science Direct; Engineering Geology Journal 75, pp. 251-262

Klohn Leonoff Ltd (1988) ‘Working paper No. 23 – Technical Report- Roseau Dam Functional Design’ Saint Lucia, pp 13-19

Ko Ko, C., Flentje, P., Chowdhury, R., (2004) ‘ Landslides Qualitative hazard and Risk Assessment Method and its Reliability’ Bulletin of Engineering Geology and the Environment, Volume 63, pp 149 - 165

Lam, L., Fredlund,D.G., Barbour, S.L., (1987) ‘ Transient Seepage Model for Saturated-Unsaturated Soil System : A geotechnical Engineering Approach,’ Canadian Geotechnical Journal, Volume 24, pp 565-580

Leach, B., Herbert, R., (1982) ‘ The Genesis of a Numerical Model for the Study of the Hydrology of a Steep Hillside in Hong Kong,’ Quarterly Journal of Engineering Geology, Volume 15, pp 243-259

Leong, E.C., Rahardjo, H., (1997) ‘ Permeability Functions for Unsaturated Soils’ Journal of Geotechnical and Geoenvironmental Engineering, Volume 123, No.12, ASCE, Paper No. 14485, pp 1118-1126.

Li, A.G., Yue, Z.Q., Tham, L.G., Lee, C.F., Law, K.T., (2005)‘ Field-monitored variations of soil moisture and matric suction in a saprolite slope’ Canadian Geotechnical Journal Vol. 42, pp 13-26

Lindsay, J., David J., Shepherd J., Ephraim, J. (2002) ‘ Scientific Supplement to the Volcanic Hazard Assessment for Saint Lucia, Lesser Antillies’ Seismic Research Unit, The University of the West Indies, St. Augustine, Trinidad and Tobago.

Little, A.L., (1969) ‘ The Engineering Classification of Residual Tropical Soils’ Proceedings of the 7th International Conference on Soil Mechanics and Foundation Engineering; Speciality Session on Engineering Properties of Lateritic Soils, Mexico, 1969, Vol 1. pp 1-10

Lo, D.O.K., Ho, K.K.S., Wong, H.N., (1998) ‘ Effectiveness of slope maintenance in reducing the likelihood of landslide’ ; Slope Engineering in Hong Kong; Proceedings of the Annual Seminar on Slope Engineering in Hong Kong; Balkema, Rotterdam/Brookfield, pp. 251-258

Locat, J., Lefebvre, G., Ballivy, G., (1984) ' Mineralogy, chemistry, and physical properties interrelationships of some sensitive clays from Eastern Canada' Canadian Geotechnical Journal, Vol. 21, pp 530-540

Loganathan, N., de Silva, S., Thurairajah, A., (1992) ' Strength Correlation Factor for Residual Soils' Journal of Geotechnical Engineering, Vol. 118, No. 4, April 1992, pp 593-609

Longworth, T.I., (1995) ' Investigation, monitoring and emergency remedial works at the La Butte landslide, Mauritius' Building Research Establishment , UK, Landslides, Bell (ed) Balkema, Rotterdam ISBN 90 5410 032X, pp 1593-1602

Low, T.H., Faisal, H.A., Saravanan, M., (2000) ' Suction and infiltration measurement on cut slope in highly heterogeneous residual soil' Unsaturated Soils for Asia; Proceedings of the Asian Conference on Unsaturated Soils, UNSAT-ASIA 2000, SINGAPORE 2000, 18-19 May, 2000, pp. 807-811

Lu, N., Likos, W.J., (2004) 'Unsaturated Soil Mechanics' John Wiley & Sons, Inc., pp. 3-43

Lumb, P. (1975) ' Slope Failures in Hong Kong,' Quarterly Journal of Engineering Geology, Volume 8, pp 31-65

Mavimbela, S.S.W., van Rensburg, L.D., (2012) ' Evaluating Models for Predicting Hydraulic Characteristics of Layered Soils' Hydrology and Earth System Sciences Discussions, Volume 9, pp 301 - 336

Moellmann, A., Vermeer, P.A., Huber, M., (2008) 'A Probabilistic Finite Element Analysis of Embankment Stability Under Transient Seepage Conditions.' Proceedings of the 6th International Probabilistic Workshop, Darmstadt, Germany pp.551- 562

Mohr, E.C.J., Van Baren, F.A., (1954) ' Tropical Soils' Interscience, London, pp. 498

Mungan, N., Jessen,F.W., (2011)' Studies in Fractionated Montmorillonite Suspensions' The University of Texas, Austin, pp 282 - 294

Nagarajan, R., Roy, A., Kumar, R. V., Mukherjee, A., Khire, M.V. (2000) ' Landslide hazard susceptibility mapping based on terrain and climatic factors for tropical monsoon regions' Bulletin of Engineering Geology & the Environment Vol 58, pp 275-287

Newill, D., (1954), 'A n Investigation into the relation for Ghanaian soils between organic matter content and the strength of soil-cement,' British Road Research Laboratory, Note 3572 (unpublished)

Newman, W.R. (1965) ' A Report on General and Economic Geological Studies of St. Lucia, West Indies' United Nations Report for The Government of Saint Lucia.

Ng, C.W.W., Shi, Q., (1998) ' A Numerical Investigation of the Stability of Unsaturated Soil Slopes Subject to Transient Seepage,' Computer and Geotechnics Volume 22, No.1 pp 1-28

Ng, C.W.W., Shi, Q. (1998) ' Influence of Rainfall Intensity and Duration on Slope Stability in Unsaturated Soils,' Quarterly Journal of Engineering Geology, Volume 31, pp 105-113

Ng, C.W.W., Pang, Y.W. (2000) ‘ Influence of Stress States on Soil-Water Characteristics and Slope Stability,’ Journal of Geotechnical and Environmental Engineering, Volume 126, No.2, pp 157-166

Ng, C.W.W., Zhan, L.T., Bao, C.G., Fredlund, D.G., Gong, B.W., (2003)‘ Performance of an unsaturated expansive soil slope subjected to artificial rainfall infiltration’ Geotechnique 53, No. 2, pp 143-157

O’Keefe, P., Conway, C., (1977) ‘Natural Hazards in the Windward Islands,’ Disaster Research Unit, Occasional Paper No. 14, University of Bradford, U.K. Appendix 3, A Disaster History of St. Lucia, pp 81-84

Pandian, N.S., Nagaraj, T.S., Sivakumar Babu, G.L., (1993) ‘ Tropical Clays: Index Properties and Microstructural Aspects’ Journal of Geotechnical Engineering, Vol. 119, No. 5, May, 1993, pp 826-838

Pedrozzi, G., (2003) ‘ Triggering of landslides in Canton Ticino (Switzerland) and prediction by rainfall intensity and duration method’ ; Bulletin of Engineering Geology & the Environment, Vol. 63, pp 281-291

Persson, H. (2008) ‘ Estimation of Pore water Pressure Levels in Slope Stability Calculations: Analyses and Modeling of Groundwater level Fluctuations in Confined Aquifers along the Swedish West Coast,’ Swedish Geotechnical Institute, LINKOPING 2008, pp 13 - 102

Poulos, S.J., (1981) ‘The Steady State of Deformation’ Journal of Geotechnical Engineering, Vol. 107, No. 5, May 1981, pp 553-562

Prior, D.B., Ho, C., (1972) ‘Coastal and Mountain Slope Instability on the Islands of St. Lucia and Barbados’ Journal of Engineering Geology, Volume 6, pp. 1-18

Quigley, R.M., Matich, A.J., Horvath, R.G., Hawson, H.H., (1971) ‘ Swelling Clay in Two Slope Failures at Toronto, Canada’ Canadian Geotechnical Journal Vol. 8, No.3 pp 417- 424

Rahardjo, H., Lim, T.T., Chang M.F., Fredlund D.G., (1995) ‘ Shear Strength Characteristics of a Residual Soil’ Canadian Geotechnical Journal, Vol 32, pp 60-77

Rahardjo, H., Leong, E.C., Rezaur, R.B., (2002) ‘ Studies of Rainfall-Induced Slope Failures’ Invited lecture, National Seminar Slope 2000, Proceedings of the National Seminar, Slope 2002, Bandung, Indonesia, pp 15 - 29

Rahardjo, H., Hritzuk, K.J., Leong, E.C., Rezaur, R.B., (2003) ‘Effectiveness of Horizontal Drains for Slope Stability’, Journal of Engineering Geology, Vol. 69, pp. 295-308

Rahardjo, H., Lee, T.T., Leong, E.C., Rezaur, R.B., (2005) ‘ Response of a Residual Soil Slope to Rainfall,’ Canadian Geotechnical Journal, Vol. 42, pp. 340-351.

Rahardjo, H., Li, X.W., Toll, D.G., Leong, E.C., (2001) ‘ The Effect of Antecedent Rainfall on Slope Stability,’ Earth And Environmental Science; Geotechnical and Geological Engineering; Volume 19, Numbers 3-4, pp 371 – 399.

Rahardjo, H., Rezaur, R.B., Hritzuk, K.J., Leong, E.C. ' Slope Failures in Singapore : Case Study of Two Landslides' Nanyang Technological University, Singapore; Pp 59 - 70

Rahardjo, H., Fredlund, D.G., Vanapalli, S.K., (1991) ' Use of Linear and Nonlinear Shear Strength Versus Matric Suction Relations in Slope Stability Analysis' Landslides, Bell (ed) Balkema, Rotterdam, pp 531 - 537

Reading, A.J., (1991) ' Stability of Tropical Residual Soils from Dominica, West Indies' Journal of Engineering Geology Vol. 31: pp 27- 44

Ridley,A.M., Dineen,K., Burland, J.B.,Vaughn, P.R.(2002) ' Soil Matrix Suction: Some samples of its measurement and application in geotechnical engineering' Geotechnique 53, No.2, pp 241-253

Rogers, C.T., (1997) ' Landslide Hazard Data for Watershed Management and Development Planning, St. Lucia, West Indies': Natural hazards and Hazard Management in the Greater Caribbean and Latin America; Unit for Disaster Studies, The University of the West Indies, Mona, Jamaica, ISBN 976-41-0115-1, Publication No.3, pp. 150-164

Rolfe, B.N., Miller, R.F., McQueen, I.S.,(1960) ' Dispersion Characteristics of Montmorillonite, Kaolinite, and Illite Clays in Waters of Varying Quality, and Their Control with Phosphate Dispersants,' Shorter Contributions to General Geology, Geological Survey Professional Paper 334-G, United States Government Printing Office, Washington 25, D.C., USA, pp 229-270

Rowe, R.K., Poulos, H.G., (1979) ' Settlement of Single Piles in Nonhomogeneous Soil', Journal of geotechnical Engineering, ASCE, Vol. 105, No.5, pp.365-415

Rulon, J.J., Freeze, R.A., (1985) ' Multiple Seepage Faces on Layered Slopes and Their Implications for Slope Stability Analysis' Canadian Geotechnical Journal, Volume 22, pp. 347-356

Sapari,N., Harahap, I.S.H., Adlan, M.N., (2008) ' The Influence of Rising Groundwater on Slope Stability and Engineering Properties of Soil,' Proceedings of EnCon 2008, 2nd Engineering Conference on Sustainable Engineering Infrastructures Development & Management, December 18-19, 2008, Kuching, Sarawak, Malaysia, pp. 1 – 6.

Sassa, K., Nagai, O., Solidum, R., Yamazaki, Y., Ohta, H. (2010) ' An Integrated Model Simulating the Initiation and Motion of Earthquake and Rain Induced Rapid landslides and its Application to the 2006 Leyte Landslide,' Springer –Verlag, DOI 10.1007/s10346-010-0230-z

Schulz, W.H., Lidke, D.J., Godt, J.W., (2008) ' Modeling the spartial distribution of landslide-prone colluvium and shallow groundwater on hillslopes of Seattle, WA, USA' ; United States Geological Survey; Earth Surface Processes and Landforms; John Wiley & Sons Ltd, Vol. 33, pp 123-141

Seismic Research Unit – University of the West Indies 2009 ' Island Profiles – Saint Lucia Seismicity' (www.uwiseismic.com/news/events)

Shen, J.M., (1998) 'Soil Suction in relation to Slope Stability: A summary of research carried out in Hong Kong in 1978-1997' Slope Engineering in Hong Kong: Proceedings of the Annual Seminar on Slope Engineering in Hong Kong; Balkema Rotterdam, 1997, pp 93-98

Sheng. D, Zou, A., Fredlund, D.G., (2011) ‘ Shear Strength Criteria for Unsaturated Soils’ Geotech Geol Eng, Volume 29, pp 145-159

Sheng, D. (2011) ‘ Review of Fundamental Principles in modeling Unsaturated Soil Behaviour’ Elsevier : Computers and Geotechnics 38 pp 757 – 776

SLOPE INDICATOR COMPANY (2006) ‘ Digitilt Inclinometer Probe Manual 50302599’ SLOPE INDICATOR COMPANY, Mukilteo, WA, USA

SLOPE INDICATOR COMPANY (2007) ‘Data Mate Manager Software Manual 50310970’, SLOPE INDICATOR COMPANY, Mukilteo, WA, USA

SOILMOISTURE EQUIPMENT CORP. (1986) ‘Model 2725A Jet Fill Tensiometer Operating Instructions’ SOILMOISTURE EQUIPMENT CORP., Santa Barbara, CA, USA

SOILVISION (Software) – A Knowledge-Based Soils Database System for Saturated/Unsaturated Soil Properties : SOILVISION SYSTEMS LTD, Saskatoon, Saskatchewan, Canada; 2006

Sparks, D.L., et al, (1996) ‘ Methods of Soil Analysis, Part 3, Chemical Methods’ SSSA, Madison,Wisconsin, USA pp 1004-1005.

Springman, S.M., Jommi, C., Teysseire, P., (2002) ‘ Instabilities on moraine slopes induced by loss of suction: a case history’; Geotechnique, Vol. 53, No. 1, pp 3-10

Sridharan, A. (1988) ‘ General Report: Engineering Properties of Tropical Soils’, Proceedings of the second International Conference on Geomechanics in Tropical Soils, Singapore, Volume 2, A.A Balkema, Rotterdam, pp 529

Staiano, T., Rinaldi, M., Paris, E. (2011) ‘ Seepage and Stability Analysis of Embankments During Flood Events’ Department of Civil Engineering, University of Florence, Italy. Via S. Marta 3, 50139 Florence, pp 1-14

Strata Engineering Consultants Ltd – Archives : 1996 – 2009 (not published) Saint Lucia, West Indies.

Taha, M.R., et al, (2000) ‘ Shear Strength of Unsaturated granite Residual Soil’ Unsaturated Soils for Asia, Balkema, Rotterdam, pp 575-580

Tang, W.H., Stark, T.D., Angulo, M., (1999) ‘ Reliability in Back Analysis of Slope Failures’ SOILS AND FOUNDATIONS, Japanese Geotechnical Society, Volume 39, No. 5, 000-000, October 1999, pp. 73 - 80

Tarantino, A., Bosco, G., Mongiovi, L., (2000) ‘Response of the IC tensiometer with respect to cavitation’ ; Unsaturated Soils for Asia; Proceedings of the Asian Conference on Unsaturated Soils; UNSAT-ASIA 2000/SINGAPORE/18-19 May 2000, pp 309-313

Terzaghi, K, Peck, R.B. (1967) ‘ Soil Mechanics in Engineering Practice’ Second Edition, John Wiley & Sons Inc., New York, U.S.A. pp 432

The American Society of Civil Engineers (1983) ‘ Seismic Design of Embankments and Caverns’ Proceedings of a Symposium sponsored by the ASCE Geotechnical Engineering Division, May 16-20, 1983

The Japanese Geotechnical Society (1998) ‘ Remedial Measures Against Soil Liquefaction’ A.A. Balkema Publishers/Rotterdam/Brookfield, pp 40–54.

Thieu, N.T.M, Fredlund, M.D., Fredlund, D.G., Hung, V.Q., (2001) ‘ Seepage Modeling in a Saturated/Unsaturated Soil System’; International Conference on Management of the Land and Water Resources, MLWR, October 20-22, 2001, Hanoi, Vietnam.

Tofani, V., Dapporto, S., Vannocci, P., and Casagli, N., (2006) ‘ Infiltration, Seepage and Slope Stability Mechanisms During the 20 – 21 November 2000 Rainstorm in Tuscany, Central Italy.’ Natural Hazards and Earth Systems Science, 6. pp. 1026-1033

Tohari, A., Sarah, D., (2006) ‘ Assessment of the Stability of Steep Volcanic Residual Soil Slopes Under Rainfall Infiltration,’ Media Teknik Sipil July 2006, pp 95-102

Toll, D.G. (1990) ‘A Framework for Unsaturated Soil Behaviour,’ Geotechnique 40, No.1, pp 31- 44

Toll, D.G., et al, (2000) ‘ Triaxial Testing of Unsaturated Samples of Undisturbed Residual Soil from Singapore’, Unsaturated Soils for Asia, Balkema, Rotterdam, pp 581-586.

Toll, D.G., (2001)‘ Rainfall-induced Landslides in Singapore’ Proceedings of the Institution of Civil Engineers, Geotechnical Engineering 149, Paper 12138, Issue 4, pp 211-216

Tommasi, P., Pellegrini, P., Boldini, D., Ribacchi, R., (2006) ‘ Influence of rainfall regime on hydraulic conditions and movement rates in the overconsolidated clayey slope of the Orvieto hill (Central Italy)’ Canadian Geotechnical Journal 43, pp 70- 86

Townsend, F.C., (1985) ‘ Geotechnical Characteristics of Residual Soils’ Journal of Geotechnical Engineering, Vol. 111, No. 1, 1985, pp 77-92

Trewin, N.H., (1988) ‘ The Use of the Scanning Electron Microscope in Sedimentology’ Techniques in Sedimentology (M. Tucker ed.) Oxford (Blackwell) pp 229-273

Tsai, T.L., Chen, H.E., Yang, J.C. (2008) Numerical Modeling of Rainstorm-Induced Shallow Landslides in saturated and unsaturated Soils’ Environmental Geology 55, DOI 10, 1007/s00254-007-1075-1, pp 1269 - 1277

Tsaparas, I., Rahardjo, H., Toll, D.G., Leong, E.C., (2002) ‘ Controlling parameters for rainfall-induced landslides’; Elsevier Science Ltd; Computers and Geotechnics 29, (2002) pp. 1-27

Tsaparas, I., Toll, D.G., Rahardjo, H., (2000) ‘ Influence of rainfall sequences on the seepage conditions within a slope: A parametric study’; Unsaturated Soils for Asia; Proceedings of the Asian Conference on Unsaturated Soils; UNSAT-ASIA 2000/SINGAPORE/18-19 May, 2000, pp. 837-842

United Nations (2011) ‘ SAINT LUCIA – Macro Socio-Economic and Environmental A Assessment of the Damage and Losses Caused by Hurricane TOMAS : Geo-Environmental Disaster’ , The Economic Commission for Latin America and the Caribbean – ECLAC, February 7, 2011.

United States of America Department of the Navy, Naval Facilities Engineering Command (NAVFAC) 1974, ‘Field Tests and Measurements’, pp 7-4-8

Vanapalli, S.K., Fredlund, D.G., Pufahl, D.E., (1999) ‘ Relationship between Soil-Water Characteristic Curves and the As-Compacted Water Content Versus Soil Suction for a Clay Till’; X1 Pan-American Conference on Soil Mechanics and Foundation Engineering, Brazil, August 8-12, 1999, pp. 991-998

Vanapalli, S.K., Sillers, W.S., Fredlund, M.D., (1998) ‘ The Meaning and Relevance of Residual State to Unsaturated Soils’, 51st Canadian Geotechnical Conference, Edmonton, Alberta, October 4 – 7, 1998, pp. 1-8

Vandamme, J., Zou, Q. (2012) ‘ Investigation of Slope Instability Induced by Seepage and Erosion by Particle Method,’ Computers and Geotechnics, Elsevier Ltd, Volume 48, pp 9-20

Vargas, M., (1983) ‘ A Brazilian Experience in Construction and maintenance of Roads on Tropical Rainy Mountainsides’ Proceedings of the Seventh Panamerican Conference on Soil Mechanics and Foundation Engineering, Vancouver, British Columbia, Canada 1983, pp 259-267

Veniale, F., Simeoni, L., Navarro, C.R., Setti, M., (2002) ‘ The Role of Fabric and Mineralogy in Planar Sliding Processes in Marly Rocks: Investigation Using Scanning Electron Microscopy (SEM) and Environmental – SEM’ REVISTA ITALIANA DI GEOTECNICA, pp. 24-39

Walker, B.F., Fell, R. (1987) ‘ Soil Slope Instability & Stabilization’, A.A.Balkema, Rotterdam, Proceedings of an Extension Course on Soil Slope Instability and Stabilisation/ Sydney, November 30 to December 2, 1987, pp 1-47.

Wang, B. , Murray, L., ‘ An Unsaturated Soil Seepage Analysis for Design of a Soil Cover System to Reduce Oxidation of a Mine Tailings Deposit’ Klohn Crippen Berger

Wen, B.P., Aydin, A. (2003) ‘ Microstructural study of a natural slip zone: qualification and deformation history’ Elsevier Science B.V.; Engineering Geology 68, pp 289-317

Wesley, L.D., (1988) ‘Engineering classification of residual soils’. Proceedings of the Second International Conference on Geomechanics in Tropical Soils, Singapore Vol. 1, pp. 77-84

Wong, J.C. et al, (2000) ‘ Shear Strength of Undisturbed Bukit Timah Granite Soils under Infiltration Conditions’, Unsaturated Soils For Asia, Balkema, Rotterdam, pp 587-591.

Xue, J., Gavin, K., (2007) ‘ Effect of Rainfall Intensity on Infiltration into Partially Saturated Slopes’ Geotech Geol Eng., Springer Science & Business Media B.V.

Yagi, N., Yatabe, R., Yokota, K., Bhandary, N.P., (2000) 'Suction measurement for the prediction of slope failure due to rainfall'; Unsaturatede Soils for Asia', Proceedings of the Asian Conference on Unsaturated Soil; UNSAT-ASIA 2000/SINGAPORE, 18-19 May, 2000, pp. 847-851

Yang, C., Sheng, D., Carter, J.P. (2011) ' Effect of Hydraulic Hysteresis on Seepage Analysis for Unsaturated Soils,' Computers and Geotechnics, Elsevier Ltd, Volume 14, pp 36-56

Yang, H., Rahardjo, H., Leong, E.C., (2006) ' Behavior of Unsaturated Layered Soil Columns during Infiltration.' Journal of Hydrologic Engineering , ASCE, Volume 11, No. 4, pp 329 - 337

Yangwen, J.I.A., Nobuyuki, T., (1997) ' Modeling Infiltration into a Multi-layered Soil during an Unsteady Rain,' Annual Journal of Hydraulic Engineering, JSCE, Vol. 41, pp 31 - 36

Yeh, T.C.J., Harvey, D.J. (1990) ' Effective Unsaturated Hydraulic Conductivity of Layered Sands' Water Resources Research, Volume 26, No. 6, pp 1271 – 1279.

Yeh, H.F., Chang,P.H., Chen, J.F., Lee,C.H., (2006) ' Instability of Unsaturated Soil Slopes Due to Infiltration' International Symposium on Geohazards Mitigation, Tainan, Taiwan, pp 1 – 6.

Yeh, H.F., Lee, C.C., Lee, C.H., (2008) ' A Rainfall-Infiltration Model For Unsaturated Soil Slope Stability,' Journal of Environmental Engineering Management, Volume 18, No. 4, pp 261-268.

Yilmaz, I., Erzin, Y., (2004) ' Selection of Core Material for an Earth dam in Lower Cekerek Basin, Tokat, Turkey' Electronic Journal of Geotechnical Engineering, Paper 0472, pp 1-10

Yunusa, G.H., Gofar, N. (2012) 'Influenceof Evaporation on Transient Suction Distribution in Unsaturated Soil,' Internationsl Journal of the Physical Sciences Volume 7, No.3, pp 508-518

Zhang, J., Jiao,J.J., Yang, J. (2000) ' In situ Infiltration Studies at a Hillside in Hubei Provence, China' Elsevier, Engineering Geology 57, pp 31 - 38

Zhan, T.L.T., Ng, C.W.W., (2004) ' Analytical Analysis of Rainfall Infiltration Mechanism in Unsaturated Soils' ; International Journal of Geomechanics, Vol. 4, No. 4, 2004, pp 273-284